Karlsruhe Institute of Technology

Proceedings of the 20th International Workshop on Ceramic Breeder Blanket Interactions (CBBI-20)

September, 18-20, 2019, KIT, Germany

Regina Knitter (ed.)

KIT SCIENTIFIC WORKING PAPERS 130

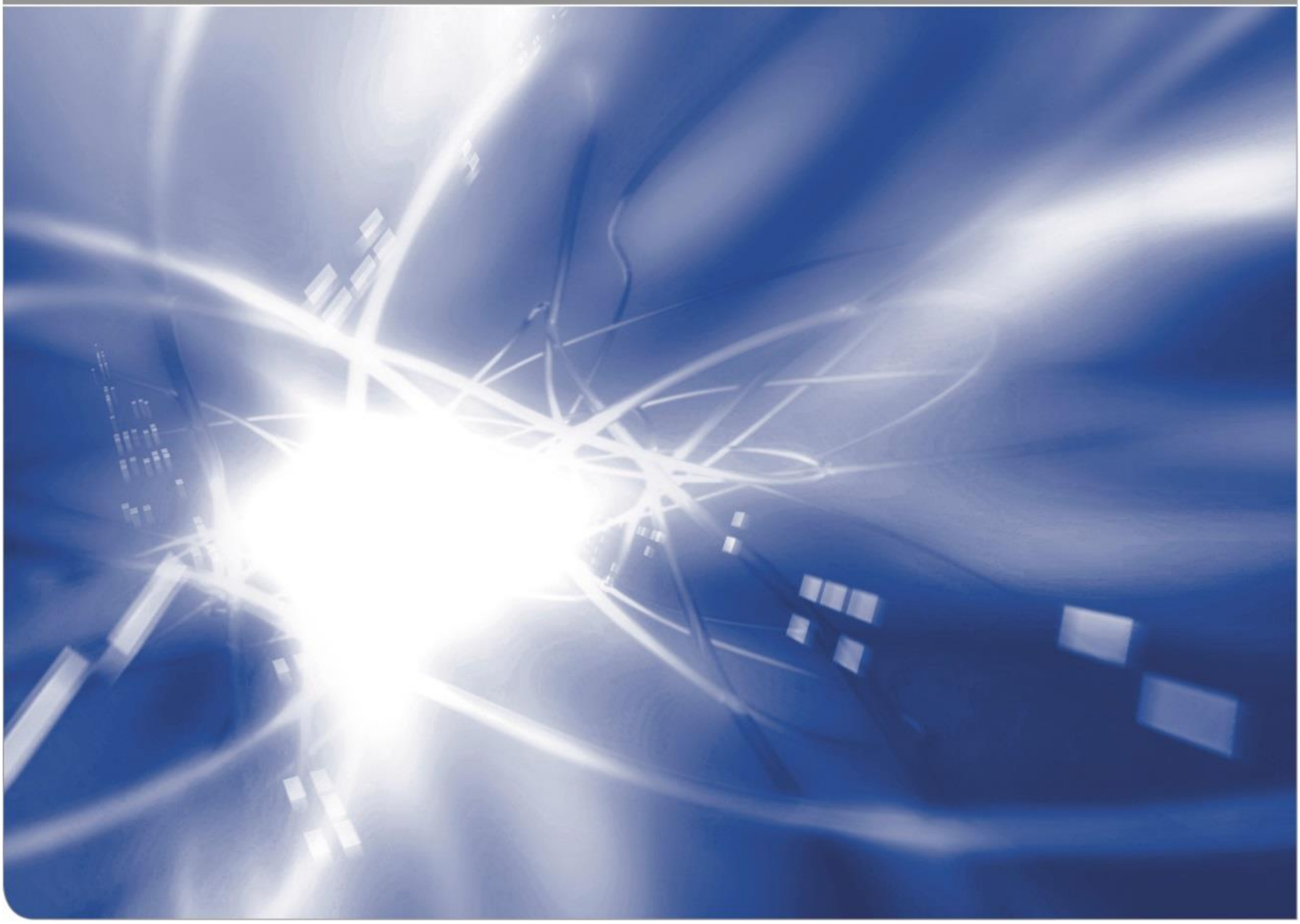

Dr. Regina Knitter
Institute for Applied Materials
P.O. Box 3640
76021 Karlsruhe

Impressum

Karlsruher Institut für Technologie (KIT)
www.kit.edu

2019

ISSN: 2194-1629

Proceedings of the

20th International Workshop on Ceramic Breeder Blanket Interactions

CBBI-20

18 – 20 September 2019, KIT, Germany

CONTENT

PREFACE

The 20th International Workshop on Ceramic Breeder Blanket Interactions (CBBI-20) was held under the auspices of the International Energy Agency (IEA) Implementing Agreement on the Nuclear Technology of Fusion Reactors at Karlsruhe Institute of Technology, Germany, on September 18-20, 2019 in conjunction with the 14th International Symposium on Fusion Nuclear Technology (ISFNT-14), in Budapest, Hungary, September 22-27, 2019.

The workshop provided a forum of specialists involved in the design, research, development and testing of materials and components for lithium ceramic based breeding blankets. It was attended by nearly 50 researchers working on ceramic breeder blankets. In 35 contributions recent results and advances in the areas of ceramic breeder material development, solid breeder blanket design, irradiation testing as well as experiments and modelling of pebble bed thermo-mechanics and Li-6 enrichment were presented.

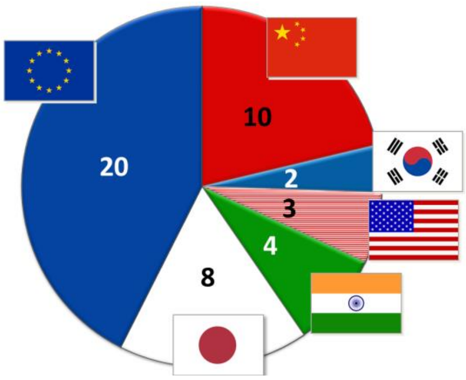

Origin of CBBI-20 participants.

EDITOR

R. Knitter (KIT)

PROGRAM ADVISORY COMMITTEE

M. Abdou (UCLA)	Y. Feng (SWIP)
M.-Y. Ahn (NFRI)	A. Ibarra (CIEMAT)
L.V. Boccaccini (KIT)	Y. Kawamura (QST)
P. Chaudhuri (IPR)	R. Knitter (KIT)
X. Chen (CAEP)	T. Terai (Univ. of Tokyo)

LOCAL ORGANIZATION

R. Knitter, M. Ionescu-Bujor, T. Mitrovic (KIT)

CBBI-20

Program

Wednesday, 18 September 2019

Session 1 – Chair: R. Knitter, KIT

Paritosh Chaudhuri, IPR
Status and progress on the activities of lithium ceramic breeder materials at IPR

Xiaojun Chen, CAEP
Progress of ceramic breeder materials in CAEP

Oliver Leys, KIT
Advanced ceramic breeder pebble production: Controlling the pebble size

Qiang Qi, ASIPP
Comparison of tritium release behavior in promising tritium breeding materials

Session 2 – Chair: M.-Y. Ahn, NFRI

Linjie Zhao, CAEP
Design, synthesis and characterization of Li4SiO4-based solid solutions as advanced tritium breeders

Juemin Yan, Sichuan U, CAEP
Design, synthesis, calculation and characterization of the tritium breeder: Li4TiO4 ceramics

Yu-Ping Xu, ASIPP
3D imaging of the microstructure of the ceramic breeding pebbles by X-ray computed tomography

Keisuke Mukai, Kyoto U
Analysis of valence electron structure of Li metal/oxides by soft X-ray emission spectroscopy

Session 3 – Chair: X. Chen, CAEP

Takumi Chikada, Shizuoka U
Compatibility of tritium permeation barrier coatings under solid breeder blanket conditions

Mario Walter, KIT
Impact of a ceramic breeder environment on the fatigue lifetime of EUROFER

Keiji Oishi, U Tokyo
Compatibility between fusion reactor blanket structural material F82H and solid breeders lithium titanate and lithium oxide

Long Wang, SWIP
Hydrogen isotope permeability of reduced activation ferritic-martensitic steel CLF-1 by Li_4SiO_4

Session 4 – Chair: R. K. Annabattula, IITM

Jae-Hwan Kim, QST
Compatibility of advanced functional materials for fusion applications

Xiaoman Cheng, ASIPP
Simulation of oxidation reaction between Be pebble beds and steam in WCCB blanket during in-box LOCA

Simon Steel, UKAEA
Test facility for tritium permeation measurements of containment materials and coatings under breeder blanket relevant conditions

CBBI-20

Thursday, 19 September 2019

Session 5 – Chair: T. Hoshino, QST

María González, CIEMAT
Behavior of ceramic breeder candidates to high-energy ion beams

Samuel J. Waters, U Sheffield
Radiation damage and helium accommodation in lithium metatitanate ceramic breeder materials

Artūrs Zariņš, U Latvia
Analysis of electromagnetic and corpuscular radiation-induced processes in advanced two-phased ceramic breeder pebbles

Satoshi Konishi, Kyoto U
Integrated neutronics experiment of breeding blanket assembly and TBR evaluation with discharge fusion source

Session 6 – Chair: K. Mukai, Kyoto U

Samuel T. Murphy, Lancaster U
Tritium and helium solubility in Li_2TiO_3 from density functional theory

Kamal Nayan Goswami, Lancaster U
A first-principles kinetic Monte Carlo investigation of tritium diffusion in Li_2TiO_3

Megha Sanjeev, Lancaster U
Thermal conductivity of Li_2TiO_3 by atomistic simulation

Narasimhan Swaminathan, IITM
Radiation damage properties of Li_4SiO_4 and Li_2TiO_3 using molecular dynamics simulations – A comparative study

Session 7 – Chair: S. Liu, ASIPP

Yi-Hyun Park, NFRI
Maximum operating temperature for Li_2TiO_3 pebble bed from sintering phenomenon

Marigrazia Moscardini, U Pisa
Discrete Element analysis of plastic deformation in pebble beds

Jörg Reimann, KIT
Influences of pebble geometry on the thermomechanical behaviour of ceramic breeder pebble beds

Session 8 – Chair: A. Ying, UCLA

Ratna Kumar Annabattula, IITM
Application of machine learning tools to study heat transfer in ceramic pebble beds

Baoping Gong, SWIP
Investigation of the packing behaviors and the effective thermal conductivity of pebble beds

Lei Chen, ASIPP
Experimental and numerical study of flow and heat transfer characteristics for pebble beds in fusion blankets

Friday, 20 September 2019

Session 9 – Chair: P. Chaudhuri, IPR

Songlin Liu, ASIPP
Design of the water cooled ceramic breeder blanket for CFETR with the latest core parameters and mission

Francisco A. Hernández, KIT
Consolidated design of the HCPB breeding blanket for the pre-conceptual design activities of the EU DEMO and harmonization with the ITER HCPB TBM program

Mu-Young Ahn, NFRI
Design and R&D status of tritium extraction system for HCCR-TBM

Session 10 – Chair: R. Knitter, KIT

Tsuyoshi Hoshino, QST
Lithium-6 enrichment using innovative electrodialysis with lithium ionic conductor for fusion reactor

Kenji Morita, QST
Computational analyses of fast ion conductors for efficient separation of lithium-6

Julia M. Heuser, KIT
Lithium-6 availability and an assessment of enrichment strategies

LIST OF PARTICIPANTS

1	Ahn	Mu-Young	NFRI
2	Annabattula	Ratna Kumar	IITM
3	Boccaccini	Lorenzo V.	KIT
4	Chauduri	Paritosh	IPR
5	Chen	Lei	ASIPP
6	Chen	Xiaojun	CAEP
7	Cheng	Xiaoman	ASIPP
8	Chikada	Takumi	Shizuoka Univ.
9	Gong	Baoping	SWIP
10	González	María	CIEMAT
11	Goraieb	Ancieto	KBHF
12	Goswami	Kamal Nayan	Lancaster Univ.
13	Gray	Rebecca	Lancaster Univ.
14	Hernandez	Francisco	KIT
15	Heuser	Julia	KIT
16	Hoshino	Tsuyoshi	QST
17	Humrickhouse	Paul	INL
18	Ionescu-Bujor	Mihaela	KIT
19	Kamlah	Marc	KIT
20	Kim	Jae-Hwan	QST
21	Knitter	Regina	KIT
22	Konishi	Satoshi	Kyoto Univ.
23	Leys	Oliver	KIT
24	Lui	Songlin	ASIPP
25	Meenakshi	Meenakshi	KIT
26	Morita	Kenji	QST
27	Moscardini	Marigrazia	Univ. Pisa
28	Mukai	Keisuke	Kyoto Univ.
29	Murphy	Samuel	Lancaster Univ.
30	Oishi	Keiji	Tokyo Univ.
31	Park	Yi-Hyun	NFRI
32	Qi	Qiang	ASIPP
33	Radloff	Dirk	KIT
34	Reimann	Jörg	KIT
35	Sanjeev	Megha	Lancaster Univ.
36	Shaw	Guinevere	DoE
37	Steel	Simon	UKAEA
38	Swaminathan	Narasimhan	IITM
39	Terai	Takayuki	Tokyo Univ.
40	Walter	Mario	KIT
41	Wang	Long	SWIP
42	Waters	Samuel	Univ. Sheffield
43	Xu	Yu-Ping	ASIPP
44	Yan	Juemin	Sichuan Univ.
45	Ying	Alice	UCLA
46	Zariņš	Artūrs	Univ. Latvia
47	Zhao	Linjie	CAEP

Further participants from KIT temporarily joint the workshop.

PHOTOGRAPHS

(by courtesy of Prof. T. Terai, Univ. Tokyo)

Participants of CBBI-20 on September, 19, 2019.

Participants of CBBI-20 on September, 20, 2019.

CBBI-20 Dinner on September, 19, 2019.

CBBI-20 Dinner on September, 19, 2019.

CONTENTS LIST OF PRESENTATIONS

The presentations are included as far as the reproduction is in agreement with the authors.

Status and progress on the activities of lithium ceramic breeder materials at IPR

Paritosh Chaudhuri[1,2*] , Maulick Panchal[1], Aroh Shrivastava[1]

[1]Institute for Plasma Research, Bhat, Gandhinagar, Gujarat – 382428, India

[2] Homi Bhabha National Institute, Anushaktinagar, Mumbai - 400094, India

Lithium meta-titanate (Li_2TiO_3) and Lithium ortho-silicate (Li_4SiO_4) are considered to be the suitable candidate materials for tritium breeders. India has developed and prepared Li_2TiO_3 as the tritium breeder materials for fusion blankets. Li_2TiO_3 power was prepared by solid state reaction using Li_2CO_3 and TiO_2 followed by ball-milling and calcination. Li_2TiO_3 pellets and pebbles are prepared from this powder followed by high temperature sintering. Effect of sintering time and temperature on the properties of pebbles has been studied. At every stage of preparation, extensive characterizations are being carried out to meet the desired properties of these materials. This includes all physical (density, porosity, phase purity, particle size etc.), mechanical (crush strength etc.), thermal (thermal diffusivity, conductivity, specific heat), thermo-mechanical characterization of pellets, pebble and pebble bed. Detail study of thermal diffusivity, and thermal conductivity of Li_2TiO_3 pellets by laser Flash technique has been performed and compared with Finite Element Analysis using ANSYS. Results obtained from these experiments and also the future scope will be discussed in this paper. Details of lithium ceramic breeder material development, their comprehensive characterizations, preparation of material database, related R&D activities and their status will be discussed in this paper.

Progress of Ceramic Breeder Materials in CAEP

Xiaojun Chen, DT fuel cycle research group

Institute of Nuclear Physics and Chemistry, CAEP

Ceramic breeder pebble will be is used as tritium production materials in CFETR. Li_4SiO_4 and Li_2TiO_3 pebble are the candidates in the present tritium production modules design. Some research works, including pebble fabrication, characterization, in-pile test and out-of-pile test experiment, are carried out in CAEP. A series of advanced tritium breeders have also been developed, for example, Li_2O pebble coated with SiO_2, Li_4SiO_4-based solid solutions and PbO_2-doped Li_4SiO_4. Freeze-drying method and melt-spraying method ware developed to fabricate ceramic pebble. In the TRINPC series tritium release experiments, the effect of 7 T MF on tritium release behavior was also carried out to prove the effect of magnetic field on the tritium release property, the result shows the tritium release property did not affected by the magnetic field in out-of-pile experiment. The behaviors of water desorption and tritium release was found to proceed simultaneously, indicating a strong correlation between the two processes. Including the hydrogen isotope separation process and purification process, an in-pile test platform is just finish constructed. Some in-pile tritium release experiment will carry out in the year using Li_4SiO_4 and Li_2TiO_3 pebble. In the presentation, some results and future challenges related to tritium ceramic breeder for TBMs will be reviewed.


核物理与化学研究所
INSTITUTE OF NUCLEAR PHYSICS AND CHEMISTRY
CBBI-20
Progress of Ceramic Breeder Materials in CAEP
Presented by: CHEN Xiaojun
E-mail Address: xiaojunchen@caep.cn
Institute of Nuclear Physics and Chemistry, CAEP
2019.09.18

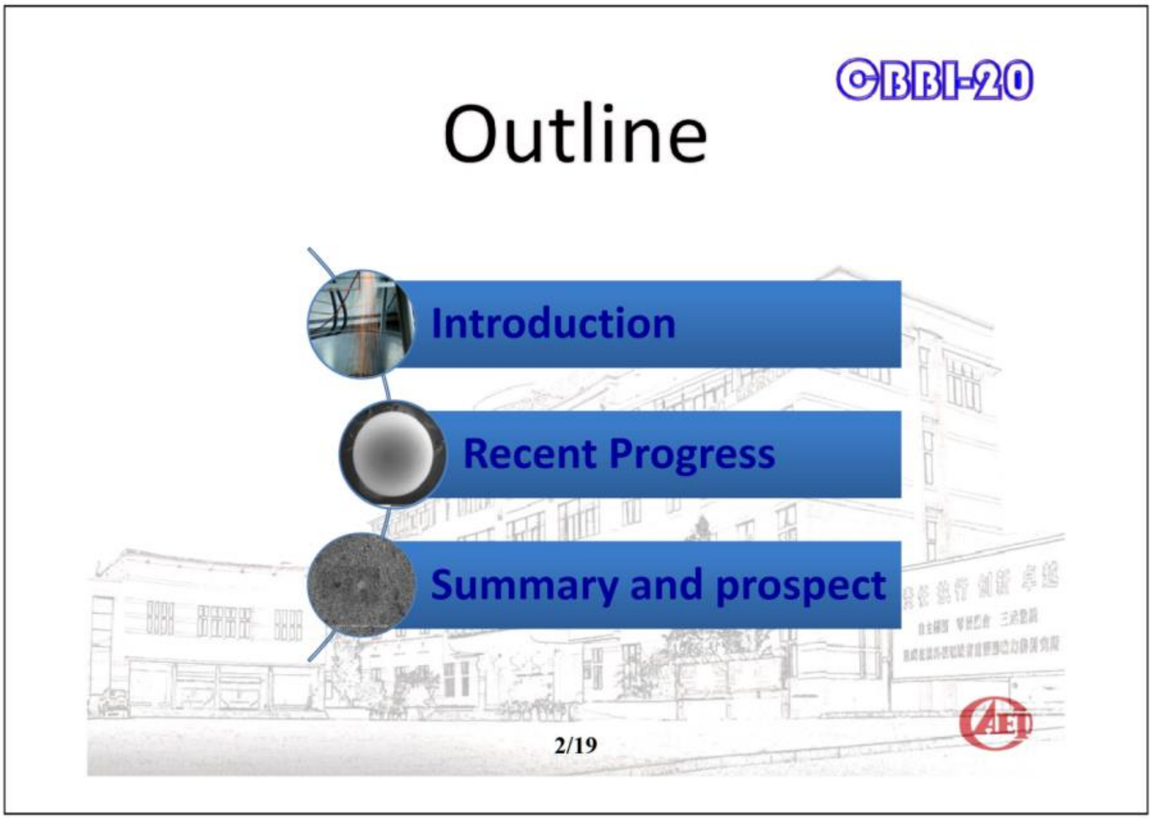
CBBI-20
Outline
Introduction
Recent Progress
Summary and prospect
2/19

1. Introduction

CBBI-20

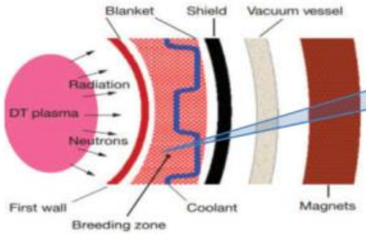

Fundamental property of solid ceramic breeder

- Tritium production — Lithium density
- Tritium extraction — Tritium inventory
- Life-span — Neutron irradiation
- Reliability — Thermo. mechanism
- Heat extraction — Thermal conductivity
- Safety — Melting point
- Lithium recycle — Radio activity
- Security — Mat. compatibility

3/19

2. Recent Progress

CBBI-20

(1) Scale-up production

-effects of pre-treatment and reagent ratio

Li:Si=4.2， phase purity≈98%

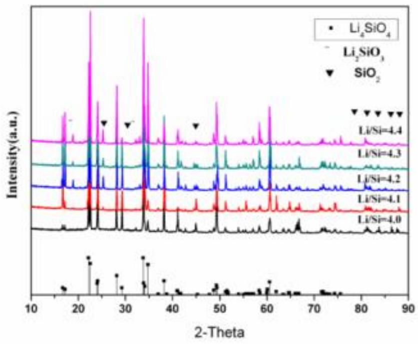

Pretreatment at 750ºC 10 h

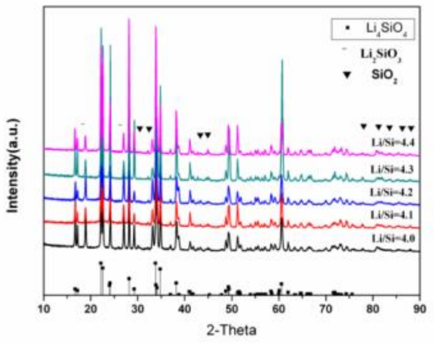

Former process with no pretreatment

From Dr. Zhao's thesis work

4/19

CBBI-20

2. Recent Progress

(1) Scale-up production

-melting process

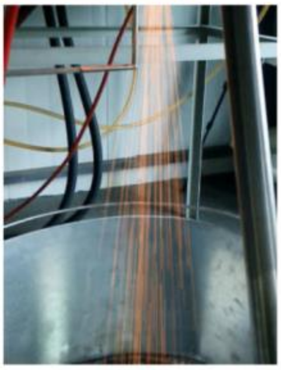

Improved process

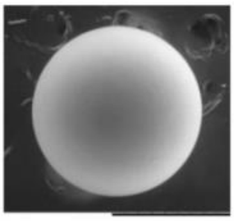

>1kg(one batch) ， >500kg(in one year)

5/19

CBBI-20

2. Recent Progress

(1) Scale-up production

Melting process

Li_4SiO_4

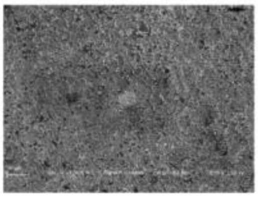

SEM

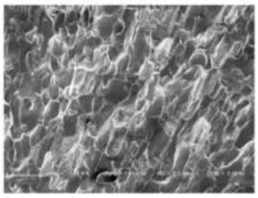

SEM

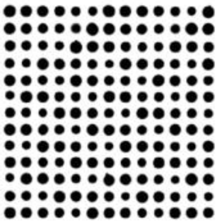

Image of the pebble

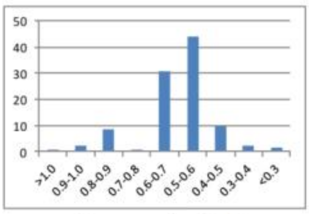

Diameter distribution

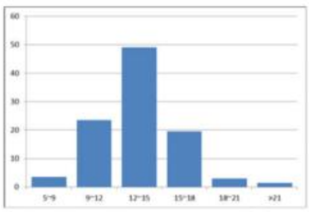

Crush load

6/19

CBBI-20

2. Recent Progress

(2) Advanced ceramic breeder

$Li_{4+x}Si_{1-x}Al_xO_4$

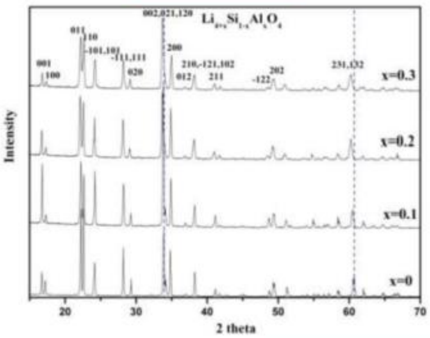

$Li_4Si_{1-x}Ti_xO_4$

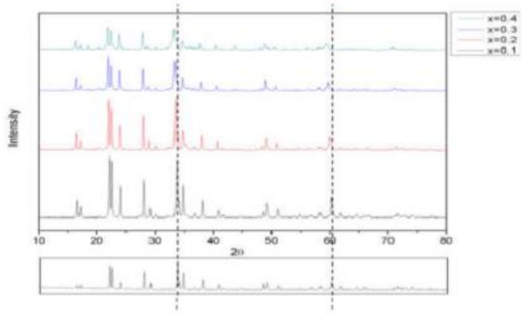

XRD of Al、Ti doped Li_4SiO_4

From Dr. Zhao's thesis work

7/19

CBBI-20

2. Recent Progress

(2) Advanced ceramic breeder

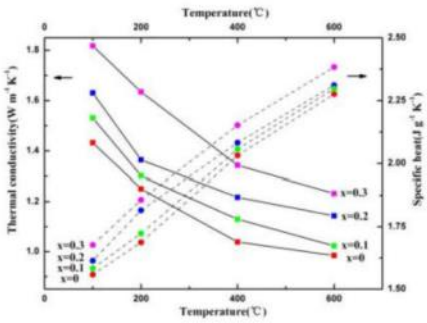

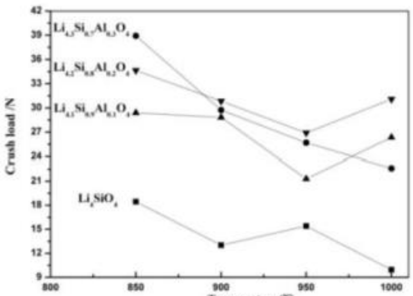

Thermal conductivity and crush load of advanced ceramic breeder

From Dr. Zhao's thesis work

8/19

CBBI-20

2. Recent Progress

(2) Advanced ceramic breeder

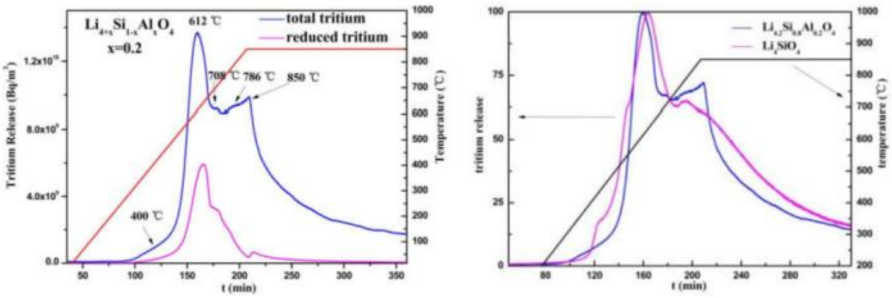

Out of pile tritium release property of $Li_{4+x}Si_{1-x}Al_xO_4$

From Dr. Zhao's thesis work

9/19

CBBI-20

2. Recent Progress

(2) Advanced ceramic breeder

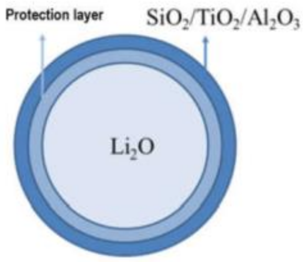

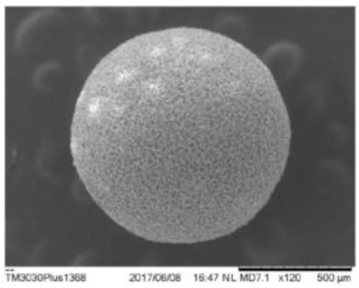

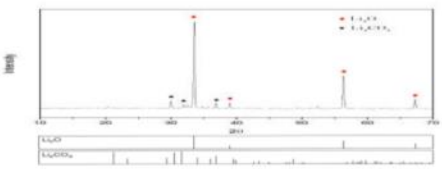

- **Newly designed advanced Ceramic breeder, Li_2O as the nucleus。**

From Mr. Ma's thesis work

10/19

CBBI-20

2. Recent Progress

(3) Tritium release property

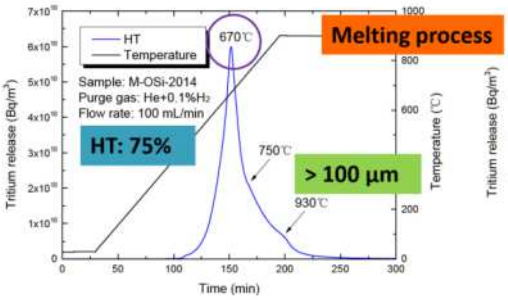

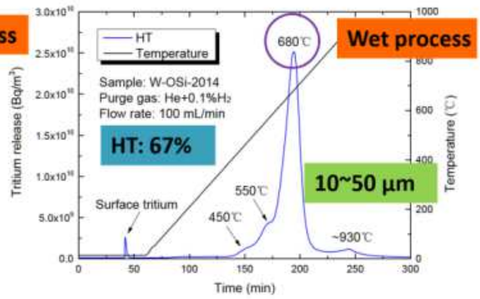

Tritium release behavior of the OSi pebbles for different process
Density, crystal size VS tritium release temp. tritium chemical form

From Dr. Ran's thesis work 11/19

CBBI-20

2. Recent Progress

(3) Tritium release property

➢ Crystal size：100~300 μm

Neutron fluence：3.9×10²² m²

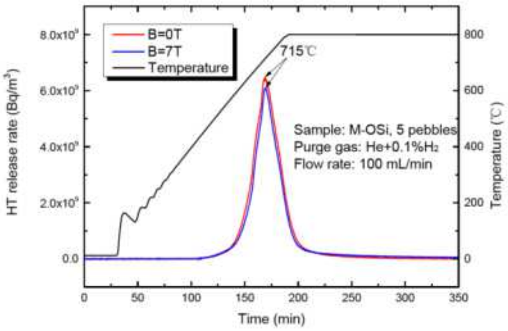

Tritium release behavior under magnetic field

Magnetic field has nearly no effects on the tritium release process

From Dr. Ran's thesis work 12/19

2. Recent Progress

CBBI-20

(3) Tritium release property

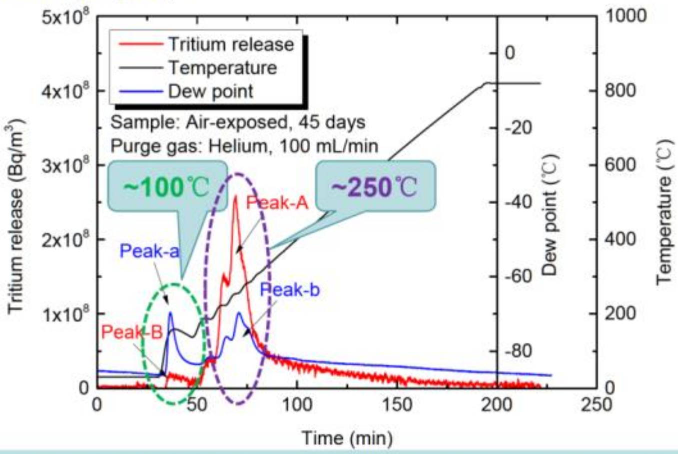

Tritium release behavior (irradiated sample exposed to air for 45

Tritium release peak ≈ water desorption peak

From Dr. Ran's thesis work

13/19

2. Recent Progress

CBBI-20

(4) Tritium release mechanism

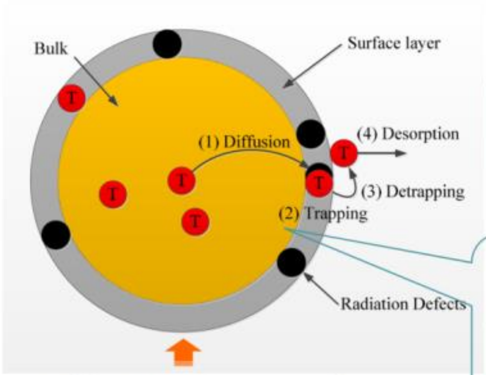

Tritium desorption on the surface is controlling preocess

Temp. for radiation defects disappear and tritium release 500~600℃

Interactions of radiation defects and tritium is at the crystal surface

1) T^+ diffusion fron the crystal
2) T^+capture in the E' center
3) T^+ detrapping with the defects disappear
4) tritium desorption on the surface

From Dr. Ran's thesis work

14/19

CBBI-20

2. Recent Progress

5. Pebble bed

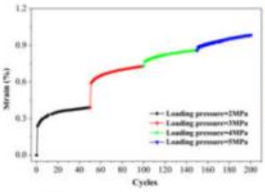

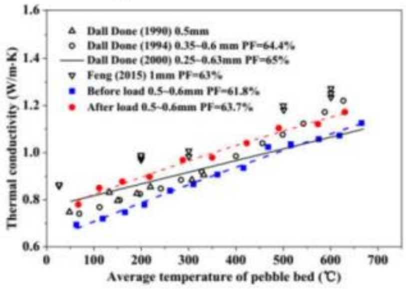

Equivalent thermal conductivity of Li_4SiO_4pebble bed after thermal-mechanical cycle

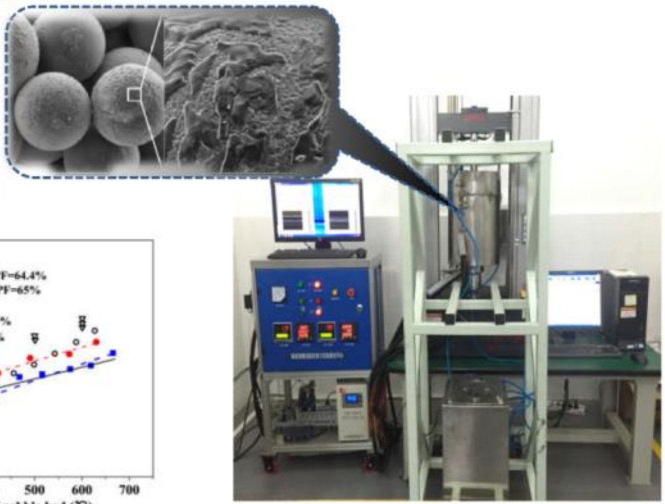

Pebble bed property test apparatus, periodical thermal –mechanical load test

From Dr. Zhang's thesis work

15/19

CBBI-20

2. Recent Progress

6. In-pile tritium extraction platform

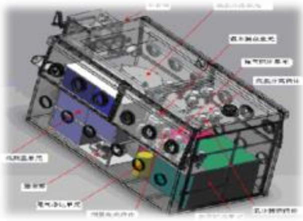

16/19

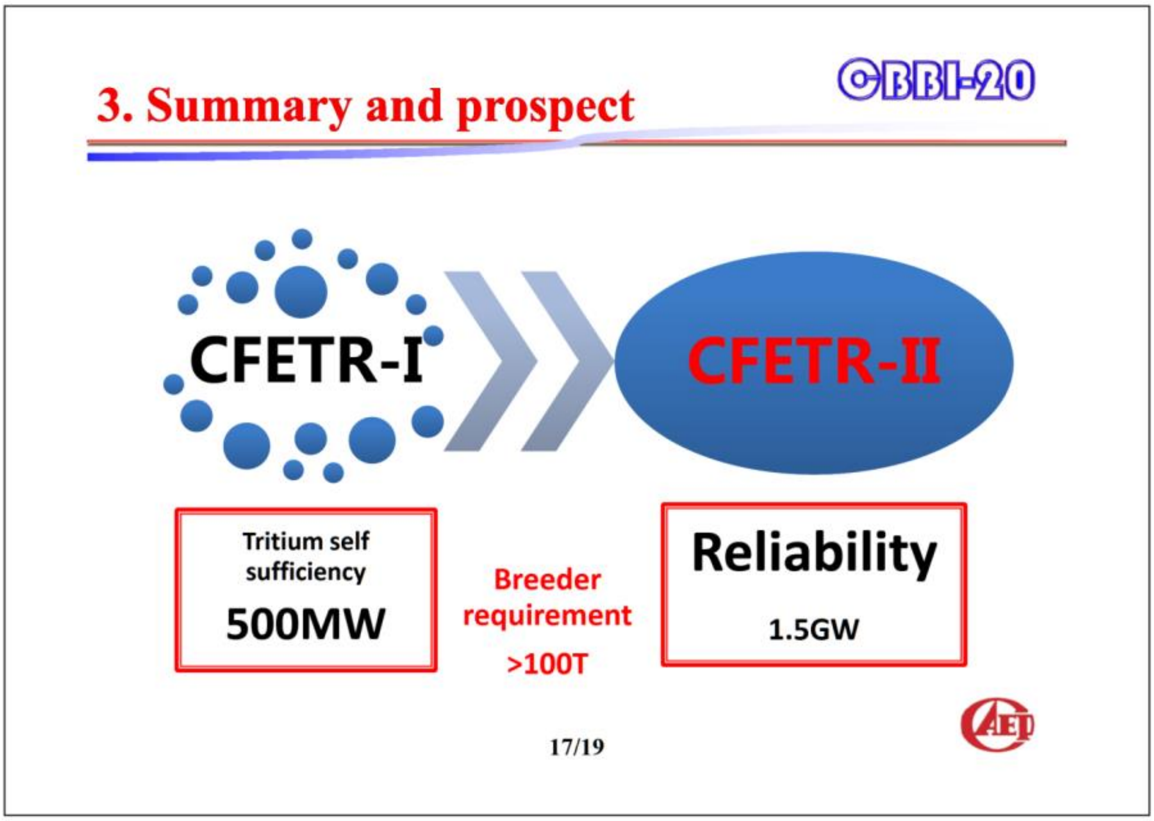
3. Summary and prospect
CBBI-20
CFETR-I
CFETR-II
Tritium self sufficiency
500MW
Breeder requirement
>100T
Reliability
1.5GW
AEP
17/19

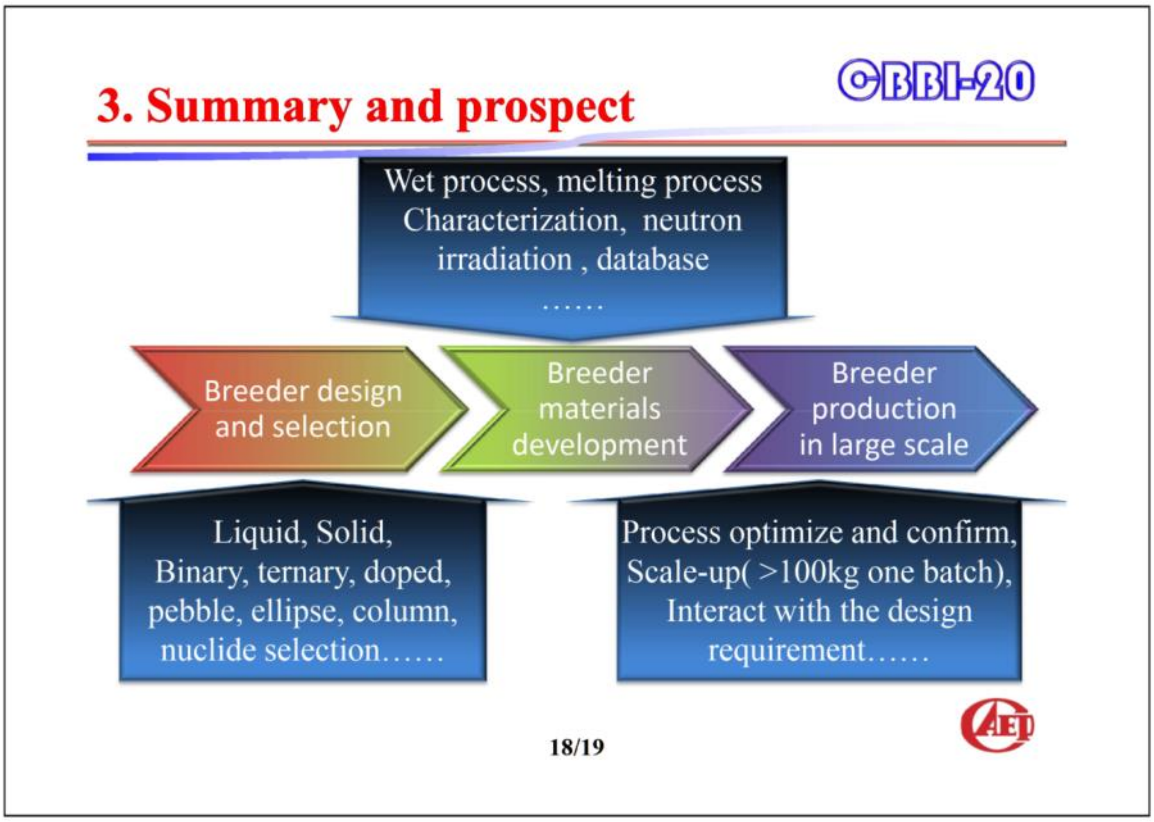
3. Summary and prospect
CBBI-20
Wet process, melting process
Characterization, neutron irradiation , database
……
Breeder design and selection
Breeder materials development
Breeder production in large scale
Liquid, Solid,
Binary, ternary, doped,
pebble, ellipse, column,
nuclide selection……
Process optimize and confirm,
Scale-up(>100kg one batch),
Interact with the design requirement……
AEP
18/19


CBBI-20
Thanks for your listening!
19/19

Advanced Ceramic Breeder Pebble Production: Controlling the Pebble Size Distribution

Oliver Leys[1], Patrick Waibel[2], Jörg Matthes[2], Regina Knitter[1]

Karlsruhe Institute of Technology (KIT), Germany, [1]Institute for Applied Materials (IAM), [2]Institute for Automation and Applied Informatics (IAI)

In order for future fusion reactors to generate the fuel component tritium, it is foreseen to install lithium rich ceramic breeder pebbles in the form of pebble beds into the wall of the reactor. Upon irradiation by neutrons generated from the fusion reaction, the lithium will be transformed to form both tritium and helium of which the former will then be extracted, processed and used to fuel the self-sufficient reactor.

The melt-based process KALOS (Karlsruhe Lithium Orthosilicate) is used for the production of so-called advanced ceramic breeder pebbles with sizes ranging from 250 to 1250 µm. Synthesis powders are heated in a platinum alloy crucible to approximately 1400 °C, thereby forming a melt. A pressure is then applied to the system to force the melt through a small nozzle on the underside of the crucible to form a molten laminar jet, which subsequently breaks up into droplets. These then enter a cooling tower where they are solidified using a liquid nitrogen spray system. At the base of the tower, the pebbles are collected and stored in inert conditions for further action.

The size distribution and yield of the process are predominantly determined during the break-up of the jet, making it one of the most important process steps. In general, random ambient disturbances grow on the surface of the jet until the surface tension forces overcome the viscous forces and a droplet breaks off. According to the theory, there is an optimum instability frequency which will grow the fastest on the jet, thereby suppressing other disturbances and resulting in a monodisperse droplet generation.

In order to control the break-up of the process jet, equipment was developed at room temperature using a replica steel crucible and a water-glycerine mixture to imitate the melt. Various tests were then performed, before successfully transferring the technology to the high-temperature process. A wide range of frequencies was then applied to the system while filming the jet break-up with a high-speed camera. The recordings were then analysed using an image processing algorithm to determine the optimum driving frequency to generate a monodisperse jet break-up. Subsequently, batches were produced using the newly determined operating frequency, resulting in very high process yields and highly discrete pebble size distributions.

KIT Karlsruhe Institute of Technology

Advanced Ceramic Breeder Pebble Production

CONTROLLING THE PEBBLE SIZE DISTRIBUTION

O. Leys, P. Waibel, J. Matthes and R. Knitter

INSTITUTE FOR APPLIED MATERIALS - FUSION CERAMICS

KIT – The Research University in the Helmholtz Association www.kit.edu

The KALOS Process Overview

KIT Karlsruhe Institute of Technology

1. Heating of synthesis powders (pre-reacted $LiOH{\cdot}H_2O$, SiO_2 and TiO_2) in a Pt-alloy crucible
2. Formation of a melt at ca. 1400 °C
3. Application of process pressure to crucible (ca. 300 mbar)

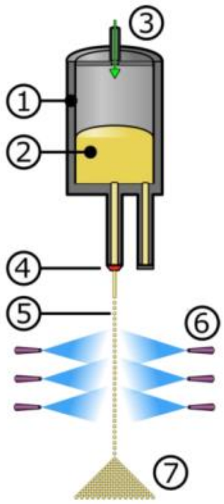

4. Formation of a laminar jet through a ca. 300 µm nozzle
5. Break-up of jet into droplets
6. Solidification of droplets into pebbles
7. Collection of pebbles

2 Karlsruhe, 18. September 2019 CBBI-20 Oliver Leys Institute for Applied Materials (IAM-ESS)

The KALOS Process Overview

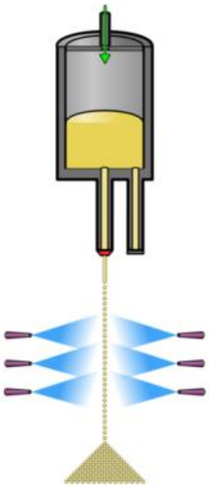

The KALOS Process Jet Break-up

- Plateau-Rayleigh instabilities on the surface of a jet lead to its break-up
- The waves grow until surface tension forces overcome viscous forces
  - ➢ Drop break off
- In general:

$$Primary\ Droplet\ Ø = 1.9\ x\ Nozzle\ Ø$$

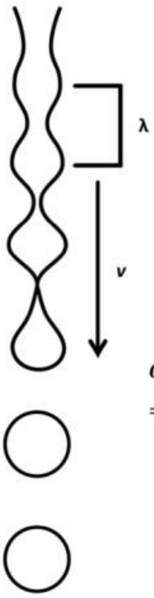

- Undersized pebbles
  - Satellite droplets
  - Shear forces
- Oversized pebbles
  - Coalescing droplets
- KALOS Process Yield
  - Pebbles 250 – 1250 µm

$$CV = \frac{\textbf{Standard Deviation } (s)}{\textbf{Mean } (s)}$$

s = **droplet spacing**

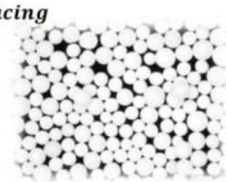

Pebble Size Distribution Nozzle Effects

- Comparison of pebble size distributions for **different nozzle sizes**
- **Pressure constant** at 400 mbar

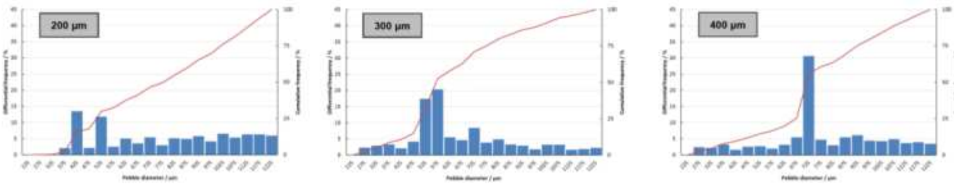

Pebble Size Distribution Pressure Effects

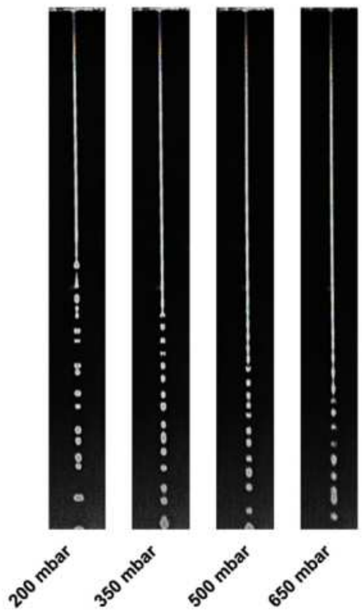

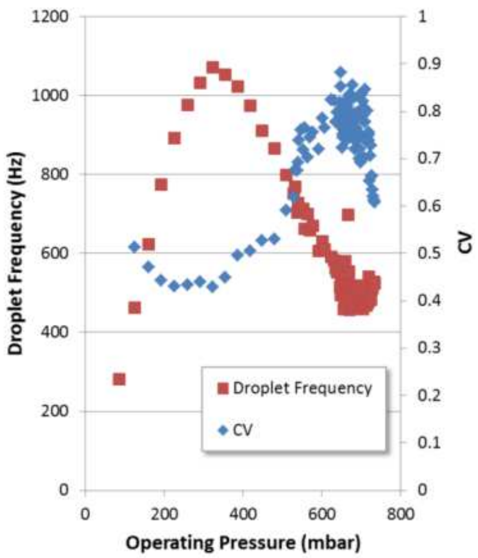

Figure (l): IJAMT_Leys2018; (r): CBBI19_Leys

Pebble Size Distribution Pressure Effects

- Comparison of pebble size distributions for **different operating pressures**
- **Nozzle diameter constant** at 300 µm

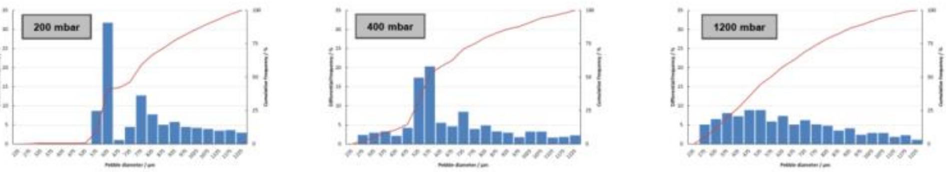

Induced Jet Break-up

- Intrinsic optimal wavelength
  - Fastest growth of instabilities
  - Suppression of ambient disturbances
  - Generation of a monodisperse jet break-up
- In order to increase the contrast between the jet/droplets and the background, an actively cooled plate was installed in the oven
- A frequency generator was developed for applying vertical instabilities directly to the air-tight pressure system within the crucible

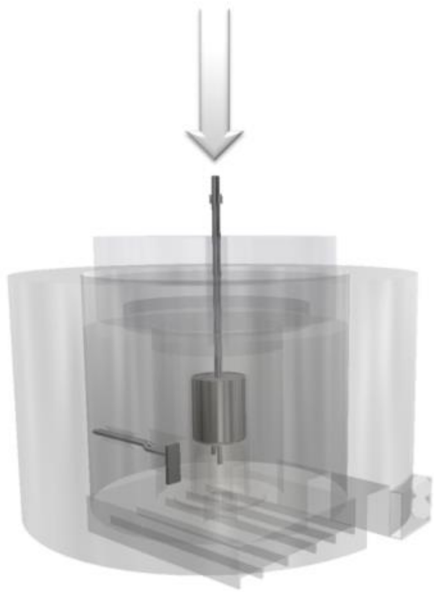

Induced Jet Break-up KALOS

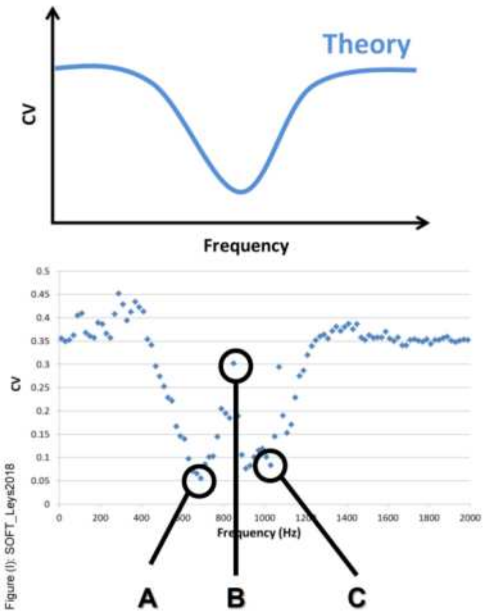

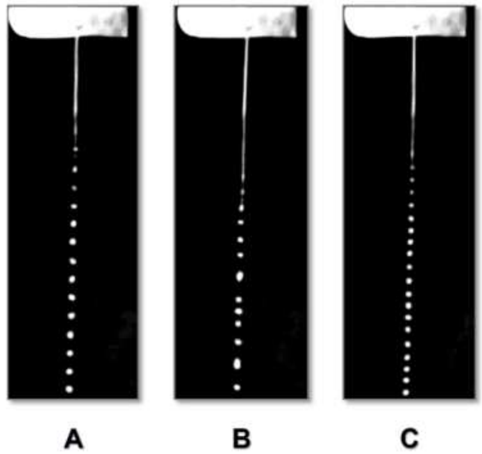

Induced Jet Break-up KALOS

- The effect of an induced jet break-up on the pebble size distribution was then studied

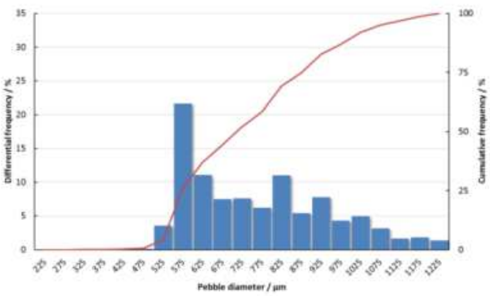

Example without excitation

Yield = 84%

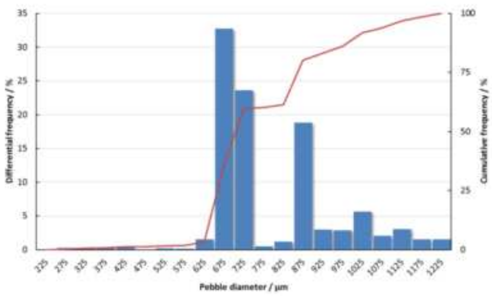

Example with *f* = 1070 Hz

Yield = 91%

Summary

- Various techniques have been developed for controlling the size distribution of the pebbles produced using the KALOS process
- Setting the nozzle diameter determines the main pebble size
- The process pressure is to be adjusted according to the nozzle diameter to ensure a stable jet whilst minimising shear forces
- The application of desired instabilities to the system results in the formation of a monodisperse jet break-up, leading to more discrete distributions and higher yields

11 Karlsruhe, 18. September 2019 CBBI-20 **Oliver Leys** Institute for Applied Materials (IAM-ESS)

Thank you for your attention!

Part of this work has been carried out within the framework of the EUROfusion Consortium and has received funding from the Euratom research and training programme 2014-2018 and 2019-2020 under grant agreement No 633053. The views and opinions expressed herein do not necessarily reflect those of the European Commission.

EUROfusion

12 Karlsruhe, 18. September 2019 CBBI-20 **Oliver Leys** Institute for Applied Materials (IAM-ESS)

Comparison of Tritium Release Behavior in Promising Tritium Breeding Materials

Qiang Qi[a], Shouxi Gu[a], Mingzhong Zhao[b], Fei Sun, Baolong Ji[a], Moeko Nakata[b], Haishan Zhou[a], Yingchun Zhang[c], Yasuhisa Oya[b], Guang-Nan Luo[a]

[a]Institute of Plasma Physics, Chinese Academy of Sciences, Hefei, 230031, China.

[b]Shizuoka University, 836, Ohya, Suruga-ku, Shizuoka 422-8529, Japan.

[c]University of Science and Technology Beijing, Beijing 100083, PR China.

In future D-T fusion reactor, tritium will be bred by tritium breeding materials to maintain steady-state operation of the reactor. Li_2TiO_3 and Li_4SiO_4 have been proposed as prominent tritium breeder candidates due to high lithium density, favorable tritium release behavior and mechanical stability. The novel tritium breeder of core-shell Li_2TiO_3-Li_4SiO_4 biphasic ceramic pebbles are promising tritium breeder which combine the advantages of Li_2TiO_3 in good mechanical property and Li_4SiO_4 in high lithium density. All the pebbles were irradiated at the same time and tritium release were performed at the same device to avoid the effects of different irradiation conditions and device on the tritium release.

Tritium breeding pebbles have been irradiated by thermal neutrons in Kyoto University with the flux of 5.5×10^{12}n/s . cm^2. Tritium release experiment was performed in Shizuoka University. There is one main tritium release peak in the tritium release spectra of Li_2TiO_3 and Li_4SiO_4. However, there are two main release peaks in the tritium release spectra of core-shell Li_2TiO_3-Li_4SiO_4. The peak temperature of Li_4SiO_4 located at 241 ^oC is lowest compared with that of the other two type pebbles at the heating rate of 10 ^oC/min. The temperature of the tritium release peak from Li_2TiO_3 is 392 ^oC at the heating rate of 10 ^oC/min. For core-shell pebbles, the temperature of the first tritium release peak is 312 ^oC and the second peak locates at 465 ^oC at the heating rate of 10 ^oC/min. From the experiment results, tritium release behavior of Li_4SiO_4 is better than the other two pebbles. The results may be different with some work reported that the tritium release performance of Li_2TiO_3 is better than Li_4SiO_4. This can be attributed to different preparation method and irradiation conditions. The studies on tritium release from the pebbles with different preparation method and different irradiation conditions are prepared. The kinetic parameters were obtained by KAS model-free-kinetics method. The activation energy of tritium release from Li_4SiO_4 was obtained as 0.29 eV and 0.49 for Li_2TiO_3. The activation energy of tritium release from core-shell Li_2TiO_3-Li_4SiO_4 was 1.78 eV for the main release peak. Almost all tritium (about 98%) released from Li_4SiO_4 pebbles when heating at 300 ^oC for 1 hour. However, almost all tritium (about 98%) released from Li_2TiO_3 and Li_2TiO_3-Li_4SiO_4 should heating at 400 ^oC for 1 hour.

CBBI-20

ASIPP

Comparison of Tritium Release Behavior in Promising Tritium Breeding Materials

Qiang Qi[a], Mingzhong Zhao[b], Shouxi Gu[a], Fei Sun[b], Baolong Ji[a], Moeko Nakata[b], Haishan Zhou[a], Yingchun Zhang[c], Yasuhisa Oya[b], Guang-Nan Luo[a]

[a]*Institute of Plasma Physics, Chinese Academy of Sciences, Hefei 230031, China*
[b]*Shizuoka University, 836, Ohya, Suruga-ku, Shizuoka 422-8529, Japan*
[c]*University of Science and Technology Beijing, Beijing 100083, China*

2019/9/18 CBBI-20 1

Outline

ASIPP

CFETR

- Introduction
- Experimental details
- Results and discussion
- Summary

2019/9/18 CBBI-20 2

Outline

ASIPP

- Introduction
- Experimental details
- Results and discussion
- Summary

2019/9/18 CBBI-20 3

Introduction

ASIPP

- **Fusion reaction:**
  $^{2}D+^{3}T \rightarrow ^{4}He+n+17.58MeV$
- **Tritium source:**
  $^{6}Li+n=^{3}H+^{4}He+4.5MeV$
  $^{7}Li+n=^{3}H+^{4}He+n'-2.9MeV$
- **Tritium breeders:**
  Solid breeder: Li_2TiO_3, Li_4SiO_4, Li_2ZrO_3, $LiAlO_2$, Li_2O …
  Liquid breeder: Li, $Li_{17}Pb_{83}$, $FLiBe$ …

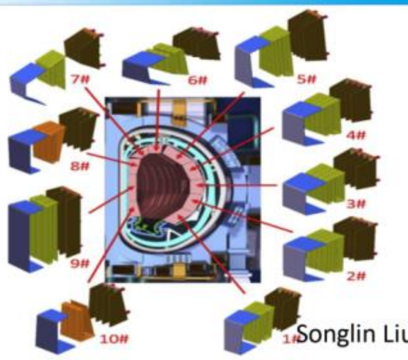

Songlin Liu et al.

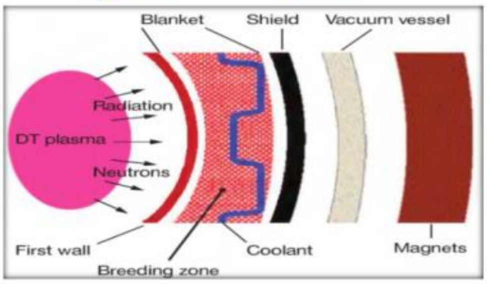

2019/9/18 CBBI-20 4

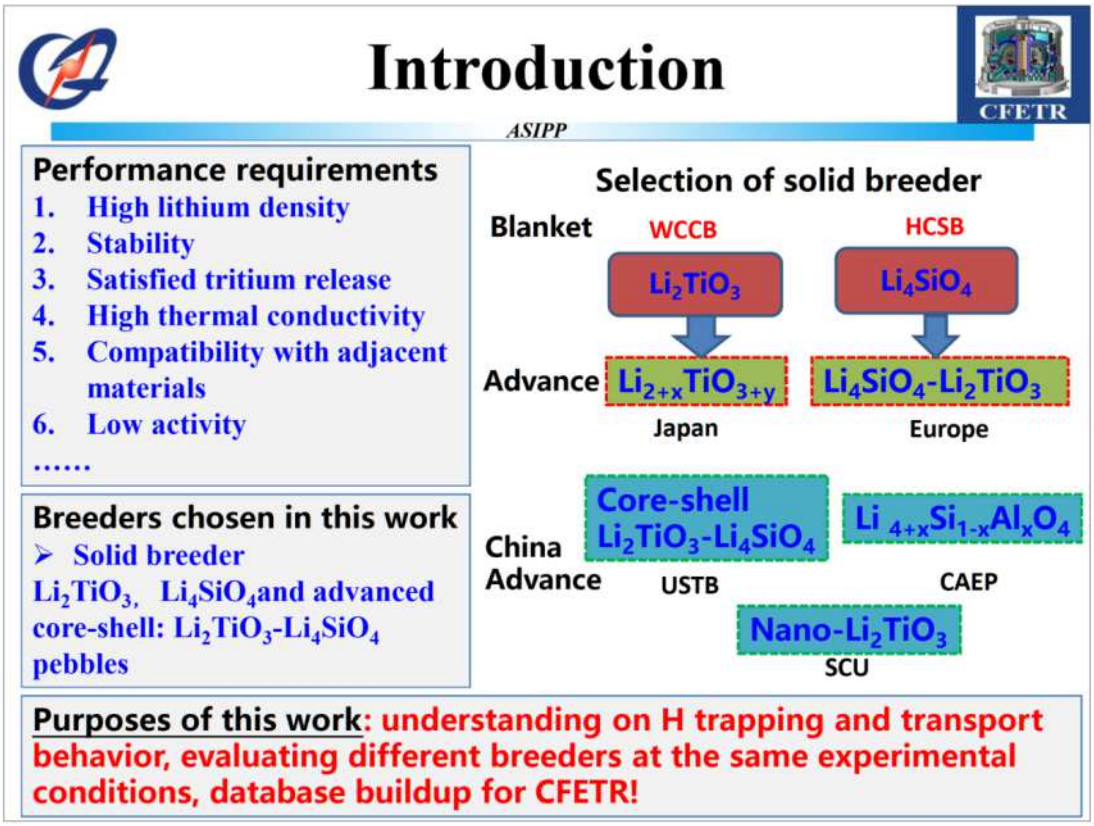
Introduction
ASIPP
CFETR
Performance requirements
1. High lithium density
2. Stability
3. Satisfied tritium release
4. High thermal conductivity
5. Compatibility with adjacent materials
6. Low activity
……
Breeders chosen in this work
➢ Solid breeder
Li_2TiO_3, Li_4SiO_4 and advanced core-shell: Li_2TiO_3-Li_4SiO_4 pebbles
Selection of solid breeder
Blanket
WCCB
HCSB
Li_2TiO_3
Li_4SiO_4
Advance
$Li_{2+x}TiO_{3+y}$
Li_4SiO_4-Li_2TiO_3
Japan
Europe
China Advance
Core-shell Li_2TiO_3-Li_4SiO_4
USTB
$Li_{4+x}Si_{1-x}Al_xO_4$
CAEP
Nano-Li_2TiO_3
SCU
Purposes of this work: understanding on H trapping and transport behavior, evaluating different breeders at the same experimental conditions, database buildup for CFETR!

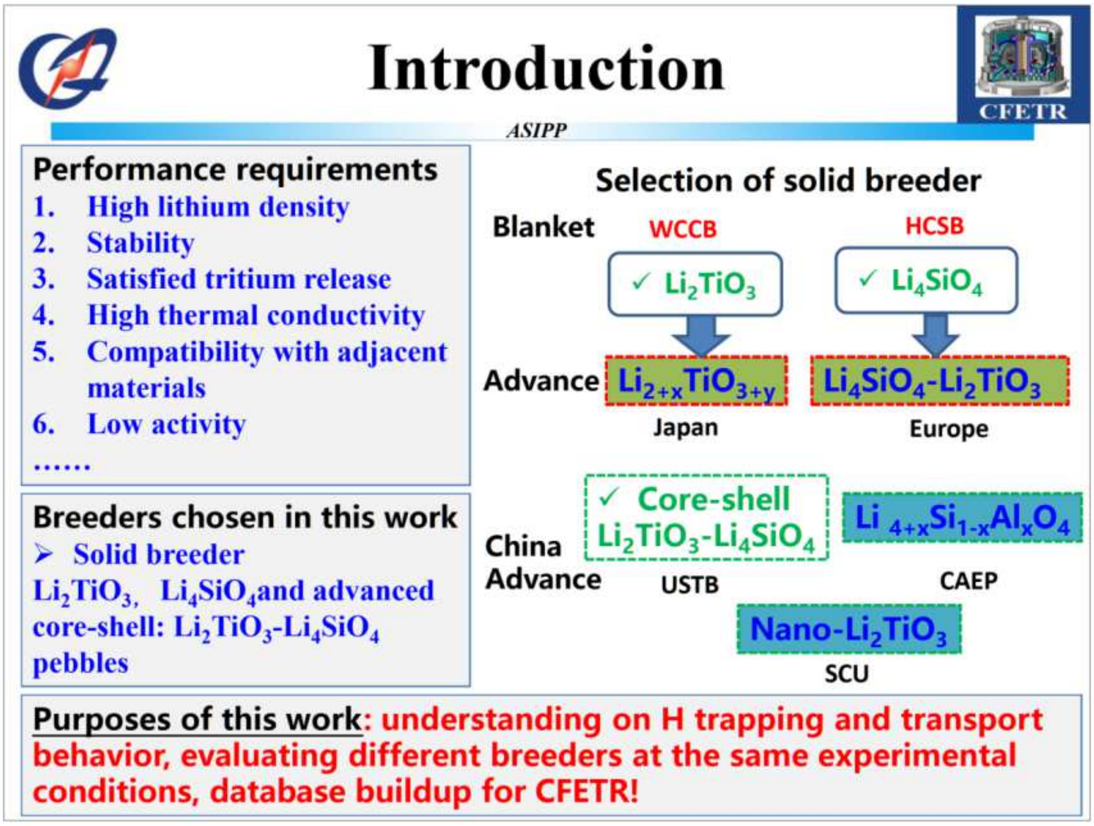
Introduction
ASIPP
CFETR
Performance requirements
1. High lithium density
2. Stability
3. Satisfied tritium release
4. High thermal conductivity
5. Compatibility with adjacent materials
6. Low activity
……
Breeders chosen in this work
➢ Solid breeder
Li_2TiO_3, Li_4SiO_4 and advanced core-shell: Li_2TiO_3-Li_4SiO_4 pebbles
Selection of solid breeder
Blanket
WCCB
HCSB
✓ Li_2TiO_3
✓ Li_4SiO_4
Advance
$Li_{2+x}TiO_{3+y}$
Li_4SiO_4-Li_2TiO_3
Japan
Europe
China Advance
✓ Core-shell Li_2TiO_3-Li_4SiO_4
USTB
$Li_{4+x}Si_{1-x}Al_xO_4$
CAEP
Nano-Li_2TiO_3
SCU
Purposes of this work: understanding on H trapping and transport behavior, evaluating different breeders at the same experimental conditions, database buildup for CFETR!

Outline

ASIPP

CFETR

- Introduction
- **Experimental details**
- Results and discussion
- Summary

Experimental (Materials)

ASIPP

CFETR

Preparation of samples

Characterization of Li_2TiO_3, Li_4SiO_4 and Li_2TiO_3-Li_4SiO_4

Breeder	Pebble diameter (mm)	Relative density (TD%)	Grain size (μm)	Porosity (%)	Crush load (N)
Li_2TiO_3	1.08	90.4	8.2	9.6	48
Li_4SiO_4	1	88.7%	5	11.3	40
Li_2TiO_3-Li_4SiO_4	0.93	90.3	1.12/1.67	9.7	104.79

JNM 441 (2013) 390–394; JNM 466 (2015) 477-483; FED 95 (2015) 72–78

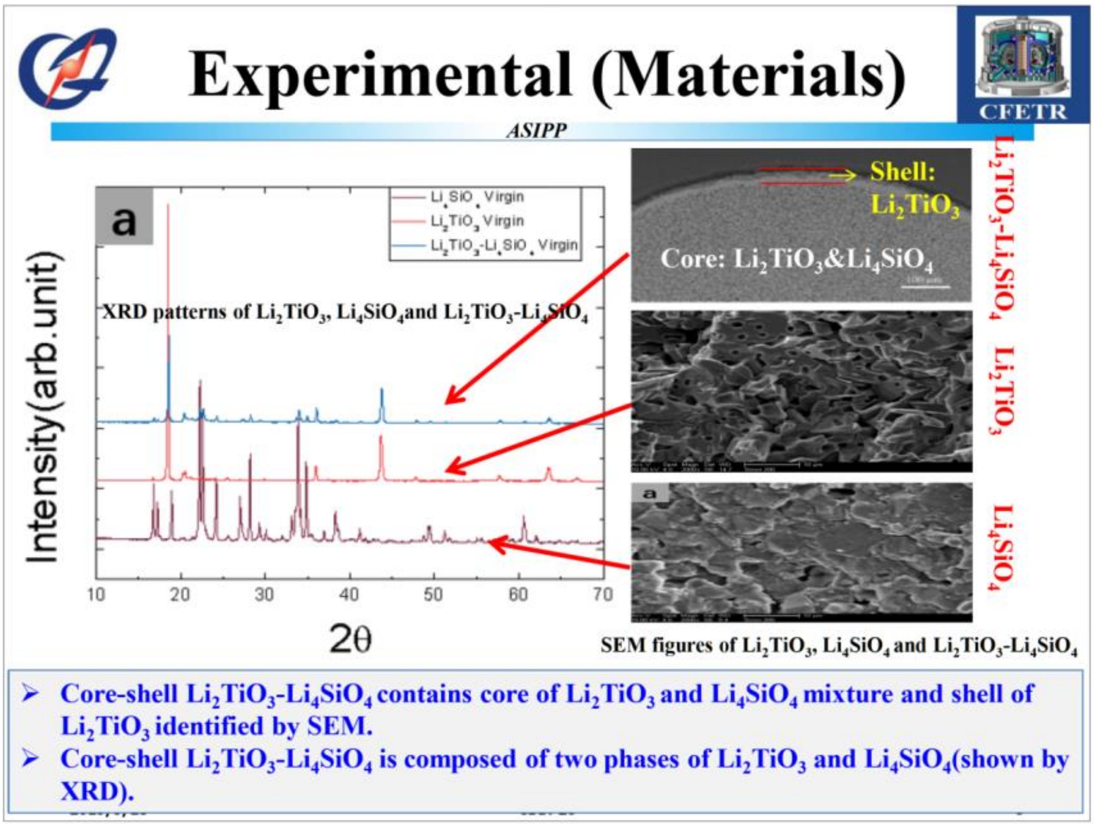
Experimental (Materials)
CFETR
ASIPP
a
Li_4SiO_4 Virgin
Li_2TiO_3 Virgin
Li_2TiO_3-Li_4SiO_4 Virgin
XRD patterns of Li_2TiO_3, Li_4SiO_4 and Li_2TiO_3-Li_4SiO_4
Intensity(arb.unit)
10 20 30 40 50 60 70
2θ
Shell: Li_2TiO_3
Core: Li_2TiO_3&Li_4SiO_4
Li_2TiO_3-Li_4SiO_4
Li_2TiO_3
Li_4SiO_4
SEM figures of Li_2TiO_3, Li_4SiO_4 and Li_2TiO_3-Li_4SiO_4
➢ Core-shell Li_2TiO_3-Li_4SiO_4 contains core of Li_2TiO_3 and Li_4SiO_4 mixture and shell of Li_2TiO_3 identified by SEM.
➢ Core-shell Li_2TiO_3-Li_4SiO_4 is composed of two phases of Li_2TiO_3 and Li_4SiO_4(shown by XRD).

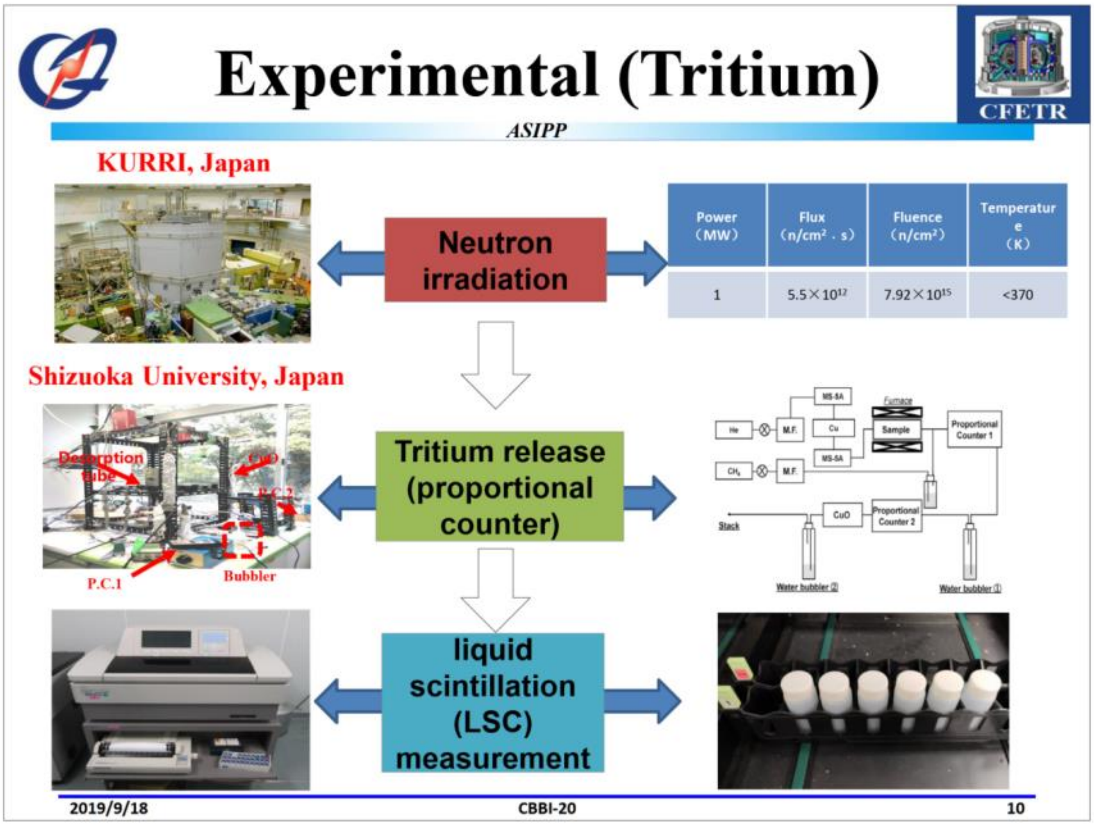
Experimental (Tritium)
CFETR
ASIPP
KURRI, Japan
Neutron irradiation
Power (MW) | Flux (n/cm²・s) | Fluence (n/cm²) | Temperature (K)
1 | 5.5×10¹² | 7.92×10¹⁵ | <370
Shizuoka University, Japan
Desorption tube
CuO
P.C.2
P.C.1
Bubbler
Tritium release (proportional counter)
He
CH₄
M.F.
MS-5A
Cu
Furnace
Sample
Proportional Counter 1
CuO
Proportional Counter 2
Stack
Water bubbler ②
Water bubbler ①
liquid scintillation (LSC) measurement
2019/9/18
CBBI-20
10

Outline

ASIPP

CFETR

- Introduction
- Experimental details
- **Results and discussion**
- Summary

Tritium release from Li_2TiO_3

ASIPP

CFETR

$$\frac{d\alpha}{dt} = kf(\alpha) = A\exp\left(\frac{-E_a}{RT}\right)f(\alpha) \Rightarrow \ln\left(\frac{\beta}{T_P^2}\right) = \ln\left(\frac{RA}{E_a g(\alpha)}\right) - \frac{E_a}{RT_P}$$

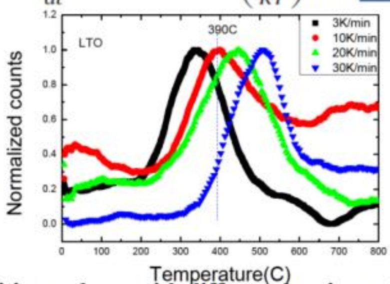

Tritium release with different heating rate

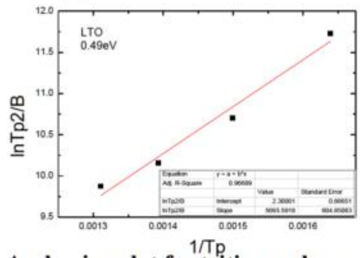

Arrhenius plot for tritium release process

Tritium diffusivity were obtained as: $5.68\times10^{-4}\exp(-0.49eV/KT)\ m^2/s$

Parameters for tritium release from Li_2TiO_3

Sample	Grain size (μm)	Fluence ($n\cdot cm^{-2}$)	Ea (eV)	Reference
Pebble	8.2	8×10^{16}	0.49	This work
Powder	3	3.3×10^{15}	0.59	Kobayashi et al.
Pebble	1	2.4×10^{17}	1.7	Kinjo et al.
Pebble	18	2.4×10^{17}	1.6	Kinjo et al.

The difference is due to different sample parameters (grain size, porosity, sample shape and so on) and irradiation conditions.

Tritium release from Li_4SiO_4

ASIPP

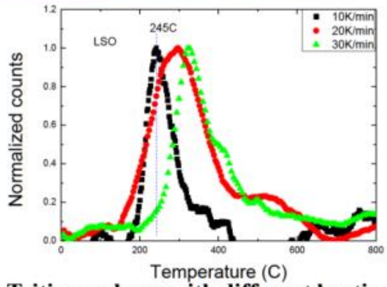

Tritium release with different heating rate

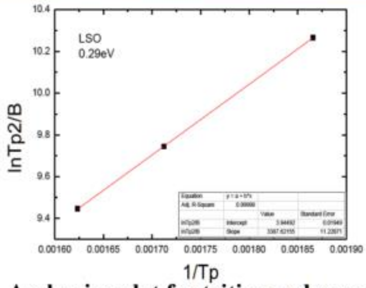

Arrhenius plot for tritium release process

Tritium diffusivity were obtained as: $6.53\times10^{-5}\exp(-0.29eV/KT)\ m^2/s$

Parameters for tritium release from Li_4SiO_4

Sample	Grain size (μm)	Fluence ($n\cdot cm^{-2}$)	Ea (eV)	Reference
Li_4SiO_4 Pebble	5	7.92×10^{15}	0.29	This work
Li_4SiO_4 Powder	-	2.5×10^{16}	0.45	Okuno et al.
Li_4SiO_4 Pebble	10	3.3×10^{14}	0.42	C. Xiao et al.

- One main release peak in the TDS spectra designated as tritium diffusion in crystal grain.
- The peak temperature (245C at 10K/min) and activation energy (0.29 eV) is lower than other reports. This may be due to mainly preparation procedure, as well as experimental conditions.

2019/9/18 CBBI-20 13

Tritium release from Li_2TiO_3-Li_4SiO_4

ASIPP

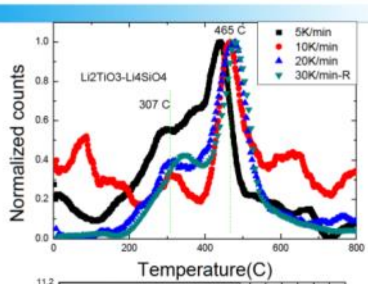

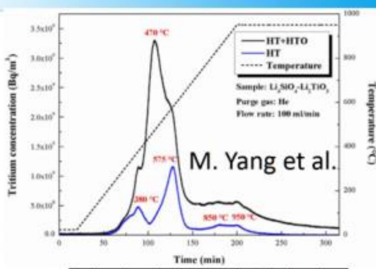

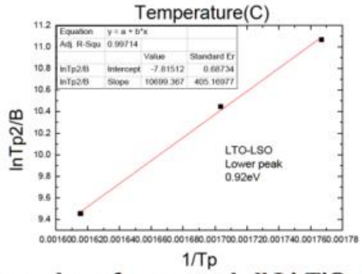

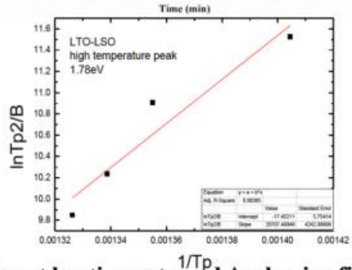

Tritium release from core-shell Li_2TiO_3-Li_4SiO_4 at different heating rate and Arrhenius fitting

- There are two distinct release peaks from the Li_2TiO_3-Li_4SiO_4 pebbles. The peak temperature is lower than the report.
- The lower temperature peak at 307C is considered as tritium diffusion from shell Li_2TiO_3. The higher temperature peak at 465C can be attributed as tritium diffusion from inner affected by mixed phases and interfaces between core and shell.

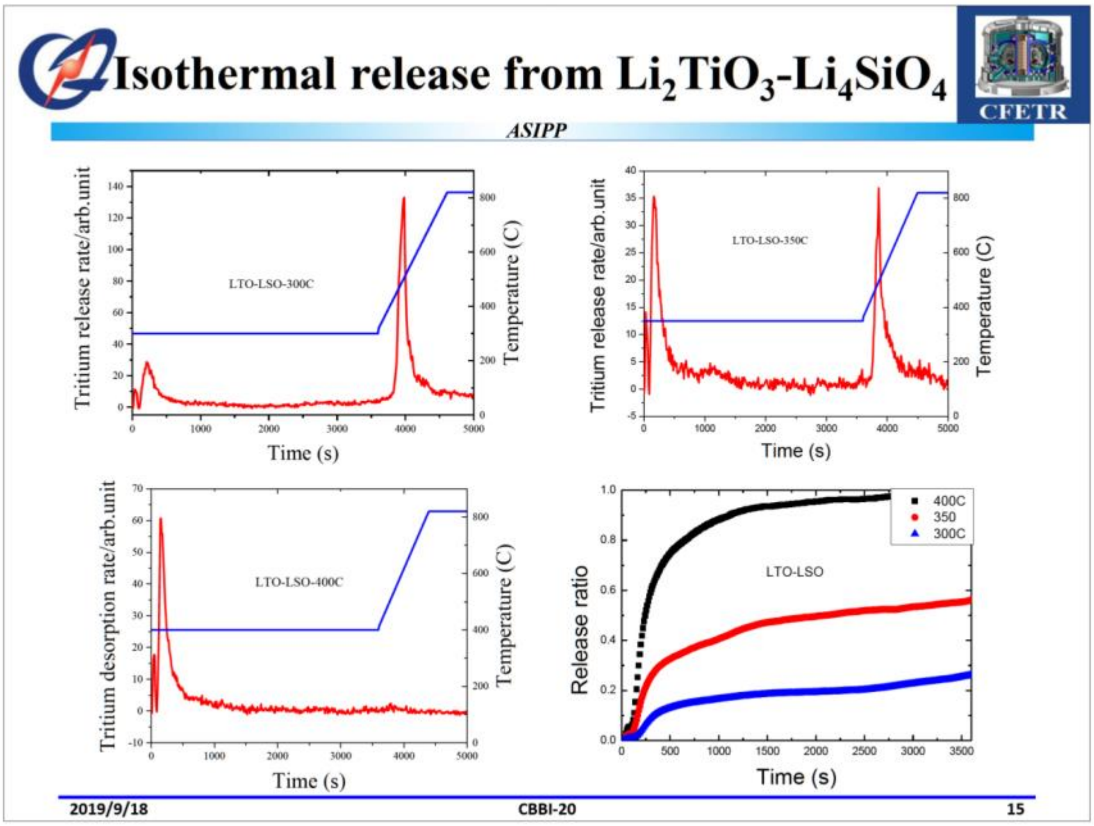
Isothermal release from Li2TiO3-Li4SiO4
CFETR
ASIPP
LTO-LSO-300C
Tritium release rate/arb.unit
Temperature (C)
Time (s)
LTO-LSO-350C
Tritium release rate/arb.unit
Temperature (C)
Time (s)
LTO-LSO-400C
Tritium desorption rate/arb.unit
Temperature (C)
Time (s)
400C
350
300C
LTO-LSO
Release ratio
Time (s)
2019/9/18
CBBI-20
15

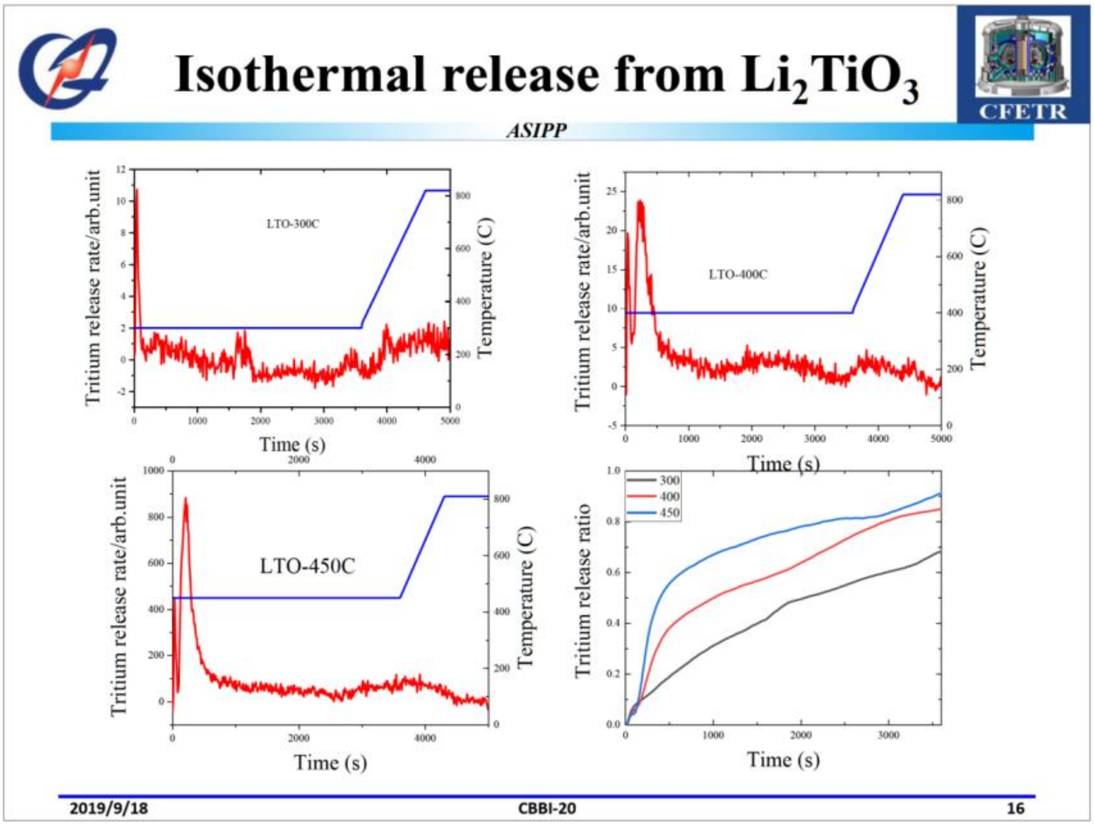
Isothermal release from Li2TiO3
CFETR
ASIPP
LTO-300C
Tritium release rate/arb.unit
Temperature (C)
Time (s)
LTO-400C
Tritium release rate/arb.unit
Temperature (C)
Time (s)
LTO-450C
Tritium release rate/arb.unit
Temperature (C)
Time (s)
300
400
450
Tritium release ratio
Time (s)
2019/9/18
CBBI-20
16

Isothermal release from Li_4SiO_4

ASIPP

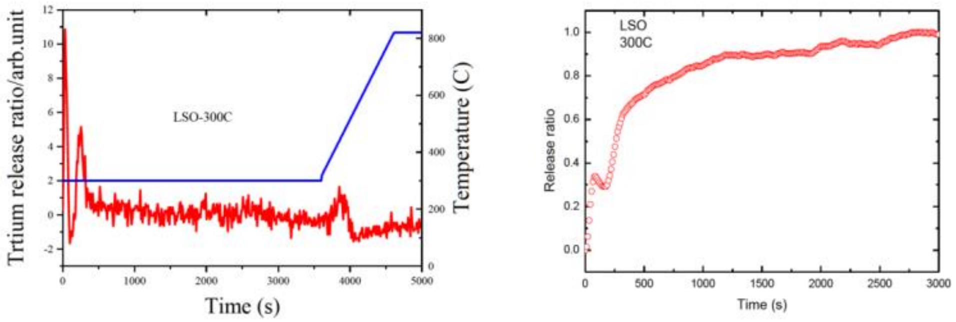

- At lower keeping temperature of 300C, 95% tritium released from Li_4SiO_4. However, a lot of tritium retained in Li_2TiO_3 and core-shell pebbles.
- The order of release amount at lower temperature (300C) are Li_4SiO_4> Li_2TiO_3>Li_2TiO_3-Li_4SiO_4.
- When the temperature increased to 400 C, almost all the tritium released. So it is still a promising candidate breeding material for core-shell Li_2TiO_3-Li_4SiO_4, especially for its excellent mechanical property of 104N crush load.

Tritium release from three pebbles

ASIPP

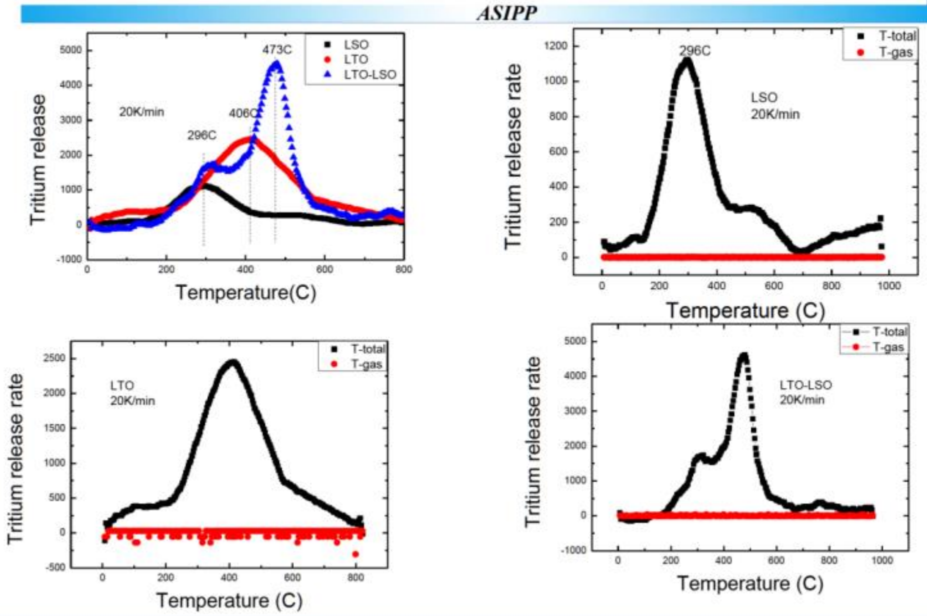

- The order of main peak temperature are Li_4SiO_4< Li_2TiO_3<Li_2TiO_3-Li_4SiO_4.
- The major form of released tritium is tritiated water, ~99% of the total amount.

Summary and future work

ASIPP

CFETR

Summary

- The kinetic parameters for tritium release in n-irradiated Li_2TiO_3, Li_4SiO_4 and core-shell Li_2TiO_3-Li_4SiO_4 were obtained.
- There are two distinct tritium release peaks for n-irradiated Li_2TiO_3-Li_4SiO_4 which are determined by core-shell structure.
- The order of release amount at lower keeping temperature (300C) are Li_4SiO_4> Li_2TiO_3>Li_2TiO_3-Li_4SiO_4 , but almost all the tritium released at 400C indicating a promising candidate breeding material for core-shell Li_2TiO_3-Li_4SiO_4 , especially for its excellent mechanical property of 104N crush load.

Future work

- Very limited n-irradiation so far for fusion society, more are needed to better understand trapping & transport behavior.
- Domestic & Int'l collaborations are welcome and inevitable!

2019/9/18 CBBI-20 19

Acknowledgements

ASIPP

CFETR

- The authors thank Kyoto University and Shizuoka University for providing neutron irradiation and tritium release experiment chance.
- This work was supported by the National Natural Science Foundation of China under contract Nos. 11605230 and 51372017.

2019/9/18 CBBI-20 20


ASIPP
CFETR
THANK YOU !
2019/9/18
CBBI-20
21

Design, synthesis and characterization of Li_4SiO_4-based solid solutions as advanced tritium breeders

Linjie Zhao, Xiaojun Chen, Chengjian Xiao, Yu Gong, Heyi Wang, Xinggui Long, Shuming Peng

Institute of Nuclear Physics and Chemistry, China Academy of Engineering Physics, Mianyang 621999, China

The breeding blanket is a key component of the fusion reactor since it involves tritium breeding and energy extraction, both of which are critically important for the development of fusion power. Different lithium based ceramics have been studied as attractive tritium breeder materials, Li_4SiO_4 has been selected as one of the most promising candidates for solid tritium breeding materials in fusion reactors because of its high lithium atom density, its high melting temperature and favorable tritium release behavior. Li_4SiO_4-based solid solutions: $Li_{4+x}(Si_{1-x}Al_x)O_4$ and $Li_4Si_{1-x}Ti_xO_4$ were prepared as advanced tritium breeder to improve the mechanical property, irradiation resistance and reduce the tritium retention. Different Li4SiO4-based solid solutions powders and pebbles containing aluminum and titanium were prepared by solid state reactions and Modified melt-spraying process. Phase analysis, microstructures and density of the ceramics were determined by XRD, SEM and Archimedes' method. Impedance spectroscopy was measured to evaluate the electrical conduction properties of the ceramics. The thermal conductivity was determined using a laser flash device. Tritium release performance in Li_{4+x} $(Si_{1-x}Al_x)O_4$ and $Li_4Si_{1-x}Ti_xO_4$ irradiated with thermal neutron was studied by out-of-pile annealing experiments. These facts would represent the following advantages to use Li4SiO4-based solid solutions in blanket system of D-T fusion reactor that the thermal conductivity is higher and tritium inventory is lower in Li_4SiO_4-based solid solutions than those in Li_4SiO_4.

核物理与化学研究所
INSTITUTE OF NUCLEAR PHYSICS AND CHEMISTRY

中国工程物理研究院
CHINA ACADEMY OF ENGINEERING PHYSICS

The tritium release performance of Li_4SiO_4-based solid solutions as advanced tritium breeders

Linjie Zhao, *Xiaojun Chen, Chengjian Xiao, Yu Gong, Guangming Ran, Heyi Wang, Xinggui Long, Shuming Peng*

Laboratory of Advanced Nuclear Energy
Institute of Nuclear Physics and Chemistry

CBBI-20, 18-20 September 2019

Outline

1. Introduction
2. Experimental details
3. Results and discussion
4. Conclusions

2/16

1. Introduction- tritium breeders

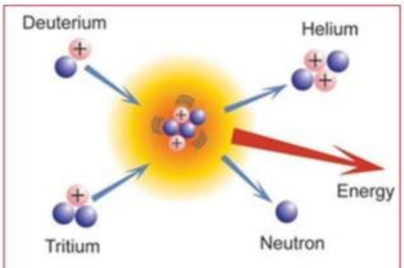

$$D + T \longrightarrow n + {}^4He + 17.6MeV$$

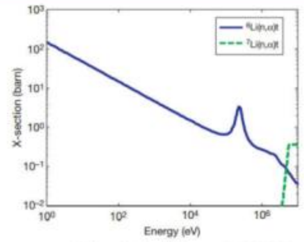

$$n + {}^6Li \rightarrow T + {}^4He + 4.78MeV$$

$$n + {}^7Li \rightarrow T + {}^4He - 2.47MeV + n$$

Deuterium： abundant (1 out of 6500 atoms) in seawater
Tritium： radioactive and can't be obtained from natural resources.
Therefore, the D-T fuel cycle requires the breeding of tritium from lithium.
Tritium breeders : solid breeder & liquid breeder

3/16

1. Introduction- Main requirements for solid breeder materials

1. **High lithium density**
2. **Suitable tritium release property**
3. **Stability (high temperature &strong irradiation)**
4. **Compatibility with adjacent materials**
5. **High thermal conductivity**
6. **High melting point**
7. **Low activity**

… …

4/16

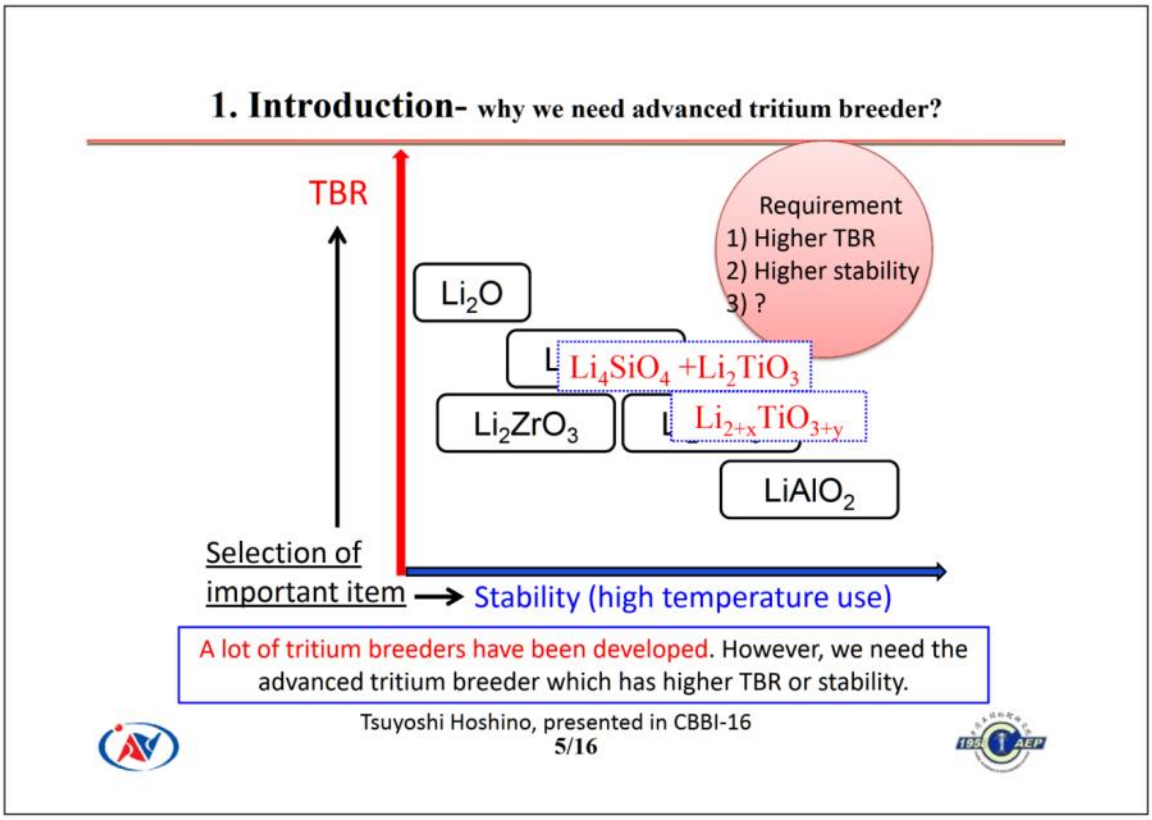
1. Introduction- why we need advanced tritium breeder?
TBR
Requirement
1) Higher TBR
2) Higher stability
3) ?
Li2O
Li4SiO4 +Li2TiO3
Li2ZrO3
Li2+xTiO3+y
LiAlO2
Selection of important item
Stability (high temperature use)
A lot of tritium breeders have been developed. However, we need the advanced tritium breeder which has higher TBR or stability.
Tsuyoshi Hoshino, presented in CBBI-16
5/16

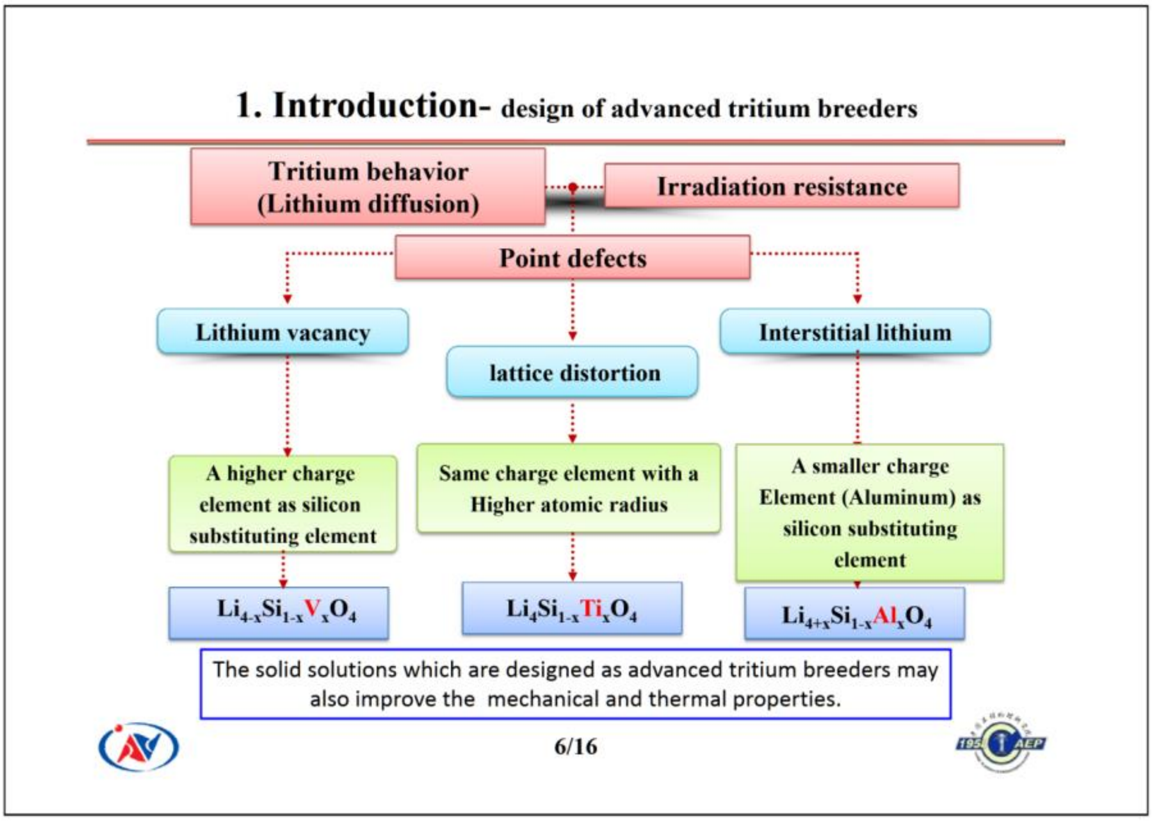
1. Introduction- design of advanced tritium breeders
Tritium behavior (Lithium diffusion)
Irradiation resistance
Point defects
Lithium vacancy
lattice distortion
Interstitial lithium
A higher charge element as silicon substituting element
Same charge element with a Higher atomic radius
A smaller charge Element (Aluminum) as silicon substituting element
Li4-xSi1-xVxO4
Li4Si1-xTixO4
Li4+xSi1-xAlxO4
The solid solutions which are designed as advanced tritium breeders may also improve the mechanical and thermal properties.
6/16

2. Experimental details

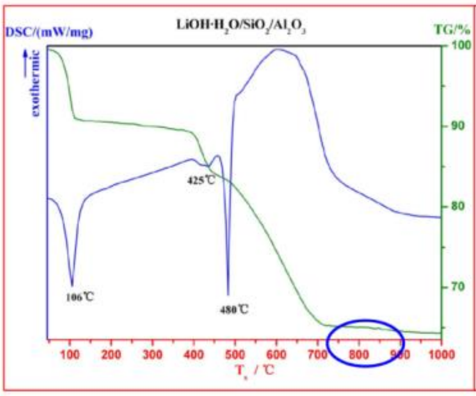

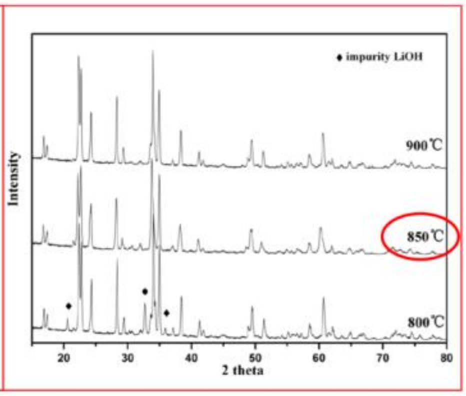

The curve does not change (No additional weight changes and endothermic or exothermic peaks) **above 800 ℃, which suggested that reaction had completely finished. Then, the powders were fired at 800, 850, 900 ℃ for 10 h. It was noted that the appropriate temperature for the preparation of samples was 850 ℃ .**

7/16

2. Experimental details

X-ray diffraction

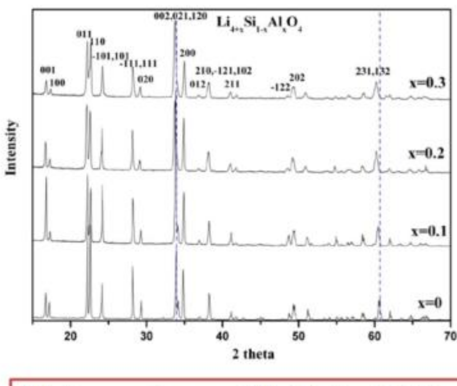

neutron diffraction

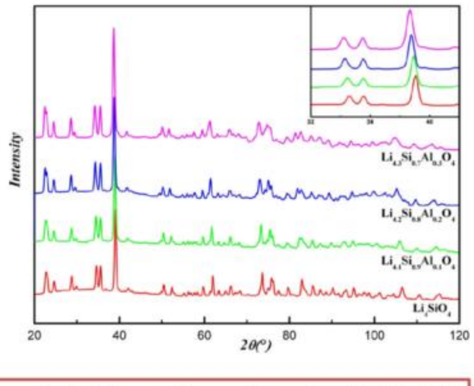

All the samples were fitted to the Li_4SiO_4 except that the patterns showed a slightly left shift, which indicated that the Aluminum-doped Li_4SiO_4 formed the expected solid solutions (Aluminum incorporation into the Li_4SiO_4 structure rather than forming impurities) **and the cell structure had been expanded.**

8/16

2. Experimental details

Rietveld structural refinement Data from ND curves

$Li_{4+x}Si_{1-x}Al_xO_4$	a	b	c	β (°)	Cell volume(Å³)	R_{wp}
ICSD#81249	11.532	6.075	16.678	99.04	1153.9	
x=0	11.555	6.09708	16.72698	99.05991	1163.744	7.33
x=0.1	11.57802	6.12485	16.7493	99.26067	1172.273	7.57
x=0.2	11.56990	6.16095	16.8260	99.24115	1183.785	6.44
x=0.3	11.58753	6.19179	16.81925	99.27601	1190.960	9.17

The cell volume increases with the Aluminum doped. It could be explained by the fact that Al^{3+} had a larger radius than Si^{4+}. Additionally, the formation of interstitial lithium, as the result of aluminum addition, might also contribute to the cell expansion.

9/16

3. Results and discussion

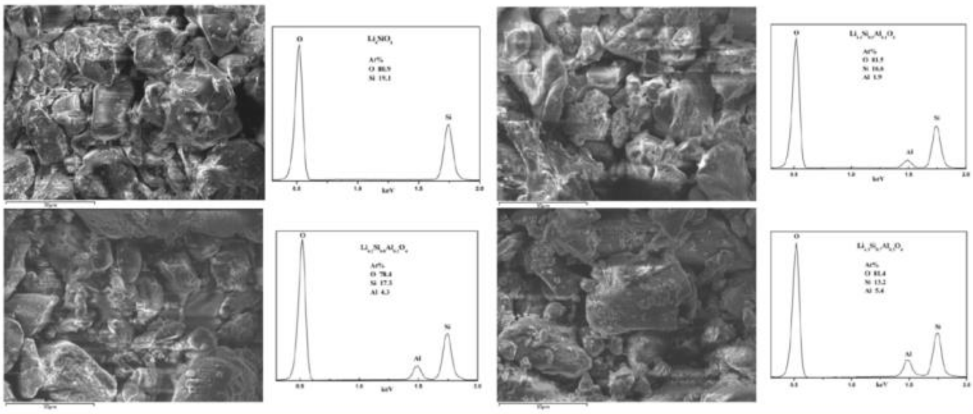

The microstructure of $Li_{4+x}Si_{1-x}Al_xO_4$ powder was observed by SEM. The particle size of the samples was about 30 μm(micron). The Si/Al ratio was 8.74, 4.02, 2.44, respectively, which was quite consistent with the theoretical data (9, 4, 2.3).

10/16

3. Results and discussion

Thermal conductivity and specific heat

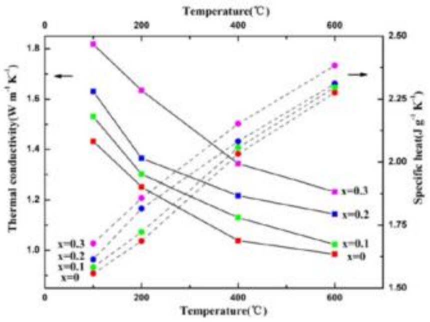

specific heat of Li_4SiO_4

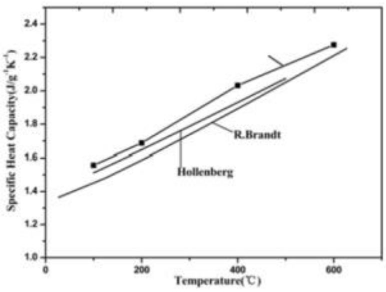

The thermal conductivity decreased and the specific heat increased as the temperature increased. It could be clearly seen that the thermal conductivity increased with the aluminum content.

11/16

3. Results and discussion

The mean crush load of pebbles

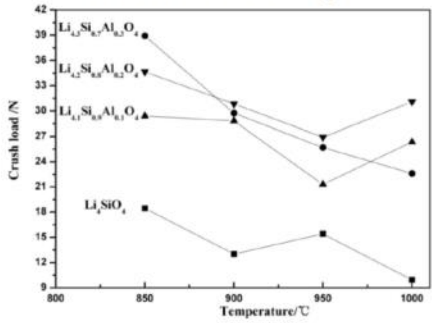

The mean crush load of the Li_4SiO_4 pebbles was 15 N while the mean crush load of Al-doped samples was about 30 N. It could be concluded that the mechanical property of Li_4SiO_4 pebbles could be significantly improved by Al-doped.

12/16

3. Results and discussion

Tritium extraction apparatus flow schematic

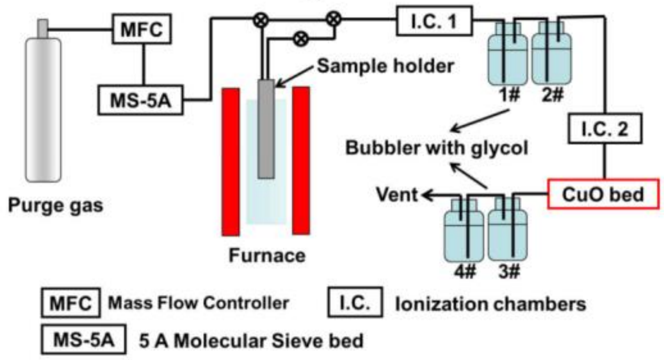

There are two ionization chambers (I.C.) used to monitor tritium release from the irradiated samples online in the system. The working volume of the I.C. used in this work is 50 mL. **I.C.1 gives the total tritium, while I.C.2 gives the reduced tritium** released from the samples online.

3. Results and discussion

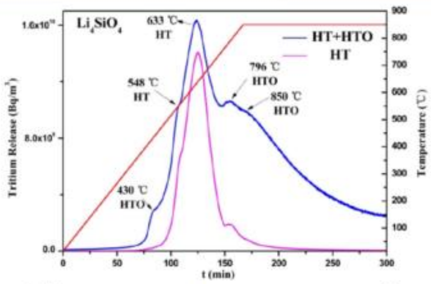

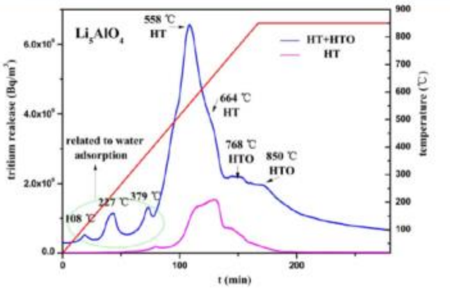

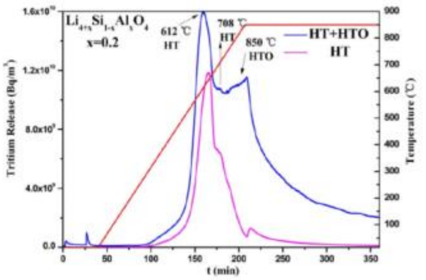

out-of-pile tritium release experiments

The tritium release curves show very similar proprities. The main peak of solid solution is around 600 ℃, which is between Li_4SiO_4 and Li_5AlO_4.

4. Conclusions

- $Li_{4+x}Si_{1-x}Al_xO_4$ solid solutions which were designed as the advanced tritium breeders were obtained by direct solid state reactions.
- The lithium atom density, thermal conductivity and the mechanical properties of the $Li_{4+x}Si_{1-x}Al_xO_4$ were improved to the Li_4SiO_4.
- The tritium performance of Al-doped sample is similar with the Li_4SiO_4. The main peak for tritium release was observed at a peak temperature between Li_4SiO_4 and Li_5AlO_4.

15/16

核物理与化学研究所
INSTITUTE OF NUCLEAR PHYSICS AND CHEMISTRY

Thanks for your attention!

16/16

Design, synthesis, calculation and characterization of the tritium breeder: Li_4TiO_4 ceramics

Juemin Yan[a,b], Tao Gao[a*], Xiaojun Chen[b,] Chengjian Xiao[b]

[a] Institute of Atomic and Molecular Physics, Sichuan University, Chengdu 610065, P.R. China

[b] Institute of Nuclear Physics and Chemistry, China Academy of Engineering Physics, Mianyang 621903, P.R. China

*Corresponding Author Information: E-mail address: gaotao@scu.edu.cn

Fusion is a potential source of safe, non-carbon emitting and virtually limitless energy. The tririum breeding blanket, which acts as the breeding zone of tritium fuel and serves as the main thermal power conversion system, is one of the most important components of a fusion reactor. The breeding materials are important as one of the key functional materials in the breeding blanket. Increased versatility in the available properties of tritium breeding materials can be of benefit to the design of TBM.

The compound Li_4TiO_4 (Tetralithium Titanium) has attracted widespread scholarly interest for its sharp nose about carbon dioxide and high lithium density in the atmosphere and tritium breeder materials. At present, this paper makes comparison on the theory and experimental data on Li_4TiO_4. First the structural, electronic, dynamical and thermodynamic properties of Li_4TiO_4 are studied by means of density functional theory (DFT) and phone lattice dynamics (get IR- and Raman-active). Thermodynamic properties (F, S, C_v, C_p, and E) are firstly evaluated ground on the phonon dynamics contribution. Then, Li_4TiO_4 solid solution was obtained by solid state reactions. Samples were systematically characterized by various techniques. XRD, UV, Infrared and Raman results were compared with the calculated values. The obtained XRD matches the standard card dovetailed together without friction. After ultraviolet diffuse characterization of Li_4TiO_4 power bandwidth of 4.45 eV, which is 7.9% higher than the density function theory calculated value. These experiments indicated that theoretical value approaches the experimental result very well.

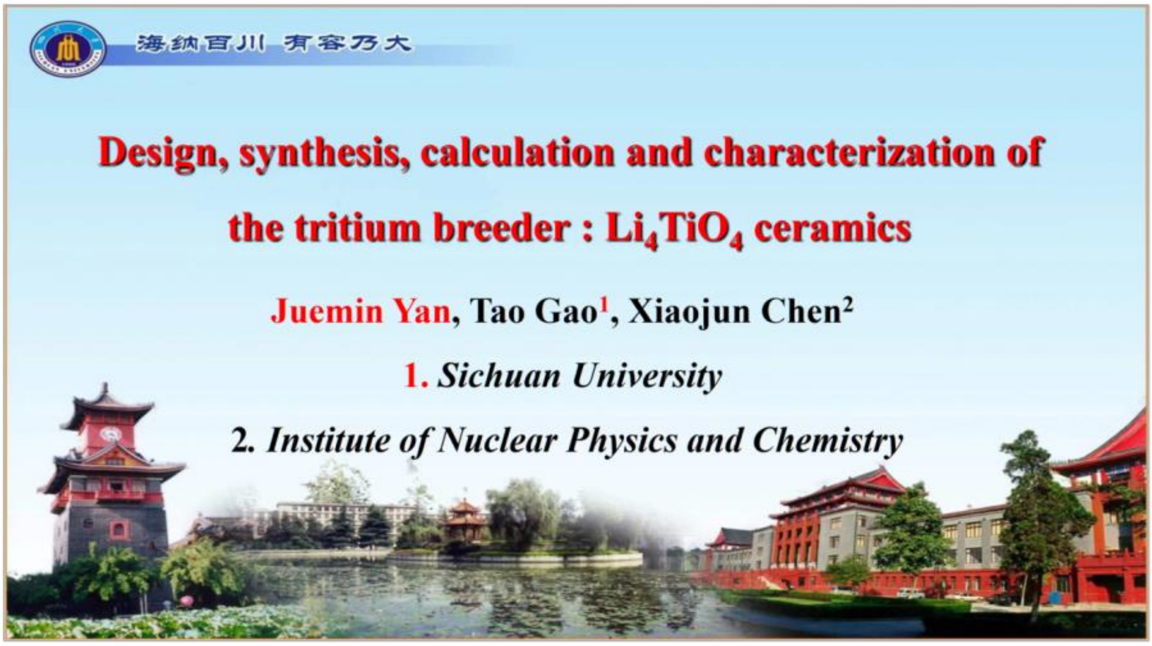
海纳百川 有容乃大
Design, synthesis, calculation and characterization of
the tritium breeder : Li_4TiO_4 ceramics
Juemin Yan, Tao Gao[1], Xiaojun Chen[2]
1. Sichuan University
2. Institute of Nuclear Physics and Chemistry


Sichuan University
目录
CONTENT
01 Background
02 Research technique
03 Research results
04 Summary and plan

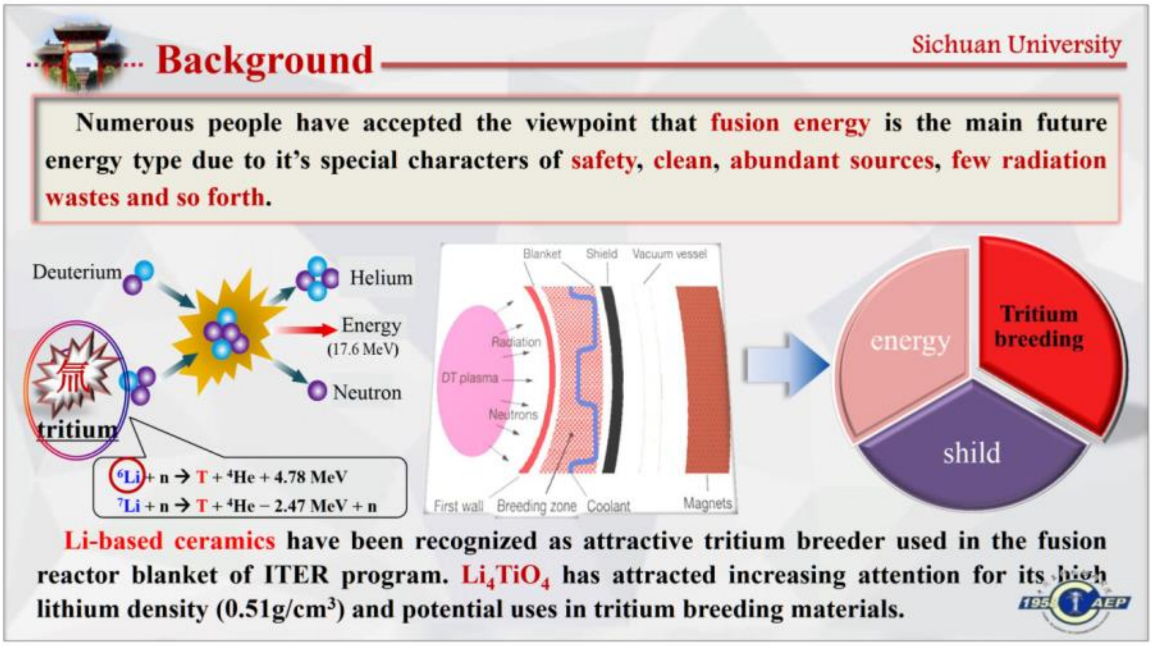
Background
Sichuan University
Numerous people have accepted the viewpoint that fusion energy is the main future energy type due to it's special characters of safety, clean, abundant sources, few radiation wastes and so forth.
Deuterium
Helium
Energy
(17.6 MeV)
Neutron
tritium
$^6Li + n \rightarrow T + {}^4He + 4.78$ MeV
$^7Li + n \rightarrow T + {}^4He - 2.47$ MeV + n
Blanket
Shield
Vacuum vessel
Radiation
DT plasma
Neutrons
First wall
Breeding zone
Coolant
Magnets
energy
Tritium breeding
shild
Li-based ceramics have been recognized as attractive tritium breeder used in the fusion reactor blanket of ITER program. Li_4TiO_4 has attracted increasing attention for its high lithium density ($0.51g/cm^3$) and potential uses in tritium breeding materials.

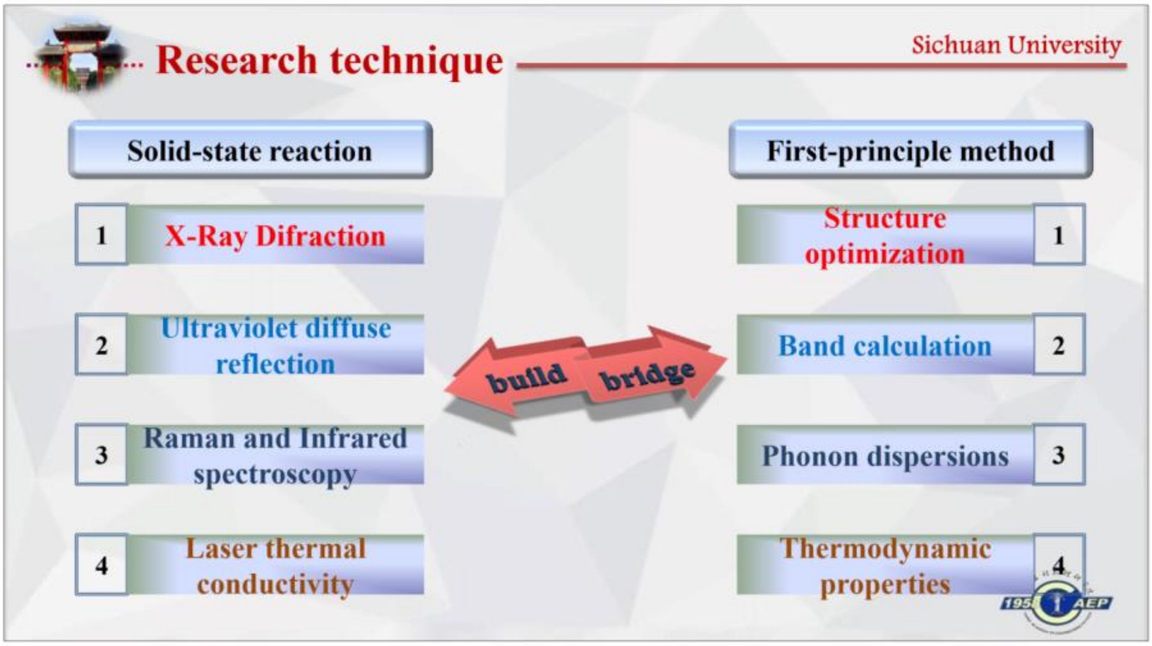
Research technique
Sichuan University
Solid-state reaction
1 X-Ray Difraction
2 Ultraviolet diffuse reflection
3 Raman and Infrared spectroscopy
4 Laser thermal conductivity
build
bridge
First-principle method
Structure optimization 1
Band calculation 2
Phonon dispersions 3
Thermodynamic properties 4

Research results — Solid-state reaction

Sichuan University

Li_4TiO_4 ceramic powder was obtained via solid state reaction.

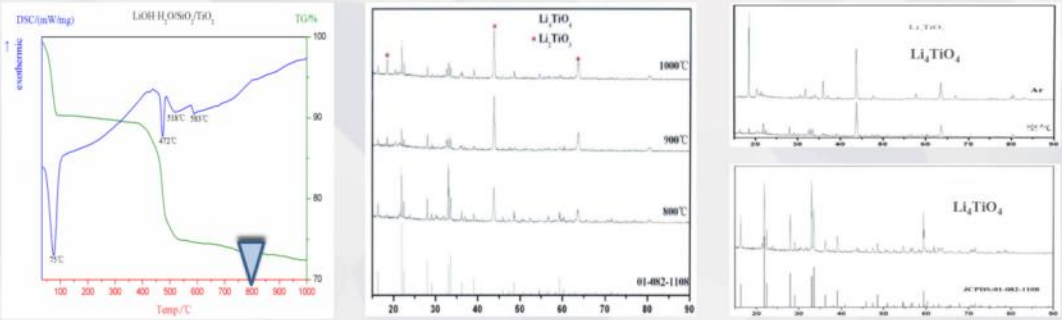

The mixtures for the preparation of Li_4TiO_4 were investigated by **TG-DSC.**
The **XRD** of samples obtained at different temperature were compared fired.
It was noted that the appropriate temperature for preparation was **800 ℃, 10h, air.**

Research results — Solid-state reaction

Sichuan University

Ultraviolet diffuse reflection

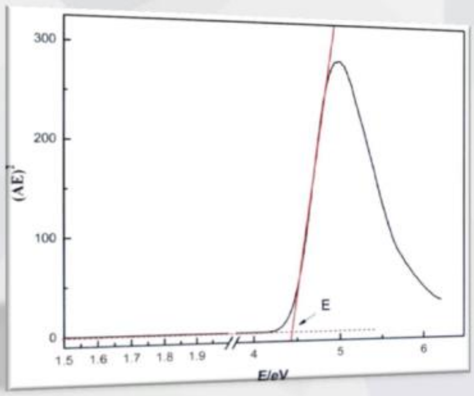

The relationship of $(AE)^2$ and E

Wavelength range:
200nm—1100nm
The linear relationship between the band and absorbance:
Ahv=(hv-Eg)1/2 E=hv=hc/λ
The point at which tangent of a curve intersects its x-coordinate:
Band value:
E_g=4.45ev

Research results — Solid-state reaction

Sichuan University

Raman and Infrared spectroscopy

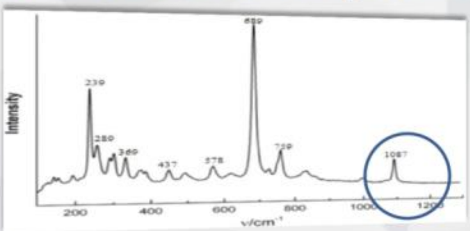

The vibration spectrum larger than 1000nm in the figure may be due to the vibration of carbon and oxygen ions in the impurity.

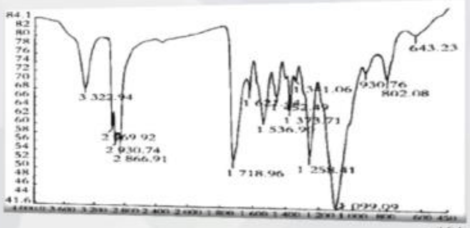

The sample structure was analyzed by IR spectrum, the characteristic absorption peak sharper with the increase of frequency, with strong chemical activity.

Research results — Solid-state reaction

Sichuan University

Laser thermal conductivity

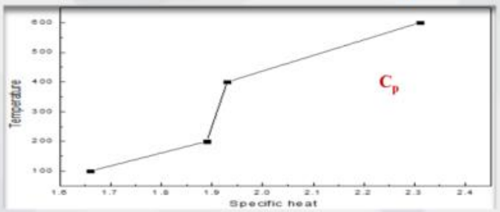

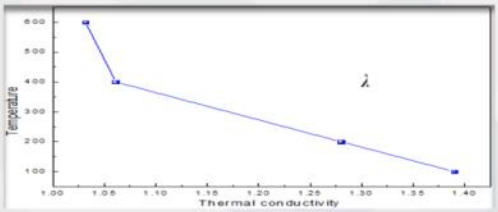

C_p increased with temperature rise

λ decreased with temperature drop

Thermal conductivity: $\lambda=\rho\times\alpha\times C_p$

Thermal diffusivity : α Dendity: ρ Constant pressure specific heat: C_p

The increase of thermal conductivity improves the thermal efficiency of fusion reactor.

Research results — First-principle method

Sichuan University

Structure optimization

	XRD	calculated	literrature
a(Å)	7.956±0.003	7.993(1.02%)	7.912
b(Å)	7.472±0.015	7.469(0.48%)	7.433
c(Å)	6.187±0.043	6.196(0.96%)	6.137
V(Å³)	143.33	141.89(0.65%)	140.97

The crystal structure of Li_4TiO_4 was detected by X-ray diffraction, and the powder diffraction data is used as a critical factor for the structure optimization. The results show that the values of calculation **agree well** with the experiment data.

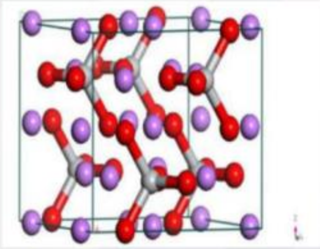

The crystal structure of Li_4TiO_4.
(**purple-Li**)、(**red-O**)、(**grey-Ti**)

Research results — First-principle method

Sichuan University

Band calculation

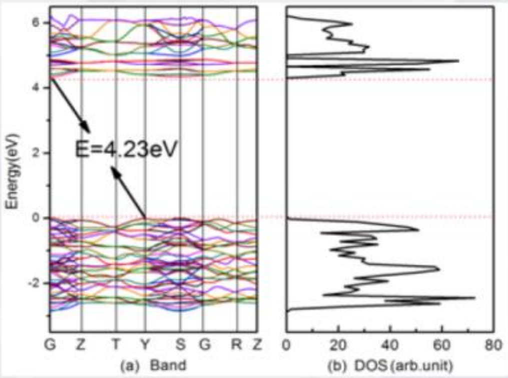

The calculated electronic band structures and the total density of states of Li_4TiO_4 are displayed. The valence band is located below Fermi energy level (set to relative zero). It takes on an indirect band gap with the value of **4.23eV**, less than experimental value **4.45eV, but within reason.**

Research results — First-principle method

Sichuan University

Phonon dispersions

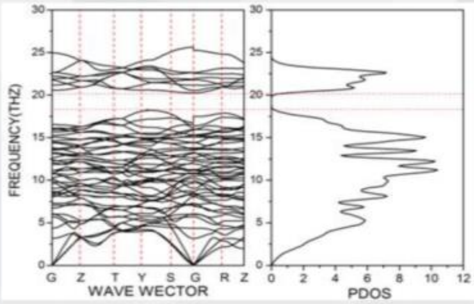

Atom	Z_1	Z_2	Z_3	Z_{aver}
Li(1)	1.2203	1.1178	0.9187	1.0856
Li(2)	1.0390	0.9965	1.2066	1.0807
Ti	3.0538	2.7365	3.4067	3.0656
O(1)	-1.3805	-1.7724	-2.5355	-1.8961
O(2)	-2.3981	-1.7051	-1.2886	-1.7972

Born effective tensor for each nonequivalent atom.

The calculated phonon dispersion curves and total phonon dendity of states of Li_4TiO_4. There are **54** branchess of phonon branches in the system, and there are **3** acoustic and **51** optical modes.

Research results — First-principle method

Sichuan University

	Raman				Infrared		
	A_g	B_{1g}	B_{2g}	B_{3g}	B_{1u}	B_{2u}	B_{3u}
Li_4TiO_4	189.9	105.8	199.1	145.6	242.5	321.2	224.5
					242.6	323.5	238.7
	279.3	201.5	272.9	289.1	283.2	327.3	338.6
					284.0	331.6	350.8
Cmcm	358.2	235.2	340.8	361.6	374.2	400.5	371.3
					412.4	415.6	372.3
	421.0	358.1	455.2	450.4	440.6	437.7	395.5
					487.4	437.9	398.4
No.63	479.6	408.8	508.2	501.5	509.3	536.8	439.8
					522.2	545.2	558.3
	530.8	481.2		725.4	674.6	550.5	729.6
					830.7	582.0	753.8
Z=4	684.8	531.7				727.7	
						731.9	
	754.1	704.6				753.8	
						852.9	

The left table summarized the calculated phonon fruquencues at k=0 together with LO-TO splitting.

$T_{aco}=B_{1u}+B_{2u}+B_{3u}$ (aco: acoustic; opt: optical)

$T_{opt}=8A_g+8B_{1g}+5B_{2g}+6B_{3g}+6B_{1u}+8B_{2u}+6B_{3u}+4A_u$

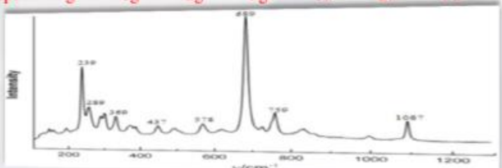

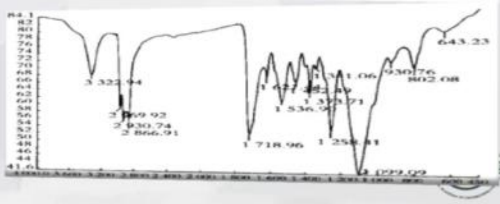

Research results — First-principle method

Sichuan University

Thermodynamic properties

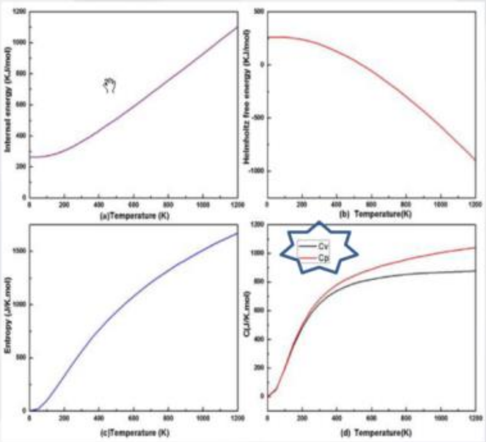

After the dynamical phonon properties, the thermodyanmic properties of Li_4TiO_4 are achieved using DFPT calculations.

The calculated helmholtz free energy, entropy, C_V, C_P and internal energy with the temperature from 0 to 1200 K are presented.

The calculated value (C_P) agree with experiment, and it increases with temperature.

Summary and Outlook

Sichuan University

Summary

1. For the advanced tritium breeders in fusion and fission-fusion reactors, the Li_4TiO_4 solid solutions had been prepared successfully by solid state reaction。

2. Samples were systemtically characterized by experimental and calculating method. And the result obtained agree well with each other.

Outlook

1. Have a deep understanding on tritium release behavior from Li_4TiO_4。

2. A theoretical model on the tritium release will be set up to explained rationally the tritium release behavior.


Sichuan University
Thanks for listening !

3D imaging of the microstructure of the ceramic breeding pebbles by X-ray computed tomography (X-ray CT)

Yu-Ping Xu[1], Xin Hu[2], Ying-Chun Zhang[2], Hai-Shan Zhou[1], Guang-Nan Luo[1]

[1]Institute of Plasma Physics, Chinese Academy of Sciences, Hefei, 230031, China

[2]University of Science and Technology Beijing, Beijing, 100083, China

Pebbles with a few millimeters in diameter have been the approaches of choice for ITER solid TBM and future DEMO solid breeder concept. The performance of ceramic breeding pebbles is controlled by their microstructure, in particular the pore network plays a critical role in determining mechanical properties and the tritium desorption behavior. Unfortunately, most of the imaging techniques used before were destructive techniques such as SEM, which settles to limited observation region and requires a large amount of sample preparation time. It is challenging but essential to find a non-destructive technique to obtain a 3D morphology of the pore network of one pebble.

Here in this work, we apply a X-ray computed tomography (X-ray CT) technique to extract and study the complete 3D pore network, both quantitatively and morphologically. As far as we know, this is the first time that an experimental technique allows the visualization and investigation of the complete 3D pore network of single lithium-containing ceramic pebbles. Calibrated by mercury intrusion method, 3D imaging of Li_2TiO_3, Li_4SiO_4 and Li_2TiO_3-Li_4SiO_4 composite pebbles prepared by agar method have been obtained. Some imaging pictures are shown in Fig. 1. Based on the CT results, we are trying to analysis the tritium transport behavior in one single pebble employing lattice Boltzmann method (LBM).

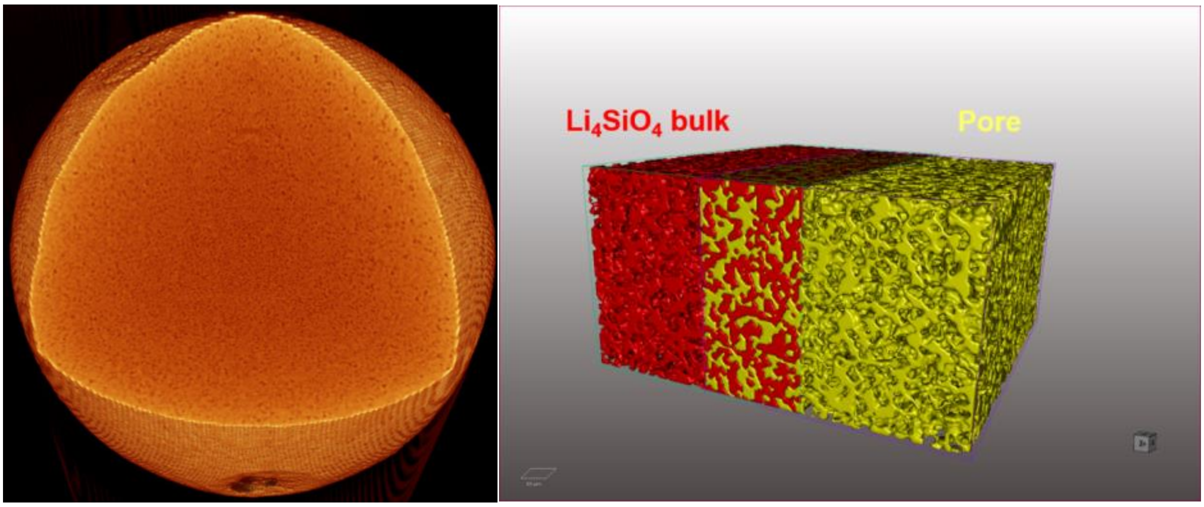

Fig.1. Left, 3D image of a Li_4SiO_4 pebble with some inner structure visible by digital image processing. Right, 3D image of the bonding of pore and the bulk in a Li_4SiO_4 pebble (red part for Li_4SiO_4 bulk, golden part for pore network).

Analysis of valence electron structure of Li metal/oxides by soft X-ray emission spectroscopy

Keisuke Mukai[1], Ryuta Kasada[2], Kazuya Sasaki[3], Satoshi Konishi[1]

[1]Institute of Advanced Energy, Kyoto University

[2]Institute for Material Research, Tohoku University

[3]Graduate School of Science and Engineering, Hirosaki University

Li-containing ceramic breeder pebbles (Li_2O, Li_2TiO_3, Li_2ZrO_3, Li_4SiO_4, and etc.) are employed in fusion reactors to produce fuel tritium by transmutation of Li in blanket. Mass transport of Li and O from the breeder pebbles to the structural steel is caused in the blanket during an operation because gas species (e.g. Li, Li_2O, and Li_2O_2) are vaporized. Previous compatibility studies between breeder materials and reduced activation ferritic/martensitic (RAFM) structural steel showed the formations of the double oxide scales on the RAFM steel specimens by element mapping using energy-dispersive X-ray spectroscopy (EDS). Due to a poor emission efficiency of X-rays from Li, however, an identification of the corrosion phase was impossible only by the compositional analysis by EDS. The identification of the Li-containing oxide required other methods such as X-ray diffraction and secondary-ion mass spectroscopy.

This study aims to develop an analytical method which visualizes distribution of Li at the micro scale. Li-Kα spectra from metallic Li, Li_2O, and Li_2TiO_3 were investigated by using soft X-ray emission spectrometer (SXES) attached to an electron probe micro-analyzer (EPMA), which covers a low energy range (50–210 eV) with ultra-high energy resolutions (0.22 eV). Density functional theory (DFT) calculations were performed to simulate the density of state (DOS) of the Li-compounds using the Perdew–Burke–Ernzerhof (PBE) generalized gradient approximation (GGA) for the exchange and correlation functional implemented in Vienna ab initio simulation package (VASP). DOSs of Li were convoluted with Gaussian functions with a full width at half-maximum (FWHM) of 0.5 eV and then compare with the experimental SXES spectra. Li-Kα spectrum from the Li_2O specimen was observed in the energy range of 47.5–51.0 eV with the peak top at 49.6 eV. The peak top was approximately 4.5 eV lower than that from metallic Li, indicating a large chemical shift by the oxidation. The experimental Li-Kα peak shape by the SXES had a good agreement with the calculated PDOS of Li 2*p* states, while the energy was largely underestimated in the calculation. The intensities of Li-Kα from the oxide specimens were much lower than that from the metallic specimen because of a considerable loss of valence electrons by ionization (Li^+). By taking advantage of the large chemical shift of Li-Ka caused by oxidation, chemical state mapping of Li metal/oxide in the oxidised Li specimen was successfully visualized.

Analysis of valence electron structure of Li metal/oxides by soft X-ray emission spectroscopy

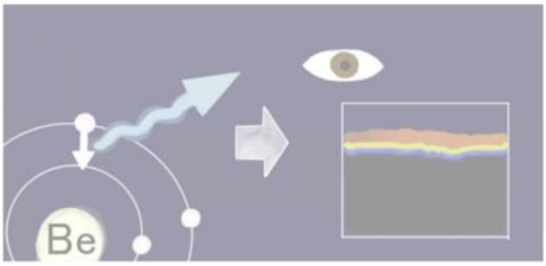

K. Mukai[1], R. Kasada[2], K. Sasaki[3], S. Konishi[1]
[1]Institute of Advanced Energy, Kyoto University
[2]Institute for Material Research, Tohoku University
[3]Graduate School of Science and Engineering, Hirosaki University
京都大学 KYOTO UNIVERSITY
15th anniversary KONISHI LAB

CBBI-20 (Karlsruhe, Germany), 18-20 September 2019

KYOTO UNIVERSITY

Functional materials in a solid breeding blanket

Neutron multiplier (Be-compounds) and ceramic breeder (Li-compounds) play vital roles in a solid breeding blanket for self-sufficient fueling.

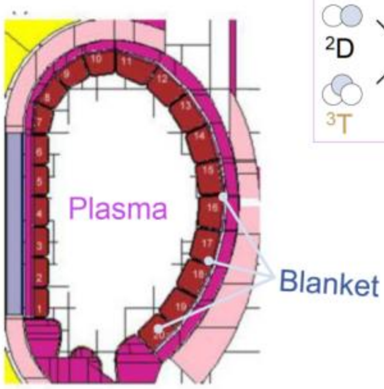

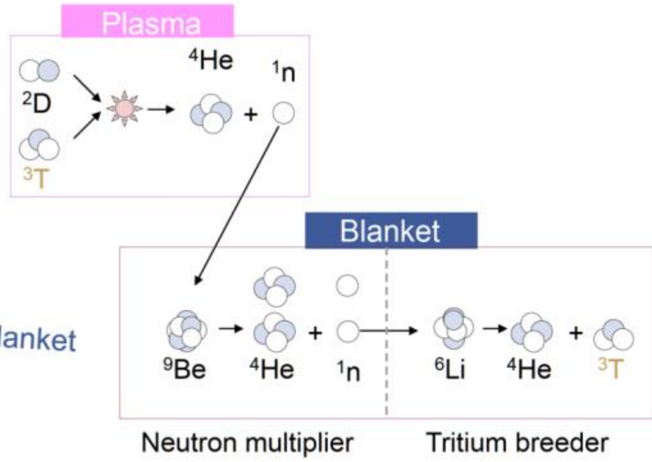

20.09.2019 Keisuke Mukai 2

KYOTO UNIVERSITY

Analysis on corrosion layer using SEM/EDX

Cross section of EUROFER contacted with KALOS (Li_4SiO_4/Li_2TiO_3) ceramic breeder for 28 days (800 °C)

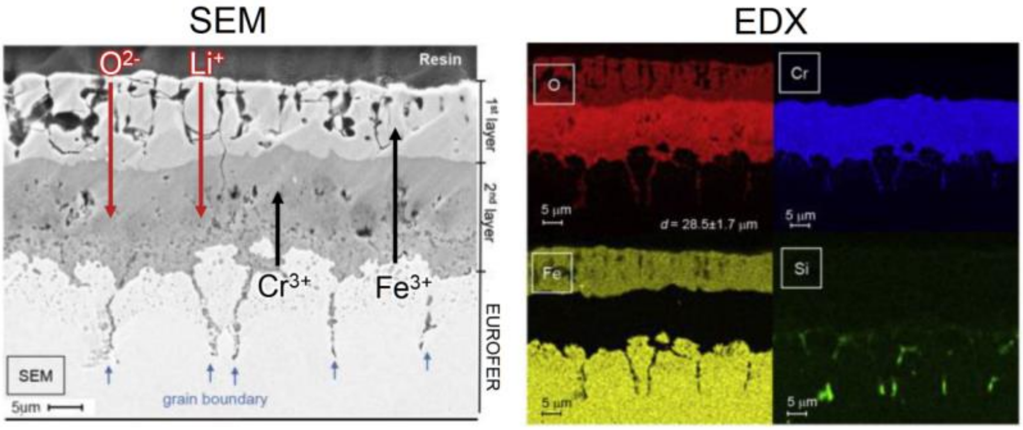

Li distribution is not given by the conventional approach (EDX).
SIMS (destructive measurement) was applied for Li detection.

20.09.2019 Keisuke Mukai K. Mukai et al., *J. Nucl. Mater.* 488 (2017) 196-203. 3

KYOTO UNIVERSITY

Objective of study

- To develop a non-destructive approach to analyze light-element compounds (Li/Be) in an electron microscope
  - Soft X-ray emission spectroscopy (SXES) attached to Electron probe micro-analyzer (EPMA)
  - Materials
    - Neutron multiplier (Be metal/intermetallics)
    - Tritium breeder (Li metal/oxide)

20.09.2019 Keisuke Mukai 4

KYOTO UNIVERSITY

Method

20.09.2019 Keisuke Mukai 5

KYOTO UNIVERSITY

Samples

Bulk samples	Method and conditions
Be	Hot press
BeO	Plasma sintering
Be−Ti and Be−V beryllides	Plasma sintering
steamed $Be_{12}V$	Single-phase $Be_{12}V$ was oxidized at 1000 °C, 24h, 15%H_2O/Ar

All of Be-specimens were prepared at QST Rokkasho by Dr. J.H. Kim & Dr. M. Nakamichi

Powder samples	Procurement
Li	Mitsuwa co.
LiO_2	Kojundo chemical laboratory co.
Li_2O_2	
Li_2TiO_3	

20.09.2019 Keisuke Mukai 6

KYOTO UNIVERSITY

EPMA-SXES at Kyoto University (Uji)

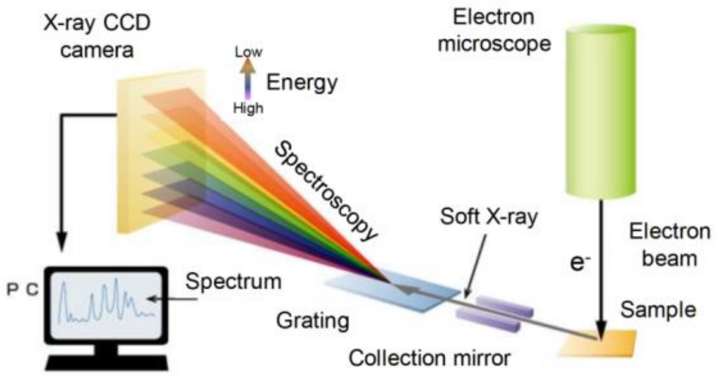

SXES by JEOL is attached to electron probe micro analyzer (EPMA) JXA-8500F.

20.09.2019 Keisuke Mukai 7

KYOTO UNIVERSITY

Advantages of the SXES

Energy resolution*

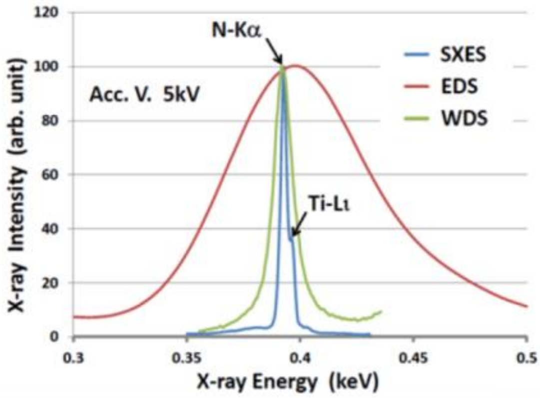

Chemical state mapping;

B_4C after steam oxidation (1250 °C, 30 min)**

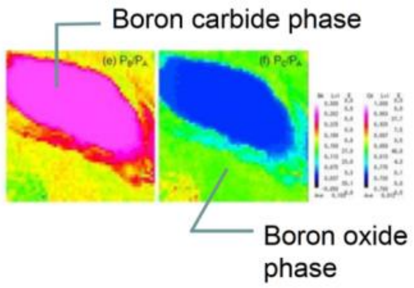

Low energy range 50～200 eV covers Li-Kα (54 eV) and Be-Kα (110 eV)
High energy resolution (0.22 eV @Al-L) enables chemical state mapping**

*JEOL web site
R. Kasada, Y. Ha, T. Higuchi, K. Sakamoto, *Sci. Rep.* **2016, 6, 25700.

20.09.2019 Keisuke Mukai 8

KYOTO UNIVERSITY

Density of State (DOS) by DFT calculations

Projected DOS for each atom was calculated using VASP code with PBE-GGA functionals.

Crystals
- Be metal (3×3×3 supercell)
- BeO (2×2×2 supercell)
- $Be_{12}Ti$ (unitcell)
- $Be_{12}V$ (unitcell)
- Li metal (3×3×3 supercell)
- Li_2O (2×2×2 supercell)
- Li_2O_2 (3×3×1 supercell)
- Li_2TiO_3 (2×1×1 supercell)

PDOS was convoluted with Gaussian (FWHM: 0.6 eV) to allow a direct comparison with soft X-ray spectra by the SXES

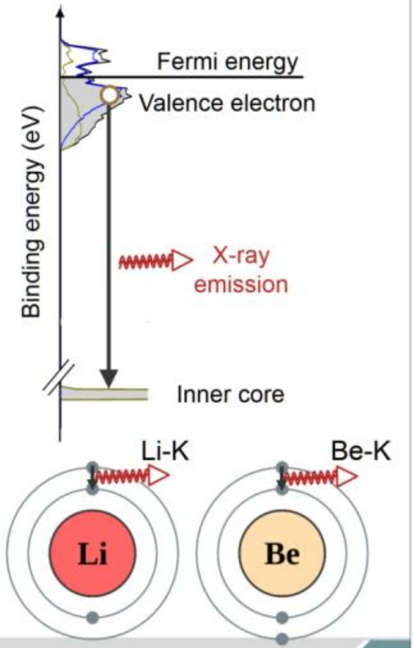

20.09.2019 Keisuke Mukai 9

KYOTO UNIVERSITY

Results

20.09.2019 Keisuke Mukai 10

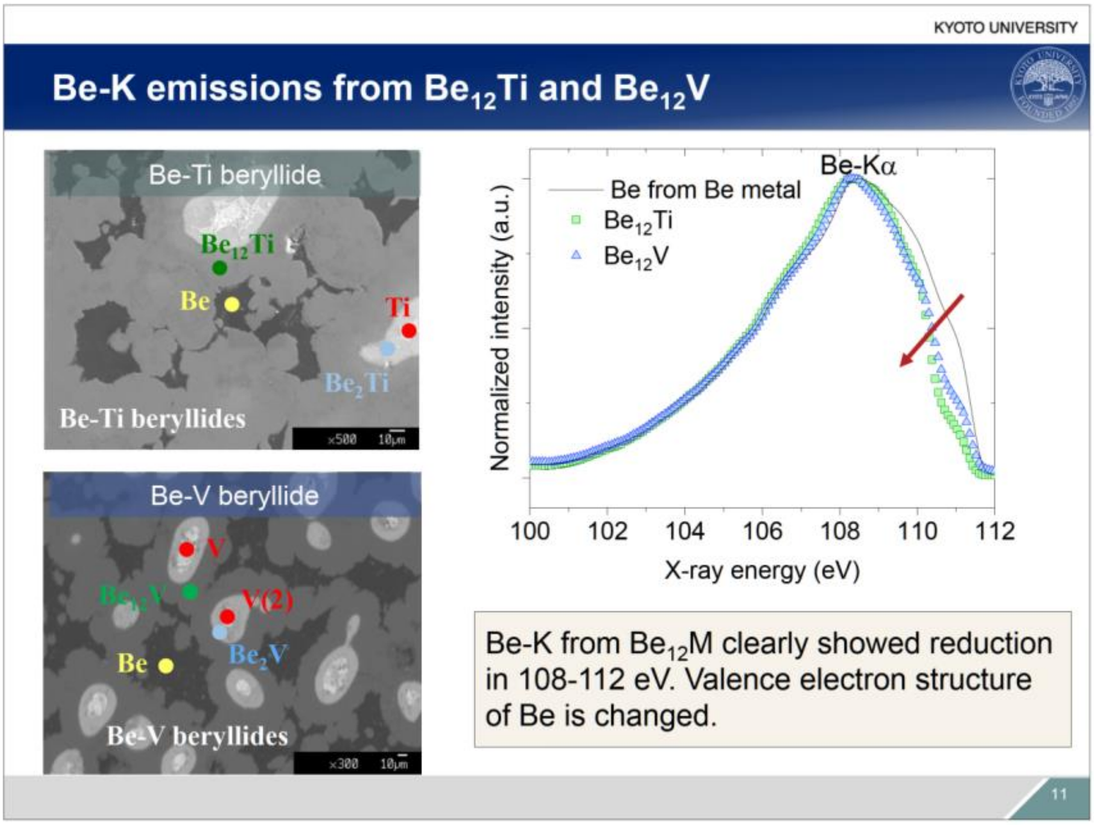
KYOTO UNIVERSITY
Be-K emissions from Be12Ti and Be12V
Be-Ti beryllide
Be12Ti
Be
Ti
Be2Ti
Be-Ti beryllides
Be-V beryllide
V
Be12V
V(2)
Be2V
Be
Be-V beryllides
Be-Kα
Be from Be metal
Be12Ti
Be12V
Normalized intensity (a.u.)
100 102 104 106 108 110 112
X-ray energy (eV)
Be-K from Be12M clearly showed reduction in 108-112 eV. Valence electron structure of Be is changed.
11

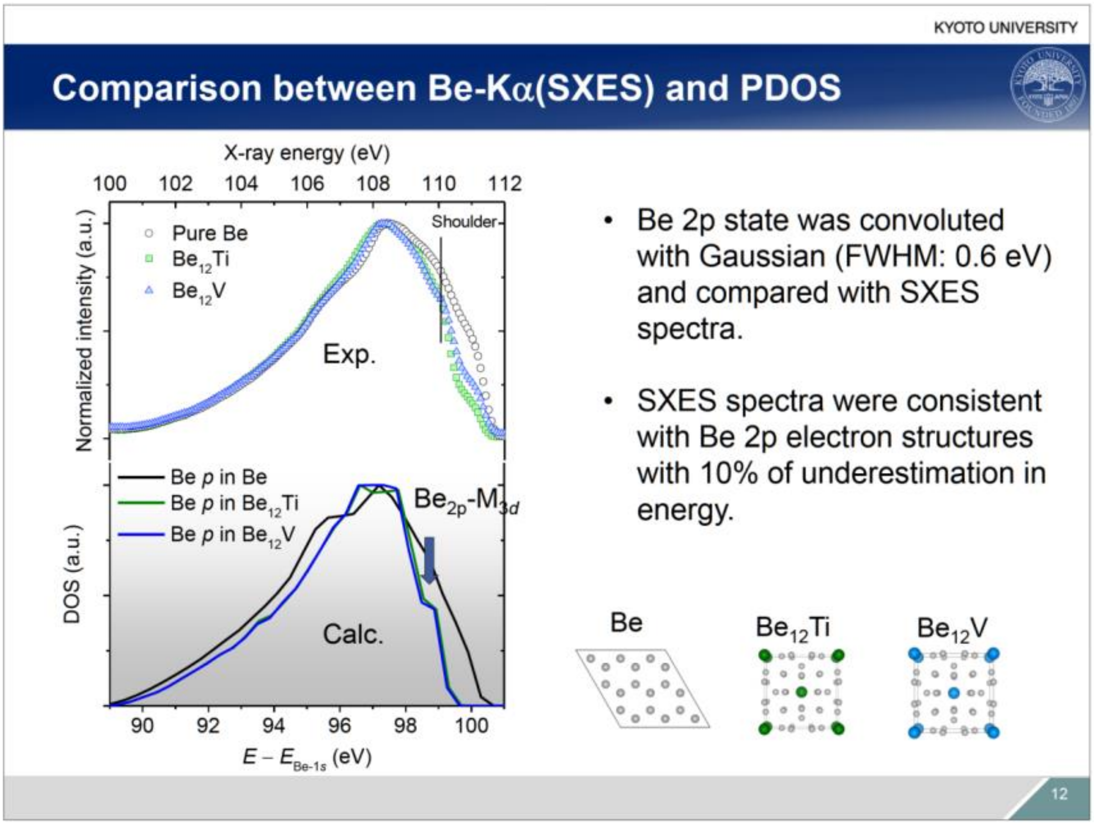
KYOTO UNIVERSITY
Comparison between Be-Kα(SXES) and PDOS
X-ray energy (eV)
100 102 104 106 108 110 112
Shoulder
Pure Be
Be12Ti
Be12V
Normalized intensity (a.u.)
Exp.
Be p in Be
Be p in Be12Ti
Be p in Be12V
Be2p-M3d
DOS (a.u.)
Calc.
90 92 94 96 98 100
E – EBe-1s (eV)
• Be 2p state was convoluted with Gaussian (FWHM: 0.6 eV) and compared with SXES spectra.
• SXES spectra were consistent with Be 2p electron structures with 10% of underestimation in energy.
Be
Be12Ti
Be12V
12

KYOTO UNIVERSITY

Chemical state mappings of steamed $Be_{12}V$

Chemical shift of BeO as large as 4 eV was observed.
Chemical state mapping in the oxidized $Be_{12}V$ was visualized using the shift.

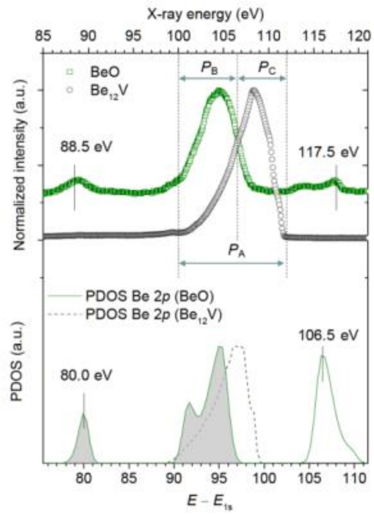

Element mappings

Chemical state mappings

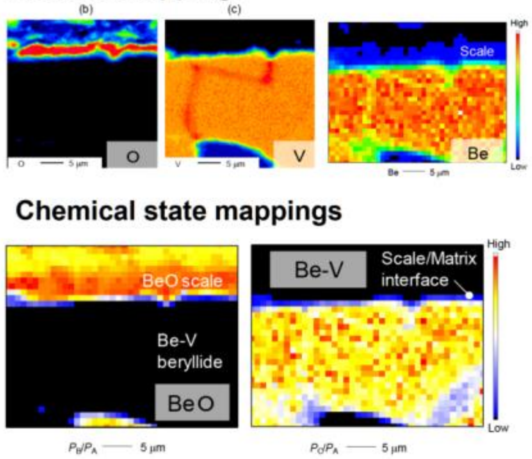

K. Mukai, R. Kasada et al. *ACS Appl. Energy Mater.* 2019, 2, 4, 2889-2895

13

KYOTO UNIVERSITY

SXES from β-Li_2TiO_3

Very low signal was obtained for VB electrons.
Signals at 55 and 57 eV are electrons in CB(?).

PDOS by DFT calculations

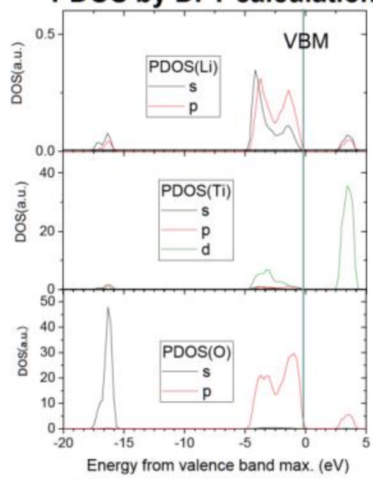

VBM: valence band maximum

β-Li_2TiO_3*

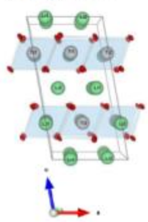

Detection limit of SXES (47 eV)

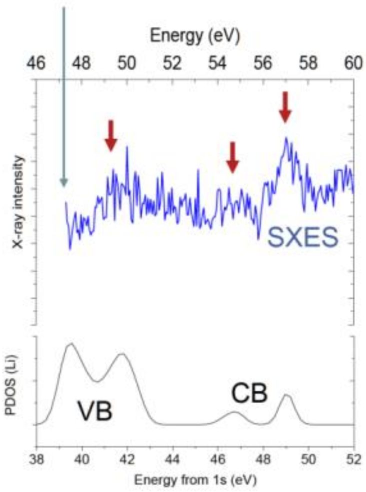

VB: valence band
CB: conduction band

20.09.2019

K. Mukai et al., *ACS Applied Energy Materials* 2019 2 (8), 5481-5489

14

KYOTO UNIVERSITY

Conclusion

- Soft X-ray emission spectroscopy (SXES) can analyze light elements (Li, Be, B; Z = 3～5) and visualize chemical state mapping.
- Be compounds (neutron multiplier)
  - The change of Be-p valence electron was successfully analyzed.
  - Chemical state mapping was shown using the chemical shift between beryllide phase and BeO.
- Li compounds (tritium breeder)
  - Li, Li_2O_2, Li_2O were successfully analyzed.
  - The Li-K signal from Li_2TiO_3 was very low
- Metallic or intermetallic sample is better for SXES analysis.
- EPMA/SXES is open for all researchers

15

Acknowledgement
This work is supported by the Joint Usage/Research Program on Zero-Emission Energy Research, Institute of Advanced Energy, Kyoto University (ZE29A-12, ZE30A-23)

Compatibility of Tritium Permeation Barrier Coatings under Solid Breeder Blanket Conditions

Takumi Chikada[1], Matthias Kolb[2], Kazuki Nakamura[1], Keisuke Kimura[1], Hikari Fujita[3], Marcin Rasinski[4], Keisuke Mukai[5], Yoshimitsu Hishinuma[6], Regina Knitter[2]

[1]Shizuoka University, Japan, [2]Karlsruhe Institute of Technology, Germany, [3]The University of Tokyo, Japan, [4]Forschungszentrum Jülich, Germany, [5]Kyoto University, Japan, [6]National Institute for Fusion Science, Japan

Strict control of tritium migration is an essential requirement for every blanket concept in a fusion reactor in terms of fuel efficiency and radiological safety. Tritium permeation barriers (TPBs), basically using ceramic coatings, have been developed in particular for liquid lithium-lead blankets; however, recent DEMO reactor design activities initiate an argument that a TPB is necessary also in solid breeder blankets. The previous studies showed that solid breeder lithium ceramics reacted with reduced activation ferritic/martensitic steels at elevated temperature, indicating the lithium reactivity of solid breeders should be taken into consideration. In this study, compatibility tests for TPBs with lithium ceramic pebbles have been carried out in order to assess the chemical stability of TPBs in the helium cooled pebble bed blanket concept.

Reduced activation ferritic/martensitic steel F82H plates were used as substrates. For the preparation of TPB coatings, erbium oxide (Er_2O_3) coatings were fabricated by filtered vacuum arc deposition and metal-organic decomposition, and chromium oxide (Cr_2O_3) layers formed on the F82H substrates by heat treatment for 10 min at 710 ºC under hydrogen-argon mixture gas (H_2:Ar = 1:1) flow of 200 standard cubic centimeter per minute. Ceramic breeder pebbles of lithium orthosilicate with 30 mol% of lithium metatitanate were put on the samples and then annealed for 2–32 days at 550 and 700 °C under 20 standard cubic centimeter per minute He with 0.1 vol% H_2 flow.

After annealing at 550 °C, no change in microstructure was confirmed for the Er_2O_3 coatings, while the Cr_2O_3-formed samples showed drastic changes in surface and cross-sectional structures including oxidation of F82H to iron oxide (Fe_2O_3) and iron-chromium spinel-type oxide ($Fe(Fe,Cr)_2O_4$)), reduction of iron oxide and chemical reactions by lithium. In the case of the Er_2O_3 coatings annealed at 700 °C, the coatings fabricated by filtered vacuum arc deposition remained on the substrates when tested without pebbles, while severely damaged with pebbles. The Er_2O_3 coatings prepared by metal-organic decomposition might vanish with and without pebbles. Further discussion on chemical reactions of the Cr_2O_3 layer and stability of Er_2O_3 coatings at 700 °C will be included in the presentation.

20th International Workshop on Ceramic Breeder Blanket Interactions (CBBI-20)
Karlsruhe Institute of Technology, Campus North
September 18, 2019

Compatibility of Tritium Permeation Barrier Coatings under Solid Breeder Blanket Conditions

Takumi Chikada[1], Matthias H.H. Kolb[2], Kazuki Nakamura[1], Keisuke Kimura[1], Hikari Fujita[3], Marcin Rasinski[4], Keisuke Mukai[5], Yoshimitsu Hishinuma[6], Regina Knitter[2]

[1]Shizuoka University [2]Karlsruhe Institute of Technology
[3]The University of Tokyo [4]Forschungszentrum Jülich
[5]Kyoto University [6]National Institute for Fusion Science

Acknowledgement: This work was supported by JSPS KAKENHI Grant Number 19H01873 and the general collaboration research with National Institute for Fusion Science (NIFS18KEMF119).

Contents

1. Introduction
   - Tritium permeation in solid breeder blanket
   - Tritium permeation barrier coating
   - Objectives of this work
2. Experimental details
   - Coating preparation
   - Solid breeder pebbles exposure test
   - Characterization
3. Results and discussion
   - Cr_2O_3-formed F82H
   - Er_2O_3 coatings
4. Summary

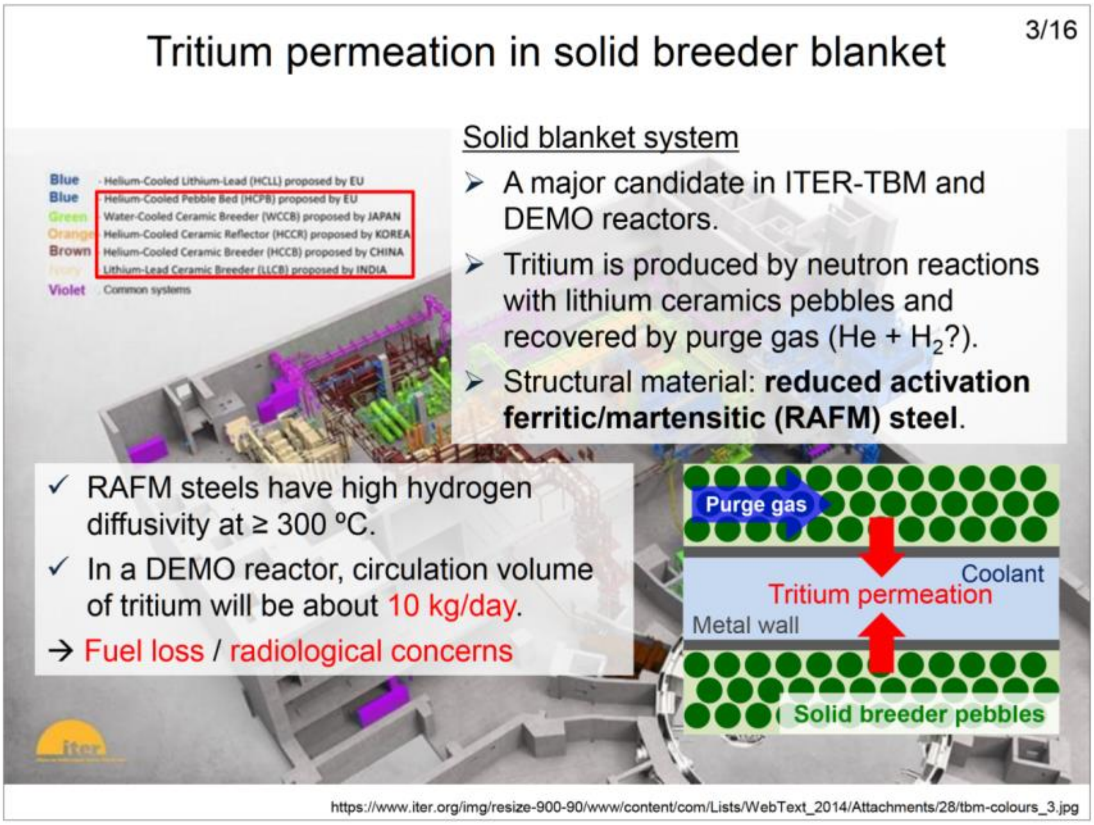
3/16
Tritium permeation in solid breeder blanket
Solid blanket system
➢ A major candidate in ITER-TBM and DEMO reactors.
➢ Tritium is produced by neutron reactions with lithium ceramics pebbles and recovered by purge gas (He + H_2?).
➢ Structural material: **reduced activation ferritic/martensitic (RAFM) steel**.
Blue - Helium-Cooled Lithium-Lead (HCLL) proposed by EU
Blue - Helium-Cooled Pebble Bed (HCPB) proposed by EU
Green - Water-Cooled Ceramic Breeder (WCCB) proposed by JAPAN
Orange - Helium-Cooled Ceramic Reflector (HCCR) proposed by KOREA
Brown - Helium-Cooled Ceramic Breeder (HCCB) proposed by CHINA
Ivory - Lithium-Lead Ceramic Breeder (LLCB) proposed by INDIA
Violet - Common systems
✓ RAFM steels have high hydrogen diffusivity at ≥ 300 °C.
✓ In a DEMO reactor, circulation volume of tritium will be about 10 kg/day.
→ Fuel loss / radiological concerns
Purge gas
Coolant
Tritium permeation
Metal wall
Solid breeder pebbles
https://www.iter.org/img/resize-900-90/www/content/com/Lists/WebText_2014/Attachments/28/tbm-colours_3.jpg

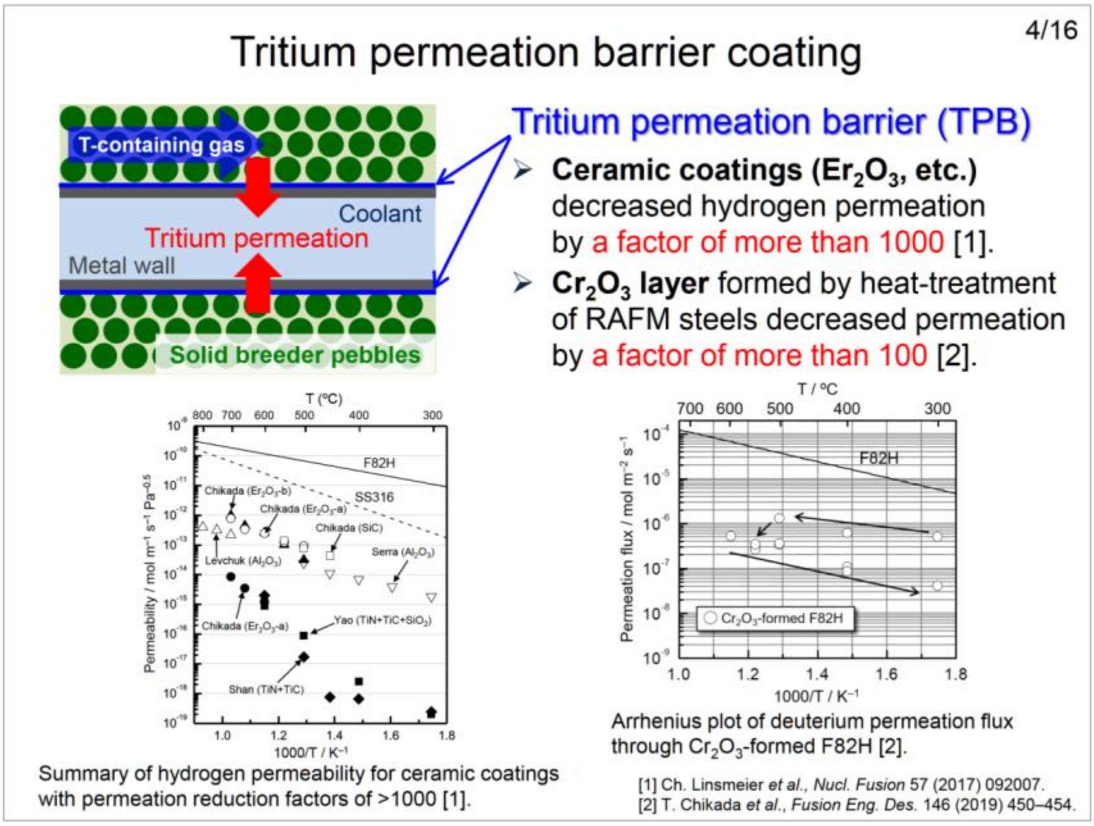
4/16
Tritium permeation barrier coating
Tritium permeation barrier (TPB)
➢ **Ceramic coatings (Er_2O_3, etc.)** decreased hydrogen permeation by a factor of more than 1000 [1].
➢ **Cr_2O_3 layer** formed by heat-treatment of RAFM steels decreased permeation by a factor of more than 100 [2].
T-containing gas
Coolant
Tritium permeation
Metal wall
Solid breeder pebbles
T (°C)
Permeability / mol m^{-1} s^{-1} Pa$^{-0.5}$
1000/T / K^{-1}
F82H
SS316
Chikada (Er_2O_3-b)
Chikada (Er_2O_3-a)
Chikada (SiC)
Levchuk (Al_2O_3)
Serra (Al_2O_3)
Chikada (Er_2O_3-a)
Yao (TiN+TiC+SiO_2)
Shan (TiN+TiC)
Summary of hydrogen permeability for ceramic coatings with permeation reduction factors of >1000 [1].
T / °C
Permeation flux / mol m^{-2} s^{-1}
1000/T / K^{-1}
F82H
Cr_2O_3-formed F82H
Arrhenius plot of deuterium permeation flux through Cr_2O_3-formed F82H [2].
[1] Ch. Linsmeier *et al.*, *Nucl. Fusion* 57 (2017) 092007.
[2] T. Chikada *et al.*, *Fusion Eng. Des.* 146 (2019) 450–454.

5/16

Objectives of this work

Requirements for TPB

- ✓ High permeation reduction factor (PRF) PRF = $J_{uncoated}$ / J_{coated} >100–1000
- ✓ Compatibility with blanket materials
- ✓ Irradiation resistance, thermal durability, accessible fabrication process, etc.

- ☐ The necessity of TPB coatings has been discussed mainly in liquid blankets. [3]
- ☐ Recent study revealed that RAFM steel was corroded by ceramic breeders [4].
- ☐ **Compatibility of TPB coatings in solid breeders** has not been considered.

In this study, compatibility of tritium permeation barrier coatings with ceramic breeder pebbles has been investigated.

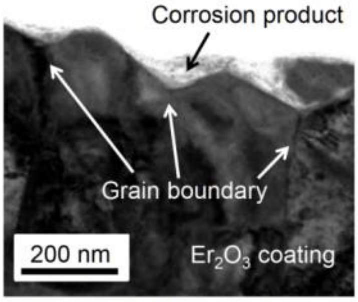

Cross-sectional TEM micrograph of Er_2O_3 coating exposed to Li-Pb at 550 °C for 400 h [3].

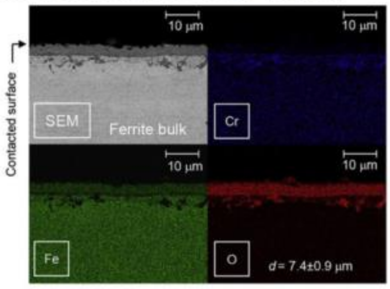

Cross-sectional SEM micrograph with elemental mapping of EUROFER97 exposed to solid breeder pellet at 550 °C for 3 weeks [4].

[3] S. Horikoshi *et al.*, *Nucl. Mater. Energy* 16 (2018) 66–70.
[4] K. Mukai *et al.*, *J. Nucl. Mater.* 488 (2017) 196–203.

6/16

Experimental details

Coating preparation (1) Formation of Cr_2O_3 layer

Substrate: RAFM steel F82H (Fe-8Cr-2W, F82H-BA07 heat)

Size: 25 mmL × 25 mmW × 0.5 mmt

Annealing parameter was optimized by our previous study. [2]

- Gas: Ar + H_2 (1:1)
- Flow rate: 200 sccm
- Temperature: 710 °C
- Time: 5 min

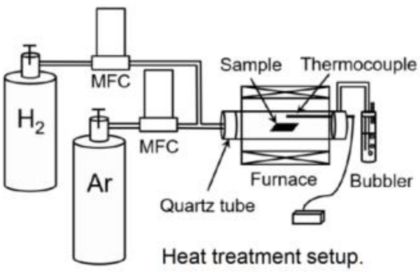

Heat treatment setup.

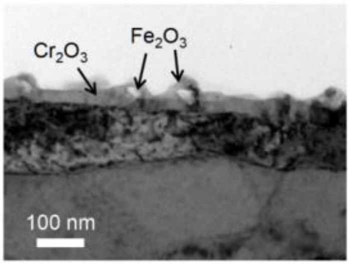

Cross-sectional TEM image of Cr_2O_3-formed F82H.

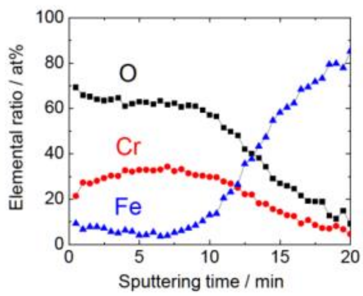

Depth profile of Cr_2O_3-formed F82H by XPS [2].

[2] T. Chikada *et al.*, *Fusion Eng. Des.* 146 (2019) 450–454.

7/16

Experimental details

Coating preparation (2) Fabrication of Er_2O_3 coatings

Substrate: RAFM steel F82H
(Fe-8Cr-2W, F82H-BA07 heat)

Size: 25 mmL × 25 mmW × 0.5 mmt

Fabrication methods:

Vacuum arc deposition (VAD)

- A gas-phase method providing high-purity metal oxides.
- Thickness: 1–3 μm

Metal organic decomposition (MOD)

- A liquid-phase method with simple procedure.
- Potential to apply plant-scale fabrication.
- Thickness: ~0.3 μm

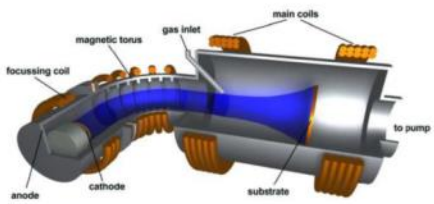

Filtered vacuum arc deposition device [5].

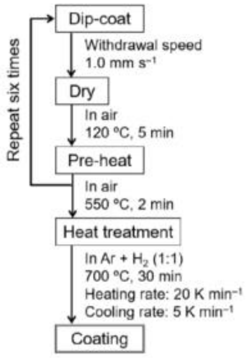

Dip coater

Heat-treatment device

Coating procedure of metal organic decomposition [6].

[5] F. Koch *et al.*, *J Nucl. Mater.* 329–333 (2004) 1403–1406.
[6] J. Mochizuki *et al.*, *Fusion Eng. Des.* 136 (2018) 219–222.

8/16

Experimental details

Solid breeder pebble exposure test

Pebble information

- Composition: 30 mol% Li_2TiO_3 in Li_4SiO_4
- Fabrication: KALOS process [7]
- Size: ~700 μm in diameter

Ceramic breeder pebbles before (left) and after (right) exposure test.

Test condition

- Temperature: 550 °C, 700 °C
- Exposure time: 2–32 days
- Gas: 0.1 vol%H_2 + He
- Flow rate: 20 sccm
- Oxygen concentration: 0.16–0.23 vol%
- Moisture: (in) 6.1 ppm
  (out) 71–375 ppm

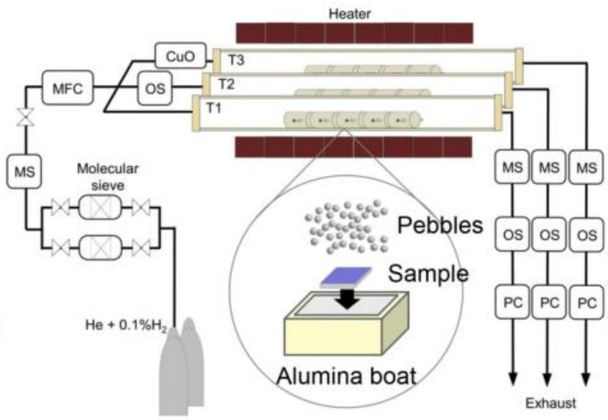

Setup of ceramic breeder pebbles exposure tests.

[7] R. Knitter *et al.*, *J. Nucl. Mater.* 442 (2013) S433–S436.

Experimental details

Characterization

- Surface and cross-sectional observation was performed using a scanning electron microscope with focused ion beam cutting (FIB-SEM).
- Elemental mapping was also available by energy dispersive X-ray spectroscopy (EDX).
  * Li cannot be analyzed by EDX.
- Depth profiles including Li were obtained by X-ray photoelectron spectroscopy (XPS).

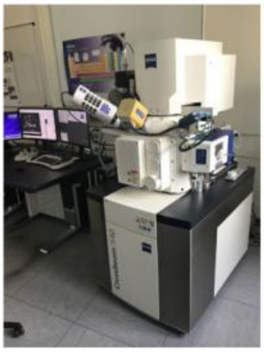

FIB-SEM (Zeiss Crossbeam 540).

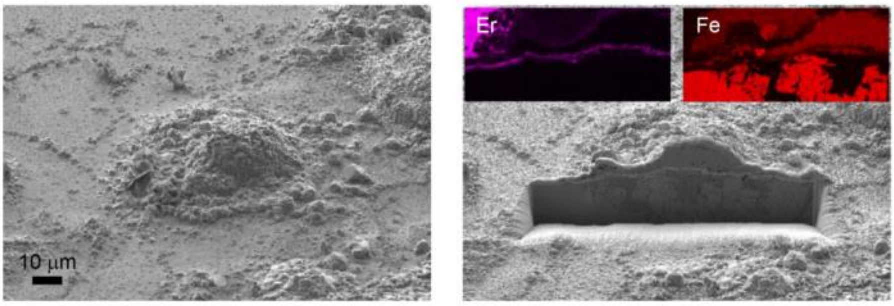

SEM micrographs with elemental mapping of Er_2O_3-coated sample before and after focused ion beam cutting.

Results and discussion Cr_2O_3 layer@550 ºC

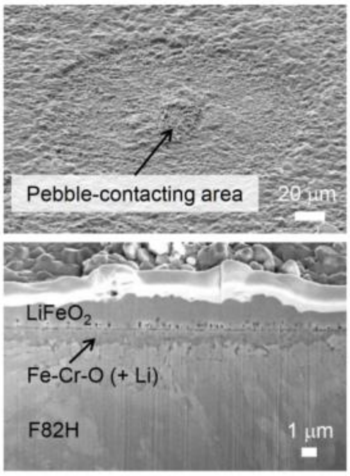

Surface and cross-sectional SEM micrographs of Cr_2O_3-formed F82H exposed to solid breeder pebbles at 550 ºC for 2 days.

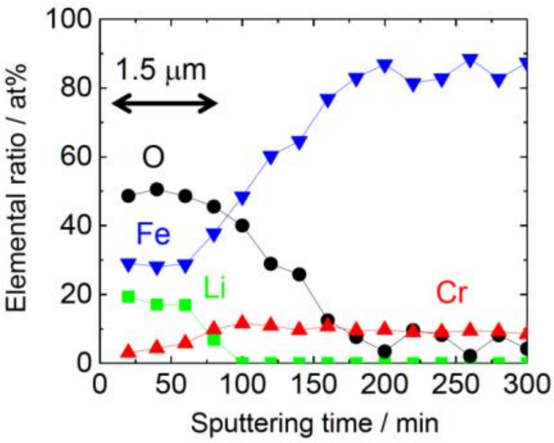

XPS depth profile of Cr_2O_3-formed F82H exposed to solid breeder pebbles at 550 ºC for 2 days.

- After 2-day exposure, a 1.5-μm-thick $LiFeO_2$ layer would form on the Fe-Cr-O (+ Li) layer, and its thickness increased with exposure time.
- $LiFeO_2$ would form at most areas of the sample surface by reaction with Li.

Results and discussion Cr_2O_3 layer@550 °C

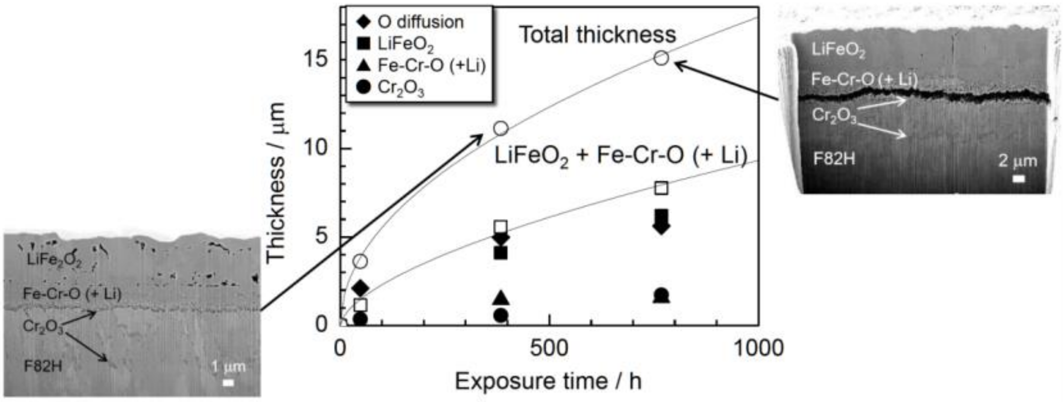

Layer thicknesses of Cr_2O_3-formed F82H after exposure to ceramic pebbles at 550 °C.

- After 32-day exposure, a gap was observed at the Cr_2O_3 layer.
- The fitting curve of "total thickness" as a function of exposure time showed a relationship of $(\text{Thickness}) \propto t^{0.5}$.

→ Diffusion limited regime can be applied.
Apparent diffusivity at 550 °C was estimated to be 8.3×10^{-13} cm^2 s^{-1}.

Results and discussion Cr_2O_3 layer@550 °C

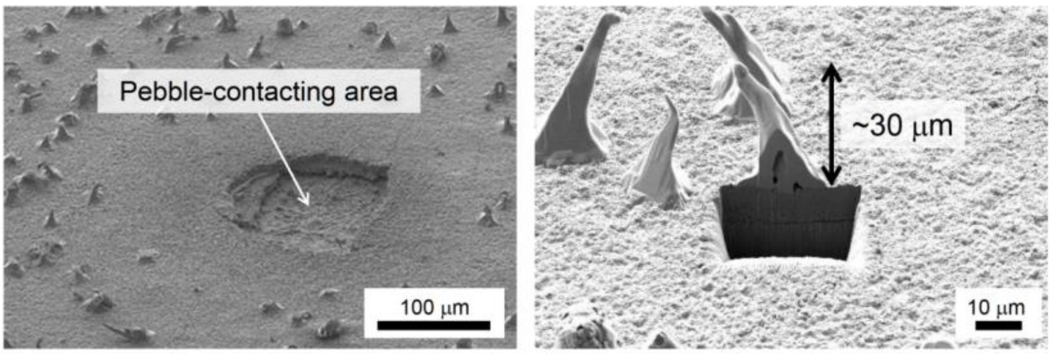

Surface and cross-sectional SEM micrographs of Cr_2O_3-formed F82H exposed to solid breeder pebbles at 550 °C for 32 days.

- After 16/32-day exposure, many pure-Fe projections formed around pebble-contacting areas.
- Cross-sectional observation revealed that the projections grew from the $LiFeO_2$ layer, suggesting reduction of $LiFeO_2$.

e.g. $2LiFeO_2 + 3H_2 \rightarrow 2Fe + 2LiOH + 2H_2O$

- These projections did not form at the pebble-contacting areas.

→ Due to the difference in physical and chemical states.

13/16

Results and discussion Er_2O_3 coating@550 °C

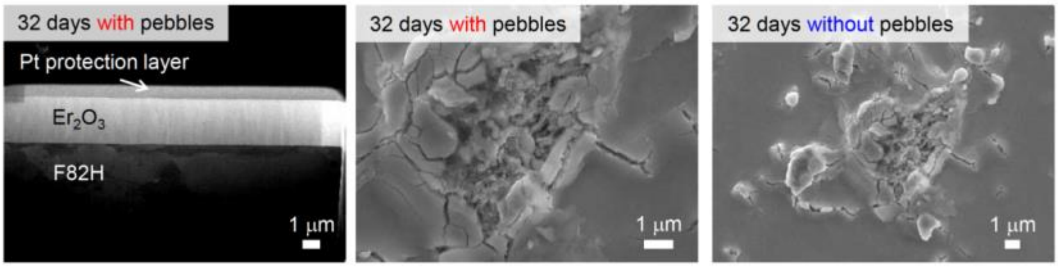

Surface and cross-sectional SEM images of Er_2O_3 coatings after exposure to ceramic pebbles at 550 °C.

Gas-phase method (VAD)

- No change in microstructure after 32-day exposure at 550 °C.

Liquid-phase method (MOD)

- After 16/32-day exposure, the formation of metal Fe at the pebble-contacting points and Fe-Cr-O (+ Li) around the areas with cracks of the Er_2O_3 coating. The cracks formed without pebbles.

→ In terms of compatibility, the thickness of the MOD coatings should be increased, even though the coating shows a high PRF.

14/16

Results and discussion VAD Er_2O_3@700 °C

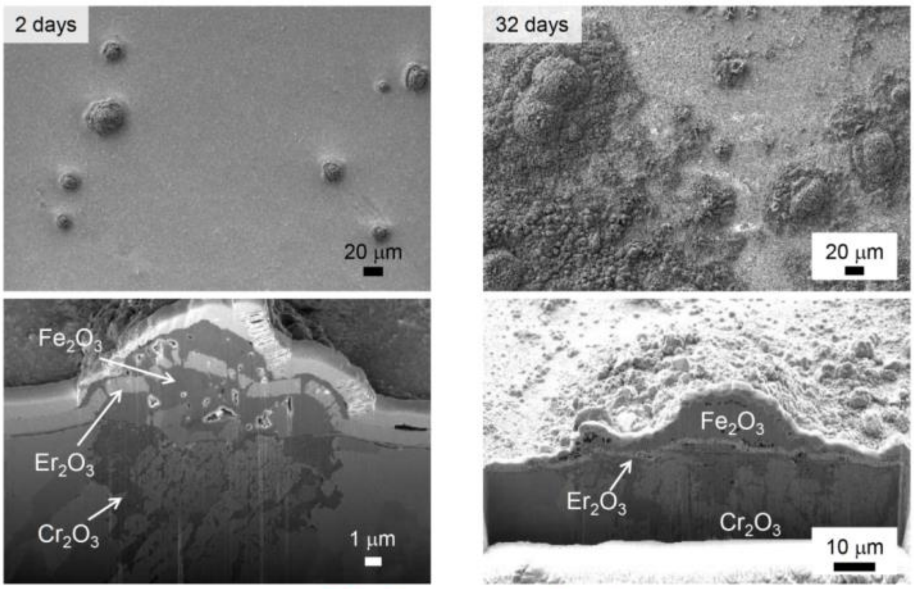

- Er_2O_3 was broken where Fe_2O_3 was prominent, and the area increased with exposure time.

→ Oxygen diffusion to the substrate would be attributed to the break.

Results and discussion MOD Er_2O_3@700 ºC

15/16

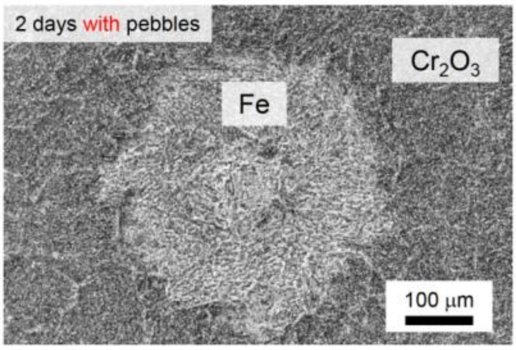

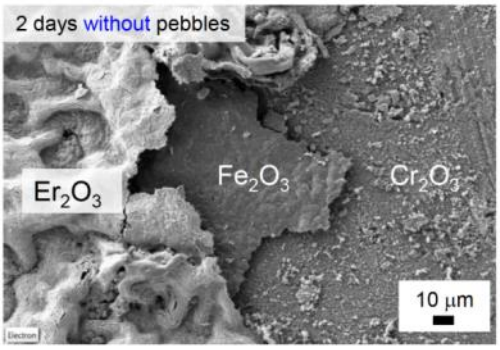

- After 2-day exposure at 700 ºC, the MOD coatings totally disappeared. In addition, reduced metal Fe at pebble-contacting points and Cr_2O_3 around the points were observed.

→ The redox state around the pebbles might be different with temperature.

- After 2-day exposure at the same temperature without pebbles, the coating was largely delaminated with the formation of Fe_2O_3 and Cr_2O_3.

→ Due to the small thickness of the MOD coatings (< 1 μm), oxygen diffused fast to the substrate, resulting in a fast Fe_2O_3 growth.

Summary

16/16

Exposure tests to the solid breeder blanket environment were carried out using ceramic breeder pebbles and TPB coatings.

Cr_2O_3-formed F82H

- The $LiFeO_2$ layer formed after exposure at 550 ºC.
  Characteristic structures formed in and around the pebble-contacting areas, indicating the difference in the physical and chemical states.

Er_2O_3 coatings

- No change in structure was confirmed for the VAD coatings after up to 32-day exposure at 550 ºC, while cracks formed for the MOD coatings. This difference would be due to the coating thickness which changes the formation rate of Fe_2O_3 at the substrate via oxygen diffusion through the coating.
- After exposure at 700 ºC, both coatings were severely damaged by Fe_2O_3 formation. In particular, the MOD coatings totally disappeared after 2-day exposure.
  Optimization of coating thickness and control of oxygen diffusion will be important to enhance compatibility of TPBs.

Impact of a ceramic breeder environment on the fatigue lifetime of EUROFER

Mario Walter, Matthias Kolb, Regina Knitter, Jarir Aktaa

Karlsruhe Institute of Technology, Institute for Applied Materials,
Hermann-von-Helmholtz-Platz 1, 76344 Eggenstein-Leopoldshafen, Germany

In advanced designs of DEMO breeding blankets, structural materials like EUROFER are in direct contact with the pebbles of a ceramic breeder made of lithium orthosilicate. From recent studies it is known, that the breeder specific environment is particularly resulting in both a chemical and morphological change of the surface of structural materials under operation relevant conditions. Especially from a dimensioning point of view, it is important to know to which extend the observed changes will lead to a degradation of mechanical properties. Due to a predominant thermo-mechanical loading of the entire blanket structure under pulsed plasma conditions, in particular the impact on the fatigue lifetime needs to be thoroughly determined. For this purpose, round bar fatigue specimens made from EUROFER97-2 were embedded in pebbles beds of the ceramic breeder material Li_4SiO_4 + 30 mol% Li_2TiO_3. The two materials in unconstrained contact were then exposed to flowing He + 0.1 vol.% H_2 atmosphere at 550°C for 8, 16 and 32 days. Subsequently, the impact of the chemical attack on the fatigue behavior of the RAFM steel was investigated by performing strain-controlled low cycle fatigue (LCF) tests at 550°C.

Within the frame of this talk, the results of the investigations will be presented and based on findings obtained in accompanied microstructural and fractographical studies, the effect of a realistic ceramic breeder environment on the fatigue behaviour of EUROFER will be discussed in detail.

20th CBBI workshop 18. – 20.09.2019, Karlsruhe, KIT/CN

Impact of a ceramic breeder environment on the fatigue lifetime of EUROFER 97

Mario Walter, Jarir Aktaa, Matthias Kolb, Regina Knitter

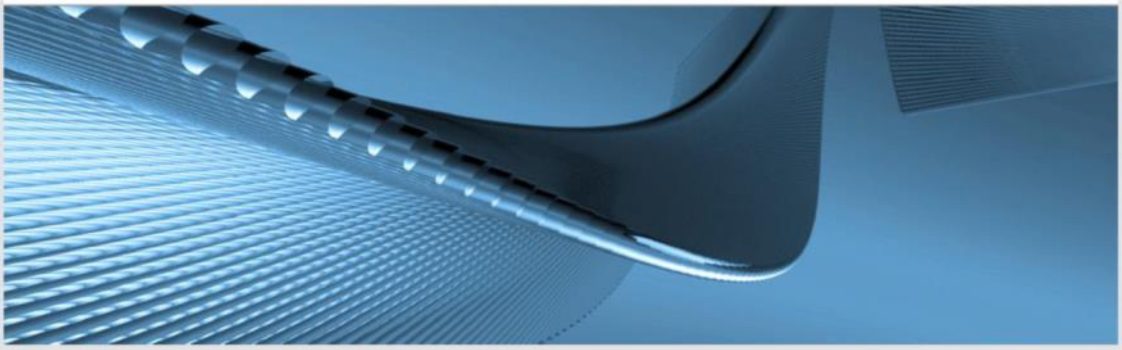

0 | IAM-WBM | Dr. Mario Walter

KIT – Universität des Landes Baden-Württemberg und nationales Forschungszentrum in der Helmholtz-Gemeinschaft

20th CBBI workshop 18. – 20.09.2019, Karlsruhe, KIT/CN

- **motivation**
- **fatigue behaviour of EUROFER 97**
- **sample preparation and test performance**
- **results of fatigue tests**
- **discussion and outlook**

1 | IAM-WBM | Dr. Mario Walter

KIT – Universität des Landes Baden-Württemberg und nationales Forschungszentrum in der Helmholtz-Gemeinschaft

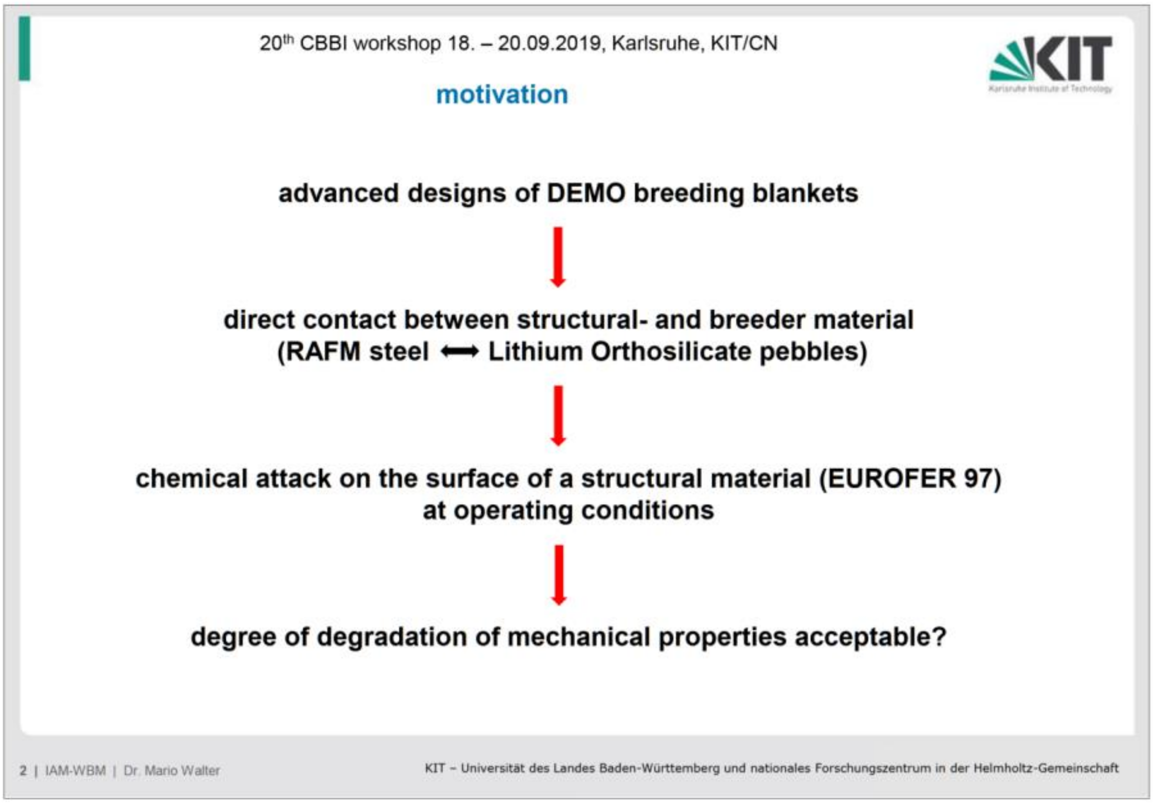
20th CBBI workshop 18. – 20.09.2019, Karlsruhe, KIT/CN
KIT
motivation
advanced designs of DEMO breeding blankets
direct contact between structural- and breeder material
(RAFM steel ⟷ Lithium Orthosilicate pebbles)
chemical attack on the surface of a structural material (EUROFER 97)
at operating conditions
degree of degradation of mechanical properties acceptable?
2 | IAM-WBM | Dr. Mario Walter
KIT – Universität des Landes Baden-Württemberg und nationales Forschungszentrum in der Helmholtz-Gemeinschaft

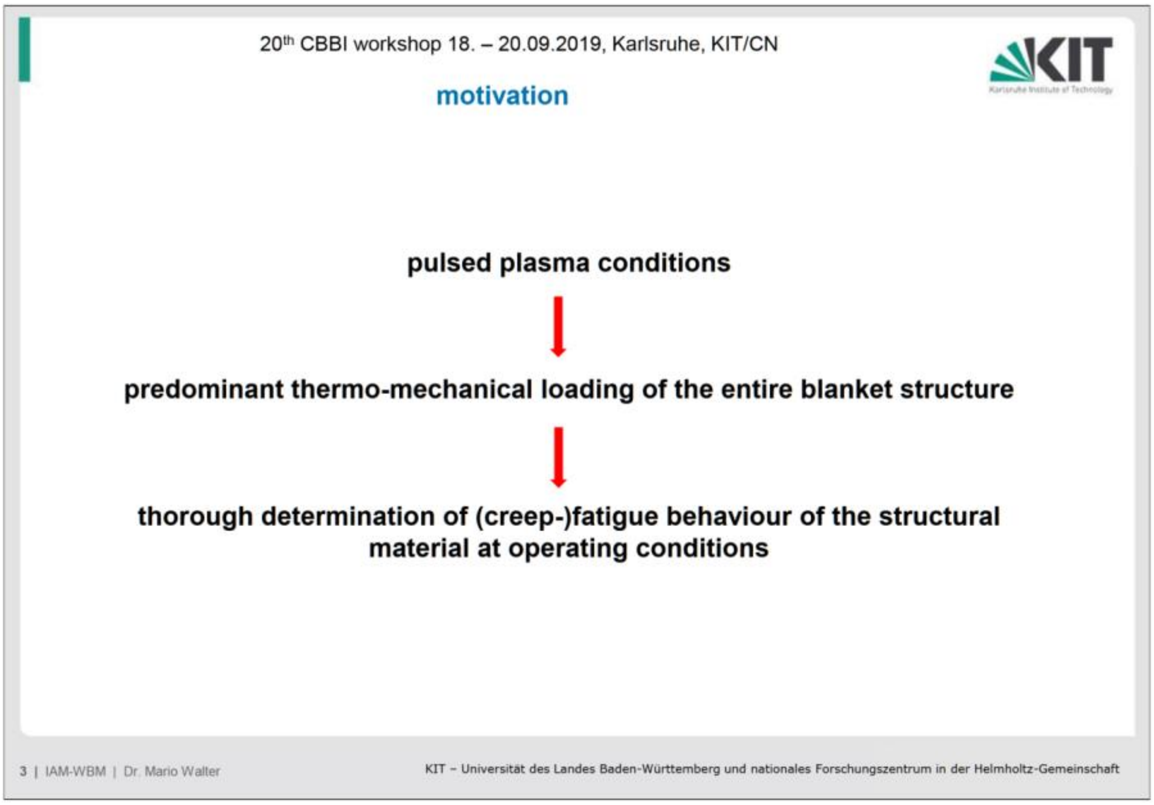
20th CBBI workshop 18. – 20.09.2019, Karlsruhe, KIT/CN
KIT
motivation
pulsed plasma conditions
predominant thermo-mechanical loading of the entire blanket structure
thorough determination of (creep-)fatigue behaviour of the structural
material at operating conditions
3 | IAM-WBM | Dr. Mario Walter
KIT – Universität des Landes Baden-Württemberg und nationales Forschungszentrum in der Helmholtz-Gemeinschaft

20th CBBI workshop 18. – 20.09.2019, Karlsruhe, KIT/CN

fatigue behaviour of EUROFER 97

EUROFER 97 → **X10Cr W Mn V Ta 8.5 1.1 (0.2) (0.15) (0.12)**

heat treatment: **normalized at 960°C for 1.5 h, quenched in oil**
annealed at 750°C for 4 h/air

↓

microstructure:

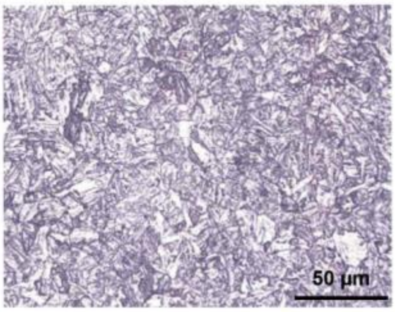

- **ferritic matrix (laths structure)**
- **carbic precipitate: $M_{23}C_6$ (on lath boundaries and former austenite grain boundaries)**

average grain size: 10 µm
$M_{23}C_6$- size between some nm and ca. 5 µm

20th CBBI workshop 18. – 20.09.2019, Karlsruhe, KIT/CN

fatigue behaviour of EUROFER 97

EUROFER 97 – general behaviour under cyclic loading:

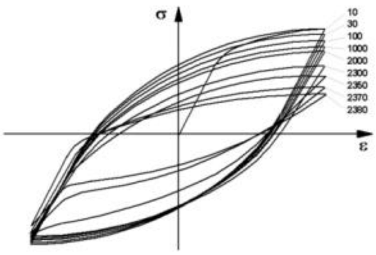

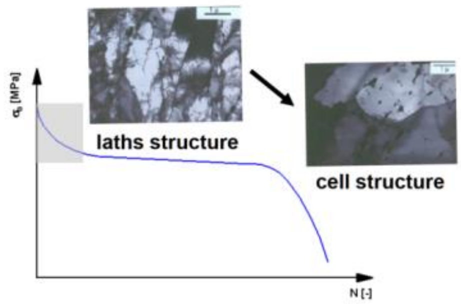

- **reorganisation of existing dislocation structures combined with dislocation annihilations**
- **coarsening/dissolution of precipitate**

→ **dislocation motion activation at lower shear stresses**

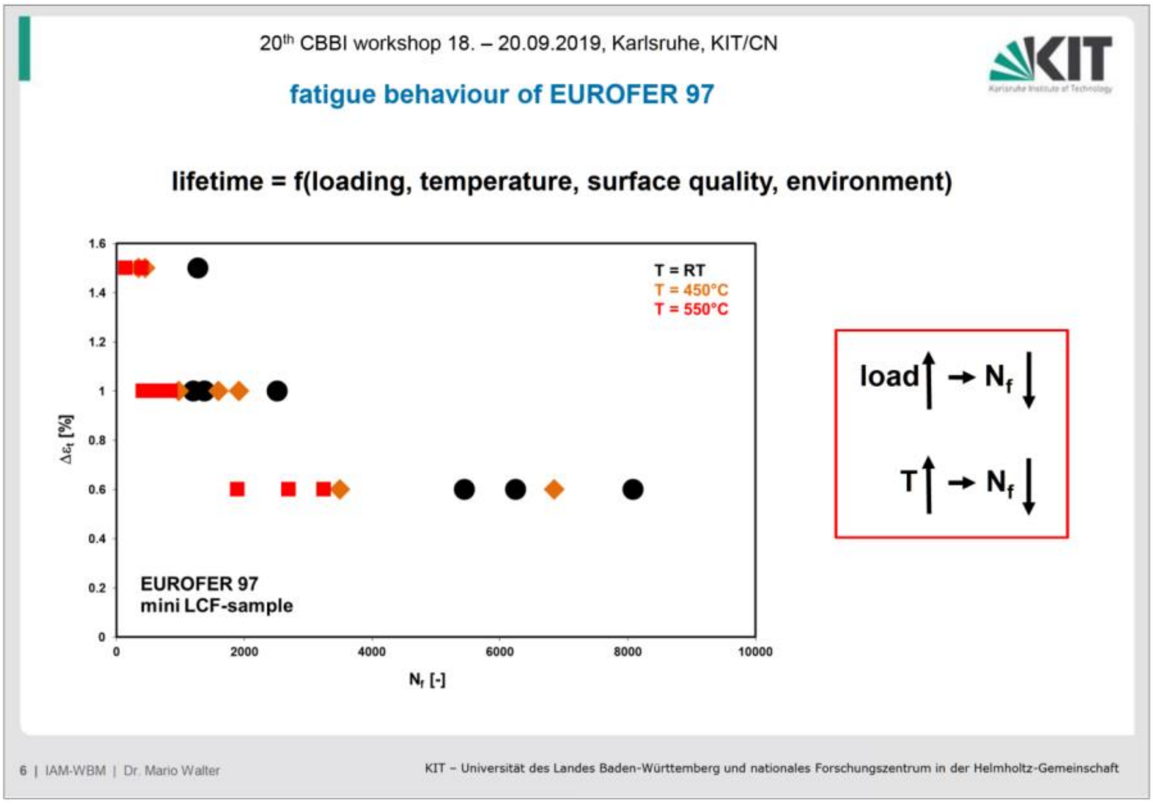
20th CBBI workshop 18. – 20.09.2019, Karlsruhe, KIT/CN
fatigue behaviour of EUROFER 97
lifetime = f(loading, temperature, surface quality, environment)
T = RT
T = 450°C
T = 550°C
EUROFER 97
mini LCF-sample
Δε_t [%]
N_f [-]
load ↑ → N_f ↓
T ↑ → N_f ↓
6 | IAM-WBM | Dr. Mario Walter
KIT – Universität des Landes Baden-Württemberg und nationales Forschungszentrum in der Helmholtz-Gemeinschaft

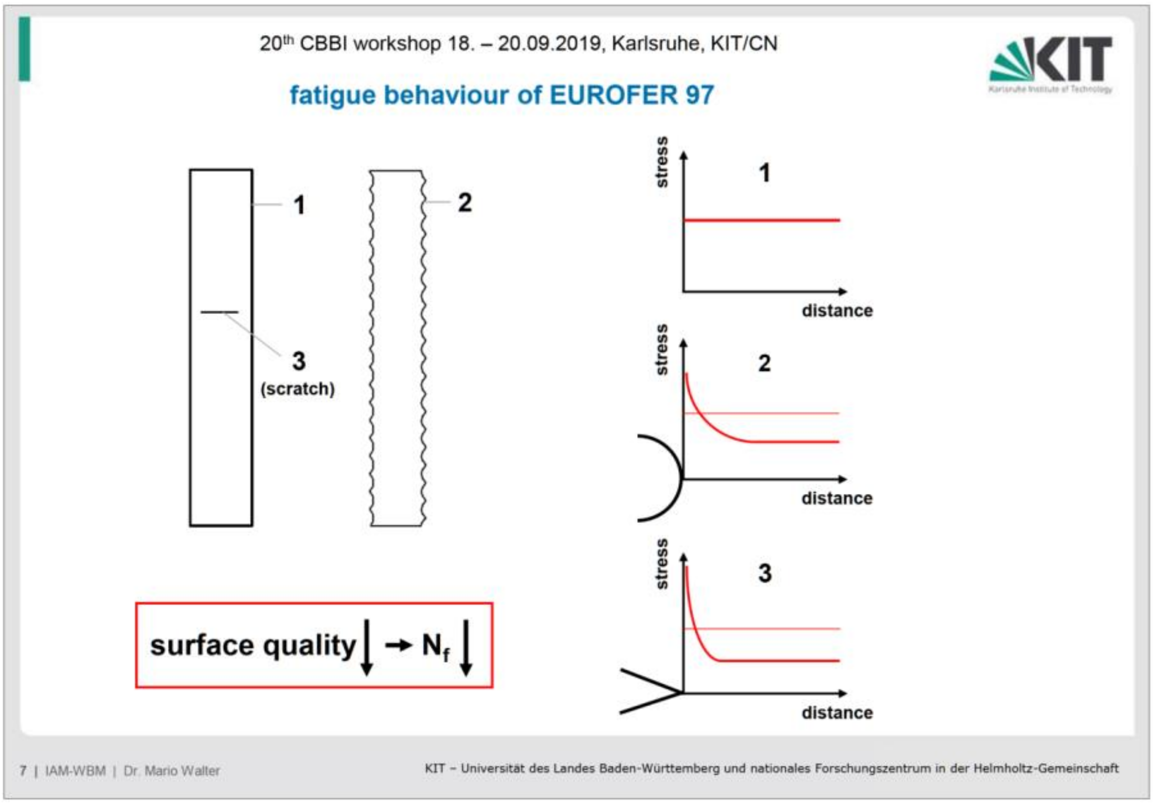
20th CBBI workshop 18. – 20.09.2019, Karlsruhe, KIT/CN
fatigue behaviour of EUROFER 97
1
2
3
(scratch)
stress
distance
surface quality ↓ → N_f ↓
7 | IAM-WBM | Dr. Mario Walter
KIT – Universität des Landes Baden-Württemberg und nationales Forschungszentrum in der Helmholtz-Gemeinschaft

20th CBBI workshop 18. – 20.09.2019, Karlsruhe, KIT/CN

sample preparation

standard LCF sample

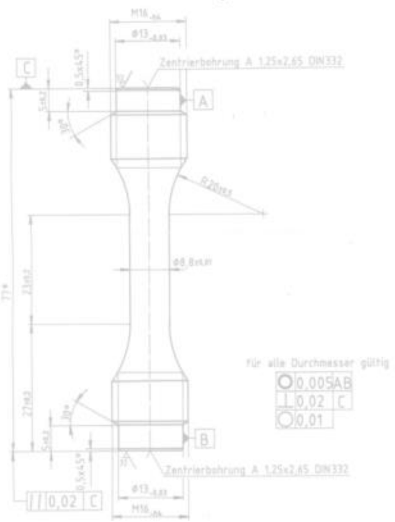

mini LCF sample

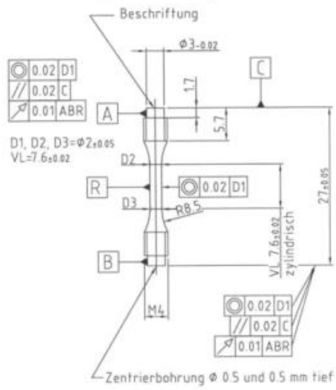

(allowing to increase # of samples related to aging process)

8 | IAM-WBM | Dr. Mario Walter

KIT – Universität des Landes Baden-Württemberg und nationales Forschungszentrum in der Helmholtz-Gemeinschaft

20th CBBI workshop 18. – 20.09.2019, Karlsruhe, KIT/CN

sample preparation

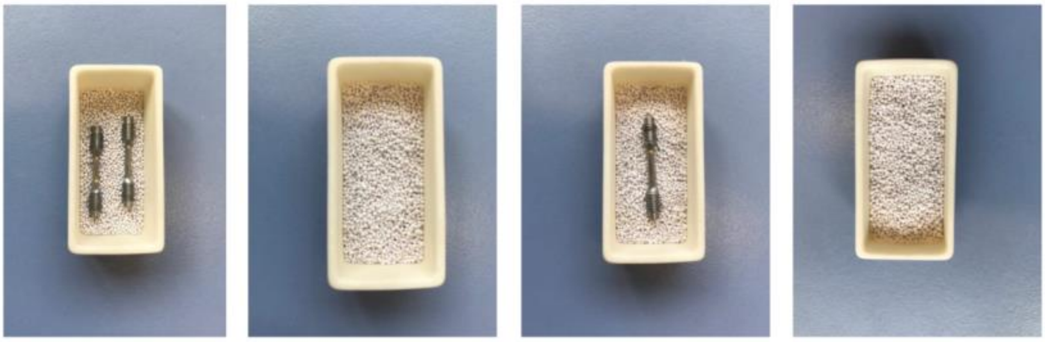

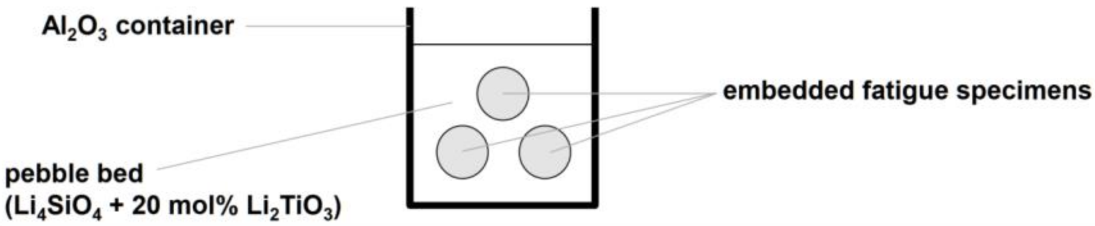

9 | IAM-WBM | Dr. Mario Walter

KIT – Universität des Landes Baden-Württemberg und nationales Forschungszentrum in der Helmholtz-Gemeinschaft

20th CBBI workshop 18. – 20.09.2019, Karlsruhe, KIT/CN

aging

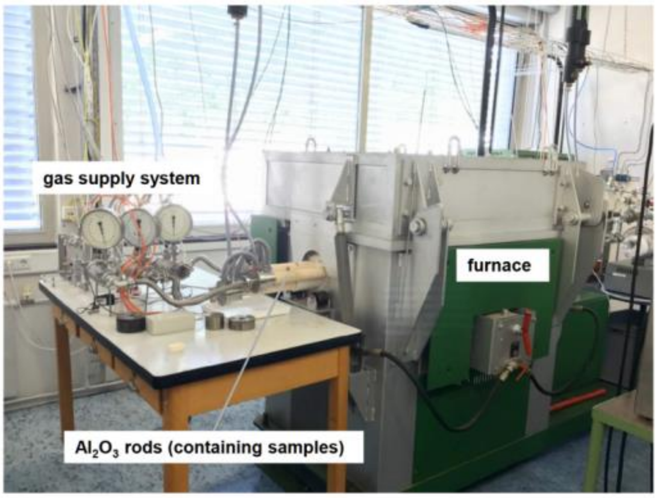

aging at:

T = 550°C
p = 1200 mbar

in:

He + 0.1 vol% H_2 atmosphere
(flow rate = 1200 ml/h)

for:

8, 16, 32 and 64 days

10 | IAM-WBM | Dr. Mario Walter

KIT – Universität des Landes Baden-Württemberg und nationales Forschungszentrum in der Helmholtz-Gemeinschaft

20th CBBI workshop 18. – 20.09.2019, Karlsruhe, KIT/CN

after aging

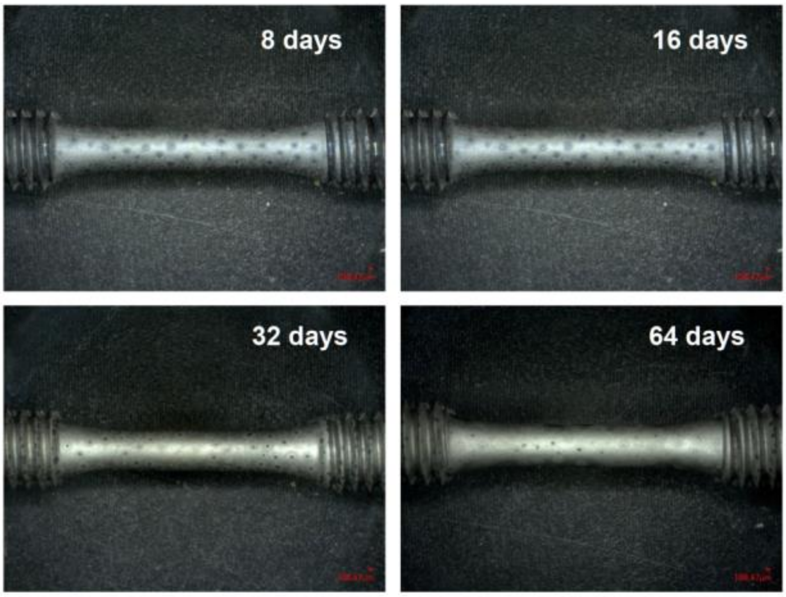

Journal of Nuclear Materials 488 (2017), 169-203

corrosion layer consists of :

Iron Oxide,

different species of Lithium-Iron-Oxide

possibly Lithium-Chrome-Oxide

11 | IAM-WBM | Dr. Mario Walter

KIT – Universität des Landes Baden-Württemberg und nationales Forschungszentrum in der Helmholtz-Gemeinschaft

20th CBBI workshop 18. – 20.09.2019, Karlsruhe, KIT/CN

after aging

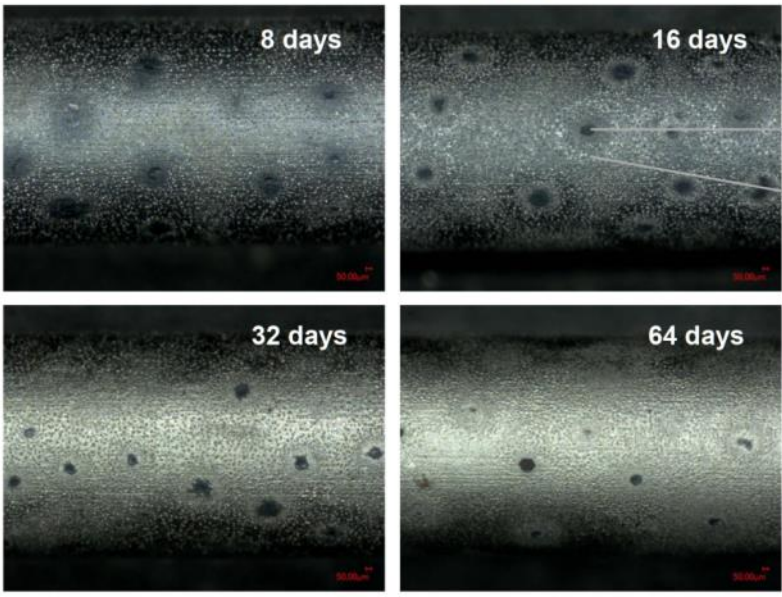

spherical voids

surrounding bubbles/particles

20th CBBI workshop 18. – 20.09.2019, Karlsruhe, KIT/CN

low cycle fatigue testing

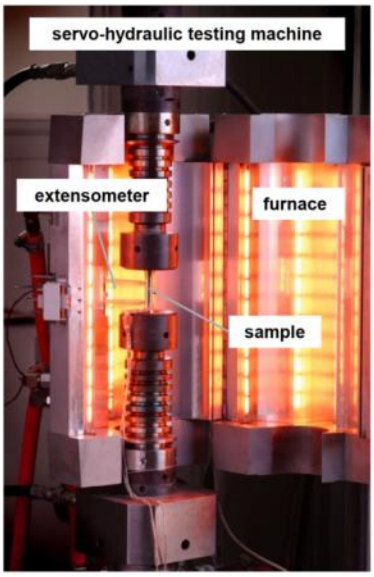

isothermal strain controlled experiments (R = -1)

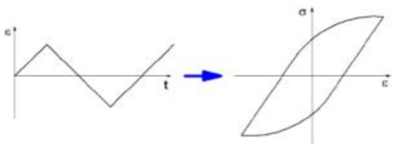

testing at:

T = 550°C in air

with:

stain rate = 3*10^{-3}/s

strain range = 0.6, 1.0 and 1.6 %

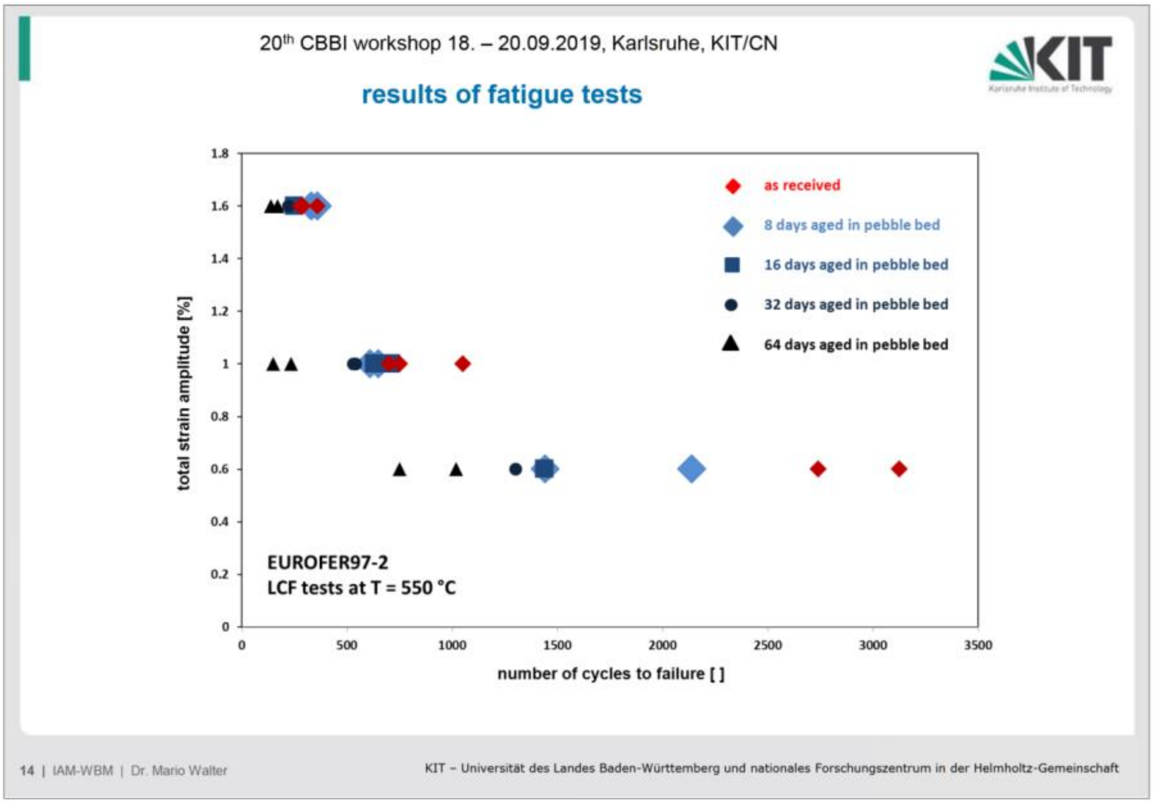
20th CBBI workshop 18. – 20.09.2019, Karlsruhe, KIT/CN
KIT
results of fatigue tests
as received
8 days aged in pebble bed
16 days aged in pebble bed
32 days aged in pebble bed
64 days aged in pebble bed
total strain amplitude [%]
1.8
1.6
1.4
1.2
1
0.8
0.6
0.4
0.2
0
0
500
1000
1500
2000
2500
3000
3500
number of cycles to failure [ ]
EUROFER97-2
LCF tests at T = 550 °C
14 | IAM-WBM | Dr. Mario Walter
KIT – Universität des Landes Baden-Württemberg und nationales Forschungszentrum in der Helmholtz-Gemeinschaft

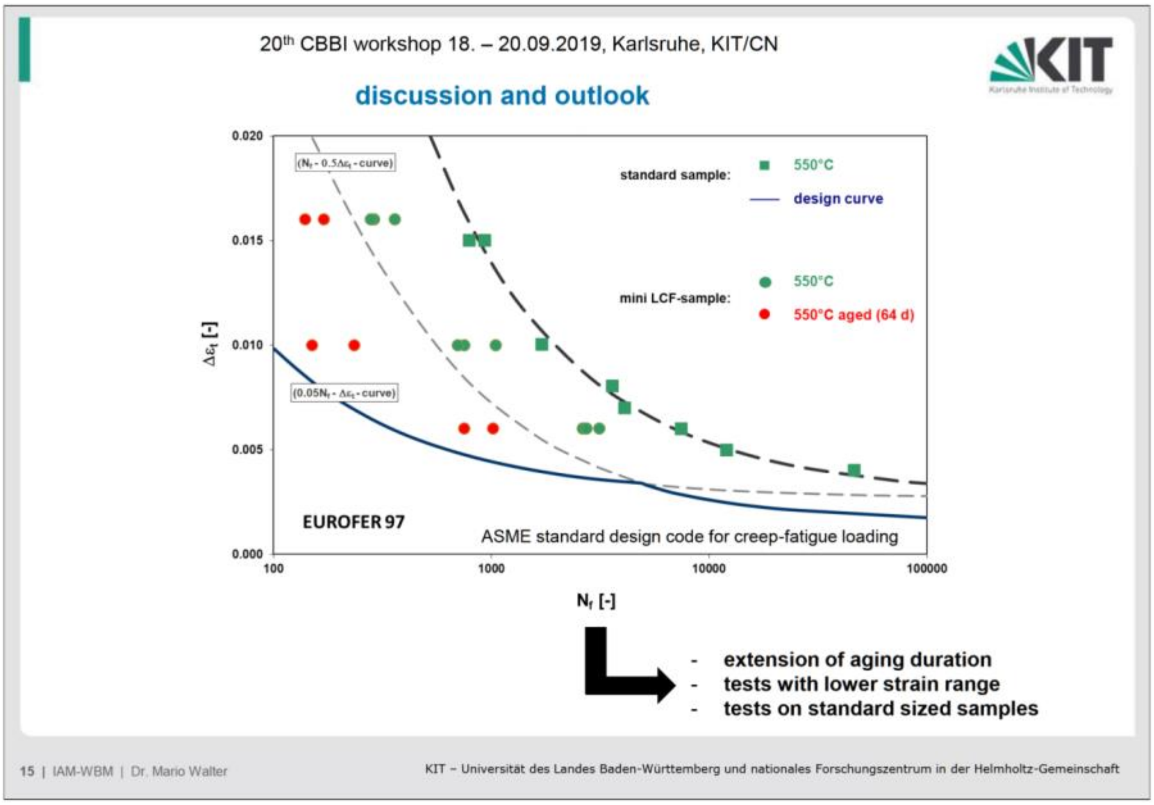
20th CBBI workshop 18. – 20.09.2019, Karlsruhe, KIT/CN
KIT
discussion and outlook
(N_f - 0.5Δε_t - curve)
(0.05N_f - Δε_t - curve)
standard sample:
550°C
design curve
mini LCF-sample:
550°C
550°C aged (64 d)
Δε_t [-]
0.020
0.015
0.010
0.005
0.000
100
1000
10000
100000
N_f [-]
EUROFER 97
ASME standard design code for creep-fatigue loading
- extension of aging duration
- tests with lower strain range
- tests on standard sized samples
15 | IAM-WBM | Dr. Mario Walter
KIT – Universität des Landes Baden-Württemberg und nationales Forschungszentrum in der Helmholtz-Gemeinschaft

20th CBBI workshop 18. – 20.09.2019, Karlsruhe, KIT/CN

discussion and outlook

structural investigations related to:

-type & thickness of corrosion layer
f (aging duration)

-evolution of damage
(interrupted tests)

-hydrogen embrittlement?

development of a protective layer concept!

16 | IAM-WBM | Dr. Mario Walter

KIT – Universität des Landes Baden-Württemberg und nationales Forschungszentrum in der Helmholtz-Gemeinschaft

20th CBBI workshop 18. – 20.09.2019, Karlsruhe, KIT/CN

thank‘s for your attention!

17 | IAM-WBM | Dr. Mario Walter

KIT – Universität des Landes Baden-Württemberg und nationales Forschungszentrum in der Helmholtz-Gemeinschaft

Compatibility between Fusion Reactor Blanket Structural Material F82H and Solid Breeders Lithium Titanate and Lithium Oxide

Keiji Oishi, Shinichi Inoue, Takayuki Terai

School of Engineering. The University of Tokyo, Yayoi, Tokyo, 113-0032, Japan

In the ITER-TBM and the DEMO reactor of Japan, the reduced activation ferritic steel F82H (Fe-8Cr-2W-0.2V-0.04Ta-0.1C) is planned to be used as the blanket structural material while Li_2TiO_3 has been considered as one of the most promising candidate materials among solid breeder materials from the view point of chemical stability, and Li-excess Li_2TiO_3 is currently regarded as an advanced tritium breeder material. The temperature of the interface between the structural material and the solid breeder material is designed from 300 C to 500 C, and the solid breeder material is planned to be used in the blanket for two years. However, it has been pointed out that the Li_2O component vaporizes from the high temperature region of Li_2TiO_3 pebble bed to be deposited on the low temperature piping wall. Therefore, we investigated the compatibility between F82H and them for the safety evaluation of the solid breeder blanket.

Li_2O, Li_2TiO_3 and Li-excess Li_2TiO_3 (Li/Ti ratio = 2.27) pellets (10 mm in diameter and 4 mm in thickness) were prepared by sintering the starting powders at 800 C under Ar gas atmosphere. The compatibility experiments were carried out by keeping F82H specimens (6 mm x 6 mm x 1 mm) in contact with lithium oxide specimens or lithium meta-titanate specimens under He + 0.1%H_2 sweep gas flow at 400 C, 600 C and 800 C for 100 to 4000 hours. After each experiment, the cross section of the reaction zone on the F82H side was observed by SEM/EDX. In addition, the apparent O diffusion coefficients were obtained from the data on different time, and the activation energies were calculated from the results at different temperatures in order to estimate the corrosion depth of F82H in the actual temperature condition. As a result, it was shown that the diffusion and corrosion depth and the reaction amount were much smaller for F82H in contact with Li_2TiO_3 than with Li_2O and Li-excess Li_2TiO_3. This can be explained by the fact that the chemical potentials of Li and O in Li_2O and Li-excess Li_2TiO_3 are much larger than those in Li_2TiO_3. Based on the results, the corrosion depth of F82H with Li_2O and Li-excess Li_2TiO_3 was estimated to be 75~110 µm and 9 µm after the operation at 400 C for two years, respectively.

Compatibility between Fusion Reactor Blanket Structural Material F82H and Solid Breeders Lithium Titanate and Lithium Oxide

Keiji Oishi, Shinichi Inoue, Takayuki Terai (U Tokyo)

1.Background 1

○Schematic of the blanket

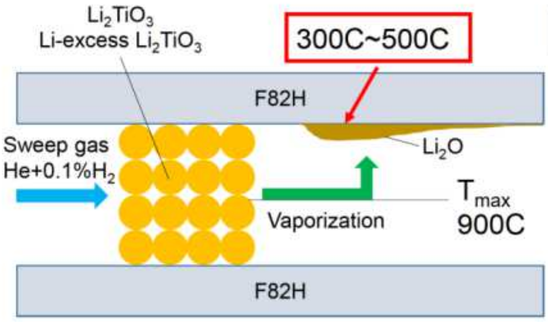

F82H-BA12 composition (wt.%)

C	Cr	W	Mn	V	Ta	B
0.99	7.88	1.78	0.45	0.19	0.093	0.004
Si	P	S	N	O	Fe	
0.1	0.11	<0.0005	0.0098	0.0012	Bal.	

Background

- The temperature of interface between structural material and breeder is designed 300C to 500C.
- Pebble beds contact with structural material directly.
- Li_2O vaporized from pebble bed deposits on the low temperature piping wall.

2.Objectives and experimental condition 2

○Objectives and experimental condition

objectives

・Clarify the compatibility between F82H and Li_2TiO_3, Li-excess Li_2TiO_3 and Li_2O.

・Estimate the corrosion depth in actual blanket condition.

Experimental condition

Temperature (C)	400	600	800
Li_2TiO_3	×	○	○
Li-excess Li_2TiO_3	○	○	○
Li_2O	○	○	○
heating period (h)	500～4000	100～500	100～500

3.Method 3

○Experimental method


Sample

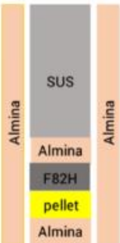

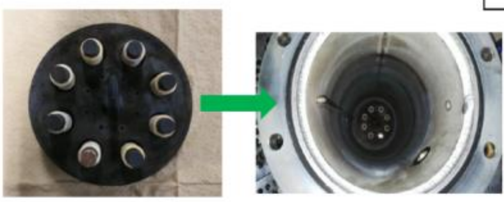
Set samples into electric furnace

1.Preparation of F82H
- ◆ Cut F82H (1mm×6mm×6mm)
- ◆ Polish the surface of F82H

2.Heat treatment of Li_2O powder
- ◆ 400C・24h in Ar gas

3.Sintering
- ◆ Compression molding of powder with mold
- ◆ 800C・5h in Ar gas (Li_2TiO_3,Li-excess Li_2TiO_3)

4.Set samples into electric furnace
- ◆After replacing He + 0.1% H_2 gas, raise the temperature

5. Sample removal
- ◆Remove the sample set when the target time is reached

4.Result 4

○Comparison between Li_2TiO_3 and Li-excess Li_2TiO_3

600C × 200h

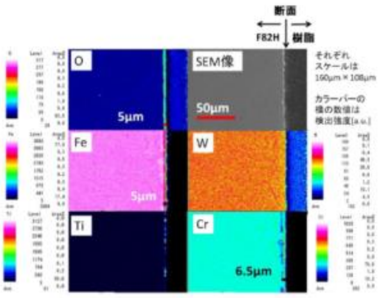

F82H contacting with Li_2TiO_3

Cr migrated to the surface of F82H.
Diffusion of O was very small.

600C × 200h

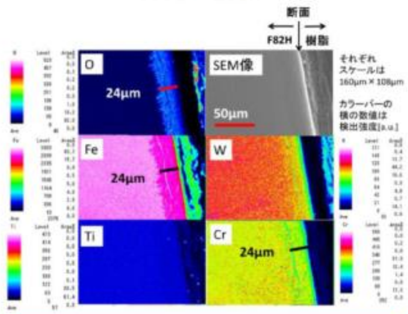

F82H contacting with Li-excess Li_2TiO_3
(Li/Ti = 2.27)

O diffused very deep area with Fe concentration decreasing.

4.Result 5

○Li_2O-SEM/EDX(600C-300h)

Corrosion depth

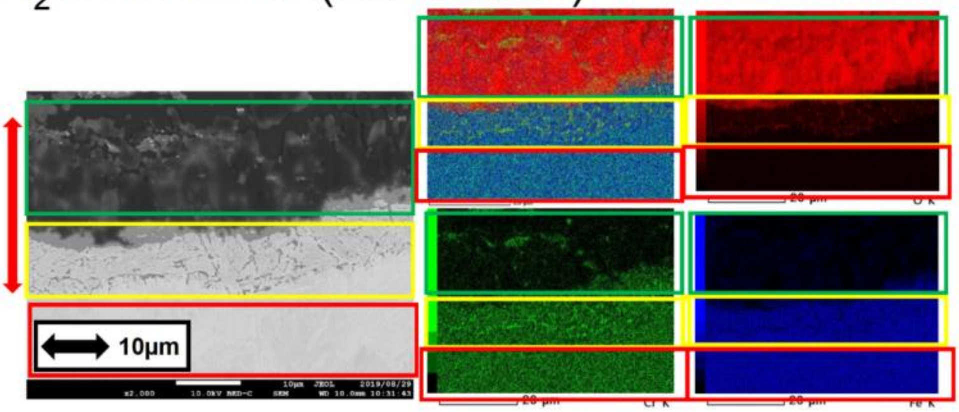

- Green region→Oxidized layer was formed.
- Yellow region→Both Cr and O were observed.
- Red region→There was no O.

4.Result 6

○Li_2O-SEM/EDX(800C-500h)

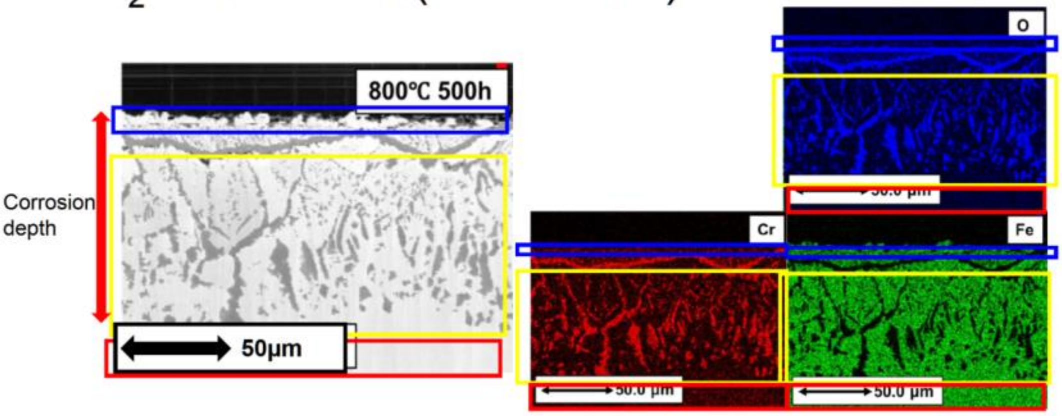

・Blue region→Both Fe and O were observed.
・Yellow region→Both Cr and O were observed and Fe was expelled.
・Red region→There was no O.

4.Result 7

○Measurement by EBSD (under 50μm from surface)

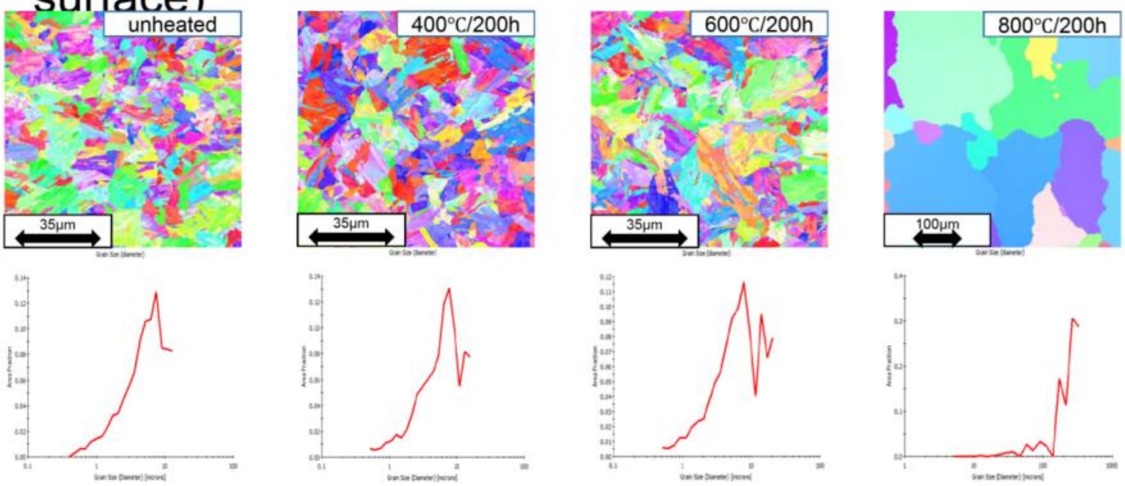

5.Discussion 8

○How to estimate corrosion depth in blanket

Step.1

- Apparent diffusion coefficient of O at 400C
- Apparent diffusion coefficient of O at 600C
- Apparent diffusion coefficient of O at 800C

↓

Step.2

The activation energy EA is calculated according to the Arrhenius plot of the diffusion coefficient obtained under different temperature conditions.

↓

Step.3

Estimate corrosion depth in actual blanket condition.

5.Discussion 9

Apparent diffusion coefficient of O (F82H contacting with Li-excess-Li_2TiO_3)

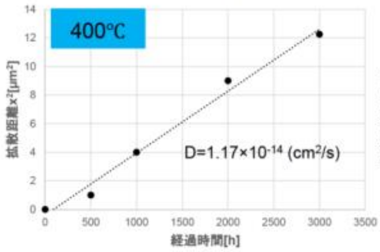

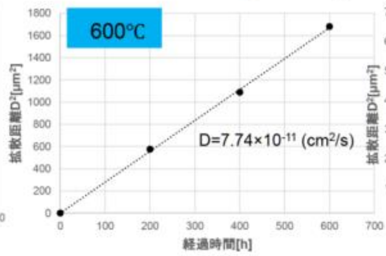

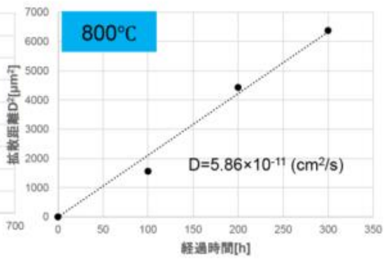

Based on diffusion rate, diffusion coefficient D is expressed as below.

$$D = \frac{x^2}{t}$$

D・・・Diffusion coefficient of O(cm^2/s)
x・・・Average diffusion depth of O (cm)
t・・・Heating period(s)

→

Diffusion coefficient of O at 400C is $D=1.17\times10^{-14}$ (cm^2/s)

When the temperature of interface between F82H and Li_2O is 400C, corrosion depth is estimated to be 9μm after two years.

5.Discussion

10

Apparent diffusion coefficient of O (F82H contacting with Li_2O)

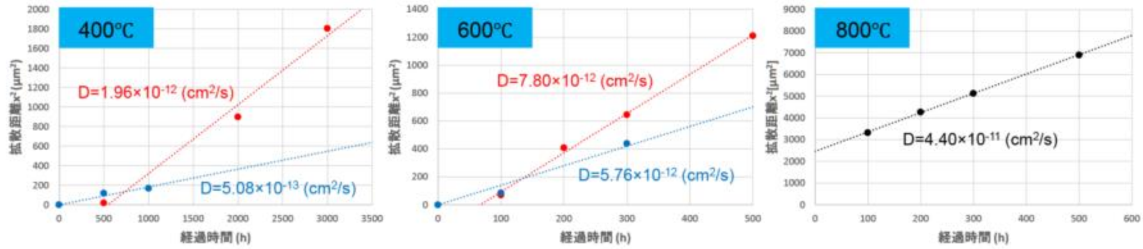

Based on diffusion rate, diffusion coefficient D is expressed as below.

$$D = \frac{x^2}{t}$$

D・・・Diffusion coefficient of O(cm^2/s)
x・・・Average diffusion depth of O (cm)
t・・・Heating period(s)

Diffusion coefficient of O at 400C is D=0.508~1.96×10^{-12} (cm^2/s)
When the temperature of interface between F82H and Li_2O is 400C, corrosion depth is estimated to be 112μm after two years.

5.Discussion

11

○Comparison of apparent diffusion coefficient

Apparent diffusion coefficient in F82H (cm^2/s)			
Temperature/Breeder	Li_2TiO_3	Li-excess Li_2TiO_3	Li_2O
400C		1.17×10^{-14}	1.96×10^{-12}
600C	5.63×10^{-13}	7.74×10^{-12}	7.80×10^{-12}
800C	9.0×10^{-12}	5.86×10^{-11}	4.40×10^{-11}

- ✓ At 400C, in terms of diffusion coefficient, there is a quite difference between Li-excess Li_2TiO_3 and Li_2O.
- ✓ As temperature increases, each diffusion coefficient becomes closer.

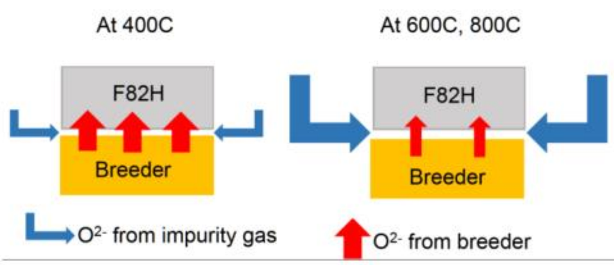

This result implies that impurity gas which includes oxygen affect diffusion coefficient effectively at high temperature.

5.Discussion

12

Step.2:Arrhenius plot

$$D = D_0 e^{-\frac{E_A}{kT}}$$

$$lnD = -\frac{E_A}{k} \times \frac{1}{T} + lnD_0$$

D・・・Diffusion coefficient of O(cm^2/s)
D_0・・・Coefficient cm^2/s)
k・・・Boltzmann constant8.617×10^{-5} (eV/K)
T・・・Temperature (K)
E_A・・・Activation energy (eV)

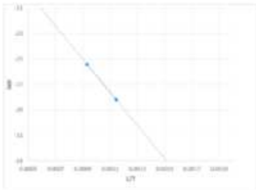

Li_2TiO_3

D_0= 1.66×10^{-6} (cm^2/s)

EA = 1.12 (eV)

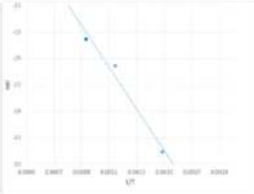

Li-excess Li_2TiO_3

D_0=2.26×10^{-4} (cm^2/s)

EA = 1.36 (eV)

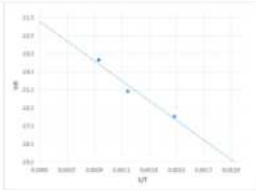

Li_2O

D_0=5.83×10^{-9} (cm^2/s)

EA = 0.472 (eV)

5.Discussion

13

○Corrosion depth in the actual blanket condition

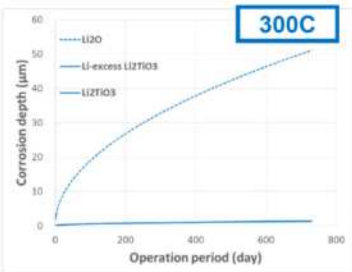

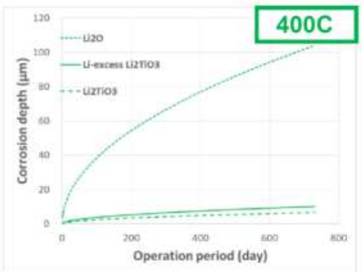

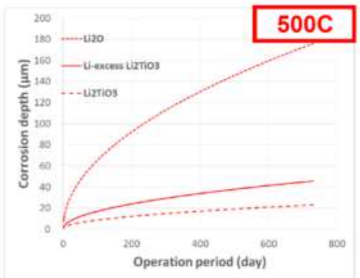

300C	Li_2TiO_3	Li-excess Li_2TiO_3	Li_2O
D (cm^2/s)	2.38×10^{-16}	2.71×10^{-16}	4.15×10^{-13}
Corrosion depth after two years (μm)	1.23	1.31	51.1

400C	Li_2TiO_3	Li-excess Li_2TiO_3	Li_2O
D (cm^2/s)	6.91×10^{-15}	1.60×10^{-14}	1.71×10^{-12}
Corrosion depth after two years (μm)	6.60	10.1	104

500C	Li_2TiO_3	Li-excess Li_2TiO_3	Li_2O
D (cm^2/s)	8.39×10^{-14}	3.29×10^{-13}	4.91×10^{-12}
Corrosion depth after two years (μm)	23.0	45.6	176

6.Conclusion

14

○Conclusion

F82H contacting with Li-excess Li_2TiO_3

✓Diffusion distance of O is large compared with F82H contacting Li_2TiO_3

✓Diffusion coefficient of O at 400C is much low compared with that at 600C (800C).

✓At 400C, the corrosion depth after two years is about 10μm.

F82H contacting with Li_2O

✓The diffusion coefficient is large even if the temperature is low.

(Corrosion depth of Li_2O at 300C > Corrosion depth of Li-excess Li_2TiO_3 at 500C)

✓At 400C, the corrosion depth is more than 100μm.

→ It is equivalent to 10% of the thickness of blanket structural material.

15

Thank you for your attention

Hydrogen isotope permeability of reduced activation ferritic-martensitic steel CLF-1 by Li_4SiO_4

Long Wang, Yongjin Feng, Baoping Gong, Hao Cheng, Xiaoyu Wang, Zhihao Hong, Kaiming Feng

Southwestern Institute of Physics, Chengdu 610225, P.R. China

Tritium permeation through structural materials is a significant issue for fusion demonstration (DEMO) reactor blankets in terms of fuel cycle efficiency and radiological safety. Reduced activation ferritic (RAFM) steel CLF-1 is a prime candidate for the China's CFETR blanket structural material, facing high permeability of hydrogen isotopes at reactor operational temperature. To confine tritium as much as possible in the reactor, surface modification of the steels including surface oxidation and fabrication of tritium permeation barrier (TPB) attracts much attention.

In the helium cooled pebble bed (HCPB) concept, ternary oxides of Li_4SiO_4 are promising candidates for ceramic breeders. They are packed in the blanket for tritium production by nuclear transmutation of Li and used for years of operational period, contacting with structural material at a high temperature of 673-773K. In this case, oxide corrosion layers tend to form on RAFM steel and gradually grow with time. Even an oxide double layer, Fe-rich outer and Cr-rich inner layer, was reportedly observed by compatibility studies between EUROFER and Li_4SiO_4 with addition of 20 mol% Li_2TiO_3. Based on current TPB researches, nano-structured or multilayered layers are beneficial for improving the permeation reduction factor (PRF). However, the effects of these oxide layer on hydrogen isotope permeability of RAFM steels is still unknown at present.

Concerning the existing interface between Li_4SiO_4 ceramic pebbles and RAFM steel CLF-1 D-T fusion reactor in China, the possibility to decrease the hydrogen isotope permeability of RAFM steel by forming an controllable oxide layer during evolution of the interface was evaluated in this study. By adopting a novel dynamic pileup-pellets method combing with static powder embedding experiments, we firstly get the evolution mechanism and deep elements diffusion law at lithium ceramics/RAFM steel CLF-1 interfaces scientifically. It finds that the $LiFe_5O_8$ was formed after statically packed in Li_4SiO_4 powder at 973K for two weeks. The thickness increased with the increase of heating periods. Adding an extra mechanical force of 10~20N, the rate of oxide layer formation was accelerated. Through analyzing and characterizing the hydrogen isotope permeation results of the special corroded RAFM samples, an internal link between hydrogen isotope permeation behavior and evolution mechanism at lithium ceramics / RAFM steel CLF-1 interfaces was established.

核工业西南物理研究院
中核集团 Southwestern Institute of Physics
CNNC

CBBI-20

Hydrogen isotope permeability of reduced activation ferritic-martensitic steel CLF-1 by Li_4SiO_4

Southwestern Institute of Physics

Long Wang, Yongjin Feng, Baoping Gong

E-mail: wanglong@swip.ac.cn
TEL: +86 18202894472

18/09/2019

SWIP Southwestern Institute of Physics

核工业西南物理研究院
中核集团 Southwestern Institute of Physics
CNNC

SWIP Southwestern Institute of Physics


核工业西南物理研究院
中核集团 CNNC Southwestern Institute of Physics
1.Brief introduction to SWIP
2.Background
3.Experiments and results
4.Conclusions
5.Future Plan
SWIP Southwestern Institute of Physics

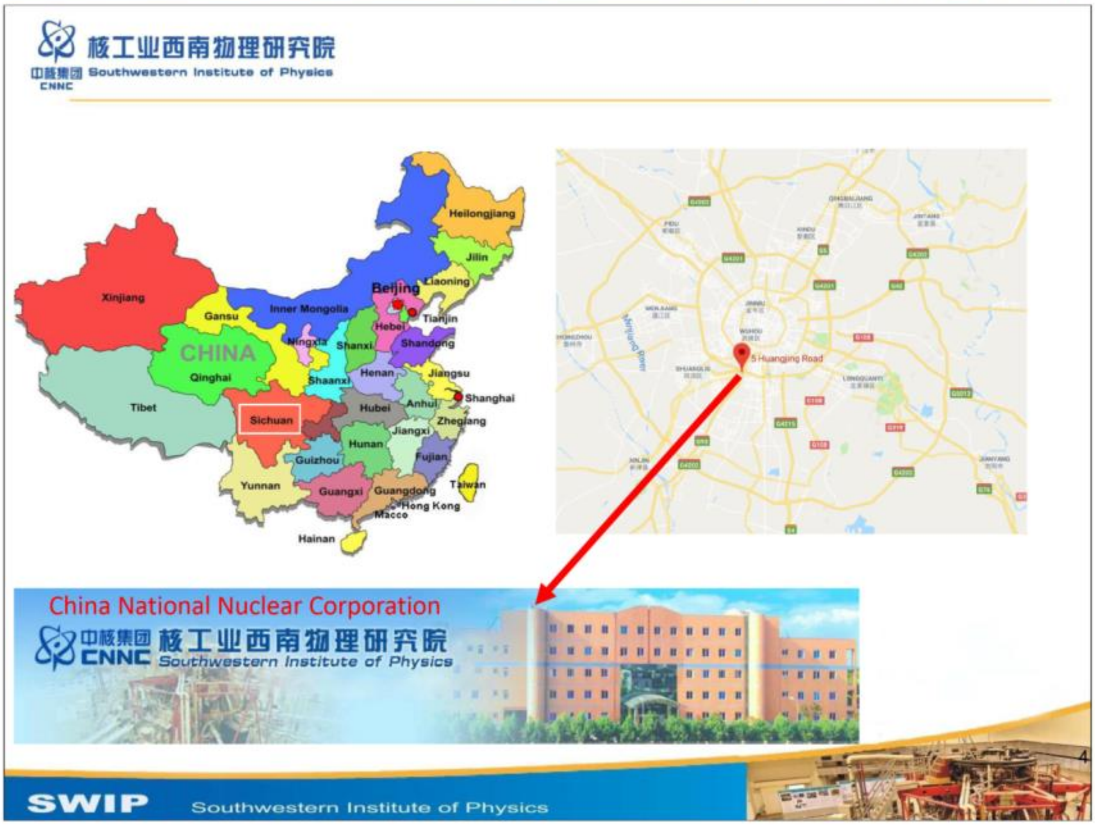
核工业西南物理研究院
中核集团 CNNC Southwestern Institute of Physics
CHINA
Heilongjiang
Jilin
Liaoning
Beijing
Tianjin
Hebei
Inner Mongolia
Xinjiang
Gansu
Ningxia
Shanxi
Shandong
Qinghai
Shaanxi
Henan
Jiangsu
Shanghai
Tibet
Sichuan
Hubei
Anhui
Zhejiang
Jiangxi
Hunan
Guizhou
Fujian
Yunnan
Guangxi
Guangdong
Taiwan
Hong Kong
Macco
Hainan
5 Huanqing Road
China National Nuclear Corporation
中核集团 CNNC 核工业西南物理研究院 Southwestern Institute of Physics
4
SWIP Southwestern Institute of Physics

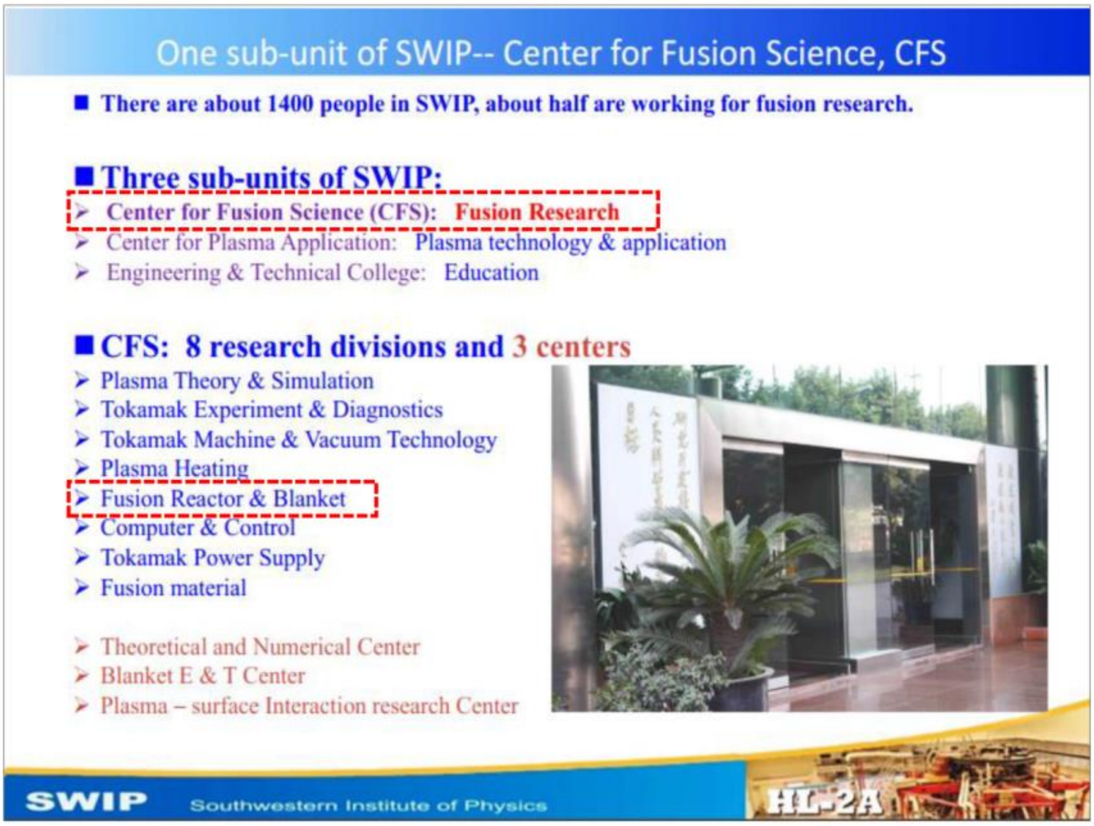
One sub-unit of SWIP-- Center for Fusion Science, CFS
There are about 1400 people in SWIP, about half are working for fusion research.
Three sub-units of SWIP:
Center for Fusion Science (CFS): Fusion Research
Center for Plasma Application: Plasma technology & application
Engineering & Technical College: Education
CFS: 8 research divisions and 3 centers
Plasma Theory & Simulation
Tokamak Experiment & Diagnostics
Tokamak Machine & Vacuum Technology
Plasma Heating
Fusion Reactor & Blanket
Computer & Control
Tokamak Power Supply
Fusion material
Theoretical and Numerical Center
Blanket E & T Center
Plasma – surface Interaction research Center
SWIP Southwestern Institute of Physics
HL-2A


核工业西南物理研究院
Southwestern Institute of Physics
Our Team
Fusion reactor design group, Center for Fusion Science, SWIP
Functional materials
HCCB TBM
HCCB TES Sub-system
Li_4SiO_4 Pebble
Be Pebble
CLF-1 steel
6
SWIP Southwestern Institute of Physics

核工业西南物理研究院
中核集团 CNNC Southwestern Institute of Physics

1.Brief introduction to SWIP

2.Background

3.Experiments and results

4.Conclusions

5.Future Plan

SWIP Southwestern Institute of Physics

核工业西南物理研究院
中核集团 CNNC Southwestern Institute of Physics

Background

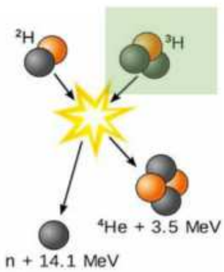

1GW fusion reactor, a tritium refuelling rate of at least 184 g/day[1]

Chinese Fusion Engineering Test Reactor, 50–200 MW, tritium consumption rate reaches over 30 g/d[2] .

The world's entire civil tritium inventory (~22 kg)

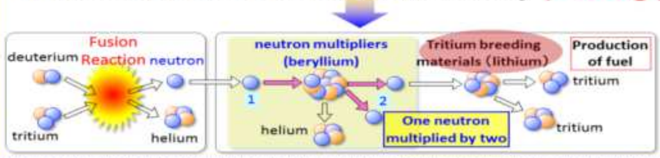

Tritium permeation

Radiological hazard
Tritium contaminated wastes
High tritium concentrations in operation areas
Hydrogen embrittlement

SWIP Southwestern Institute of Physics

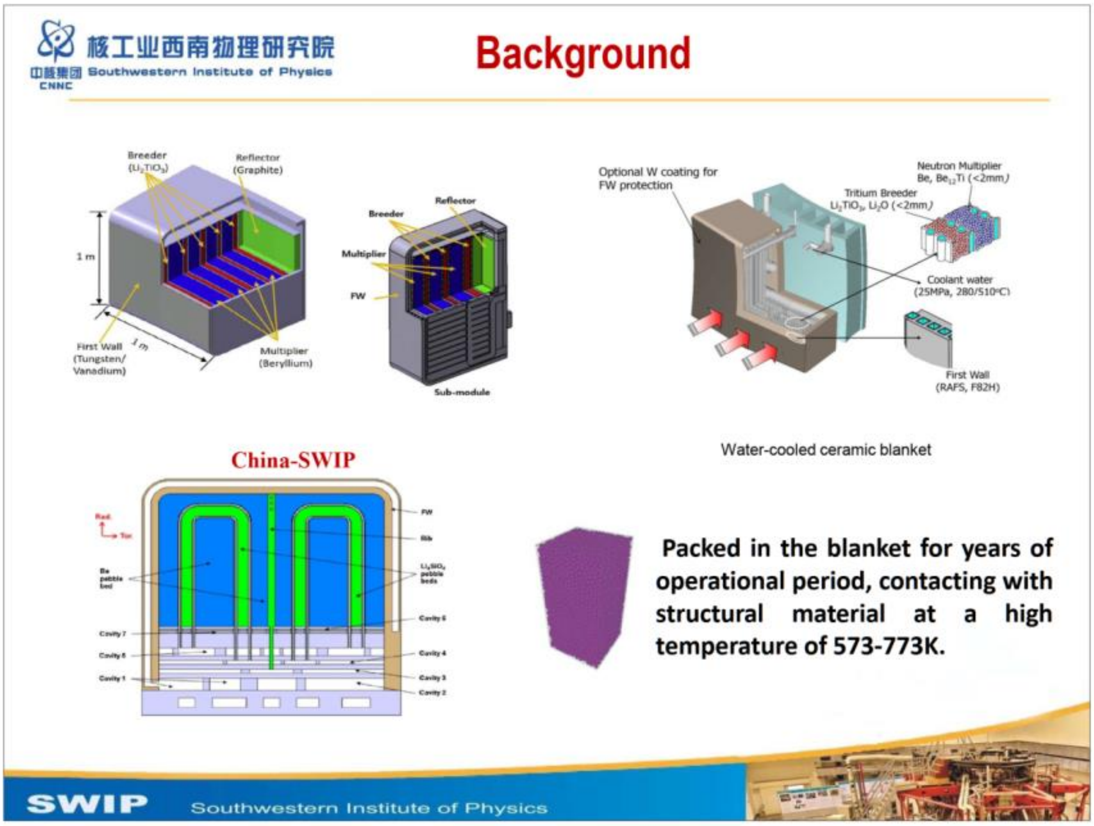
核工业西南物理研究院
Southwestern Institute of Physics
Background
Breeder
Reflector (Graphite)
1 m
First Wall (Tungsten/ Vanadium)
Multiplier (Beryllium)
Reflector
Breeder
Multiplier
FW
Sub-module
Optional W coating for FW protection
Neutron Multiplier
Tritium Breeder
Coolant water
First Wall (RAFS, F82H)
Water-cooled ceramic blanket
China-SWIP
Packed in the blanket for years of operational period, contacting with structural material at a high temperature of 573-773K.
SWIP Southwestern Institute of Physics

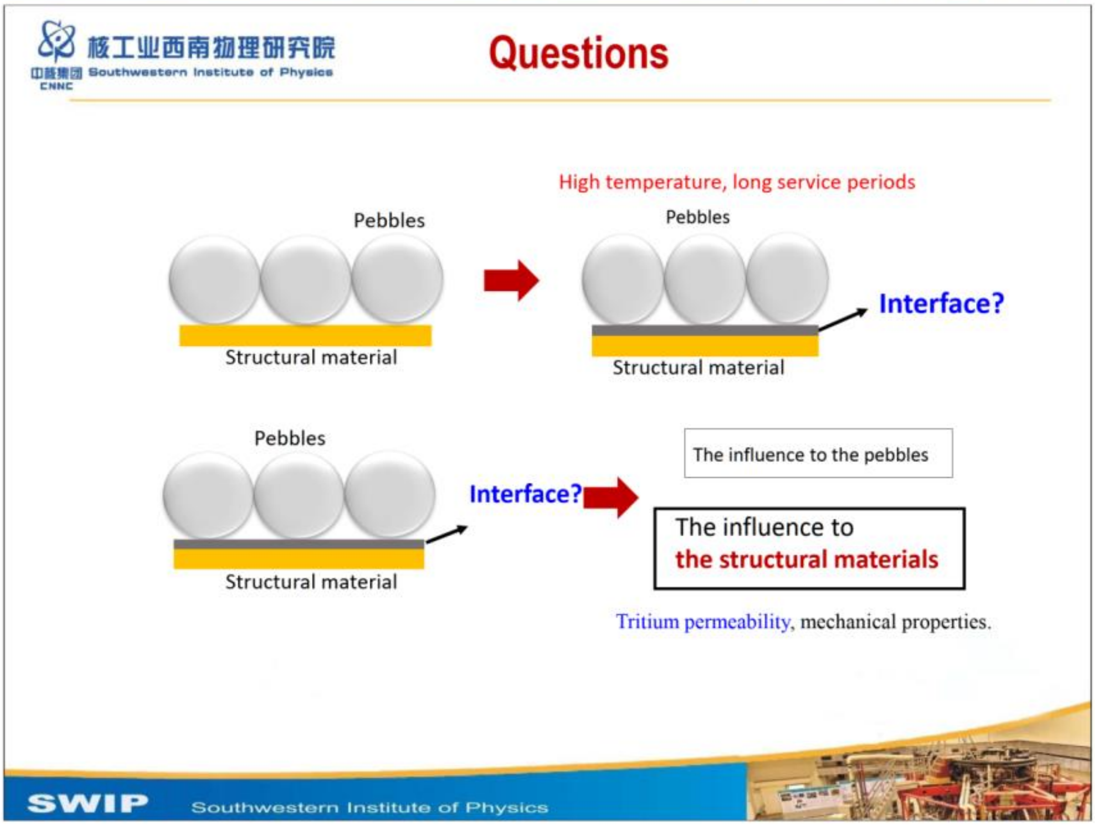
核工业西南物理研究院
Southwestern Institute of Physics
Questions
High temperature, long service periods
Pebbles
Structural material
Pebbles
Interface?
Structural material
Pebbles
Structural material
Interface?
The influence to the pebbles
The influence to the structural materials
Tritium permeability, mechanical properties.
SWIP Southwestern Institute of Physics


核工业西南物理研究院
中核集团 Southwestern Institute of Physics
CNNC
1.Brief introduction to SWIP
2.Background
3.Experiments and results
4.Conclusions
5.Future Plan
SWIP Southwestern Institute of Physics

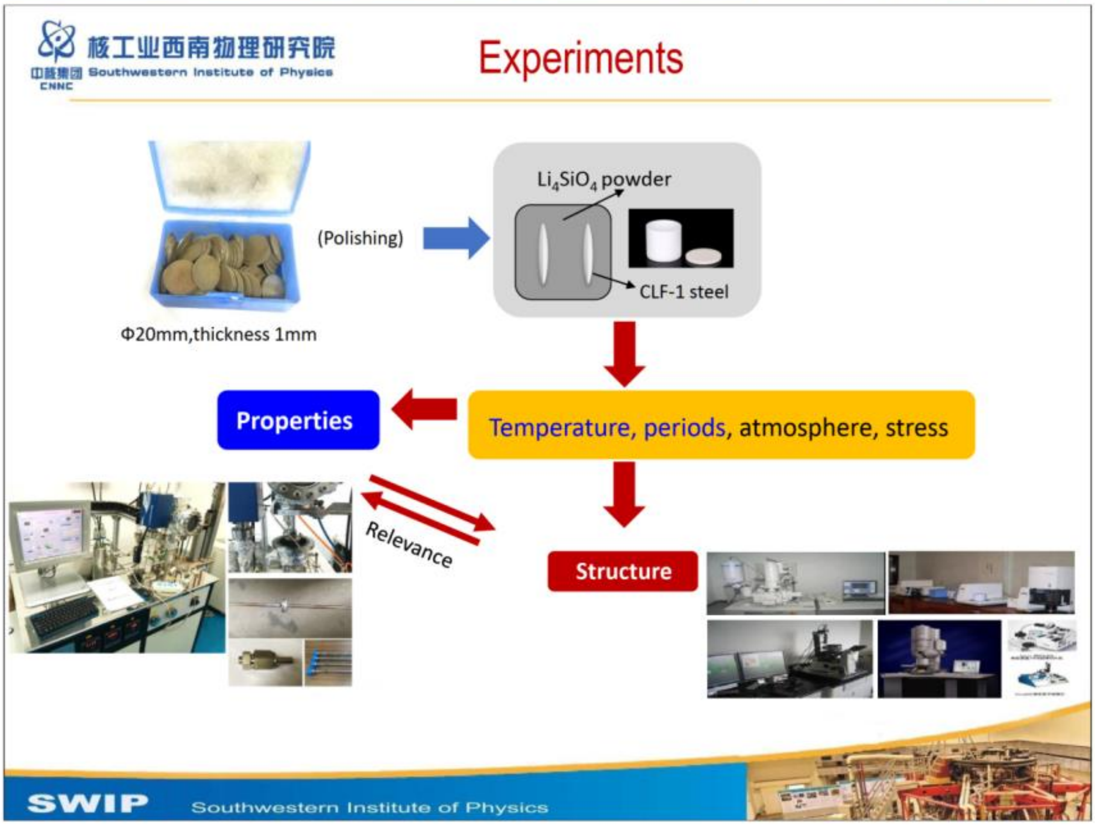
核工业西南物理研究院
中核集团 Southwestern Institute of Physics
CNNC
Experiments
(Polishing)
Φ20mm,thickness 1mm
Li_4SiO_4 powder
CLF-1 steel
Properties
Temperature, periods, atmosphere, stress
Relevance
Structure
SWIP Southwestern Institute of Physics

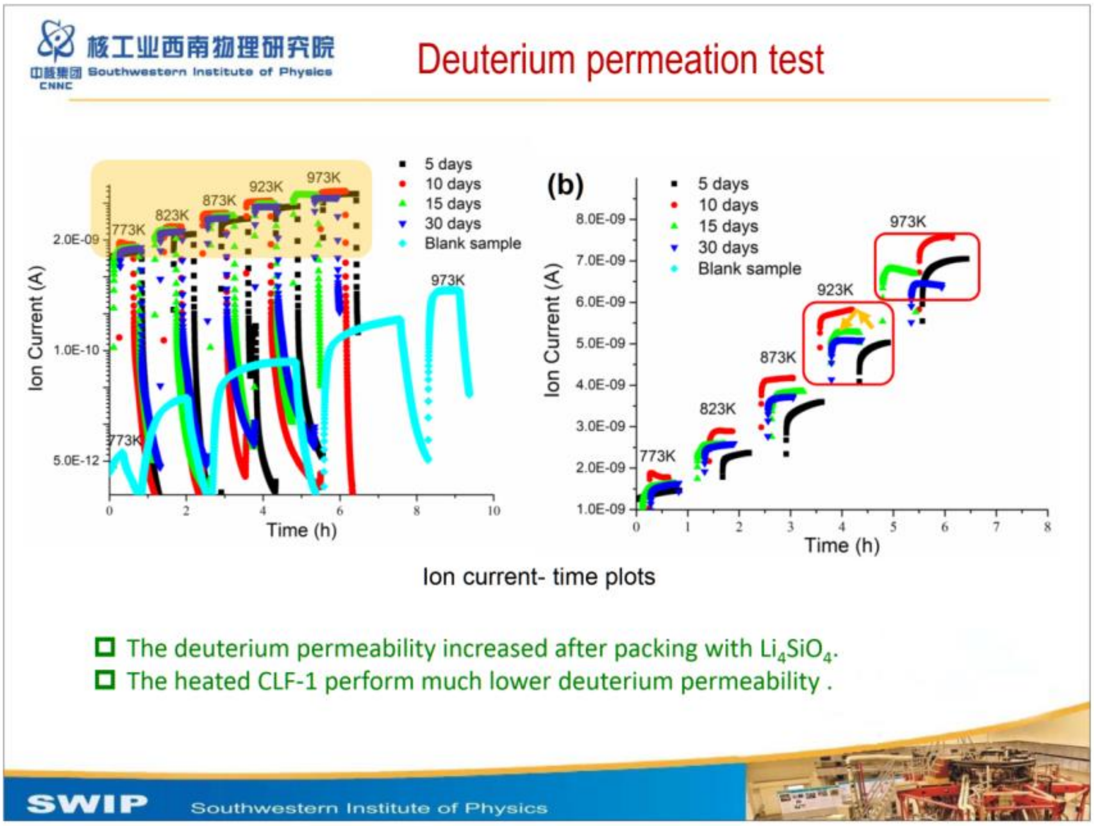
核工业西南物理研究院
Southwestern Institute of Physics
Deuterium permeation test
5 days
10 days
15 days
30 days
Blank sample
Ion Current (A)
Time (h)
(b)
Ion current- time plots
The deuterium permeability increased after packing with Li_4SiO_4.
The heated CLF-1 perform much lower deuterium permeability .
SWIP Southwestern Institute of Physics

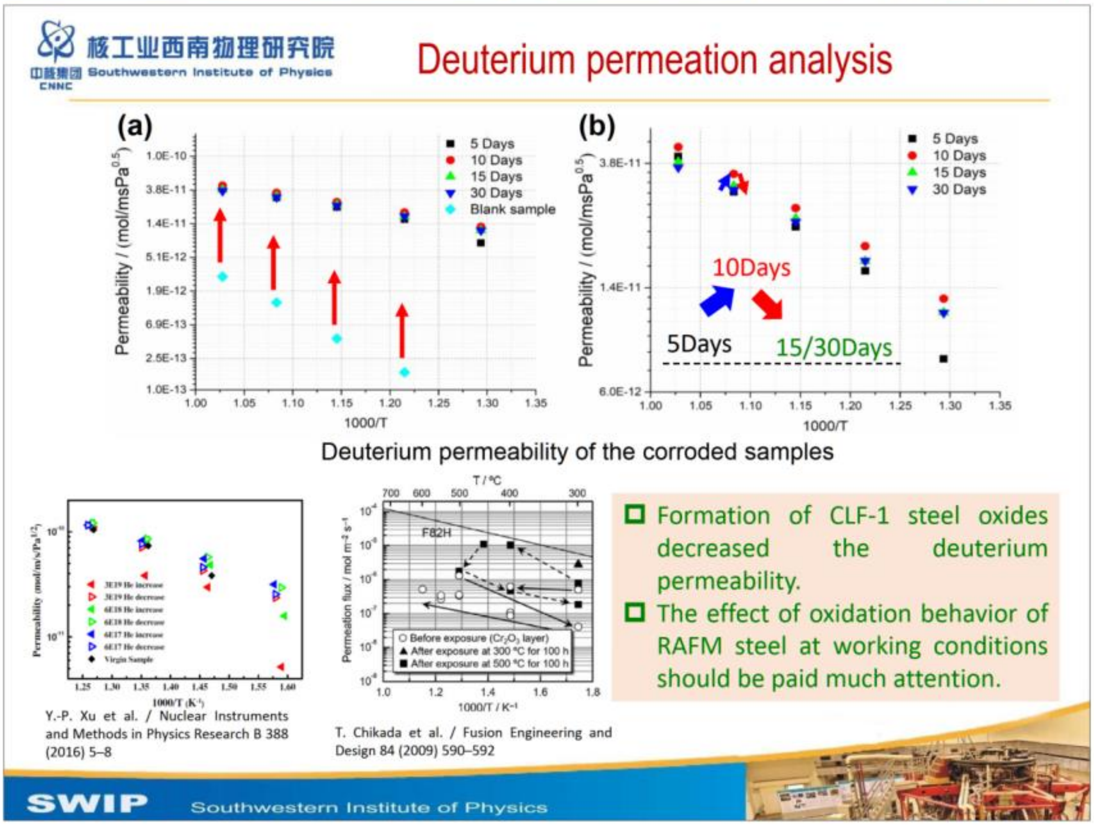
核工业西南物理研究院
Southwestern Institute of Physics
Deuterium permeation analysis
(a)
(b)
5 Days
10 Days
15 Days
30 Days
Blank sample
Permeability / (mol/msPa$^{0.5}$)
1000/T
10Days
5Days
15/30Days
Deuterium permeability of the corroded samples
Y.-P. Xu et al. / Nuclear Instruments and Methods in Physics Research B 388 (2016) 5–8
T. Chikada et al. / Fusion Engineering and Design 84 (2009) 590–592
Formation of CLF-1 steel oxides decreased the deuterium permeability.
The effect of oxidation behavior of RAFM steel at working conditions should be paid much attention.
SWIP Southwestern Institute of Physics

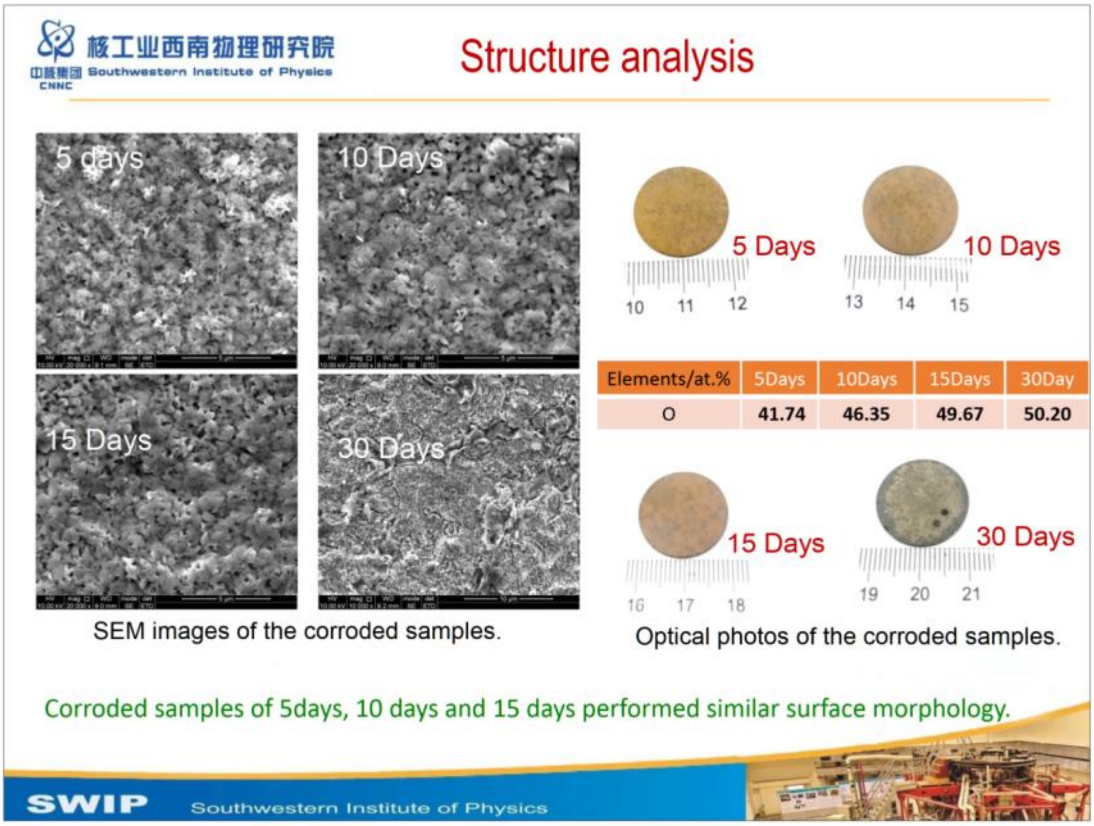
核工业西南物理研究院
Southwestern Institute of Physics
Structure analysis
5 days
10 Days
15 Days
30 Days
SEM images of the corroded samples.
5 Days
10 Days
15 Days
30 Days
Optical photos of the corroded samples.
Elements/at.% | 5Days | 10Days | 15Days | 30Day
O | 41.74 | 46.35 | 49.67 | 50.20
Corroded samples of 5days, 10 days and 15 days performed similar surface morphology.
SWIP Southwestern Institute of Physics

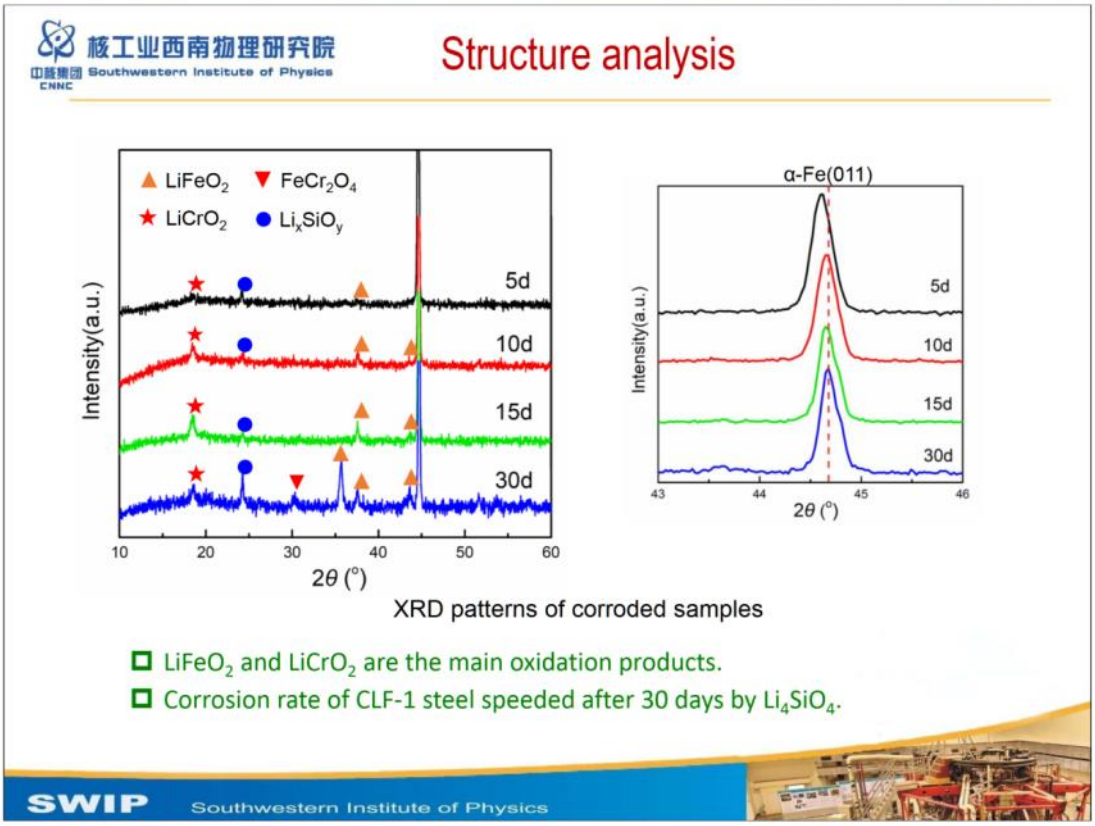
核工业西南物理研究院
Southwestern Institute of Physics
Structure analysis
LiFeO2
FeCr2O4
LiCrO2
LixSiOy
5d
10d
15d
30d
Intensity(a.u.)
2θ (°)
α-Fe(011)
XRD patterns of corroded samples
LiFeO2 and LiCrO2 are the main oxidation products.
Corrosion rate of CLF-1 steel speeded after 30 days by Li4SiO4.
SWIP Southwestern Institute of Physics

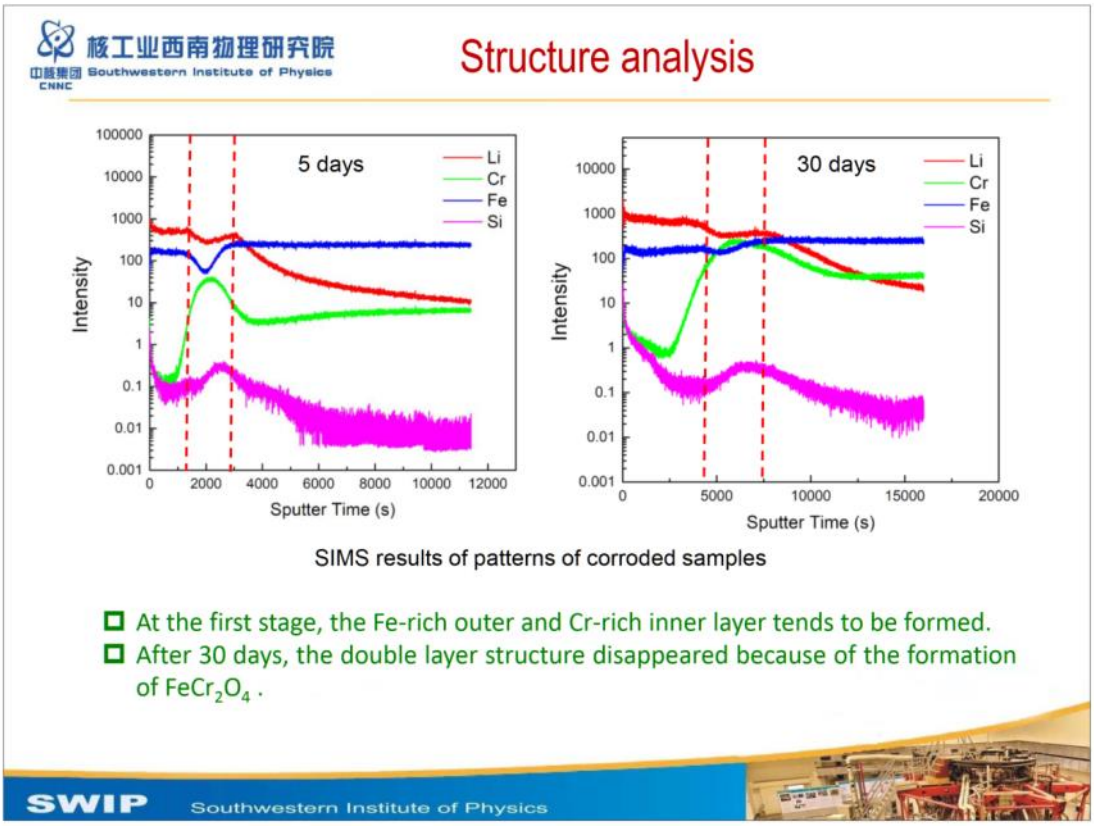
核工业西南物理研究院
中核集团 Southwestern Institute of Physics
CNNC
Structure analysis
5 days
30 days
Li
Cr
Fe
Si
Intensity
Sputter Time (s)
SIMS results of patterns of corroded samples
At the first stage, the Fe-rich outer and Cr-rich inner layer tends to be formed.
After 30 days, the double layer structure disappeared because of the formation of $FeCr_2O_4$.
SWIP
Southwestern Institute of Physics

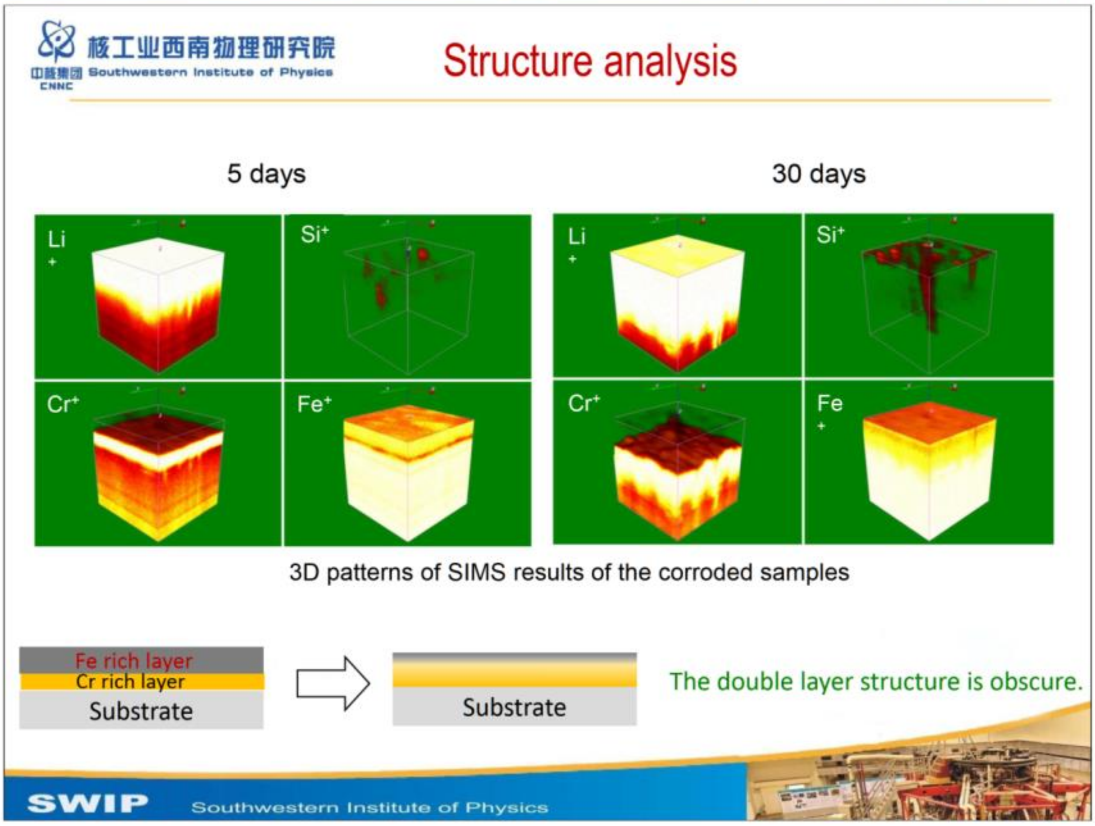
核工业西南物理研究院
中核集团 Southwestern Institute of Physics
CNNC
Structure analysis
5 days
30 days
Li+
Si+
Cr+
Fe+
3D patterns of SIMS results of the corroded samples
Fe rich layer
Cr rich layer
Substrate
Substrate
The double layer structure is obscure.
SWIP
Southwestern Institute of Physics

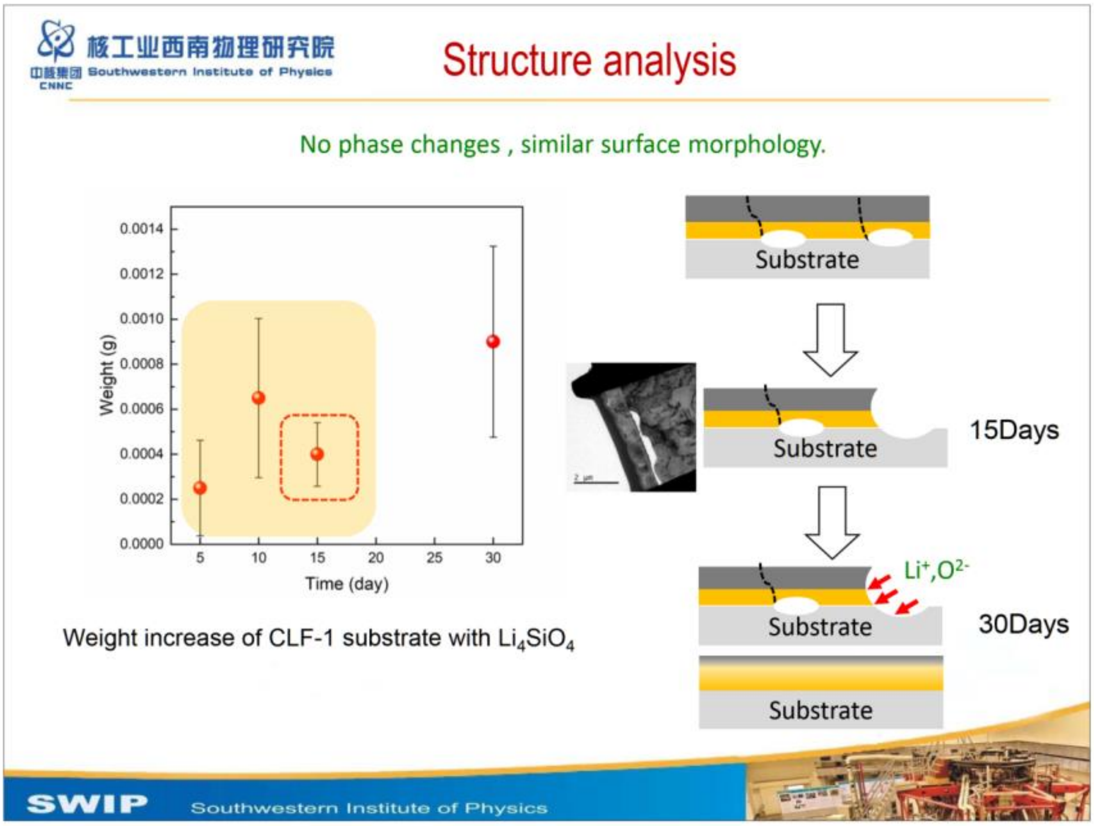
核工业西南物理研究院
中核集团 Southwestern Institute of Physics
CNNC
Structure analysis
No phase changes , similar surface morphology.
Weight (g)
Time (day)
Substrate
15Days
Li+,O2-
30Days
Weight increase of CLF-1 substrate with Li4SiO4
SWIP Southwestern Institute of Physics

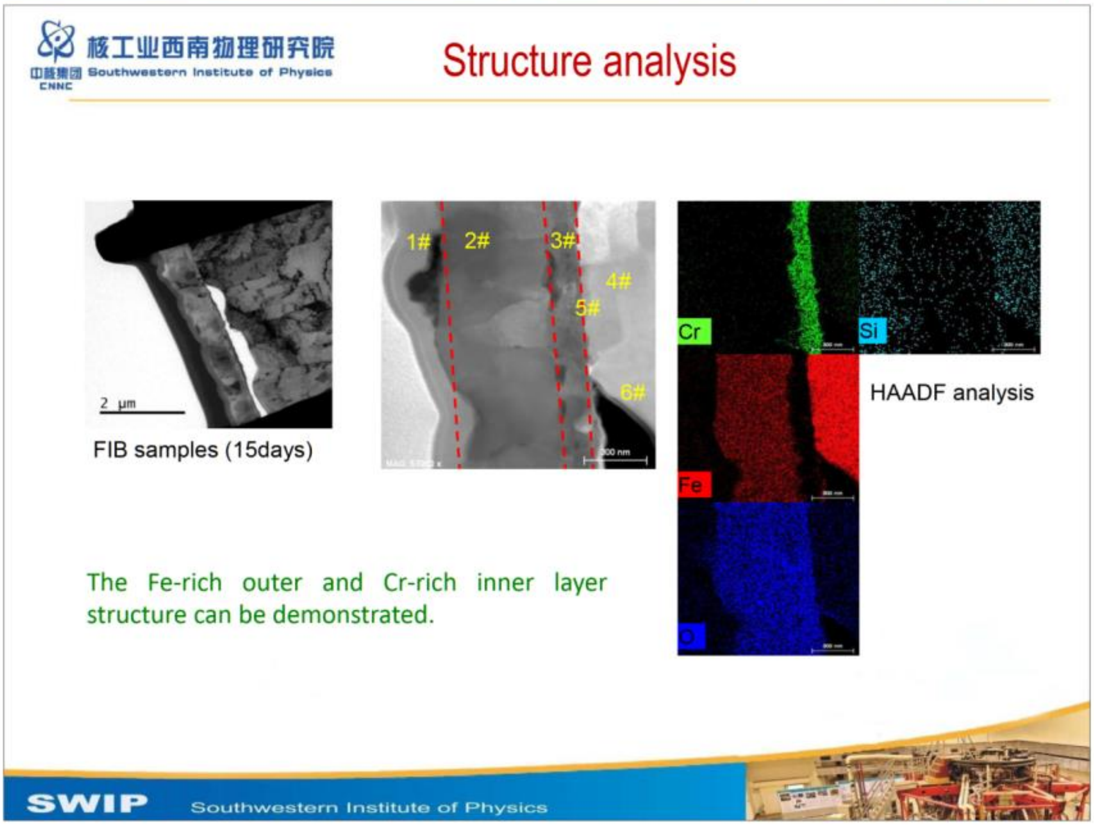
核工业西南物理研究院
中核集团 Southwestern Institute of Physics
CNNC
Structure analysis
2 μm
FIB samples (15days)
1#
2#
3#
4#
5#
6#
Cr
Si
Fe
O
HAADF analysis
The Fe-rich outer and Cr-rich inner layer structure can be demonstrated.
SWIP Southwestern Institute of Physics

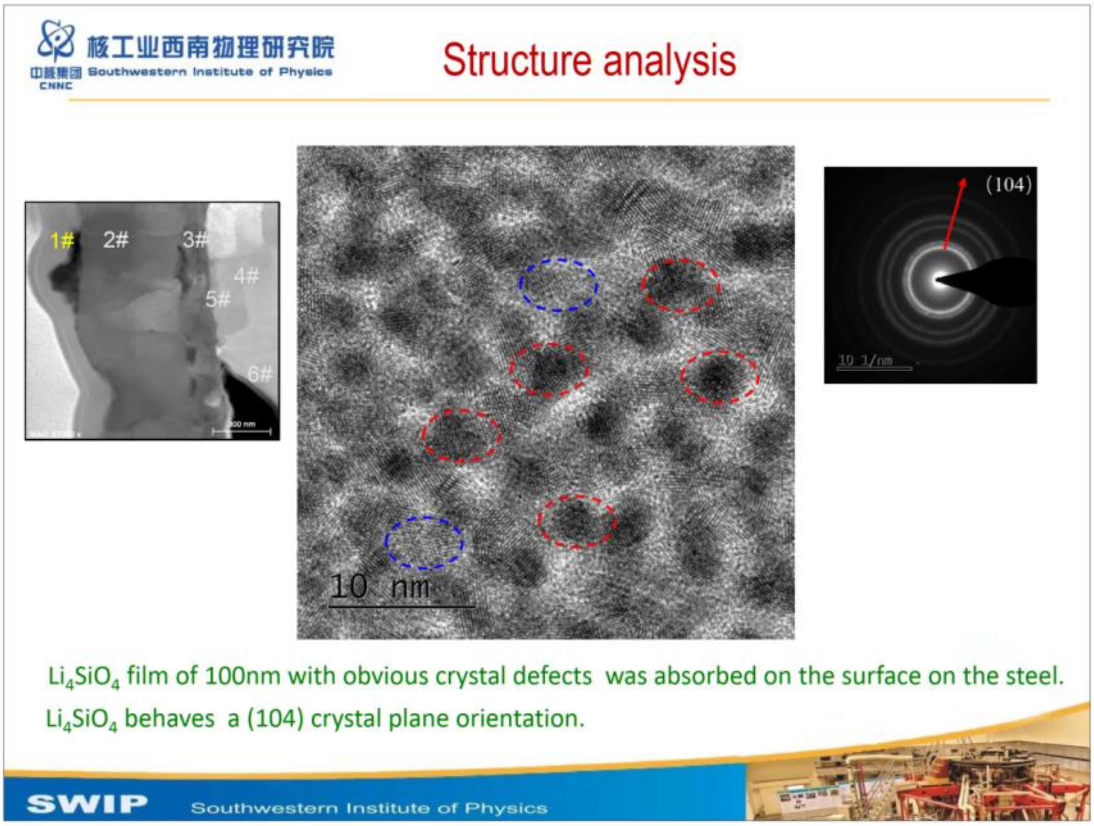
核工业西南物理研究院
中核集团 Southwestern Institute of Physics
CNNC
Structure analysis
1#
2#
3#
4#
5#
6#
10 nm
(104)
10 1/nm
Li_4SiO_4 film of 100nm with obvious crystal defects was absorbed on the surface on the steel.
Li_4SiO_4 behaves a (104) crystal plane orientation.
SWIP Southwestern Institute of Physics

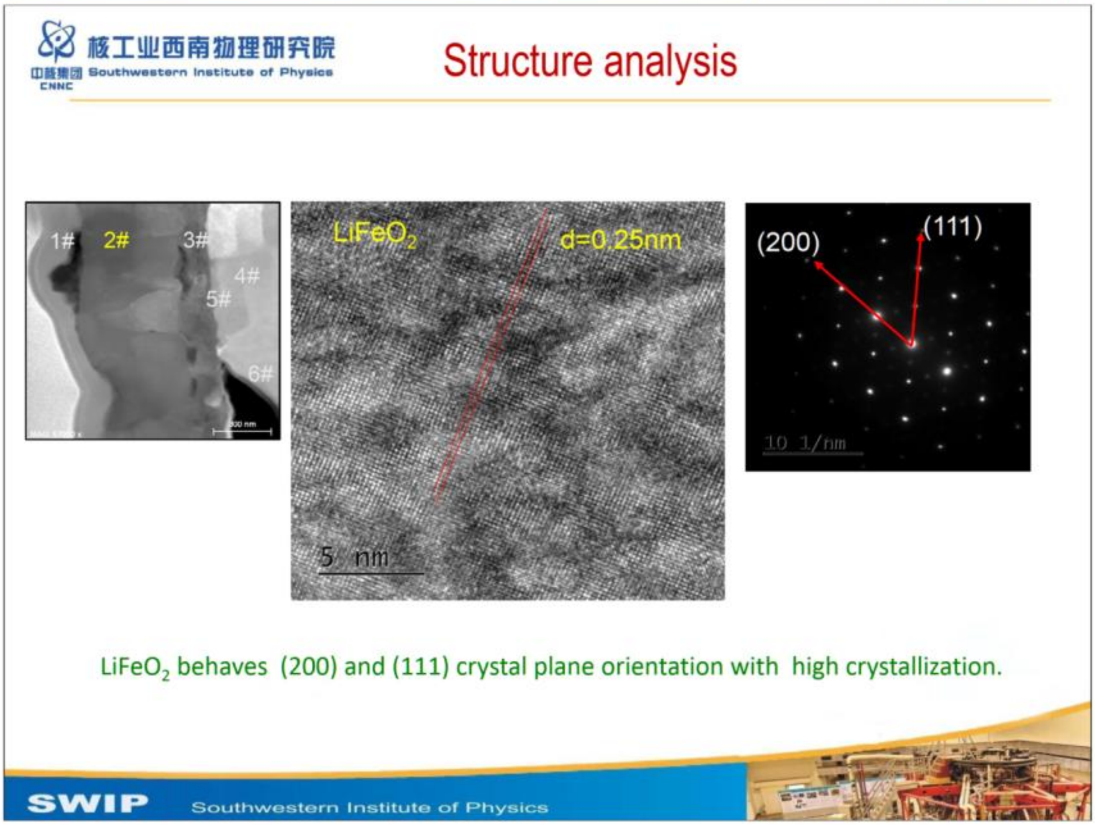
核工业西南物理研究院
中核集团 Southwestern Institute of Physics
CNNC
Structure analysis
1#
2#
3#
4#
5#
6#
$LiFeO_2$
d=0.25nm
5 nm
(200)
(111)
10 1/nm
$LiFeO_2$ behaves (200) and (111) crystal plane orientation with high crystallization.
SWIP Southwestern Institute of Physics

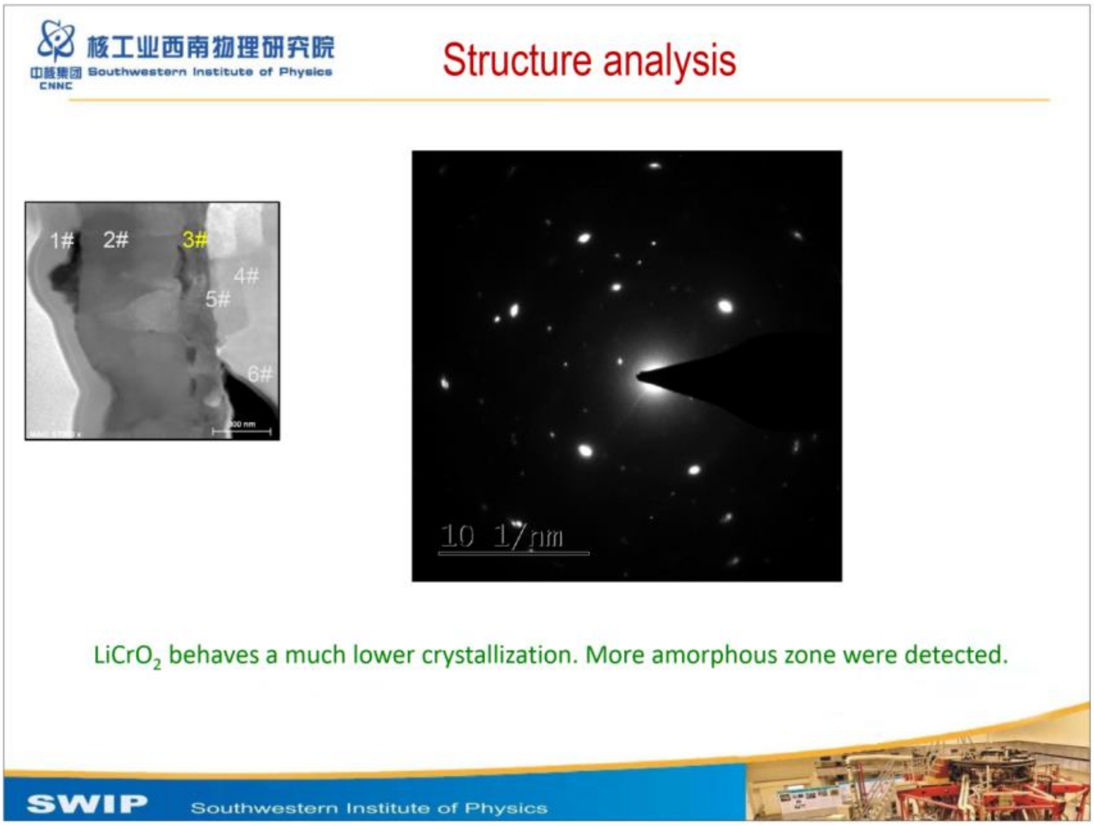
核工业西南物理研究院
中核集团 CNNC
Southwestern Institute of Physics
Structure analysis
1#
2#
3#
4#
5#
6#
10 1/nm
LiCrO$_2$ behaves a much lower crystallization. More amorphous zone were detected.
SWIP
Southwestern Institute of Physics

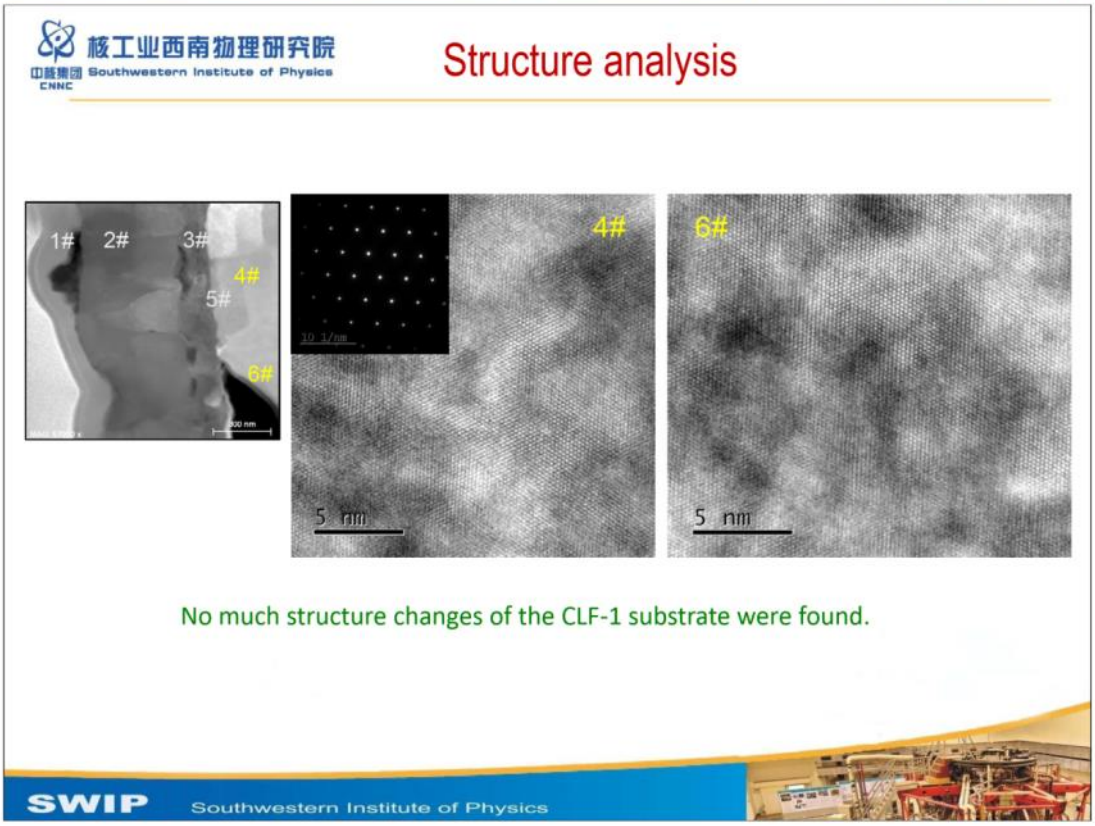
核工业西南物理研究院
中核集团 CNNC
Southwestern Institute of Physics
Structure analysis
1#
2#
3#
4#
5#
6#
4#
6#
5 nm
5 nm
No much structure changes of the CLF-1 substrate were found.
SWIP
Southwestern Institute of Physics

核工业西南物理研究院
中核集团 CNNC Southwestern Institute of Physics

Structure analysis

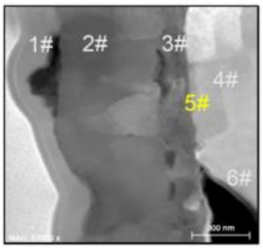

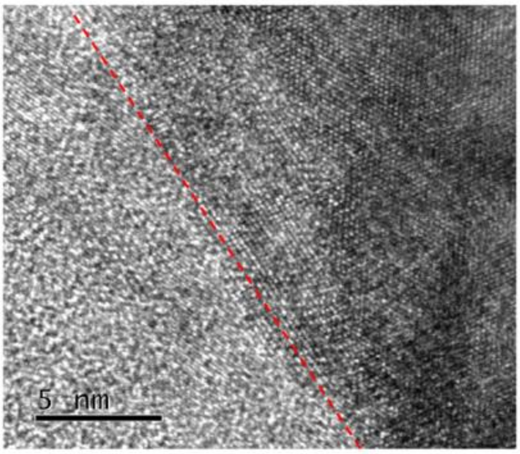

The crystal misfit at the interface could accelerate the peeling-off rate of the oxide film.

SWIP Southwestern Institute of Physics

核工业西南物理研究院
中核集团 CNNC Southwestern Institute of Physics

1.Brief introduction to SWIP

2.Background

3.Experiments and results

4.Conclusions

5.Future Plan

SWIP Southwestern Institute of Physics

核工业西南物理研究院
中核集团 Southwestern Institute of Physics
CNNC

1.The deuterium permeability of CLF-1 increased of 2 magnitude order by Li_4SiO_4 .

2. An oxide layer, Fe-rich outer and Cr-rich inner layer, was formed on the surface of CLF-1 steel by Li_4SiO_4 .

3.With the increase of periods, the double layer structure became obscure after 30 days.

4. Li_4SiO_4 film with crystal defects can be absorbed on the surface on the steel.

SWIP Southwestern Institute of Physics

核工业西南物理研究院
中核集团 Southwestern Institute of Physics
CNNC

1.Brief introduction to SWIP

2.Background

3.Experiments and results

4.Conclusions

5.Future Plan

SWIP Southwestern Institute of Physics

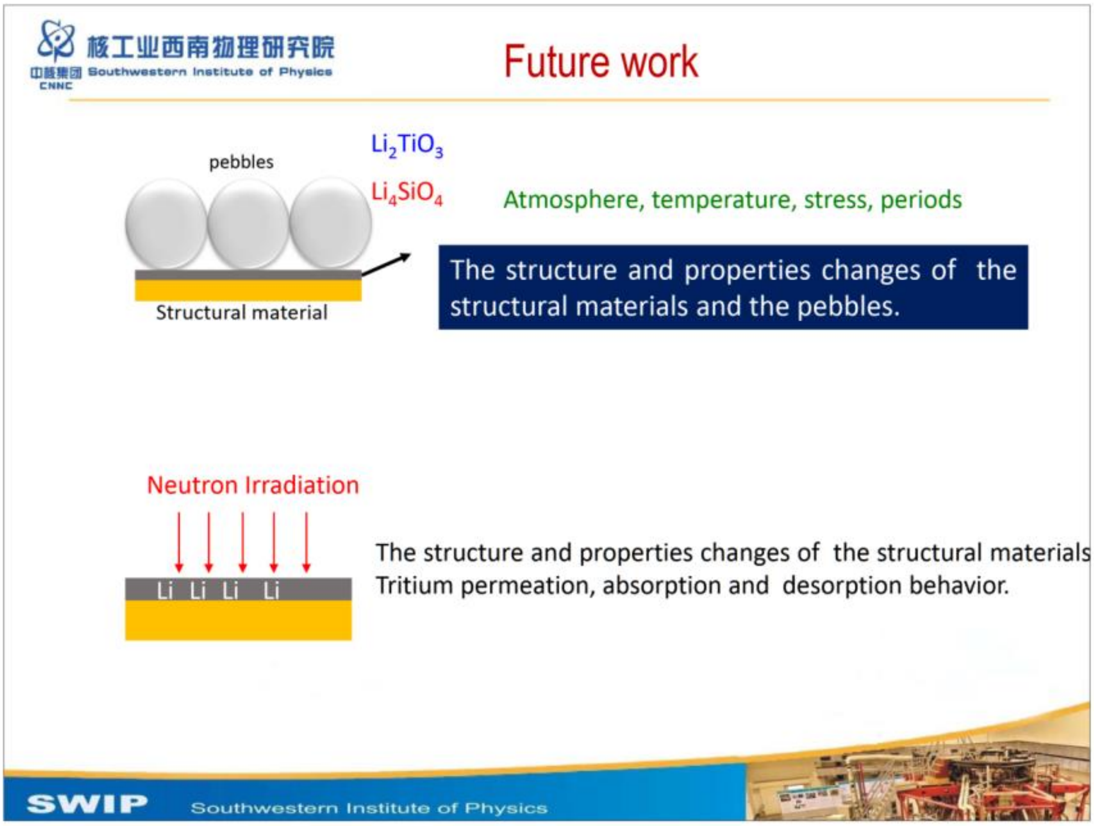
核工业西南物理研究院
中核集团 Southwestern Institute of Physics
CNNC
Future work
pebbles
Li_2TiO_3
Li_4SiO_4
Atmosphere, temperature, stress, periods
Structural material
The structure and properties changes of the structural materials and the pebbles.
Neutron Irradiation
Li Li Li Li
The structure and properties changes of the structural materials
Tritium permeation, absorption and desorption behavior.
SWIP Southwestern Institute of Physics

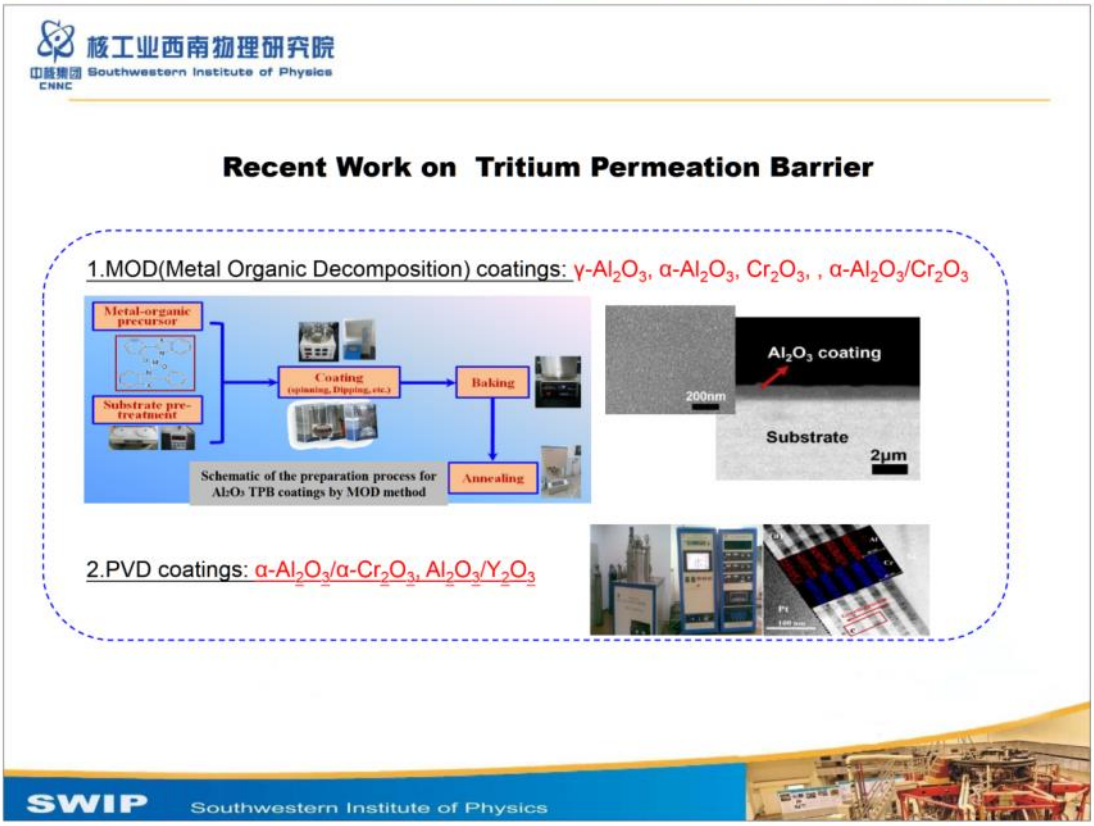
核工业西南物理研究院
中核集团 Southwestern Institute of Physics
CNNC
Recent Work on Tritium Permeation Barrier
1.MOD(Metal Organic Decomposition) coatings: γ-Al_2O_3, α-Al_2O_3, Cr_2O_3, , α-Al_2O_3/Cr_2O_3
Metal-organic precursor
Substrate pre-treatment
Coating (spinning, Dipping, etc.)
Baking
Annealing
Schematic of the preparation process for Al_2O_3 TPB coatings by MOD method
200nm
Al_2O_3 coating
Substrate
2μm
2.PVD coatings: α-Al_2O_3/α-Cr_2O_3, Al_2O_3/Y_2O_3
SWIP Southwestern Institute of Physics

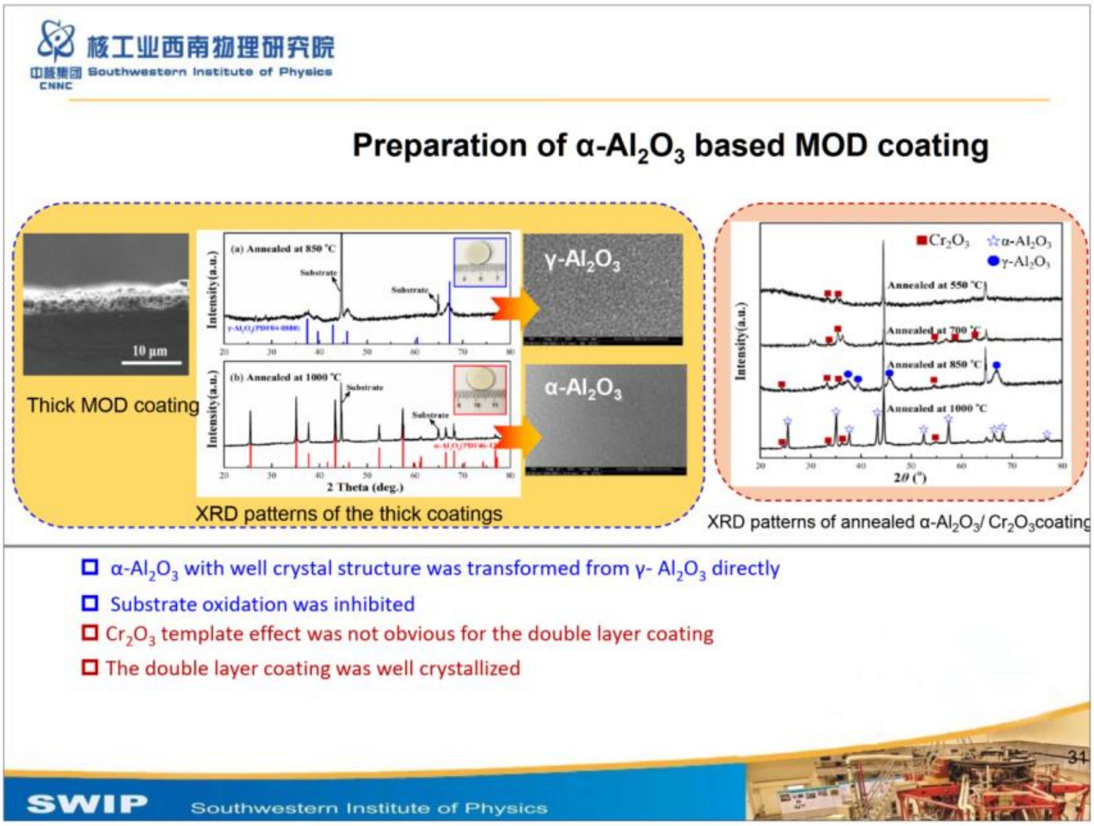
核工业西南物理研究院
中核集团 Southwestern Institute of Physics
CNNC
Preparation of α-Al2O3 based MOD coating
10 μm
Thick MOD coating
(a) Annealed at 850 °C
Substrate
(b) Annealed at 1000 °C
2 Theta (deg.)
Intensity(a.u.)
γ-Al2O3
α-Al2O3
XRD patterns of the thick coatings
Cr2O3 α-Al2O3 γ-Al2O3
Annealed at 550 °C
Annealed at 700 °C
Annealed at 850 °C
Annealed at 1000 °C
2θ (°)
XRD patterns of annealed α-Al2O3/ Cr2O3coating
α-Al2O3 with well crystal structure was transformed from γ- Al2O3 directly
Substrate oxidation was inhibited
Cr2O3 template effect was not obvious for the double layer coating
The double layer coating was well crystallized
SWIP Southwestern Institute of Physics
31

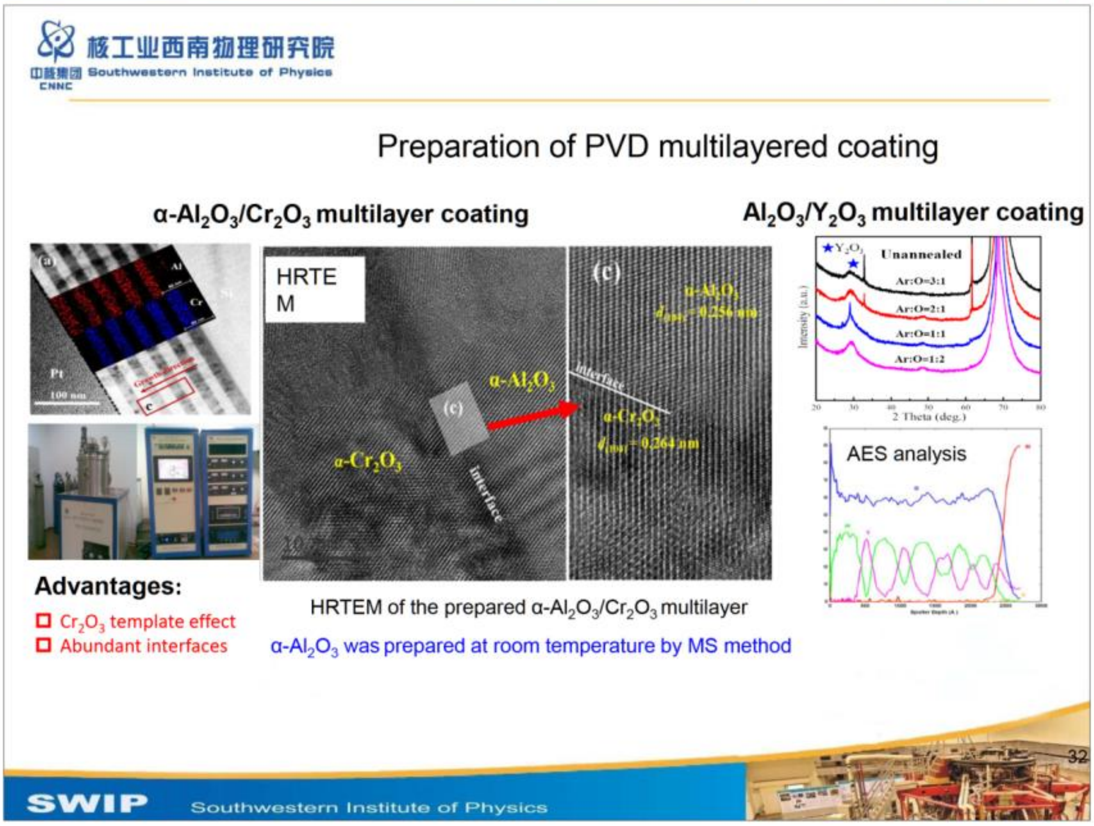
核工业西南物理研究院
中核集团 Southwestern Institute of Physics
CNNC
Preparation of PVD multilayered coating
α-Al2O3/Cr2O3 multilayer coating
Al2O3/Y2O3 multilayer coating
HRTE
M
α-Al2O3
α-Cr2O3
Interface
Unannealed
Ar:O=3:1
Ar:O=2:1
Ar:O=1:1
Ar:O=1:2
2 Theta (deg.)
AES analysis
Advantages:
Cr2O3 template effect
Abundant interfaces
HRTEM of the prepared α-Al2O3/Cr2O3 multilayer
α-Al2O3 was prepared at room temperature by MS method
SWIP Southwestern Institute of Physics
32

核工业西南物理研究院
Southwestern Institute of Physics

Y_2O_3/Al_2O_3 multilayer (MS)

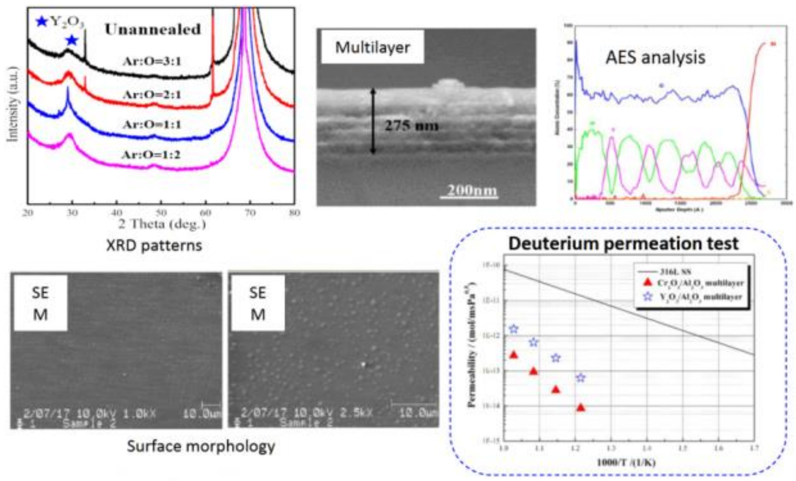

33

SWIP Southwestern Institute of Physics

核工业西南物理研究院
Southwestern Institute of Physics

Thank you for your attention.

SWIP Southwestern Institute of Physics

Compatibility of advanced functional materials for fusion applications

Jae-Hwan Kim, Masaru Nakamichi

Fusion Energy Research and Development Directorate,
National Institutes for Quantum and Radiological Science and Technology,
QST, Japan
2-166, Omotedate, Obuchi, Rokkasho, Aomori, 039-3212, Japan

Fusion reactors require advanced functional materials, such as tritium breeders and neutron multipliers owing to higher tritium breeding ratio as well as higher stability at high temperature.

In Japan, researches and developments on not only new functional materials with different chemical compositions but also new designs of the blanket systems with loading of mixed functional materials for demonstration (DEMO) fusion reactors have been performed for the higher tritium breeding ratio. To realize this new design for mixture packing, however, stability at high temperatures between breeders and multipliers should be clarified from viewpoints of mechanical degradation of materials due to formation of new compounds by reactions between those and recycling process of materials after operating for long term.

In this study, compatibility tests of advanced tritium breeders and advanced neutron multipliers were carried out at 1173 K and those preliminary experimental results will be presented.

Compatibility of advanced functional materials for fusion applications

Outline

1. Current status of R&Ds on multiplier and breeder
2. An objective of compatibility test
3. Experimental results
4. Recycling process
5. Summary

Jae-Hwan Kim, Masaru Nakamichi

National Institutes for Quantum and Radiological Science and Technology

Necessity of Advanced Breeding Functional Materials (ABFMs)

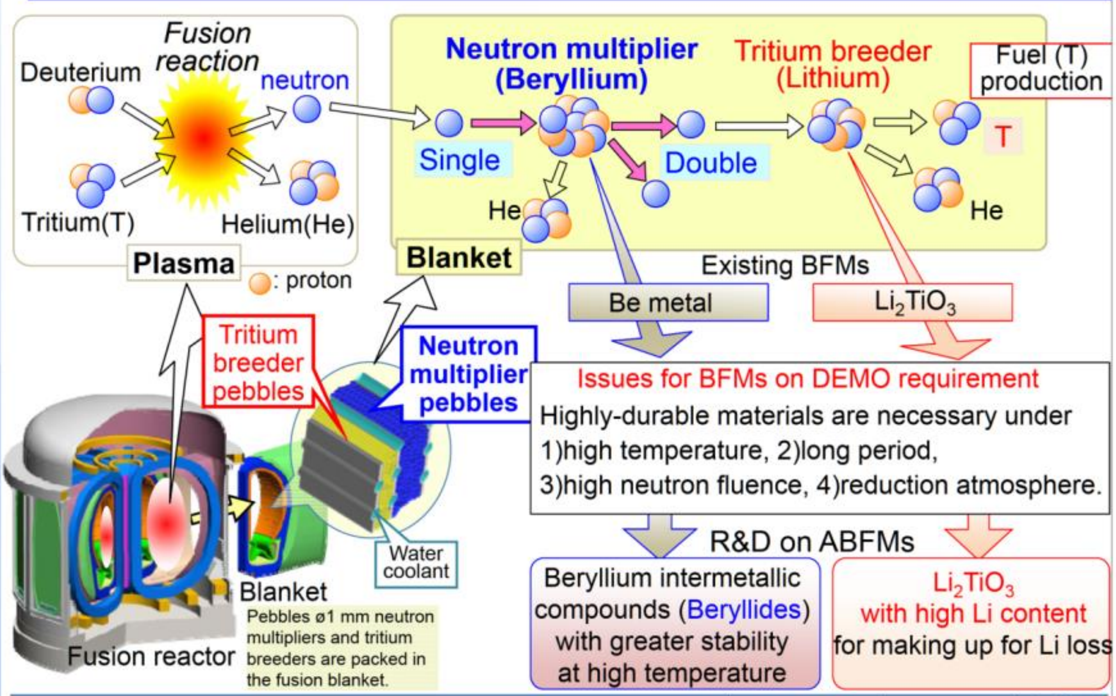

Jae-Hwan Kim | CBBI-20, KIT | 20190918 | (2/18)

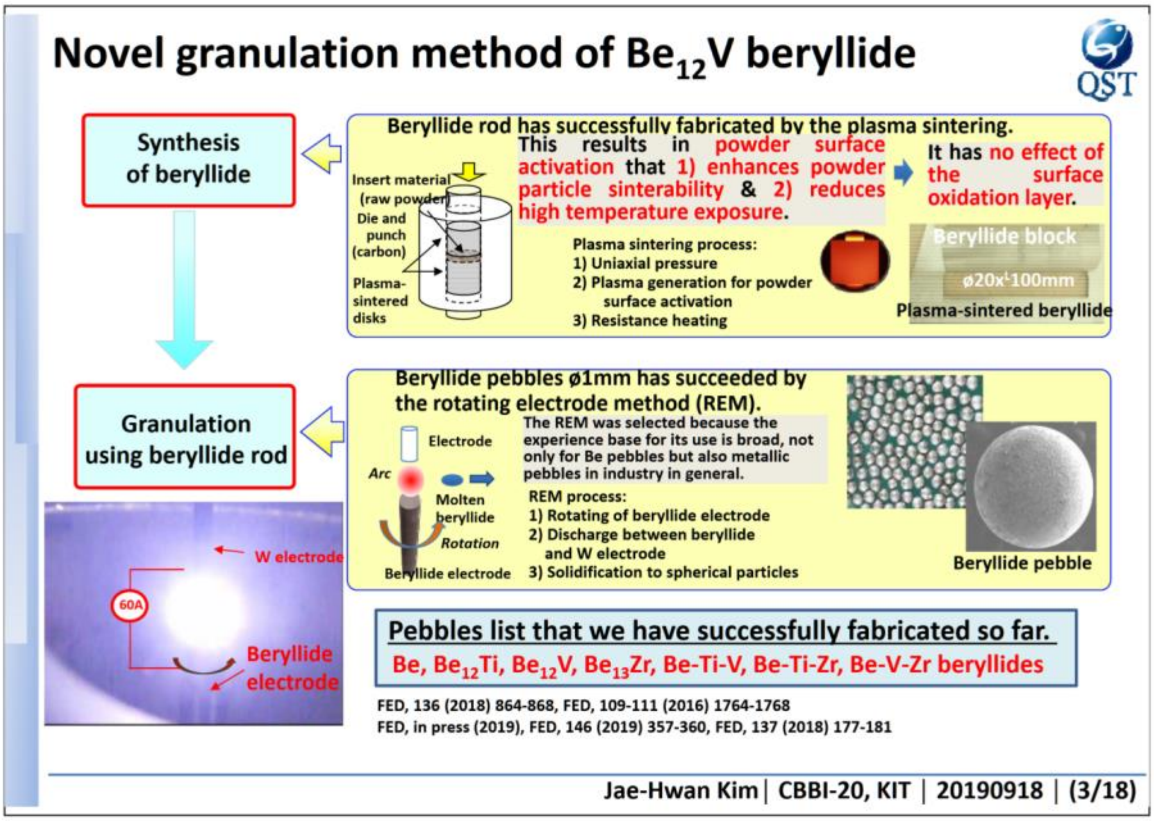
Novel granulation method of Be12V beryllide
Synthesis of beryllide
Beryllide rod has successfully fabricated by the plasma sintering.
This results in powder surface activation that 1) enhances powder particle sinterability & 2) reduces high temperature exposure.
It has no effect of the surface oxidation layer.
Insert material (raw powder)
Die and punch (carbon)
Plasma-sintered disks
Plasma sintering process:
1) Uniaxial pressure
2) Plasma generation for powder surface activation
3) Resistance heating
Beryllide block
ø20x100mm
Plasma-sintered beryllide
Granulation using beryllide rod
Beryllide pebbles ø1mm has succeeded by the rotating electrode method (REM).
The REM was selected because the experience base for its use is broad, not only for Be pebbles but also metallic pebbles in industry in general.
Electrode
Arc
Molten beryllide
Rotation
Beryllide electrode
REM process:
1) Rotating of beryllide electrode
2) Discharge between beryllide and W electrode
3) Solidification to spherical particles
Beryllide pebble
W electrode
60A
Beryllide electrode
Pebbles list that we have successfully fabricated so far.
Be, Be12Ti, Be12V, Be13Zr, Be-Ti-V, Be-Ti-Zr, Be-V-Zr beryllides
FED, 136 (2018) 864-868, FED, 109-111 (2016) 1764-1768
FED, in press (2019), FED, 146 (2019) 357-360, FED, 137 (2018) 177-181
Jae-Hwan Kim | CBBI-20, KIT | 20190918 | (3/18)

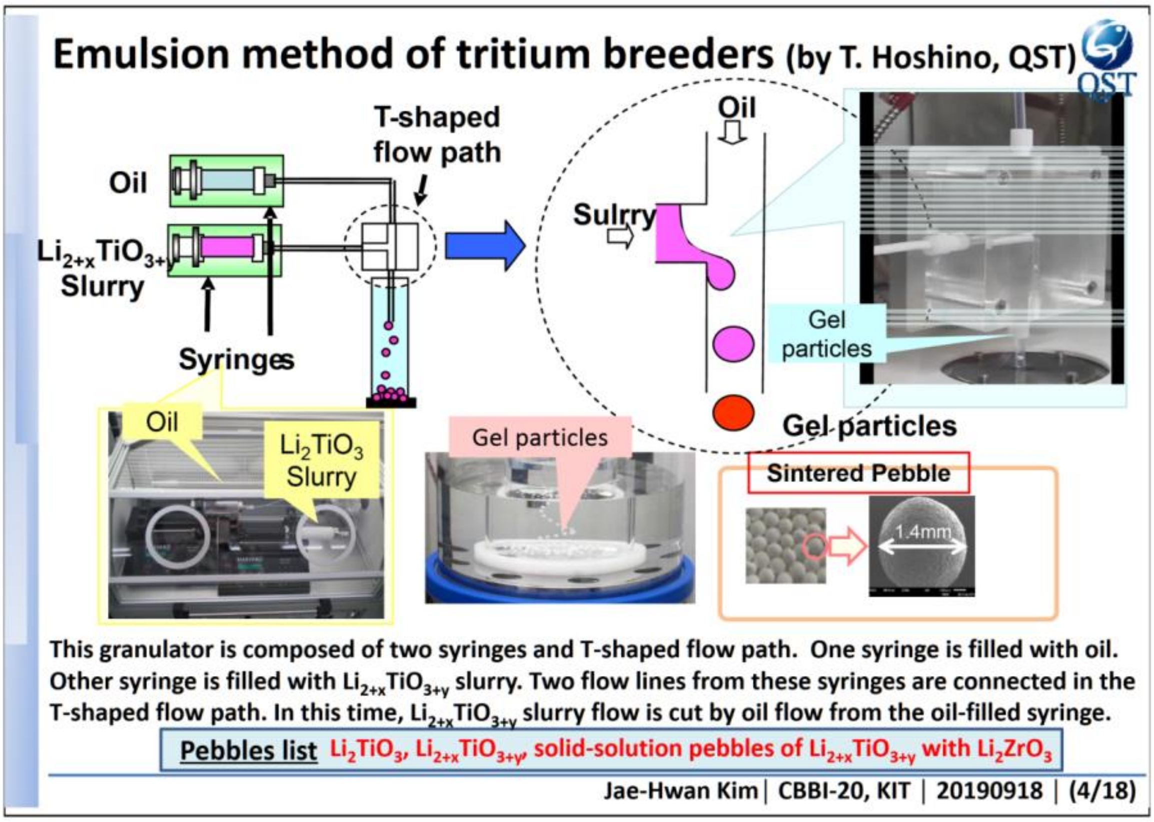
Emulsion method of tritium breeders (by T. Hoshino, QST)
T-shaped flow path
Oil
Li2+xTiO3+y Slurry
Syringes
Sulrry
Gel particles
Gel particles
Oil
Li2TiO3 Slurry
Gel particles
Sintered Pebble
1.4mm
This granulator is composed of two syringes and T-shaped flow path. One syringe is filled with oil. Other syringe is filled with Li2+xTiO3+y slurry. Two flow lines from these syringes are connected in the T-shaped flow path. In this time, Li2+xTiO3+y slurry flow is cut by oil flow from the oil-filled syringe.
Pebbles list Li2TiO3, Li2+xTiO3+y, solid-solution pebbles of Li2+xTiO3+y with Li2ZrO3
Jae-Hwan Kim | CBBI-20, KIT | 20190918 | (4/18)

An objective of compatibility test

New concept of the solid breeder blanket

A feasible DEMO blanket concept based on water cooled solid breeder

[Y. Someya et al. Plasma and Fusion Research, 6, 2405108 (2011)]

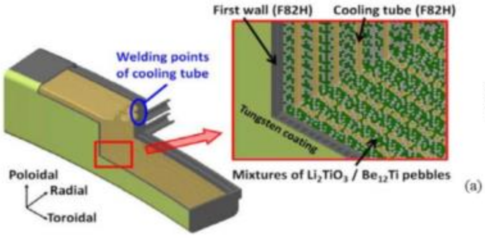

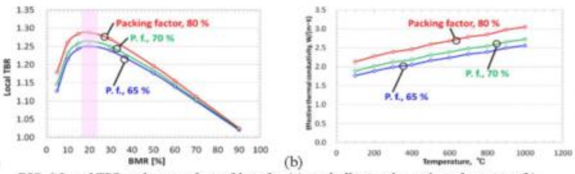

FIG. 2 Local TBR with ratio of mixed breeder (a), and effective thermal conductivities (b).

A mixing pebble packing resulted in increase of TBR.
Considering the mixing pebble packing concept, some issues should be clarified as follows,

(1) Mixing ratio of breeders and multipliers by neutronics
(2) Compatibility of each at high temperatures
(3) Recycling process after operation for several years

Preparation of compatibility tests

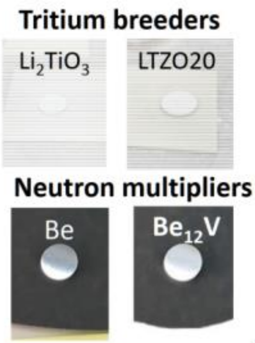

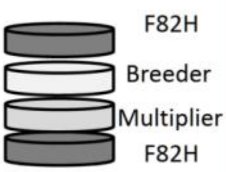

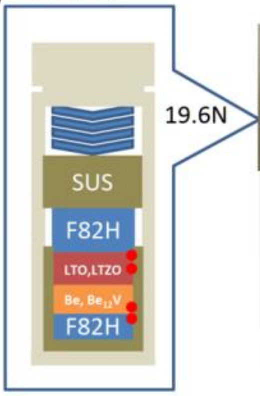

973, 1073, 1173 K
100, 300, (1000) h

Experimental schedule

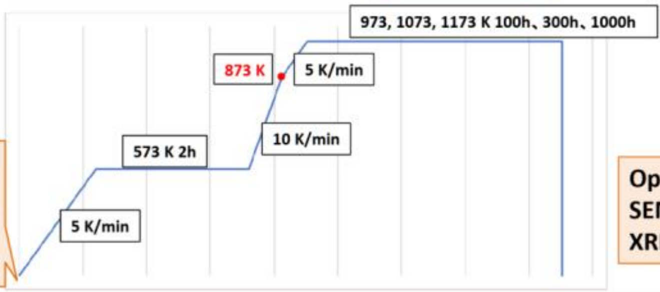

Before heating vacuuming up to 1 Pa was carried out.

Optical observation
SEM observation
XRD analysis and so on.

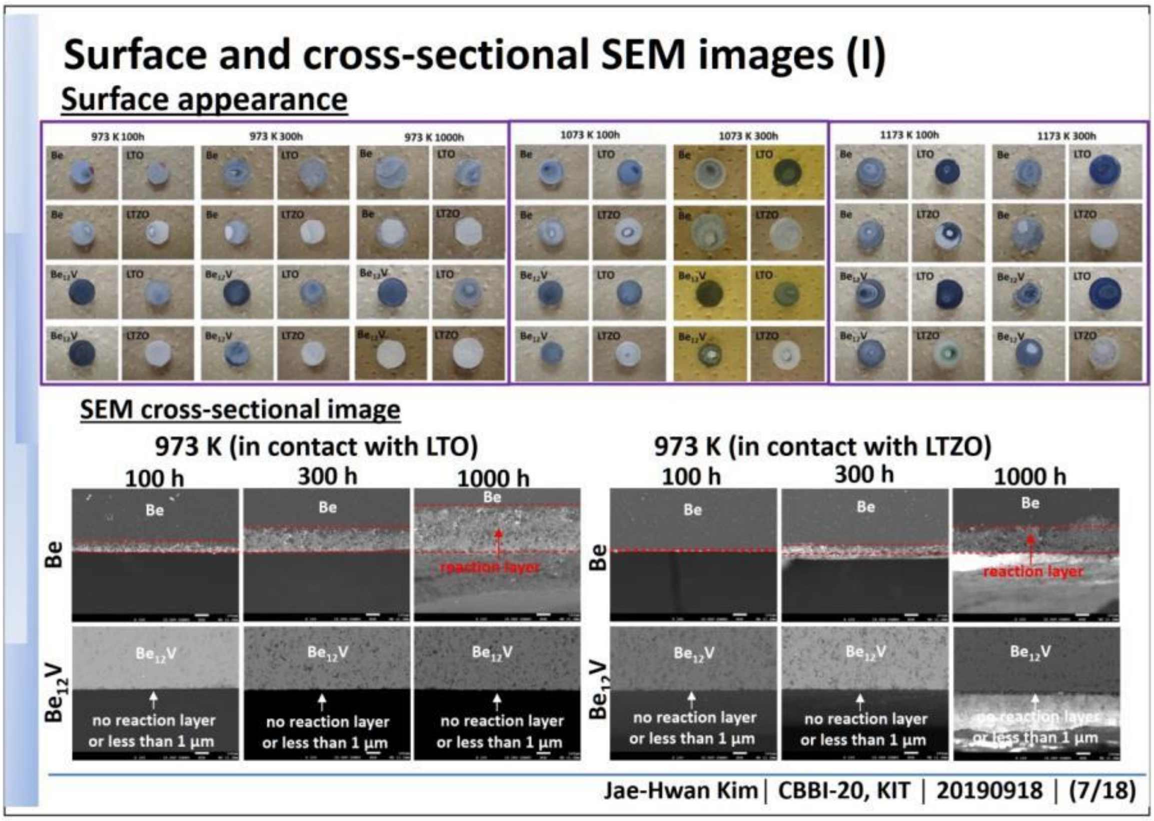
Surface and cross-sectional SEM images (I)
Surface appearance
973 K 100h
973 K 300h
973 K 1000h
1073 K 100h
1073 K 300h
1173 K 100h
1173 K 300h
SEM cross-sectional image
973 K (in contact with LTO)
973 K (in contact with LTZO)
100 h
300 h
1000 h
Be
Be12V
reaction layer
no reaction layer or less than 1 μm
Jae-Hwan Kim | CBBI-20, KIT | 20190918 | (7/18)

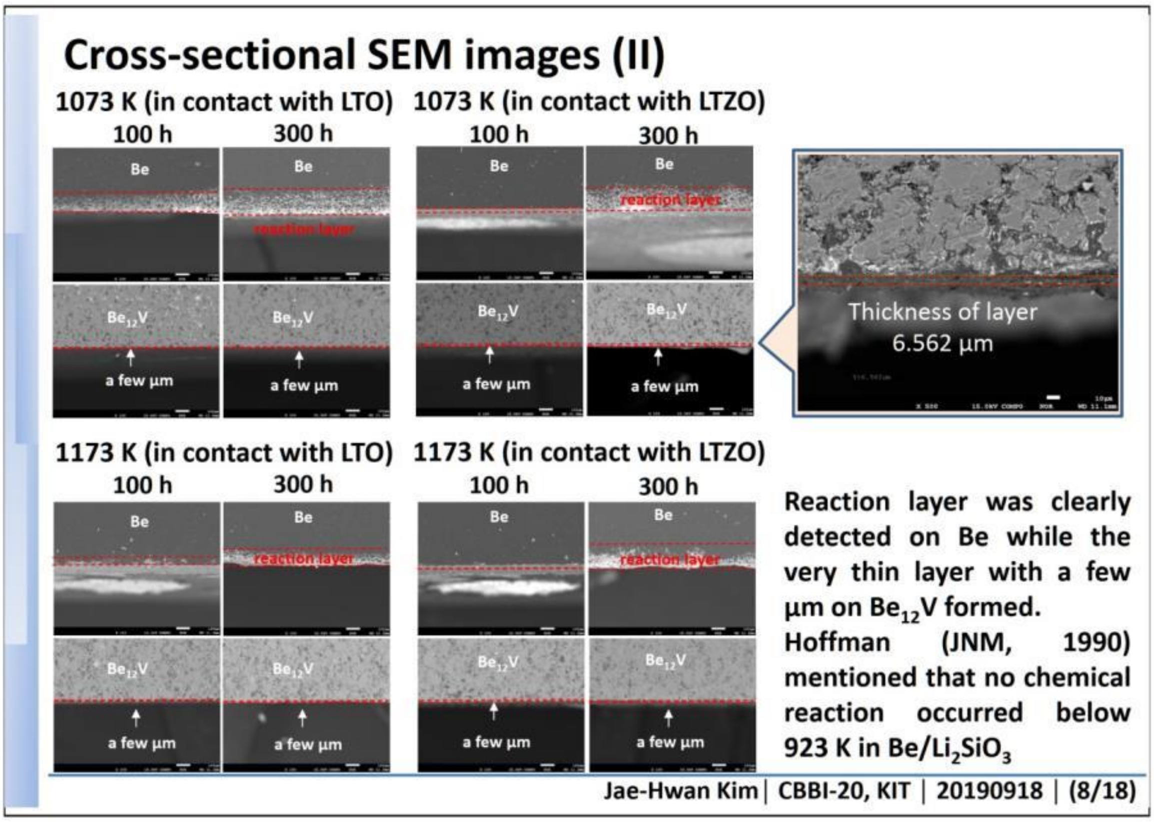
Cross-sectional SEM images (II)
1073 K (in contact with LTO)
1073 K (in contact with LTZO)
1173 K (in contact with LTO)
1173 K (in contact with LTZO)
100 h
300 h
Be
Be12V
reaction layer
a few μm
Thickness of layer 6.562 μm
Reaction layer was clearly detected on Be while the very thin layer with a few μm on Be12V formed.
Hoffman (JNM, 1990) mentioned that no chemical reaction occurred below 923 K in Be/Li2SiO3
Jae-Hwan Kim | CBBI-20, KIT | 20190918 | (8/18)

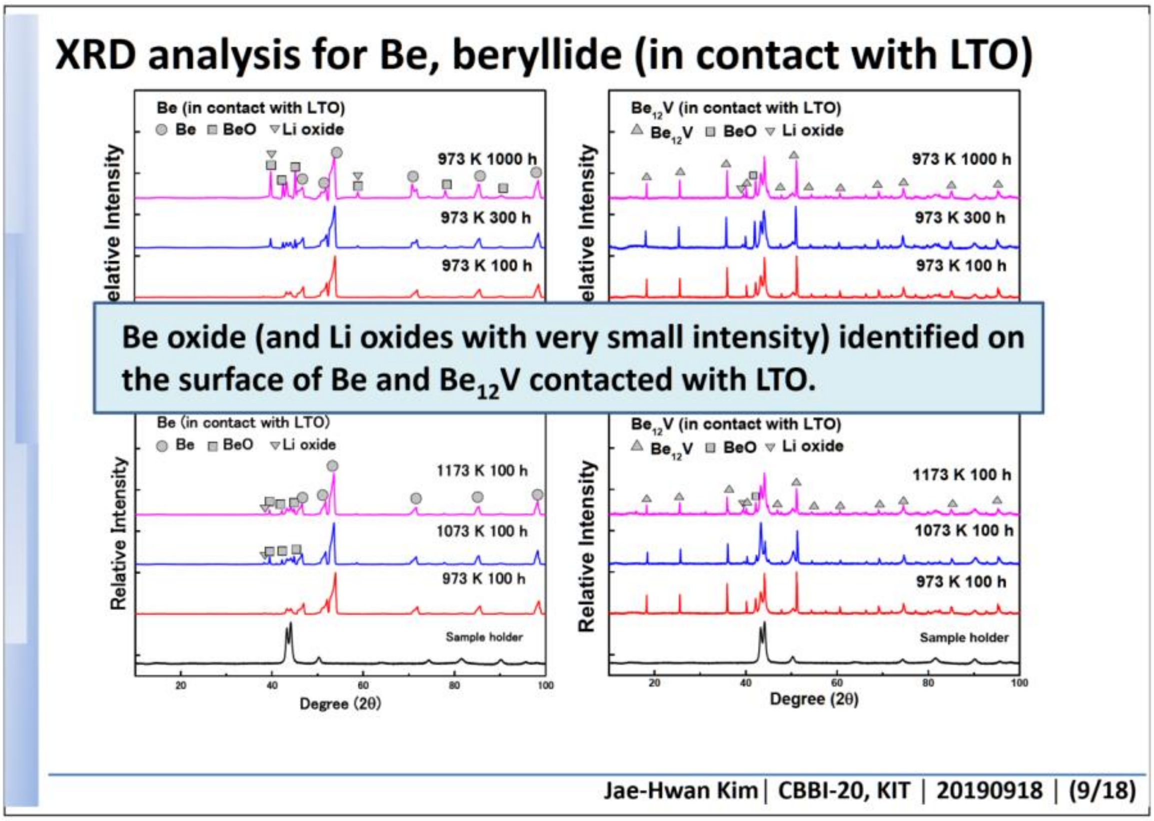
XRD analysis for Be, beryllide (in contact with LTO)
Be (in contact with LTO)
Be BeO Li oxide
973 K 1000 h
973 K 300 h
973 K 100 h
1173 K 100 h
1073 K 100 h
Sample holder
Relative Intensity
Degree (2θ)
Be12V (in contact with LTO)
Be12V BeO Li oxide
Be oxide (and Li oxides with very small intensity) identified on the surface of Be and Be12V contacted with LTO.
Jae-Hwan Kim | CBBI-20, KIT | 20190918 | (9/18)

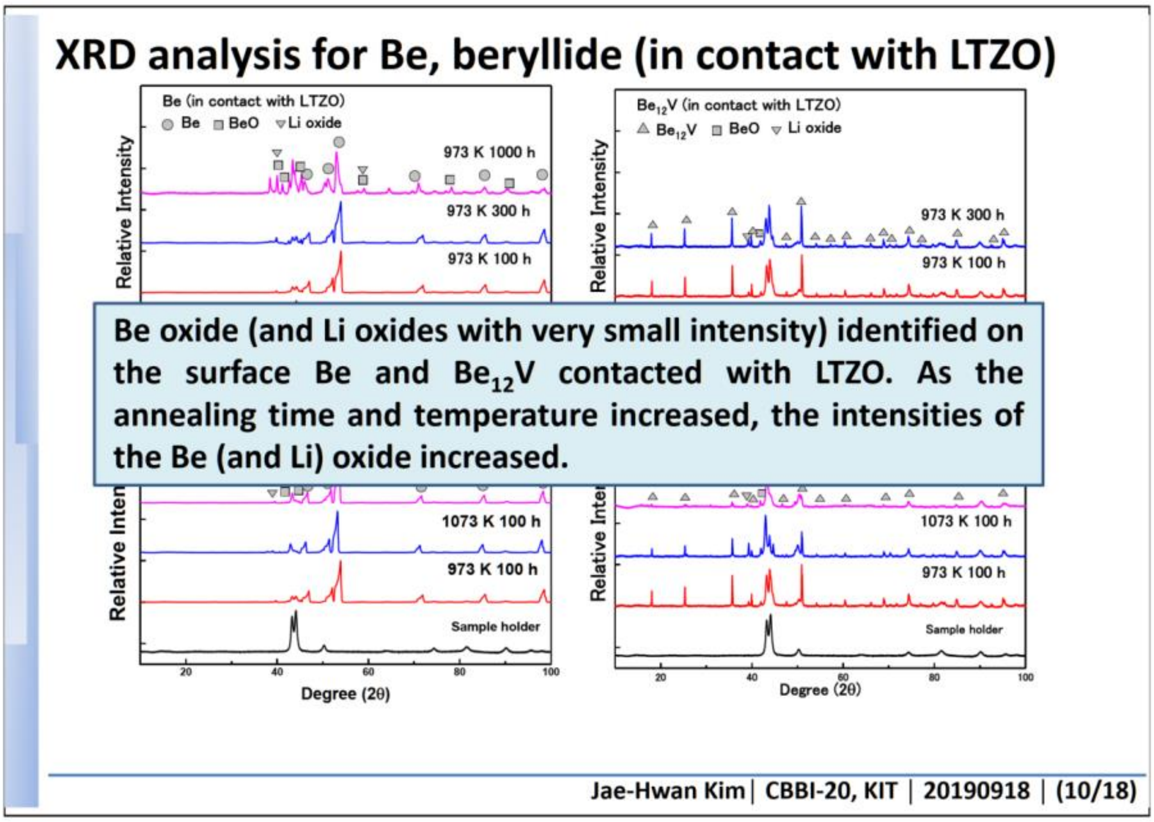
XRD analysis for Be, beryllide (in contact with LTZO)
Be (in contact with LTZO)
Be BeO Li oxide
973 K 1000 h
973 K 300 h
973 K 100 h
1073 K 100 h
Sample holder
Relative Intensity
Degree (2θ)
Be12V (in contact with LTZO)
Be12V BeO Li oxide
Be oxide (and Li oxides with very small intensity) identified on the surface Be and Be12V contacted with LTZO. As the annealing time and temperature increased, the intensities of the Be (and Li) oxide increased.
Jae-Hwan Kim | CBBI-20, KIT | 20190918 | (10/18)

XRD analysis for LTO,LTZO (in contact with Be, $Be_{12}V$)

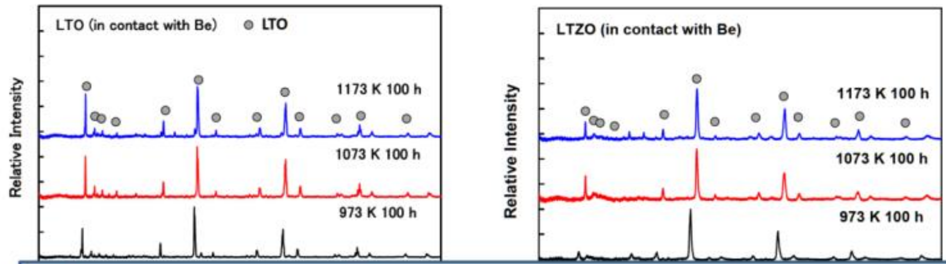

There was no new peaks as temperature and time increases.

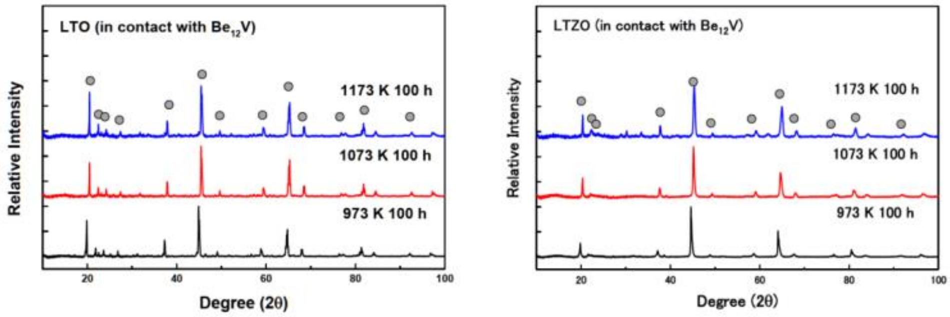

XRD analysis for LTO (in contact with Be, $Be_{12}V$)

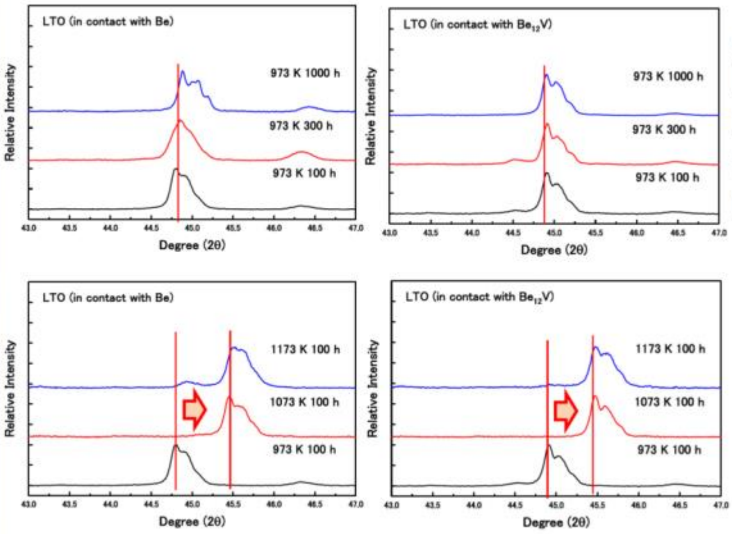

At 973 K, there was no big variation of LTO peak. However, above 1073 K, the peak shifted to higher degree.

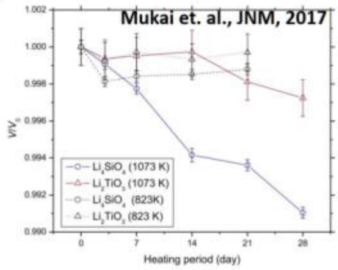

As the Li evaporated as a oxide type, the lattice shrinks and the lattice constant decreases. The decrease contributes the increase of degree. This is in a good agreement with results previously reported.

Summary

Taking into account the mixing pebble packing concept, compatibility test of each functional material should be clarified. In this study, Be/LTO, Be/LTZO, $Be_{12}V$/LTO, $Be_{12}V$/LTZO samples were tested at 973, 1073, 1173 K for 100, 300, and 1000 h. The results obtained as follows,

(1) Oxides (relating Be, Li) were formed on the surface of multipliers (Be, $Be_{12}V$) as results of XRD and EPMA analyses.

(2) It was clear that the thickness zone of Be in contact with breeders may reach into 2000 μm, which is not allowable at 973 K for the mixing pebble concept while that of beryllide does about 30~77 μm.

Jae-Hwan Kim | CBBI-20, KIT | 20190918 | (17/18)

(3) $Be_{12}V$ indicated lower reaction growth rates by one to three orders of magnitude than Be

(4) With respect to the recycling process of multiplier,
Li elimination as an impurity from multipliers would be available by means of the plasma sintering process, which is one of processes for pebbles fabrication (combination of plasma sintering and rotating electrode process for rods and pebbles, respectively).

For the future plans, compatibility tests using pebbles (Be, $Be_{12}V$, LTO, LTZO) will be performed and the results will be presented soon.

Jae-Hwan Kim | CBBI-20, KIT | 20190918 | (18/18)

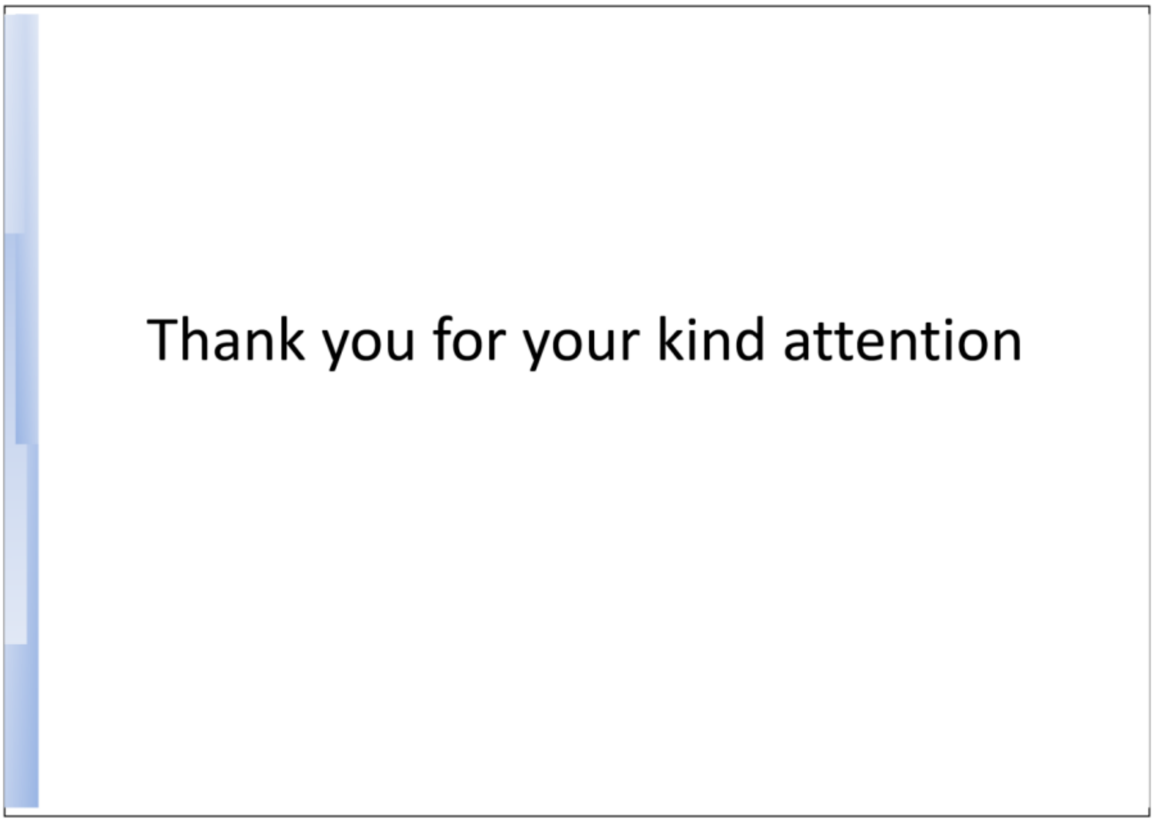
Thank you for your kind attention

Simulation of oxidation reaction between Be pebble beds and steam in WCCB blanket during in-box LOCA

Xiaoman Cheng[1], Andrei Khodak[2], Lei Chen[1], Songlin Liu[1]

[1] Institute of Plasma Physics, Chinese Academy of Sciences, Hefei, 230031, China.

[2] Princeton Plasma Physics Laboratory, Princeton, NJ08543, USA.

The Water Cooled Ceramic Breeder (WCCB) blanket is one of the blanket candidates for Chinese Fusion Engineering Test Reactor (CFETR). The WCCB blanket employs Beryllium/Beryllide as neutron multiplier in the form of pebble beds. In case of in-box Loss of Coolant Accident (LOCA), cooling channels inside the blanket module are broken, causing leakage of high temperature and high pressure water coolant into Beryllium pebble beds. The water coolant will vaporize instantly. Then the Be-steam reaction will take place. The reaction is exothermic and produces hydrogen, threatening the safety of the blanket system, as well as the fusion reactor. Therefore safety analyses of Be-steam reaction in the WCCB blanket during in-box LOCA should be investigated to prevent serious damage.

The simulation of Be-steam reaction was carried out by two steps. In Step 1, system analysis code RELAP5 was employed to model the WCCB blanket modules and the Primary Heat Transfer System (PHTS) of blankets. Then in-box LOCA with different break areas was simulated to figure out responses of the blanket module and the PHTS. Transient thermal hydraulic parameters were analyzed, including mass flow rate at the break, pressure of the gas in the pebble beds, temperature of steam, etc.

In Step 2, a 3D model of the whole blanket module was analyzed using computational fluid dynamic code ANSYS CFX. In the numerical model, pebble beds were introduced as porous media. The Be-steam reaction rate was obtained from experiment results in literature, depending on temperature and reactant concentration. For in-box LOCA transient, multicomponent flow was considered, consisting of a homogenous mixture of helium purge gas, steam and hydrogen. Sink and source terms of reactants and products were defined for the transient process involving multi-fluids and solids. The breach on the coolant channel was introduced into the 3D geometry as a steam volume source and coolant volume sink. Results from Step 1 were applied as boundary conditions. According to the current result, the local high pressure and high steam velocity should be the major concern and mitigation methods should be put forward. As for the impact of Be-steam reaction, the initial temperature is relatively low for acceleration of the reaction. The impact is limited at the initial stage. More analyses and optimization should be carried out in the next step.

ASIPP PPPL

Simulation of oxidation reaction between Be pebble beds and steam in WCCB blanket during in-box LOCA

Xiaoman Cheng[1], Andrei Khodak[2], Lei Chen[1], Songlin Liu[1]

[1] *Institute of Plasma Physics, Chinese Academy of Sciences, Hefei, 230031, China.*

[2] *Princeton Plasma Physics Laboratory, Princeton, NJ 08543, USA*

CBBI-20, 18-20 September 2019, Karlsruhe, Germany

2019/11/22 1

ASIPP

Outline

- Introduction
- Be-steam reaction mechanism
- RELAP5 simulation
- CFX simulation
- Conclusions

2019/11/22 2

Introduction: Overview of the WCCB

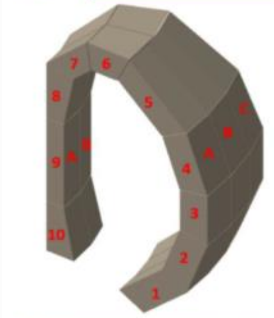

Blanket sector segmentation

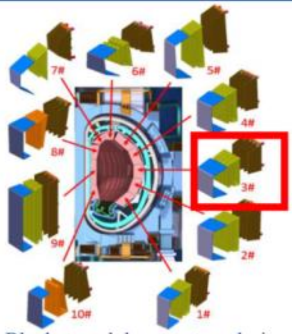

Blanket modules structure design

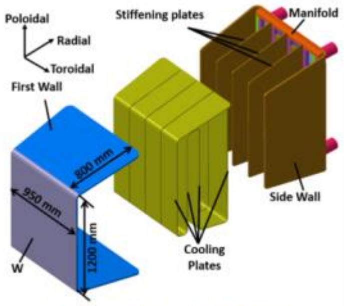

Blanket 3# exploded view

- Based on previous version (R=5.7 m)
- 16 blanket sectors in CFETR
- 5×3 outboard blankets (OBs) and 5×2 inboard blankets (IBs) in one sector
- 3~4 layers of mixed pebble beds of Li_2TiO_3 and $Be_{12}Ti$ as breeder
- 2 layers of Be pebble beds as separate multiplier in every blanket module
- W armor, RAFM steel structure

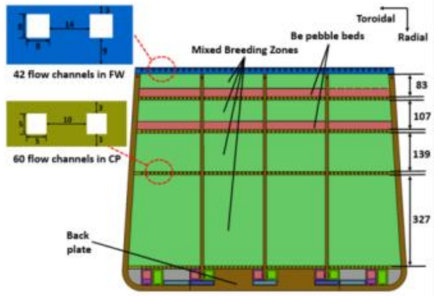

2019/11/22

Blanket 3# sectional view

Introduction: Purge gas system

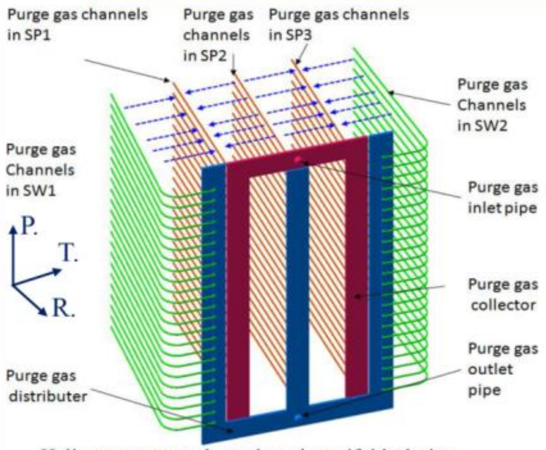

Helium purge gas channels and manifolds design

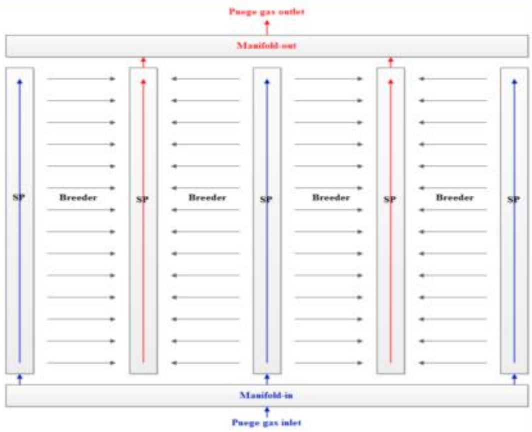

Helium purge gas flow scheme

- Helium gas flowing toroidally to reduce pressure drop
- System pressure 0.1-0.3 MPa-- 0.2 MPa in calculation
- Inlet velocity 0.01-0.1 m/s-- 0.05 m/s as target
- Inlet temperature 600 K -- TBD, water coolant at ~598 K in SPs

2019/11/22 4

Be-steam reaction mechanism

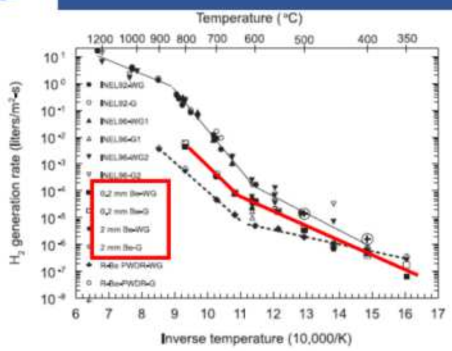

Fig. 3. Comparison of average H_2 generation rates for Be pebble and powder material with those for fully dense CPM-Be.

Table 1
BET specific surface area analyses

Sample type	Nominal diameter	Specific surface area (m^2/g)
2 mm pebble	2 mm	0.12
0.2 mm pebble	0.2 mm	0.24
CBP-56-1 powder	31.3 μm	0.69
CBP-56-2 powder	30.1 μm	0.66
CBP-56-3 powder	29.1 μm	0.67
CBP-30-1 powder	14.1 μm	1.21
CBP-30-2 powder	19.1 μm	1.05
DBP-30 powder	20.5 μm	1.04

R. A. Anderl, et al. Steam chemical reactivity of Be pebbles and Be power. J Nuc. Mater. 283-287 (2000) 1463-1467.

$Be+H_2O \rightarrow BeO+H_2$-370 kJ/mol

- Reaction rate proportional to temperature, for 0.2 mm pebbles:
  - <673 K, parabolic
  - 723-873 K, combination of parabolic and paralinear
  - 973 K, paralinear and accelerating
  - 1073 K, autocalitytic
- Reaction rate proportional to surface area of Be
- Experimental data for 1 mm pebbles not found, use experimental data of 0.2 mm pebbles for conservative consideration

RELAP5 simulation: System model

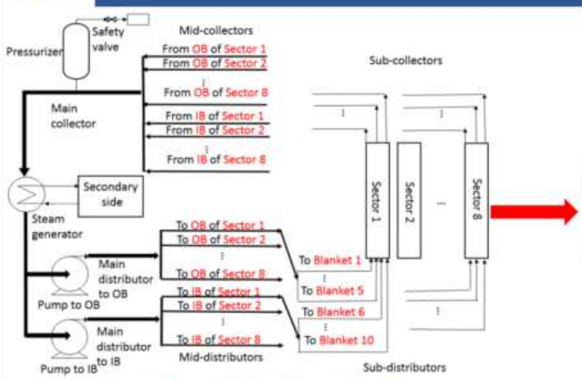

One loop of Primary Heat Transfer System

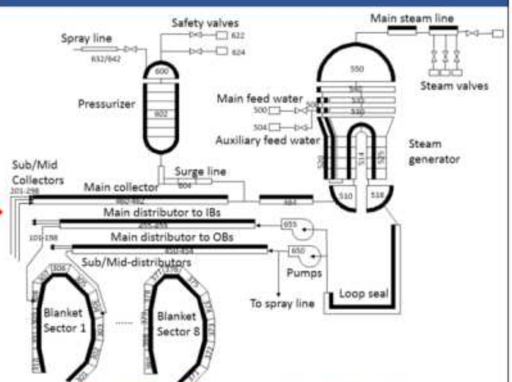

RELAP5 nodalization of one PHTS loop

- 2 identical and independent loops in WCCB blanket PHTS, each feeding 8 sectors
- IB line and OB line fed by 2 pumps
- System components like pumps, pressurizer and steam generator referring to PWR design for the current design stage
- 8 sectors modeled separately with same geometry but different space angles

Main parameters of WCCB PHTS

Items	Unit	Parameters
Operation pressure	MPa	15.5
I/O temperature	K	553/598
Total mass flow	kg/s	1050.0
Total water volume	m^3	~175
Total water inventory	kg	~1.26e5
Pressure drop of IB/OB sector	MPa	0.68
Total pressure drop	MPa	0.89

2019/11/22 6

RELAP5 simulation: In-box LOCA

In-box Loss of Coolant Accident process

Time (s)	Events	Heat load
t=0	Initial condition from the steady state	Full loads
$0 \leq t < 10$	Normal operation	
$t_0=10$	Break of 1/15/180 CP1 channels in blanket 3 sector 1	
t_1	Pressure in purge gas pipe > 0.4 MPa, TES isolated Be-steam reaction	
$t_2=t_1+3$	Plasma disruption Pump coast down	Decay heat with additional plasma disruption loads, reaction heat
$t_3>t_2$	Pressure > 2 MPa, rupture disks open	Decay heat

- Break of one lumped module considered
- Consecutive break for 1 channel break of CP1
- Double-ended break for 15 channels break and 180 channels break
- Porosity of all pebble beds lumped as one volume

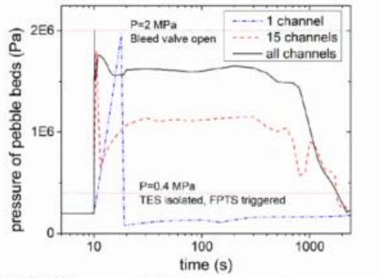

Pebble beds porosity pressure

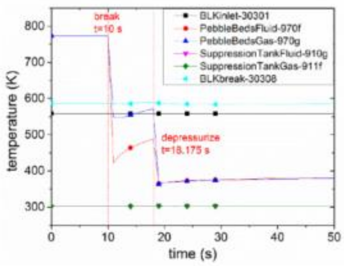

Temperature in case of 1 channel break

2019/11/22 7

RELAP5 simulation: BC for CFX

- Important timing
  - 0 s, break flow
  - 0.775 s, TES isolated, He inlet flow=0 kg/s
  - 3.775 s, plasma disruption
- Heat sources
  - Decay heat: Be, breeder, steel, water (from 3.775s)
  - FW surface heat flux (from 3.775 s)
- Boundary conditions (fit as red dots)
  - Break steam flow rate (ramp-up in 1s, 1/3 of lumped flow)
  - Break steam temperature
  - Water coolant inlet flow rate (1/3 of lumped flow)
  - Water coolant inlet flow temperature

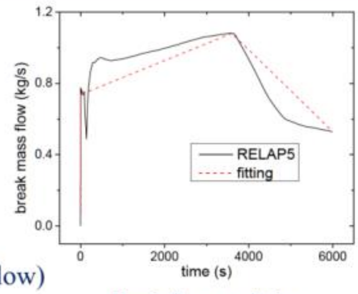

Break flow rate fitting

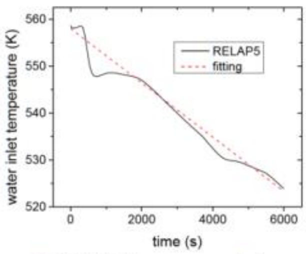

Water inlet temperature fitting

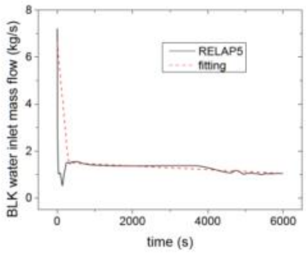

Water inlet flow rate fitting

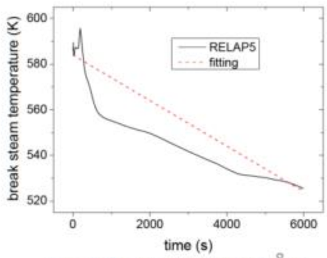

Break flow temperature fitting

2019/11/22 8

CFX simulation: Numerical model

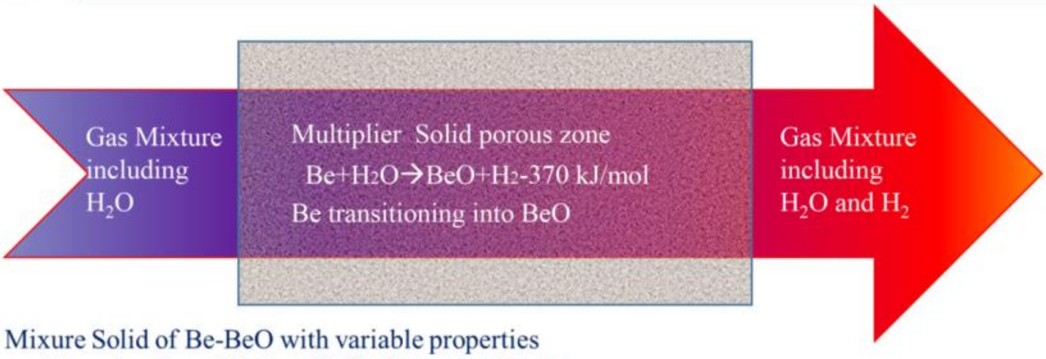

Mixure Solid of Be-BeO with variable properties

- Mass fraction of BeO: $\varkappa(0,1)$~time, temperature
- Mixture density: $\rho_s = \frac{1}{\frac{(1-\varkappa)}{\rho_{Be}}+\frac{\varkappa}{\rho_{BeO}}}$
- Mixture molar mass: $\mu_s = \frac{1}{\frac{(1-\varkappa)}{\mu_{Be}}+\frac{\varkappa}{\mu_{BeO}}}$
- Mixture specific heat capacity: $c_p = c_{pBe}(1-\varkappa) + c_{pBeO}\varkappa$
- Volume fraction of BeO: $\epsilon = \frac{\varkappa\rho_s}{\rho_{BeO}} = \frac{\varkappa}{\frac{(1-\varkappa)\rho_{BeO}}{\rho_{Be}}+\varkappa}$
- Mixture thermal conductivity: $\lambda = \lambda_{Be}(1-\epsilon) + \lambda_{BeO}\epsilon$

2019/11/22 9

CFX simulation: Numerical model

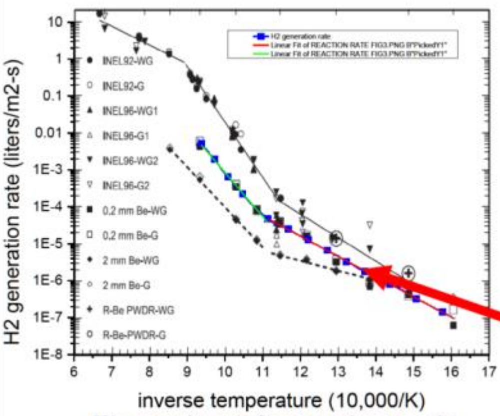

H2 generation rate from experiment results

$$\begin{cases} \dot{\rho}_{BeO} = \mu_{BeO} A_{fs} \frac{\dot{V}_{c\,linear}}{AC_s}[H_2O]^x[Be]^y \\ \dot{\rho}_{BeO} = \frac{\partial \rho_s \gamma_s \varkappa}{\partial t} \end{cases}$$

where:

$\dot{\rho}_{BeO}$-volumetric mass source of BeO [kg/m3-s]

μ_{BeO}-Molar mass of BeO [kg/mol]

A_{fs}-interface area density [1/m]

$\frac{\dot{V}_{c\,linear}}{A}$-H2 generation rate[m3/m2-s]

C_s-standard gas ratio, 0.0224 m3/mol

γ_s-solid volume ratio

Definition of source term for additional variable $\varkappa$:

$$\frac{\partial \rho_s \gamma_s \varkappa}{\partial t} = A_{fs} \frac{\dot{V}_{c\,linear}}{AC_s}[H_2O]^x[Be]^y$$

$$S_{BeO} = A_{fs} \frac{\dot{V}_{c\,linear}}{AC_s}[H_2O]^x[Be]^y$$

$$S_{H_2} = \frac{\mu_{H_2}}{\mu_{BeO}} S_{BeO}$$

$$S_{H_2O} = -\frac{\mu_{H_2O}}{\mu_{BeO}} S_{BeO}$$

$$\dot{q} = -\frac{Q}{\mu_{BeO}} S_{BeO}$$

2019/11/22 10

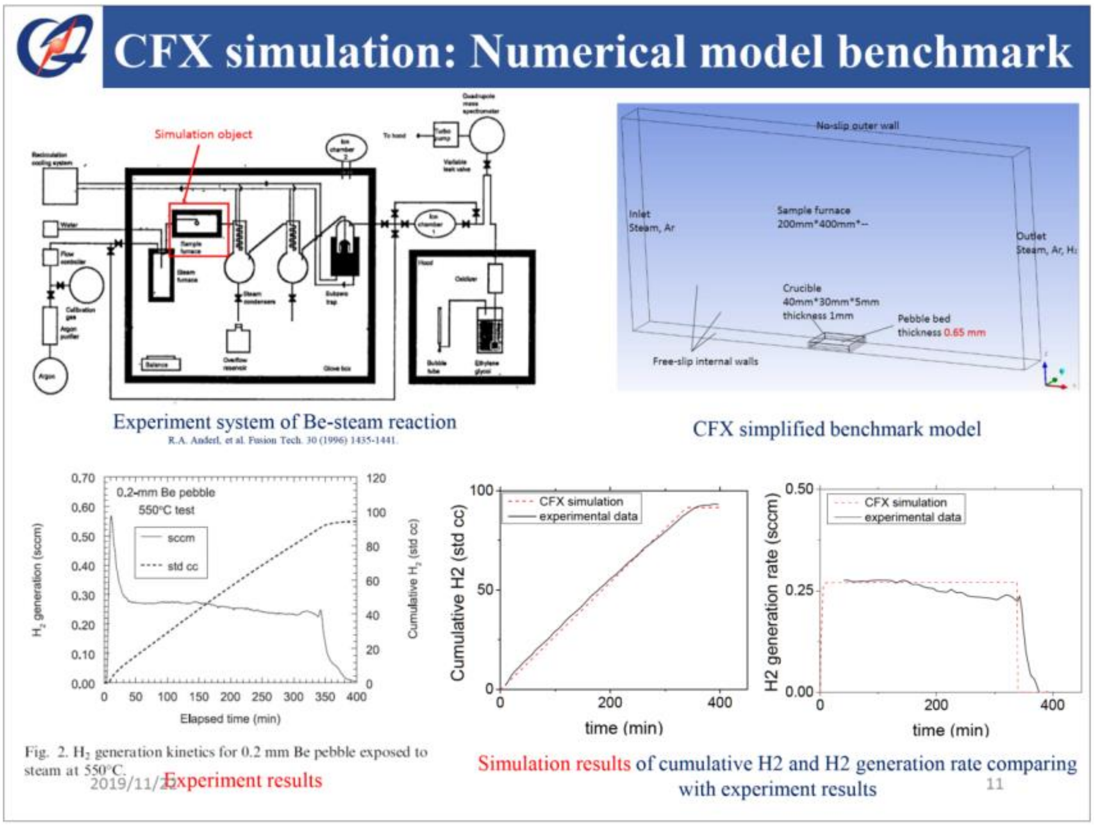
CFX simulation: Numerical model benchmark
Simulation object
Experiment system of Be-steam reaction
R.A. Anderl, et al. Fusion Tech. 30 (1996) 1435-1441.
No-slip outer wall
Inlet
Steam, Ar
Sample furnace
200mm*400mm*--
Outlet
Steam, Ar, H2
Crucible
40mm*30mm*5mm
thickness 1mm
Pebble bed
thickness 0.65 mm
Free-slip internal walls
CFX simplified benchmark model
0.2-mm Be pebble
550°C test
sccm
std cc
H2 generation (sccm)
Cumulative H2 (std cc)
Elapsed time (min)
Fig. 2. H2 generation kinetics for 0.2 mm Be pebble exposed to steam at 550°C.
2019/11/22
Experiment results
CFX simulation
experimental data
Cumulative H2 (std cc)
time (min)
H2 generation rate (sccm)
Simulation results of cumulative H2 and H2 generation rate comparing with experiment results
11

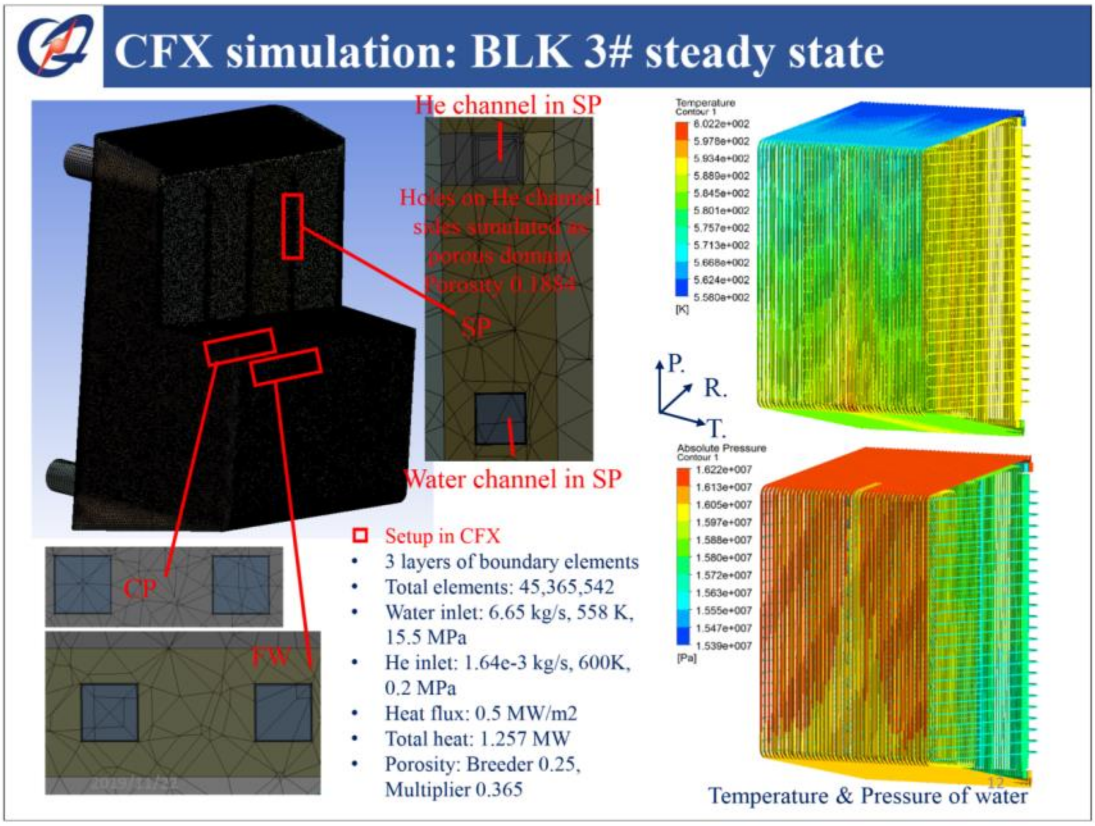
CFX simulation: BLK 3# steady state
He channel in SP
Holes on He channel sides simulated as porous domain
Porosity 0.1884
SP
Water channel in SP
CP
FW
Setup in CFX
3 layers of boundary elements
Total elements: 45,365,542
Water inlet: 6.65 kg/s, 558 K, 15.5 MPa
He inlet: 1.64e-3 kg/s, 600K, 0.2 MPa
Heat flux: 0.5 MW/m2
Total heat: 1.257 MW
Porosity: Breeder 0.25, Multiplier 0.365
Temperature
Contour 1
[K]
Absolute Pressure
Contour 1
[Pa]
P.
R.
T.
Temperature & Pressure of water
2019/11/22
12

CFX simulation: BLK 3# steady state

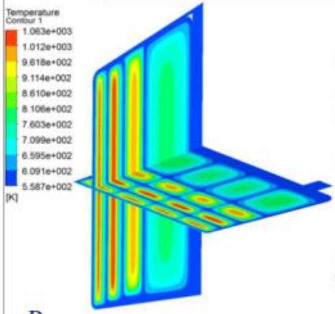

Temperature of each part

Part	Min temp.	Max temp.
Be	554 K	804 K
Breeder	544 K	1063 K
Steel	551 K	805 K
Water	558 K	602 K
He	564 K	664 K

✓ Temperature within the allowable limits

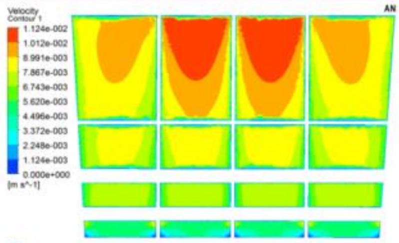

Velocity of purge gas in Breeder

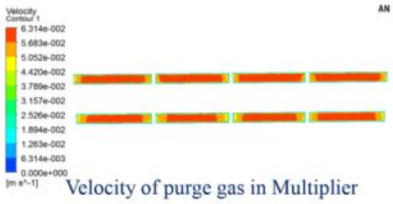

Velocity of purge gas in Multiplier

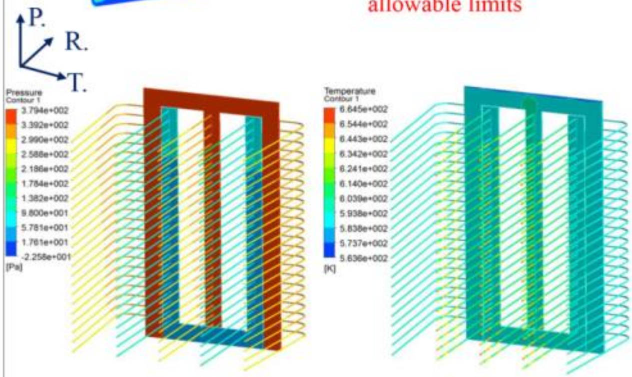

- Pressure drop in pebble beds ~380 Pa
- Ave. velocity in Be ~0.066 m/s
- Ave. velocity in breeder ~0.01 m/s

He manifolds & channels temperature & pressure

2019 13

CFX simulation: Transient setup V.1

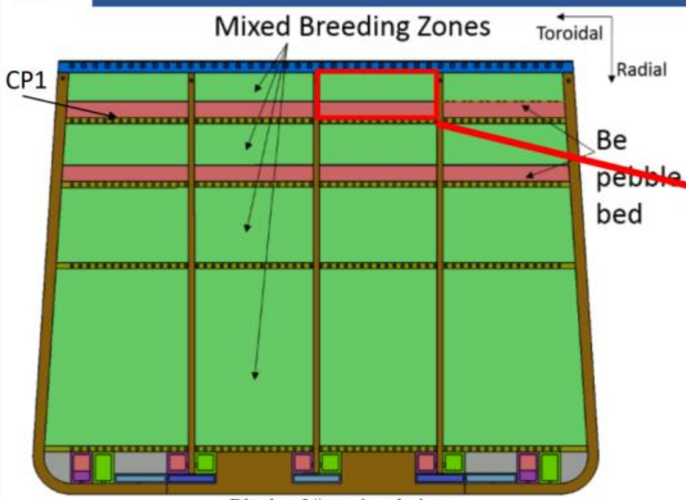

Blanket 3# sectional view

- 1 Channel break assumed on CP1
- 5*5 mm^2 square in the middle of Be1 as steam surface source, 5*5 mm^2 square in the middle of CP as water surface sink
- Multicomponent flow in pebble beds, including He, H_2 & steam
- Sink and source terms of reactants and products in Be pebble beds to simulate reaction

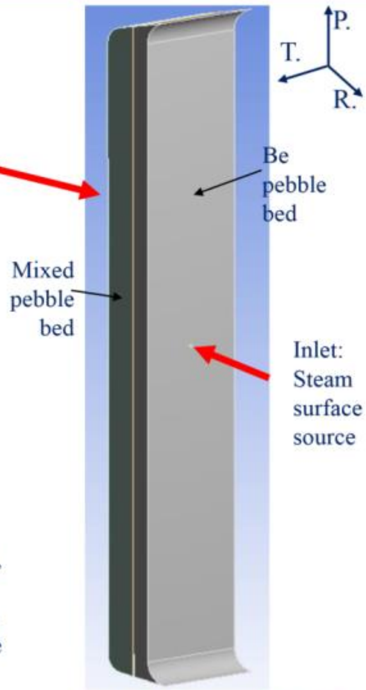

Be1 & BZ1 in one sub-module

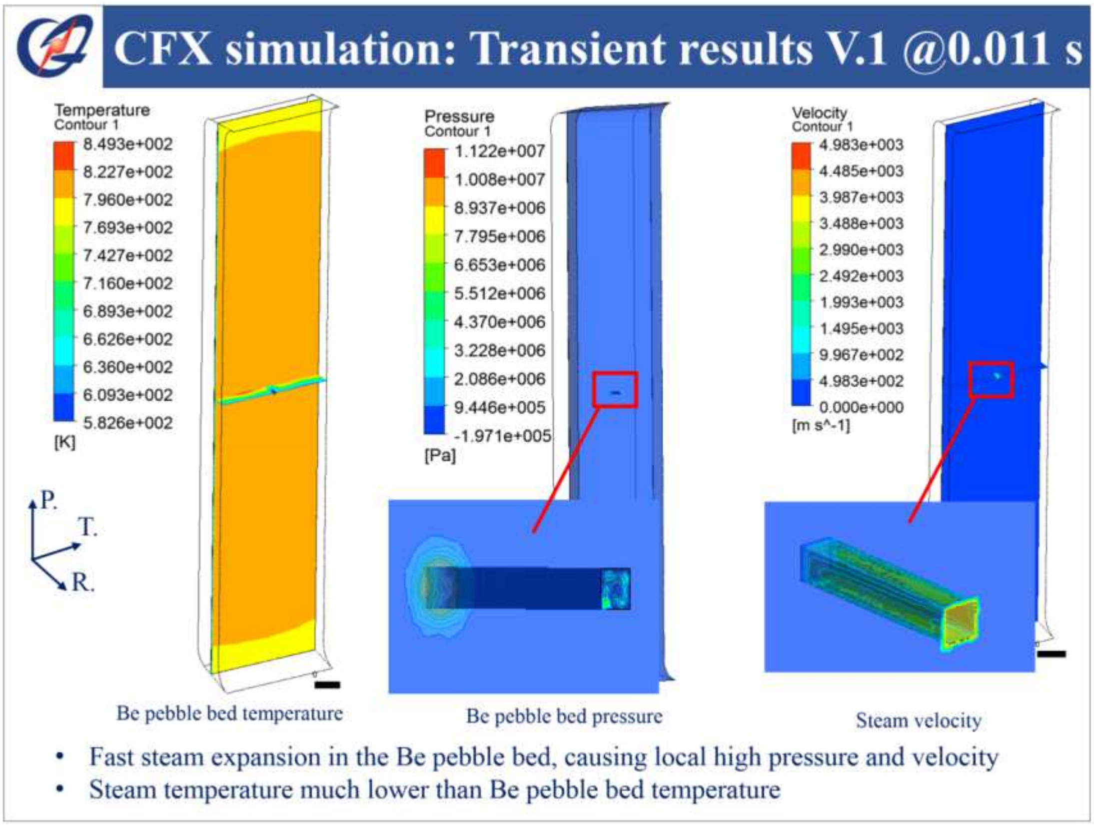
CFX simulation: Transient results V.1 @0.011 s
Temperature
Contour 1
8.493e+002
8.227e+002
7.960e+002
7.693e+002
7.427e+002
7.160e+002
6.893e+002
6.626e+002
6.360e+002
6.093e+002
5.826e+002
[K]
P.
T.
R.
Pressure
Contour 1
1.122e+007
1.008e+007
8.937e+006
7.795e+006
6.653e+006
5.512e+006
4.370e+006
3.228e+006
2.086e+006
9.446e+005
-1.971e+005
[Pa]
Velocity
Contour 1
4.983e+003
4.485e+003
3.987e+003
3.488e+003
2.990e+003
2.492e+003
1.993e+003
1.495e+003
9.967e+002
4.983e+002
0.000e+000
[m s^-1]
Be pebble bed temperature
Be pebble bed pressure
Steam velocity
• Fast steam expansion in the Be pebble bed, causing local high pressure and velocity
• Steam temperature much lower than Be pebble bed temperature

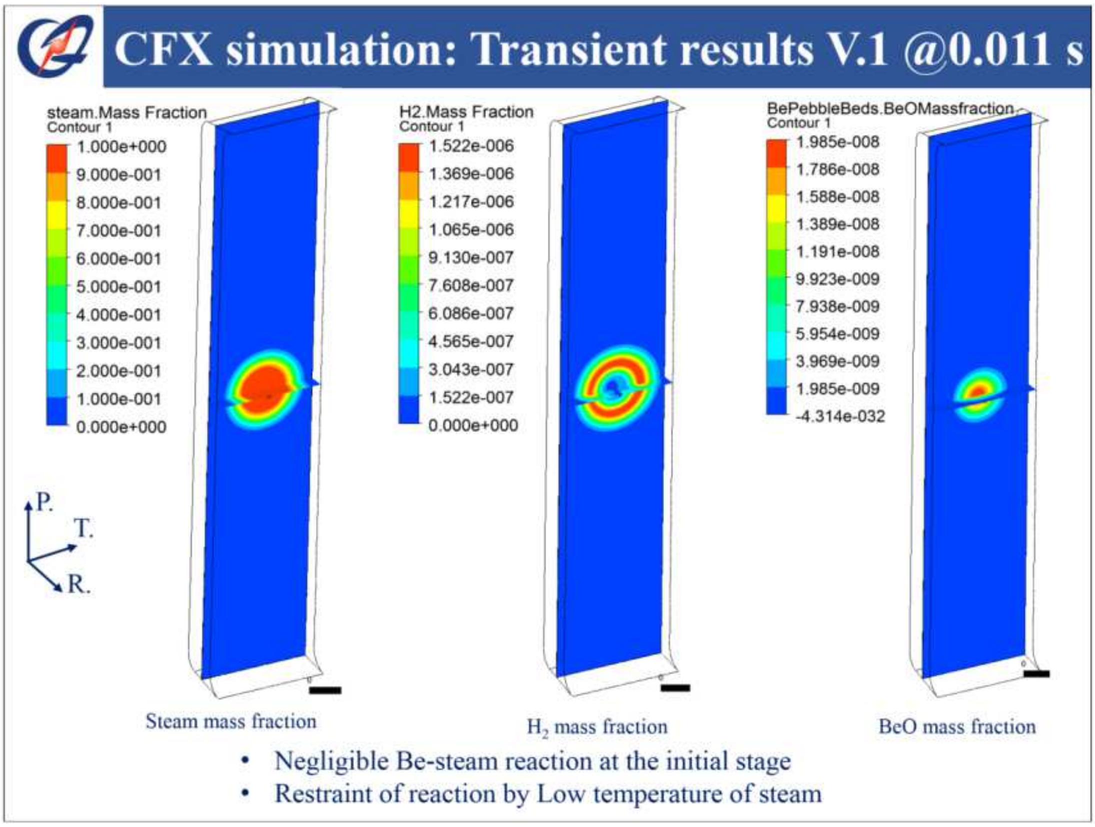
CFX simulation: Transient results V.1 @0.011 s
steam.Mass Fraction
Contour 1
1.000e+000
9.000e-001
8.000e-001
7.000e-001
6.000e-001
5.000e-001
4.000e-001
3.000e-001
2.000e-001
1.000e-001
0.000e+000
P.
T.
R.
H2.Mass Fraction
Contour 1
1.522e-006
1.369e-006
1.217e-006
1.065e-006
9.130e-007
7.608e-007
6.086e-007
4.565e-007
3.043e-007
1.522e-007
0.000e+000
BePebbleBeds.BeOMassfraction
Contour 1
1.985e-008
1.786e-008
1.588e-008
1.389e-008
1.191e-008
9.923e-009
7.938e-009
5.954e-009
3.969e-009
1.985e-009
-4.314e-032
Steam mass fraction
H_2 mass fraction
BeO mass fraction
• Negligible Be-steam reaction at the initial stage
• Restraint of reaction by Low temperature of steam

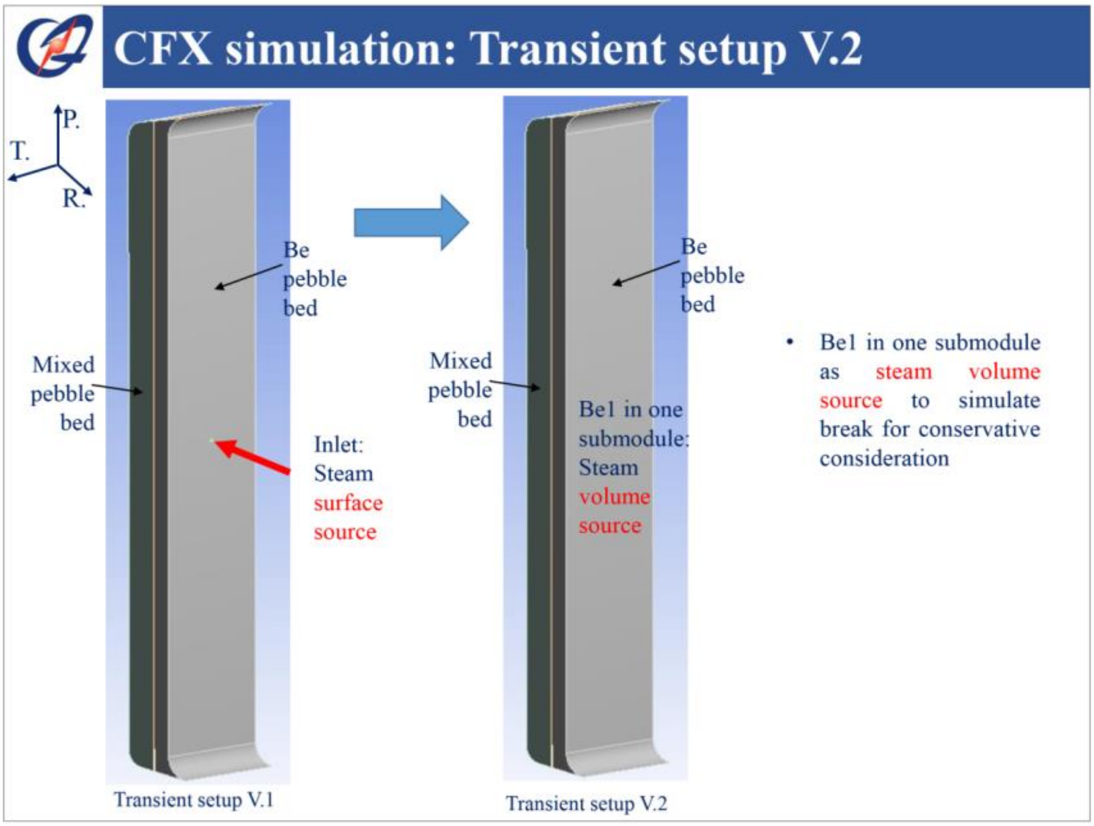
CFX simulation: Transient setup V.2
P.
T.
R.
Be pebble bed
Mixed pebble bed
Inlet: Steam surface source
Be pebble bed
Mixed pebble bed
Be1 in one submodule: Steam volume source
• Be1 in one submodule as steam volume source to simulate break for conservative consideration
Transient setup V.1
Transient setup V.2

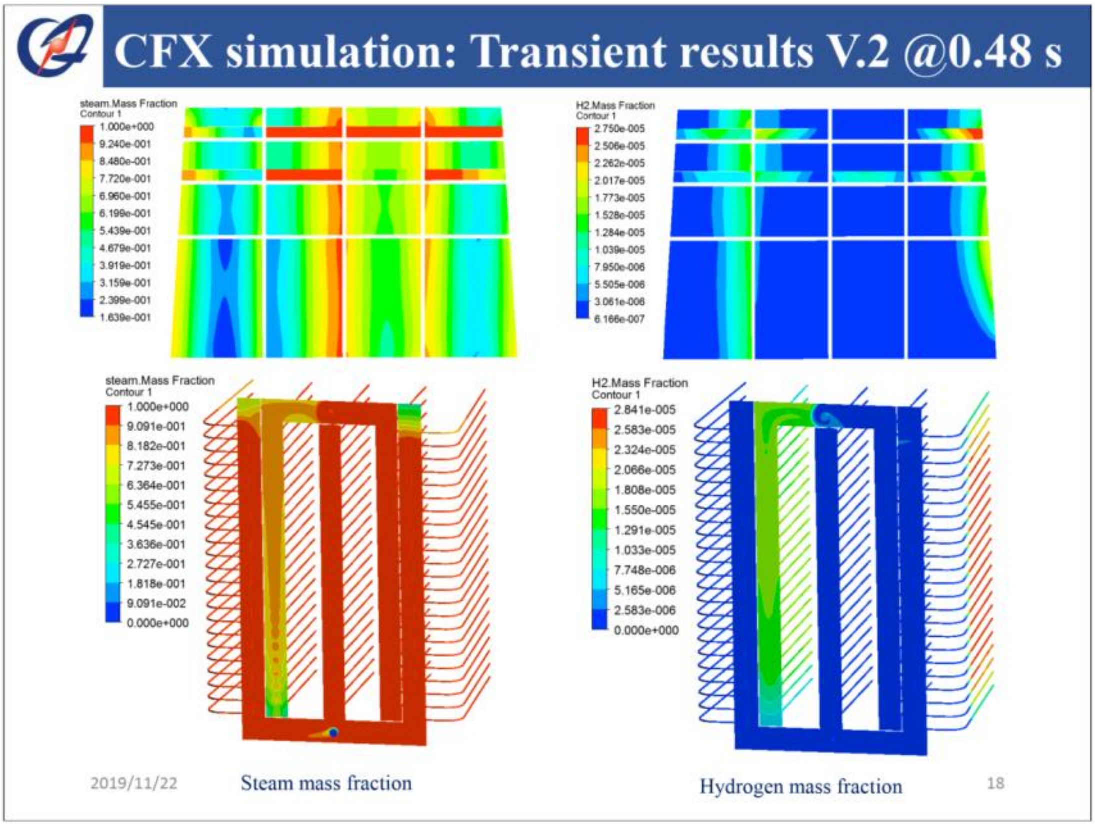
CFX simulation: Transient results V.2 @0.48 s
steam.Mass Fraction
Contour 1
H2.Mass Fraction
Contour 1
steam.Mass Fraction
Contour 1
1.000e+000
9.091e-001
8.182e-001
7.273e-001
6.364e-001
5.455e-001
4.545e-001
3.636e-001
2.727e-001
1.818e-001
9.091e-002
0.000e+000
H2.Mass Fraction
Contour 1
2.841e-005
2.583e-005
2.324e-005
2.066e-005
1.808e-005
1.550e-005
1.291e-005
1.033e-005
7.748e-006
5.165e-006
2.583e-006
0.000e+000
2019/11/22
Steam mass fraction
Hydrogen mass fraction
18

CFX simulation: Transient results V.2 @0.48 s

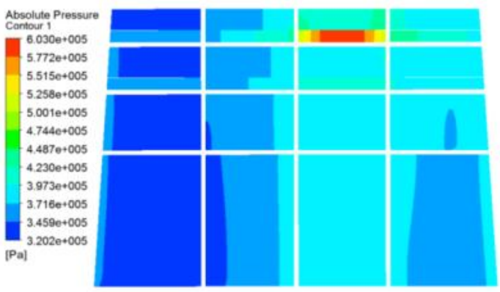

Pressure of pebble beds

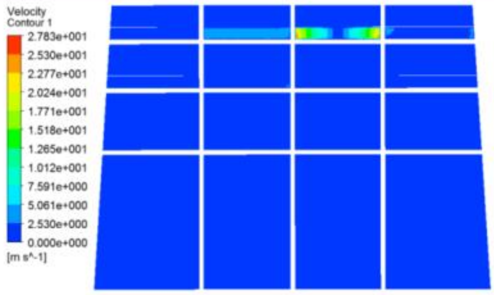

Velocity of pebble beds

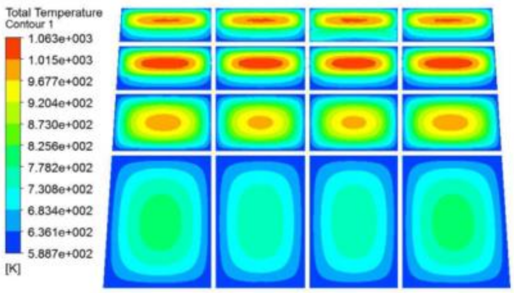

Temperature of pebble beds

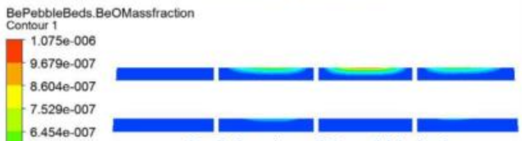

BeO fraction of Be pebble beds

- Steam permeation into all pebble beds through SP due to toroidal purge gas scheme
- Local high pressure and velocity
- Calculation to be continued

Conclusions

- Be-steam reaction during in-box LOCA of WCCB blanket was simulated in two steps.
- In Step 1, RELAP5 was used to model the WCCB PHTS and simulate in-box LOCA so as to provide boundary conditions for CFX simulation.
- In Step 2, a numerical model was proposed for Be-steam simulation. Benchmark results agreed well with the experimental data.
- Then whole 3D module of BLK 3# was modeled in CFX to simulate the Be-steam reaction during in-box LOCA.
- The initial temperature is relatively low for acceleration of the Be-steam reaction. The impact is limited at the initial stage.
- More consideration should be taken to the issue of local high pressure and velocity during the transient.
- WCCB blanket has been updated to avoid the use of Be. The oxidation reaction of $Be_{12}Ti$ and steam will be evaluated in the next step.

ASIPP PPPL

Thank you for your attention!

2019/11/22 21

Test facility for tritium permeation measurements of containment materials and coatings under breeder blanket relevant conditions

Simon Steel, Richard Walker, Zoltan Kollo

United Kingdom Atomic Energy Authority, Culham Science Centre, Oxfordshire, UK

Here we present a forthcoming automated test system for investigating tritium permeation through proposed breeder blanket containment materials (with / without coatings) under conditions specifically relevant to ceramic breeder blanket modules.

Hydrogen isotope permeation is problem throughout the fusion fuel cycle. It leads to difficulty with inventory monitoring, complications in coolant processing, changes to material properties, reduced breeder module efficiency, and increased total tritium inventory. Much of the work investigating permeation reduction has been conducted with protium and deuterium however, due to the differences in the sorption and diffusion characteristics of the hydrogen isotopes, and the specific radio-chemistry issues associated with tritium, it is vital that these materials be examined in operation relevant conditions.

The first phase of this work will deliver the ability to subject one surface of 100mm discs of structural material (such as Eurofer 97, SS316-L, etc.) to bespoke mixtures of tritium and helium (maximum total pressure of 1 Bar) where the desired composition can be maintained for long periods (upwards of one month). The sample region can be heated to around 500°C (in line with ITER and DEMO expected conditions). The mounting flange for the sample has been specially designed to protect deposited coatings while providing a high level of containment. The other side of the sample is exposed to high vacuum where a turbomolecular pump draws permeated molecules to a suite of measurement instruments (Beta Induced X-ray Spectroscope, Ionisation Chamber, Quadrupole Mass Spectrometer). The design also incorporates a dedicated measurement suite for the gas feedstock and the ability to sample the upstream gas with the QMS.

Investigations are already underway to extend the capability of this system to incorporate water vapour in the gas mixture, gas flow across the sample surface, and expanded pressure / temperature ranges.

Phase one is expected to be operational in late 2019. The results of the first full experimental runs (conducted with samples provided by ENEA - Brasimone) should be available by Q3 2020.

This work has been carried out within the framework of the EUROfusion Consortium and has received funding from the Euratom research and training programme 2014-2018 and 2019-2020 under grant agreement No 633053. The views and opinions expressed herein do not necessarily reflect those of the European Commission.

Behavior of ceramic breeder candidates to high-energy ion beams

M. González, M. Malo and F. Sánchez

LNF_CIEMAT, Avda Complutense, 40. 28040 Madrid, Spain

Following an experimental approach towards the progress on the simulation of tritium diffusion and release, accelerated ions were used to implant hydrogen isotopes but also to produce damage on the ceramic breeder crystalline structure. Experimental results based on characterization of the irradiated structure and depth profile analytical techniques are discussed aiming to approach the transport mechanisms of hydrogen isotopes through the breeder crystalline network and to those features able to trap the bred tritium.

Ion irradiation on candidate ceramic breeders was performed at the CMAM's high-energy ion accelerator facility, Madrid, Spain. Although compacted discs from milled pebbles were firstly used, the direct implantation on pebbles was the main objective and therefore a special sampleholder was previously designed to assure the implantation pebble volume directly exposed to the subsequent analytical techniques. H and D ions were implanted at energies ranging from few keV to several MeV, while damage was achieved using O and Si self-ion beams in the MeV energy scale.

Several techniques were applied to characterize the structural modifications and the produced defects due to the high-energy ion beam interaction. SIMS in-depth profiles and initial EPR analyses indicate that ion irradiation does not induce new defects although the concentration of intrinsic defects increases. Thermal-induced gas desorption was also applied. Results denote the sequential release of the implanted deuterium trapped in intrinsic and ion induced defects but also its self-diffusion towards surface at room temperature. By means of GIXRD, the high resistance to ion irradiation of these materials is concluded: even after high radiation dose, a high degree of crystallinity is conserved, the crystalline network distortion only being represented. Nevertheless, it is suggested the need of further studies using analytical techniques to systematically correlate the ion radiation-induced defects with their role in the diffusion of hydrogen isotopes through a damaged breeder structure.

EUROfusion

Behavior of ceramic breeder candidates under high-energy ion beams

M. González, M. Malo, F. Sánchez

Experimental approach to the understanding of
T transport into and release out of the solid breeder microstructure
Study H-isotopes – He synergies
Assess the active trapping centres involved

Simulation of bred T presence after n transmutation
Using characterization and analytical techniques to evaluate the irradiated structure and analyze the ions depth profiles.

OUTLINE

- INTRODUCTION
- AIM
- EXPERIMENTAL APPROACH
- WHY USING IONS?
- PRELIMINARY RESULTS ON H IMPLANTATION
- FIRST CONCLUSIONS
- 2020 ACTIVITIES

INTRODUCTION

From previous studies ….

- On ACB pebbles supplied by KIT but previously on commercial LOS and LMT
- On D surface absorption followed by thermally induced desorption
- at different environments (temp, rad, …)

results indicate that …

- D desorption is almost completed at relevant reactor's temperature (>500 °C) .
- Ionizing radiation during desorption give rise to a more efficient release process.

AIM

PROGRESSING on
the definition of H-isotopes and He ion diffusion and release processes
through candidate ceramic breeder microstructure
(from inside grains towards surface)
at close to the HCPB BB operational conditions

retention due to damage?
role of defects?

EXPERIMENTAL APPROACH

- **Ion implantation**
- **Structural characterization**
- **Thermal-induced desorption**

EXPERIMENTAL APPROACH

✧ Ion implantation

KIT supplied
Advanced Ceramic Breeder (ACB) pebbles:
Li4SiO4+ X% Li2TiO3

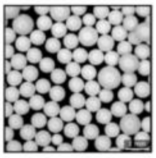

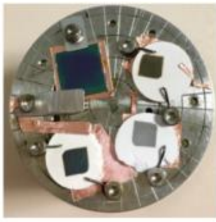

pellets-from-pebbles samples

1.- dehydrated @400ºC/2hs in vacuum
2.- crushed to powder
3.- pressed into 15 mm dia discs

EXPERIMENTAL APPROACH

✧ Ion implantation

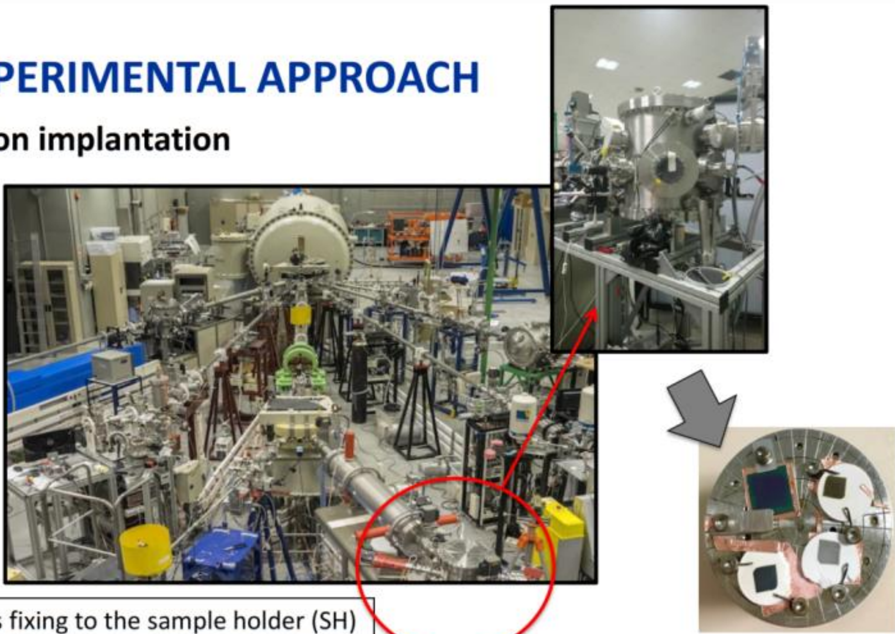

I. Discs fixing to the sample holder (SH)
II. SH location in the irradiation chamber
III. ion irradiation at RT in high vacuum

why use ions?

an experimental tool recommended in the Fusion Roadmap to simulate neutron effect

PROS

- rapid
- low cost,
- no radioactive final samples = immediate use
- control of variables such as dose, dose rate, temperature, chemical and mechanical environment;

CONS

- local high temperatures could be generated
- small sample volumes are affected
- compared to that of neutrons collisions, events may vary

Results on H implantation

Thermal induced desorption of H isotopes

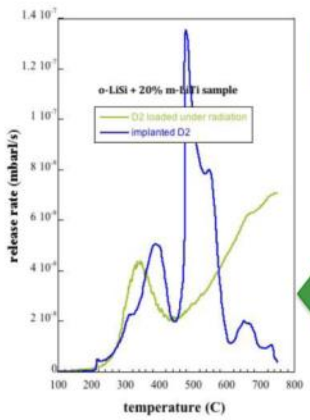

ceramic pellets-from-pebbles

deeply

D2 implantation

D2 desorption monitoring by TID

The surface structure, damaged during implantation, affects the desorption process by delaying the temperature for the maximum desorption rate up to 500ºC

Results on H implantation

Thermal induced desorption of H isotopes

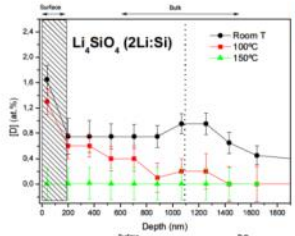

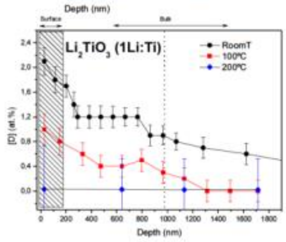

ceramic pellets-from-pebbles

deeply

D2 implantation

D2 depth profile by NRA (IBA technique)

- ***efficient diffusion***
- ***surface storage due to a wall effect***

E. Carella, M. González, R. Gonzalez-Arrabal. ***J.Nucl.Mater.****, 438 (2013) 193-198.*

Results on H implantation

Thermal induced desorption of H isotopes

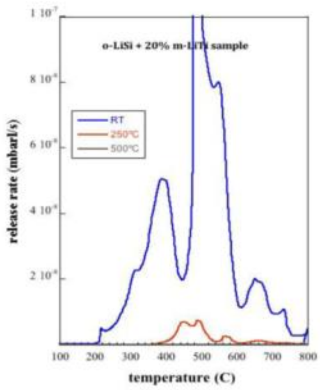

ceramic pellets-from-pebbles

deeply

D2 implantation

D2 desorption monitoring by TID

As expected, the higher the implantation temperature, the poor the desorption obtained as a consequence of an active release during implantation.

Easy gas release at high temperatures

Results on H implantation

Thermal induced desorption of H isotopes
on a pre-damaged structure

ceramic pellets-from-pebbles

Self-ion (O, Si) damage

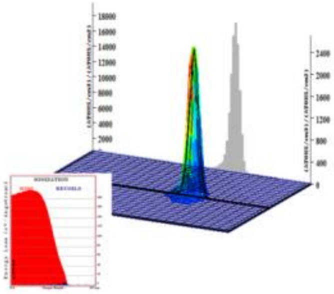

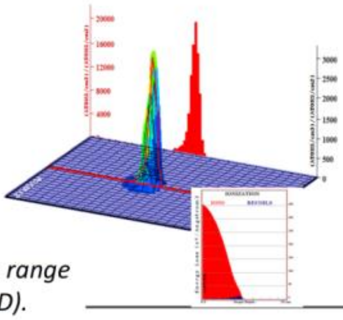

SRIM calculation of the ion profile
10 MeV O^{3+} (left) and 10 MeV Si^{3+} projected ion range
in a 10% porous Li_4SiO_4 sample (2,2 g/cm^3 TD).

Results on H implantation

Thermal induced desorption of H isotopes
on a pre-damage structure

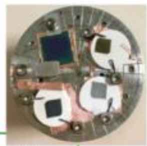

ceramic pellets-from-pebbles

Self-ion (O, Si) damage

IBIL Characterization

O^{3+} irradiation
emission at 420 nm

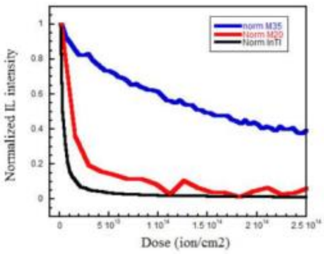

luminescence decay,
due to the annihilation of defect centres
or the induced matrix distortion

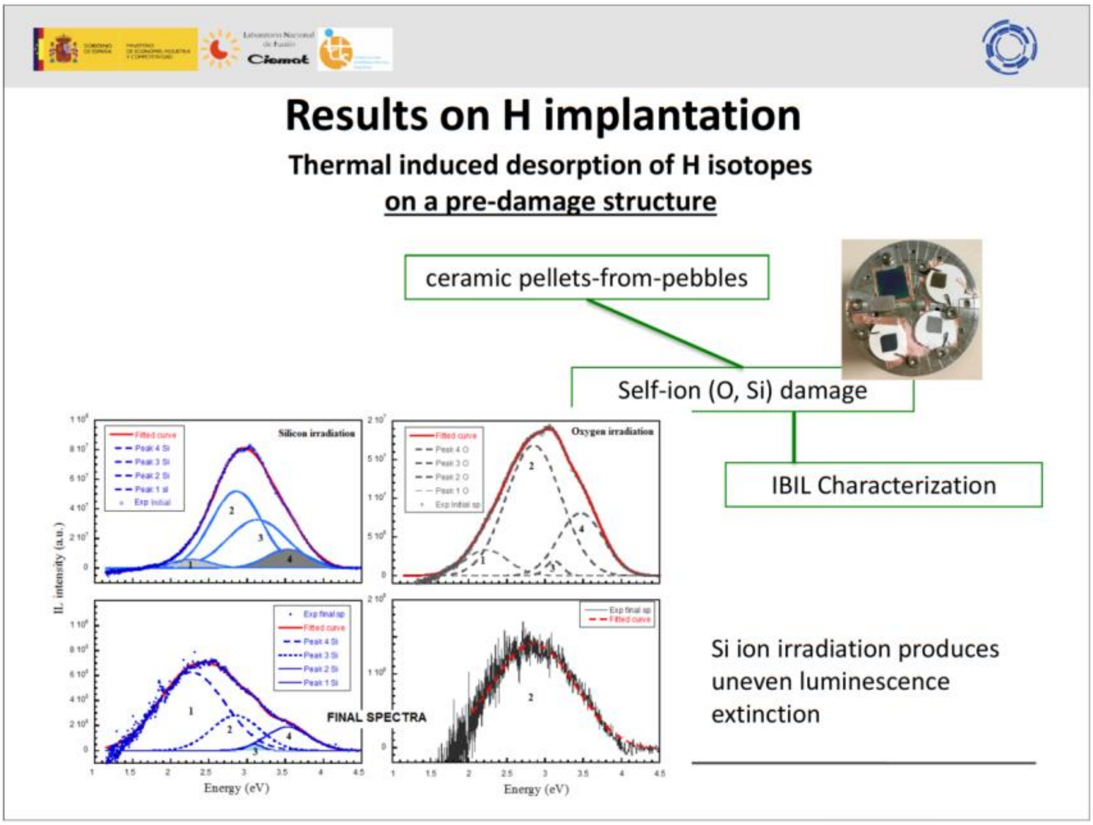
Results on H implantation
Thermal induced desorption of H isotopes
on a pre-damage structure
ceramic pellets-from-pebbles
Self-ion (O, Si) damage
IBIL Characterization
Silicon irradiation
Oxygen irradiation
FINAL SPECTRA
IL intensity (a.u.)
Energy (eV)
Si ion irradiation produces uneven luminescence extinction

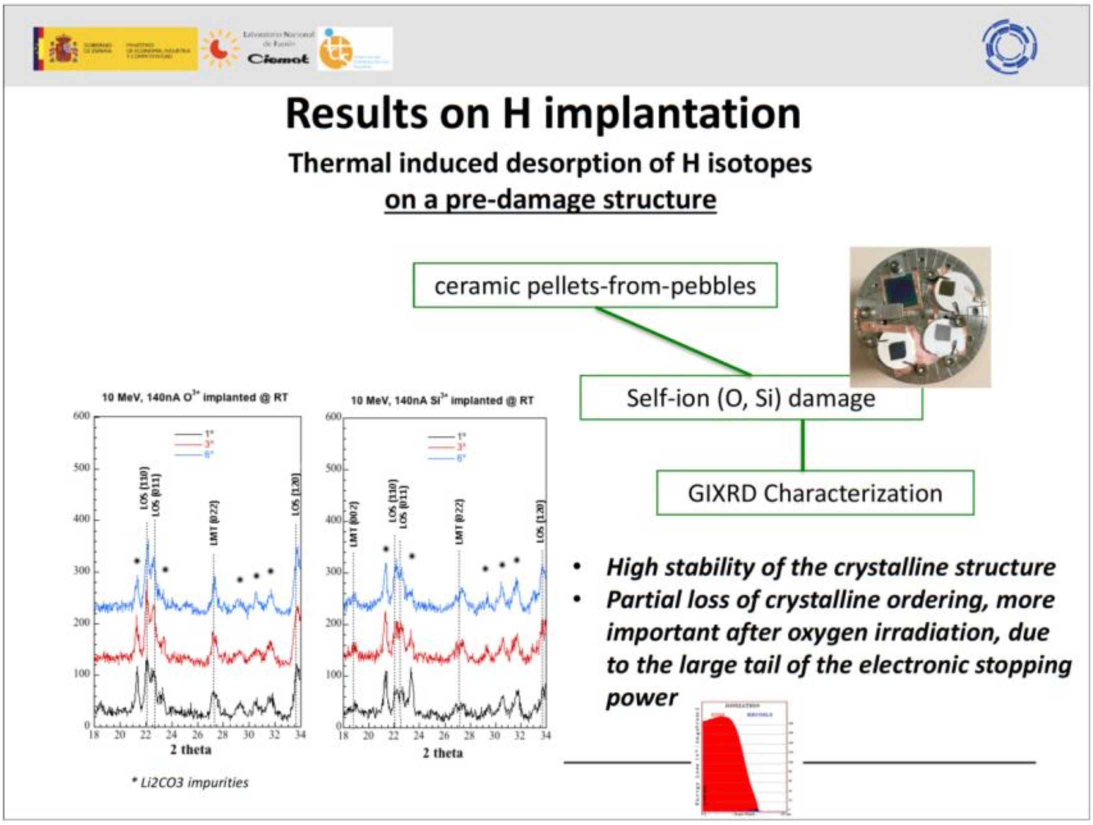
Results on H implantation
Thermal induced desorption of H isotopes
on a pre-damage structure
ceramic pellets-from-pebbles
Self-ion (O, Si) damage
GIXRD Characterization
10 MeV, 140nA O3+ implanted @ RT
10 MeV, 140nA Si3+ implanted @ RT
2 theta
* Li2CO3 impurities
High stability of the crystalline structure
Partial loss of crystalline ordering, more important after oxygen irradiation, due to the large tail of the electronic stopping power

Results on H implantation

Thermal induced desorption of H isotopes
on a pre-damage structure

ceramic pellets-from-pebbles

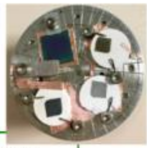

Self-ion (O, Si) damage

ESR Characterization

LATVIJAS UNIVERSITĀTE

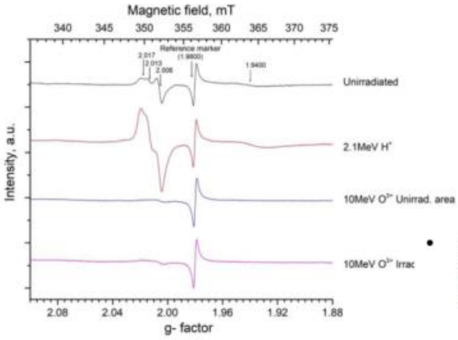

- ***Defects assigned on unirradiated sample: non-bridging oxygen hole centres (HC1 and HC2), E' centres, Si^{3+}/Ti^{3+} centres.***

Results on H implantation

Thermal induced desorption of H isotopes
on a pre-damage structure

ceramic pellets-from-pebbles

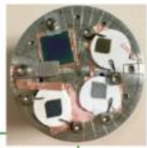

Self-ion (O, Si) damage

in-depth D addition

H-isotopes shallow implantation

Results on H implantation

Thermal induced desorption of H isotopes
on a pre-damage structure

LATVIJAS UNIVERSITĀTE

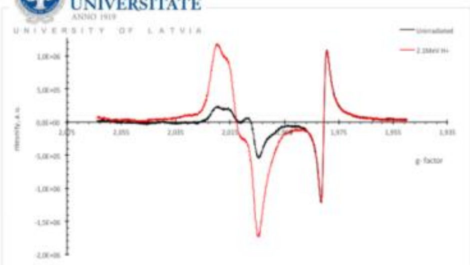

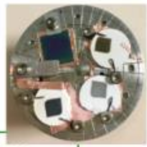

ceramic pellets-from-pebbles

Self-ion (O, Si) damage

in-depth D addition

H-isotopes shallow implantation

ESR Characterization

- ***Defects assigned: non-bridging oxygen hole centres (HC1 and HC2), E' centres plus Si^{3+}/Ti^{3+} centres in H-implanted.***
- ***Intensity increasing.***
- ***No differential features, concluding that implanted H may be bonded or in its molecular form (H_2) = diamagnetic, not detectable.***

Results on H implantation

Thermal induced desorption of H isotopes
on a pre-damage structure

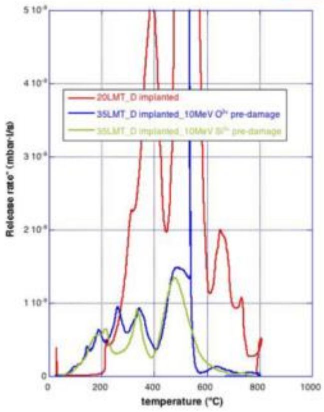

ceramic pellets-from-pebbles

Self-ion (O, Si) damage

in-depth D addition

H-isotopes shallow implantation

TID Characterization

On previously damaged structures, defects will favour the diffusion

From results of H-isotope implantation release from
pellets-from-pebbles samples
as-processed or ion-damaged

it can be concluded that

at close to operational conditions,
implanted D is efficiently release from damaged breeder structures,
although the radiation induced defects swift the release temperature

conclusion on the defects involved is still pendant

What was left to be addressed
on the study of H-isotopes diffusion and release?

2019-2020 EUROfusion objectives at CIEMAT

- Apply the analytical methodology directly on pebbles
- Approach the co-existence of both neutron transmutation products ….
  important synergies of He + H at least in metals !!
- Use the purge gas as atmosphere for release exps

Starting up

Implantation on breeder pebbles

advanced ceramic pebbles

Ion implantation
high energy H or low energy D,
He,
both simultaneously

Matrix characterization

Gas release monitoring

Starting up

Implantation on breeder pebbles

advanced ceramic pebbles

Ion implantation
high energy H or low energy D,
He,
H + He simultaneously

Matrix characterization

Gas release monitoring

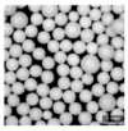

Samples of dehydrated pebbles
@400ºC/2hs in vacuum:

- ✓ Advanced KALOS: LOS + X% LMT. Supplied by KIT


Starting up
Implantation on breeder pebbles
advanced ceramic pebbles
Ion implantation
high energy H or low energy D,
He,
H + He simultaneously
Matrix characterization
Gas release monitoring
pebbles located in
a vertical sample holder
CBBI-20, Karlsruhe, Germany. 18-20 September 2019.

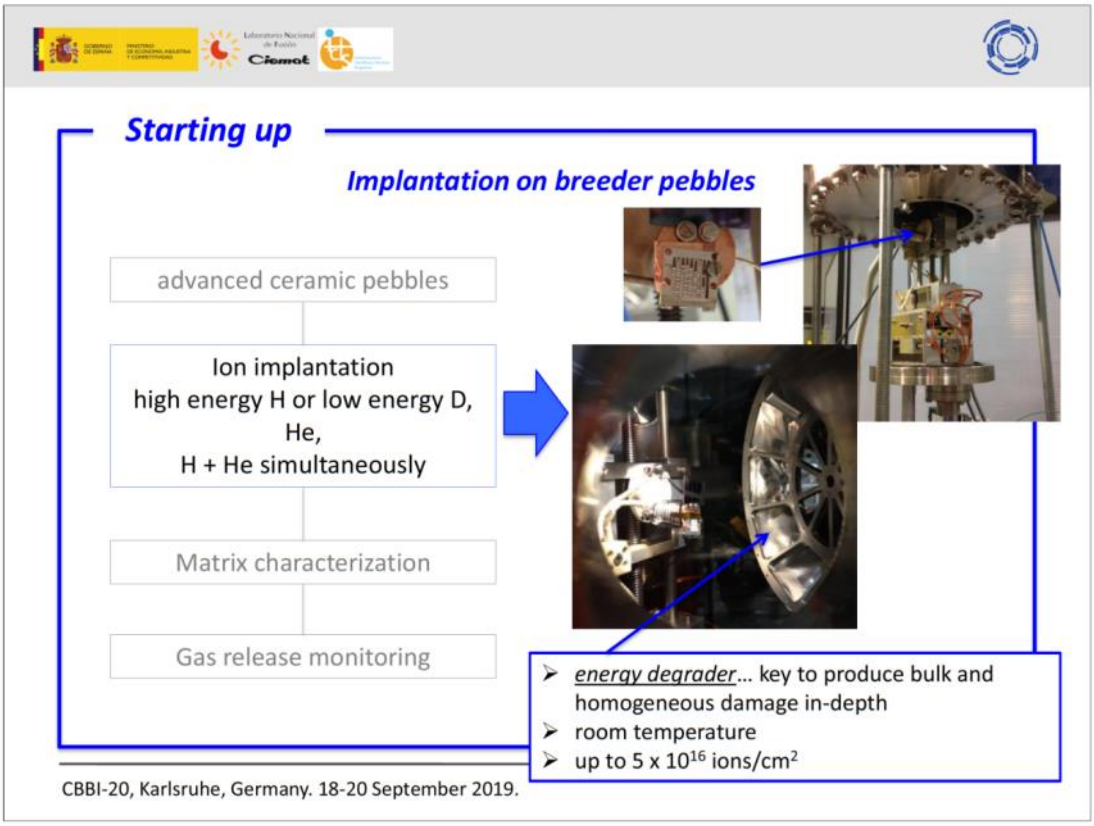
Starting up
Implantation on breeder pebbles
advanced ceramic pebbles
Ion implantation
high energy H or low energy D,
He,
H + He simultaneously
Matrix characterization
Gas release monitoring
energy degrader… key to produce bulk and homogeneous damage in-depth
room temperature
up to 5 x 10^16 ions/cm^2
CBBI-20, Karlsruhe, Germany. 18-20 September 2019.

Starting up

Implantation on breeder pebbles

advanced ceramic pebbles

Ion implantation
high energy H or low energy D,
He,
H + He simultaneously

Matrix characterization

Gas release monitoring

On going
Applying different techniques at CIEMAT
In collaboration with UoL

LATVIJAS UNIVERSITĀTE

CBBI-20, Karlsruhe, Germany. 18-20 September 2019.

Starting up

Implantation on breeder pebbles

advanced ceramic pebbles

Ion i
high energy
H + He

Matrix c

Gas release monitoring

Results and conclusions
on H / He / H + He implantation,
gas release efficiency,
and their effects on the breeder matrix

will be delivered
through 2019-2020

CBBI-20, Karlsruhe, Germany. 18-20 September 2019.

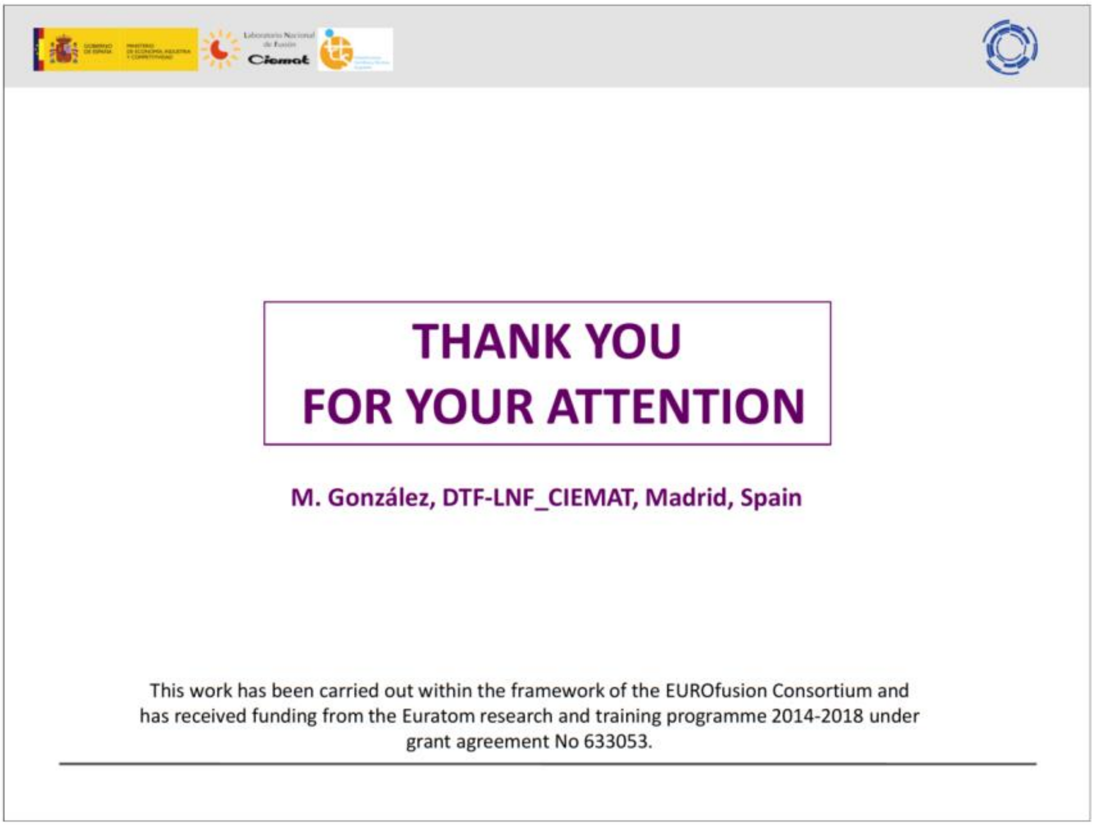
THANK YOU
FOR YOUR ATTENTION
M. González, DTF-LNF_CIEMAT, Madrid, Spain
This work has been carried out within the framework of the EUROfusion Consortium and has received funding from the Euratom research and training programme 2014-2018 under grant agreement No 633053.

Radiation Damage and Helium Accommodation in Lithium Metatitanate Ceramic Breeder Materials

Samuel J. Waters[1], Yiqiang Wang[2], Ionut Jepu[2], Graeme Greaves[3], Ron Smith[4], Nik Reeves-McLaren[1], Amy S. Gandy[1]

[1]Department of Materials Science and Engineering, University of Sheffield, UK.

[2]Culham Centre for Fusion Energy (CCFE), Culham Science Centre, UK.

[3]MIAMI Facility, University of Huddersfield, UK.

[4]ISIS Neutron and Muon Source, STFC, Rutherford Appleton Laboratory, UK.

Lithium metatitanate (Li_2TiO_3) is one of the leading candidates for application as a tritium breeder blanket material, either as a single-phase material or as a secondary phase in advanced Li_4SiO_4 / Li_2TiO_3 breeder pebbles in current EU studies.

During operation, Incident neutrons and recoil nuclei will induce ballistic damage due to energetic collisions with lattice atoms, resulting in atomic displacement and the production of defects; the He by-product to may also accumulate within the ceramic.

Evidence of the breakdown of long- and short-range order in structural units of Li_2TiO_3 resulting from ion-implantations has been reported, and a number of studies suggest that tritium release is impeded by both high levels of radiation-induced damage and the presence of He; although few studies focus on the influence of ceramic microstructure. Furthermore, while a substantial amount of research has been carried out concerning tritium diffusion and release from candidate ceramic breeders, comparatively little is known about the mechanisms of He accommodation in these materials.

The purpose of this work was to identify the influence of ceramic crystal- and microstructure (e.g. native disorder, grain size, morphology, porosity) on radiation damage resistance and He accommodation (and any correlation between the two) in Li_2TiO_3. Li_2TiO_3 samples with progressively different microstructural properties have been characterised using a combination of electron microscopy, Raman spectroscopy, X-ray and neutron diffraction studies. Suites of these samples were implanted with heavy ions (Ti^+) to induce displacement damage analogous to that caused by fusion neutrons, and He^+ ions to simulate the production of He within the ceramic; implantations were carried out in both bulk format and in-situ inside a TEM.

In this contribution, in addition to presenting evidence of structural modifications and He bubble formation resulting from ion implantations, we report the discovery and thermal evolution of nanoscale vacancy-type defects in as-prepared and He^+ implanted Li_2TiO_3. The results of thermal desorption spectroscopy experiments detailing the desorption behaviour of gaseous species from ion-implanted samples will also be discussed.

Analysis of electromagnetic and corpuscular radiation-induced processes in advanced two-phased ceramic breeder pebbles

Arturs Zarins[1,2], Janis Cipa[1,3], Gunta Kizane[1], Arnis Supe[1], Larisa Baumane[1,4], Aleksejs Zolotarjovs[5], Laima Trinkler[3], Oliver Leys[6], Julia Heuser[6], Regina Knitter[6]

1 - University of Latvia, Institute of Chemical Physics, Department of Radiation Processes, 1 Jelgavas street, LV-1004, Riga, Latvia

2 - Daugavpils University, Faculty of Natural Sciences and Mathematics, Department of Chemistry and Geography, 1a Parades street, LV-5401, Daugavpils, Latvia

3 - University of Latvia, Institute of Solid State Physics, Laboratory of Spectroscopy, 8 Kengaraga street, LV-1063, Riga, Latvia

4 - University of Latvia, Institute of Solid State Physics, Laboratory of Optical Materials, 8 Kengaraga street, LV-1063, Riga, Latvia

5 - Latvian Institute of Organic Synthesis, 21 Aizkraukles street, LV-1006, Riga, Latvia

6 - Karlsruhe Institute of Technology, Institute for Applied Materials (IAM), 76021, Karlsruhe, Germany

Advanced lithium orthosilicate (Li_4SiO_4) pebbles with additions of lithium metatitanate (Li_2TiO_3) as a secondary phase have attracted international attention as an alternative solid-state candidate for the tritium breeding in future nuclear fusion reactors. In this research, the formation and accumulation of radiation-induced defects (RD) and radiolysis products (RP) in the Li_4SiO_4 pebbles with various contents of Li_2TiO_3 was analysed under actions of both electromagnetic and corpuscular radiation (X-rays and accelerated electrons). The accumulated RD and RP were analysed by using thermally stimulated luminescence, powder X-ray diffractometry, scanning electron microscopy, electron spin resonance, absorption and Fourier transformation infrared spectrometry. On the basis of the obtained results, it is concluded that the formation mechanism and structure of RD and RP (except Ti^{3+} centres) in the advanced Li_4SiO_4 pebbles with additions of Li_2TiO_3 is similar to the single-phase silicate ceramics. The advanced pebbles have a good radiation stability in comparison to the EU reference Li_4SiO_4 pebbles (without additions of Li_2TiO_3), and the concentration of the accumulated paramagnetic RD and RP decreases with an increasing content of Li_2TiO_3. The accumulated RD and RP in the advanced pebbles annihilate between 300 K and 650 K (except large colloidal lithium particles), and it can be expected that the tritium release starts in this temperature range.

Analysis of electromagnetic and corpuscular radiation induced processes in advanced two-phased ceramic breeder pebbles

Arturs Zarins[1,2], Janis Cipa[1,3], Gunta Kizane[1], Arnis Supe[1], Larisa Baumane[1,4], Aleksejs Zolotarjovs[3], Laima Trinkler[3], Oliver Leys[5], Julia Heuser[5] and Regina Knitter[5]

1 – University of Latvia, Institute of Chemical Physics, Riga, Latvia
2 – Daugavpils University, Faculty of Natural Sciences and Mathematics, Daugavpils, Latvia
3 – University of Latvia, Institute of Solid State Physics, Riga, Latvia
4 – Latvian Institute of Organic Synthesis, Riga, Latvia
5 – Karlsruhe Institute of Technology, Institute for Applied Materials, Karlsruhe, Germany

20th International Workshop on Ceramic Breeder Blanket Interactions (CBBI-20)
18-20 September 2019, Karlsruhe Institute of Technology, Campus North

Motivation

- Advanced ceramic breeder (ACB) pebbles consisting of lithium orthosilicate (Li_4SiO_4) with additions of lithium metatitanate (Li_2TiO_3) as a secondary phase have been suggested as a potential solid-state material for the tritium breeding in the European Helium Cooled Pebble Bed (HCPB) concept
- The ACB pebbles under operational conditions will be exposed to the simultaneous action of an intense neutron and gamma radiation, a high magnetic field and an elevated temperature
- The accumulated radiation-induced defects and radiolysis products, which will be created by atomic displacements, ionization and excitation mechanism (radiolysis), in the ACB pebbles can interact with the generated tritium and thus influence the tritium release diffusion and release processes
- The **aim of this research** is to analyse and describe the formation and accumulation of radiation-induced defects and radiolysis products in the Li_4SiO_4 pebbles with various contents of Li_2TiO_3 under action of X-rays and accelerated electrons
- **Practical significance.** Such research is necessary: **(1)** to understand the formation mechanism and structure of the formed radiation-induced defects and radiolysis products, **(2)** to determine the parameters, which characterise the radiation stability, and **(3)** to evaluate the high-temperature radiation-induced processes in the ACB pebbles

2/17

UNIVERSITY OF LATVIA
ANNO 1919

Investigated samples

- Three types of ACB pebbles were investigated together with the former EU reference pebbles, Li_4SiO_4 with 2.5 wt.% excess of silicon dioxide (SiO_2)
- The reference pebbles were produced by a melt-spraying processes (Schott AG), while the ACB pebbles were fabricated by a melt-based process (KIT)
- The pebbles before irradiation were thermally treated at 1170 K for 3 weeks in air

Optical microscopy

Scanning electron microscopy (SEM)

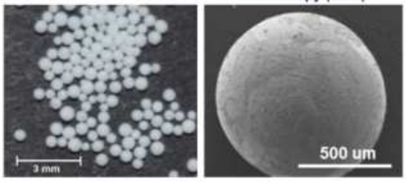

Fig. 1 Former EU reference pebbles, Li_4SiO_4 with 2.5 wt.% excess of SiO_2

Table 1. Specification of the investigated Li_4SiO_4 pebbles with various contents of Li_2TiO_3

Sample	Pebbles	Phase composition			Pebble diameter, μm	Pebble colour
		mcl Li_4SiO_4, mol%	*mcl* Li_2TiO_3, mol%	*orh* Li_2SiO_3, mol%		
#1	Reference	90	0	10	250-900*	«Pearl» white
#2	ACB	90	10	0	500-1000	Light-yellow
#3	ACB	80	20	0	500-1000	Light-yellow
#4	ACB	70	30	0	500-1000	Light-yellow

** Two batches: 250-630 μm and 560-900 μm*
mcl – monoclinic; orh - orthorhombic

3/17

UNIVERSITY OF LATVIA
ANNO 1919

Study of X-ray induced effects

(small absorbed doses & room temperature)

J. Cipa et al. *X-ray induced defects in advanced lithium orthosilicate pebbles with additions of lithium metatitanate. Fusion Engineering and Design, 143 (2019) 10-15.*

4/17

UNIVERSITY OF LATVIA ANNO 1919

Experimental

- Pebbles before irradiation were crushed into fine powders and pressed into 10 mm pellets ← *due to vertical sample holder*
- X-ray induced luminescence (XRL) technique ← *irradiation & in situ luminescence measurements*
- In cooperation with the Institute of Solid State Physics, University of Latvia (Riga, Latvia)
- After irradiation:
  - Absorption spectrometry ← *pellets*
  - Electron spin resonance (ESR) spectrometry ← *crushed powders*
  - Thermally stimulated luminescence (TSL) technique
    TSL glow curves ← crushed powders
    TSL spectra ← pellets
- Isochronal annealing experiments ← *will be started next year*

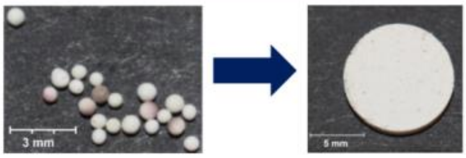

X-ray source: W anode, 40 kV, 10 mA
Distance (sample-source): 15 cm
Irradiation time: up to 1 h
Absorbed dose: up to 40 kGy
Irradiation temperature: room
Atmosphere: vacuum ($<10^{-2}$ Pa)

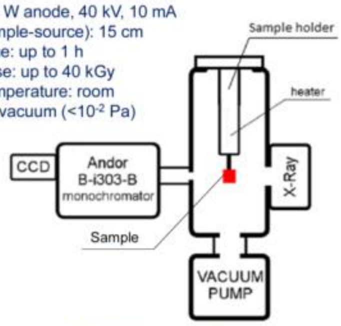

Fig. 2 XRL device block scheme

5/17

UNIVERSITY OF LATVIA ANNO 1919

X-ray induced luminescence (XRL) technique

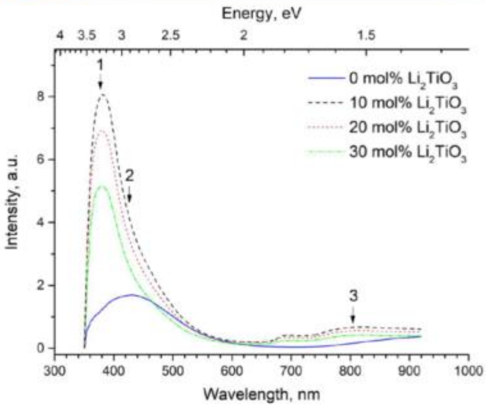

Fig. 3 XRL spectra of the Li_4SiO_4 pebbles with various contents of Li_2TiO_3

- XRL bands in the spectra were separated using Gaussian function: $f(x) = Ae^{-\frac{(x-B)^2}{2C^2}}$

- The ACB pebbles are biphasic without solid solutions, and thus the formation mechanism and structure of primary radiation-induced defects is similar to the single-phase ceramics, Li_4SiO_4 and Li_2TiO_3

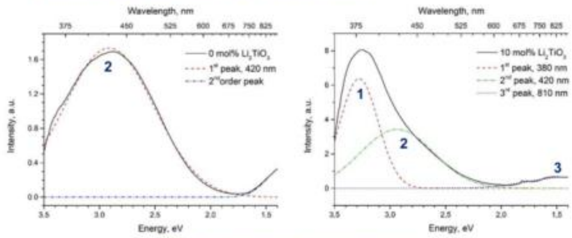

Fig. 4 XRL spectra with separated bands

Table 2 Possible origins of XRL bands

Band	Wavelength	Energy	Possible origin
1	380 nm	3.3 eV	L-centre (excited SiO_4^{4-} units)
2	420 nm	2.9 eV	E' centre (≡Si• or SiO_3^{3-})
3	810 nm	1.55 eV	Ti^{3+} centre

6/17

UNIVERSITY OF LATVIA

Electron spin resonance (ESR) spectrometry

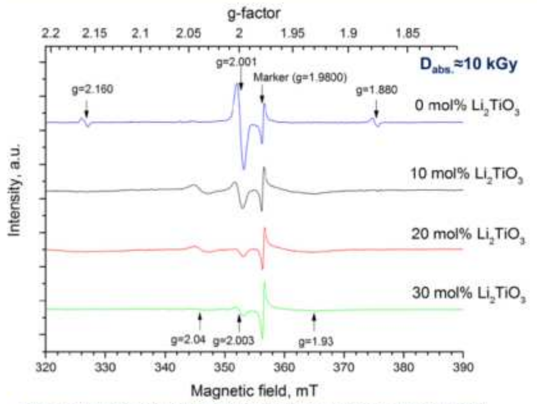

Fig. 5 ESR spectra of the Li_4SiO_4 pebbles with various contents of Li_2TiO_3 after irradiation with X-rays

- In the ACB pebbles, the formation of primary radiation-induced defects was detected, which are characteristic for Li_4SiO_4 (except Ti^{3+} centres)

Table 3 Possible origins of ESR signals

Signal	g-factor	Possible origin	Structure
1	2.16±0.01	Atomic hydrogen	H°
2	2.040±0.001	O related defects	O^- or O_2^-
3	2.003±0.001	E' centre	≡Si• or SiO_3^{3-}
4	1.93±0.01	Ti^{3+} centre	Ti^{3+}
5	1.88±0.01	Atomic hydrogen	H°

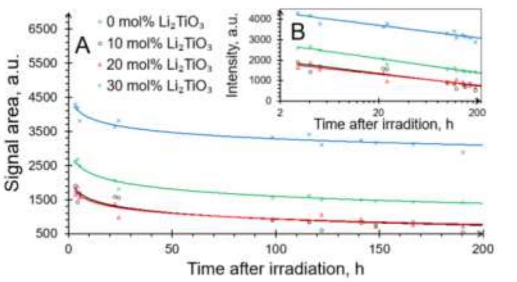

Fig. 6 Area of ESR signal with a g-factor 2.003 as a function of time after irradiation

UNIVERSITY OF LATVIA

Absorption spectrometry

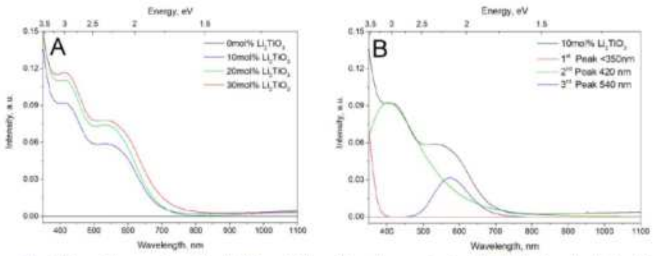

Fig. 7 Absorption spectra of the Li_4SiO_4 pebbles with various contents of Li_2TiO_3 before irradiation (A). Absorption spectrum with separated bands for the ACB pebbles before irradiation (B)

Table 4 Possible origins of absorption bands

Band	Wavelength	Possible origin	Comments
1	230 nm	E' centre (≡Si• or SiO_3^{3-})	Not observed
2	<350 nm	Fe^{3+} ions (?)	Before & after irrad.
3	410 nm	HC_1 centre (≡Si-O• or SiO_4^{3-})	After irrad.
4	420 nm	Fe^{3+} ions (?)	Before & after irrad.
5	570 nm	Ti^{3+} centre (?)	Before & after irrad.
6	630 nm	HC_2 centre (≡Si-O• or SiO_4^{3-})	After irrad.

- In the ACB pebbles before irradiation, at least three overlapped absorption bands were detected with maxima at around 350 nm, 420 nm and 540 nm
- The difference spectrum of the pebbles before and after irradiation consists of at least three wide and overlapped absorption bands

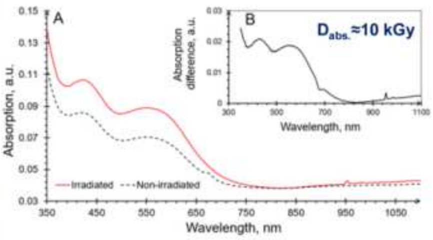

Fig. 8 Absorption spectra of the ACB pebbles with 10 mol% Li_2TiO_3 before and after irradiation with X-rays

UNIVERSITY OF LATVIA
ANNO 1919

Thermally stimulated luminescence (TSL) technique

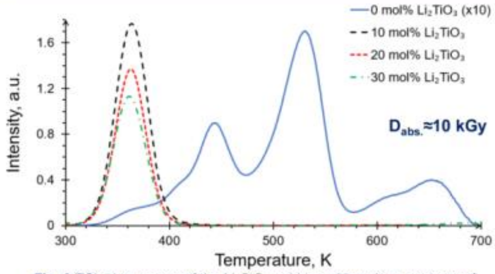

Fig. 9 TSL glow curves of the Li_4SiO_4 pebbles with various contents of Li_2TiO_3 after irradiation with X-rays (heating rate: 2 K s^{-1})

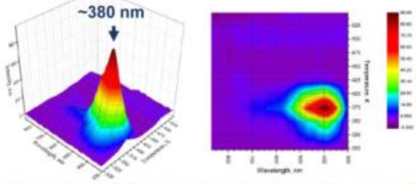

Fig. 10 TSL spectra of the ACB pebbles with 10 mol% Li_2TiO_3 after irradiation with X-rays (heating rate: 1 Ks^{-1})

- In the ACB pebbles after irradiation, one main TSL peak with a maximum at around 360 K was detected
- TSL peak is not stable at room temperature
- TSL spectra consist of one main band with a maximum at around 380 nm (3.3 eV)

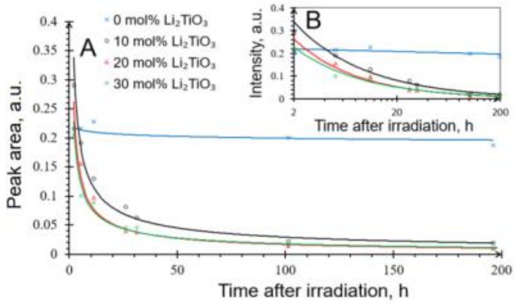

Fig. 11 Area of TSL glow curves as a function of time after irradiation

9/17

UNIVERSITY OF LATVIA
ANNO 1919

Study of accelerated electron induced effects

(small, medium and high absorbed doses & room and elevated temperature)

A . Zarins et al. *Study of accelerated electron induced processes in lithium orthosilicate pebbles with various contents of lithium metatitanate. Journal of Nuclear Materials (2019/2020) prepared for submission.*

A. Zarins et al. *Characterisation and radiolysis of modified lithium orthosilicate pebbles with noble metal impurities. Fusion Engineering and Design, 124 (2017) 934-939.*

J.M. Heuser et al. *Radiation stability of long-term annealed bi-phasic advanced ceramic breeder pebbles. Fusion Engineering and Design, 138 (2019) 395-399.*

A. Zarins et al. *Behaviour of advanced tritium breeder pebbles under simultaneous action of accelerated electrons and high temperature. Fusion Engineering and Design, 121 (2017) 167-173.*

A. Zarins et al. *Formation and accumulation of radiation-induced defects and radiolysis products in modified lithium orthosilicate pebbles with additions of titanium dioxide. Journal of Nuclear Materials, 470 (2016) 187-196.*

10/17

UNIVERSITY OF LATVIA

ANNO 1919

Experimental

- Pebbles were irradiated with 5 MeV accelerated electrons ← *linear electron accelerator ELU-4 (Salaspils, Latvia)*

Fig. 12 Encapsulated pebbles in quartz ampules with dry argon (before irradiation)

Fig. 13 Linear electron accelerator ELU-4

Fig. 14 Encapsulated pebbles in quartz ampules with dry argon (after irradiation)

Fig. 15 Li_4SiO_4 pebbles with various contents of Li_2TiO_3 before and after irradiation

Table 5 Specification of irradiation conditions (D –absorbed dose, T – irradiation temperature, P – dose rate)

Parameter	Irradiation conditions																				
	#1	#2	#3	#4	#5	#6	#7	#8	#9	#10	#11	#12	#13	#14	#15	#16	#17	#18	#19	#20	#21
D, MGy	0.01	0.05	0.15	0.5	1.5	2	3	6	6	12	24	42	42	84	100	100	193	249	1000	3700	5000
$T_{aver.}$, K	300	300	300	300	300	300	305	305	-	310	320	520	670	630	710	730	710	940	460	520	520
T_{min}, K	-	-	-	-	-	-	300	300	-	300	300	460	630	533	580	500	690	875	380	440	380
T_{max}, K	-	-	-	-	-	-	310	310	1285	315	345	580	730	720	840	950	730	990	560	670	650
P, kGy s^{-1}	0.67	0.67	0.67	0.83	0.64	0.64	0.85	0.85	33	0.85	0.85	11.7	11.7	11.7	2.6	2.6	13.4	21.3	11.7	13.4	11.6

11/17

UNIVERSITY OF LATVIA

ANNO 1919

Electron spin resonance (ESR) spectrometry (1)

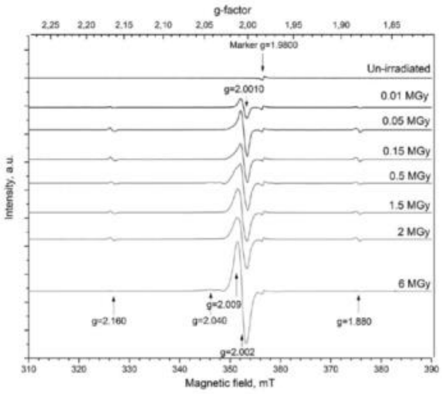

Fig. 16 ESR spectra of the reference pebbles (0 mol% Li_2TiO_3) before and after irradiation with various absorbed doses

- Radiation chemical yield (G): 0.15 defects/products per 100 eV

* Low probability in case of 5 MeV accelerated electrons

- The formation of radiation-induced defects and radiolysis products takes place through two main stages.
- In the first stage (fast process), the formed electrons and holes are self-trapped on intrinsic and extrinsic defects.
- In the second stage (slow process), atomic displacements* and excitation mechanism (radiolysis) dominates.

ESR signal origins:

(1) E' centres (≡Si• or SiO_3^{3-})
singlet, g=2.0010, ΔB_{pp}=1 mT

(2) HC_1 and HC_2 centres (≡Si-O• or SiO_4^{3-})
anisotropic singlet, g=2.009
HC_1 centre: g_1= 2.0026, g_2=2.0088 and g_3=2.0213
HC_2 centre: g_1=2.0118, g_2=2.0127 and g_3=2.0158

(3) Oxygen related defects (O^-, O_2^-) or peroxide radicals (≡Si-O-O•)
g=2.040, ΔB_{pp}≈2 mT

(4) Atomic hydrogen (H•)
g=2.160 and g=1.880

(5) Small Li_n particles (<1 um)
narrow singlet g=2.0030, ΔB_{pp} <0.1 mT
(detected only after annealing >570 K)

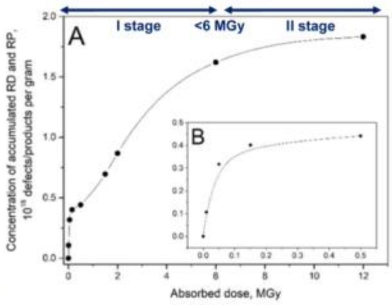

Fig. 17 Total concentration of the detected paramagnetic RD and RP as a function of the absorbed dose

12/17

UNIVERSITY OF LATVIA ANNO 1919

Electron spin resonance (ESR) spectrometry (2)

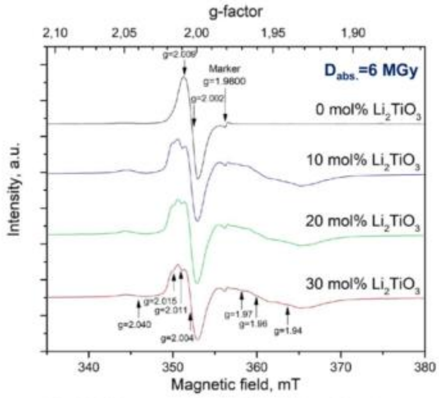

Fig. 18 ESR spectra of the Li_4SiO_4 pebbles with various contents of Li_2TiO_3 after irradiation

Table 6 Possible origins of ESR signals

Signal	g-factor	Possible origin	Structure
1	2.040±0.001	O related defects or peroxide radicals	O^-, O_2^- or ≡Si-O-O•
2	2.015±0.001 and 2.011±0.001	HC_2 centres	SiO_4^{3-} and TiO_3^-
3	2.004±0.001	E' centre	SiO_3^{3-} and TiO_3^{3-}
4	1.97±0.01, 1.96±0.01 and 1.94±0.01	Ti^{3+} centre	Ti^{3+}

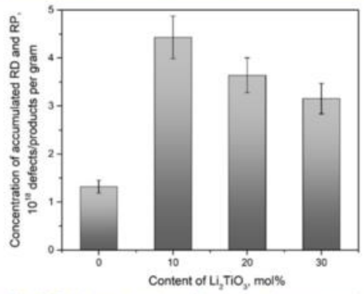

Fig. 19 Total concentration of the detected paramagnetic RD and RP as a function of the content of Li_2TiO_3

Intrinsic defects
(crystalline lattice imperfections)

Extrinsic defects
(impurity atoms)

$Ti^{4+} + e^- \rightarrow Ti^{3+}$

- In the ACB pebbles, Ti^{4+} ions can be incorporated into the crystalline lattice of the primary phase, Li_4SiO_4, during the fabrication processes

- Radiation chemical yield (G): <0.8 defects/products per 100 eV

13/17

UNIVERSITY OF LATVIA ANNO 1919

Electron spin resonance (ESR) spectrometry (3)

- Irradiation temperature has a significant impact on the formation and accumulation of radiation-induced defects and radiolysis products
- The concentration of the accumulated radiation-induced defects and radiolysis products decreases with increasing irradiation temperature.

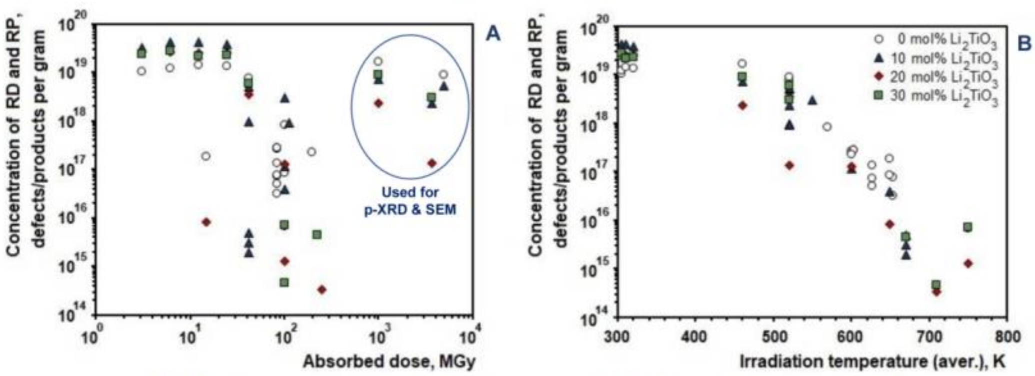

Fig. 20 Total concentration of detected paramagnetic radiation-induced defects and radiolysis products as a function of absorbed dose (A) and irradiation temperature (B).

14/17

UNIVERSITY OF LATVIA ANNO 1919

Powder X-ray diffractometry (p-XRD) and scanning electron microscopy (SEM)

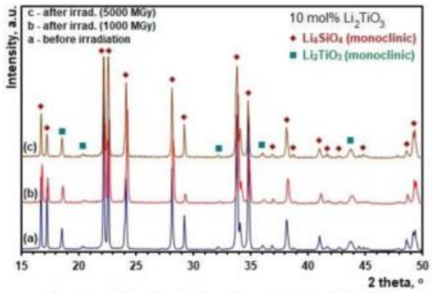

Fig. 21 p-XRD of the ACB pebbles with 10 mol% Li_2TiO_3 before and after irradiation

- ❑ Major changes in phase composition were not detected after irradiation, due to small radiolysis degree
- ❑ Microstructure is only slightly changed during irradiation

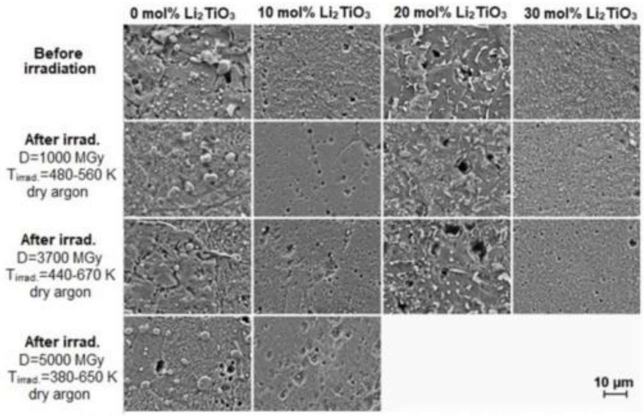

Fig. 22 Microstructure at the chemically etched cross-section of the Li_4SiO_4 pebbles with various contents of Li_2TiO_3 before and after irradiation

- ❑ Radiolysis degree (α): ≤1 mol% (5000 MGy)

15/17

UNIVERSITY OF LATVIA ANNO 1919

Conclusions

- ❑ The ACB pebbles are biphasic without solid solutions, and the formation mechanism and structure of the formed radiation-induced defects and radiolysis products (except Ti^{3+} centres) during irradiation is similar to the single-phase ceramics.
- ❑ The additions of Li_2TiO_3 as a secondary phase in the ACB pebbles slightly increase the total concentration of the accumulated radiation-induced defects and radiolysis products in comparison to the former EU reference pebbles, Li_4SiO_4 with 2.5 wt.% excess of SiO_2.
- ❑ The ACB pebbles have a good radiation stability, and the radiation chemical yield (G) of paramagnetic radiation-induced defects and radiolysis products is below 0.8 defects/products per 100 eV and the radiolysis degree (α) is under 1 mol% after irradiation up to 5000 MGy absorbed dose.
- ❑ The irradiation temperature has a significant impact on the formation and accumulation of radiation-induced defects and radiolysis products in the ACB pebbles, and the concentration of the accumulated radiation-induced defects and radiolysis products decreases with increasing irradiation temperature.

16/17


UNIVERSITY OF LATVIA
INSTITUTE OF SOLID STATE PHYSICS
UNIVERSITY OF LATVIA
Latvian Institute of Organic Synthesis
KIT
Baltisch-Deutsches HOCHSCHULKONTOR
Thank you for your attention!
This research of the Baltic-German University Liaison Office is supported by the German Academic Exchange Service (DAAD) with funds from the Foreign Office of the Federal Republic Germany. The views and opinions expressed herein do not reflect those of the Baltic-German University Liaison Office.
17/17

Integrated Neutronics Experiment of Breeding Blanket Assembly and TBR Evaluation with Discharge Fusion Source

Satoshi Konishi[1], Keisuke Mukai[1], Yasuyuki Ogino[2],

[1]Institute of Advanced Energy, Kyoto University

[2]Graduate School of Energy Science, Kyoto University

One of the most important issues of breeding blanket is accurate evaluation of TBR to certify the tritium self-sufficiency of the entire reactor. Although Monte Carlo simulation provides detailed neutron transport data, actual blanket is always different from ideal assumption. Lithium containing ceramic breeder pebbles (Li_2O, Li_2TiO_3, Li_2ZrO_3, Li_4SiO_4, and etc.) are particularly anticipated to have some error in this tritium economy because of the non-uniform packing density and complicated structure of pebble bed with coolant pipes and multiplier. Accurate experimental measurement of tritium production in a realistic blanket module assembly is needed to verify the blanket designs. The authors have pointed out it is possible with relatively small number (flux) of neutron is sufficient for its purpose if they are well confined by an assembly of realistic blanket structure. It is essential that all the neutron contained in the blanket modules are not lost by streaming or absorption by the surrounding structure for irradiation test. Neutron economy in the fully covering DEMO blanket is expected to be close to this condition.

For the purpose of neutronics experiments, we developed two techniques. One is a small discharge fusion neutron source that typically generates ~10^{-7} neutron/sec. Another new technique is 2D/3/D neutron measurement with imaging plate assisted by various activation foils/wires for the neutron energy measurement, like "Mesh tally" in transport codes. Neutron distribution profile in the assembly is first recorded by the imaging plate and then read out by digital scanning. Different activation metals provide unique sensitivity for a certain range of neutron energy.

The early results of the neutron generation by the fusion source and the measurement of neutron with imaging plate were reported in the previous CBBI meeting. Recent progress will be reported together with the future plan to assemble more realistic materials such as lithium ceramics, reactor grade graphite, beryllium, lithium compounds and steel. Special materials such as pebbles of breeder, multiplier needs international round robin tests for benchmarking. After the test apparatus and procedure would be established, DT fusion neutron will be used to actually measure the multiplication function.

Integrated Neutronics Experiment of Breeding Blanket Assembly and TBR Evaluation with Discharge Fusion Source

Satoshi Konishi, Keiske Mukai and Yasuhisa Oginoi

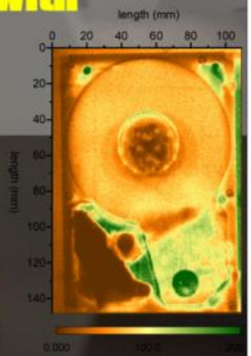

CBBI-20

KIT North Campus
18-20 Sep, 2019

京都大学
KYOTO UNIVERSITY

Partially supported by JSPS grant in aid (17H06794)

KYOTO UNIVERSITY

Introduction

Tritium consumption
$^{2}D + ^{3}T \rightarrow ^{1}n + ^{4}He$

Tritium production
$^{6}Li + ^{1}n \rightarrow ^{3}T + ^{4}He$

$$TBR = \frac{T_{generated}}{T_{lost}} > 1.05$$

Tritium Breeding Ratio（TBR）> 1.05 is crucial for fusion programs, but nobody has ever attempted to verify it before DEMO

Compact neutron sources with special neutron measurement can evaluate tritium ^{6}Li(n,t) production in blanket modules
"Experimental Mesh Tally"

04.12.2019 2

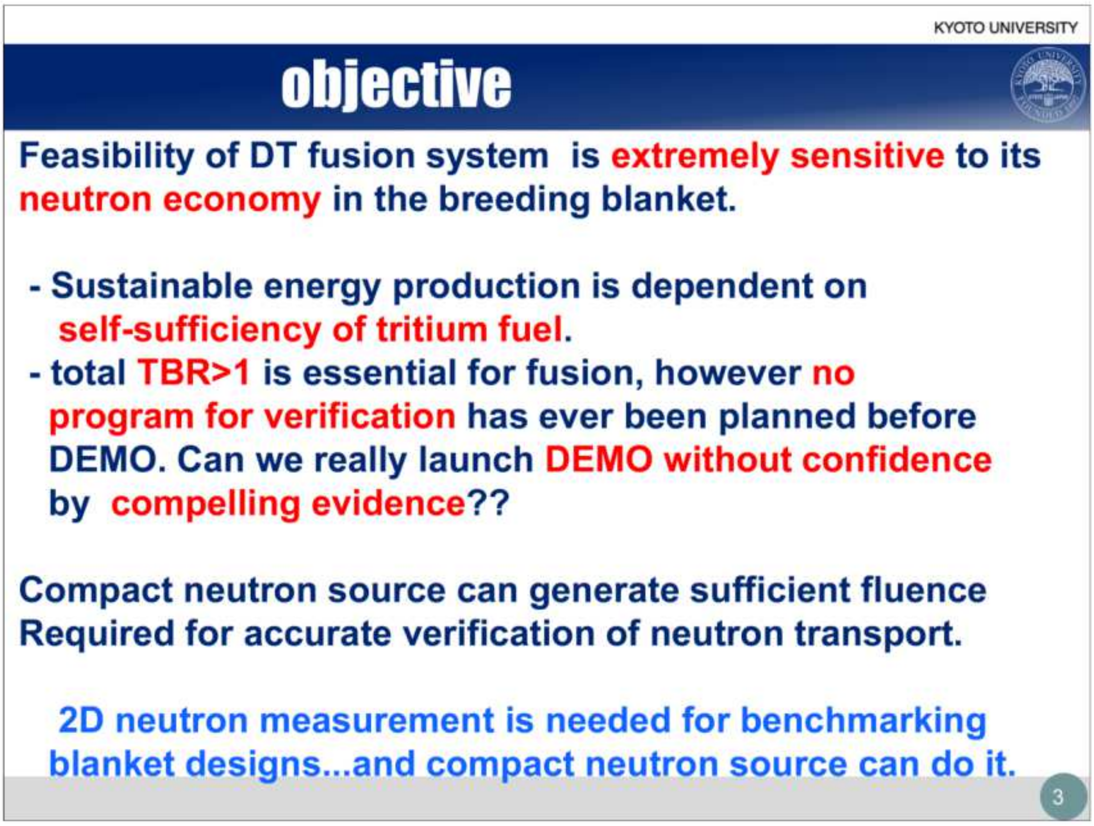
KYOTO UNIVERSITY
objective
Feasibility of DT fusion system is extremely sensitive to its neutron economy in the breeding blanket.
- Sustainable energy production is dependent on self-sufficiency of tritium fuel.
- total TBR>1 is essential for fusion, however no program for verification has ever been planned before DEMO. Can we really launch DEMO without confidence by compelling evidence??
Compact neutron source can generate sufficient fluence Required for accurate verification of neutron transport.
2D neutron measurement is needed for benchmarking blanket designs...and compact neutron source can do it.
3

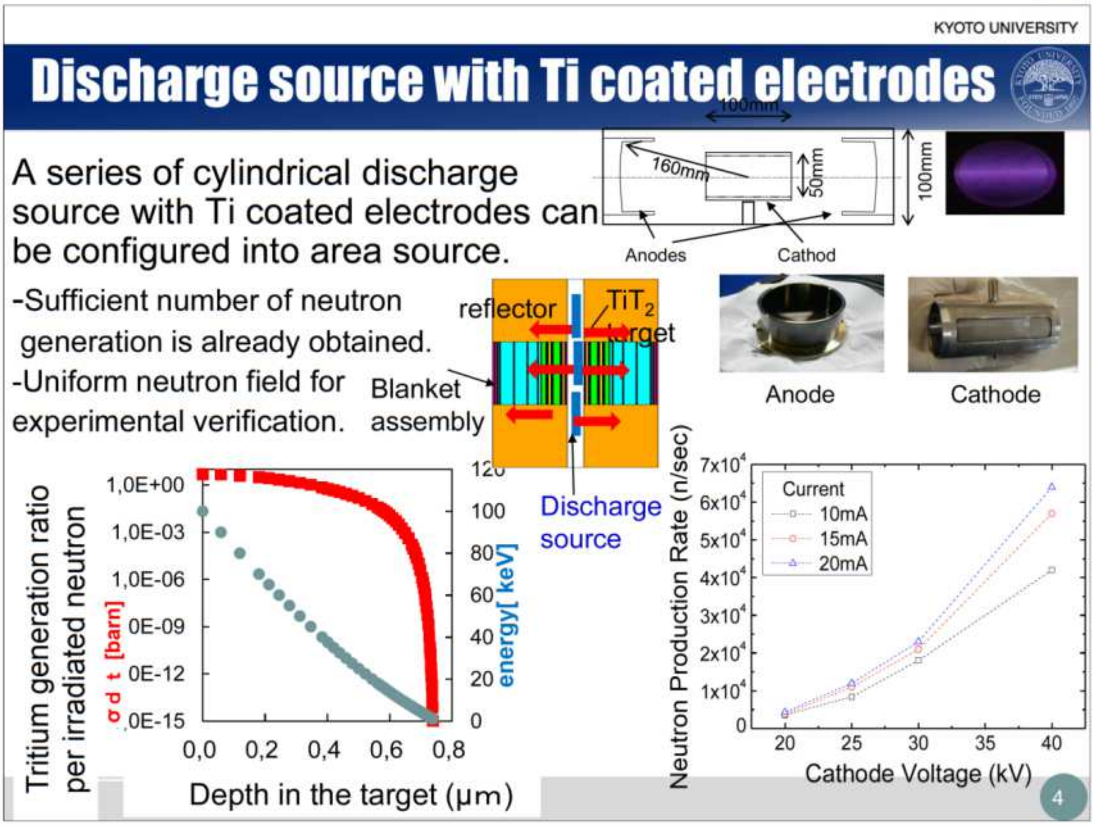
KYOTO UNIVERSITY
Discharge source with Ti coated electrodes
A series of cylindrical discharge source with Ti coated electrodes can be configured into area source.
-Sufficient number of neutron generation is already obtained.
-Uniform neutron field for experimental verification.
100mm
160mm
50mm
100mm
Anodes
Cathod
Anode
Cathode
reflector
TiT2 target
Blanket assembly
Discharge source
Tritium generation ratio per irradiated neutron
σ d t [barn]
energy[keV]
Depth in the target (μm)
Neutron Production Rate (n/sec)
Cathode Voltage (kV)
Current
10mA
15mA
20mA
4

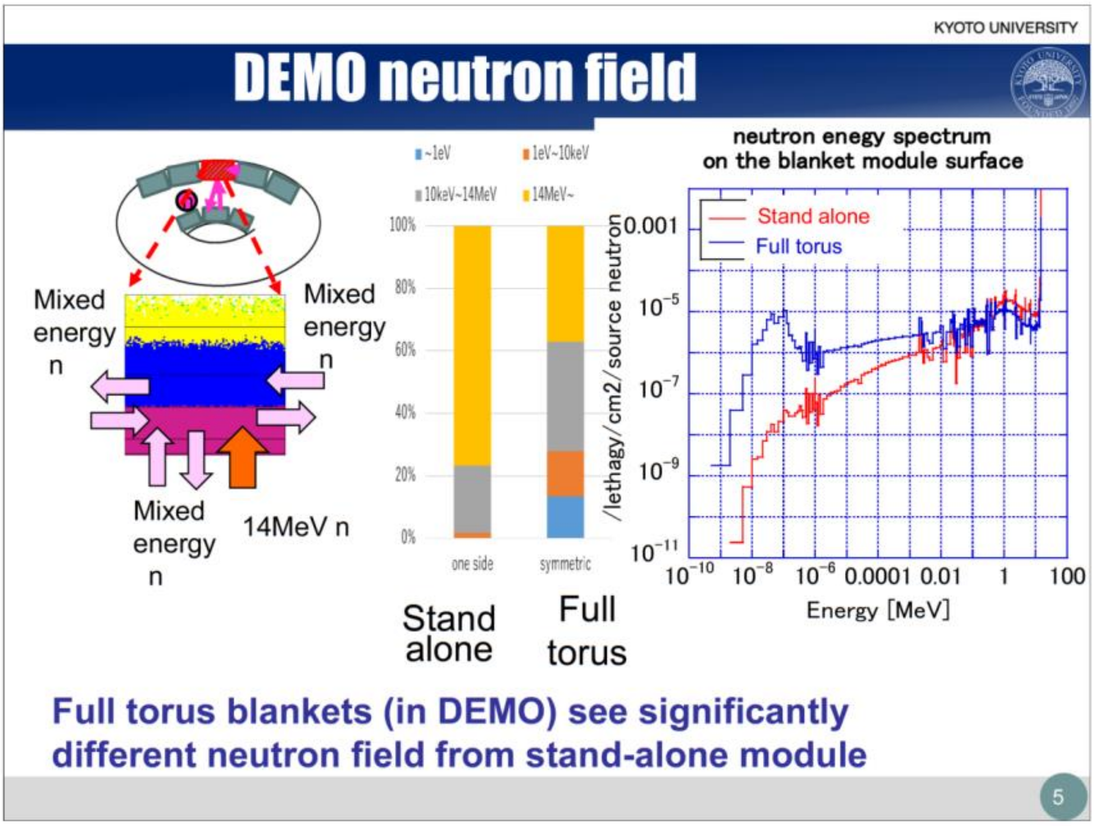
KYOTO UNIVERSITY
DEMO neutron field
Mixed energy n
Mixed energy n
Mixed energy n
14MeV n
~1eV
1eV~10keV
10keV~14MeV
14MeV~
100%
80%
60%
40%
20%
0%
one side
symmetric
Stand alone
Full torus
neutron enegy spectrum on the blanket module surface
Stand alone
Full torus
/lethagy/cm2/source neutron
0.001
10^{-5}
10^{-7}
10^{-9}
10^{-11}
10^{-10} 10^{-8} 10^{-6} 0.0001 0.01 1 100
Energy [MeV]
Full torus blankets (in DEMO) see significantly different neutron field from stand-alone module
5

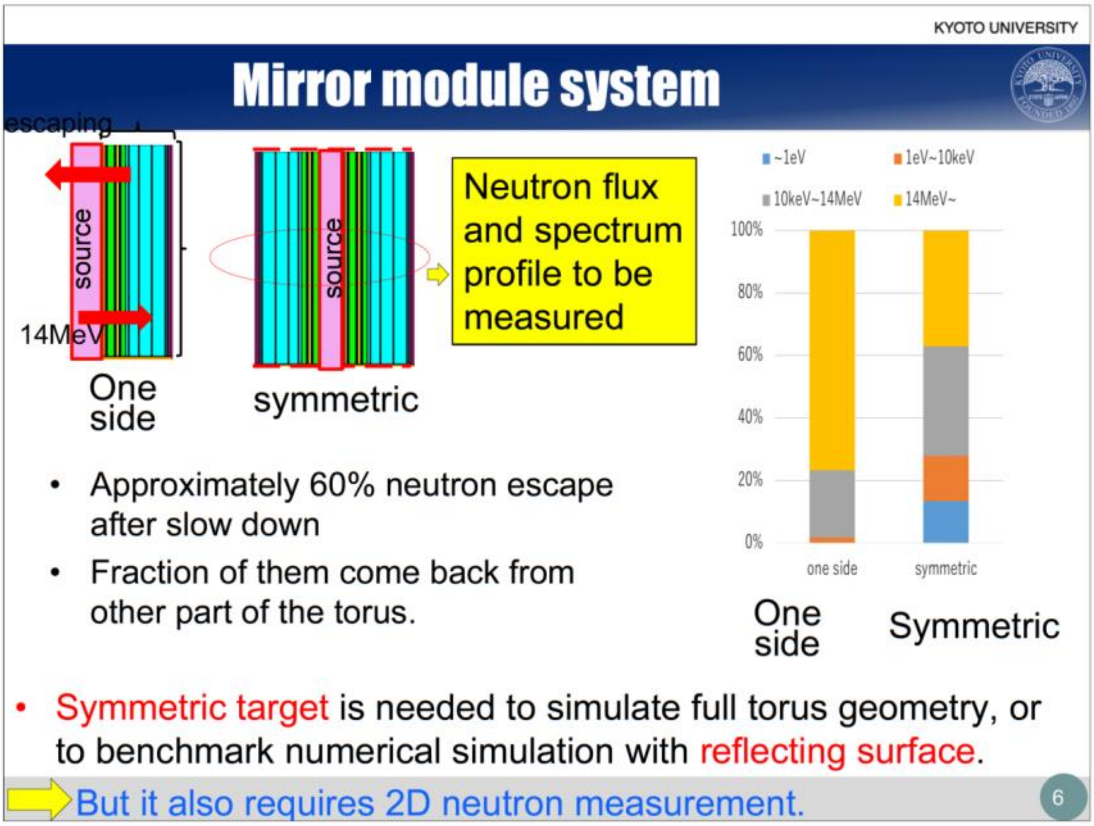
KYOTO UNIVERSITY
Mirror module system
escaping
source
14MeV
One side
source
symmetric
Neutron flux and spectrum profile to be measured
~1eV
1eV~10keV
10keV~14MeV
14MeV~
100%
80%
60%
40%
20%
0%
one side
symmetric
One side
Symmetric
• Approximately 60% neutron escape after slow down
• Fraction of them come back from other part of the torus.
• Symmetric target is needed to simulate full torus geometry, or to benchmark numerical simulation with reflecting surface.
But it also requires 2D neutron measurement.
6

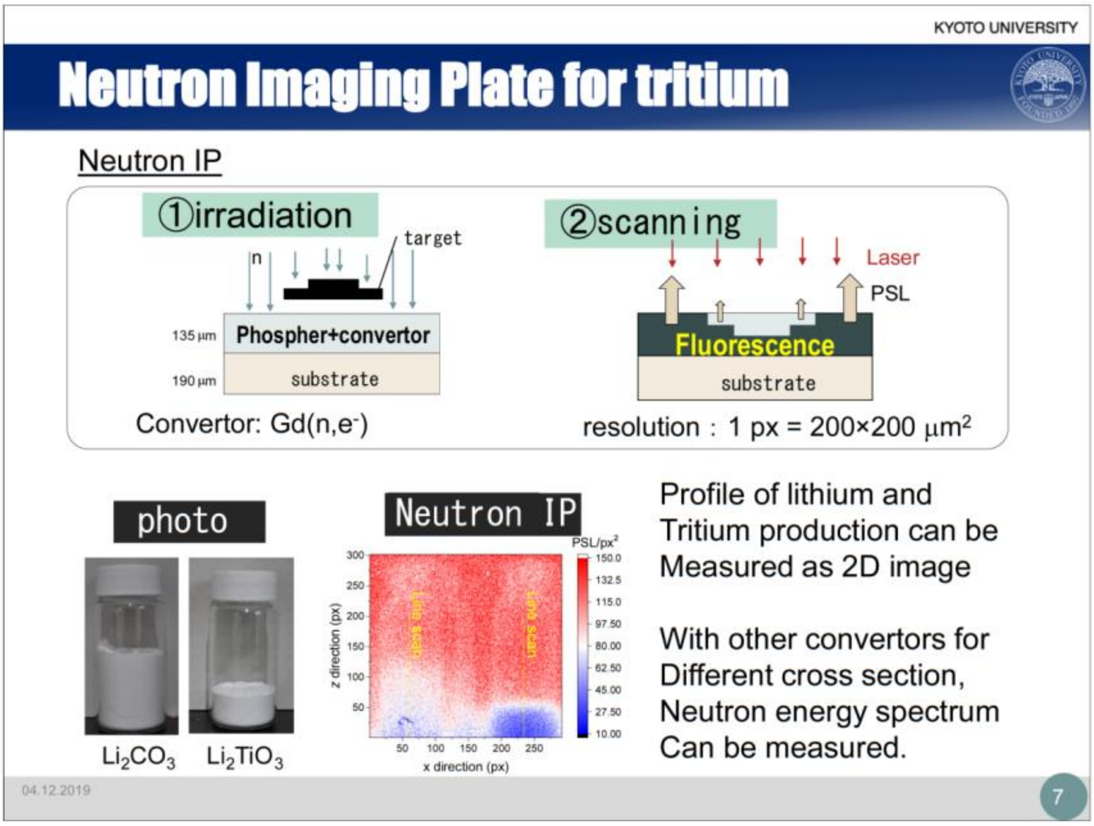
KYOTO UNIVERSITY
Neutron Imaging Plate for tritium
Neutron IP
①irradiation
n
target
135 μm
Phospher+convertor
190 μm
substrate
Convertor: Gd(n,e-)
②scanning
Laser
PSL
Fluorescence
substrate
resolution : 1 px = 200×200 μm²
photo
Li₂CO₃ Li₂TiO₃
Neutron IP
PSL/px²
z direction (px)
x direction (px)
Profile of lithium and
Tritium production can be
Measured as 2D image
With other convertors for
Different cross section,
Neutron energy spectrum
Can be measured.
04.12.2019
7

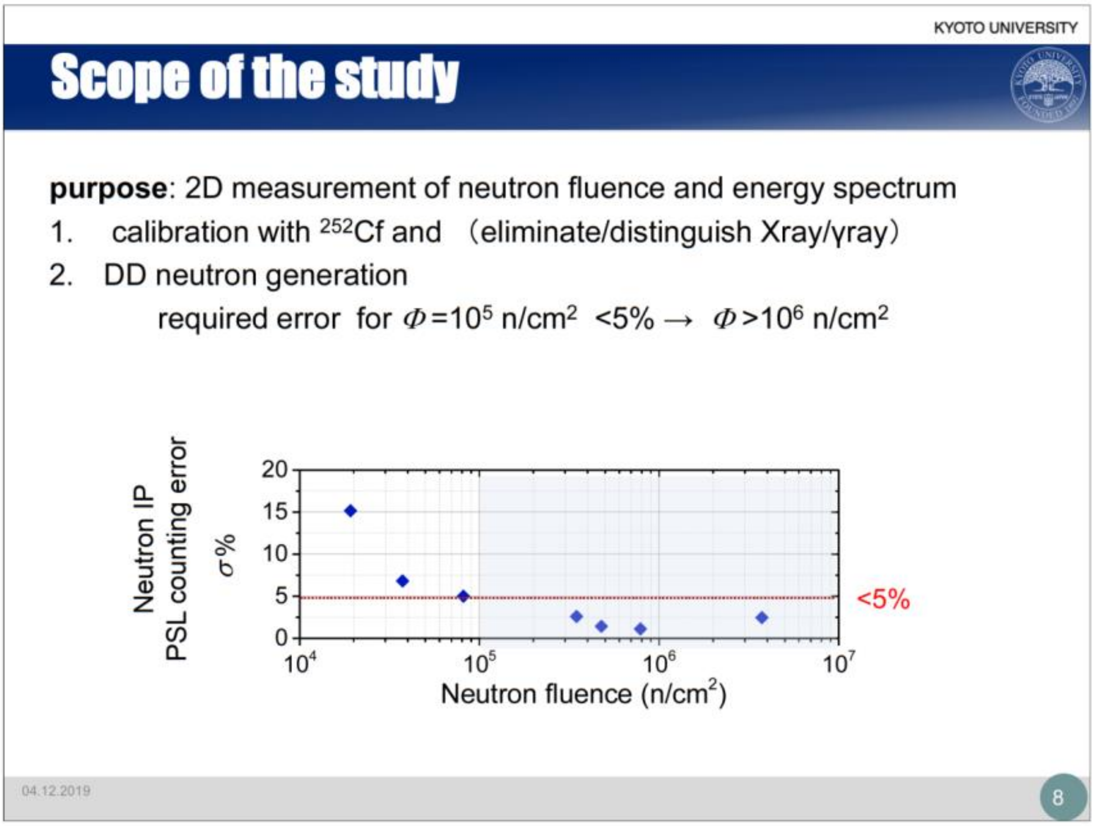
KYOTO UNIVERSITY
Scope of the study
purpose: 2D measurement of neutron fluence and energy spectrum
1. calibration with 252Cf and (eliminate/distinguish Xray/γray)
2. DD neutron generation
required error for Φ=10⁵ n/cm² <5% → Φ>10⁶ n/cm²
Neutron IP
PSL counting error
σ%
<5%
Neutron fluence (n/cm²)
04.12.2019
8

KYOTO UNIVERSITY

Experimental set up

^{3}He counter was uncovered by Pb.

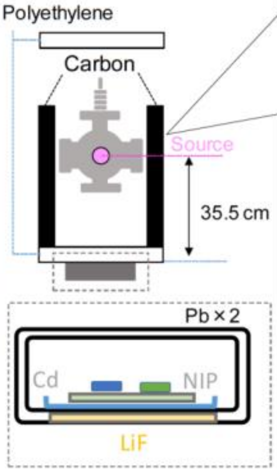

Discharge-type DD neutron source[1,2]

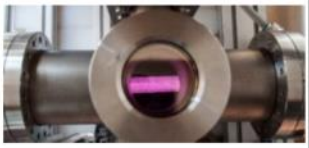

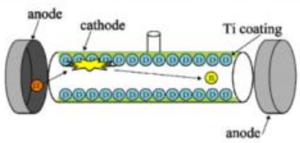

D + D → He + n(2.45 MeV)

Neutron imaging plate (NIP)	BAS-ND2025 Fuji film
Neutron measurement	^{3}He gas-filledcounter
Image analyzer	STORM8200 (Molecular dynamics)

9

KYOTO UNIVERSITY

Target materials

NIP

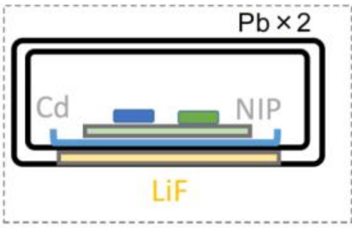

Li_2TiO_3	5.58 g (18% T.D.)
Li_2O	9.19 g (50% T.D.)
B_4C	5.59 g (24% T.D.)

V of PMMA container : 17.39 cm^3
V of target materials : 9.67 cm^3

04.12.2019 Keisuke Mukai 10

KYOTO UNIVERSITY

Procedure

^{252}Cf source

activity	1.4×10^4 Bq
NPR:	1.8×10^3 n/s
Energy E_{av}	2.3 MeV
accompanied	γ線(>1 MeV)

5 cm PB (μ = 0.87 cm^{-1})

Discharge DD source

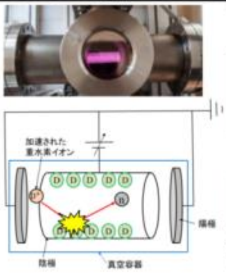

Energy E	2.45 MeV
Pressure of D2	0.5–1.0 Pa
current	<30 mA
voltage	<125 kV (X ray)

Low current with higher voltage

Neutron transport simulation and benchmark

Neutron IP	BAS-ND2025 (Gd 含有) Fuji film
counting	^{3}He
scanning	STORM8200 (GE Health care)

code	MCNP 5
library	FENDL 2.1 FENDL 3.0 IRDFF-1.05

04.12.2019 11

KYOTO UNIVERSITY

Calibration with ^{252}Cf

^{252}Cfirradiation for（1 h～10days）for (P vs Φ)

MCNP

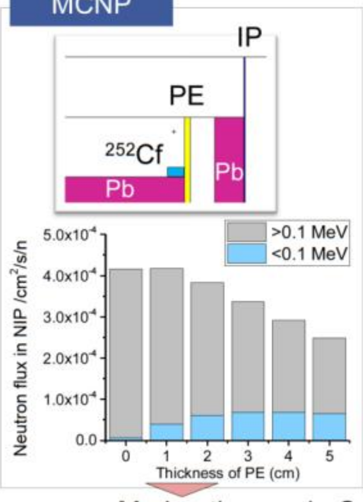

Moderation made Gd(n,γ) reaction
→ enhanced sensitivity

exposure

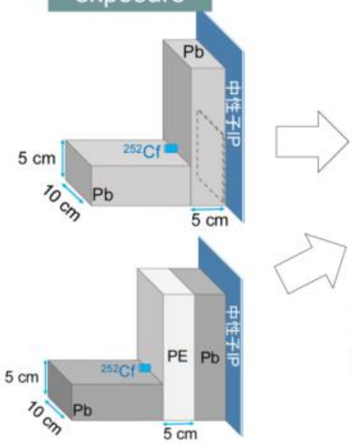

scanning

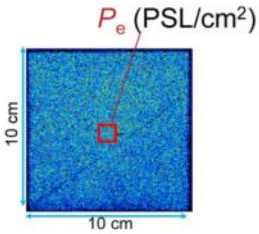

- P (PSL/cm^2): $P_e - P_{BG}$
- Φ (n/cm^2): $\phi \times t$

ϕ: flux (n/cm^2/s)

t: exposure time(s)

04.12.2019 12

KYOTO UNIVERSITY

Gamma ray from 252Cf source

J. Phys. G: Nucl. Part. Phys. **42** (2015) 034025 — P Talou *et al*

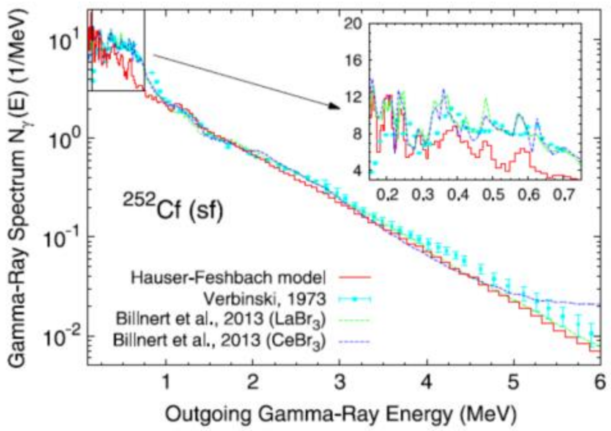

Figure 6. The average prompt fission γ-ray spectrum in the spontaneous fission of ^{252}Cf measured by Billnert *et al* [49] and by Verbinski *et al* [51] are compared to recent calculations [52, 53] using a Monte Carlo implementation of the Hauser-Feshbach statistical theory of nuclear reactions.

13

KYOTO UNIVERSITY

Comparison of IP counting with ^{252}Cf

10^3–10^7 n/cm^2 4orders of linearity ($P \propto \Phi^{0.95\pm0.02}$) observed

5 cm thick polyethylene enhanced total sensitivity for Neutron IP

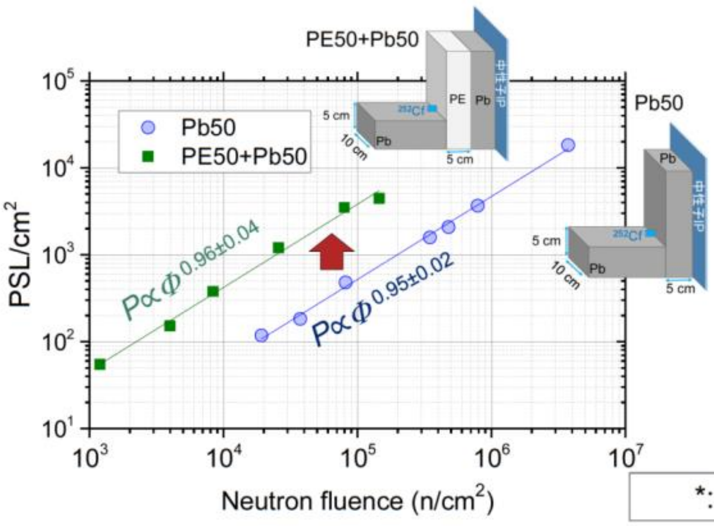

*: PSL$\propto \Phi^{0.974}$

*H. Kobayashi *et al*., *Nucl. Instrum. Methods Phys. Res. A* 424, 1-8 (1999).

14

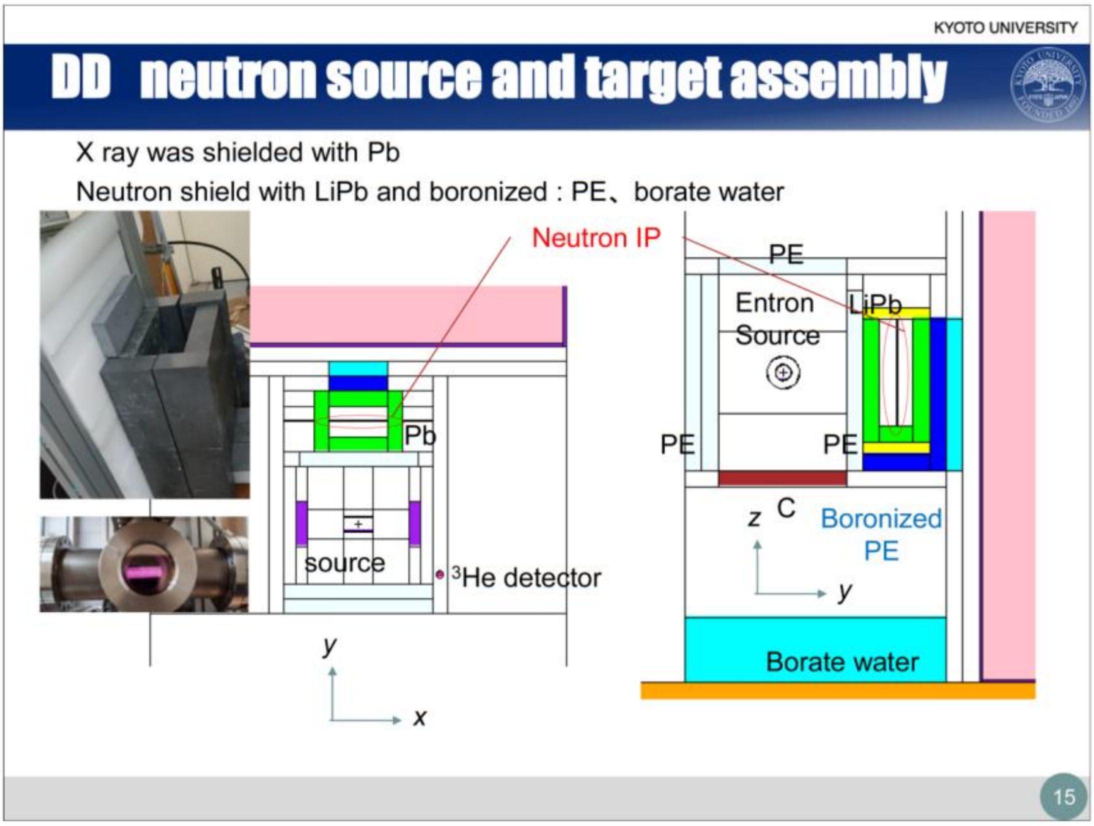
KYOTO UNIVERSITY
DD neutron source and target assembly
X ray was shielded with Pb
Neutron shield with LiPb and boronized : PE、borate water
Neutron IP
Pb
source
³He detector
y
x
PE
Entron Source
LiPb
PE
PE
z
C
Boronized PE
y
Borate water
15

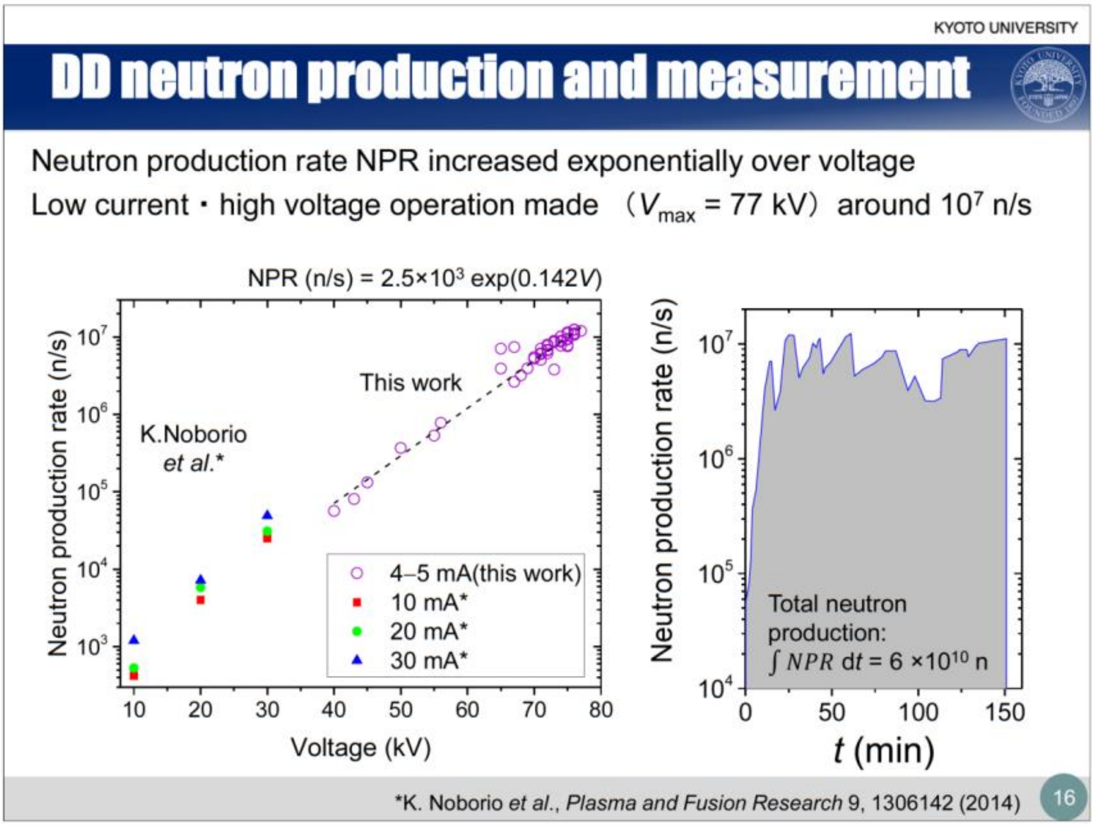
KYOTO UNIVERSITY
DD neutron production and measurement
Neutron production rate NPR increased exponentially over voltage
Low current・high voltage operation made （V_max = 77 kV）around 10⁷ n/s
NPR (n/s) = 2.5×10³ exp(0.142V)
Neutron production rate (n/s)
This work
K.Noborio et al.*
4–5 mA(this work)
10 mA*
20 mA*
30 mA*
Voltage (kV)
Neutron production rate (n/s)
Total neutron production:
∫NPR dt = 6 ×10¹⁰ n
t (min)
*K. Noborio et al., Plasma and Fusion Research 9, 1306142 (2014)
16

KYOTO UNIVERSITY

Influence of PE thickness on Neutron flux in NIP

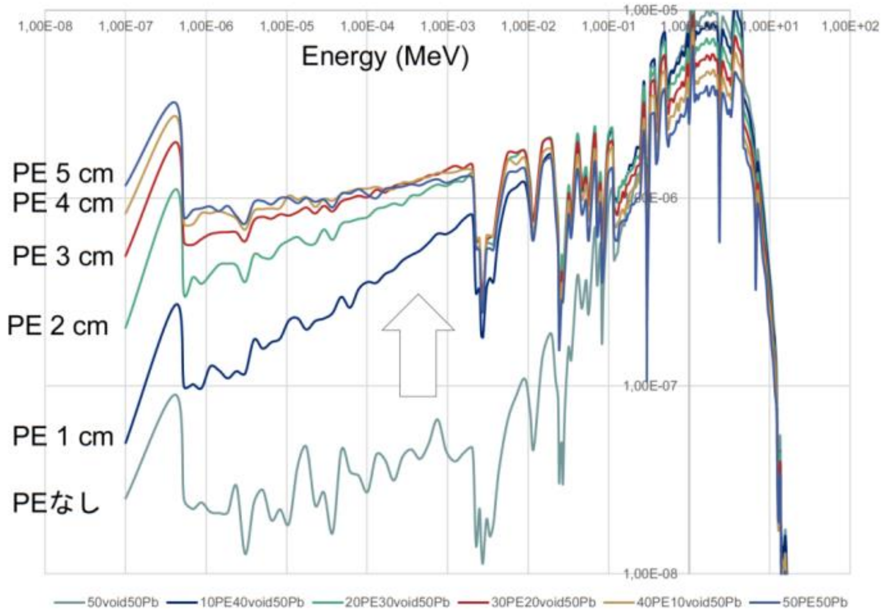

17

KYOTO UNIVERSITY

Neutron fluence and energy spectrum

Approximately 1 h exposure was sufficient for imaging with NIP at $\Phi > 10^6$ n/cm^2.

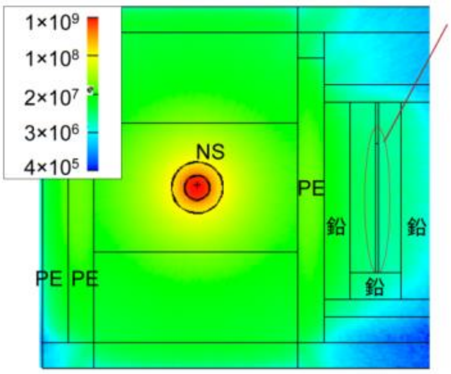

Neutron fluence n/cm^2

NIP: $\Phi = 6\times10^6$ n/cm^2

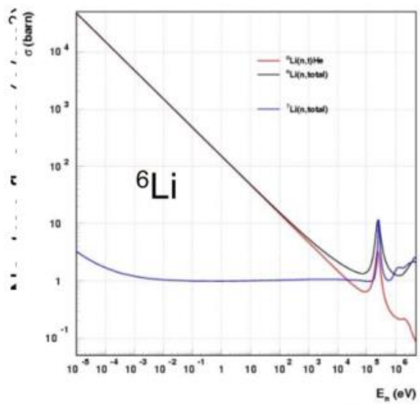

elastic scattering by ^{6}Li can be avoided by eliminating >10 keV

18

KYOTO UNIVERSITY

Energy spectrum measurement

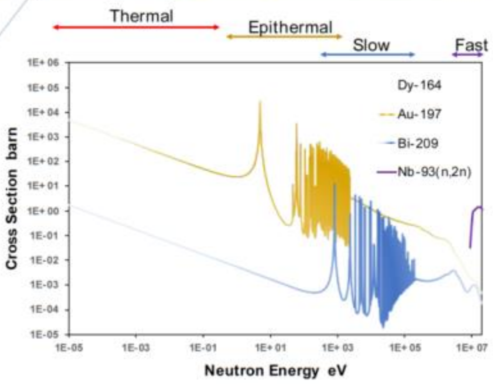

Cross sections of different activation materials
for higher energy neutrons

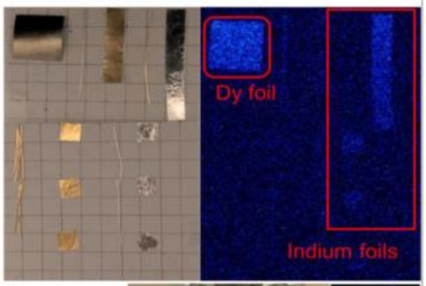

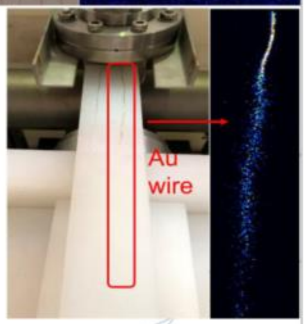

various activation materials are tested for
detection of higher energy neutron followed by unfolding
Au,In and Dy

Aug.07.2019 19

19

KYOTO UNIVERSITY

Conclusion

- For the 2D measurement of neutron, (1) neutron IP was calibrated with ^{252}Cf and discharge neutron source. (2) Discharge source was conditioned to generate 10^7 n/s. X and γ shielded.
- Neutron was moderated for the converter Gd(n, γ), and good lineality (PSL$\propto\Phi^{1.02\pm0.05}$) was obtained in the range of $10^3<\Phi<10^7$ n/cm^2.
  →for faster neutrons, different convertors are planned to be used to measure the energy spectrum.
- Low current high voltage glow discharge yielded $>10^7$ n/s .
  → ca. 1 h exposure is sufficient to make $\Phi>10^6$ n/cm^2 imaging.
- for the neutronics benchmarking of fusion blanket, ^{6}Li(n,t) will be measured with a pair of realistic modules and neutron spectrum.
- For further study, IP with different energy sensitivity will be developed.
- Both neutron and γ ray will be either shielded or utilized depending on the target nucli. Neutron and /X ray are distinguished by shielding

This technique may be applied for 2D/3D detection of various elements.

JSPS grant (17H06794) partially supported.

20

Tritium and helium solubility in Li_2TiO_3 from density functional theory

Samuel T. Murphy

Engineering Department, Lancaster University, Bailrigg, Lancaster LA1 4YW, UK

An understanding of the fundamental processes governing the behaviour of tritium and helium in a ceramic breeder materials is a requirement for the development of breeder blanket technologies for future fusion reactors. Here, density functional theory (DFT) is used to study tritium and helium accommodating defects in one of the leading breeder blanket candidate materials, Li_2TiO_3. Defect formation energies are combined with simple thermodynamics to predict the mechanisms of tritium/helium solubility across a range of conditions relevant to a fusion reactor. The simulations predict very different modes of tritium accommodation depending on the stoichiometry of the crystal and the oxygen partial pressure. In addition, results appear to support the idea that the presence of helium can increase the release rate of tritium by displacing tritium atoms from lithium vacancy defects. Finally, the simulations show how the incorporation of a significant tritium concentration can modify the defect chemistry of the host matrix.

Lancaster University

Tritium and helium solubility in Li_2TiO_3 from density functional theory

Samuel T. Murphy (samuel.murphy@lancaster.ac.uk)

Where on earth is Lancaster?

Lancaster University

Lancaster Castle was Europe's longest serving prison, finally closing in 2011.

The multiscale modelling approach

Lancaster University

"Simulation is a means of scientific discovery that employs a computer system to simulate a physical system according to laws from theory and experiment"

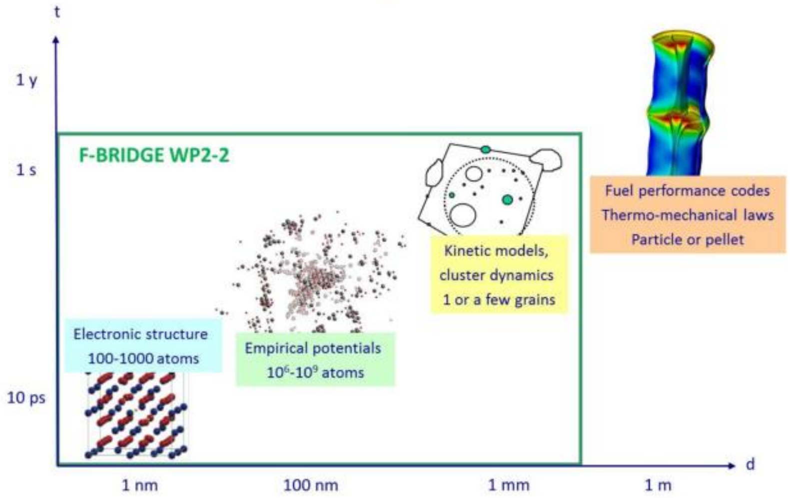

Sustaining nuclear fusion

Lancaster University

- Employ to so called D-T reaction:

$$^{2}_{1}D + ^{3}_{1}T \rightarrow ^{4}_{2}He + ^{1}_{0}n + energy!$$

- Deuterium can be easily extracted from sea-water.
- Tritium is radioactive and has a half-life of 12.32 years so does not occur naturally.
- Can generate tritium *in-situ* from the transmutation of lithium, via:

$$^{6}_{3}Li + ^{1}_{0}n \rightarrow ^{4}_{2}He + ^{3}_{1}T$$

- Lithium is abundant.

Ceramic pebbles

Lancaster University

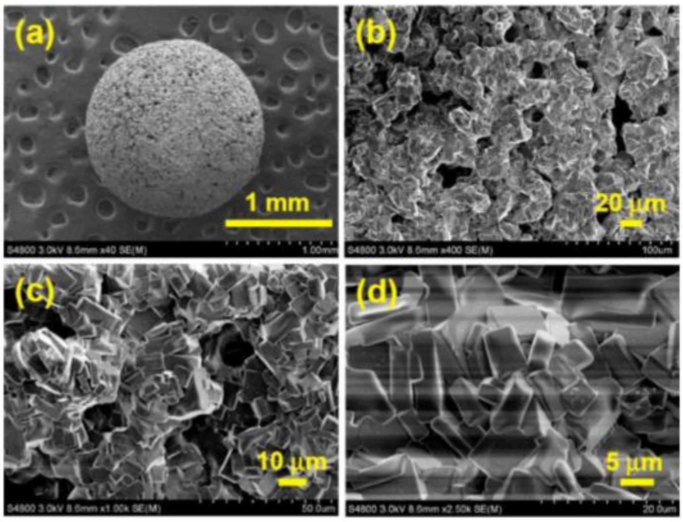

Li_2TiO_3 pebbles fabricated by a modified indirect wet chemistry method (Yu *et al.* Fus. Eng. Des. 101 (2015) 73).

Tritium release process

Lancaster University

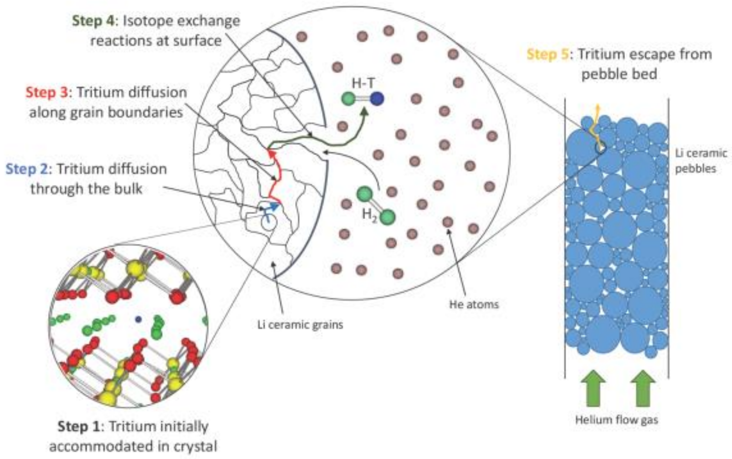

- The rate limiting step in this process is tritium diffusion in the bulk.
- Activation energies for the release process vary significantly 0.63-1.5 eV for Li_2TiO_3 to 0.4-0.88 eV for Li_4SiO_4.

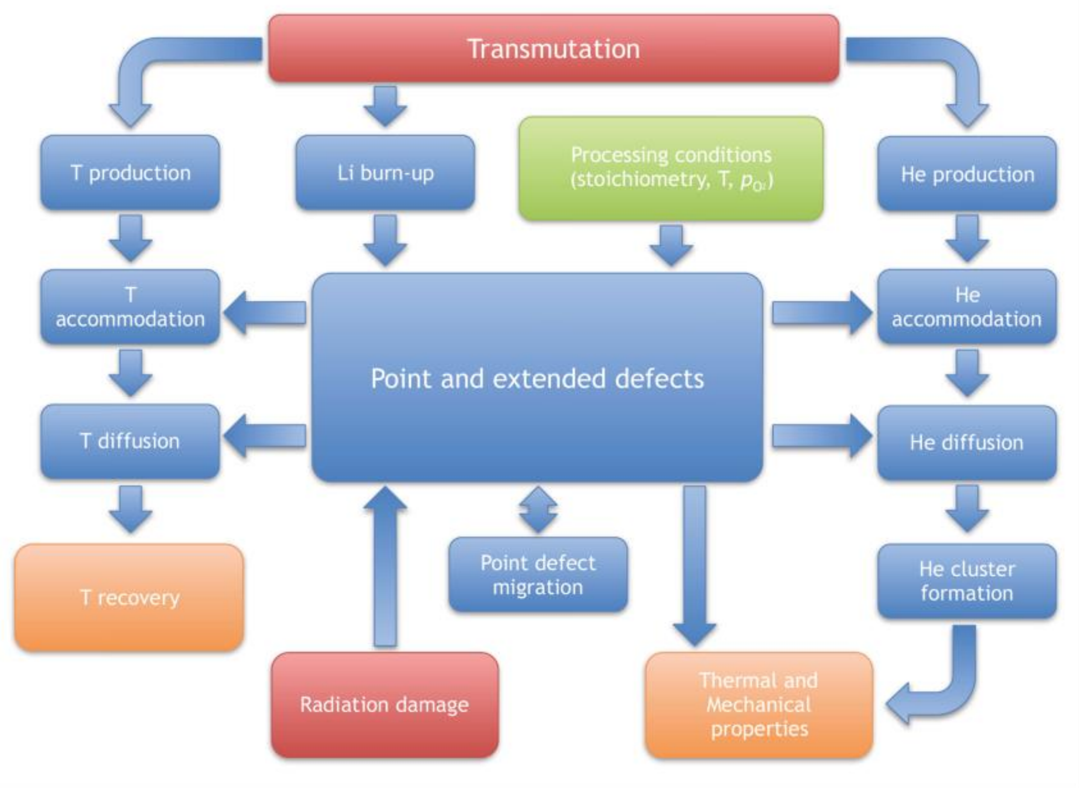

Lithium metatitanate

Lancaster University

- Lithium metatitanate (Li_2TiO_3) is a leading ceramic breeder candidate.
- According to the phase diagram Li_2TiO_3 can extend from 47.5-51.5% TiO_2.
- Can fabricate Li_2TiO_3 with Li excess to enhance tritium breeding.
- As burn-up proceeds material will become lithium deficient.
- The important question is will this change affect tritium extraction?

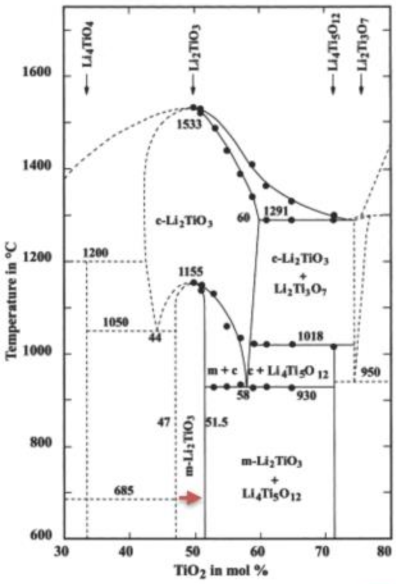

Lithium metatitanate

Lancaster University

- Li_2TiO_3 has a complex crystal structure that can be best thought of as a rocksalt structure with alternating Li_6 ,O_6 , Li_2Ti_4 , O_6 (111) planes.

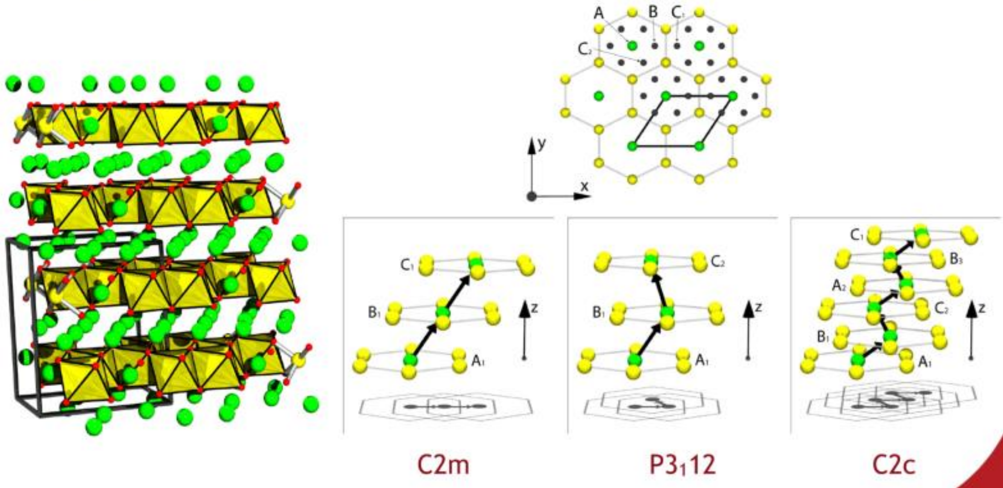

Lithium metatitanate

Lancaster University

- Li_2TiO_3 has a complex crystal structure that can be best thought of as a rocksalt structure with alternating Li_6 ,O_6 , Li_2Ti_4 , O_6 (111) planes.

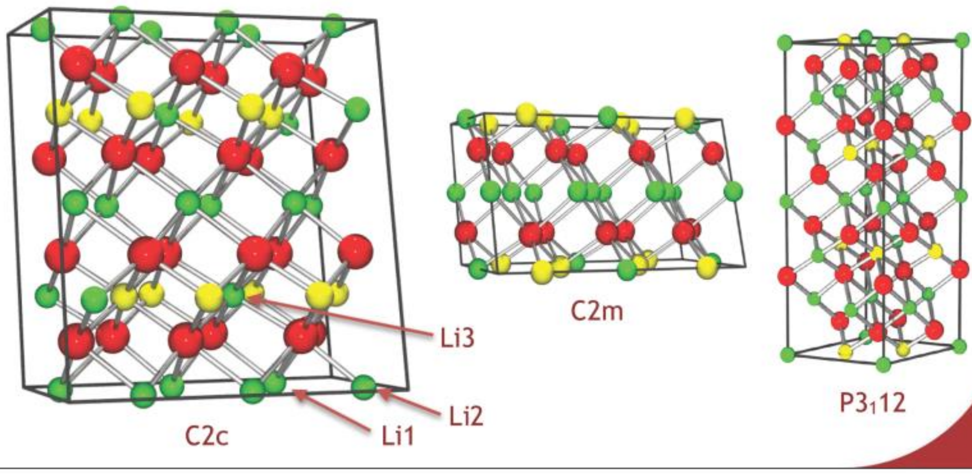

Simulation methodology

Lancaster University

- Perform *ab initio* density functional theory (DFT) simulations using the CASTEP code.
- Exchange correlation represented using the GGA-PBE.
- Ultrasoft pseudopotentials generated using CASTEP's *on-the-fly* pseudopotential generator (cutoff energy 550 eV).
- Sample the Brillouin zone using a Monkhorst-Pack grid of points with the spacing between points maintained at 0.05 A^{-1} in all directions.
- Perform defect calculations in supercells of different sizes to overcome finite size effects.
- Lattice parameters fixed for defect containing supercells.

Note as we use the GGA-PBE there are some issues with the bandgap (3.27 eV versus 3.9 eV from experiment)

Bulk Li_2TiO_3

Lancaster University

Lattice parameters for the three Li_2TiO_3 crystal structures calculated using DFT and the empirical pair potential of Vijanakumar *et al*. J. Phys. Chem. C 113 (2009) 20108.

Property	C2/m		P_3112		C2/c		
	DFT	Emp	DFT	Emp	DFT	Emp	Exp
Volume / Å	216.65	208.51	324.98	312.82	**433.22**	417.10	**427.01**
a /Å	5.10	5.08	5.09	5.07	**5.09**	5.07	**5.06**
b/Å	8.80	8.77	5.09	5.07	**8.83**	8.80	**8.79**
c /Å	5.13	4.98	14.47	14.04	**9.80**	9.51	**9.75**
α/◦	90.00	90.00	90.03	90.00	**90.00**	90.00	**90.00**
β/◦	109.88	109.93	89.98	90.00	**100.25**	100.24	**100.21**
γ/◦	90.00	90.00	119.99	120.00	**90.00**	90.00	**90.00**

Bulk Li_2TiO_3

Lancaster University

Atomisation and interaction energies for the three three Li_2TiO_3 crystal structures calculated using DFT and the empirical pair potential of Vijanakumar *et al.* J. Phys. Chem. C 113 (2009) 20108.

Property	C2/m		$P3_112$		C2/c		
	DFT	Emp	DFT	EMP	DFT	Emp	Exp
E_a /eV	33.12	-	33.12	-	33.12	-	33.03
$\Sigma E(r_{ij})$	-	50.23	-	50.23	-	50.23	

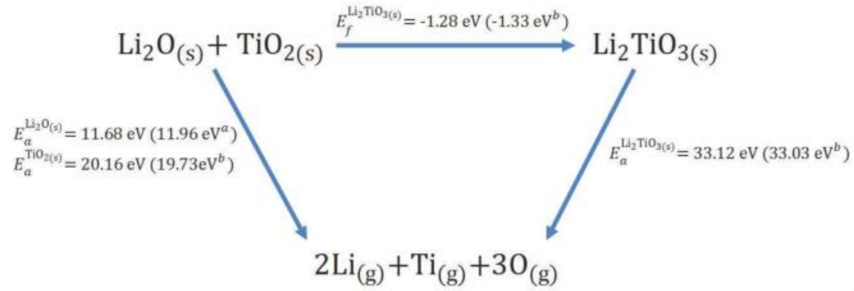

Defect formation energies

Lancaster University

- The concentration of a defect is related to the energy required to form the defect, E_f:

$$[c_i] \propto m_i \exp\left(\frac{-\Delta E_f}{k_B T}\right)$$

- The defect formation energy can be calculated using DFT and the supercell approach, according to:

$$\Delta E_f = E^{defect} - E^{perfect} \pm \sum_i n_i \mu_i + q\mu_e$$

- The crystal must be charge neutral, therefore:

$$\underbrace{\boxed{\sum_i q_i c_i}}_{\text{Defect contribution}} + \underbrace{\boxed{N_c \exp\left(\frac{E_g - \mu_e}{k_B T}\right)}}_{\text{Electron contribution}} + \underbrace{\boxed{N_v \exp\left(\frac{-\mu_e}{k_B T}\right)}}_{\text{Hole contribution}} = 0$$

Chemical potentials

Lancaster University

- The starting point for the chemical potentials is to assume:

$$Li_2O_{(s)} + TiO_{2(s)} \rightarrow Li_2TiO_{3(s)}$$

- Under any given conditions the sum of the chemical potentials must equal the energy of the product, i.e.:

$$\mu_{TiO_2}\left(p_{O_2},T\right) + \mu_{Li_2O}\left(p_{O_2},T\right) = \mu_{Li_2TiO_{3(s)}}$$

- Then define limits, for example Li_2O-rich:

$$\mu_{Li_2O}\left(p_{O_2},T\right) = \mu_{Li_2O_{(s)}} \qquad \mu_{TiO_2}\left(p_{O_2},T\right) = \mu_{Li_2TiO_{3(s)}} - \mu_{Li_2O_{(s)}}$$

- This can then be further decomposed:

$$\mu_{Li_2O_{(s)}} = 2\mu_{Li}\left(p_{O_2},T\right) + \mu_{1/2O_{2(g)}}\left(p_{O_2},T\right)$$

Chemical potentials

Lancaster University

- We then run into a problem with the DFT description of the O_2 molecule, so we reference the experimental free energy:

$$\Delta G_f^{Li_2O}\left(p^{\circ}_{O_2},T^{\circ}\right) = \mu_{Li_2O_{(s)}} - 2\mu_{Li_{(s)}} - \mu_{1/2O_{2(g)}}\left(p^{\circ}_{O_2},T^{\circ}\right)$$

- The oxygen chemical potential can be extrapolated using ideal gas relations:

$$\mu_{1/2O_{2(g)}}\left(p_{O_2},T\right) = \mu_{1/2O_{2(g)}}\left(p^{\circ}_{O_2},T^{\circ}\right) + \Delta\mu(T) + \frac{1}{2}k_B T \log\left(\frac{p_{O_2}}{p^{\circ}_{O_2}}\right)$$

where

$$\Delta\mu(T) = -\frac{1}{2}\left(S^{\circ}_{O_2} - C^{\circ}_P\right)\left(T - T^{\circ}\right) + C^{\circ}_P \log\left(\frac{T}{T^{\circ}}\right)$$

- From the the oxygen chemical potential the other can be easily determined.

Non-stoichiometry in Li_2TiO_3

Lancaster University

- Li_2O-rich Li_2TiO_3

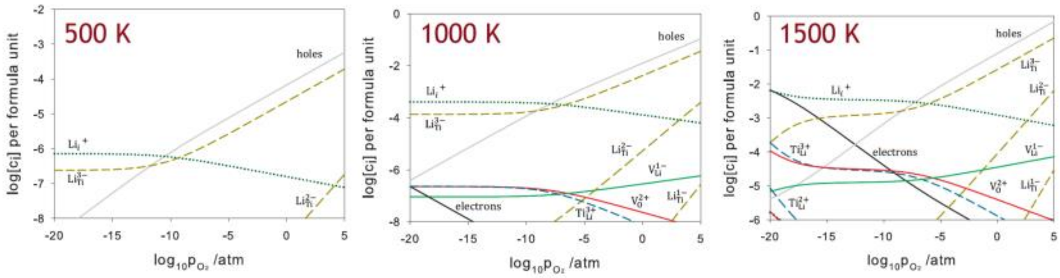

- Defect chemistry dominated by lithium interstitial and antisite defects.
- At high temperature and low oxygen partial pressure the Lithium interstitial compensated for by electrons (i.e. Ti^{3+} ions) dominates in excellent agreement with experiment.

Non-stoichiometry in Li_2TiO_3

Lancaster University

- TiO_2-rich Li_2TiO_3

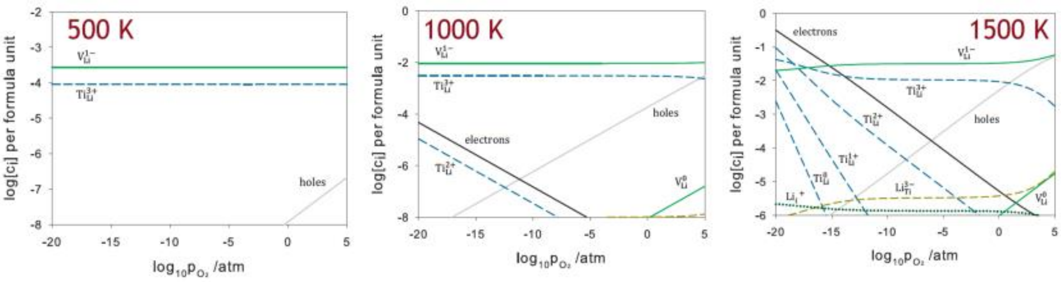

- Defect chemistry completely dominated by lithium vacancies and titanium antisites in excellent agreement with experiment.

Non-stoichiometry in Li_2TiO_3

Lancaster University

- Defect chemistry as a function of stoichiometry (@ p_{O2} = 10^{-20} atm).

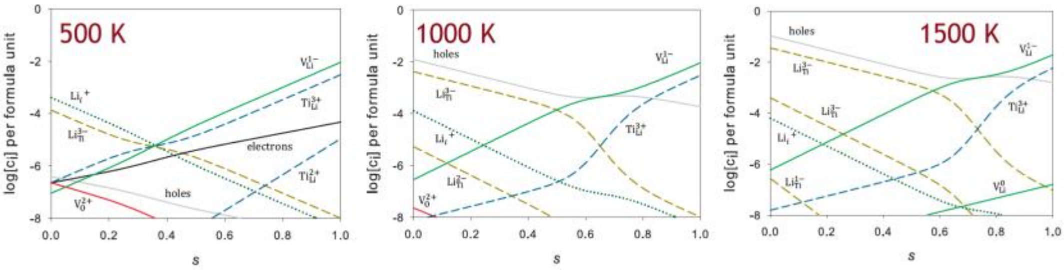

T accommodation in Li_2TiO_3

Lancaster University

- Tritium will be accommodated at these point defects, so as the availability of point defects changes so does the mechanism of tritium solubility.

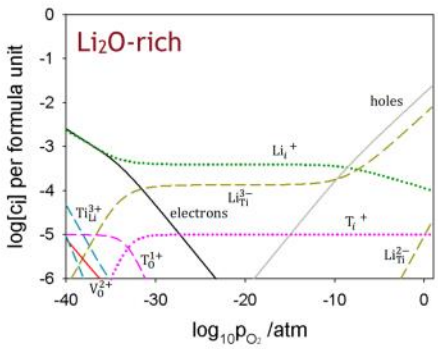

Brouwer diagram showing defect concentrations in Li_2O-rich Li_2TiO_3 as a function of the oxygen partial pressure with a tritium concentration of 10^{-5} per formula unit.

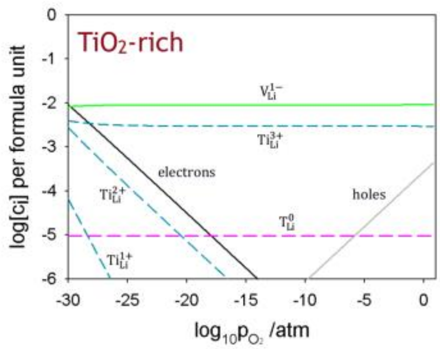

Brouwer diagram showing defect concentrations in Li_2O-rich Li_2TiO_3 as a function of the oxygen partial pressure with a tritium concentration of 10^{-5} per formula unit.

T accommodation in Li_2TiO_3

Lancaster University

- At high tritium concentrations the tritium will start to dominate the intrinsic defect chemistry in Li_2O-rich Li_2TiO_3.

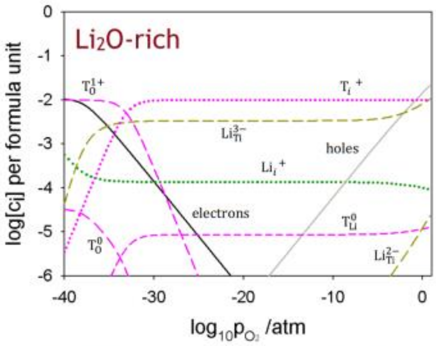

Brouwer diagram showing defect concentrations in Li_2O-rich Li_2TiO_3 as a function of the oxygen partial pressure with a tritium concentration of 10^{-2} per formula unit.

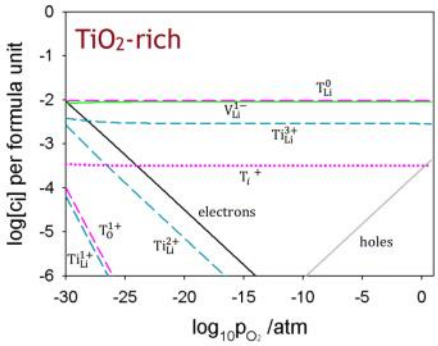

Brouwer diagram showing defect concentrations in Li_2O-rich Li_2TiO_3 as a function of the oxygen partial pressure with a tritium concentration of 10^{-2} per formula unit.

He accommodation in Li_2TiO_3

Lancaster University

- Similarly helium must be accommodated at point defects.

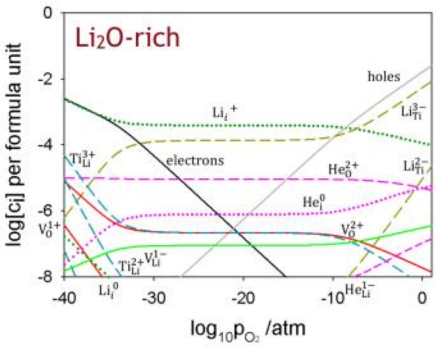

Brouwer diagram showing defect concentrations in Li_2O-rich Li_2TiO_3 as a function of the oxygen partial pressure with a helium concentration of 10^{-5} per formula unit.

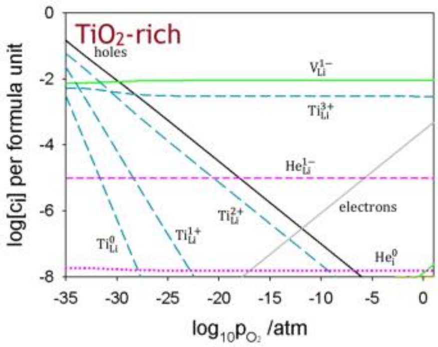

Brouwer diagram showing defect concentrations in Li_2O-rich Li_2TiO_3 as a function of the oxygen partial pressure with a helium concentration of 10^{-5} per formula unit.

Non-stoichiometry and T and He accommodation in Li_2TiO_3

Lancaster University

- During operation the fuel will move from being Li_2O-rich to TiO_2 rich and consequently the mode of tritium accommodation will change.
- Under TiO_2-rich conditions T may become bound to lithium vacancies, thereby slowing down diffusion and extraction.

$$T_{Li}^{0} \xrightarrow{0.6\ \mathrm{eV}} T_{i}^{1+} + V_{Li}^{1-}$$

- However, the presence of helium may help displace tritium from these lithium vacancies, via:

$$T_{Li}^{0} + He_{i}^{0} \xrightarrow{-0.2\ \mathrm{eV}} T_{i}^{1+} + He_{Li}^{1-}$$

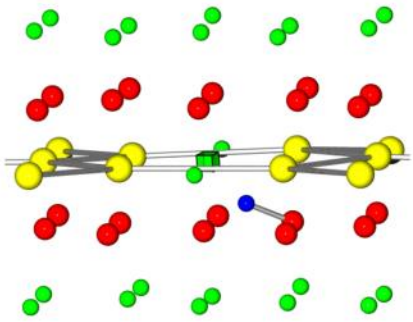

Tritium interstitial bound to a lithium vacancy defect (Murphy J. Phys. Chem. C 2016).

Conclusions

Lancaster University

- Defect chemistry under Li_2O-rich conditions dominated by antisite defects and Li interstitials.
- Under TiO_2-rich conditions the defect chemistry dominated by lithium vacancies and titanium antisites.
- Tritium accommodated as either T_O or T_i defect under Li_2O-rich conditions and T_{Li} defect under TiO_2-rich conditions
- He accommodated on oxygen site under Li_2O-rich conditions and on lithium site under TiO_2-rich conditions.
- Both of these have implications for T release.

Thank you for your attention

Lancaster University

- I would like to thank people who have helped with this work:
  - Dr. Nicholas Hine (Warwick University)
  - Dr. Laurent van Brutzel (CEA Saclay)
  - Dr. Alain Chartier (CEA Saclay)
  - Dr. Phillipe Zeller (CEA Saclay)
  - Imperial College High Performance Computing Centre

archer

EPSRC

Engineering and Physical Sciences Research Council

A first-principles kinetic Monte Carlo investigation of tritium diffusion in Li_2TiO_3

Kamal Nayan Goswami and Samuel T. Murphy

Department of Engineering, Lancaster University, Lancaster LA1 4YW, United Kingdom

The nuclear fusion reactors of the future will be based on the reaction between deuterium and tritium. Since there is no naturally occurring source of tritium, it is expedient to generate it *in-situ* from the transmutation of Li using the high energy neutron ejected from the plasma. This will be done by surrounding the reactor by a blanket region containing the lithium breeder material such as lithium metatitanate (Li_2TiO_3). Li_2TiO_3 is a promising candidate for a breeder material given its high Li density, high melting temperature and excellent tritium-release performance amongst others. However, in order to ensure a self-sustaining plasma, a tritium breeding ratio of at least unity is essential. The tritium release from a solid breeder material is the limiting step in the tritium recovery process and thus it is important to understand the atomic scale mechanisms responsible for tritium diffusion in the breeder material. The activation energy for tritium diffusion in Li_2TiO_3 has been reported with considerable uncertainty in previous experimental studies.

In this work, we have used kinetic Monte Carlo (kMC) simulations to study tritium diffusion in single crystal Li_2TiO_3. Inside the Li_2TiO_3 matrix, tritium is either incorporated as an interstitial defect or trapped at a vacant lattice site. Here we study tritium accommodation at six different interstitial sites and three types of Li vacancies to represent different levels of Li burn-up. The exact positions of tritium adsorption sites in these defects have been identified and mapped on to a lattice, where a tritium atom performs a diffusive jump at each step and the system evolves over time. A number of diffusion barriers have been calculated from density-functional theory (DFT) with values as low as 0.3 eV along the Li_6 layer to about 1 eV crossing the Li_2Ti_4 layer making some of these diffusive jumps more likely than others. Furthermore, the barriers for tritium diffusion within a Li vacancy were lower than that for de-trapping. The trajectory of the tritium atom was tracked and the diffusion coefficient was calculated from its displacement over time. The kMC results reveal the anisotropic nature of tritium diffusion in Li_2TiO_3.

Thermal Conductivity of Li_2TiO_3 by Atomistic Simulation

Megha Sanjeev, Samuel T. Murphy

Lancaster University, Lancaster, LA1 4YW, UK

Breeder materials in a fusion reactor are subjected to irradiation by high energy neutrons leading to the formation of defects, such as vacancies and interstitials. The presence of these defects changes the efficiency of heat transfer through the blanket to the coolant, directly affecting the overall electricity generating efficiency of the reactor. The impact on heat transfer can be predicted by calculating how the thermal conductivity changes upon incorporation of defects. Measuring the impact of specific defects on the thermal conductivity of materials is experimentally complex. Therefore, we employ atomistic simulation, principally non-equilibrium thermodynamics (NEMD) to study the evolution of the thermal conductivity in the leading candidate ceramic Li_2TiO_3.

Previous experimental results show that the thermal conductivity of Li_2TiO_3 initially decreases with temperature before increasing close to the melting point. Our simulations are capable of reproducing this effect indicating the efficacy of the model used. By introducing defects into our simulation supercells, we show how the formation of defects in the material impacts the thermal conductivity and discuss how this may impact reactor efficiency as the blanket material ages.

Radiation damage properties of Li_4SiO_4 and Li_2TiO_3 using molecular dynamics simulations – A comparative study

Deepak Ranjan Sahoo*, Mohammed Suhail*, Ratnakumar Annabattula*, Paritosh Chaudhuri**, Narasimhan Swaminathan*

* Department of Mechanical Engineering, Indian Institute of Technology Madras, Chennai, 600036, India

**Institute for Plasma Research, Bhat, Gandhinagar-382428, Gujarat, India

Among the available lithium containing ceramics, Li_4SiO_4 and Li_2TiO_3 are popular candidates for breeding tritium due to their high lithium density, low activation energy, favorable tritium release and good thermal conductivity. Previous works have mentioned that Li diffusion in both Li_4SiO_4 and Li_2TiO_3 are affected by point defects. The accumulation of point defects also alters the mechanical properties and causes the material to amorphize. In this work, molecular dynamics (MD) simulations on Li_4SiO_4 and Li_2TiO_3 were conducted to estimate several important radiation related properties. In particular, the defect evolution, threshold displacement energies (E_d), primary damage, diffusion coefficient and mechanical properties (pre and post radiation) are considered. Finally, the material is amorphized by explicitly displacing atoms to determine its resistance to radiation induced amorphization (RIA). The response of Li_4SiO_4 is then compared with that of β-Li_2TiO_3. Our simulations indicate that, point defect production is hardly dependent of on the PKA directions in case of Li_2TiO_3 whereas in case of Li_4SiO_4 the defect production in [010] direction is higher than other two directions. While calculating the threshold displacement energy it is observed that O has highest E_d whereas Ti (Li_2TiO_3) and Li (Li_4SiO_4) have the lowest. Further, the dose to amorphization for Li_4SiO_4 was found to be nearly half of that of Li_2TiO_3.

Molecular Dynamics based comparison of radiation damage in Li_2TiO_3 and Li_4SiO_4

Deepak Ranjan Sahoo†, Mohammed Suhail†, Paritosh Chaudhuri⋆, Narasimhan Swaminathan†

† **Department of Mechanical Engineering, Indian Institute of Technology Madras**
⋆**Institute for Plasma Research, Bhat, Gandhinagar, India**

September 19, 2019, CBBI-20, KIT

Introduction

Li based ceramics

- Li based ceramics ⇒ T breeding in fusion reactors
- Good *thermal stability* and *chemical inertness*
- Li_2O, Li_2TiO_3, Li_4SiO_4 and Li_2ZrO_3 ⇒ Researched breeder materials

Essential qualities of breeder materials

- T release ⇒ Diffuse within the material → release from surface [1]
- Thermo-physical/material considerations ⇒ Heat transfer, material interactions, mechanical integrity [2]
- Long-term radiation resistance at ↑ Temperature (gradients) [3] ⇒ Structural/Performance integrity [2], RIA [4], T yield [5]

[1] Journal of Nuclear Materials, **(1994) 210**, 1-2. pp. 143–160.
[2] Fusion Engineering and Design, **(2015) 100**, pp. 2–43.
[3] Journal of Nuclear Materials, **(1998) 258**, pp. 140–148.
[4] The Journal of Physical Chemistry C, **(2017) 121**, 14. pp. 7635–7642.
[5] Journal of Nuclear Materials, **(2014) 447**, 1. pp. 1–8.

Motivation

Choice of Li_2TiO_3 and Li_4SiO_4

- Excellent T release, insensitivity to moisture, low activation [3]
- Very high hardness [6]

Radiation induced effects Li_2TiO_3 and Li_4SiO_4

- $\uparrow n$ flux $\uparrow$ T inventory [7]
- T release kinetics $\Rightarrow$ damage density [5]
- Trapping of T by O $\Rightarrow$ hydroxyl groups $\downarrow$ T release [8]
- Accommodation and diffusion of T (and Li) influenced by defects [9–11]
- Radiation induced disorder (Amorphization) [12]

[3] Journal of Nuclear Materials, **(1998) 258**, pp. 140–148.
[6] The Journal of Physical Chemistry C, **(2011) 115**, 44. pp. 21874–21881.
[7] Journal of Nuclear Materials, **(2015) 458**, pp. 22–28.
[5] Journal of Nuclear Materials, **(2014) 447**, 1. pp. 1–8.
[8] Journal of Nuclear Materials, **(2017) 487**, pp. 84–90.
[9] The Journal of Physical Chemistry C, **(2009) 113**, 46. pp. 20108–20116.
[10] Chemistry of Materials, **(2014) 26**, 4. pp. 1629–1638.
[11] The Journal of Physical Chemistry C, **(2014) 118**, pp. 29525–29532.
[12] Nucl. Instr. Meth. Phys. Res. B, **(2003) 206**, pp. 166–170.

Research Gaps and Goals

Gap

- Primary damage in Li_2TiO_3 and Li_4SiO_4 not studied
- Radiation Induced Amorphization : *which is better?*
- *Performance of existing interatomic potentials for these materials for radiation damage?*

Goals

- Displacement cascades in β-Li_2TiO_3 and Li_4SiO_4 $\Rightarrow$ MD
  - Primary damage $\Rightarrow$ Point defects and Point defect clusters
- Repeatedly move atoms and amorphize $\Rightarrow$ Compare DTA
- Evaluate TDE of atoms in the two materials

Crystal structures and Interatomic potentials [13,14]

Li_2TiO_3: Monoclinic Structure

a = 5.06 Å
b = 8.78 Å
c = 9.90 Å
$\alpha = \gamma = 90^\circ$
$\beta = 100.05^\circ$

Cohesive energy

≈50.23 eV PFU

Li_4SiO_4: Monoclinic Structure

a = 11.89 Å
b = 6.27 Å
c = 17.38 Å
$\alpha = \gamma = 90^\circ$
$\beta = 99.37^\circ$

Cohesive energy

≈119.10 eV PFU

Interatomic potential

Coulombic interaction; Buckingham; Close range; **C-S** for 'O' in Li_2TiO_3 [6]

$$U_{ij} = \frac{1}{4\pi\epsilon_0}\frac{q_i q_j}{r_{ij}} + A_{ij}\exp\left(-\frac{r_{ij}}{\rho_{ij}}\right) - \frac{C_{ij}}{r_{ij}^6} + \phi(x)_{ZBL}; \quad U_{c-s} = k \times r_{c-s}^2$$

[6] The Journal of Physical Chemistry C, **(2011) 115**, 44. pp. 21874–21881.
[13] Molecular Simulation, **(1991) 6**, 4-6. pp. 239–244.
[14] Materials Chemistry and Physics, **(2018) 214**, pp. 548–556.

Simulation parameters

Simulation parameters

- 8 (10) (Li_2TiO_3) and 5(6) (Li_4SiO_4) unit cells + PBCs
- Temperature 583K 0GPa (Li_2TiO_3) [15]
- For comparision: 0K and 0Gpa (Both)
- 2keV and 4keV PKA energies
- Directions [110], [100] and [001] , 10 cascades each

Common simulation box

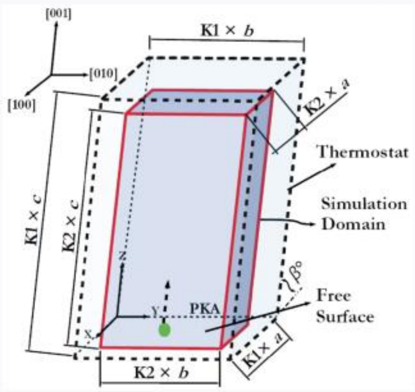

Point defects (Wigner-Seitz [16]), Defect clusters (Hoshen-Kopelman [17])

[15] Journal of Nuclear Materials, **(1988) 155**, pp. 188–201.
[16] Acta Materialia, **(2010) 58**, 8. pp. 2843 –2853.
[17] Physica A, **(2003) 321**, pp. 665–678.

Cascade simulation phases

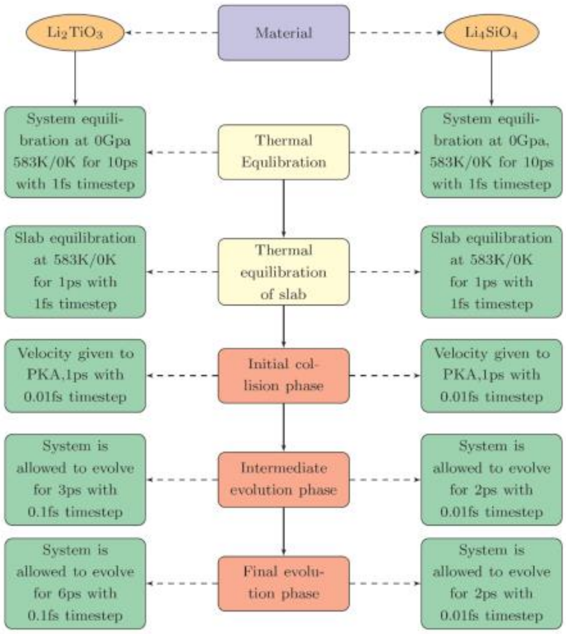

Effect of core-shell in Li_2TiO_3

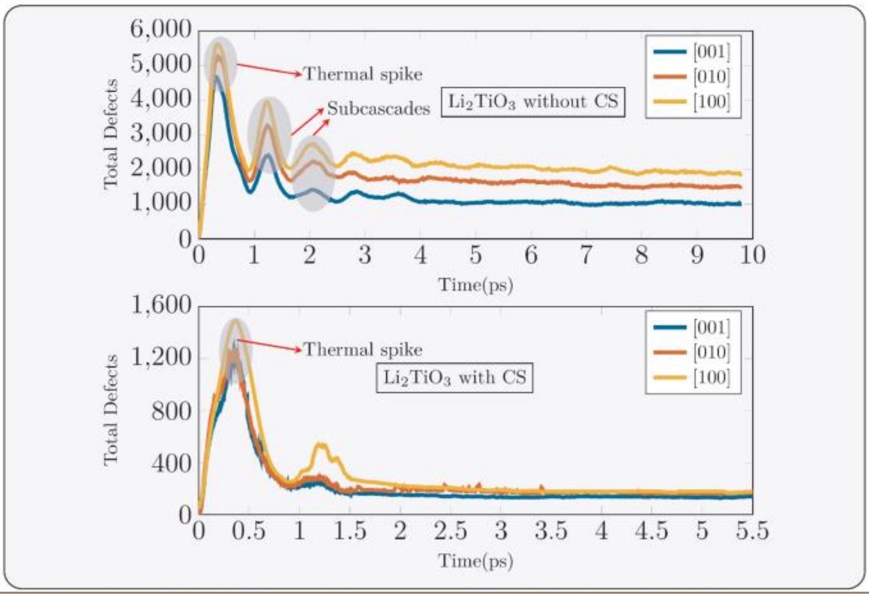

Accounting for polarization affects cascade behavior and defect production

Comparison between Li_2TiO_3 and Li_4SiO_4 @583K

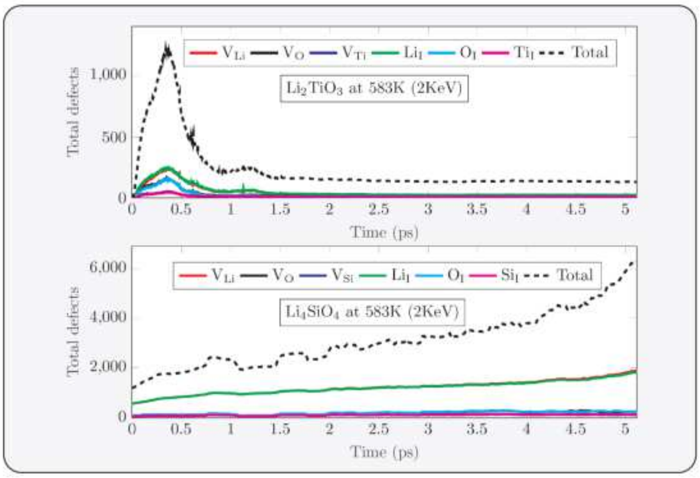

Lithium sub-lattice seems to be diffusing at 583K in Li_4SiO_4

It has been suggested that Li defects can be mobile at 8-80K [18]

[18] Nucl. Instrum. Meth. B, **(2006) 250**, 1-2. pp. 159–163.

Comparison between Li_2TiO_3 and Li_4SiO_4

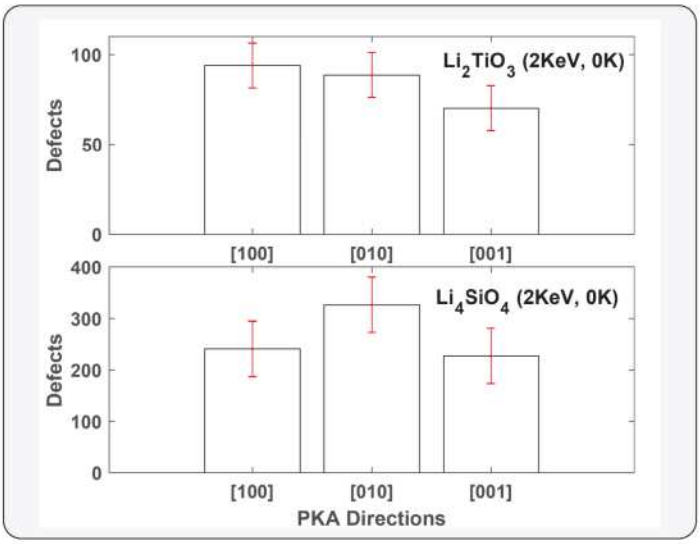

Directional dependence is observed for both materials

Defect Clusters

Clusters in Li_2TiO_3

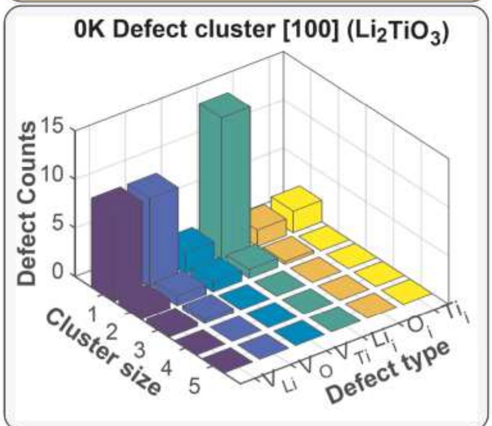

Clusters in Li_4SiO_4

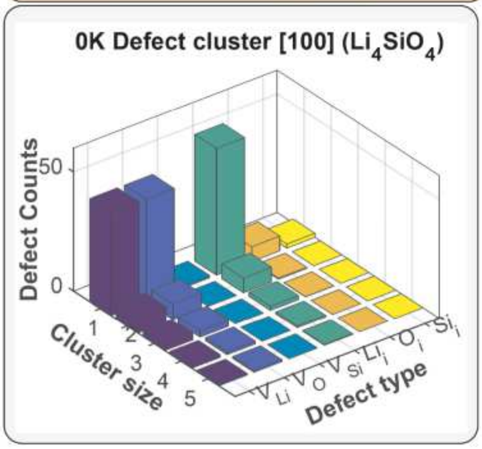

Clusters of size 2 are produced for 2keV PKA energy. No major clustering were observed even for 4keV.

Comparison between Li_2TiO_3 and Li_4SiO_4

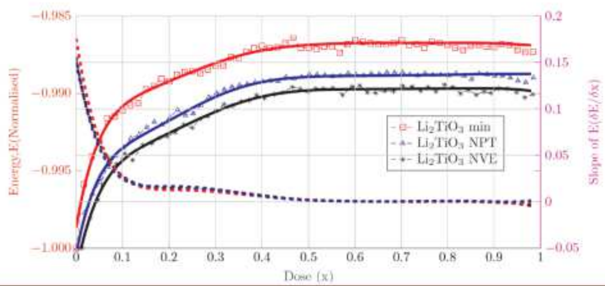

DTA unaffected by temperature or volume confinement

Comparison between Li_2TiO_3 and Li_4SiO_4

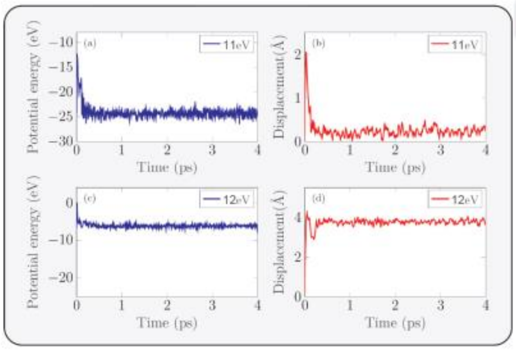

Threshold displacement energy

Directions	Li_2TiO_3 (Li_4SiO_4)		
	Li (Li)	Ti (Si)	O (O)
100	06 (6)	20 (14)	63 (36)
010	12 (17)	58 (23)	70 (34)
001	18 (10)	16 (11)	43 (41)

- O has the highest TDE among others
- In general all atoms in Li_4SiO_4 have lower TDE than atoms in Li_2TiO_3

Li_2TiO_3 seems to have higher resistance to radiation damage

Conclusions

POTENTIALS

Core-Shell interactions affects the behaviour of damage in Li_2TiO_3

Diffusion of Li in Li_4SiO_4 at 583K

RADIATION EFFECTS

More defects in Li_4SiO_4 than in Li_2TiO_3

Intracascade recombination $\Uparrow$ for Li_2TiO_3 $\sim$ peak values are seen

No clusters, Complex dependence on PKA direction

AMORPHIZATION

Li_2TiO_3 DTA is 0.5dpa, while 0.3dpa for Li_4SiO_4


Thank you
THANK YOU
IITM (Narasimhan Swaminathan)
Presentation for CBBI-20
MD-Radiation damage
15 / 15

Maximum Operating Temperature for Li_2TiO_3 Pebble Bed from Sintering Phenomenon

Yi-Hyun Park, Jongil Kim, Mu-Young Ahn, Youngmin Lee, Seungyon Cho

National Fusion Research Institute, Daejeon, 34133 Republic of Korea

In the solid-type of breeding blanket for fusion reactor, the functional materials, such as tritium breeders and neutron multipliers, are used as pebble bed form. The bred tritium from the nuclear reaction between neutron and lithium is extracted by purge gas that flow inside the pebble bed. Therefore, the flow path of the purge gas should be secured and maintained in the pebble bed for the stable tritium extraction. In general, the maximum temperature of the breeder region in the solid-type of breeding blanket has been designed as about 900 °C. However, when the lithium metatitanate (Li_2TiO_3) pebbles are fabricated, the sintering temperature is about 900 °C ~ 1200 °C. Therefore, the $L_{i2}TiO_3$ pebbles in the breeding blanket are possible to be connected with neighbored pebbles by sintering phenomenon. It means that the flow path of purge gas is to be changed in the pebble bed and the tritium extraction is to be not stable. Accordingly, the maximum operating temperature of Li_2TiO_3 pebble bed should be determined for the stable tritium extraction from the viewpoint of sintering phenomenon in the pebble bed.

To investigate the sintering phenomenon of the Li_2TiO_3 pebble bed, the densification curve of the Li_2TiO_3 pebble bed during heating up to 1300 °C under the compression pressure of 4 MPa was obtained by the Hot-press system, which was able to apply the heating and pressure simultaneously. The shrinkage of Li_2TiO_3 pebble bed was started from about 800 °C. The shrinkage rate of the Li_2TiO_3 pebble bed at 850 °C was only about 0.2 mm. However, the shrinkage rate was rapidly increased from 850 °C. Therefore, the initial stage region of sintering on the Li_2TiO_3 pebble bed was able to be determined from 800 °C to 850 °C. From the results of only this conditions, the maximum operating temperature of Li_2TiO_3 pebble bed for stable tritium extraction is able to be estimated at 800 °C. In addition, the effects of compression pressure and holding time on the maximum operating temperature of Li_2TiO_3 pebble bed will be discussed.

20th International Workshop on Ceramic Breeder Blanket Interactions (CBBI-20)

KIT Campus North, 18 - 20 September, 2019

Maximum Operation Temperature for Li_2TiO_3 Pebble Bed from Sintering Phenomenon

Yi-Hyun Park
on behalf of KO TBM Team

National Fusion Research Institute, Republic of Korea

Ministry of Science and ICT

NFRI

KOREA DOMESTIC AGENCY

Outline

I Introduction

II Experimental Method

III Sintering of the Li_2TiO_3 Pebble Bed

IV Creep Deformation of the Li_2TiO_3 Pebble Bed

V Summary

HCCR TBM Concept

◆ Helium Cooled Ceramic Reflector (HCCR) TBM (DEMO-relevant Breeding Blanket Concept)

<Main Design Parameters and Materials>

Parameter	Values
FW heat flux	0.3 MW/m^2
Neutron wall load	0.78 MW/m^2
Thermal Power	0.98 MW (TBD)
Structural material	KO-RAFM (ARAA) (< 550 °C), 1.3 ton 0.01% Zr, Improved creep and impact resistances
Breeder	Li_2TiO_3 (< 920 °C, TBD), 80 kg Li-6 Enrichment Ratio : 70 %
Multiplier	Be (< 650 °C), 100 kg
Reflector	Graphite (<1200 °C), 40 kg Reduce the Be multiplier up to 50 %
Size	1670(P) x 462(T) x 605(R) (mm)
Coolant	8 MPa He / 1.14 kg/s (Nominal) 300 °C inlet / 500 °C outlet
Purge gas	He with 0.1 % H_2
TBM-shield	316L(N)-IG Block / Cooling Channels ITER FW/BLK-PHTS (40 °C, 4 MPa)

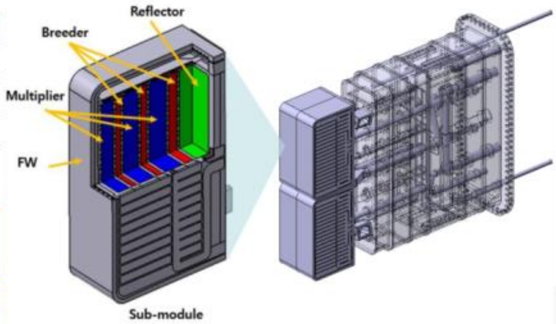

- Four Sub-module Concept
  - Manufacturability, PIE & Transportation of Irradiated TBM
  - EM Force Reduction, Endurance of Internal Over-Pressure
- Graphite as Neutron Reflector
  - Reduce the Amount of Be Multiplier
  - Reduce the difficulty of handling Be
  - Comparable Nuclear Performance
  - Decrease of Cost

Ministry of Science and ICT NFRI iter CBBI-20, KIT Campus North, 18 - 20 Sep., 2019 2

Design Parameters and Li_2TiO_3 Pebble Bed after HT Test

◆ Design Parameters of HCCR TBM

Parameter	Values
FW heat flux	0.3 MW/m^2
Neutron wall load	0.78 MW/m^2
Thermal Power	0.98 MW (TBD)
Structural material	KO-RAFM (ARAA) (< 550 °C), 1.3 ton 0.01% Zr, Improved creep and impact resistances
Breeder	Li_2TiO_3 (< 920 °C, TBD), 80 kg Li-6 Enrichment Ratio : 70 %
Multiplier	Be (< 650 °C), 100 kg
Reflector	Graphite (<1200 °C), 40 kg Reduce the Be multiplier up to 50 %
Size	1670(P) x 462(T) x 605(R) (mm)
Coolant	8 MPa He / 1.14 kg/s (Nominal) 300 °C inlet / 500 °C outlet
Purge gas	He with 0.1 % H_2
TBM-shield	316L(N)-IG Block / Cooling Channels ITER FW/BLK-PHTS (40 °C, 4 MPa)

◆ Li_2TiO_3 Pebble Bed after HT Test

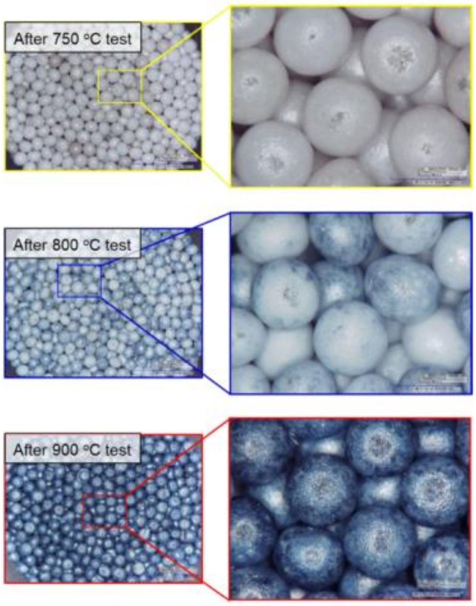

Ministry of Science and ICT NFRI iter CBBI-20, KIT Campus North, 18 - 20 Sep., 2019 3

Design Parameters and Li_2TiO_3 Pebble Bed after HT Test

◆ Design Parameters of HCCR TBM

Parameter	Values
FW heat flux	0.3 MW/m²
Neutron wall load	0.78 MW/
Thermal Power	0.98 MW (
Structural material	KO-RAFM 0.01% Zr, Imp
Breeder	Li_2TiO_3 (Li-6 Enrich
Multiplier	Be (< 650
Reflector	Graphite (Reduce the
Size	1670(P) x
Coolant	8 MPa He 300 °C inlet / 500 °C outlet
Purge gas	He with 0.1 % H_2
TBM-shield	316L(N)-IG Block / Cooling Channels ITER FW/BLK-PHTS (40 °C, 4 MPa)

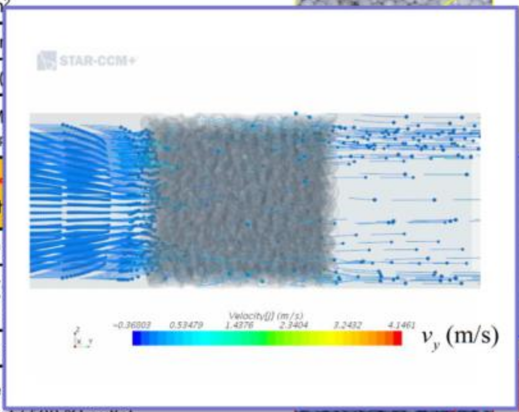

◆ Li_2TiO_3 Pebble Bed after HT Test

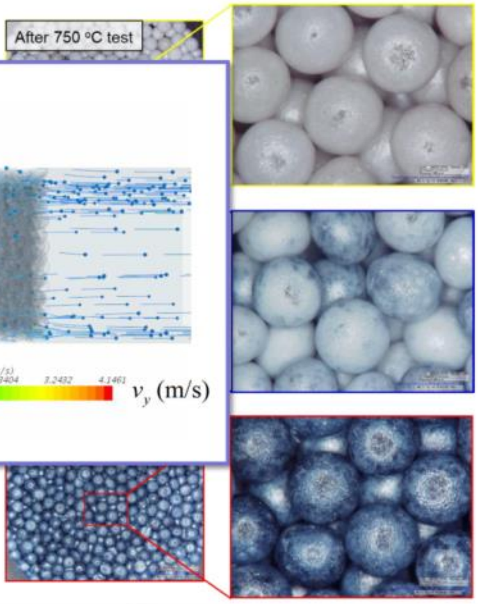

CBBI-20, KIT Campus North, 18 - 20 Sep., 2019 4

Design Parameters and Li_2TiO_3 Pebble Bed after HT Test

◆ Design Parameters of HCCR TBM

Parameter	Values
FW heat flux	0.3 MW/m²
Neutron wall load	0.78 MW/m²
Thermal Power	0.98 MW (TBD)
Structural material	KO-RAFM (ARAA) (< 550 °C), 1.3 ton 0.01% Zr, Improved creep and impact resistances
Breeder	Li_2TiO_3 (< 920 °C,
Multiplier	
Reflector	
Size	(P) x 462(T) x 605(R) (mm)
Coolant	8 MPa He / 1.14 kg/s (Nominal) 300 °C inlet / 500 °C outlet
Purge gas	He with 0.1 % H_2
TBM-shield	316L(N)-IG Block / Cooling Channels ITER FW/BLK-PHTS (40 °C, 4 MPa)

What is the maximum operating temperature for Li_2TiO_3 pebble bed?

◆ Li_2TiO_3 Pebble Bed after HT Test

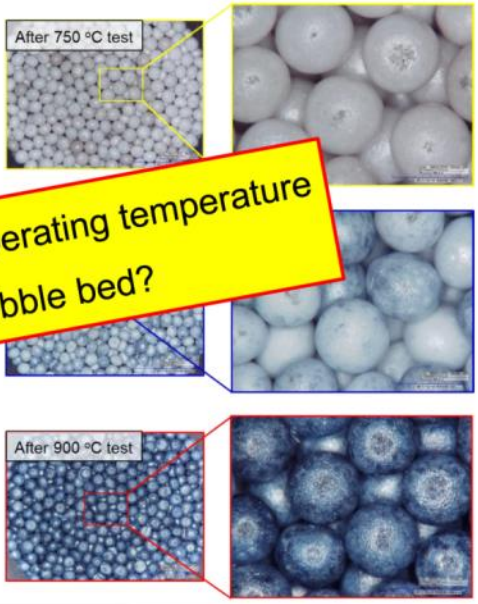

CBBI-20, KIT Campus North, 18 - 20 Sep., 2019 5

Outline

I Introduction

II Experimental Method

III Sintering of the Li_2TiO_3 Pebble Bed

IV Creep Deformation of the Li_2TiO_3 Pebble Bed

V Summary

Fabrication Method of Li_2TiO_3 Pebbles in KO

- Slurry Droplet Wetting Method based on the Cross-linking Reaction between PVA and Boric-acid

Fabrication Process

Li_2TiO_3 Powder → Mixing ← PVA Solution

Mixing → Dropping into Glycerin including Boric Acid → Drying → Sintering

Mixing

Shaping

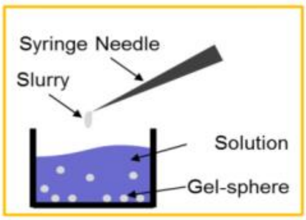

Sintering

Mass-production for Li_2TiO_3 Pebbles

- Automatic Slurry Dispensing System

Dispensing Unit

; for instillation of Li_2TiO_3 slurry

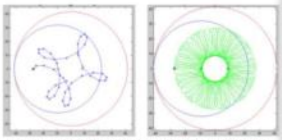

Trace of Drop Point through the Moving Needle

Glycerin Bath

; for hardening of droplets

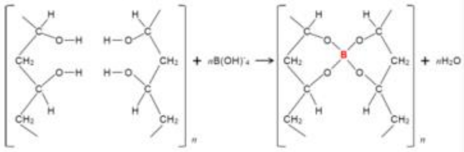

Automatic maintaining Unit

; for constant distance between syringe needle and glycerin surface

Hot Press Test for Sintering of Li_2TiO_3 Pebble Bed

- Test Conditions
  - Apparatus : Hot Press System
  - Materials : Li_2TiO_3 pebbles with 1 mm diameter
  - Temperature : ~ 1300 °C
  - Heating Rate : 10 °C/min
  - Atmosphere : Vacuum, Ar
  - Applied Pressure : 1 MPa, 4 MPa
  - Measuring Method for Displacement : LVDT

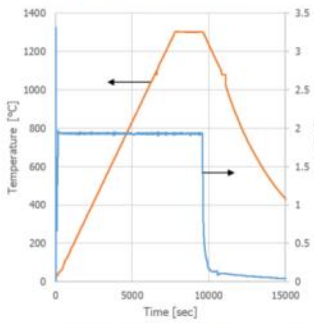

<History of Hot Pressing>

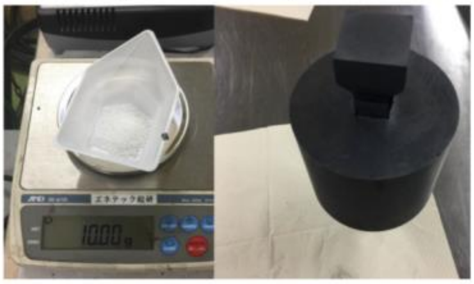

<Li_2TiO_3 pebbles and Hot Press Mold>

Hot Press System

- Schematic Diagram of the Inside of the Hot Press Chamber

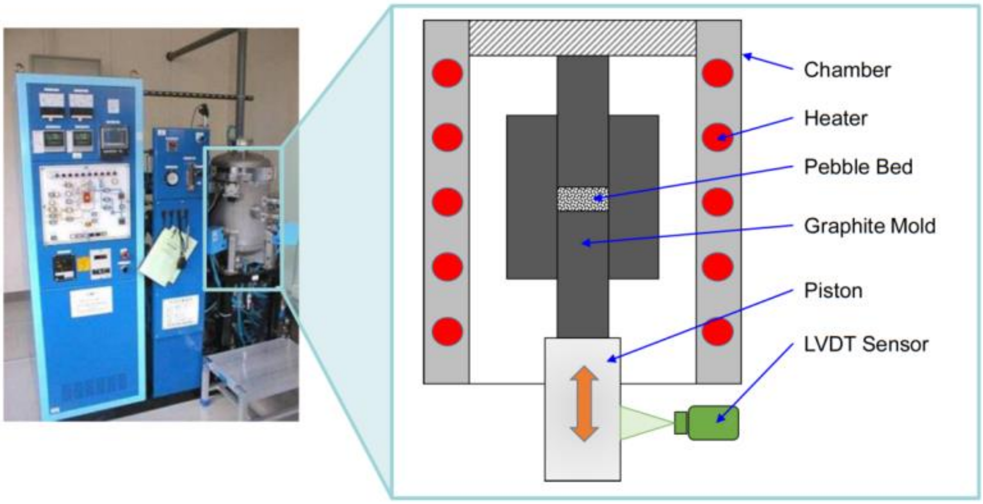

- Dimension of Pebble Bed : 22 X 22 X 10 mm^3
- Weight of Pebble Bed : 10 g

Outline

Ⅰ Introduction

Ⅱ Experimental Method

Ⅲ Sintering of the Li_2TiO_3 Pebble Bed

Ⅳ Creep Deformation of the Li_2TiO_3 Pebble Bed

Ⅴ Summary

Displacement Change during Hot Pressing under 4 MPa

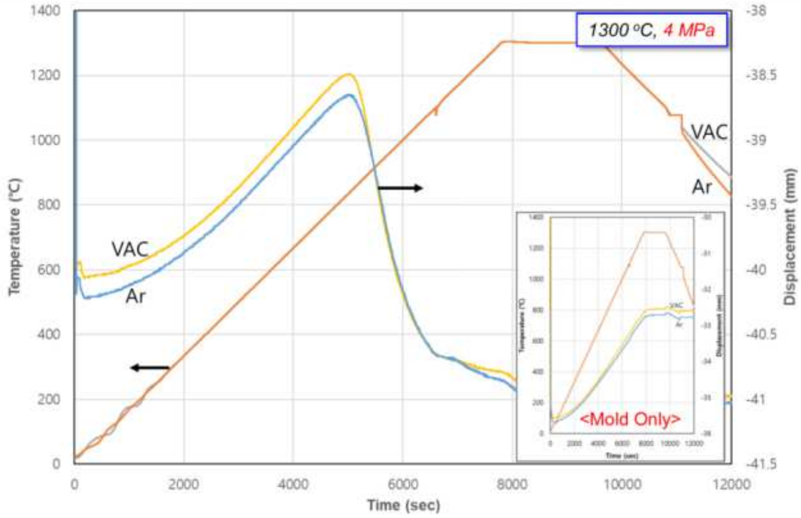

- Sintering atmosphere did not affected the densification of pebble bed.
- Displacement of the graphite mold was linearly changed with increasing temperature until 1300 °C.

Densification Curve of Li_2TiO_3 Pebble Bed under 4 MPa

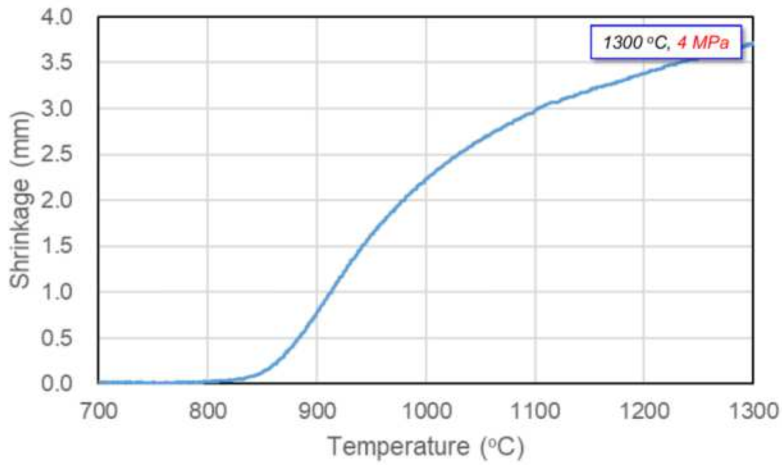

Densification Curve of Li_2TiO_3 Pebble Bed under 4 MPa

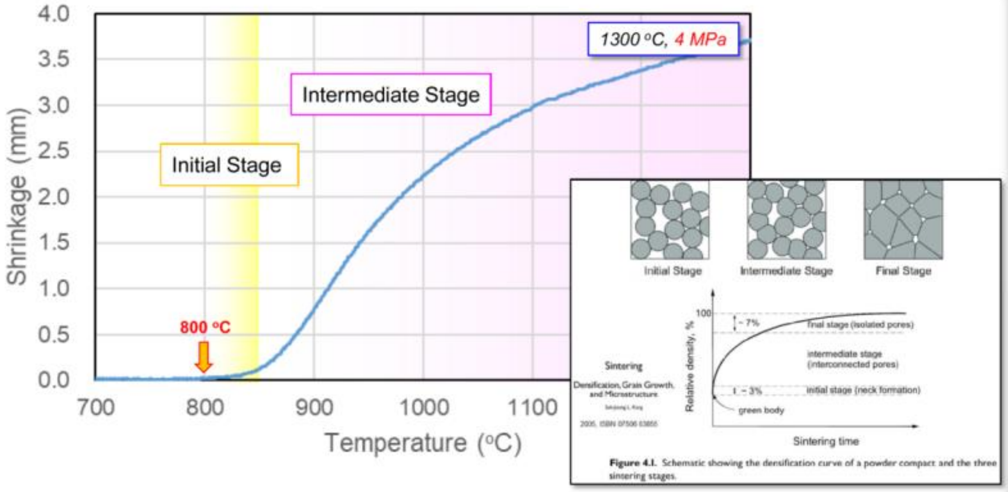

- Sintering of Li_2TiO_3 pebble bed was stared at about 800 °C.
- Initial stage of sintering on the Li_2TiO_3 pebble bed under 4 MPa was estimated at from 800 °C to 850 °C.

Displacement Change and Densification Curve under 1 MPa

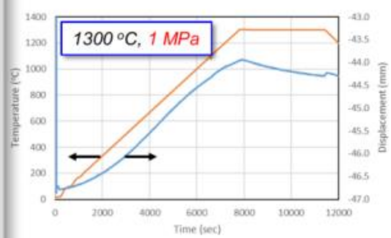

<Raw data from Hot-press>

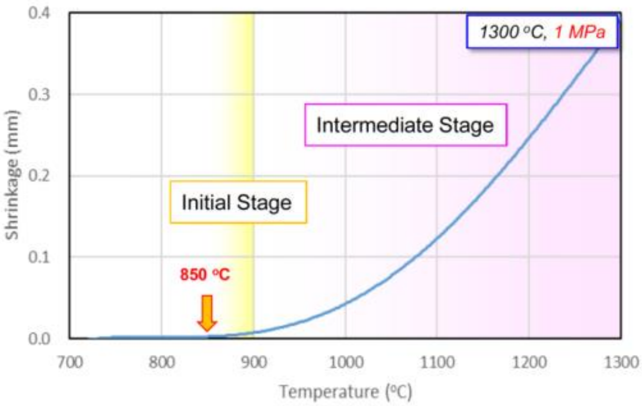

- The starting temperature of sintering was dependent on the applied pressure.
- Sintering of Li_2TiO_3 pebble bed under 1 MPa was started at about 850 °C.
- Initial stage of sintering on the Li_2TiO_3 pebble bed under 1 MPa was estimated at from 850 °C to 900 °C.

Outline

Hot Press Test for Creep Deformation of Li_2TiO_3 Pebble Bed

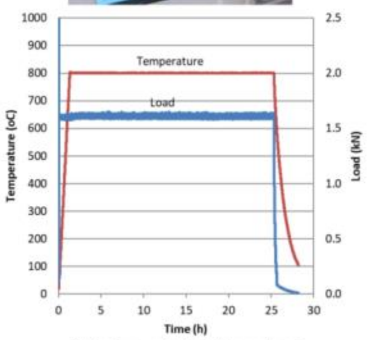

<History of Hot Pressing>

- Test Conditions
  - Apparatus : Hot Press System
  - Materials : Li_2TiO_3 pebbles with 1 mm diameter
  - Temperature : 800 °C, 850 °C, 900 °C
  - Applied Pressure : 1 MPa, 2 MPa, 3 MPa, 4 MPa
  - Holding Time : 24 hrs
  - Atmosphere : Ar
  - Measuring Method for Displacement : LVDT

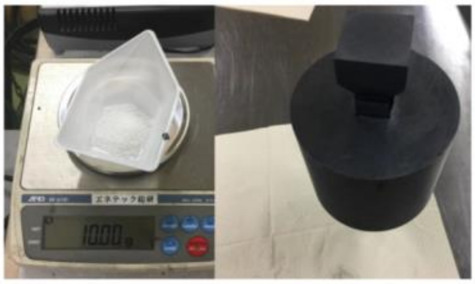

<Li_2TiO_3 pebbles and Hot Press Mold>

Effects of Temperature on Densification of Pebble Bed

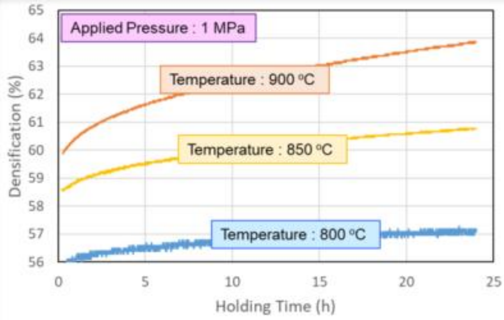

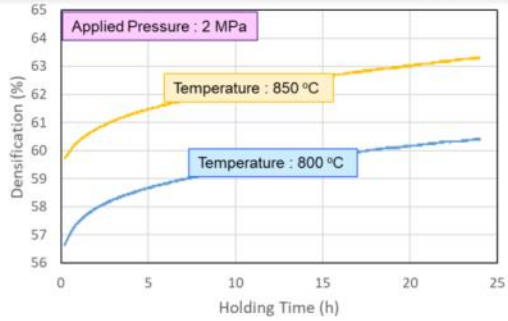

- Under the applied pressure of 1 MPa…
  - The shrinkage of Li_2TiO_3 pebble bed at 800 °C after 24 hrs was less than 2 % and had a trend of saturation after 24 hrs.
  - The densification of Li_2TiO_3 pebble bed at more than 800 °C has been still progressed even if after 24 hrs.
- Under the applied pressure of 2 MPa…
  - The densification of Li_2TiO_3 pebble bed at 800 °C after 24 hrs was about 5 % and has been still progressed even if after 24 hrs.

Ministry of Science and ICT NFRI iter CBBI-20, KIT Campus North, 18 - 20 Sep., 2019 18

Effects of Pressure on Densification of Pebble Bed

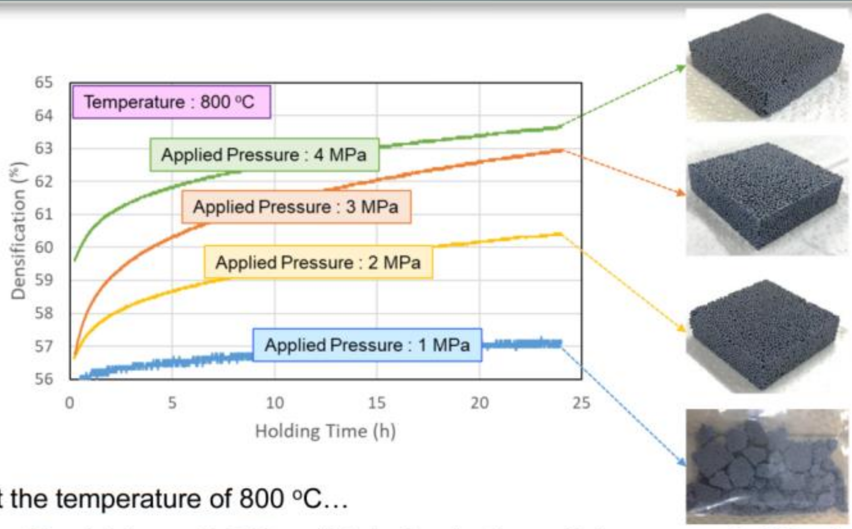

- At the temperature of 800 °C…
  - The shrinkage of Li_2TiO_3 pebble bed under the applied pressure of 1 MPa after 24 hrs was less than 2 % and had a trend of saturation.
  - The densification of Li_2TiO_3 pebble bed under more than 1 MPa was still ongoing even if after 24 hrs.

Ministry of Science and ICT NFRI iter CBBI-20, KIT Campus North, 18 - 20 Sep., 2019 19

Effects of Pressure on Densification of Pebble Bed

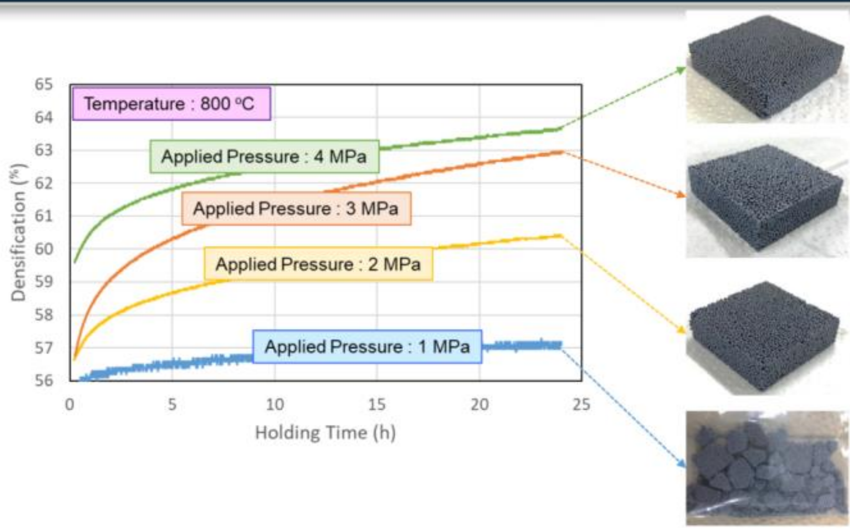

- From the viewpoint of the purge gas flow, it is better to the operation conditions of Li_2TiO_3 pebble bed are not exceeding **800 °C and 1 MPa** to keep the uniform flow path inside the pebble bed.

Outline

I Introduction

II Experimental Method

III Sintering of the Li_2TiO_3 Pebble Bed

IV Creep Deformation of the Li_2TiO_3 Pebble Bed

V Summary

4. Summary

- Starting Temperature of Sintering on Li_2TiO_3 Pebble Bed
  - Under 4 MPa : 800 °C
  - Under 1 MPa : 850 °C
- Initial Stage of Sintering Phenomena on Li_2TiO_3 Pebble Bed
  - Under 4 MPa : 800 °C ~ 850 °C
  - Under 1 MPa : 850 °C ~ 900 °C
- Creep Deformation of Li_2TiO_3 Pebble Bed
  - *Under 1 MPa* : The densification of Li_2TiO_3 pebble bed at more than 800 °C has been still progressed even if after 24 hrs.
  - *Under 2 MPa* : The densification of Li_2TiO_3 pebble bed at 800 °C after 24 hrs was about 5 % and has been still progressed even if after 24 hrs.
  - *At 800 °C* : The shrinkage of Li_2TiO_3 pebble bed under the applied pressure of 1 MPa after 24 hrs was less than 2 % and had a trend of saturation.
- From the viewpoint of the purge gas flow, it is better to the operation conditions of Li_2TiO_3 pebble bed are not exceeding **800 °C and 1 MPa** to keep the uniform flow path inside the pebble bed.

Ministry of Science and ICT NFRI iter CBBI-20, KIT Campus North, 18 - 20 Sep., 2019 22

20th International Workshop on Ceramic Breeder Blanket Interactions (CBBI-20)

KIT Campus North, 18 - 20 September, 2019

Thank you for your attention!!!

Yi-Hyun Park

yhpark@nfri.re.kr

Ministry of Science and ICT

NFRI iter KOREA DOMESTIC AGENCY

23

Discrete Element analysis of plastic deformation in pebble beds

Marigrazia Moscardini[1,2], Simone Pupeschi[1,3], Matthias Kolb[1,4], Marc Kamlah[1]

[1]Institute for Applied Materials, Karlsruhe Institute of Technology, Germany

Present address: [2]University of Pisa, Pisa, Italy; [3]Baker Hughes, a GE Company, Florence, Italy; [4]Helmut Fischer GmbH, Sindelfingen, Germany

For the solid blanket component, tritium breeder and neutron multiplier are both used in the form of pebble beds. Due to their discrete nature, the macroscopic behavior of the bed is the result of the individual interactions between particle-particle and particle-wall. In this framework, the Discrete Element Method (DEM) turns to be a powerful tool allowing investigating the evolution of the individual contacts by accounting for the influence of parameters characterizing the bed at the microscale level such as the particles' size, particles' shape and the packing factor.

At KIT, an in-house DEM code is constantly updated to accurately determine the behavior of pebble beds under fusion relevant conditions. Recently, the code was further extended to simulate the plastic behavior of assemblies of packed particles under uniaxial compression determined by the plastic deformation of the individual pebbles. Including the plastic deformation, the mechanical behavior of beryllium can be investigated. Thornton and Ning's contact theory was implemented to simulate the contact evolution through a hysteretic cycle, thus the normal force is determined by means of three consecutive steps: non-linear elastic loading, linearly hardening plastic loading and non-linear elastic unloading. The non-linear Hertzian elastic model describes the mechanics of the individual contact up to the yield point, while the yielding behavior is modelled by means of two different correlations for the loading and unloading/reloading phase. In particular, a truncated Hertzian pressure distribution is assumed to model the yielding behavior. During the loading phase a linearly hardening plasticity model is applied, while the phase of unloading/reloading is simulated by a non-linear elastic theory, which is based on a modified contact curvature generated by the permanent plastic deformation. The numerical simulations were conducted in strain control by setting the maximum displacement of the bed as an input parameter. Therefore, the code evaluates the stress generated in the bed by the uniaxial compression, accounting for both pebble rearrangement and plastic deformation in the contact area of pebbles.

As next step, an experimental campaign is planned with the aim to validate the results of the DEM code. The experiments will be carried out by means of the existing experimental setup at KIT, which was used to investigate the behavior of ceramic breeder pebble beds. Three different materials, with three different yield points will be considered as potential candidates for the experimental campaign. In particular, particles made of a CoCr alloy are now under consideration to reproduce the behavior of beryllium pebbles.

Karlsruhe Institute of Technology

EUROfusion

Discrete Element analysis of plastic deformation in pebble beds

M. Moscardini*, S. Pupeschi, M. Kolb, M. Kamlah

Karlsruhe Institute of Technology
Institute for Applied Materials (IAM-WBM)

CBBI-20

KIT – University of the State of Baden-Wuerttemberg and National Research Center of the Helmholtz Association

*Currently at University of Pisa, Department of Civil and Industrial Engineering
Email: marigrazia.moscardini@dici.unipi.it

Outline

- Background
- Motivation
- Plastic deformation in pebble beds:
  - Theory
  - Numerical analysis
- Conclusions and future steps

2 04.12.2019 Marigrazia Moscardini Email: marigrazia.moscardini@dici.unipi.it

Background

- In-house KIT DEM code → evaluating the thermo-mechanical behaviour of pebble beds

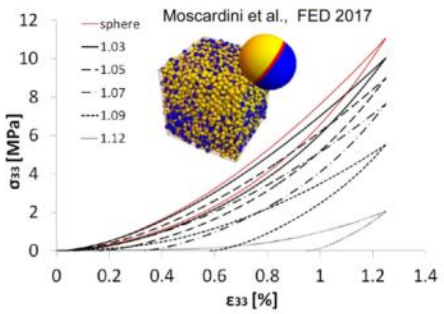

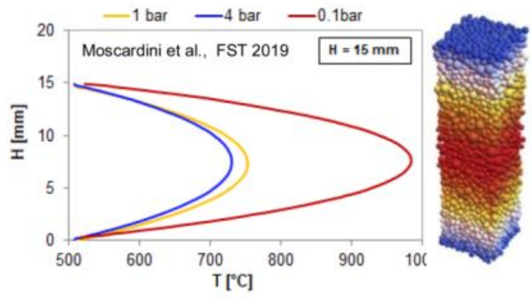

- KIT DEM code currently under development to implement the plastic deformation of pebble beds

Motivation

- Pebble beds plastic deformation = pebbles rearrangement + plastic deformation of individual pebbles in contact

Reimann and Behnke, FT 2000

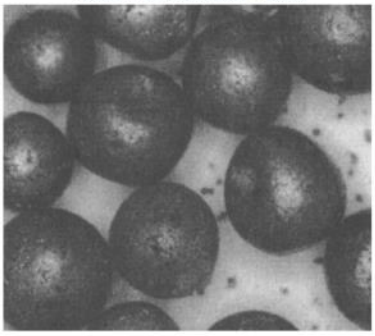

Reimann and Behnke, FT 2000

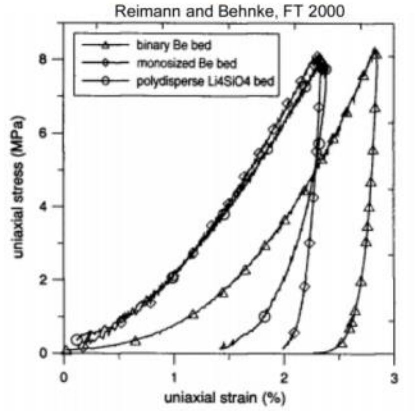

Plastic deformation in pebble beds: Theory

Thornton (1998): Truncated Hertzian pressure distribution

One fitting parameter, fast convergence, supported by extended literature

$$F^n = \begin{cases} \mathbf{F_{el}} & \xi_{i,max} < \xi_y \\ \mathbf{F_{pl}} & \xi_{i,max} \geq \xi_y,\ \dot{\xi} \geq 0 \\ \mathbf{F_{un}} & \xi_{i,max} \geq \xi_y,\ \dot{\xi} < 0 \end{cases}$$

$$\xi_y = f(\tilde{p}_y, \mathrm{R_{eff}}, \mathrm{E_{eff}})$$

$$\tilde{p}_y = \mathcal{T}\sigma_y \qquad 1.6 \leq \mathcal{T} \leq 3$$

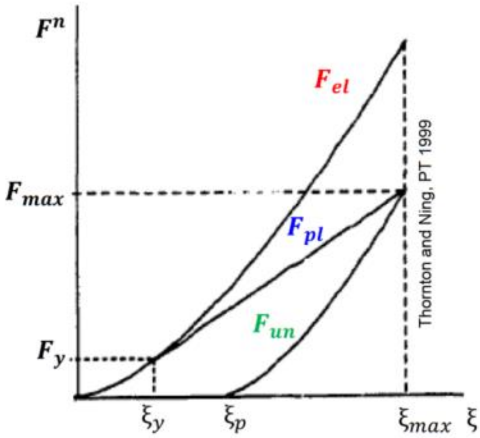

Plastic deformation in pebble beds: Theory

$$F^n = \begin{cases} \mathbf{F_{el}} = -k^n\, \xi^{3/2} \\ \mathbf{F_{pl}} = -[\mathbf{F_y} + \pi\, \tilde{p}_y\, \mathrm{R_{eff}}\, (\xi - \xi_y)] \\ \mathbf{F_{un}} = -k^n{}_{un}\, (\xi - \xi_p)^{3/2} \end{cases}$$

$$k^n{}_{un} \propto R_{eff,un} = R_{eff} \frac{\mathbf{F_{el}}^{max}}{\mathbf{F_{pl}}^{max}}$$

$$\xi_p = \xi_{max} - \xi_{max} \frac{R_{eff}}{R_{eff,un}}$$

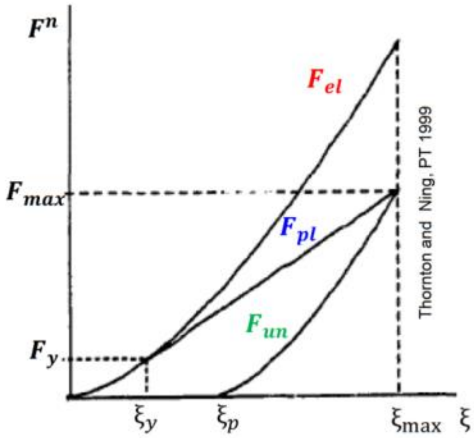

Plastic deformation in pebble beds: Numerical analysis

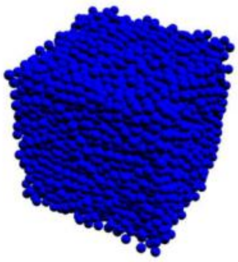

Stress generated in the bed

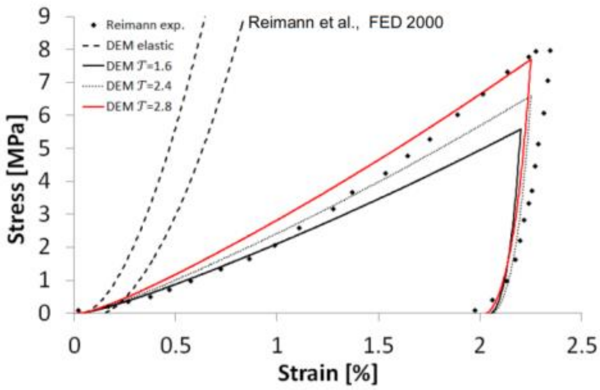

Main parameters
- 5000 pebbles of Be
- Periodic boundary
- PF = 63%
- r = 1.0 mm
- E = 306 GPa, ν = 0.07
- σy = 395MPa

Email: marigrazia.moscardini@dici.unipi.it

Plastic deformation in pebble beds: Numerical analysis

Individual contact

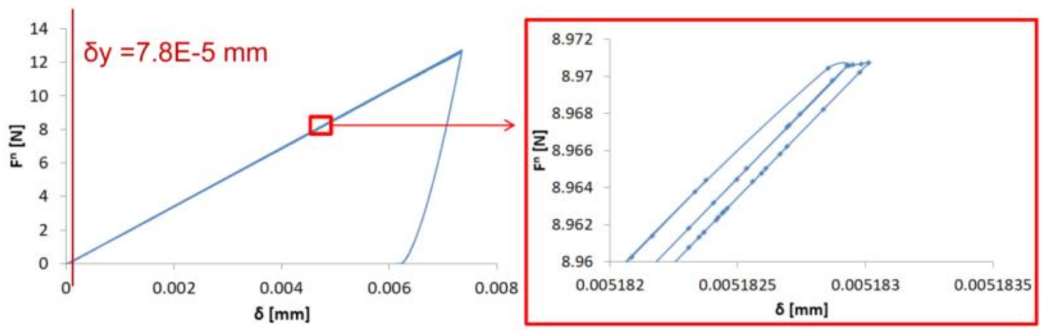

Email: marigrazia.moscardini@dici.unipi.it

Plastic deformation in pebble beds: Numerical analysis

Karlsruhe Institute of Technology

Influence of the walls

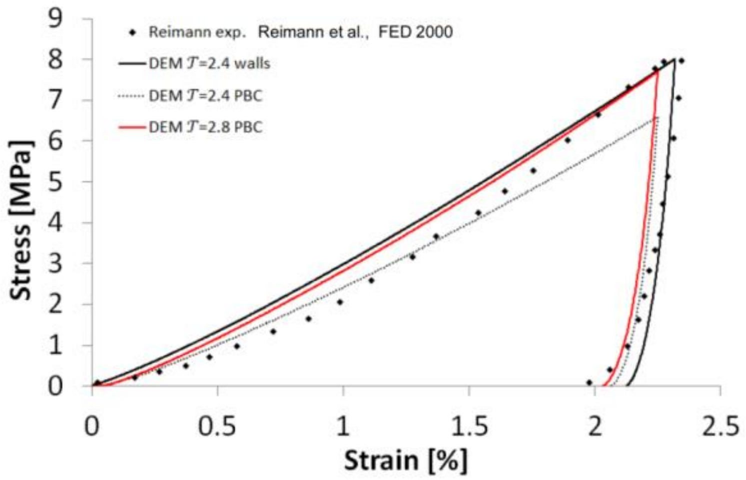

9 04.12.2019 Marigrazia Moscardini Email: marigrazia.moscardini@dici.unipi.it

Plastic deformation in pebble beds: Numerical analysis

Karlsruhe Institute of Technology

Vu-Quoc et al., JAM 2000

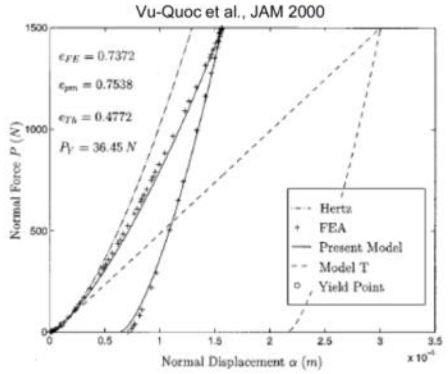

Rathbone et al., PT 2015

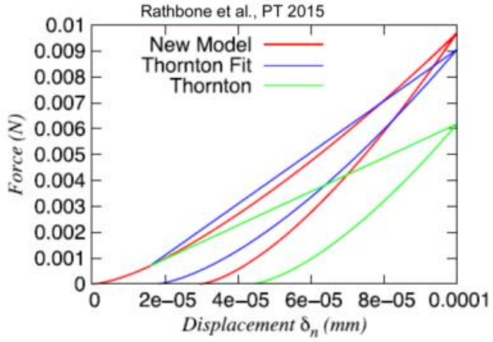

10 04.12.2019 Marigrazia Moscardini Email: marigrazia.moscardini@dici.unipi.it

Plastic deformation in pebble beds: Numerical analysis

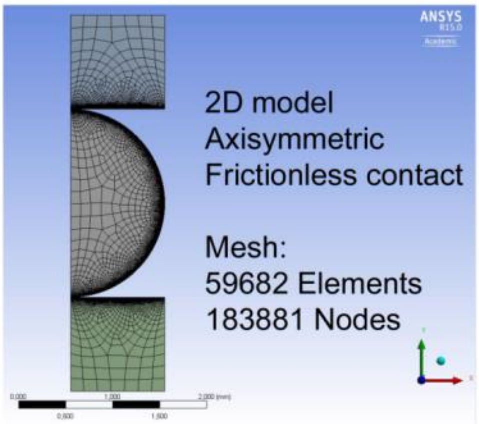

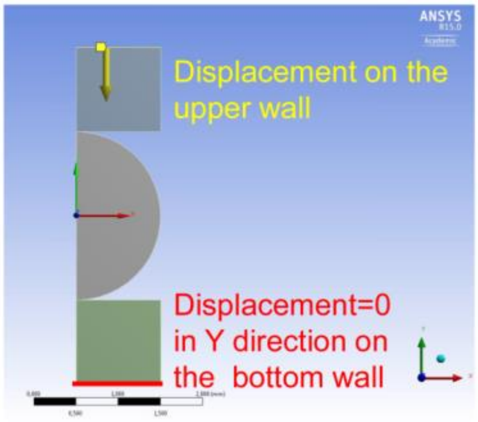

11 04.12.2019 Marigrazia Moscardini Email: marigrazia.moscardini@dici.unipi.it

Plastic deformation in pebble beds: Numerical analysis

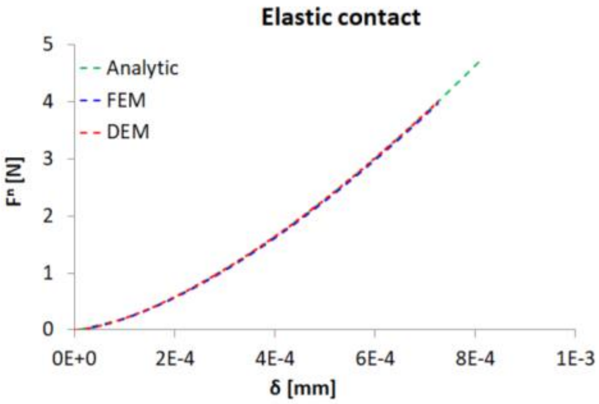

Be pebble compressed between 2 walls

Main parameters:
- r = 1.0 mm, E = 306 GPa, ν = 0.07, σ_y = 395.5MPa

12 04.12.2019 Marigrazia Moscardini Email: marigrazia.moscardini@dici.unipi.it

Plastic deformation in pebble beds: Numerical analysis

Main parameters: r = 1.0 mm, E = 306 GPa, v = 0.07, σy = 395.5MPa, Tangent modulus = 0 (FEM plastic)

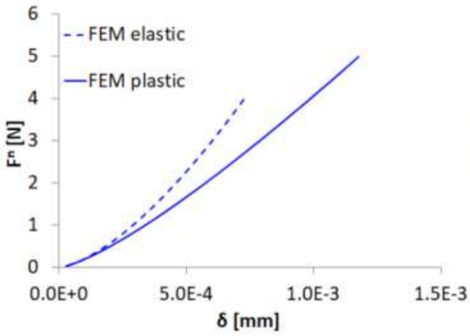

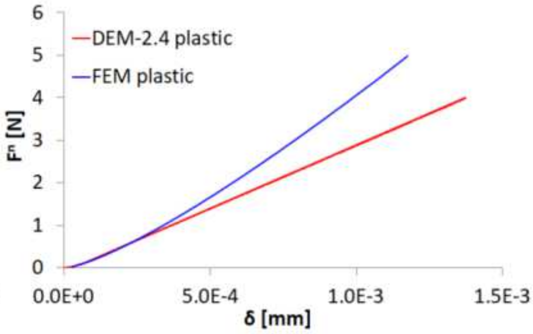

Plastic deformation in pebble beds: Numerical analysis

$$F^n = \begin{Bmatrix} \mathbf{F_{el}} = -\,k^n\,\xi^{3/2} \\ \mathbf{F_{pl}} = -\,[\mathbf{F_y} + \pi\,\tilde{p}_y\,R_{eff}\,(\xi - \xi_y)] \\ \mathbf{F_{un}} = -\,k^n{}_{un}\,(\xi - \xi_p)^{3/2} \end{Bmatrix}$$

$\tilde{p}_y = \mathcal{T}\sigma_y$ with $1.6 \le \mathcal{T} \le 3$

Condition defining $\mathbf{F_{pl}}$

$$\mathcal{T}_i = f(\mathcal{T}_{in}, \delta_i, E_{eff}, \sigma_y, R_{eff})$$

$\mathcal{T}_{in}$ *is the fitting parameter*
$1.6 \le \mathcal{T}_{in} \le 3$

$\mathcal{T}_i$ replaces $\mathcal{T}$ and changes during the contact evolution as a function of the overlap

Plastic deformation in pebble beds: Numerical analysis

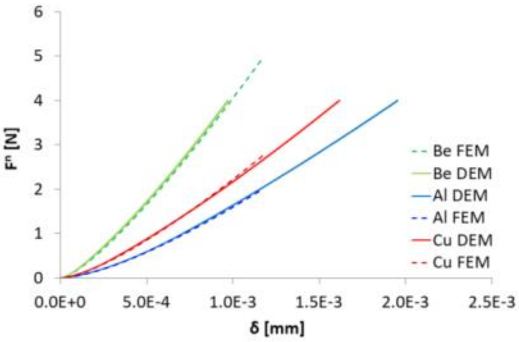

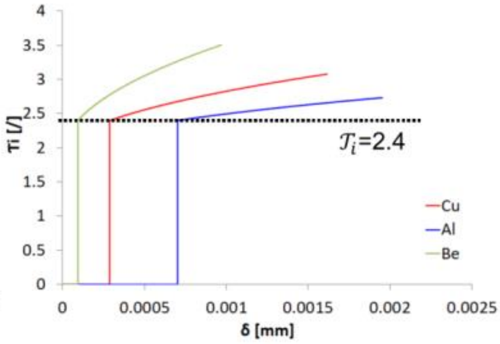

Material	E [MPa]	v	σy [MPa]	R [mm]
Be	306.0 E+3	0.07	395.5	1
Al	70.0 E+3	0.33	280.0	1
Cu	110.0 E+3	0.34	430.0	1

Plastic deformation in pebble beds: Numerical analysis

Main parameters: r = 1.0 mm, E = 306 GPa, v = 0.07, σy = 395.5MPa, tangent modulus = 0 (in FEM)

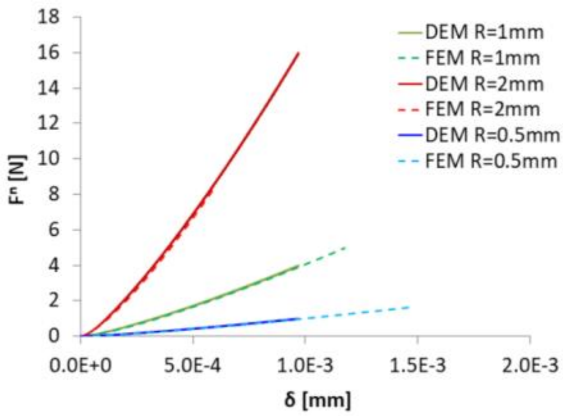

Conclusions and future steps

- The in-house KIT DEM code is constantly under development to sustain the R&D of the solid breeder blanket concept.
- Currently, the implementation of the plastic deformation of pebble beds is under development.
- The Thornton theory based on a truncated Hertzian theory was selected and applied. The theory defines a linear behaviour in the plastic region.
- In the current work the theory was slightly modified to adjust the linear behaviour according to experimental results reported in literature.
- The code is currently under validation.

17 04.12.2019 Marigrazia Moscardini Email: marigrazia.moscardini@dici.unipi.it

Conclusions and future steps

Future step: coupled thermo-mechanical DEM code by including the thermal expansion.

$$\Delta V = 3 * \alpha(T) * V * \Delta T$$

Main parameters:
- Twalls=500°C
- OSI=polydispersion
- Be=monosized, R=1 mm
- 5000 particles

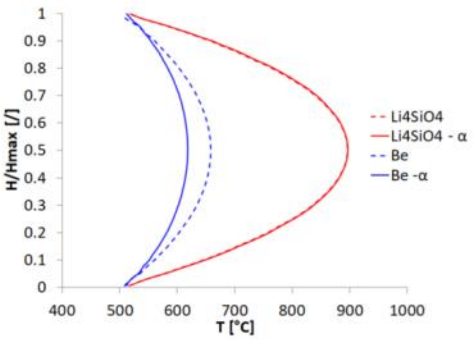

"This work has been carried out within the framework of the EUROfusion Consortium and has received funding from the Euratom research and training programme 2014-2018 and 2019-2020 under grant agreement No 633053. The views and opinions expressed herein do not necessarily reflect those of the European Commission."

18 04.12.2019 Marigrazia Moscardini Email: marigrazia.moscardini@dici.unipi.it

Influences of pebble geometry on the thermomechanical behaviour of ceramic breeder pebble beds

Joerg Reimann

Karlsruhe Institute of Technology, Institute for Nuclear and Energy Technologies

In helium-cooled pebble bed blankets, HCPBs, both the ceramic breeder and the beryllium-based neutron multiplier materials consist of pebbles, contained in corresponding cavities. The knowledge of the thermomechanical behavior of these pebble beds during blanket operation is fundamental for the design of HCPBs.

The main geometrical pebble parameters are pebble shape (spherical, non-spherical), size distribution (mono-sized, binary, polydisperse) and surface roughness. The primary design quantity is the container volume averaged packing fraction γ_t because it is a direct measure for the amount of breeder/multiplier in the relevant zones. The packing fraction γ_t depends in a complex way on the pebble parameters given above and furthermore on filling/densification procedures and on container dimensions. γ_t is also an important global parameter influencing the thermomechanical parameters such as stress-strain relationships, thermal conductivity, thermal creep strain, pebble crush fractions. However, γ_t is not sufficient for modelling these dependences but local pebble packing structures must be analysed including pebble to pebble and pebble to wall interactions (contact numbers, forces, etc.). A characteristic of contained pebble packings is that the local packing structure in the bulk zone differs characteristically from that in wall zones.

In the paper, an overview is given on recent results from experimental investigations and DEM simulations.

Karlsruhe Institute of Technology

Influences of pebble geometry on the thermomechanical behaviour of pebble beds

Joerg Reimann*
Karlsruhe Institute of Technology

presented at
CBBI-20, Sept. 18-20, 2019, KIT, Karlsruhe, Germany

INSTITUTE FOR APPLIED MATERIALS – APPLIED MATERIALS PHYSICS (IAM-AWP)

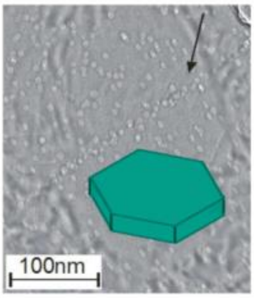

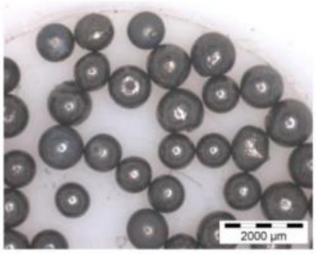

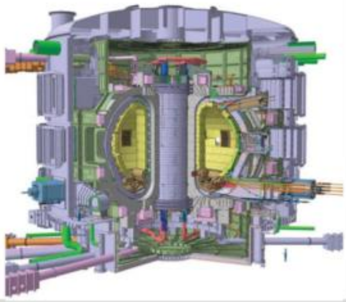

KIT – The Research University in the Helmholtz Association

www.kit.edu

PARAMETERS OF PEBBLE GEOMETRY

- shape: spherical, non-spherical
- surface roughness
- size, size distribution: mono-sized (one pebble diameter d), binary (two ds), polydisperse (d-spread).

- **Problem: often, pebbles are considered as mono-sized spheres but are polydisperse pebbles with non-spherical shapes**

- Primary pebble bed, PB, quantity: container volume averaged **packing fraction γ_t**
- γ_t is a direct measure for the amount of breeder/multiplyer: large γ_t desired
- γ_t is dependent of pebble parameters given above, and container geometry and filling/vibration procedures

- **Quantities relevant for the PB thermomechanical behavior, TMB**
- stress-strain, $\sigma-\varepsilon$, dependence
- pebble crush loads, Fc
- effective thermal conductivity, k
- thermal creep strain, εcreep
- irradiation effects

ANALYSES OF PACKING STRUCTURES

- The pebbles are nonhomogeneously distributed in containers (wall zones, bulk zone)
- These **local characteristics (**local **pebble structures)** complicate the modelling of TMB

Methods to analyse pebble structures:

- DEM simulations
- X-ray computed tomography, CT, experiments,
  - with DEM techniques, parameters can be easily varied.
  - CT data are important for validating DEM simulations

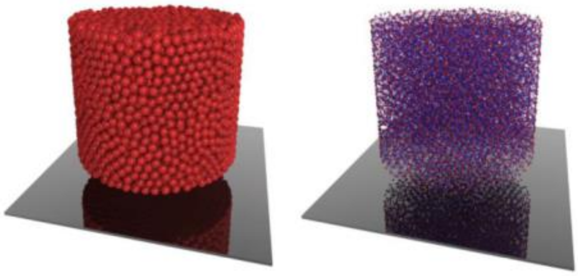

CT results*: 3D view of reconstructed volume, sphere connection network

*Reimann et al, FZKA 7120, 2005

PEBBLE BED STRUCTURES, „visualized" by packing/void fraction distributions, prismatic containers, polydisperse spheres; small d spread

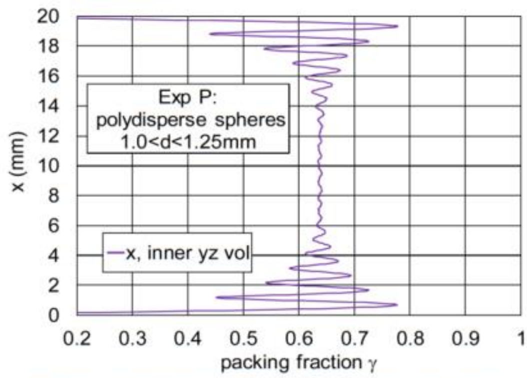

CT exp*: slender prismatic container, sphere d spread 1.0<d<1.25mm, $\gamma_t \approx 0.625$.

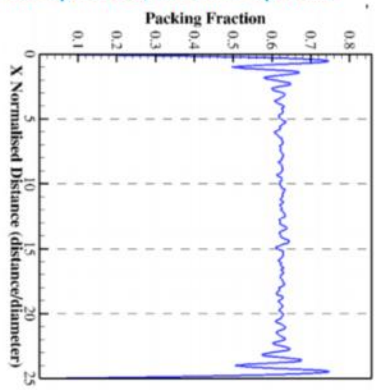

DEM simulations**: cubic container with 25d,sphere d spread 0.8<d<1.2mm, $\gamma_t \approx 0.62$

Wall zones of about 4d thickness

* Reimann, Int. J. Mat. Res, doi.org/10.3139/146.111814

**Annabattula, CBBI-19 (2017)

PEBBLE STRUCTURES, mono-sized spheres

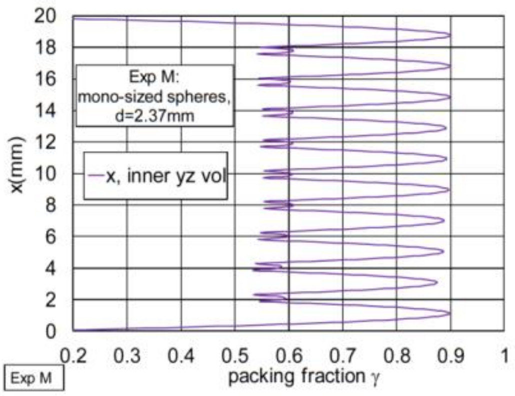

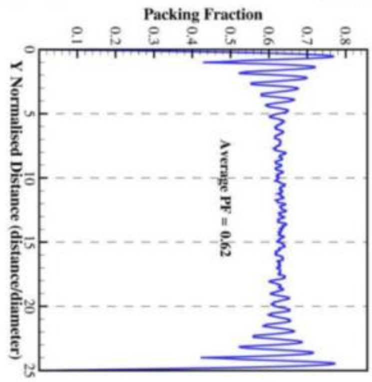

CT result*: slender prismatic container
d=2.37mm; $\gamma_{t\text{-}CT} = 0.714$, $\gamma_{t\text{-}hex} = 0.724$
CT result confirmed by DEM**

DEM result***: cubic container with 25d
d=1mm; $\gamma_{t\text{-}CT} = 0.62$

With ideal mono-sized spheres, large γ_t values can be obtained in slender containers.

* Reimann, Int. J. Mat. Res, doi.org/10.3139/146.111814 **Reddy (2019) to be publ. *** Desu, Fus Eng Des 127(2018)259-266

PEBBLE STRUCTURES, 1st wall layer, mono-sized + polydisp sphs

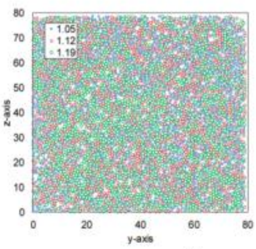

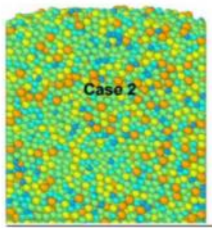

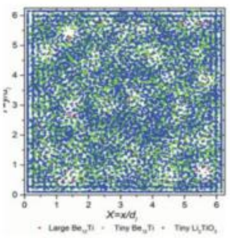

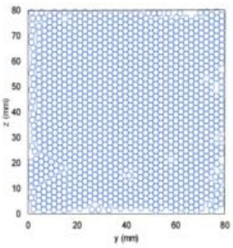

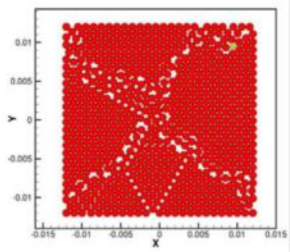

polydisperse sphs* **

binary spheres****

mono-sized sphs:
a) shallow container* perfectly structured
b) cubic container*** large structured zones

Mono-sized ⟷ polydispered spheres:
What is d-tolerance for large regularity?

polydispered/binary sphs: no homogeneous distributions but clusters

*Reimann, Int. J. Mat. Res, doi.org/10.3139/146.111814 . **Annabattula, CBBI-19 (2017)
Desu, Fus Eng Des 127(2018) * Chen, Nucl Sc Techn 53(2016)803-808

PEBBLE STRUCTURES, nonspherical pebbles

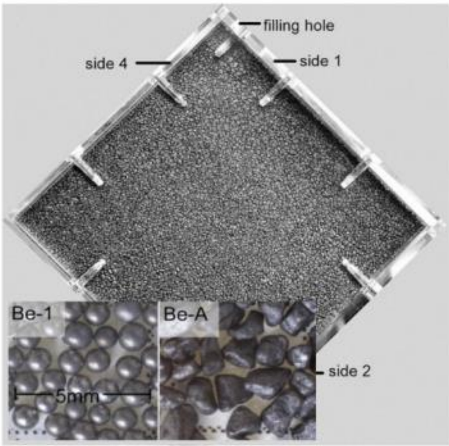

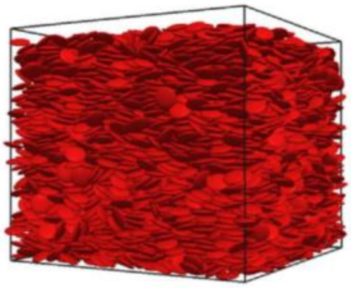

Brick-type Be-A pebbles*: largest particle side aligned with wall

Oblate spheroids**: Ordered structure due to gravity on bottom wall

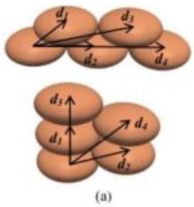

* Reimann, KIT SR 7631 (2012)

** J. Gan, Chem Eng Science 156(2016)64-76

PACKING FRACTIONS, binary spheres, bulk zone*

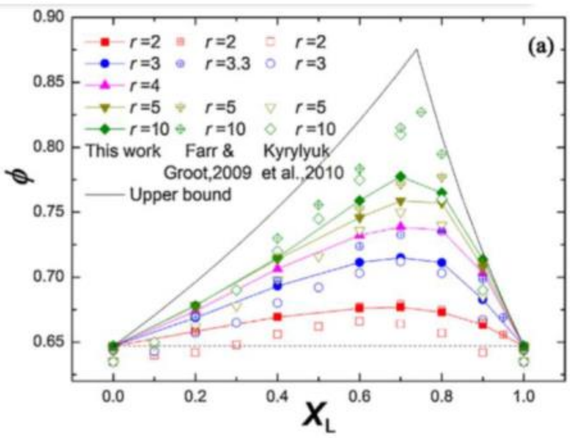

- Packing fraction (in Fig.: ϕ) = f(X_L); X_L= volumetric fraction of large spheres; r=d_l/d_s
- Results for bulk zone (no wall effects)
- Maximum packing fraction at $X_L \approx 0.7$; for small d_l/d_s: small effect.
- Separation effects during filling/vibration must be avoided.
- For d_l/d_s>5: first large spheres are filled in, vibrated and fixed. Then, small sphs are filled in interstices between large sphs.

Binary PB blankets selected by Ja and C.

Very large packing factors achievable for d_l/d_s >5. Concern: during thermal cycling rearrangement of spheres cannot be excluded (thermal ratcheting) resulting in non-defined thermomechanical behaviour.

* Meng, Particuology 16(2014)155–166

PACKING FRACTIONS, polydisperse spheres, bulk zone, DEM results*

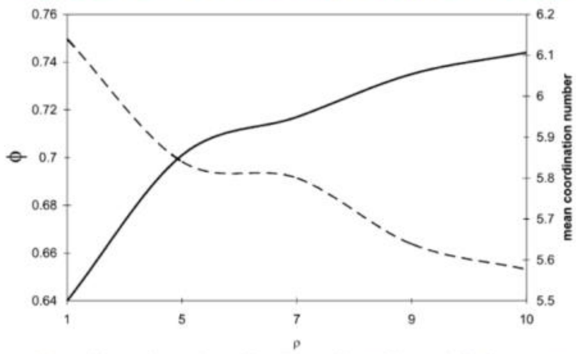

Packing fraction (in Fig.:ϕ) = f(ρ=dl/ds); power law for d distribution.

- Results for bulk zone (no wall effects)
- With increasing dl/ds: γ_t increases, mean contact number decreases.
- For small dl/ds : no large effects

*Lochmann, Solid State Sciences 8 (2006)1397-1413

see also Farr, Powder Techn 245(2013)330-343

Meng, Particuology 16(2014)155–166

PACKING FRACTIONS, irregular particles, shallow containers

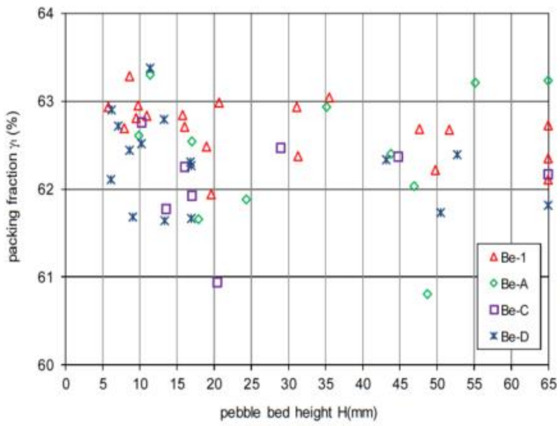

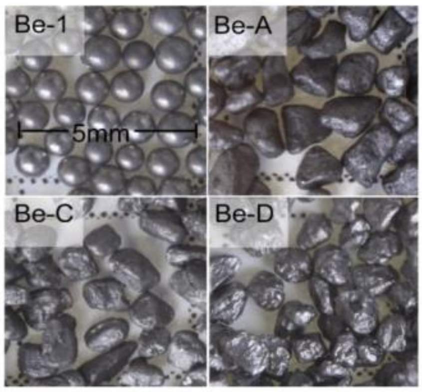

- No remarkable difference between the different materials.
- γ_t does not decrease significantly with decreasing H because of the increased influence of ordered pebble structures close to the walls.

* Reimann, KIT SR 7631 (2012)

PACKING FRACTIONS, non-spherical particles, DEM results*

KIT Karlsruhe Institute of Technology

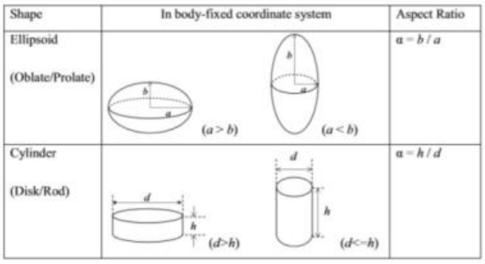

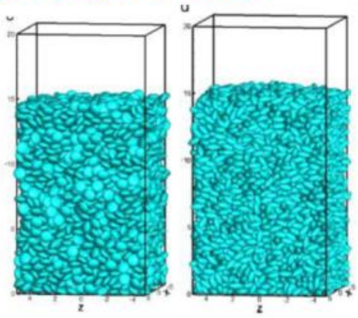

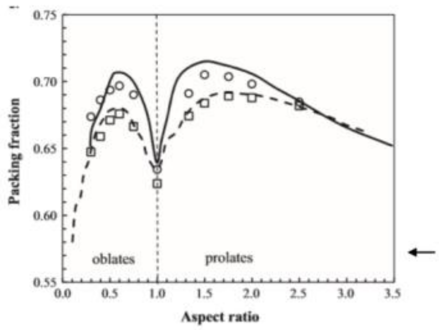

- For non-spherical particles, much larger packing fractions can be achieved
- Already small deviations of sphericity influence sensitively packing fraction and mechanical behaviour**
- Results valid for bulk zone (no wall effect)

*Dong, Chem Eng Science 126 (2015)500-516,
see also Moscardini, Fus Eng Des 121(2017)22-31

STRESS-STRAIN DEPENDENCE, THERMAL CREEP,

results from uniaxial compression tests, UCTs*

KIT Karlsruhe Institute of Technology

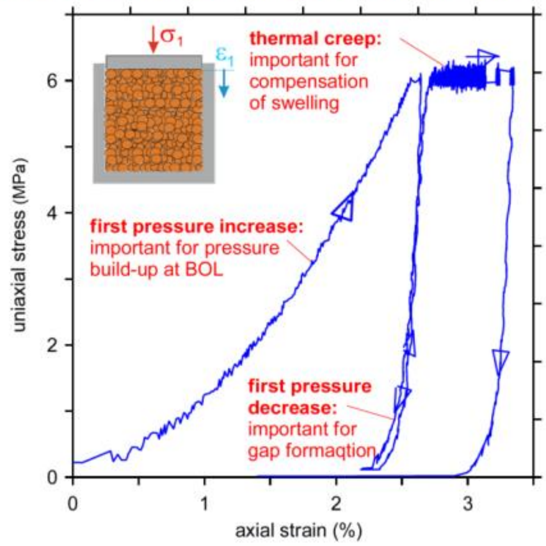

- First stress increase:
- This curve determines the stress build-up during the first blanket operation.
- First stress decrease, second stress increase:
- These curves and the curve"1st pi" determine the formation of gaps during blanket operation.
- Thermal creep strain (high T):
- Is important for stress relaxation during the first days of blanket operation and later for compensation of irradiation induced swelling

* Reimann, Fus Eng Des 49-50(2000)643-649

STRESS-STRAIN DEPENDENCE, DEM results

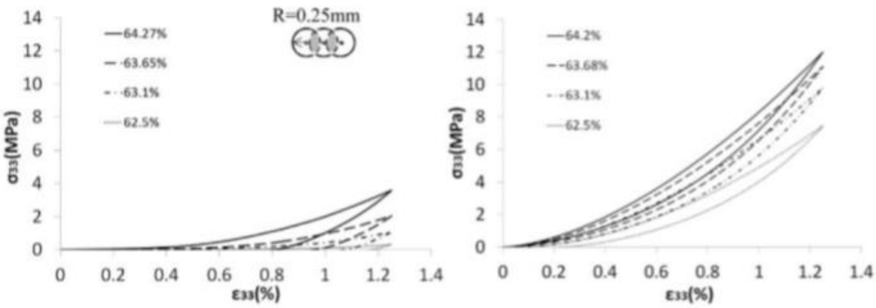

Ellipsoids R=0.25mm, a=1.12 Spheres R=0.25mm

- Ellipsoidal PBs behave significantly softer than mono-sized sphere PBs but residual strains are larger*
- Binary and polydisperse sph PBs** are softer than mono-sized sph PBs**

Soft PBs: (+) in respect to pebble crush (brittle materials), (-) in respect to the increase of thermal conductivity, relevant for ductile materials (Be) with large ks/kg

*Moscardini, Fus Eng Des 121(2017)22-31, **Annabattula, Fus Eng Des 87(2017)853-858

CRUSH LOADS, Exps, DEM results

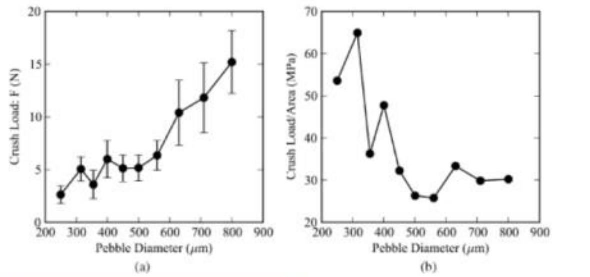

Crush loads increase with d, however, equivalent crush stress increases with decreasing d
→ in blankets small d more favourable*

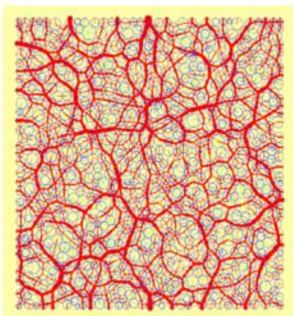

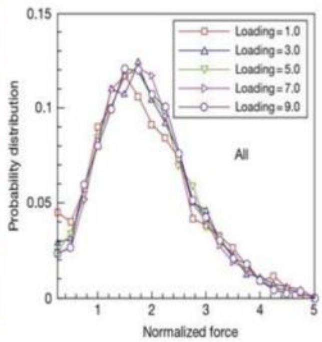

Forces between pebbles: force branches with much higher values than average values;

From force distribution curve, fraction of crushed pebbles is assessed**

No significant differences are observed for ellipsoidal particles***

* Annabattula, Fus Science Techn 66 (2014)
** An et al, Fus Eng Des 82 (2007)
*** J.Gan, Powder Techn 320 (2017)

THERMAL CONDUCTIVITY, Role of coordination number, Nc, monosized spheres

The effective thermal conductivity k in PBs is dependend on thermal conductivities of the gas k_g, the pebbles, k_s, etc, see e.g *,**. In this context, Nc is an important quantity.

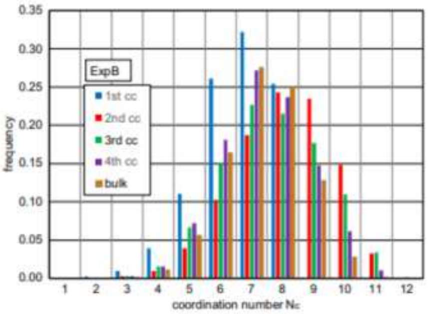

Nc distribution for exp with γ_t=0.64***
(non-ordered bulk zone, small wall zone)

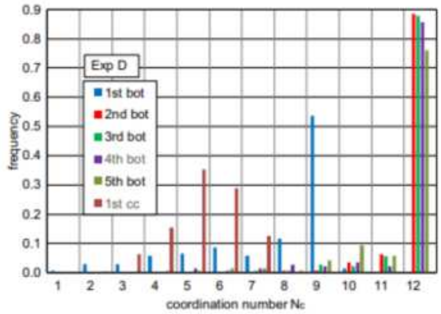

Nc distribution for exp with γ_t=0.67***,****
(ordered structure in total volume)

Nc distributions are very different for ordered and non-ordered zones!
DEM simulations can take into account these effects! See e.g. **,****

* Moscardini, Fus Eng Des 127(2018)192-201, **Desu, Comp Part Mech 6 (2019)503-514

***Reimann, Powder Techn 318(2017)471–483, ****Dai, Gran Mattter (2019) https://doi.org/10.1007/s1003

THERMAL CONDUCTIVITY, bulk zones, k = f(T, strain ε)

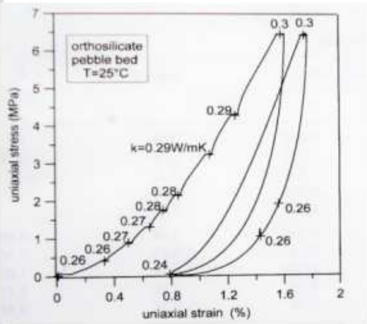

Osi PB in air atmosphere*

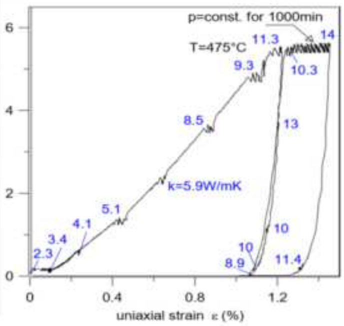

Be PB in He atmosphere**

Essential parameter: k_s/k_g
Osi/He at T=700°C: k_s/k_g= 6.5
Be/He at T=650°C: k_s/k_g= 350

For small k_s/k_g (Osi): negligible increase of k with stress (strain)

For large k_s/k_g (Be): strong k increase because of increasing contact surfaces.

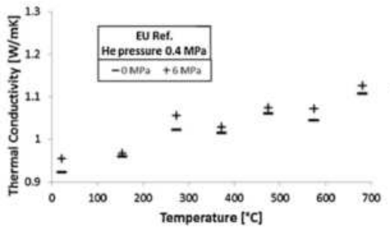

← Osi PB in He ***

* Reimann, Fus Eng Des 61-62(2002)345-351
** Reimann, Fus Eng Des 81(2006)449-454
*** Pupeschi, Fus Eng Des 116 (2017)803-808

THERMAL CONDUCTIVITY, binary Be PBs; exps*

KIT Karlsruhe Institute of Technology

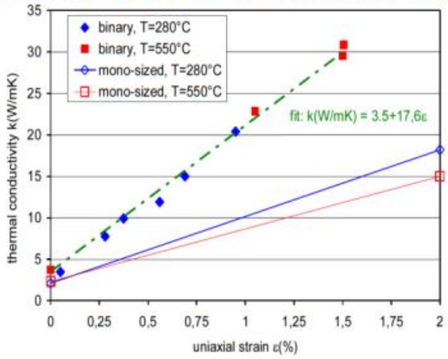

- In blankets, the build-up of stresses by thermal expansion is determined by strain, therefore, ε is considered as prime parameter.
- Binary PBs: both for large and small pebbles: d-spread, non-spherical pebbles
- Compared to mono-sized Be PBs**, the slope of the binary PB curve is larger by a factor of 2!

*Reimann et al, QST-P-3 (2018) 178-192 **Reimann Fus Eng Des 81(2006) 449-454

THERMAL CONDUCTIVITY, non-spherical particles, DEM sim.*

KIT Karlsruhe Institute of Technology

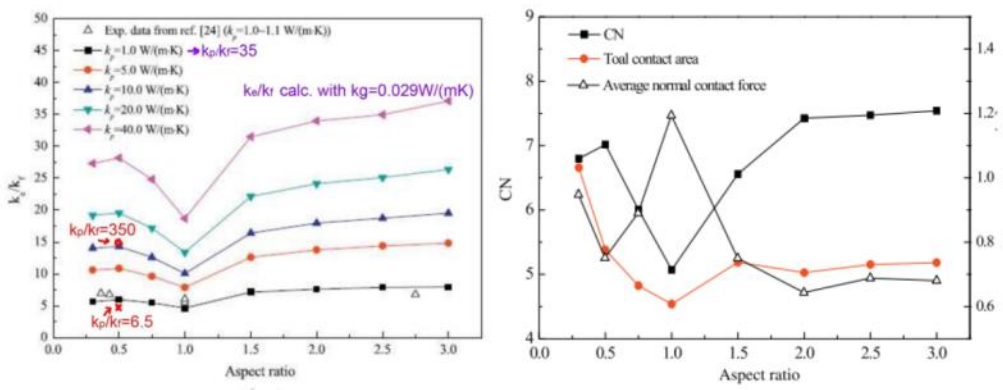

- Increase of k because of increase on Nc
- Significant increase of thermal conductivity for large ks/kf values.

*J.Gan, Powder Techn 311 (2017)157-166

THERMAL CONDUCTIVITY, irregular Be pebbles, exps*

KIT Karlsruhe Institute of Technology

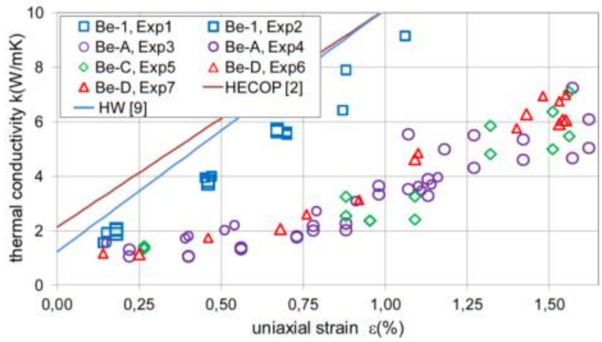

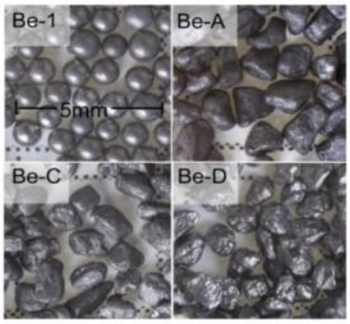

- The PBs with irreg. pebbles behave significantly softer than those with rather spherical pebbles, Be-1.
- For k=f(ε), k for PBs with irreg. pebbles is significantly lower than for Be-1.
- For k=f(σ), the differences become negligible.

* Reimann, Fus Eng Des 88 (2013) 2343-2347

THERMOMECHANICAL BEHAVIOUR, state of the art

KIT Karlsruhe Institute of Technology

For blanket designs, the TMB parameters must be known both for the beginning of life, BOL and for the neutron fluences at end of live, EOL.

State of the art

Candidate spherical pebble materials (breeder: Li4SiO4, Li2TiO3; neutron multiplyer: Be): data base for BOL sufficient; for EOL, the influence of fluence on k, F_c not sufficiently known.

- Nonspherical pebbles: only DEM simulations for BOL; experiments required!

CONCLUSIONS

- Polydisperse spheres with small d-spread generally used in blankets: moderate build-up of regular structures in wall zones. DEM simulations should take into account the d-variation and simulate relevant vibration methods.
- Mono-sized spheres: strong effect of regular structures on all thermomechanical quantities. Strong nonhomogeneous distribution of these structures (non-isotropic conditions)!
- Binary pebble systems ($d_l/d_s>5$) attractive in respect to γ_t and k; issues: compatibility, homogeneity, thermal cycling (BOL), irradiation swelling, brittleness (EOL).
- Nonspherical particles: larger γ_t already for small deviations from sphericity. Increase of k for systems with large k_s/k_g. Improved wall heat transfer expected (not yet investigated).
- In the last years increasing attention was payed to
  - nonhomogeneous pebble distributions in containers (DEM simulation, X-ray CT exps)
  - defined (repeatable) PB filling/vibration procedures.

Work should go on in this direction…

Application of machine learning tools to study heat transfer in ceramic pebble beds

Ratna Kumar Annabattula, Raghuram Karthik Desu and Akhil Reddy Peeketi

Mechanics of Materials Laboratory, Department of Mechanical Engineering, Indian Institute of Technology Madras, Chennai - 600036, India

The knowledge of effective thermal conductivity (ETC) of the pebble beds is vital for a reliable design of the breeder units. The effective thermal conductivity of a granular bed depends on various parameters pertaining to both bulk material and microstructural properties. Establishing a parametric correlation between the ETC and micro-macro properties of pebble assemblies through experiments is very expensive and not feasible in some cases as the microscopic data is not readily available. Hence, DEM along with Resistor Network (RN) model is employed to study the influence of various micro and macro structural parameters on the ETC of the pebble assemblies. The RN model is modified to include the effect of gas pressure (Smoluchowski effect) on the effective thermal conductivity.

Estimation of the effective thermal conductivity through DEM simulations with the help of the Resistor Network model is shown to be in good accordance with the experimental results, strengthening the efficacy of the numerical simulations. However, the method has its limitations for application to larger pebble assemblies. Numerical heat transfer simulations of larger assemblies through DEM needs huge computational resources and time. Resistor Network model requires the pebble configuration as input from DEM. Thus, the heat transfer simulation for a large-scale assembly through DEM-RN model is not practically feasible.

The influence of various microstructural parameters on the effective thermal conductivity is often lost during the homogenization process while simulating through a continuum approach. The present work aims at the numerical analysis of heat transfer in large-scale systems accounting for the microstructural effects on the ETC. The large-scale heat transfer simulations are carried out with the help of the artificial neural networks (ANN). The ANN is trained with the help of DEM-RN model. The fast and instant predictions of the effective thermal conductivity of an RVE at various bed conditions through ANN enables the possibility to extend the methodology to larger systems. The trained ANN is coupled with finite element simulations to study the heat transfer in pebble beds in full-scale breeder units in future.

Application of machine learning tools for thermal analysis of pebble beds

Akhil Reddy Peeketi, Raghu Ram Karthik Desu, Pramod Kumbhar
Ratna Kumar Annabattula

Mechanics of Materials (MoM) Lab,
Department of Mechanical Engineering,
Indian Institute of Technology (IIT) Madras,
Chennai, INDIA.

International Workshop on Ceramic Breeder Blanket Interactions (**CBBI-20**), KIT, Germany

Effective Thermal Conductivity (ETC)

- ETC of pebble beds is vital in designing the breeder units
- Influence of microstructural and bulk properties
  - Bulk conductivities of pebbles and stagnant gas
  - Packing fraction, coordination number, pebble configuration
- Pebble beds : Granular assembly with stagnant gas
  - Conduction through pebbles and gas
- Existing models for ETC estimation
  - **Resistance Network Model# (Numerical approach)**
  - **Semi-analytical Models#**

#M. Moscardini, Y. Gan and M. Kamlah, "Discrete element method for effective thermal conductivity of packed pebbles accounting for the Smoluchowski effect", Fusion Engineering and Design, 127, 192-201, (2008)
#Peeketi, A R , et al. "Effective thermal conductivity of a compacted pebble bed in a stagnant gaseous environment: An analytical approach together with DEM." Fusion Engineering and Design, 130, 88-88 (2018)
#Akhil Reddy Peeketi, Marigrazia Moscardini, Simone Pupeschi, Yixiang Gan, Marc Kamlah and Ratna K. Annabattula Analytical estimation of the effective thermal conductivity of a granular bed in a stagnant gas including the Smoluchowski effect, Granular Matter, 21:93 (2019)

Resistance Network Model

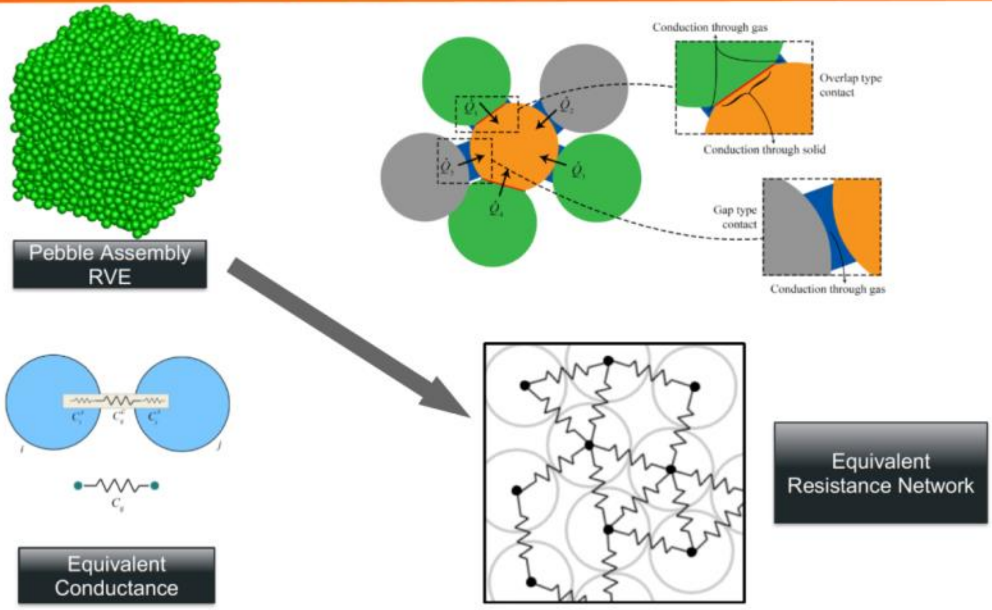

Resistance Network Model

- Contact conductance
  - Batchelor and O'Brien (1997): contacting particles in presence of gas
  - Modified by Peeketi AR (2018)
  - Overlap : solid and gas conductance
  - Gap: gas conductance

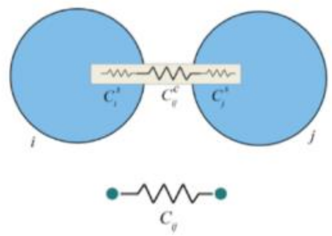

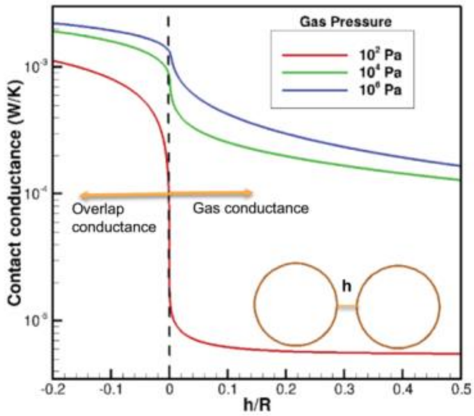

Influence of pressure on gas conductivity (Smoluchowski Effect)#

*Peeketi, A R , et al. "Effective thermal conductivity of a compacted pebble bed in a stagnant gaseous environment: An analytical approach together with DEM." Fusion Engineering and Design (2018)
#M. Moscardini, Y. Gan and M. Kamlah, "Discrete element method for effective thermal conductivity of packed pebbles accounting for the Smoluchowski effect", Fusion Engineering and Design, 127, 192-201, (2008)

Resistance Network Model

- Heat flow between each neighboring pair (i, j)
  - $\dot{q}_{ij} = C_{ij}\,(T_i - T_j)$
- Boundary conditions
  - Temperature to top and bottom layer
  - Adiabatic conditions on lateral sides
- Solving the resistance network

$$k_{\text{eff}} = \frac{\dot{Q}H}{A}$$

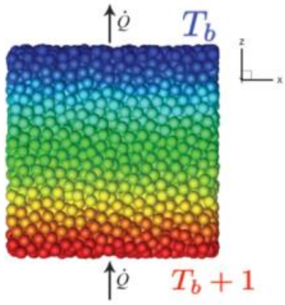

H : height of the assembly
A : cross-sectional area

Resistance Network Model…

- Comparison with experimental results*

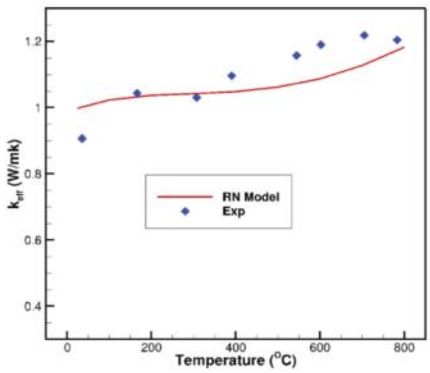

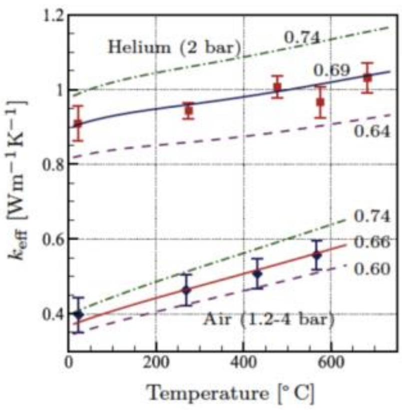

Panchal, M. et al. "Experimental measurement and numerical modeling of the effective thermal conductivity of lithium meta-titanate pebble bed". Fusion Engineering and Design (2018)
Akhil R Peeketi, M. Moscardini, S. Pupeschi, Y. Gan, M. Kamlah and R. K. Annabattula, Analytical estimation of the effective thermal conductivity of a granular bed in a stagnant gas including the Smoluchowski effect, Computational Particle Mechanics, 21:93 (2019)

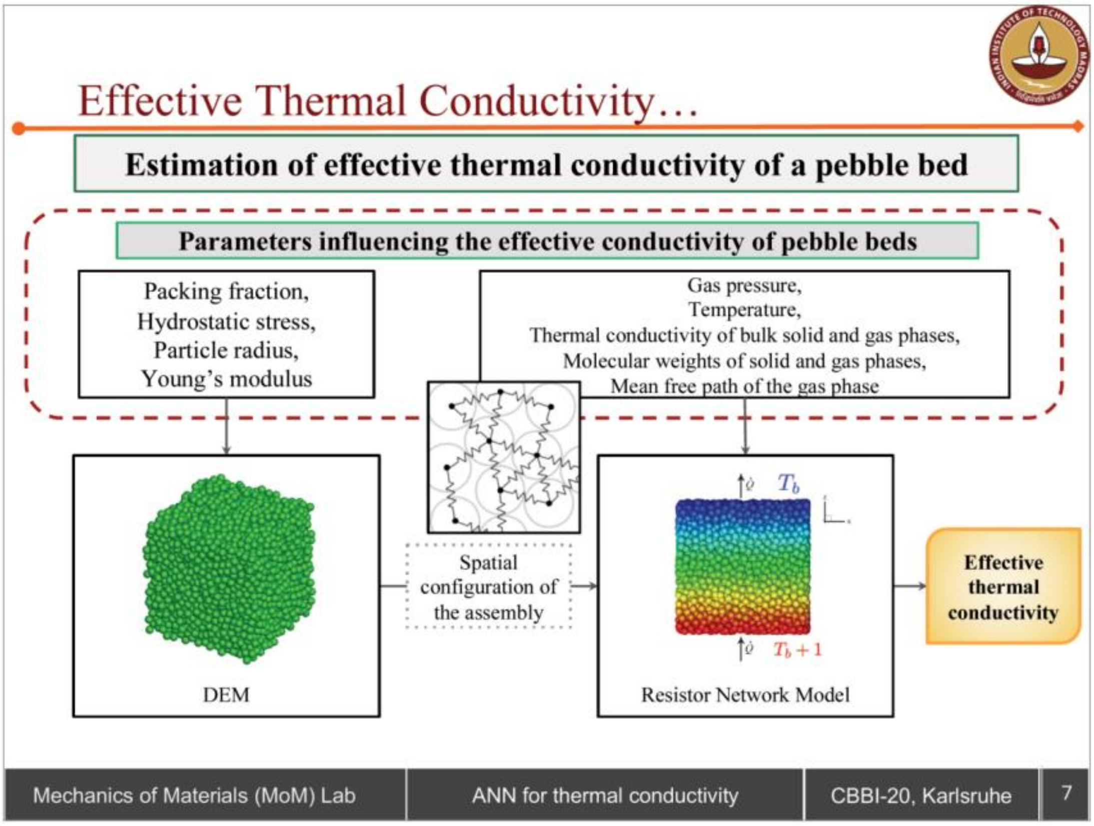

Limitations…

- DEM
  - Small scale simulations → Representative volume element
  - Higher number of particles→ computationally very intensive and time consuming
  - Large scale simulations → Not practically feasible
- Resistance Network model
  - Needs the configuration from DEM
  - Increase in particle number → computationally intensive calculations
  - ETC of pebble assembly at a given bed temperature (present model)
- Example (calculating ETC)
  - Bed size: 1000 x 50 x 50 mm^3
  - PF : 64
  - Number of pebbles (of diameter 500 μm) = 24 million (almost impossible to simulate with conventional DEM)
  - RN model: 24 million X 7 (CN) = 168 million resistors

Mechanics of Materials (MoM) Lab | ANN for thermal conductivity | CBBI-20, Karlsruhe | 8

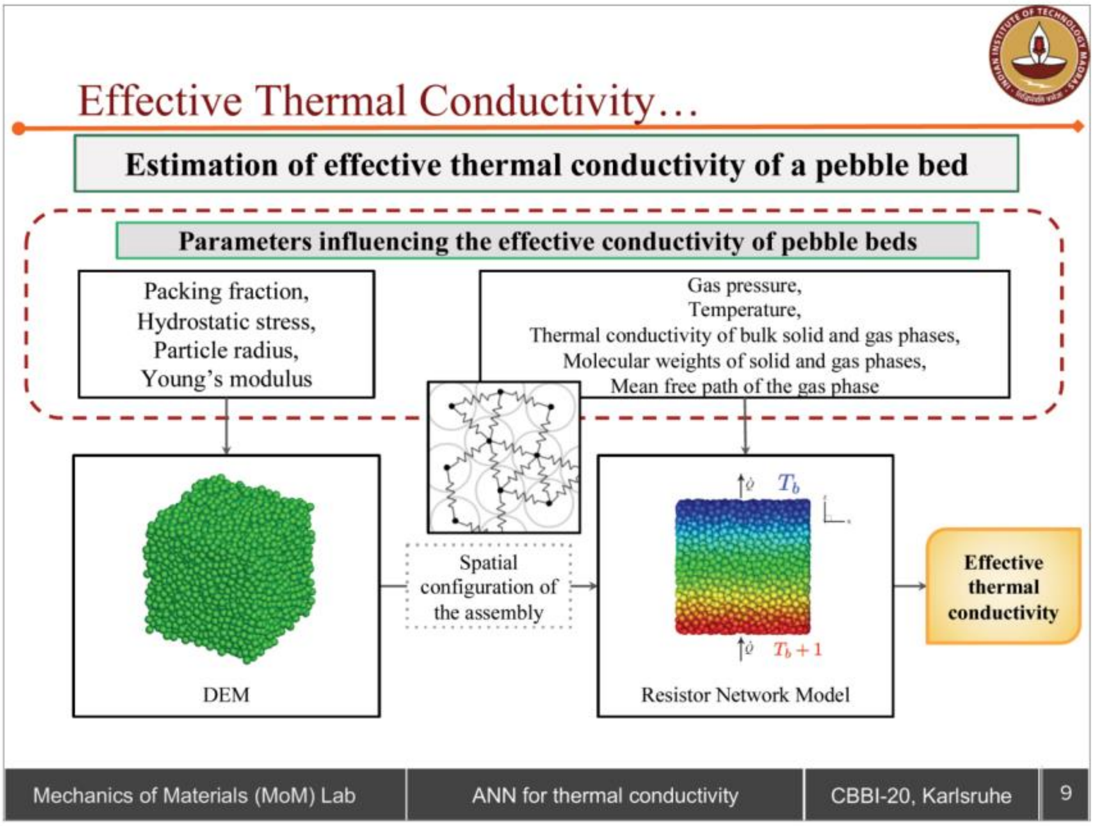
Effective Thermal Conductivity…
Estimation of effective thermal conductivity of a pebble bed
Parameters influencing the effective conductivity of pebble beds
Packing fraction, Hydrostatic stress, Particle radius, Young's modulus
Gas pressure, Temperature, Thermal conductivity of bulk solid and gas phases, Molecular weights of solid and gas phases, Mean free path of the gas phase
DEM
Spatial configuration of the assembly
T_b
$T_b + 1$
Resistor Network Model
Effective thermal conductivity
Mechanics of Materials (MoM) Lab
ANN for thermal conductivity
CBBI-20, Karlsruhe
9

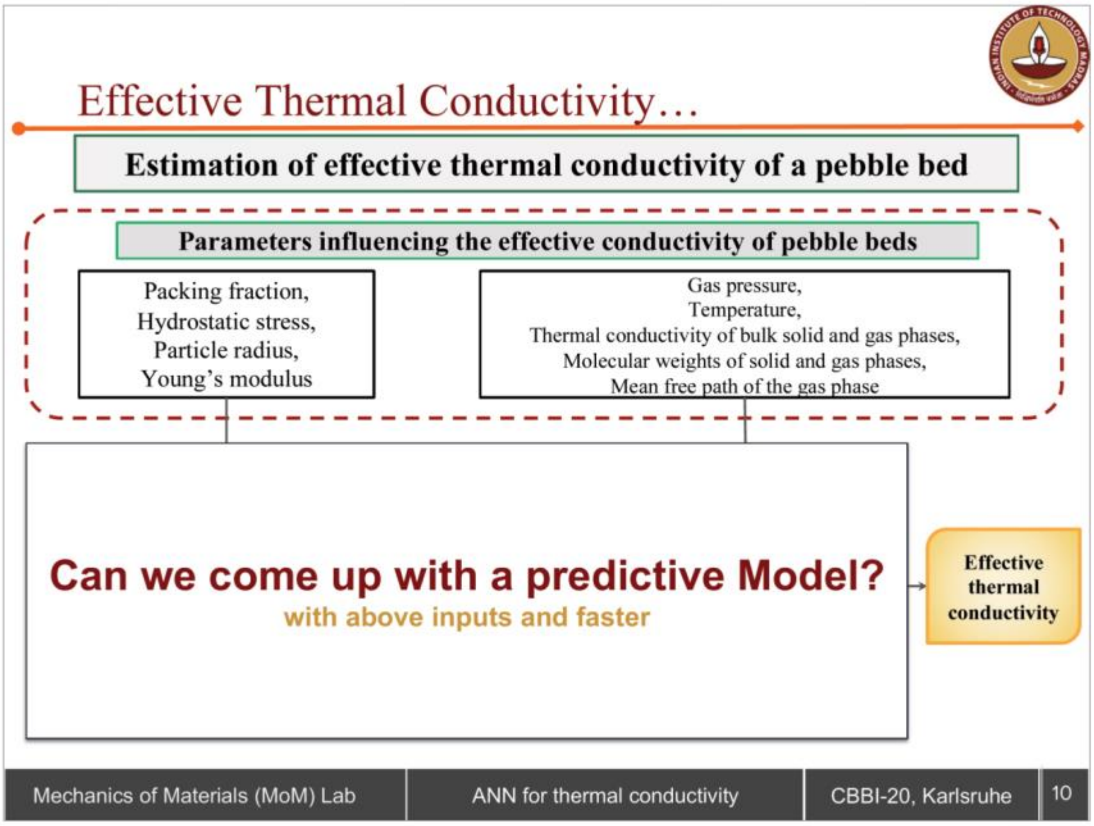
Effective Thermal Conductivity…
Estimation of effective thermal conductivity of a pebble bed
Parameters influencing the effective conductivity of pebble beds
Packing fraction, Hydrostatic stress, Particle radius, Young's modulus
Gas pressure, Temperature, Thermal conductivity of bulk solid and gas phases, Molecular weights of solid and gas phases, Mean free path of the gas phase
Can we come up with a predictive Model?
with above inputs and faster
Effective thermal conductivity
Mechanics of Materials (MoM) Lab
ANN for thermal conductivity
CBBI-20, Karlsruhe
10

Artificial Neural Networks

- Raghuram Karthik Desu, Akhil Reddy Peeketi, Ratna Kumar Annabattula, Artificial neural network-based prediction of effective thermal conductivity of a granular bed in a gaseous environment, Computational Particle Mechanics (2019)

Mechanics of Materials (MoM) Laboratory, Indian Institute of Technology Madras, Chennai.

Artificial Neural Network

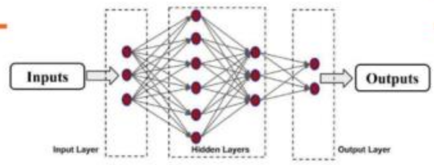

- Artificial Neural Network
  - Machine learning technique
  - Recognize complex relations and patterns → faster analysis and predictions
  - Inspired by biological neural network
  - Neuron: Basic unit
  - Network: collection of layers consisting of neurons
- Effective Thermal Conductivity
  - Supervised learning and Regression: predictions based on learning → known inputs and outputs
  - Predictive model with ANN reducing dependency on simulations
  - Inputs : Set of measurable experimental parameters

Mechanics of Materials (MoM) Lab | ANN for thermal conductivity | CBBI-20, Karlsruhe | 12

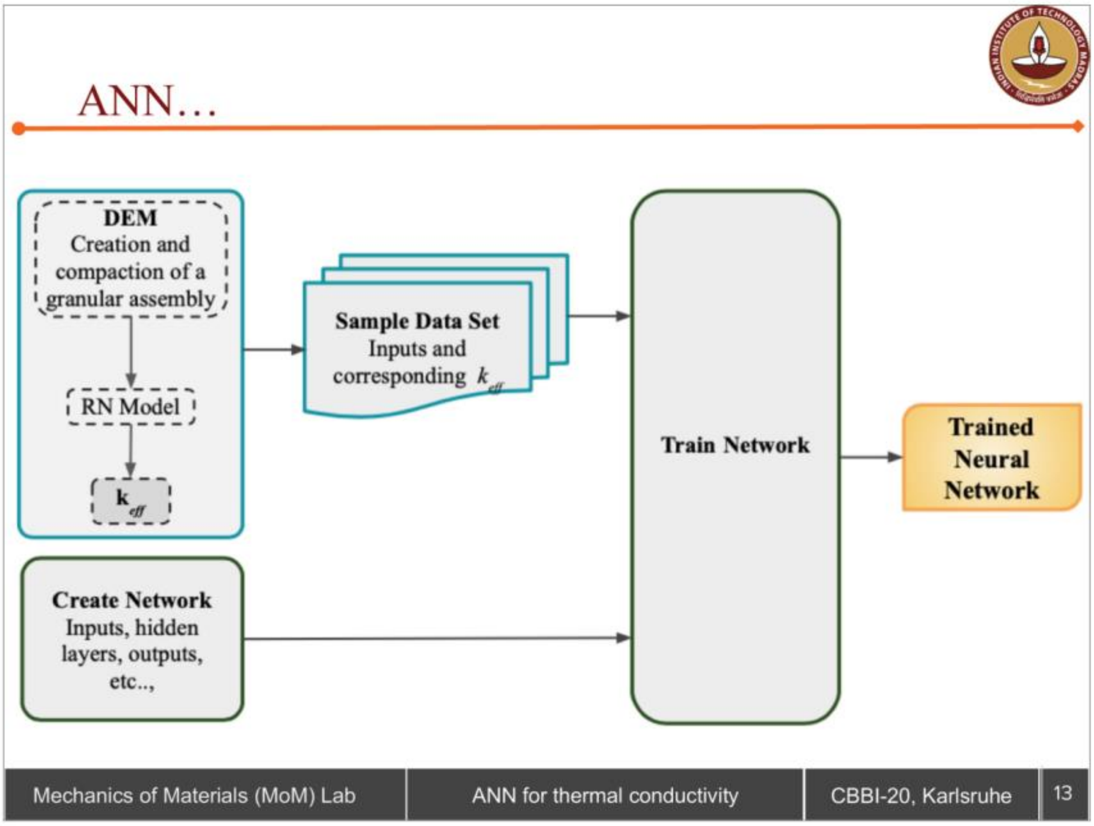
ANN…
DEM
Creation and compaction of a granular assembly
RN Model
k_{eff}
Sample Data Set
Inputs and corresponding k_{eff}
Train Network
Trained Neural Network
Create Network
Inputs, hidden layers, outputs, etc..,
Mechanics of Materials (MoM) Lab
ANN for thermal conductivity
CBBI-20, Karlsruhe
13

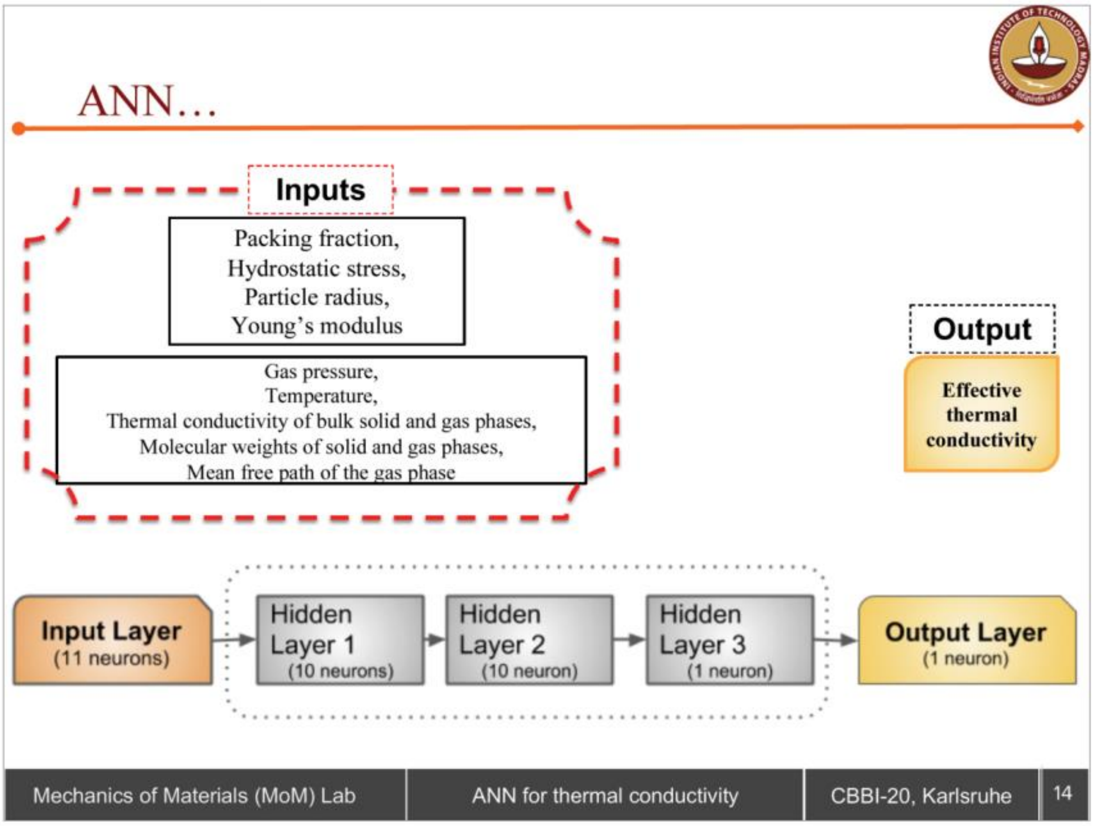
ANN…
Inputs
Packing fraction,
Hydrostatic stress,
Particle radius,
Young's modulus
Gas pressure,
Temperature,
Thermal conductivity of bulk solid and gas phases,
Molecular weights of solid and gas phases,
Mean free path of the gas phase
Output
Effective thermal conductivity
Input Layer
(11 neurons)
Hidden Layer 1
(10 neurons)
Hidden Layer 2
(10 neuron)
Hidden Layer 3
(1 neuron)
Output Layer
(1 neuron)
Mechanics of Materials (MoM) Lab
ANN for thermal conductivity
CBBI-20, Karlsruhe
14

ANN…

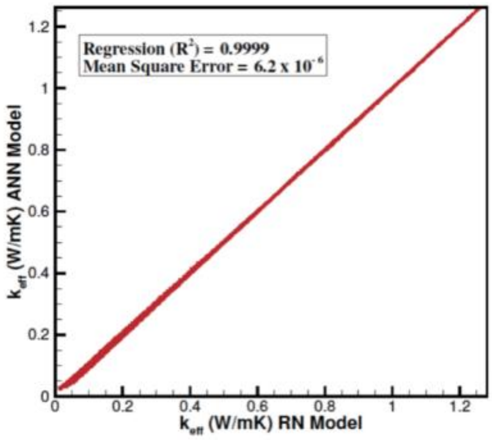

Training Data

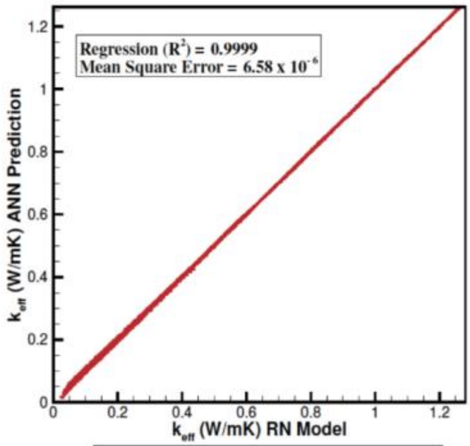

Prediction for new inputs

ANN..

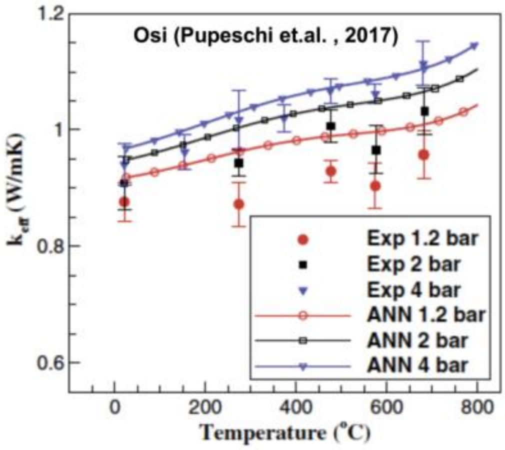

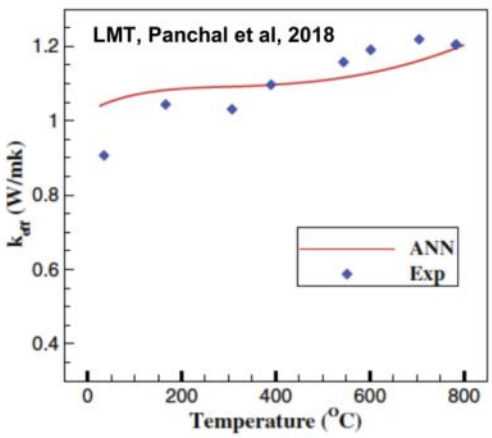

1. Pupeschi S, Knitter R, KamlahM(2017) Effective thermal conductivity of advanced ceramic breeder pebble beds. Fusion Eng Des 116:73–80
2. Panchal M, Kang C, Ying A, Chaudhuri P (2018) Experimental measurement and numerical modeling of the effective thermal conductivity of lithium metatitanate pebble bed. Fusion Eng Des 127:34–39

ANN…

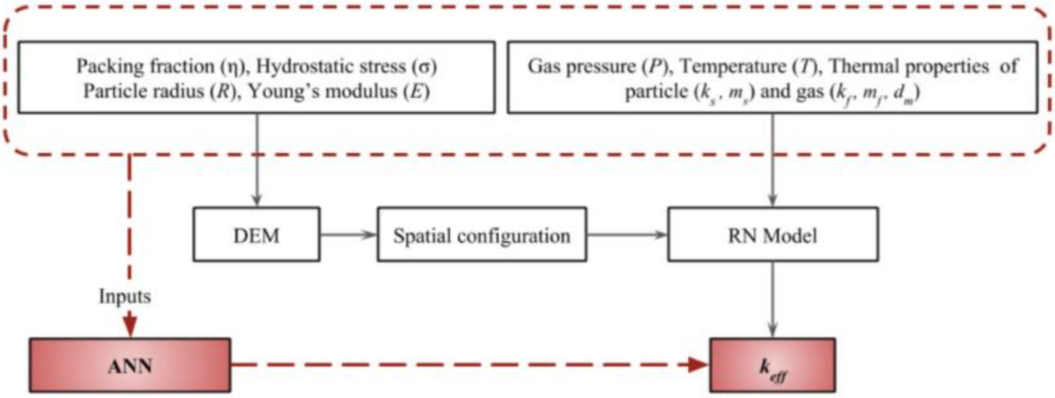

Mechanics of Materials (MoM) Lab | ANN for thermal conductivity | CBBI-20, Karlsruhe | 17

Full-scale breeder unit heat transfer Simulations

- Raghuram Karthik Desu, Akhil Reddy Peeketi, Ratna Kumar Annabattula, Artificial neural network-based prediction of effective thermal conductivity of a granular bed in a gaseous environment, Computational Particle Mechanics (2019)
- Akhil Reddy Peeketi, Raghuram Karthik Desu, Pramod Kumbhar and Ratna Kumar Annabattula, Thermal analysis of large granular assemblies using a hierarchical approach coupling the macro-scale finite element method and micro-scale discrete element method through artificial neural Networks, Computational Particle Mechanics (2019)

Mechanics of Materials (MoM) Laboratory, Indian Institute of Technology Madras, Chennai.

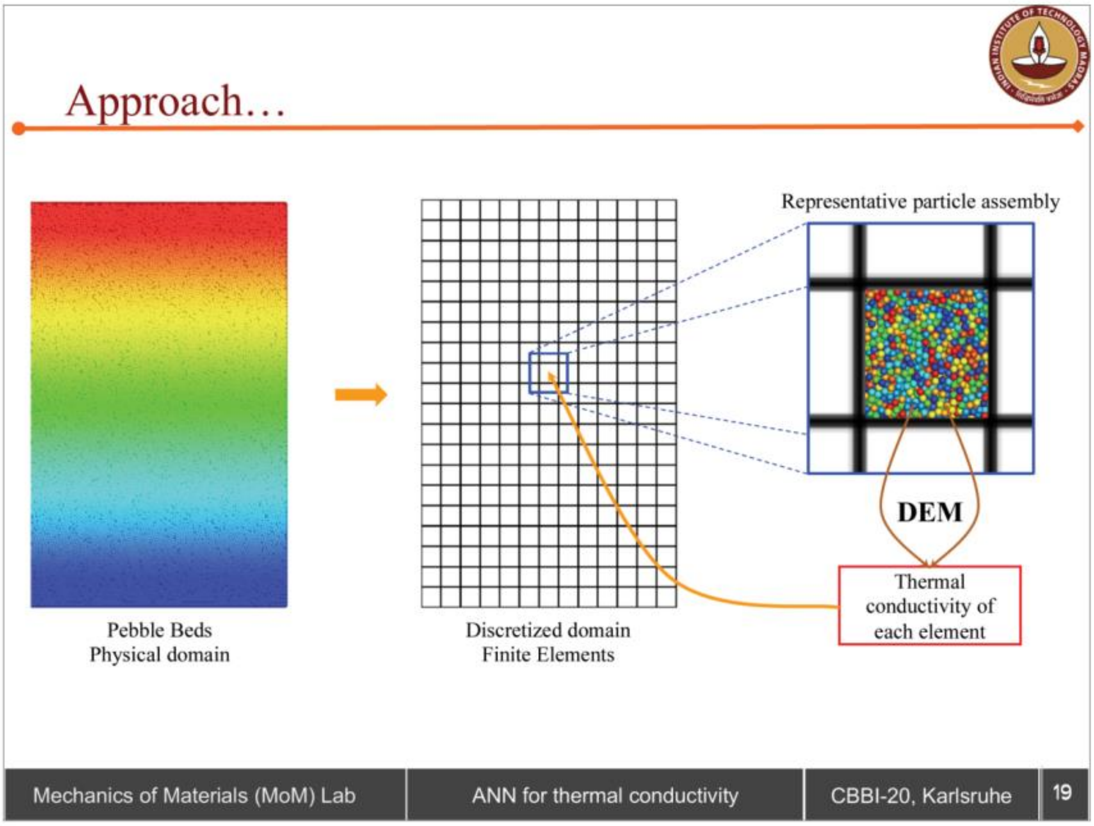
Approach…
Representative particle assembly
DEM
Thermal conductivity of each element
Pebble Beds
Physical domain
Discretized domain
Finite Elements
Mechanics of Materials (MoM) Lab
ANN for thermal conductivity
CBBI-20, Karlsruhe
19

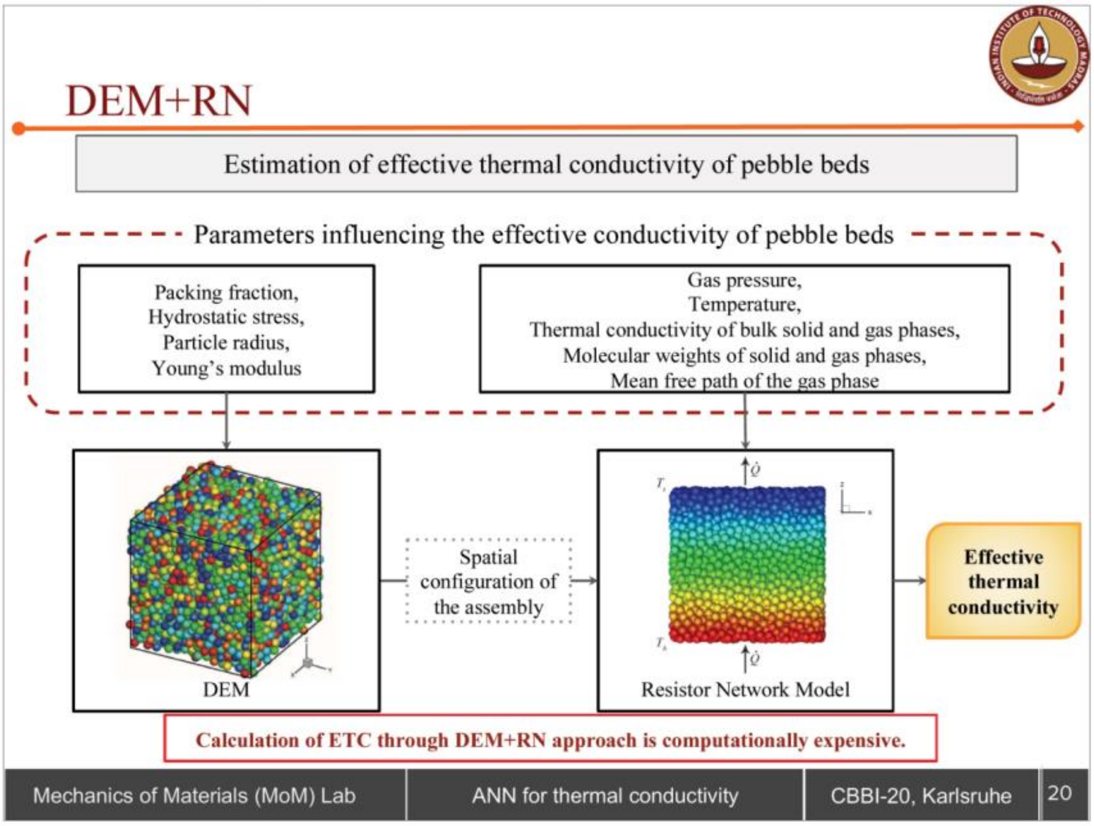
DEM+RN
Estimation of effective thermal conductivity of pebble beds
Parameters influencing the effective conductivity of pebble beds
Packing fraction, Hydrostatic stress, Particle radius, Young's modulus
Gas pressure, Temperature, Thermal conductivity of bulk solid and gas phases, Molecular weights of solid and gas phases, Mean free path of the gas phase
DEM
Spatial configuration of the assembly
Resistor Network Model
Effective thermal conductivity
Calculation of ETC through DEM+RN approach is computationally expensive.
Mechanics of Materials (MoM) Lab
ANN for thermal conductivity
CBBI-20, Karlsruhe
20

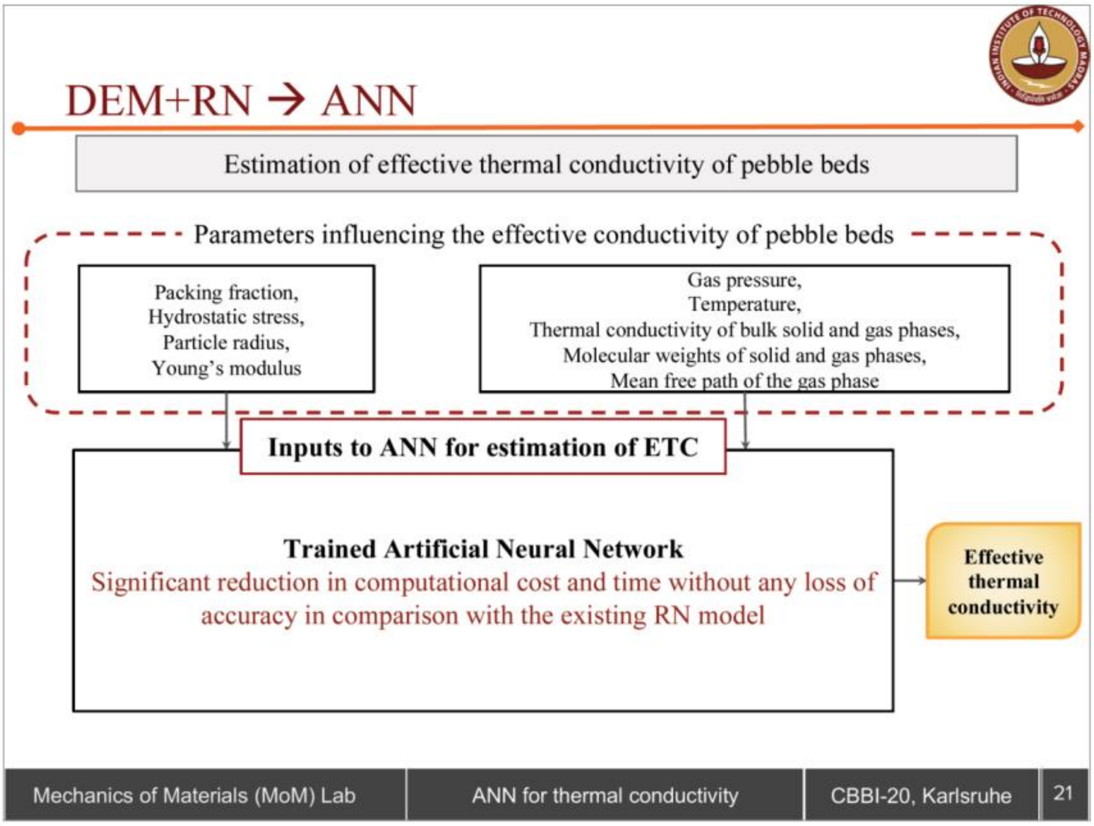
DEM+RN → ANN
Estimation of effective thermal conductivity of pebble beds
Parameters influencing the effective conductivity of pebble beds
Packing fraction,
Hydrostatic stress,
Particle radius,
Young's modulus
Gas pressure,
Temperature,
Thermal conductivity of bulk solid and gas phases,
Molecular weights of solid and gas phases,
Mean free path of the gas phase
Inputs to ANN for estimation of ETC
Trained Artificial Neural Network
Significant reduction in computational cost and time without any loss of accuracy in comparison with the existing RN model
Effective thermal conductivity
Mechanics of Materials (MoM) Lab
ANN for thermal conductivity
CBBI-20, Karlsruhe
21

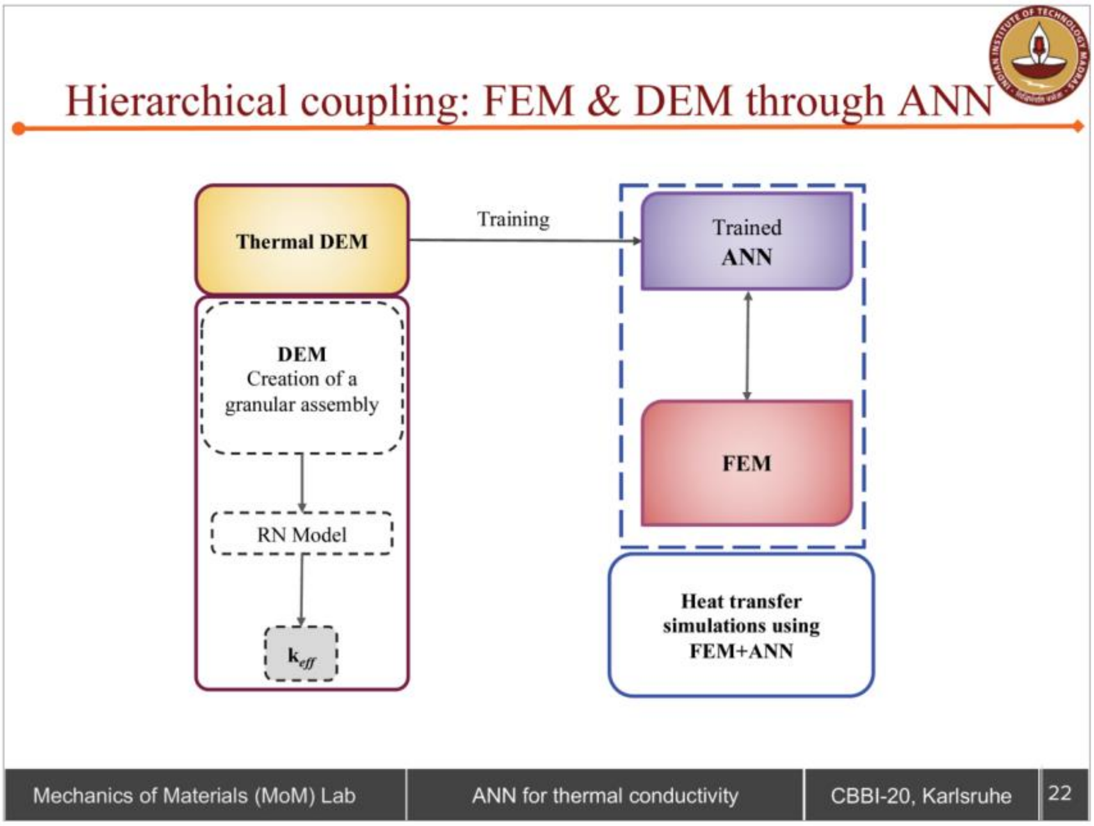
Hierarchical coupling: FEM & DEM through ANN
Thermal DEM
Training
Trained ANN
DEM
Creation of a granular assembly
RN Model
k_{eff}
FEM
Heat transfer simulations using FEM+ANN
Mechanics of Materials (MoM) Lab
ANN for thermal conductivity
CBBI-20, Karlsruhe
22

Breeder Unit

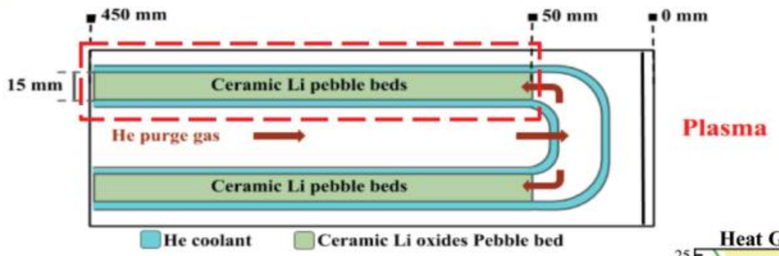

400 x 400 x 15 mm ⟶ 400 x 50 x 15 mm (simulation)
Hydrostatic stress state of 1 Mpa
Packing fraction: 0.629, porosity $\eta = 0.371$
Particle diameter $D = 0.4$ mm
Equivalent to 12 million particles
$P_{in} = 250$ kPa; $U = 1$ m/s,
$T_{z=0} = T_{z=15} = 500$C

Pressure Drop in Breeder Unit: Ergun's Formulation

$$P(x) = P_{\text{in}} - x\left[150 \times \frac{(1-\eta)^2 \mu U}{\eta^3 D^2} + 2 \times \frac{(1-\eta)\rho U^2}{\eta^3 D}\right]$$

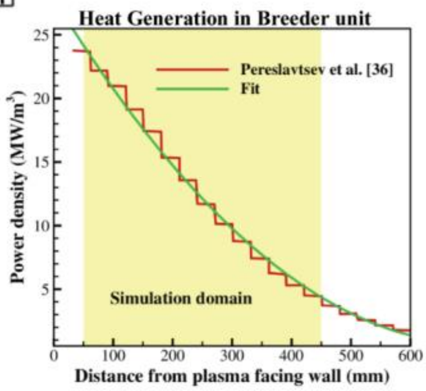

Results

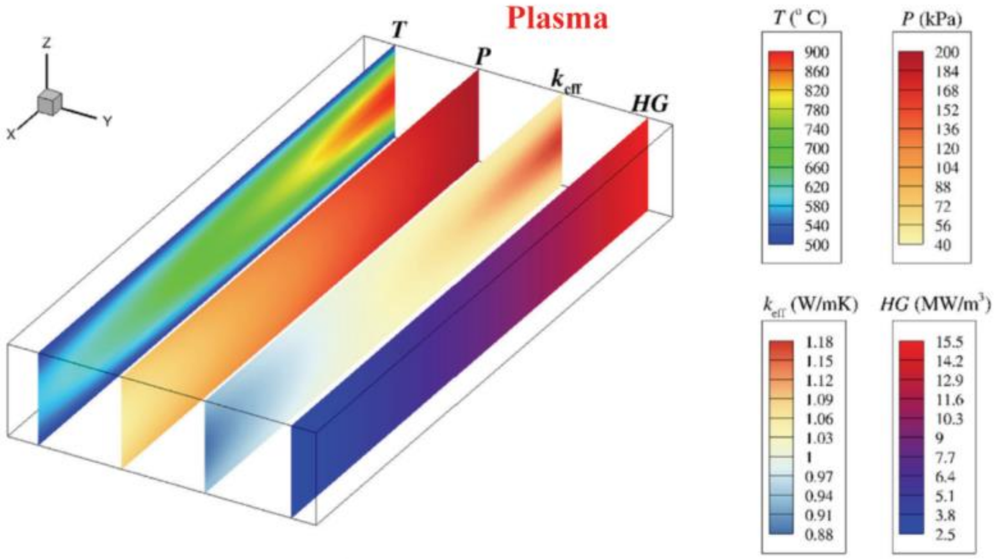

Comparison…

DEM simulation at different sections

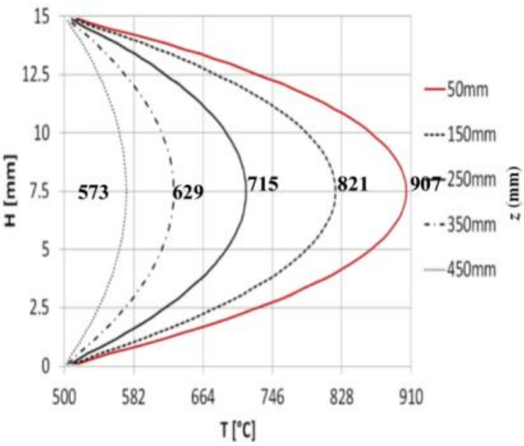

Full-scale simulations using FEM-ANN-DEM

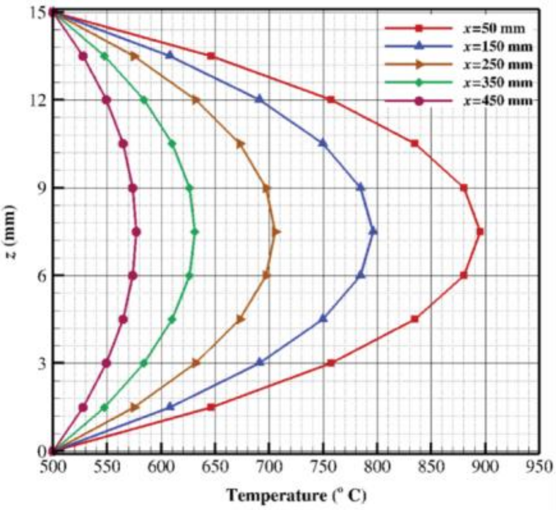

Moscardini, M., et al. "Discrete Element Analysis of Heat Transfer in the Breeder Beds of the European Solid Breeder Blanket Concept." *Fusion Science and Technology* 75.4 (2019): 283-298.

Mechanics of Materials (MoM) Lab | ANN for thermal conductivity | CBBI-20, Karlsruhe | 25

Summary and Conclusions

- The ANN tool is able to predict the temperature distribution with reasonable accuracy.
- The time taken for full-scale simulation is reduced significantly.
- The new methodology allows for estimating the heat transfer in full-scale breeder units.

Mechanics of Materials (MoM) Lab | ANN for thermal conductivity | CBBI-20, Karlsruhe | 26

Acknowledgements

- Dr. Paritosh Chaudhury, IPR
- Prof. Marc Kamlah, KIT
- Dr. Marigrazia Moscardini, KIT, (now with U. Pisa)
- Dr. Simone Pupeschi, KIT (now with General Electric)
- Dr. Simone Pupeschi, KIT
- Prof. Yixiang Gan, University of Sydney

Mechanics of Materials (MoM) Lab | ANN for thermal conductivity | CBBI-20, Karlsruhe | 27

Thank you for your attention

Mechanics of Materials (MoM) Lab | ANN for thermal conductivity | CBBI-20, Karlsruhe | 28

Investigation of the packing behaviors and the effective thermal conductivity of pebble beds

Baoping Gong, Yongjin Feng, Hao Cheng, Long Wang, Xiaoyu Wang, Kaiming Feng

Southwest Institute of physics, Chengdu, 610225, China

The tritium breeding blankets play a crucial role on the function of tritium self-sufficiency in the fusion power reactor. The tritium breeder and neutron multiplier are usually used in form of pebbles in blanket for CN HCCB TBM. The packing behaviors of pebble beds are important to estimate the thermal mechanical properties of the tritium breeder pebble beds and the neutron multiplier pebble beds.

In this work, the experiment and the discrete element method (DEM) simulation were used to investigate the packing behaviors of mono-sized and binary-sized pebble beds, respectively. The results obtained in this study show that with the increase of aspect ratios the average packing factors can be significantly increased. And the pebble size distributions have great influence on the packing structures of pebble bed. By optimizing the pebble size component, a higher packing factor can be obtained by using binary-sized pebbles and the maximum packing efficiency state appear at the volume fraction 70% of larger pebbles. But the obvious segregation effect was observed when the binary-sized pebble bed was vibrated. And the homogenization of binary-sized pebble bed is very poor. Thus the mono-sized beryllium pebbles was suggested in neutron multiplier pebble beds for HCCB TBM.

In further, the U-shaped tritium breeder Li_4SiO_4 pebble beds were investigated by DEM simulation. Close to the U-shaped container walls, the oscillating and damping characteristics of local packing factors were observed. And the oscillation is limited within about 5 pebble diameters near the wall. The contact force distributions show that close to bottom wall the pebbles suffer greater contact forces and may be more easily crushed. The results give more information about the packing structure of pebble bed, and that can be as inputs of further analyses of the thermal properties of pebble bed. Moreover, the packing behaviors of pebble beds under vibration were investigated experimental. The influences of the vibration amplitude and frequency on the packing fraction were analyzed to optimize the pebble packing techniques for the helium cooled ceramic breeder blanket. In addition, the influences of pebble size, temperature, packing factor on the effective thermal conductivity of pebble bed were investigated by using the transient plane source (TPS) method.


CBBI-20
核工业西南物理研究院
Southwestern Institute of Physics
Investigations of the packing behaviors and the effective thermal conductivity of pebble beds
Baoping Gong, Yongjin Feng, Hao Cheng, Long Wang, Xiaoyu Wang, Kaiming Feng
Southwestern Institute of Physics (SWIP), Chengdu, China
20th International Workshop on CERAMIC BREEDER BLANKET INTERACTIONS
KIT Campus North, Karlsruhe, Germany
September 18~20,2019
This work was supported by the National Key Research and Development Program of China under grant number 2017YFE0300602, and by the Sichuan Science and Technology Program of Sichuan Province of China under grant number 2018JZ0014.
1
CNNC China National Nuclear Corporation

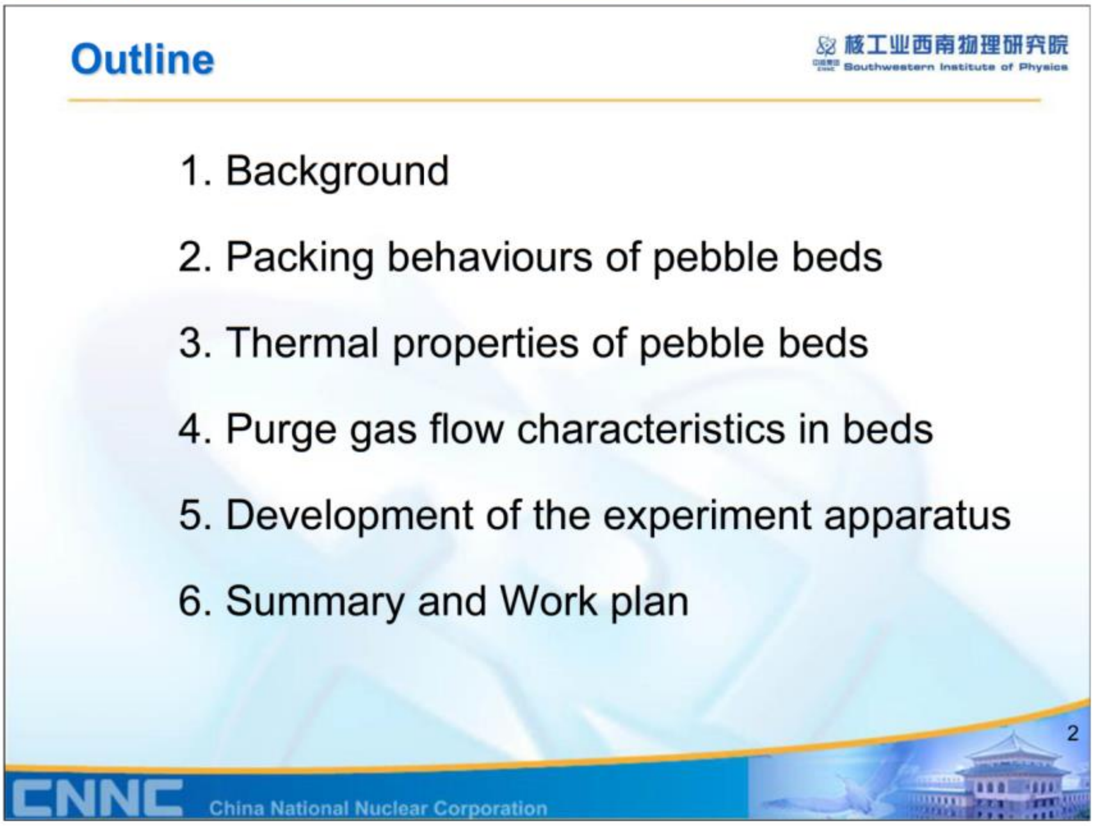
Outline
核工业西南物理研究院
Southwestern Institute of Physics
1. Background
2. Packing behaviours of pebble beds
3. Thermal properties of pebble beds
4. Purge gas flow characteristics in beds
5. Development of the experiment apparatus
6. Summary and Work plan
2
CNNC China National Nuclear Corporation


1. Background
核工业西南物理研究院
Southwestern Institute of Physics
Roadmap for Chinese
MCF Development
One of the Challenge:
Tritium self-sufficiency
PFPP
(2050's)
1GWe, Power
Plant Validation
CFETR
(2030's start operation)
I: Q=1-5, steady state、TBR>1, >200MW, 10dpa
II: DEMO validation, Q>10; CW, 1GW, >50dpa
ITER
(2025)
Phase I : Q=10, 400s, 500MW, Hybrid burning plasma
Phase I I: Q=5, 3000s, 350MW, steady-state burning plasma
EAST Advance PFC, steady-state advanced opration
HL-2M Advanced divertor, high power H&CD, diagnostics
J-TEXT Disruption mitigation, basic plasma
2015 2020 2025 2030 2035 2040 2045 2050 2055 2060
3
Jiangang Li, et al., Journal of Fusion Energy, 2019, 38(1):113-124
CNNC China National Nuclear Corporation

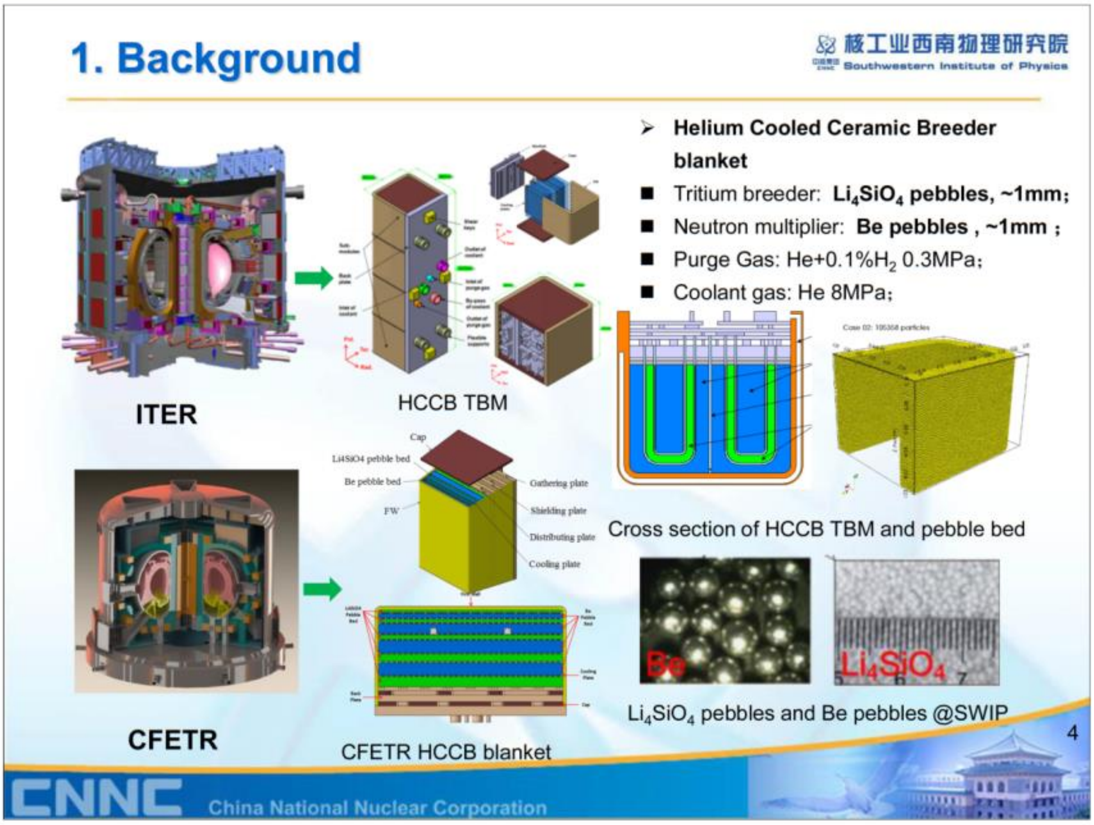
1. Background
核工业西南物理研究院
Southwestern Institute of Physics
Helium Cooled Ceramic Breeder blanket
Tritium breeder: Li4SiO4 pebbles, ~1mm;
Neutron multiplier: Be pebbles , ~1mm ;
Purge Gas: He+0.1%H2 0.3MPa;
Coolant gas: He 8MPa;
ITER
HCCB TBM
Cross section of HCCB TBM and pebble bed
Cap
Li4SiO4 pebble bed
Be pebble bed
FW
Gathering plate
Shielding plate
Distributing plate
Cooling plate
CFETR
CFETR HCCB blanket
Be
Li4SiO4
Li4SiO4 pebbles and Be pebbles @SWIP
4
CNNC China National Nuclear Corporation

Outline

核工业西南物理研究院 Southwestern Institute of Physics

1. Introduction
2. Packing behaviors of pebble beds
3. Thermal properties of pebble beds
4. Purge gas flow characteristics in beds
5. Development of the experiment apparatus
6. Summary and Work plan

5

CNNC China National Nuclear Corporation

2. Packing behaviors of pebble beds

核工业西南物理研究院 Southwestern Institute of Physics

➢ Packing factors of **mono-sized pebble beds**

- The packing behaviour of mono-sized pebble bed were investigeted by packing experiments and Discrete Element Modelling.

✓ Mono-sized pebble bed

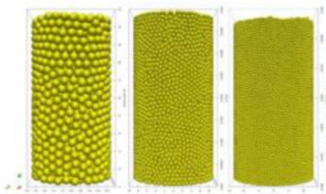

DEM result

✓ Average packing factor

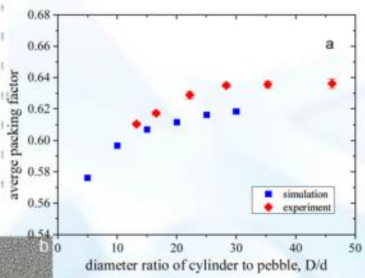

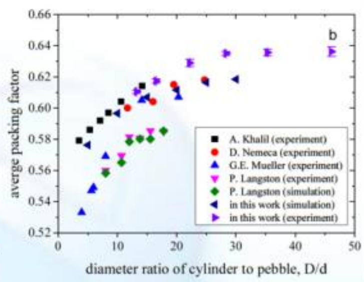

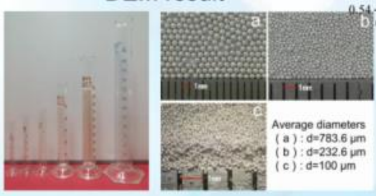

Packing experiment result

- With the increase of D/d , the average packing factors increased. The packing factor is ≥0.62 when D/d > 20.
- The simulation results are agreement well with experimental results.

6

Baoping GONG, et al., Fusion Engineering and Design 136 (2018) 1444–1451
Baoping GONG, et al., Fusion Engineering and Design 121 (2017) 256–264

CNNC China National Nuclear Corporation

2. Packing behaviors of pebble beds

➢ Packing factors of **binary-sized pebble beds**

- The packing factor can be increased significantly by using binary-sized pebble packing with larger size ratio. And the packing factor can reach 0.8. when size ratio is equal to 7 and volume fraction of large pebble is ~70%.
- However, the obvious segregation effect was observed after vibrating in the binary-sized pebble bed. Thus, the neutron multiplier pebbles changed from binary-sized pebble to mono-sized pebbles for HCCB-TBM.

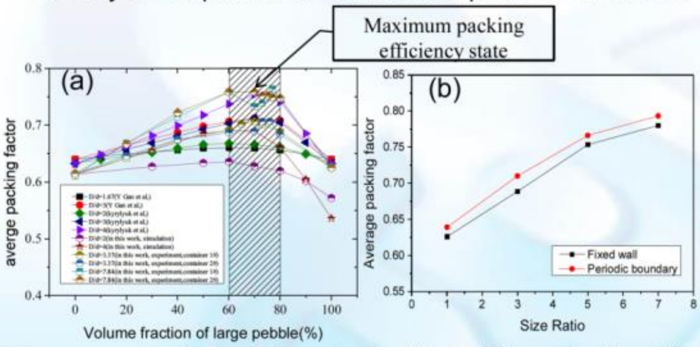

● Average packing factor of binary-sized pebble bed (a)as a function of the volume fraction of large pebble bed and (b) as a function of size ratio

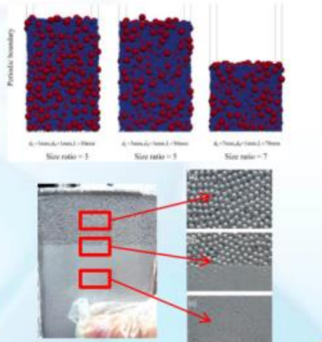

● Binary-sized pebble packing

Baoping GONG, et al., Nuclear Fusion and Plasma Physics, 2018,38(4):256–264

CNNC China National Nuclear Corporation

2. Packing behaviors of pebble beds

➢ Packing factors of **U-shaped Li_4SiO_4 pebble bed**

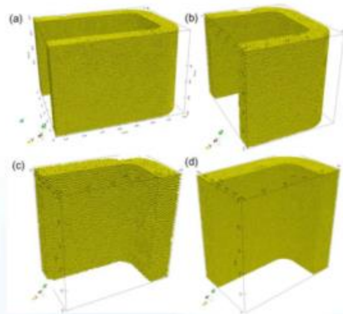

● Packing structures of four kinds of U-shaped Li_4SiO_4 pebble beds

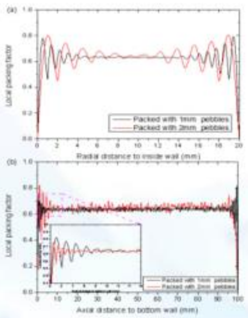

Packing factor distribution

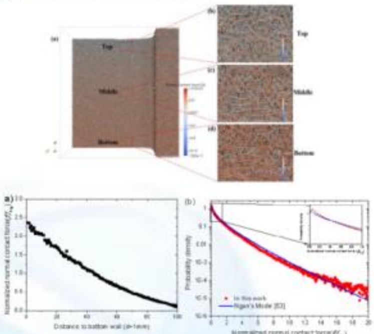

Normal contact force distribution

● Average packing factors of Four kinds of Li_4SiO_4 pebble beds

Case	Dimensions	Pebble beds	Pebble diameter	Number of pebbles	AVG. Packing Factor
1	a	a	2mm	105358	0.6153
2	b	b	2mm	76193	0.6145
3	c	c	2mm	38128	0.6193
4		d	1mm	308083	**0.6278**

8

Baoping GONG, et al., Fusion Engineering and Design 136 (2018) 1444–1451
Baoping GONG, et al., Fusion Engineering and Design 121 (2017) 256–264

CNNC China National Nuclear Corporation

2. Packing behaviors of pebble beds

- Effect of **pebble bed width** on the Packing factor between two parallel wall

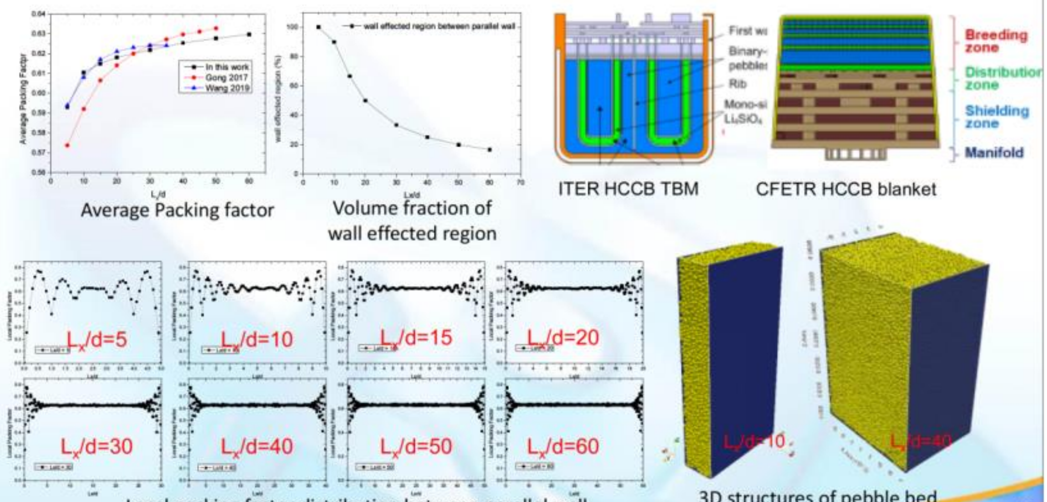

Local packing factor distribution between parallel wall

3D structures of pebble bed

9

2. Packing behaviors of pebble beds

- The **crushing characteristics** of ceramic pebbles inside the pebble bed (the experiments are ongoing)
  - The X-ray computed tomography (CT) was used to investigate the packing structures of mono-sized and binary-sized pebble beds experimentally. The results of X-ray CT experiments are in good agreement with the DEM simulation results.
  - Thus, the method can characterizes the crushing characteristics of internal pebbles under compresion. **More pebble crushing experiment inside the pebble bed under conpression are ongoing.**

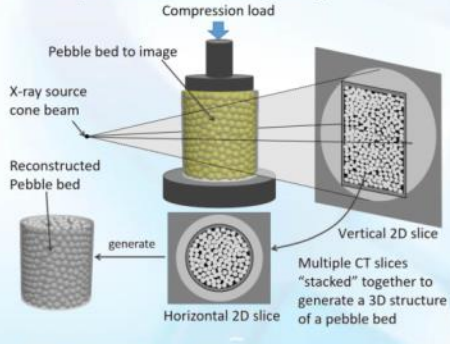

Schematic of the pebble crushing experiment in pebble bed based on the x-ray CT and the UCT.

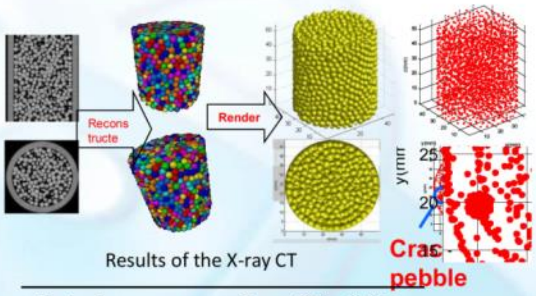

Results of the X-ray CT

Methods	X-ray CT	DEM
AVG. Packing Factor	0.6254	0.6240

10

Outline

11

CNNC China National Nuclear Corporation

3. Thermal properties of pebble beds

➢ Thermal properties of Li_4SiO_4 pebble beds

- The transient plane source (TPS) method was applied to measure the thermal properties of uncompressed mono-sized Li_4SiO_4 pebble beds.
- It was found that the effective thermal conductivity (ETC) increase with the increase of the temperature of the bed. While the thermal diffusivity decreased with the increase of the temperature of the bed.
- The **ETC measurement** of Li_4SiO_4 pebble beds under **thermal cycling** are ongoing.

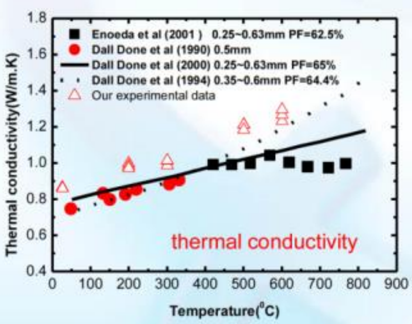

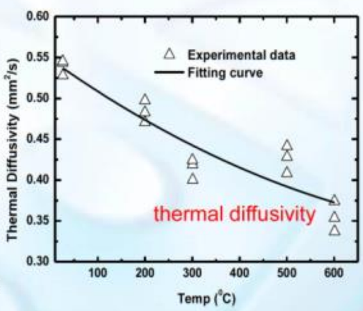

Effective thermal properties of **mono-sized Li_4SiO_4** pebble beds

Yongjin FENG, et al., J. Plasma Fusion Res. SERIES, 2015,11:49-52

12

CNNC China National Nuclear Corporation

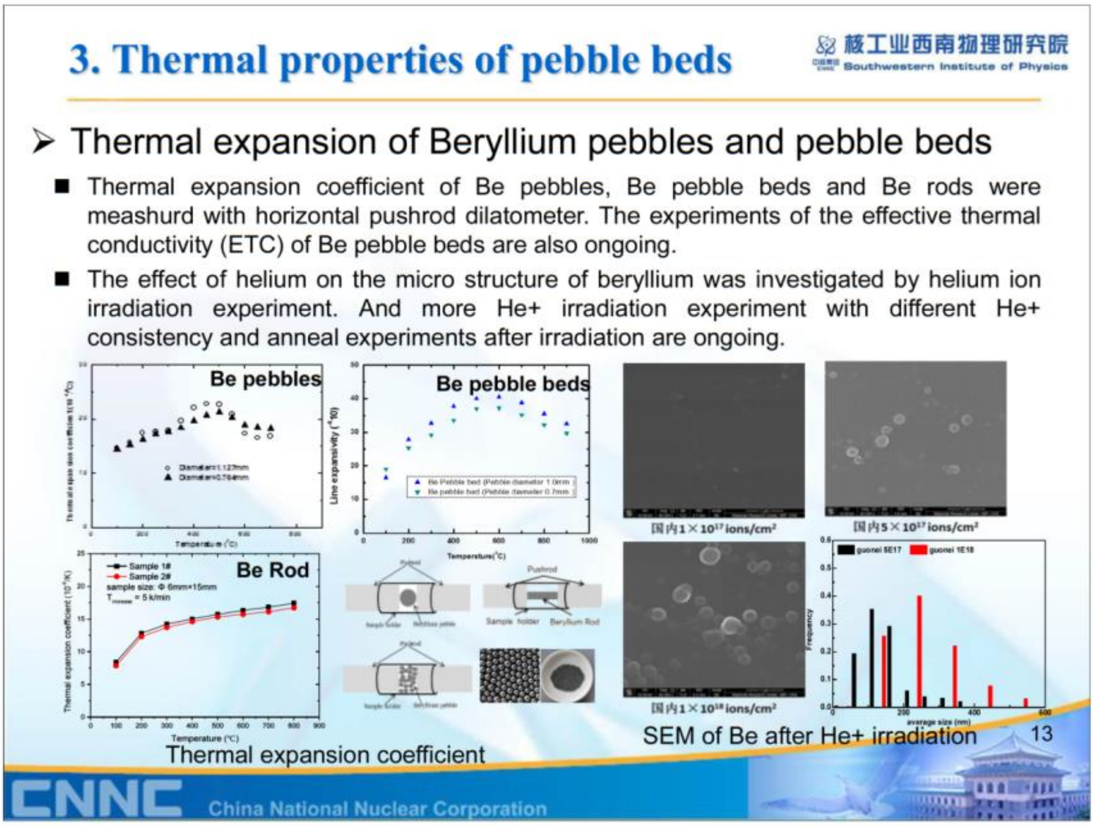
3. Thermal properties of pebble beds
核工业西南物理研究院
Southwestern Institute of Physics
➢ Thermal expansion of Beryllium pebbles and pebble beds
■ Thermal expansion coefficient of Be pebbles, Be pebble beds and Be rods were meashurd with horizontal pushrod dilatometer. The experiments of the effective thermal conductivity (ETC) of Be pebble beds are also ongoing.
■ The effect of helium on the micro structure of beryllium was investigated by helium ion irradiation experiment. And more He+ irradiation experiment with different He+ consistency and anneal experiments after irradiation are ongoing.
Be pebbles
Be pebble beds
Be Rod
国内1×10¹⁷ions/cm²
国内5×10¹⁷ions/cm²
国内1×10¹⁸ions/cm²
Thermal expansion coefficient
SEM of Be after He+ irradiation
13
CNNC
China National Nuclear Corporation

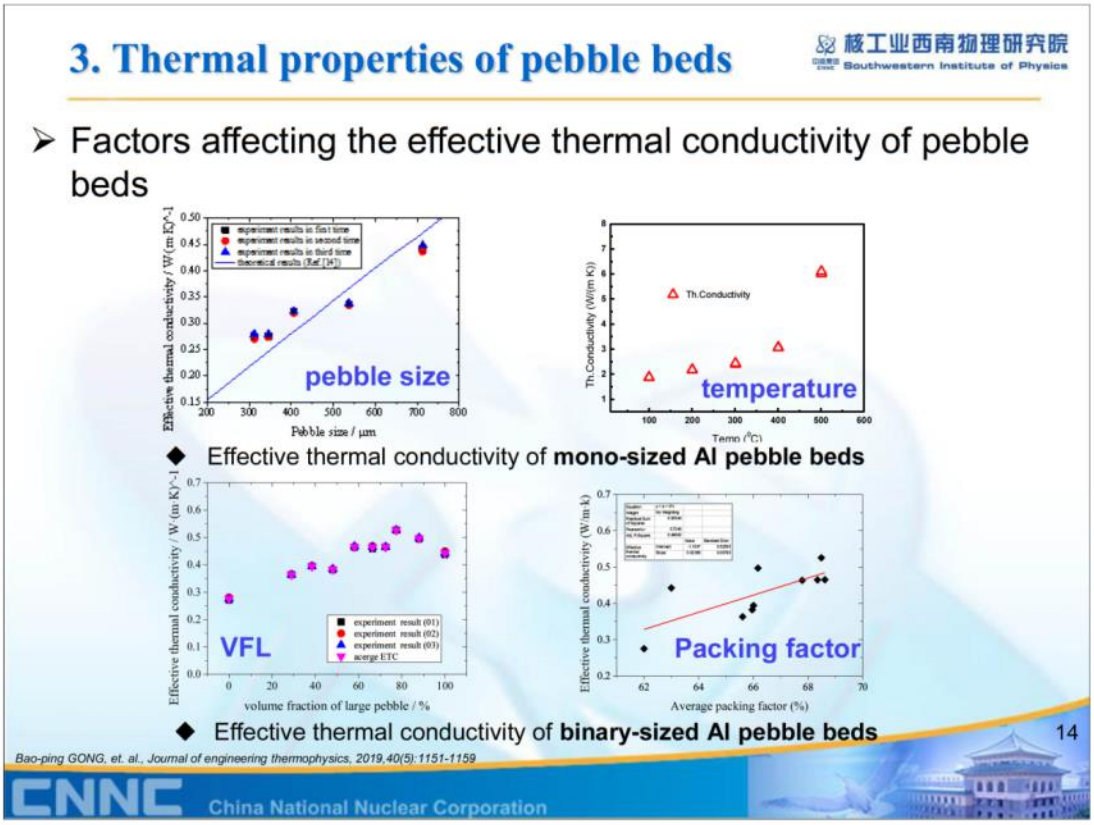
3. Thermal properties of pebble beds
核工业西南物理研究院
Southwestern Institute of Physics
➢ Factors affecting the effective thermal conductivity of pebble beds
pebble size
Pebble size / μm
Effective thermal conductivity / W (m K)^-1
temperature
Th.Conductivity
Temp (°C)
◆ Effective thermal conductivity of mono-sized Al pebble beds
VFL
volume fraction of large pebble / %
Packing factor
Average packing factor (%)
◆ Effective thermal conductivity of binary-sized Al pebble beds
14
Bao-ping GONG, et. al., Journal of engineering thermophysics, 2019,40(5):1151-1159
CNNC
China National Nuclear Corporation

4. Purge gas flow characteristics

核工业西南物理研究院 Southwestern Institute of Physics

➢ Flow characteristics through the pebble bed

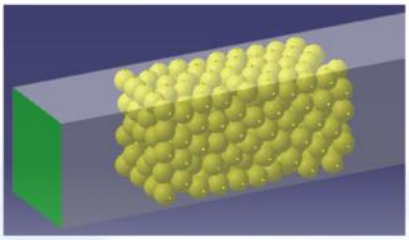

Pebble beds with 5*5*10 mm³

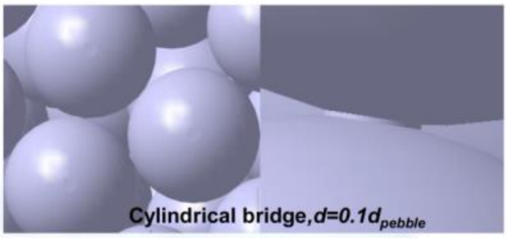

Details of the contact treatment between two pebbles

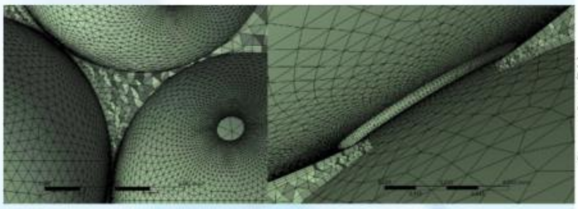

Details of the contact and the mesh between two pebbles

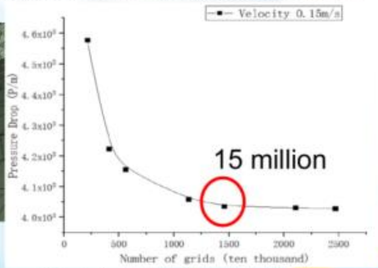

Mesh independence verification

15

CNNC China National Nuclear Corporation

4. Purge gas flow characteristics

核工业西南物理研究院 Southwestern Institute of Physics

➢ Flow characteristics through the pebble bed

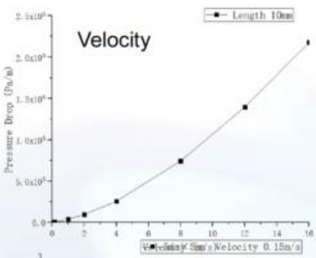

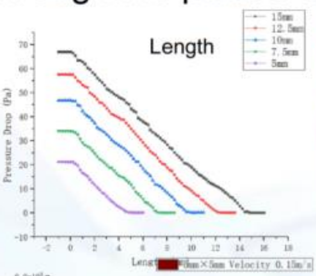

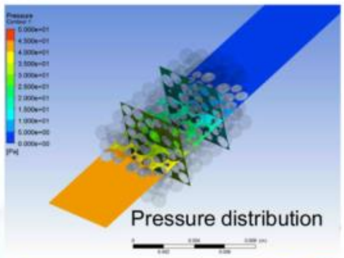

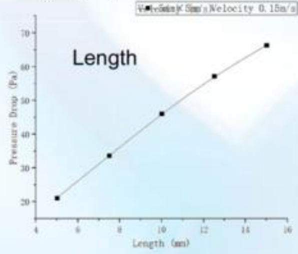

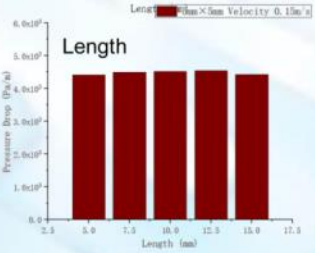

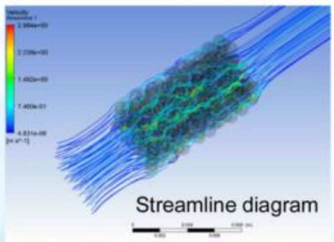

■ More analyses about the influence of the porosity distribution and wall effect on the flow characteristics and heat transfers of pebble beds are ongoing. A facility for measuring pressure drop is under construction.

16

CNNC China National Nuclear Corporation

5. Development of the test apparatus

核工业西南物理研究院 Southwestern Institute of Physics

➢ High temperature compression test equipment for measuring crush load of tritium breeder pebbles at High temperature

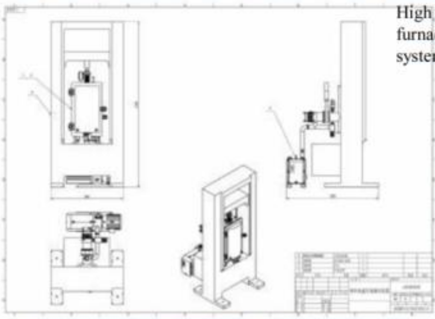

◆ High temperature compression test facility

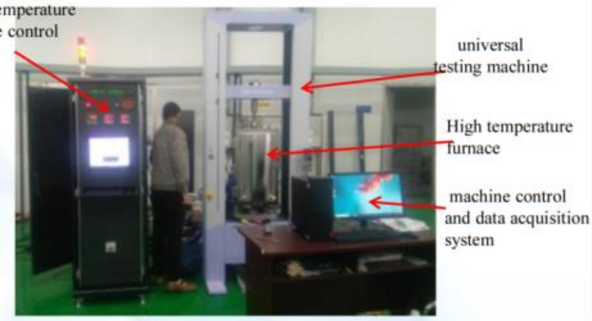

◆ Overall of the high temperature compression facility

◆ Parameters:

Test region: Φ100mm×300mm

Temperature: RM-800℃;

Maximum Load: ≥ 50kN;

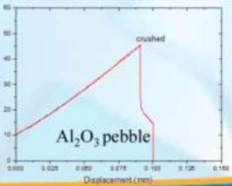

The new facility for measuring the high temperature crush load of tritium breeder pebbles have been construction. Now the facility is in the stage of commissioning.

5. Development of the test apparatus

核工业西南物理研究院 Southwestern Institute of Physics

➢ Development of the facility for measuring thermo-mechanical of pebble beds under the Multi-physics field.

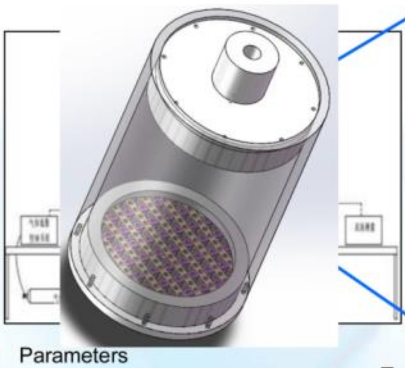

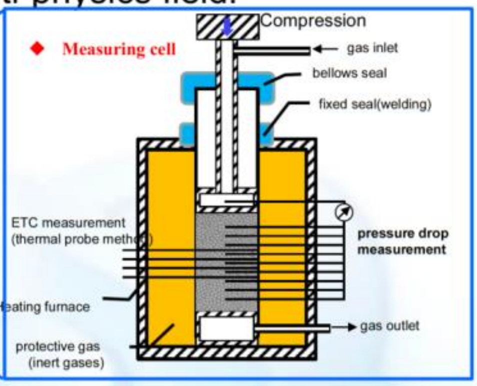

■ Parameters
- Test region: Φ150mm×200mm;
- Temperature: RM-800℃;
- Mechanical Load: ≥ 8MPa;
- Maximum gas pressure at the inlet of the pebble bed: 0.5MPa.
- Pebbles: Li_4SiO_4, Li_2TiO_3, Be, $Be_{12}Ti$

■ The new facility is being designed and manufactured for measuring the thermal-mechanical properties of pebble beds under the Multi-physics field.

■ The **thermal conductivity** and **thermal-mechanical behavior** of Li_4SiO_4 pebble bed, **pressure drop of purge gas** can be measured in the facility at the same time.

■ Movement of crushed pebbles.

6. Summary and plans

核工业西南物理研究院 Southwestern Institute of Physics

➢ Summary

✓ Packing behaviors of pebble beds

- The packing behaviors of mono-sized pebble bed in cylinder and rectangle container were investigated by packing experiment and DEM simulation.

✓ Thermal properties of pebble beds

- The thermal properties of Li_4SiO_4 pebble beds were measured by TPS method. the Factors affecting the effective thermal conductivity of pebble beds were investigated experimentally.

✓ Purge gas flow characteristics in beds

- The flow characteristics of purge gas helium were simulated and analyzed based on CFD and DEM.
- A new facility for measuring pressure drop is under construction. the experiment will be carried out in the next year.

✓ Development of the experiment apparatus

- A new facility for measuring thermo-mechanical of pebble beds under the Multi-physics field is being designed and manufactured.
- By then, more measurement experiments of tritium breeder and neutron multiplier pebble beds will be carried out.

19

CNNC China National Nuclear Corporation

6. Summary and plans

核工业西南物理研究院 Southwestern Institute of Physics

➢ Work plans

✓ Crush load of Li_4SiO_4 pebbles at high temperature (high temperature compression device)

✓ Crushing characteristics of ceramic pebbles inside the pebble bed (based on the UCT & x-ray CT)

✓ **Effective thermal conductivity** of ceramic pebble bed under **thermal cycling** and **cyclic compression** (Hot disk & UCT)

✓ **Thermal mechanical properties** of ceramic pebble bed (High temperature compression device)

✓ **Pressure drop** of the purge gas flowing through the different dimensional pebble bed and the sub-model of HCCB-TBM. (The facility is under construction)

20

CNNC China National Nuclear Corporation

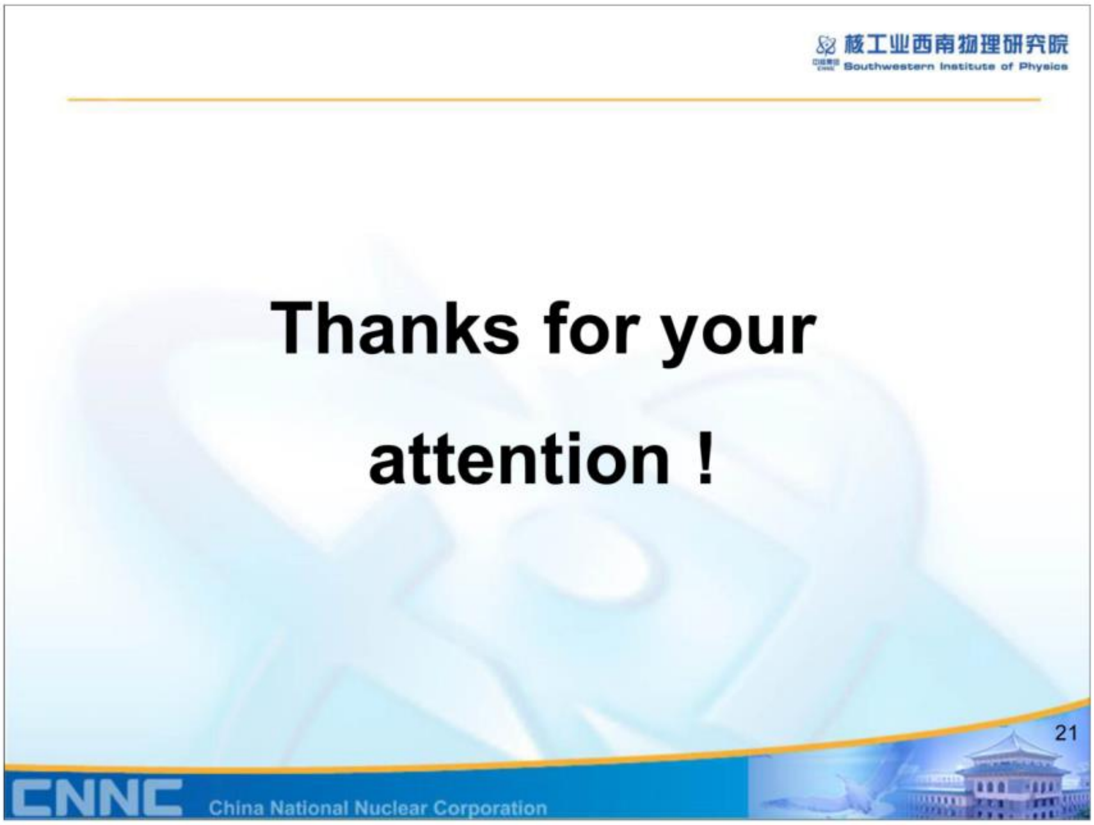
核工业西南物理研究院
Southwestern Institute of Physics
Thanks for your
attention !
21
CNNC
China National Nuclear Corporation

Experimental and numerical study of flow and heat transfer characteristics for pebble beds in fusion blankets

Lei Chen[1], Cong Wang[1, 2], Xiaoman Cheng[1], Songlin Liu[1]

[1] Institute of Plasma Physics, Chinese Academy of Sciences, Hefei, 230031, China.

[2] University of Science and Technology of China, Hefei, 230027, China.

Pebble beds composed of lithium ceramic and beryllium/beryllide particles are under consideration for solid breeding blankets used in fusion reactors to realize tritium breeding and neutron multiplication. The purge gas (helium mixed with about 0.1% content of H_2) flows through the lithium ceramic pebble beds in order to extract tritium produced by the Li(n, α)T reaction. Therefore, studies of the purge gas flow and heat transfer characteristics in pebble beds are necessary to analyze and evaluate the thermo-hydraulic performance of fusion blankets.

In the current work, an experimental platform was constructed to measure the helium pressure drop and the temperature distribution in both unitary and binary pebble beds. In the platform, a pebble bed test section was integrated into a helium loop which can provide a helium flow at 0.1~2.0 MPa and 20~500 ℃ with a maximum flow rate of 80 Nm^3/h. The helium pressure at different inlet helium velocities was measured at the inlet, middle, and outlet of the pebble bed. Besides, five thermocouples were configured along the axial direction of the pebble bed to detect its temperature distribution. The investigated pebble beds include the unitary pebble beds of 0.4~0.9/0.9~1.6 mm Li_2TiO_3, 1.0~2.1 mm Li_4SiO_4, and 1.0~5.0 mm glass particles, as well as the binary glass pebble beds with a large-to-small particle diameter ratio up to 5.

In addition, a porous media model was proposed to study the flow and heat transfer characteristics of pebble beds. In the numerical model, the porosity-dependent permeability was introduced to evaluate the influence of the wall effect. Besides, heat transfer mechanisms including the solid contact conduction, solid-fluid-solid conduction, radiation and convection were considered in the model. The suitability and validity of the numerical model were evaluated by comparing with previous empirical formulas and the current experimental data. The velocity distribution, the helium pressure drop, and the temperature profile of both unitary and binary pebble beds were eventually obtained by the numerical model. According to the current results, both the velocity profile in both unitary and binary pebble beds shows a fluctuation trend in the near-wall region. Comparing with the unitary pebble bed, the binary bed shows a dramatic increase of helium pressure drop but has a well-proportioned temperature profile.

ASIPP

Experimental and Numerical Study of Flow and Heat Transfer Characteristics for Pebble Beds in Fusion Blankets

Lei Chen [1], Cong Wang [1, 2], Xiaoman Cheng [1], Songlin Liu [1]

[1] Institute of Plasma Physics, Chinese Academy of Sciences, Hefei, 230031, China.
[2] University of Science and Technology of China, Hefei, 230026, China.

2019/9/19 CBBI-20, 18-20 September 2019, Karlsruhe, Germany 1

ASIPP

Outline

- Introduction
- Measured pressure drop of purge gas
  - Experimental Setup
  - Experimental results
- Flow and heat transfer simulation by porous media approach
  - Governing Equations for Porous Media
  - Unitary pebble bed
  - Binary pebble bed
- Summary

2019/9/19 2

Introduction

➢ Background

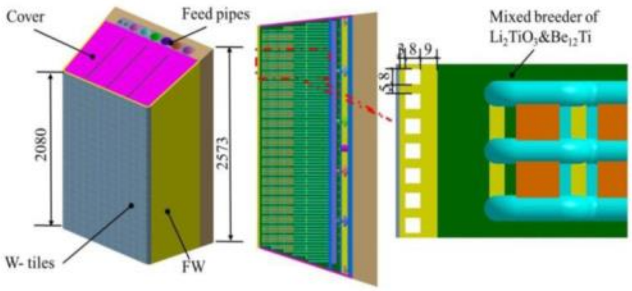

CFETR-WCCB (Water cooled ceramic breeder)

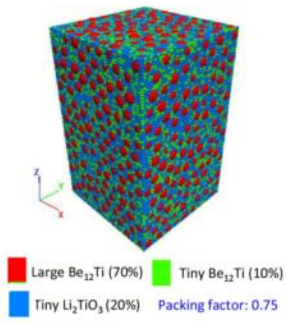

Li_2TiO_3&$Be_{12}Ti$ mixed pebble bed

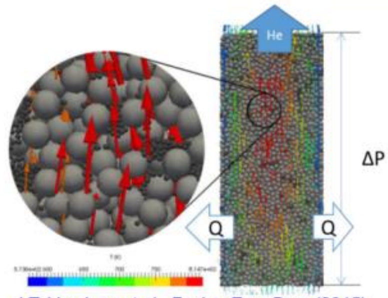

J.T. Van Lew et al., Fusion Eng. Des. (2015).

- **Purge gas for tritium extraction in WCCB**

(1) He+0.1%H_2, Velocity: ~0.1-10 cm/s,

(2) Inlet temperature : 300-500 ℃, Pressure: 0.1-0.3 MPa.

- **Flow and heat transfer characteristics of pebble beds are important in**

(1) Design of Tritium Extraction System (TES);

(2) Thermal hydraulic analysis of WCCB;

(3) Tritium transport analysis in blankets.

ASIPP

Outline

➢ Introduction

➢ **Measured pressure drop of purge gas**

- **Experimental Setup**
- **Experimental results**

➢ Flow and heat transfer simulation by porous media approach

- Governing equations for porous media
- Unitary pebble bed
- Binary pebble bed

➢ Summary

2019/9/19 4

Measured pressure drop of purge gas

➤ Experimental setup

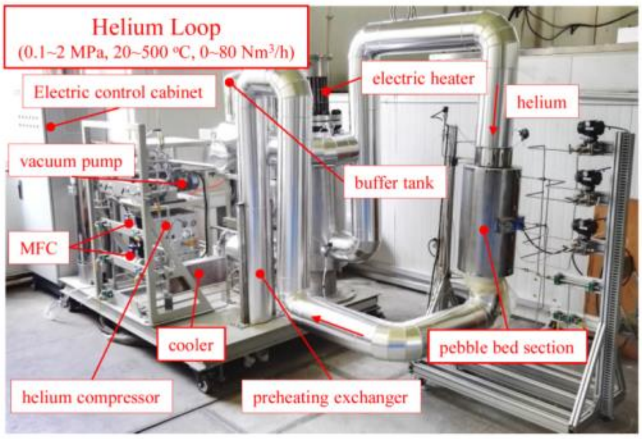

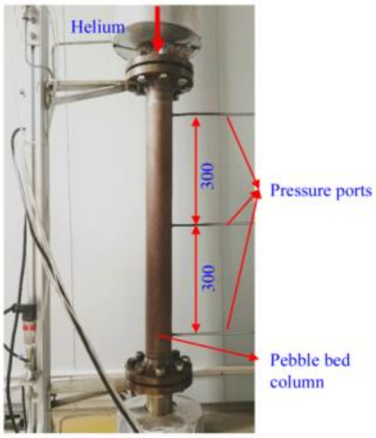

(1) Helium loop

- Helium flow, 0.1~2 MPa, 20-500℃, 80 Nm³/h
- Heat power, 10KW
- Regenerative cycle including two-stage heating and cooling
- Vacuum system for evacuation before experiments

2019/9/19

(2) Pebble bed test section

- 310S steel, Φ73mm×5mm, H700mm
- 3 pressure ports spacing 300mm
- Filters and buffer chambers at inlet/outlet
- Sealed by flanges, supported by filter screen
- Heated by electric stove (up to 500 ℃)

Measured pressure drop of purge gas

➤ Measured pressure drop - Li_2TiO_3 pebble bed

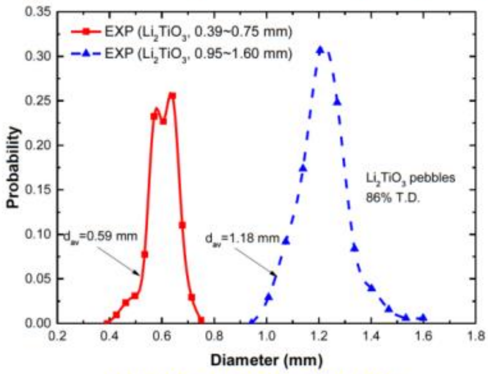

(a) size distribution of Li_2TiO_3 pebbles

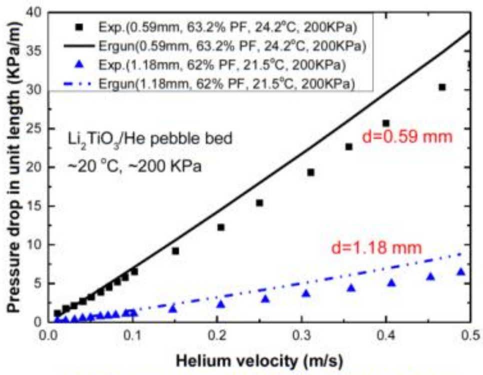

(b) Helium pressure drop in Li_2TiO_3 pebble beds

(c) $\triangle$P in Li_2TiO_3 bed (20℃, 200 KPa)

d (mm)	0.59	1.18
Packing factor	0.63	0.62
U_0 (m/s)	0.05	0.05
ΔP (KPa/m)	3.23	0.60

Ergun: $\frac{\Delta P}{L} = 150\frac{(1-\varepsilon)^2}{\varepsilon^3}\frac{\mu U_0}{d^2} + 1.75\frac{(1-\varepsilon)}{\varepsilon^3}\frac{\rho_f U_0^2}{d}$

Helium pressure drop in Li_2TiO_3 pebble beds

- About 10%~25% lower than Ergun-predicted value.
  possible reasons: size distribution and shape of Li_2TiO_3 pebbles.
- 0.59 mm Li_2TiO_3 bed: 3.23 KPa/m@5 cm/s, ~20 ℃, ~200 KPa
- 1.18 mm Li_2TiO_3 bed: 0.60 KPa/m@5 cm/s, ~20 ℃, ~200 KPa

Measured pressure drop of purge gas

➢ Measured pressure drop - mixed beds (Li_2TiO_3&Glass&Steel)

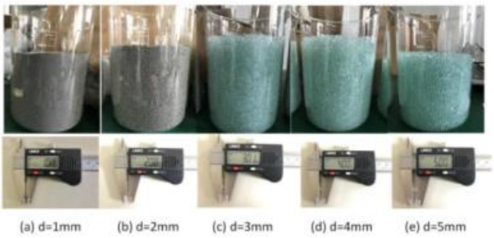

(a) Steel pebbles (1-2mm) and glass beads (3-5mm)

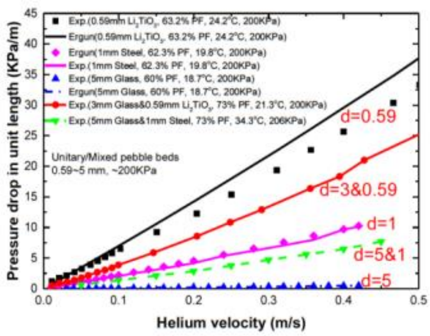

(b) Helium pressure drop in mixed beds

(c) Pressure drop in unitary/mixed beds

(~20℃, ~200 KPa)

d (mm)	Packing factor	U_0 (m/s)	ΔP (KPa/m)
0.59	0.63	0.05	3.23
1.18	0.62	0.05	0.60
3	0.62	0.05	0.12
5	0.60	0.05	0.037
3&0.59	0.73	0.05	1.77
5&1	0.73	0.05	0.61

Helium pressure drop in mixed beds

- ΔP of the mixed bed is between ΔP of the larger pebble bed and that of smaller pebble bed.
- ΔP decreases with increasing average particle size.
- Mixed bed of 3mm Glass&0.59mm Li_2TiO_3: 1.77KPa/m@5cm/s, ~20℃, ~200 KPa

2019/9/19 7

Measured pressure drop of purge gas

➢ Measured pressure drop - particle size, temperature and pressure

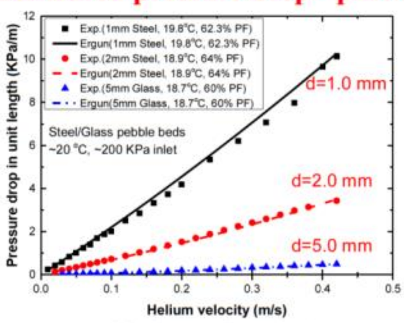

(a) Influence of particle size

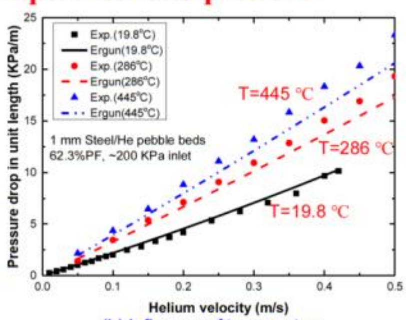

(b) Influence of temperature

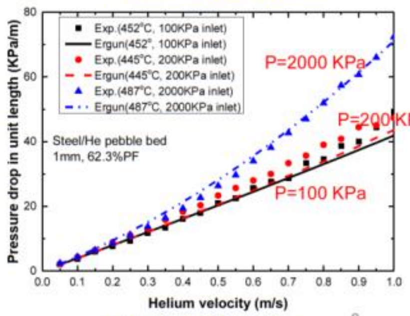

(c) Influence of pressure

Factors impacting helium pressure drop

- Particle size: d↑, ΔP↓
- Temperature: T↑, μ↑, ΔP↑
- Pressure: P↑, ρ_f↑, ΔP↑

Ergun: $\frac{\Delta P}{L} = 150\frac{(1-\varepsilon)^2}{\varepsilon^3}\frac{\mu U_0}{d^2} + 1.75\frac{(1-\varepsilon)}{\varepsilon^3}\frac{\rho_f U_0^2}{d}$

2019/9/19 8

ASIPP

Outline

- Introduction
- Measured pressure drop of flowing helium
  - Experimental Setup
  - Experimental results
- **Flow and heat transfer simulation by porous media approach**
  - **Governing equations for porous media**
  - **Unitary pebble bed**
  - **Binary pebble bed**
- Summary

2019/9/19 9

Flow and heat transfer simulation by porous media approach

Governing equations for porous media

- **Flow equation (Brinkman Model, No gravity, No Stokes flow)**

$$\frac{\partial}{\partial t}(\varepsilon\rho_f) + \nabla\cdot(\rho_f\boldsymbol{u}) = 0$$

$$\frac{\rho_f}{\varepsilon}\frac{\partial\boldsymbol{u}}{\partial t} + \frac{\rho_f}{\varepsilon}(\boldsymbol{u}\cdot\nabla)\left(\frac{\boldsymbol{u}}{\varepsilon}\right) = -\nabla P + \frac{\mu_{\mathrm{eff}}}{\varepsilon}\nabla^2\boldsymbol{u} + \boldsymbol{F_D}$$

$\boldsymbol{F_D} = -\frac{\mu}{\kappa}\boldsymbol{u} - \beta|\boldsymbol{u}|\boldsymbol{u}$ ($\varepsilon\boldsymbol{F_D}$ is drag force in unit volume)

$\kappa = \frac{d^2\varepsilon^3}{150(1-\varepsilon)^2}$ (Permeability) , $\beta = \frac{1.75\rho_f(1-\varepsilon)}{d\varepsilon^3}$ (Forchheimer Coeff.)

- **Heat transfer equation (convection heat transfer included)**

$$\frac{\partial}{\partial t}(\rho C_p)_{\mathrm{eff}}T + (\rho C_p)_{\mathrm{f}}\boldsymbol{u}\cdot\nabla T = \nabla\cdot(k_{\mathrm{eff}}\nabla T) + Q$$

$k_{\mathrm{eff}} = k_{\mathrm{eff}}^0 + k_D$ *C.T. Hsu, P. Cheng, Int. J. Heat Mass Transfer (1990)*

$\boldsymbol{k_D} = \begin{cases} \boldsymbol{D_1}k_{\mathrm{f}}\mathrm{Pe}^2, & \mathrm{Re} < 10 \\ \boldsymbol{D_2}k_{\mathrm{f}}\mathrm{Pe}, & \mathrm{Re} > 10 \end{cases}$ (Effective conductivity tensor due to thermal dispersion)

$\mathrm{Pe} = \mathrm{RePr} = \frac{|\boldsymbol{u}|d}{\alpha_{\mathrm{f}}}$ (Péclet number), $\mathrm{Re} = \frac{\rho_{\mathrm{f}}|\boldsymbol{u}|d}{\mu_{\mathrm{f}}}$ (Reynolds number)

2019/9/19 10

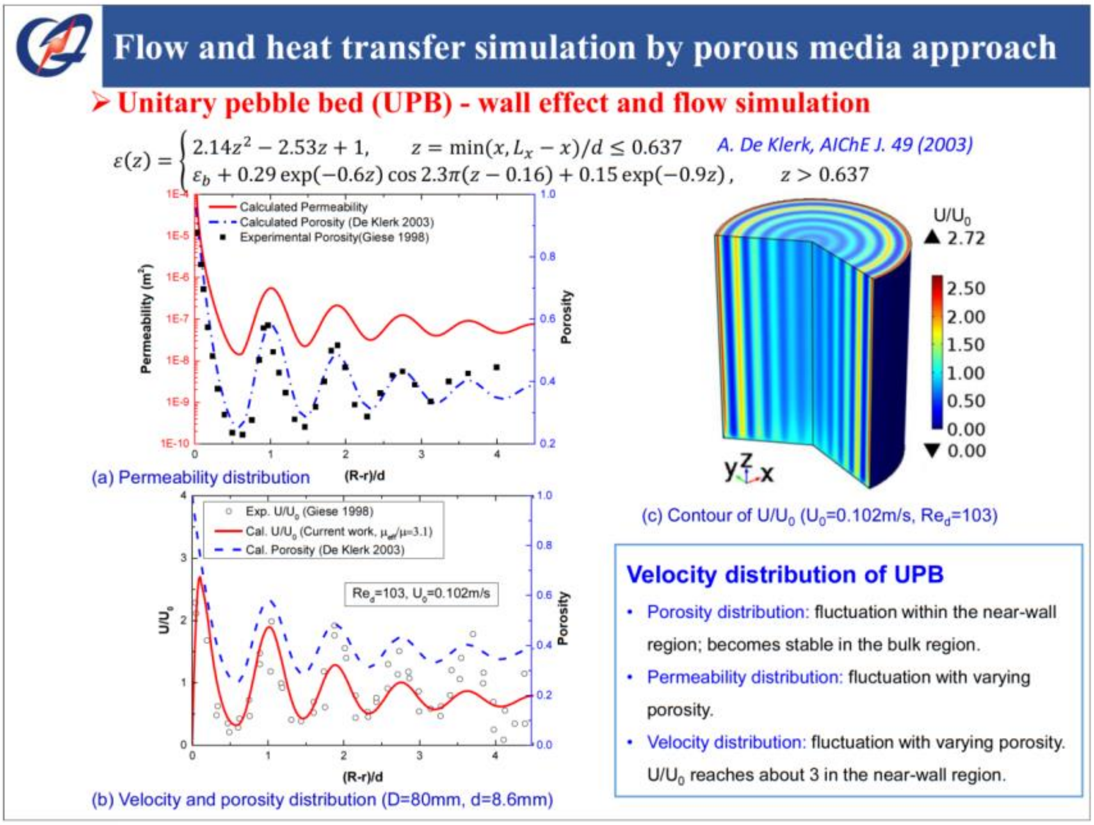
Flow and heat transfer simulation by porous media approach
➤Unitary pebble bed (UPB) - wall effect and flow simulation
$\varepsilon(z) = \begin{cases} 2.14z^2 - 2.53z + 1, & z = \min(x, L_x - x)/d \le 0.637 \\ \varepsilon_b + 0.29\exp(-0.6z)\cos 2.3\pi(z - 0.16) + 0.15\exp(-0.9z), & z > 0.637 \end{cases}$
A. De Klerk, AIChE J. 49 (2003)
Calculated Permeability
Calculated Porosity (De Klerk 2003)
Experimental Porosity(Giese 1998)
Permeability (m²)
Porosity
(R-r)/d
(a) Permeability distribution
Exp. U/U0 (Giese 1998)
Cal. U/U0 (Current work, μeff/μ=3.1)
Cal. Porosity (De Klerk 2003)
Red=103, U0=0.102m/s
U/U0
(b) Velocity and porosity distribution (D=80mm, d=8.6mm)
U/U0
▲ 2.72
2.50
2.00
1.50
1.00
0.50
0.00
▼ 0.00
(c) Contour of U/U0 (U0=0.102m/s, Red=103)
Velocity distribution of UPB
• Porosity distribution: fluctuation within the near-wall region; becomes stable in the bulk region.
• Permeability distribution: fluctuation with varying porosity.
• Velocity distribution: fluctuation with varying porosity. U/U0 reaches about 3 in the near-wall region.

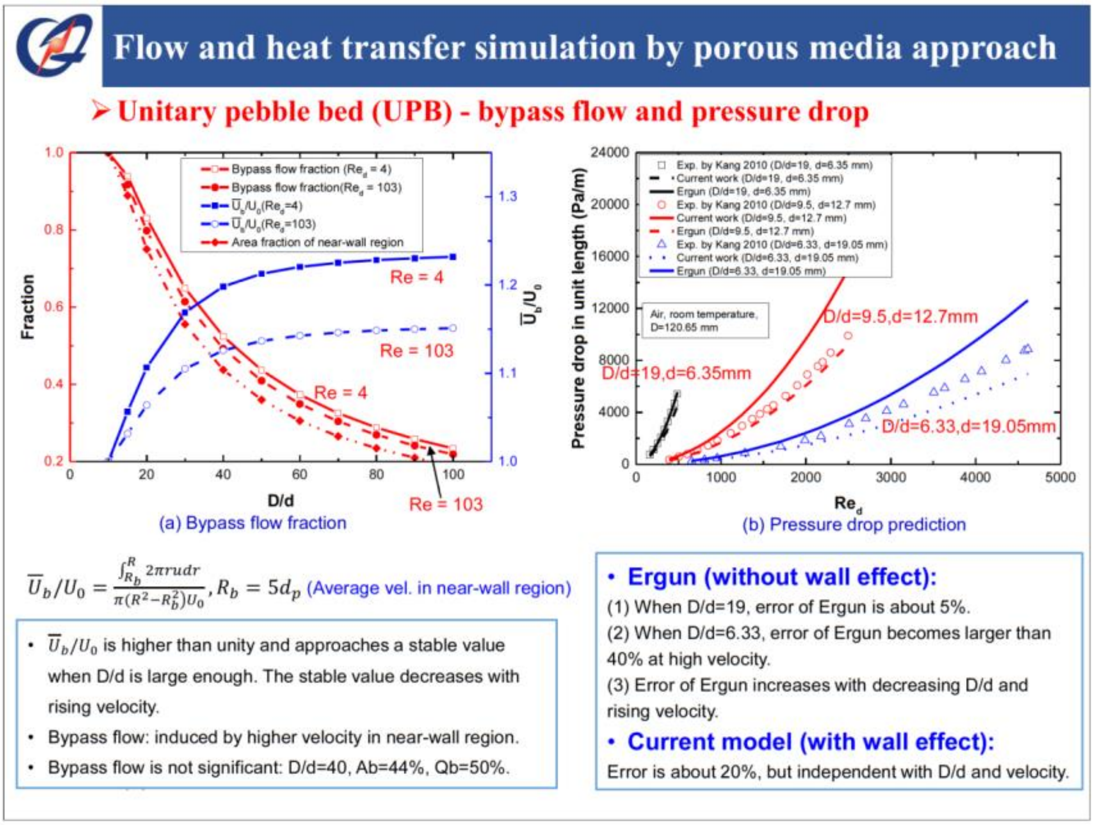
Flow and heat transfer simulation by porous media approach
➤Unitary pebble bed (UPB) - bypass flow and pressure drop
Bypass flow fraction (Red = 4)
Bypass flow fraction(Red = 103)
Ub/U0(Red=4)
Ub/U0(Red=103)
Area fraction of near-wall region
Re = 4
Re = 103
Re = 4
Re = 103
Fraction
D/d
(a) Bypass flow fraction
Exp. by Kang 2010 (D/d=19, d=6.35 mm)
Current work (D/d=19, d=6.35 mm)
Ergun (D/d=19, d=6.35 mm)
Exp. by Kang 2010 (D/d=9.5, d=12.7 mm)
Current work (D/d=9.5, d=12.7 mm)
Ergun (D/d=9.5, d=12.7 mm)
Exp. by Kang 2010 (D/d=6.33, d=19.05 mm)
Current work (D/d=6.33, d=19.05 mm)
Ergun (D/d=6.33, d=19.05 mm)
Air, room temperature, D=120.65 mm
D/d=9.5,d=12.7mm
D/d=19,d=6.35mm
D/d=6.33,d=19.05mm
Pressure drop in unit length (Pa/m)
Red
(b) Pressure drop prediction
$\overline{U}_b/U_0 = \frac{\int_{R_b}^{R} 2\pi r u dr}{\pi(R^2 - R_b^2)U_0}, R_b = 5d_p$ (Average vel. in near-wall region)
• $\overline{U}_b/U_0$ is higher than unity and approaches a stable value when D/d is large enough. The stable value decreases with rising velocity.
• Bypass flow: induced by higher velocity in near-wall region.
• Bypass flow is not significant: D/d=40, Ab=44%, Qb=50%.
• Ergun (without wall effect):
(1) When D/d=19, error of Ergun is about 5%.
(2) When D/d=6.33, error of Ergun becomes larger than 40% at high velocity.
(3) Error of Ergun increases with decreasing D/d and rising velocity.
• Current model (with wall effect):
Error is about 20%, but independent with D/d and velocity.

Flow and heat transfer simulation by porous media approach

➢ Unitary pebble bed – heat transfer model validation

- Experimental data of glass packed bed by Wen et al. were used to validate the heat transfer model.
- Stagnant effective thermal conductivity is calculated by SZB model.
- Thermal dispersion conductivity tensor is determined by fitting with exp. data.
- The heat transfer model predicted the axial and radial temperature profile well.

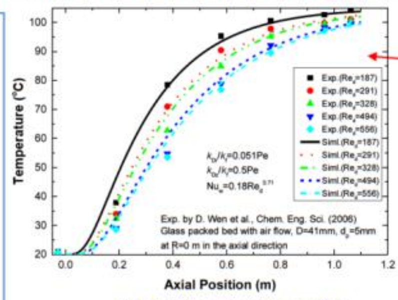

(a) Axial temperature profile

$$\frac{k_{\text{eff}}^0}{k_g} = 1 - \sqrt{1-\varepsilon} + \frac{2\sqrt{1-\varepsilon}}{1-\lambda B} \cdot \left[\frac{(1-\lambda)B}{(1-\lambda B)^2}\ln\frac{1}{\lambda B} - \frac{B+1}{2} - \frac{B-1}{1-\lambda B}\right] \quad \text{(SZB model)}$$

$$\lambda = \frac{k_g}{k_s}, B = 1.25\left(\frac{1-\varepsilon}{\varepsilon}\right)^{\frac{10}{9}}$$

$$\frac{k_{Dz}}{k_f} = 0.5\text{Pe}, \frac{k_{Dr}}{k_f} = 0.051\text{Pe}$$

$$\text{Nu}_w = \frac{h_w d}{k_f} = 0.18\text{Re}^{0.71}$$

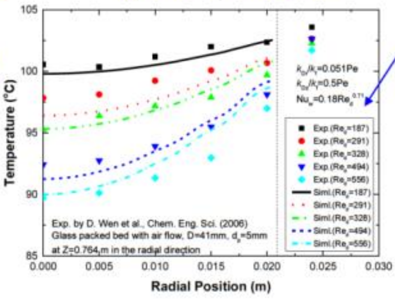

(b) Radial temperature profile

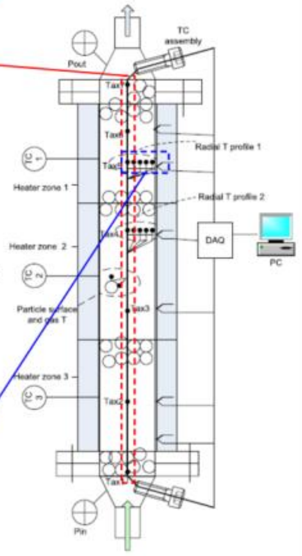

(c) Experimental setup by D. Wen

D. Wen et al., Chem. Eng. Sci. (2006)

2019/9/19 13

Flow and heat transfer simulation by porous media approach

➢ Binary pebble bed – porosity distribution and wall effect

- **DEM simulation of Li_2TiO_3&$Be_{12}Ti$ mixed bed (2mm/0.4mm)**

$$\varepsilon = \varepsilon_D \varepsilon_d, \quad X_D = \min(x, L_x - x)/D_p, \ X_d = \min(x, L_x - x)/d_p$$

$$\varepsilon_D = 0.4572 + 0.4956\exp(-8.08X_D) + 0.1201\exp(-0.6298X_D)\cos(2.4256\pi(X_D - 0.1723))$$

$$\varepsilon_d = 0.5199 + 0.0959\exp(-0.7491X_d) + 0.2575\exp(-0.9413X_d)\cos(2.3036\pi(X_d - 0.0147))$$

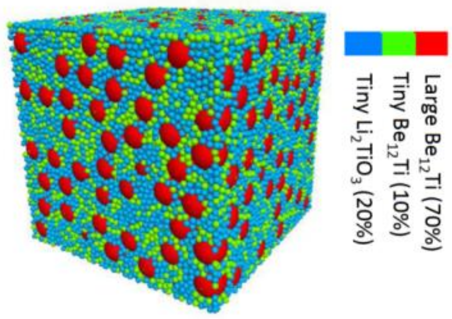

(a) $Be_{12}Ti$&Li_2TiO_3 mixed bed obtained by DEM simulation (2mm/0.4mm, P_f = 0.75, V_L=0.7)

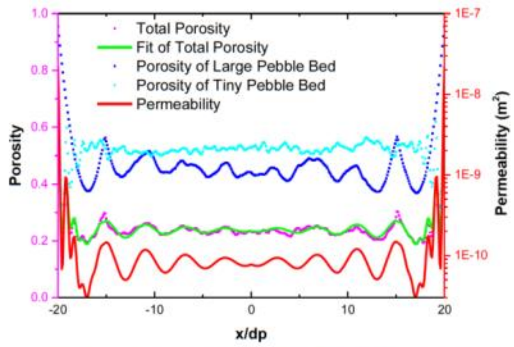

(b) Permeability distribution in $Be_{12}Ti$&Li_2TiO_3 mixed bed (2mm/0.4mm, P_f = 0.75, V_L=0.7)

2019/9/19 14

Flow and heat transfer simulation by porous media approach

➢ Binary pebble bed - flow simulation and pressure drop

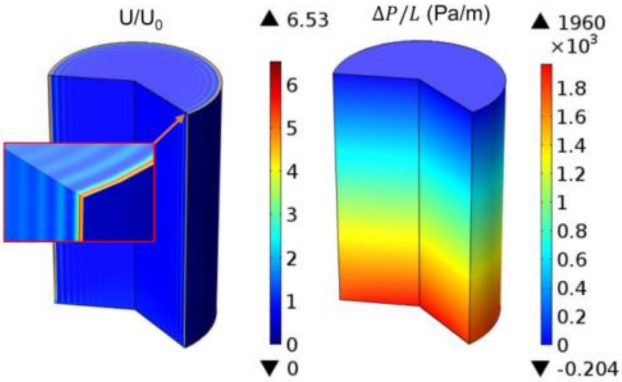

(a) Velocity field and pressure contour in mixed beds
(3mm/0.59mm, P_f = 0.75, V_L=0.7, U_0=5cm/s, He@20℃, 200 KPa)

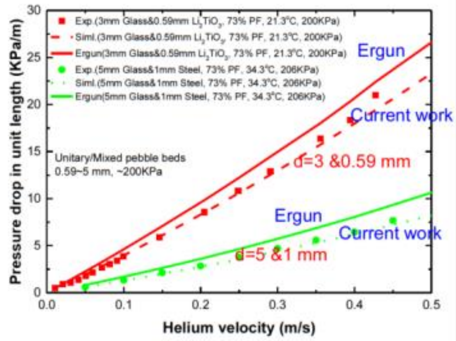

(b) Pressure drop prediction for mixed beds

Equivalent particle diameter: $d_m = \frac{1}{\frac{V_L}{d_L}+\frac{V_S}{d_S}}$

- **Velocity distribution**

(1) Fluctuation in a narrow near-wall region (3d-5d away from the wall); (2)U/U_0 reaches a peak value of 5 at about 0.5d.

- **Pressure drop:** When using the equivalent particle diameter,

(1) Error of Ergun is about 20%; (2) Results of current model with wall effect are closer to experimental data.

Flow and heat transfer simulation by porous media approach

➢ Binary pebble bed – preliminary simulation of a typical WCCB breeder zone

- **Heat transfer modelling of a Li_2TiO_3&$Be_{12}Ti$ mixed bed (2mm/0.4mm) in WCCB(Version2015)**

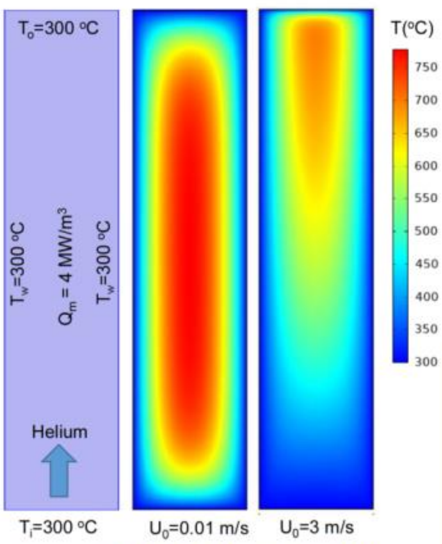

(a) Geometry and temperature field
(mixed bed, 50*220mm)

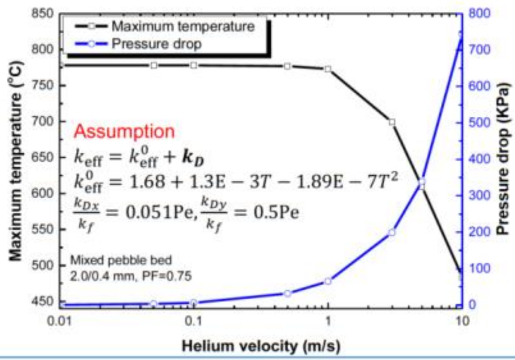

Temperature profiles at different inlet velocities

(1) Convection heat transfer is negligible at low velocity(<0.1 m/s);

(2) At high velocity(>1 m/s), the maximum temperature decreases with rising velocity;

(3) Convection might be non-negligible under the in-box LOCA accident conditions where the high-pressure water vaper (WCCB) or helium (HCCB) might flow fast into the pebble bed through a broken hole.

2019/9/19 16

Summary

- **Measurement of helium pressure drop in pebble beds**
  - 0.59mm Li_2TiO_3 pebble bed: 3.23 KPa/m@5 cm/s, ~20 ℃, ~200 KPa
  - 1.18mm Li_2TiO_3 pebble bed: 0.60 KPa/m@5 cm/s, ~20 ℃, ~200 KPa
  - 3mm & 0.59mm mixed bed : 1.77 KPa/m@5 cm/s, ~20 ℃, ~200 KPa

- **Flow and heat transfer simulation and model validation**
  - Model for unitary pebbe beds is validated by comparision to existing exp. data
  - Influences of wall effect on velocity and temperature distribution are evaluated
  - Convection heat transfer including thermal dispersion is considered
  - Implementation for binary pebble beds: Influences of wall effect and convection heat transfer are estimated

- **Future work**
  - Measurement of thermal dispersion coefficients and the near-wall heat transfer coefficient at large velocities for binary pebble beds

2019/9/19 17

Other related work

- **Simulation of tritium transport for CFETR-WCCB(version 2015)**

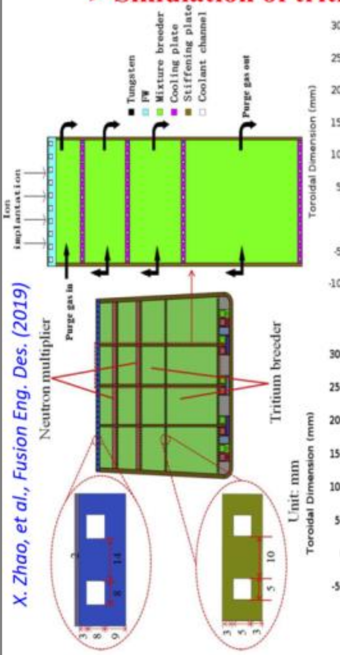

(a) Structure of blanket module 1#

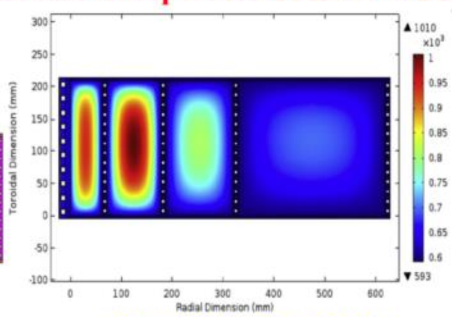

(b) Temperature distribution (K)

Coupled Model

- Flow field of purge gas
- Heat transfer with nuclear heat
- Tritium transport

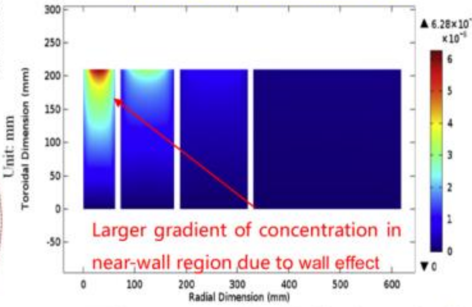

(c) Tritium concentration distribution (mol/m³)

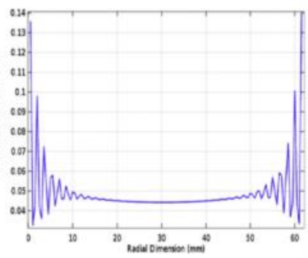

(d) Velocity profile in BZ1

18

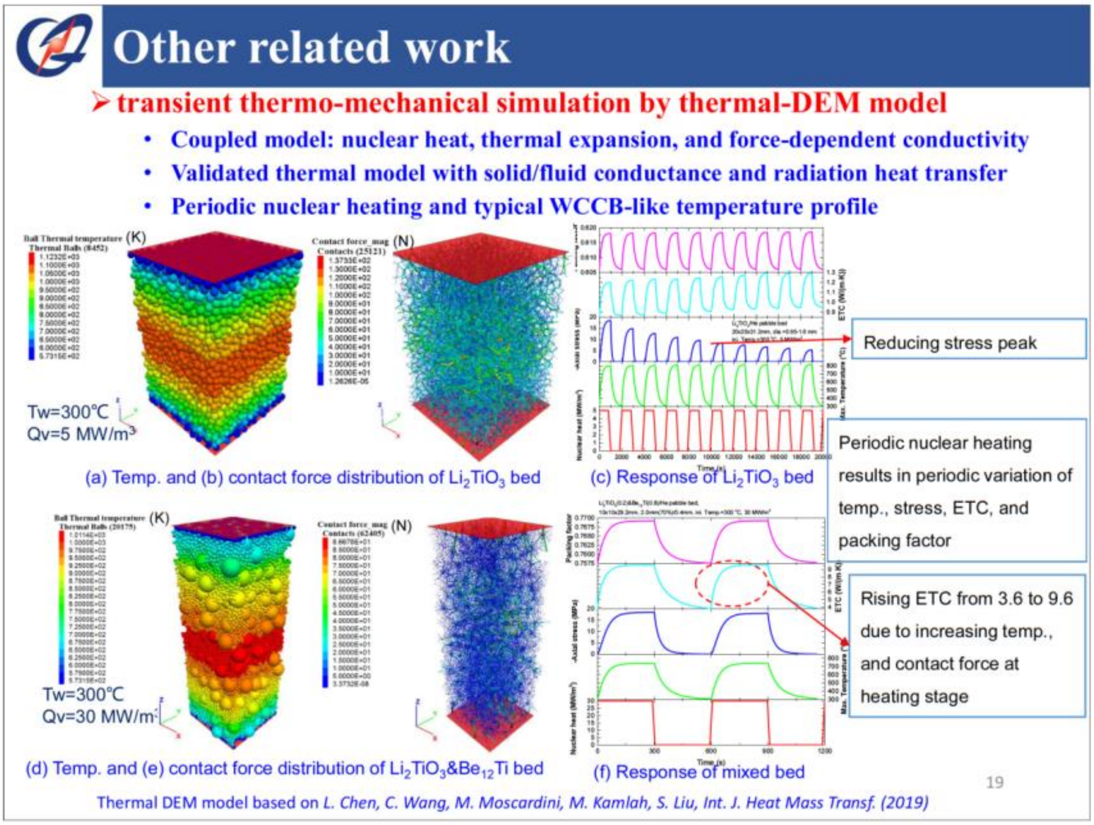
Other related work
➤transient thermo-mechanical simulation by thermal-DEM model
• Coupled model: nuclear heat, thermal expansion, and force-dependent conductivity
• Validated thermal model with solid/fluid conductance and radiation heat transfer
• Periodic nuclear heating and typical WCCB-like temperature profile
Tw=300°C
Qv=5 MW/m³
(a) Temp. and (b) contact force distribution of Li2TiO3 bed
(c) Response of Li2TiO3 bed
Reducing stress peak
Periodic nuclear heating results in periodic variation of temp., stress, ETC, and packing factor
Rising ETC from 3.6 to 9.6 due to increasing temp., and contact force at heating stage
Tw=300°C
Qv=30 MW/m³
(d) Temp. and (e) contact force distribution of Li2TiO3&Be12Ti bed
(f) Response of mixed bed
19
Thermal DEM model based on L. Chen, C. Wang, M. Moscardini, M. Kamlah, S. Liu, Int. J. Heat Mass Transf. (2019)

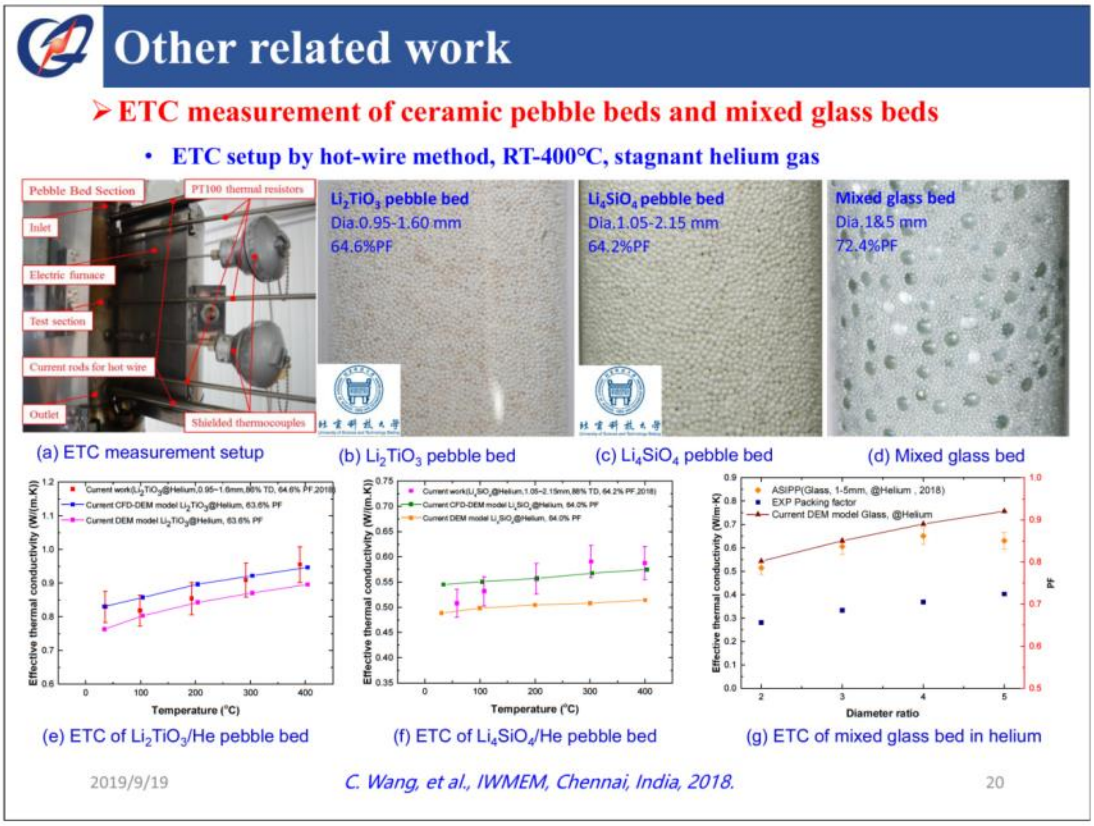
Other related work
➤ETC measurement of ceramic pebble beds and mixed glass beds
• ETC setup by hot-wire method, RT-400°C, stagnant helium gas
Pebble Bed Section
PT100 thermal resistors
Inlet
Electric furnace
Test section
Current rods for hot wire
Outlet
Shielded thermocouples
Li2TiO3 pebble bed
Dia.0.95-1.60 mm
64.6%PF
Li4SiO4 pebble bed
Dia.1.05-2.15 mm
64.2%PF
Mixed glass bed
Dia.1&5 mm
72.4%PF
(a) ETC measurement setup
(b) Li2TiO3 pebble bed
(c) Li4SiO4 pebble bed
(d) Mixed glass bed
Effective thermal conductivity (W/(m.K))
Temperature (°C)
Diameter ratio
(e) ETC of Li2TiO3/He pebble bed
(f) ETC of Li4SiO4/He pebble bed
(g) ETC of mixed glass bed in helium
2019/9/19
C. Wang, et al., IWMEM, Chennai, India, 2018.
20


ASIPP
Thank you for your attention !
Lei Chen, chlei@ipp.ac.cn
2019/9/19
21

Design of the water cooled ceramic breeder blanket for CFETR with the latest core parameters and mission

Songlin Liu, Xiaoman Cheng, Lei Chen, Xuebin Ma, Kecheng Jiang, Peng Lu

Institute of Plasma Physics, Chinese Academy of Sciences, Hefei, Anhui, 230031, China

The Chinese Fusion Engineering Testing Reactor (CFETR) is aiming to demonstrate fusion energy production up to 200 MW initially and to eventually reach DEMO relevant power level, to manifest high duty factor of 0.3~0.5, and to pursuit tritium self-sufficiency with tritium breeding ratio (TBR) > 1. The size of CFETR core parameters has been updated from R=5.7 m, a=1.6 m to R=7.2 m, a=2.2 m. More specific and challenging requirements are accordingly proposed to the reactor design.

The water-cooled ceramic breeder (WCCB) blanket is one candidate for the Chinese Fusion Engineering Testing Reactor (CFETR). The WCCB blanket concept has been developing for over five years at Institute of Plasma Physics Chinese Academy of Sciences (ASIPP). It employs a mixed pebble bed of Li2TiO3 and Be12Ti as tritium breeder and neutron multiplier, a reduced activation ferritic/martensitic steel as structural material, and tungsten as armor material for the first wall (FW). Pressurized water at 15.5MPa is chosen as coolant with 285oC inlet/325oC outlet temperature.

This contribution reviews the WCCB blanket design evolution and features changes, and presents the latest WCCB blanket concept design and integration with the primary heat transfer system with the latest core parameters (major radius R = 7.2 m; minor radius a = 2.2 m) and mission. It is expected to cover the CFETR operation modes of 200 MW, 500 MW, 1 GW, and 1.5 GW fusion power and achieve tritium self-sufficiency. This concept adopts a dual-wall cooling tube array instead of the original cooling plates. To adjust and control the temperature of the FW and the breeder zone at different fusion powers, a thermal-hydraulic scheme is proposed in which the FW uses one independent coolant circulating system and the breeder zone employs two such systems. When CFETR operates at higher fusion power (≥500MW), the three coolant systems are operated together. This can enhance the heat transfer and ensure that the material temperatures remain below the allowable limits. When the CFETR operates at a fusion power of 200MW, one coolant system is shut down. This can elevate the temperature of the breeder, which benefits the tritium release process. The feasibility of the new blanket design is evaluated considering neutronics, thermal-hydraulics, and thermal-mechanics aspects. The development plan of the WCCB blanket technologies will also be reported.

Design of the water cooled ceramic breeder blanket for CFETR with the latest core parameters and mission

Songlin Liu, Xiaoman Cheng, Lei Chen, Xuebin Ma, Kecheng Jiang, Peng Lu， et al.

Institute of Plasma Physics, Chinese Academy of Sciences

The 20th International Workshop on Ceramic Breeder Blanket Interactions ,Karlsruhe, Germany, Sept.18~21,2019

Outline

- Background
- Design description
- Performance analyses
- R&D activities

Blanket configuration and its objectives

CFETR will be operated in multiple operation modes to achieve fusion burning plasma scientific mission with the tritium self-sufficiency, fusion power from 500MW to 1.5GW, and duty time fraction >=0.5

□ Configuration

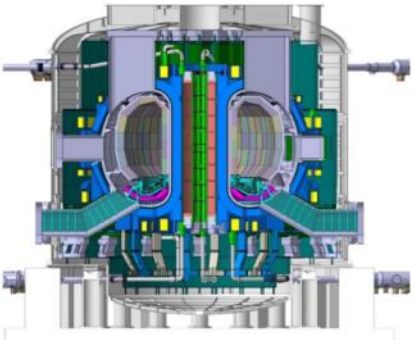

R=7.2m，a=2.2m，k=2，Bt=6.5T

- CFETR has 16 sectors of each 22.5° for blanket system.
- Each sector along toroidal direction is divided into 2 inboard and 3 outboard blanket segments.

□ Design objectives

1. **Tritium production** ➔ Fuel for fusion（self-sufficiency, TBR>=1.1）
2. **Shielding** ➔ Enough shielding capability to protect super-conducting coils.
3. **Remove nuclear heat** ➔ Generating electricity （Thermal cycle efficiency high)
4. **Operation** ➔ To meet different operation power from 500MW to 1.5GW.
5. **Maintaenace** ➔ modules integrated as one single segment, replacement from the vertical port.

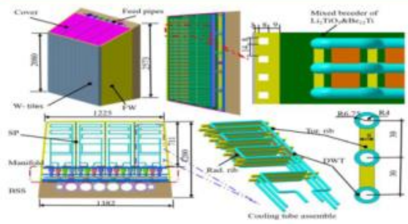

-30th Symposium on fusion technology, *Giardini Naxos, Sicily, Italy,* September 16-21, 2018

Changes in material selection

2018 version

- Pressurized wate : 15.5MPa, 285 C/ 325 C Inlet/outlet
- Li2TiO3 和 Be12Ti mixed breeder
- RAFM steel as structural material.
- Tungsten as armor material

2019 version

- Pressurized wate : 15.5MPa, 285 C/ 325 C Inlet/outlet
- Li2TiO3 和 Be12Ti mixed breeder
- RAFM-ODS steel as structural material.
- Tungsten as armor material

Item	Temp. limit，℃
Tungsten	≤1300
RAFM steel	≤550
RAFM -ODS钢	≤650
Li_2TiO_3 & $Be_{12}Ti$ mixed pebble bed	≤900

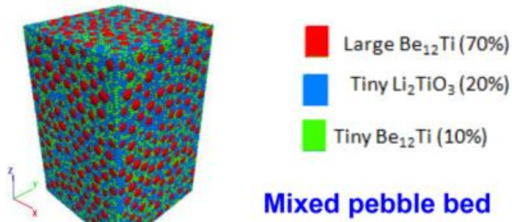

Mixed pebble bed

Temp (℃)	density（kg/m³）		thermal conductivity（W/(m·K)）		thermal expansion（K⁻¹）		Young modulus（Pa）		poisson ratio		yield strength（MPa）	
	RAFM	ODS	RAFM	ODS	RAFM	ODS	RAFM	ODS	RAFM	ODS	RAFM	ODS
200	7819	7540	32.9	26.0	1.10E-5	1.19E-5	2.07E+11	2.11E+11	0.3	0.24	-	-
300	7786	7510	33.4	25.3	1.12E-5	1.26E-5	2.03E+11	2.09E+11	0.3	0.23	-	-
400	7752	7480	33.0	24.1	1.17E-5	1.32E-5	1.97E+11	2.05E+11	0.3	0.25	-	-
500	7715	7470	32.7	23.4	1.20E-5	1.36E-5	1.89E+11	1.96E+11	0.3	0.27	-	-
600	7676	7440	32.3	23.6	1.23E-5	1.41E-5	1.78E+11	1.78E+11	0.3	0.29	281	387

Change of WCCB design

- **Heat load distribution in one typical BLK under different fusion power**

200MW		500MW		1GW		1.5GW	
FW	BZ	FW	BZ	FW	BZ	FW	BZ
1.46 MW	0.56 MW	1.65 MW	1.40 MW	1.96 MW	2.80 MW	2.26 MW	4.19 MW

Note: The Wall Load Specification for CFETR is not available, heat flux of 0.5MW /m2 from plasma chamber is assumed.

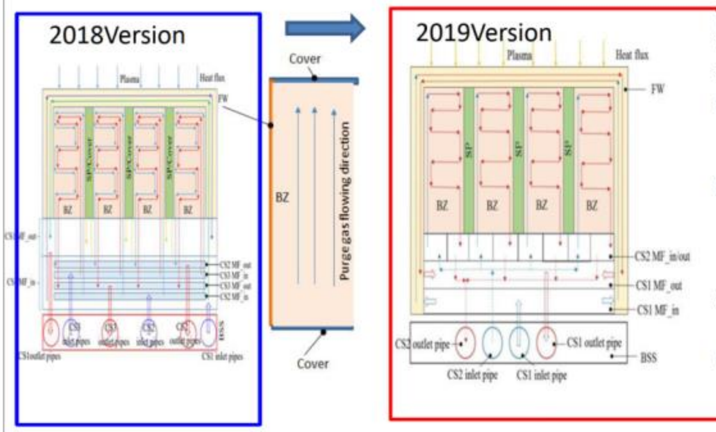

The blanket module has two sets of independent coolant circulating systems.

- The cooling system 1 (CS1) removes the heat in the structure of the FW,
- The colling system 2 (CS2) removes the heat in the structure of the breeder zone (BZ) , Covers, and stienffening plates (SPs),
- There is no coolant channels in Covers and SPs
- Purge gas flows from lower cover into BZ, and collects in upper covers .

Structure scheme

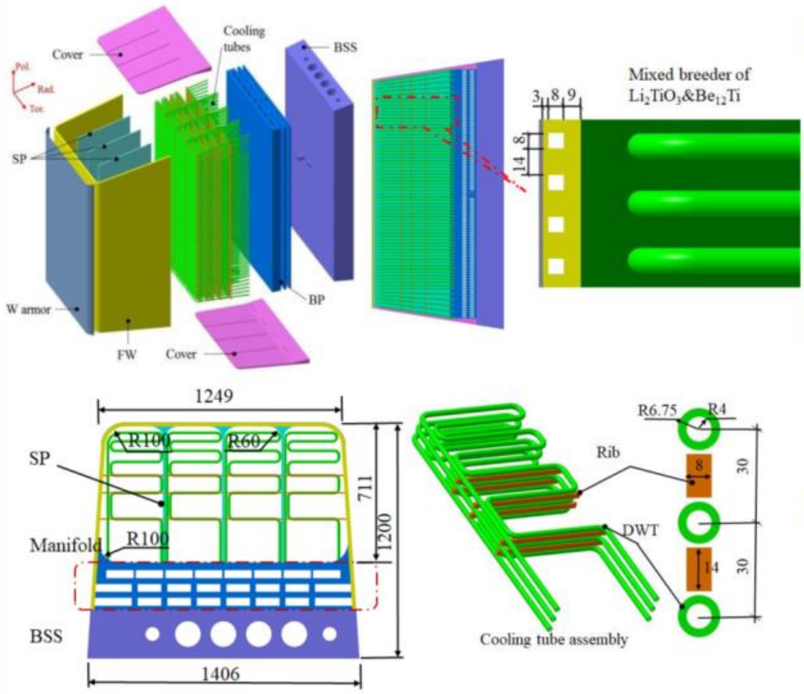

- **The FW is a U-shaped plate bended in the radial-toroidal direction.**
- **cooling tubes are embedded in the mixed breeder pebble bed zone of each sub-module**
- **The stiffening plates (SPs) are incorporated to enhance the steel box mechanical resistance**
- **the ribs are bonded with SW/ SP to enhance the blanket box structure**

6

Analysis model and material properties

Slice analysis model

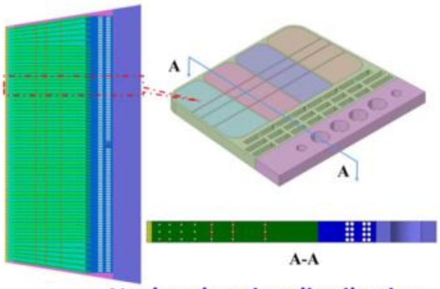

Nuclear heating distribution

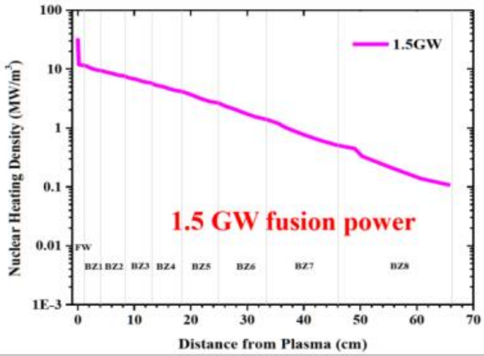

Thermophysical properties for material

Item	Thermal physical parameters
Tungsten	$\lambda_{tungsten}$=2017.98-0.136(T+273)+5.649×10^{-5}(T+273)2-7.835°C×$10^{-9}$$(T+273)^2$
RAFM steel	λ_{F82H}=33.0 (400°C)
ODS steel	λ_{ODS}=24.1 (400°C)
Li_2TiO_3&$Be_{12}Ti$ Mixed Pebble bed	$\lambda_{Mixed\ breeder}$=1.68215+0.0013(T+273)-1.894×10^{-7}(T+273)
Water	λ_{water}=1.587-0.0018（T+273）
	ρ_{water}=1902.14-2.054（T+273）
	C_{p_water}=-7733+23（T+273）
	μ_{water}=0.000314706-3.9505510-7（T+273）

Boundary conditions

FW	Velocity inlet	2.571 m/s Inlet temp. 558 K
	Pressure outlet	15.5 MPa
BZ	Velocity inlet	1.503 m/s Inlet temp. 558 K
	Pressure outlet	15.5 MPa
Front wall armor		0.5 MW/m²
MF inner wall		558 K
BSS inner wall		558 K
BP wall		558 K

Thermal analysis results

□ RAFM steel is used

□ RAFM-ODS steel is used

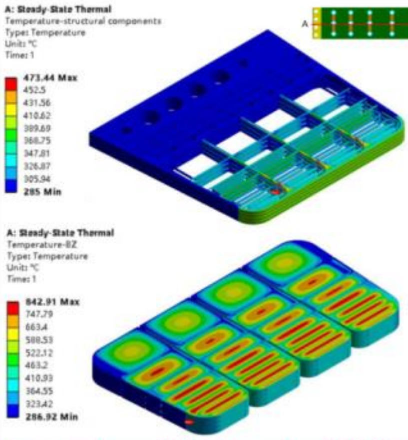

Temperature distribution on stratural material

Temperature distribution on mixed breeder

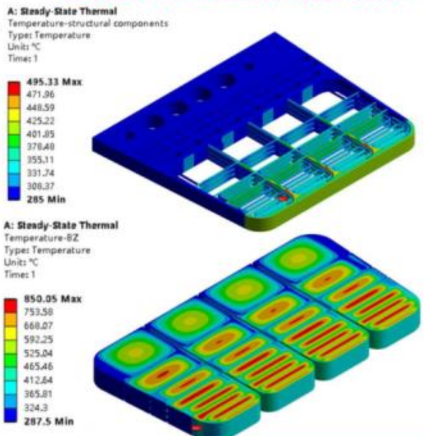

Structure material	RAFM steel		RAFM-ODS steel	
	Max. temp（°C）	Temp. limit（°C）	Max. temp.（°C）	Temp. limt（°C）
FW	425	550	466	650
SP	473		495	
DWT	342		351	
rib	396		409	
manifold	307		310	
Mixed breeder	843	900	850	900

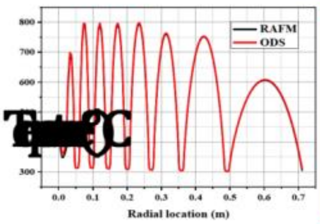

- □ Temp. on materials fulfills their limit
- □ Temp. on ODS steel is higher than that on RAFM steel due to lower thermal conductivity of ODS steel

Thermal-mechanical analysis

Under normal operation for 1.5GW

- Load:
  - ☐temp field on components
  - ☐15.5 MPa pressure on coolant channel wall
- Boundary condition:
  - ☐Fixed constrains at rear of PB
  - ☐Periodic boundary condition on lower and upper surface of model
- Stress assessment code:
  - ☐ITER SDC-IC standard

Stress assessment when RAFM steel is used

	Temp at Max. stress (℃)	Max. stress (MPa)	limit (MPa)	result
FW	309	285	503	√
SP	374	118	474	√
DWT	296	269	508	√
rib	298	304	508	√
Manifold	285	475	512	√

Stress assessment when RAFM-ODS steel is used

	Temp at Max. stress (℃)	Max. stress (MPa)	limit (MPa)	result
FW	454	400	634	√
SP	387	158	674	√
DWT	297	278	728	√
rib	306	303	722	√
Manifold	285	499	735	√

Stress distribution when RAFM is used

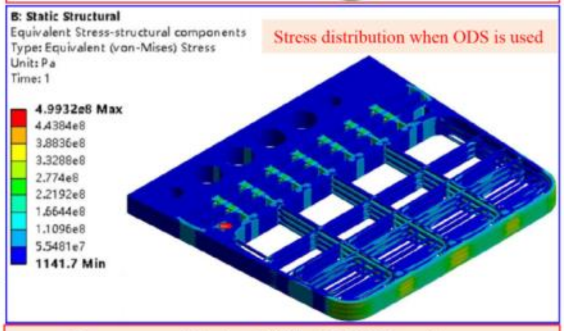

Stress distribution when ODS is used

- The stress on blanket fulfills SDC-IC' requirement
- When ODS steel is employed, the safety margin of stress is high.

Thermal-mechanical analysis

Under in-box LOCA accident for 1.5GW

- Load:
  - ☐temp on components
  - ☐17.2 MPa pressure on structural wall of componnets surrounding breeder zone
- Boundary condition:
  - ☐Fixed constrains at rear of PB
  - ☐Periodic boundary condition on lower and upper surface of model
- Stress assessment code:
  - ☐ITER SDC-IC standard

Stress assessment when RAFM steel is used

	Temp at Max. stress (℃)	Max. stress (MPa)	limit (MPa)	result
FW	332	857	1069	√
SP	424	600	984	√
DWT	285	239	1101	√
rib	389	682	1033	√
Manifold	285	498	1101	√

Stress assessment when RAFM-ODS steel is used

	Temp at Max. stress (℃)	Max. stress (MPa)	limit (MPa)	result
FW	336	868	1479	√
SP	446	602	1379	√
DWT	285	259	1543	√
rib	397	686	1402	√
Manifold	285	521	1543	√

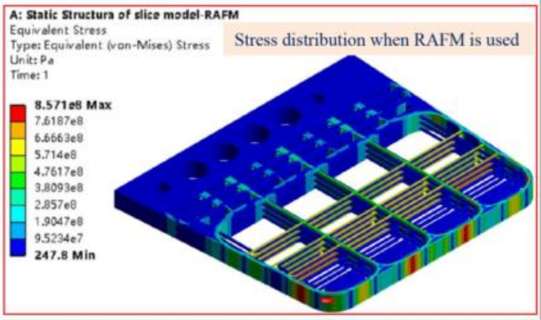

Stress distribution when RAFM is used

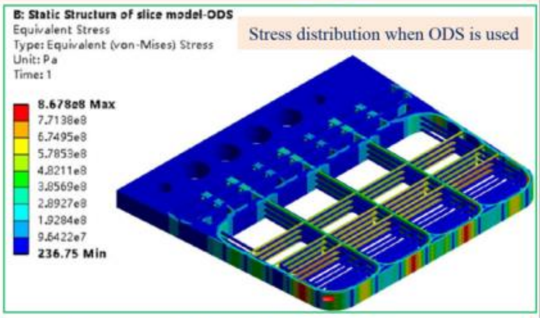

Stress distribution when ODS is used

- The stress on blanket fulfill SDC-IC' requirement
- When ODS steel is employed, the safety margin of stress is high.

Pressure drop of purge gas in breeder zones

Purge gas flow scheme and pressure drop

- Breeder zones: Li_2TiO_3&$Be_{12}Ti$ mixed bed, $d_l/d_s \geq 5$, $V_{Li2TiO3}/V_{Be12Ti} \approx 0.25$, Pf ≥ 0.75;
- Purge gas: He+0.1%H_2 ; in poloidal direction; inlet P, 0.1-0.3 MPa; Vel. 0.1-5 cm/s.

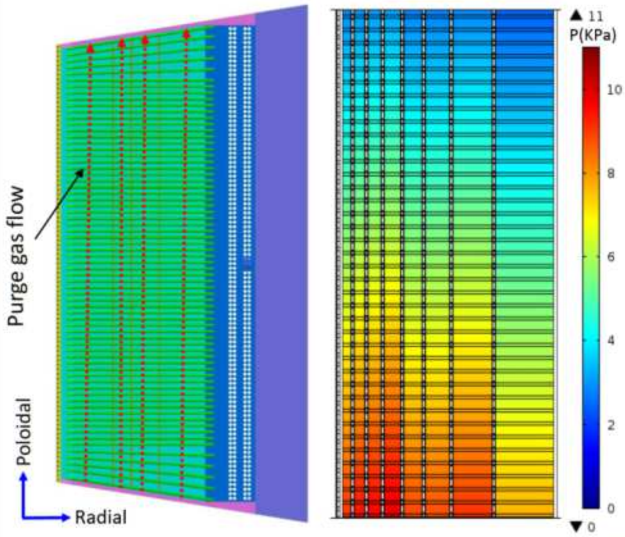

(a) Purge gas flow in Blanket 3#   (b) Pressure field of purge gas (1 cm/s, 2.0/0.4mm mixed bed)

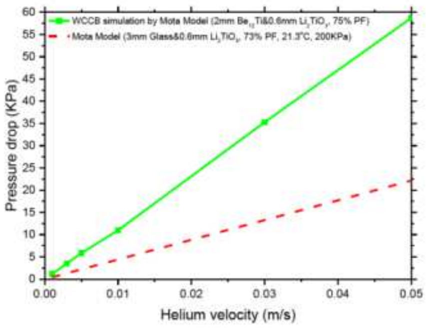

(c) Pressure drop at different velocities

Pressure drop of purge gas

(1) If inlet velocity is 1cm/s, (by Mota model)
for 2.0/0.4 mm mixed bed, △P=11KPa;
for 3.0/0.6 mm mixed bed, △P=4.4KPa.
(2) △P is proportional to velocity at low vel.。

Mota Model: M. Mota, et al., Trans. Filt. Soc. (2001)

1111

Tritium breeding radio

- the MCNP code
- the IAEA Fusion Evaluated Nuclear Data Library FENDL2.1

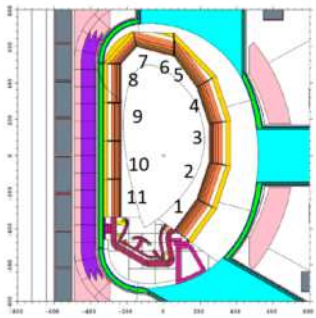

TBR with 432 BLK modules: 1.51

The composition of material

Item	Composition
W	100% Tungsten
First Wall	14.55% H2O, 85.45% CLAM steel;
Breeder zone	14.4% Li_2TiO_3, 65.6% $Be_{12}Ti$, 20% He;
Cooling Tubes zone	12.412% H2O, 45.763% CLAM Steel, 6.023% Li_2TiO_3, 27.437% $Be_{12}Ti$, 8.365% He;
Manifold	53.55% H2O, 46.12% CLAM steel, 1.65% He;
BSS	11.06% H2O, 87.29% CLAM steel, 1.65% He;
SP	100% CLAM steel;
SW	29.09% H2O, 70.91% CLAM steel;
Cover	96.23% CLAM steel, 3.77% He.

Local TBR

BLK No.	Local TBR
1	0.0374
2	0.0539
3	0.0661
4	0.0598
5	0.0437
6	0.0453
7	0.0198
8	0.0257
9	0.0365
10	0.0346
11	0.0226

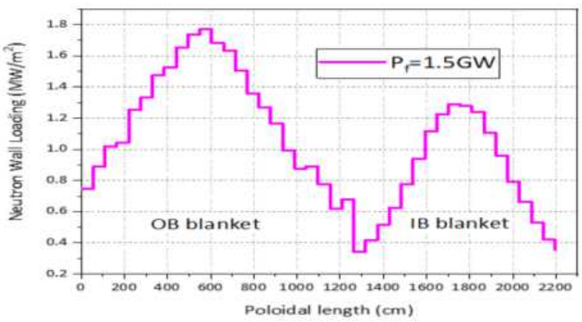

12

Shielding capability

	Fast neutron fluence in magnet conductor (n/cm2) （10 FPY）	Fast neutron fluence in insulator (n/cm2) （10 FPY）	Nuclear heating in magnet steel case (W/cm3)	Nuclear heating in magnet conductor (W/cm3)
ITER Design Limit	1×10^{19}	2×10^{18}	6×10^{-4}	3×10^{-4}

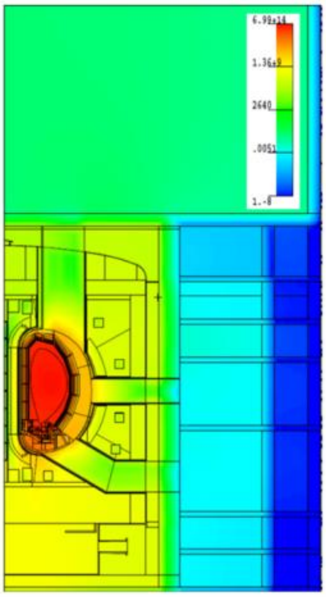

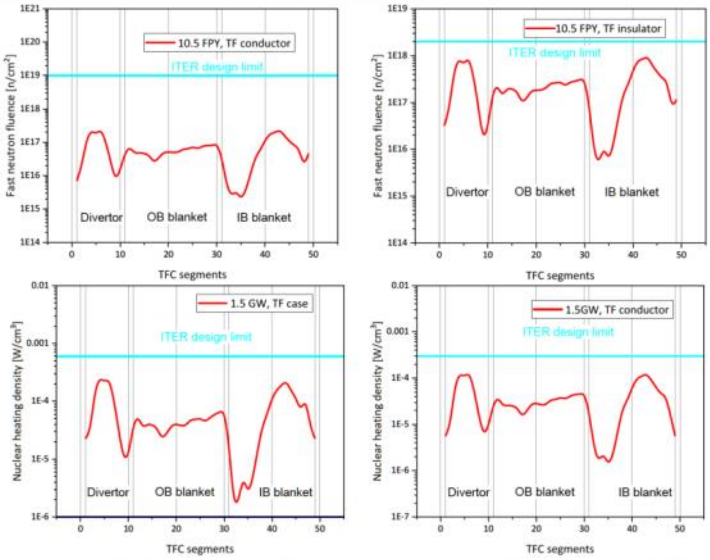

In current design phase, WCCB can provide better shielding capability

Neutronics Experiments of WCCB mockup

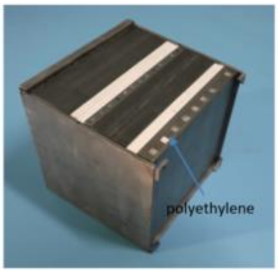

Mock up

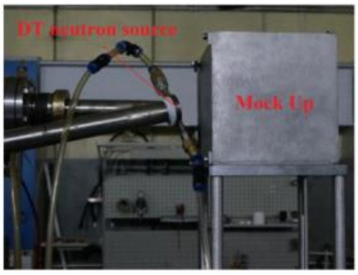

Experiment setup

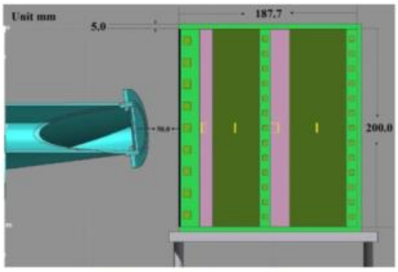

Monte Carlo model

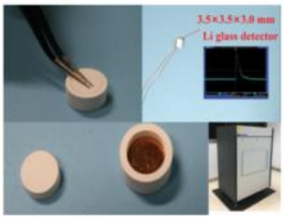

Detector

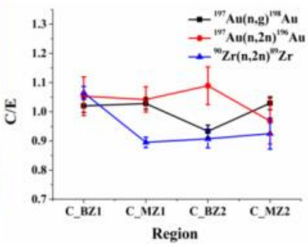

C/E of activation foils

Position	Calculation	Experiment	C/E
TPR in Li_2TiO_3 off-line measurement			
C_BZ1	1.220E-05	1.062E-05	1.15
C_BZ2	8.030E-06	7.609E-06	1.06
TPR in 6Li glass on-line mesurement			
C_BZ1	3.492E-05	3.773E-05	1.08
C_BZ2	4.069E-05	4.245E-05	1.04

C/E of TPR

14

R&D of WCCB FW Mockups

➢1/7-W/RAFM of WCCB First Wall Mockups

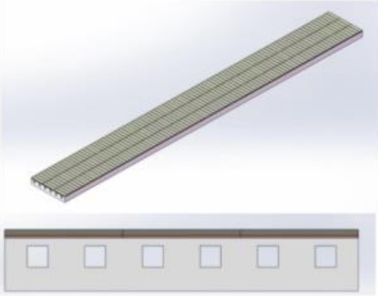

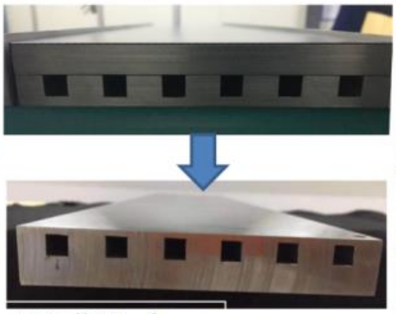

➢High Heat Flux Testing of First-Wall Mockups

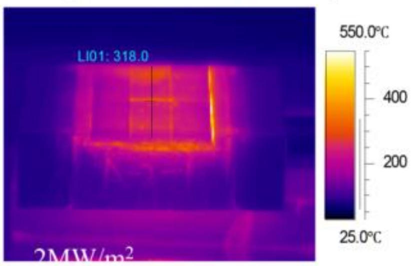

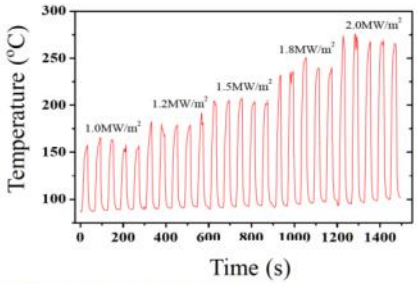

P1-126， Wanjing Wang， Progress on Manufacture Technology of CFETR WCCB at ASIPP- ISFNT conference

Construction of engineering experimental facility for BLK

CFETR WCCB PHTS design

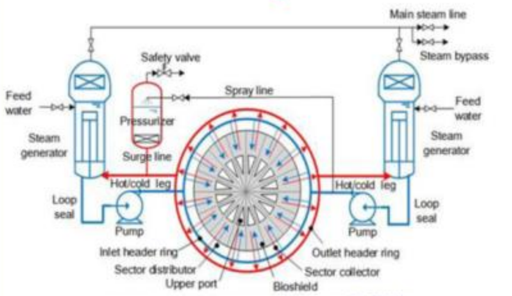

CFETR WCCB PHTS CS1/CS2示意图

PHTS's parameters

Parameter	CS	Value (RELAP5 simulation)			
		FP 200 MW	FP 500 MW	FP 1.0 GW	FP 1.5 GW
PHTS total mass flow [kg/s]	CS1	4795.4	4792.0	4746.0	4648.0
	CS2	4804.0	4800.0	4788.0	4540.0
SG total steam mass flow[kg/s]	CS1	300.2	338.0	408.3	479.5
	CS2	76.8	188.8	372.4	564.0
PHTS hot leg temperature [°C]	CS1	305.5	307.4	310.7	317.5
	CS2	296.0	300.6	307.3	325.0
PHTS cold leg temperature [°C]	CS1	284.7	283.5	281.6	283.3
	CS2	290.7	287.4	280.6	285.3
Total pressure drop [MPa]	CS1	0.591	0.588	0.575	0.554
	CS2	0.515	0.509	0.497	0.450

P1-125， Xiaoman Cheng， presented in ISFNT conference

Experiment facility: One part of Comprehensive Research Facility for Fusion Technology (**CRAFT**)

- Pressure: 15.5MPa，
- Coolant Temp.:Inlet 285℃， outlet 325℃，
- Mass flow rate:2*60m³/h

- This project has been approved by government this year
- The civil engineering will be started this year.

Summary

- One updated WCCB blanket concept is proposed corresponding to the latest core parameters (R=7.2m, a=2.2m) and mission of CFETR. ODS-steel is required as structure material.
- Main features are that the thermo-hydraulics scheme of the FW (including SP and Cover) and the breeder zone is de-coupled; SPs and Covers don't contain coolant channel to simple structure. DWT pipe is employed to embed in mixed breeder zone.
- The results of 3-D neutronics investigation show TBR is 1.15 and WCCB can provide better shielding capacity. The thermal and stress analysis indicates that the blanket are compliant with the material temperatures and stress limit.
- The R&D activities supporting design are on going, including neutronics mockup experiment, BLK fabrication, and thermal-hydraulics experiment facility.

17

Thank you for your attention !

Slliu@ipp.ac.cn

Consolidated Design of the HCPB Breeding Blanket for the Pre-Conceptual Design Activities of the EU DEMO and Harmonization with the ITER HCPB TBM Program

Francisco A. Hernández[a], Pavel Pereslavtsev[a], Guangming Zhou[a], Salvatore D'Amico[a], Heiko Neuberger[a], Jörg Rey[a], Qinlan Kang[a], Evaldas Bubelis[a], Lorenzo V. Boccaccini[a], Béla Kiss[b], Ivo Moscato[c], Gábor Nádasi[d], Fabio Cismondi[e], Yves Poitevin[f]

[a]Karlsruhe Institute of Technology, Karlsruhe, Germany

[b]Budapest University of Technology and Economics, Budapest, Hungary

[c]Università degli Studi di Palermo, Palermo, Italy

[d]Wigner Research Center for Physics, Budapest, Hungary

[e]EUROfusion Programe Management Unit, Garching, Germany

[f]Fusion for Energy, Barcelona, Spain

From the period 2014-2020, the pre-Conceptual Design Activities (pre-CDA) of the EU DEMO have taken place. These pre-CDA differ from past exercises in their strong Systems Engineering methodology, as well as for the pragmatic approach in their technology choices. The Helium Cooled Pebble Bed (HCPB) is one of the 2 candidates as driver blanket for the EU DEMO in the pre-CDA. Several design iterations have been required during the pre-CDA to adjust the design to the demanding DEMO requirements, to the very challenging systems integration and to the need to keep near-term technologies. To this respect, the design has evolved to a so-called fuel-breeder pin architecture built in single-module segments. The pins are filled with a pebble bed of an advanced ceramic breeder mixture of Li_4SiO_4 + 35mol % Li_2TiO_3 with improved mechanical properties and are embedded in prismatic blocks of $Be_{12}Ti$ acting as neutron multiplier. He gas at 8 MPa is used as coolant with a temperature window of 300-520 °C. This architecture has proven to achieve a large tritium breeding performance (≈1.20), a remarkably low plant circulating power (<100 MW) and its design for manufacturing paves the way for a better industrialization of its components and functional materials. This paper describes the consolidated design of the HCPB for the pre-CDA, shows its main performance figures and presents the ongoing realignment of the DEMO pre-CDA HCPB with the ITER HCPB TBM program.

Karlsruhe Institute of Technology

This work has been carried out within the framework of the EUROfusion Consortium and has received funding from the Euratom research and training programme 2014-2018 and 2019-2020 under grant agreement No 633053. The views and opinions expressed herein do not necessarily reflect those of the European Commission

EUROfusion

Consolidated Design of the HCPB Breeding Blanket for the Pre-Conceptual Design Phase of the EU DEMO and Harmonization with the ITER HCPB TBM Program

F. A. Hernández[a], P. Pereslavtsev[a], G. Zhou[a], Q. Kang[a], S. D'Amico[a], H. Neuberger[a], L. V. Boccaccini[a]
B. Kiss[b], G. Nádasi[c], L. Maqueda[d], I. Cristescu[a], I. Moscato[e], I. Ricapito[f], F. Cismondi[g]

[a]KIT, Germany *[b]BUTE, Hungary* *[c]Wigner RCP, Hungary* *[d]ESTEYCO, Spain* *[e]University of Palermo, Italy* *[f]F4E, Spain* *[g]EUROfusion, Germany*

20th International Workshop on Ceramic Breeder Blanket Interactions, Karlsruhe, 18-20 September 2019

KIT – The Research University in the Helmholtz Association www.kit.edu

Outline

Karlsruhe Institute of Technology

1. HCPB BL2017 v1: Design Architecture
2. Performance: Neutronics, Thermo-hydraulics, Thermo-mechanics
3. Plant Integration: HCPB TER and HCPB PHTS & BoP
4. DEMO Relevancy of the ITER HCPB-TBS
5. Summary and Outlook Towards the CD Phase

2 20/09/2019 Francisco A. Hernández et al., 20th International Workshop on CBBI, KIT CN EUROfusion

Outline

1. HCPB BL2017 v1: Design Architecture
2. Performance: Neutronics, Thermo-hydraulics, Thermo-mechanics
3. Plant integration: HCPB TER and HCPB PHTS & BoP
4. DEMO Relevancy of the ITER HCPB-TBS
5. Summary and Outlook Towards the CD Phase

2. HCPB BL2017 v1: Design Architecture

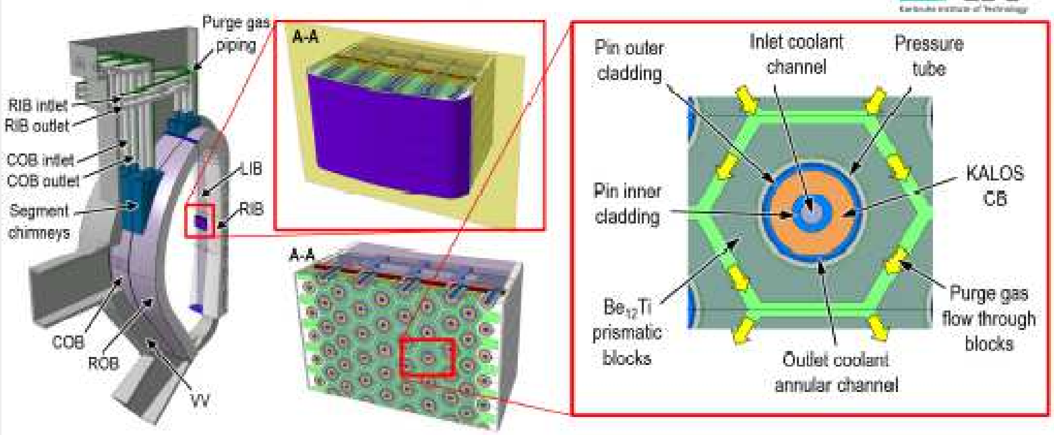

- HCPB integrated into DEMO1 BL2017 (16 sectors, R_0=9m, A=3.1, P_{fus}≈2GW)
- 1 sector = 3 outboard (OB) + 2 inboard (IB) (single module) segments
- Arrangement of fuel-breeder pins containing KALOS CB (Li_4SiO_4 + 35mol% Li_2TiO_3)
- Pins inserted into hexagonal prismatic blocks of $Be_{12}Ti$ neutron multiplier
- Structural steel: EUROFER97

2. HCPB BL2017 v1: Design Architecture

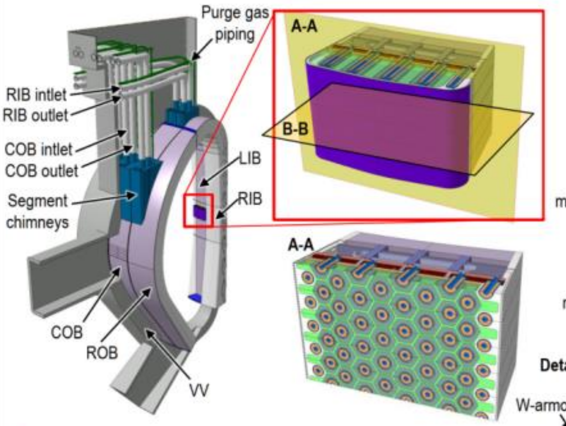

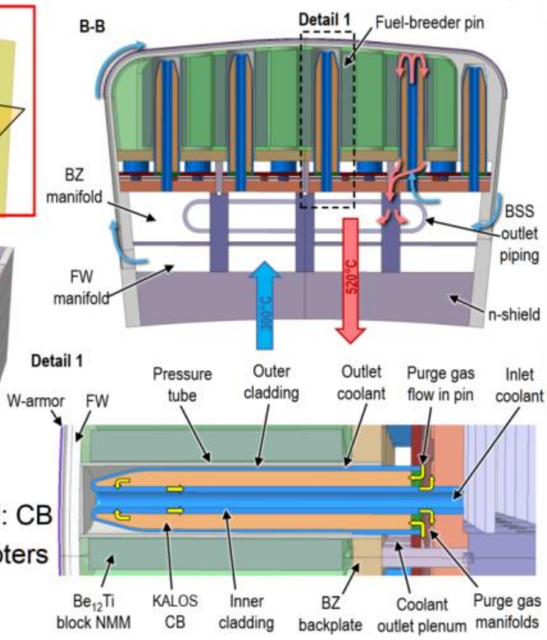

- Coolant: He @80bar, 300°C-520°C
- Purge gas: He + 0.1vol% H_2 @2bar ($He+H_2O$ as alternative); 1st: NMM, 2nd: CB
- FW roof-top shaped, turbulence promoters in FW and BZ
- Easier filling of functional materials

5 20/09/2019 Francisco A. Hernández et al., 20th International Workshop on CBBI, KIT CN

Outline

1. HCPB BL2017 v1: Design Architecture
2. Performance: Neutronics, Thermo-hydraulics, Thermo-mechanics
3. Plant Integration: HCPB TER and HCPB PHTS & BoP
4. DEMO Relevancy of the ITER HCPB-TBS
5. Summary and Outlook Towards the CD Phase

6 20/09/2019 Francisco A. Hernández et al., 20th International Workshop on CBBI, KIT CN

3. Performance: Neutronics

- Fully heterogeneous MCNP model
- Tritium Breeding:
  - ^{6}Li 60%: TBR ≈ 1.20, ^{6}Li 40%: TBR ≈ 1.16
- Neutron shielding:
  - Increased concern on VV activation: BB should contribute to ALARA-activate VV
  - dpa_{VV} ≈ 0.130dpa/fpy (WCLL ≈ 1/10 HCPB)
  - Best mats.: TiH_2, $ZrH_{1.6}$, $YH_{1.75}$, WC, B_4C
  - 18cm external shield => WCLL-like dpa_{VV}

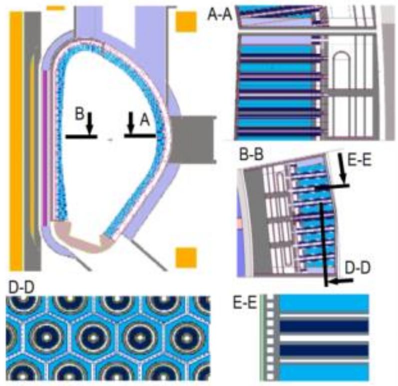

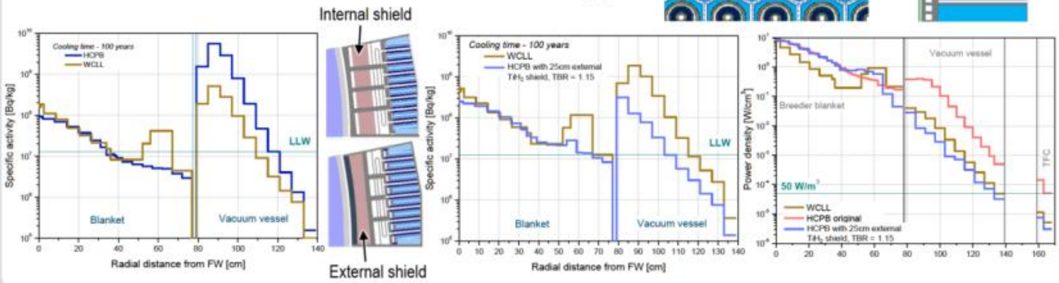

3. Performance: Thermo-hydraulics (TH)

- Global FEM TH analyses

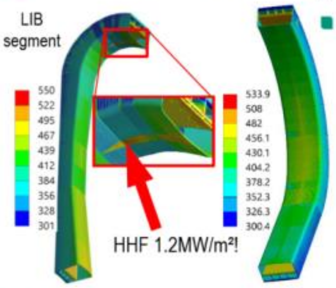

- Goals:
  - Assessment on adequacy of coolant parameters, even under HHF laods
  - Input for further global TM analyses

- Global CFD hydraulic analyses

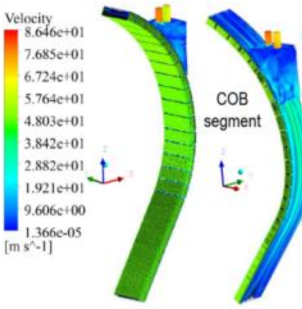

- Goals:
  - Assessment of total BB pressure drops (0.8 bar!)
  - Benchmark and calibration of global TH models with RELAP5 for WPBOP and WPSAE

- Detailed local CFD TH analyses

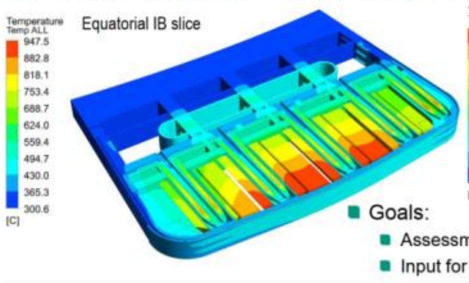

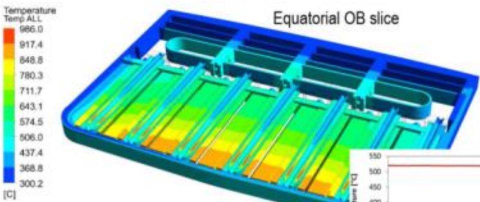

Transient: Power excursions

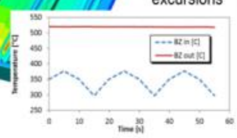

- Goals:
  - Assessment of temperature limits compliance
  - Input for further local TM analyses

3. Performance: Thermo-mechanics (TM)

KIT Karlsruhe Institute of Technology

- Local FEM TM analyses (Cat. I & IV)

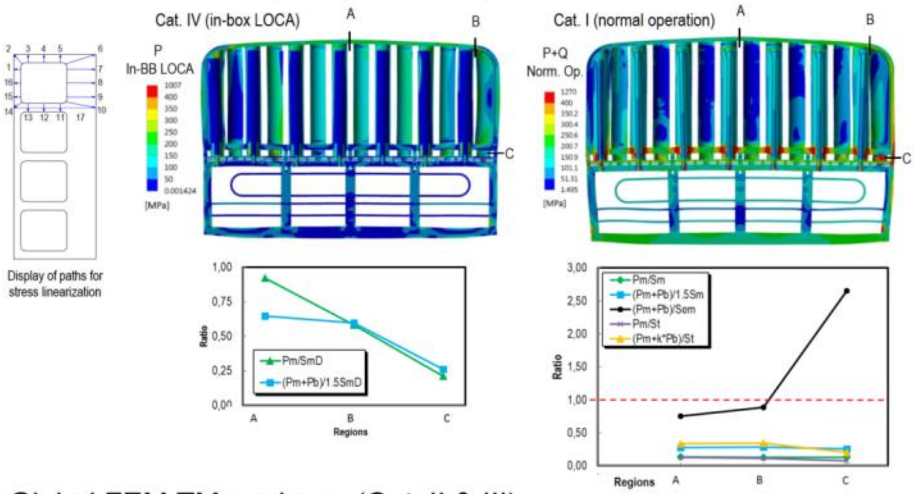

- Global FEM TM analyses (Cat. II & III)
  - Analyses involving VDE scenarios
  - EM inputs recently finished; Ongoing work with focus on BB attachment

Outline

KIT Karlsruhe Institute of Technology

1. HCPB BL2017 v1: Design Architecture
2. Performance: Neutronics, Thermo-hydraulics, Thermo-mechanics
3. Plant Integration: HCPB TER and HCPB PHTS & BoP
4. DEMO Relevancy of the ITER HCPB-TBS
5. Summary and Outlook Towards the CD Phase

4. Plant Integration: HCPB TER System

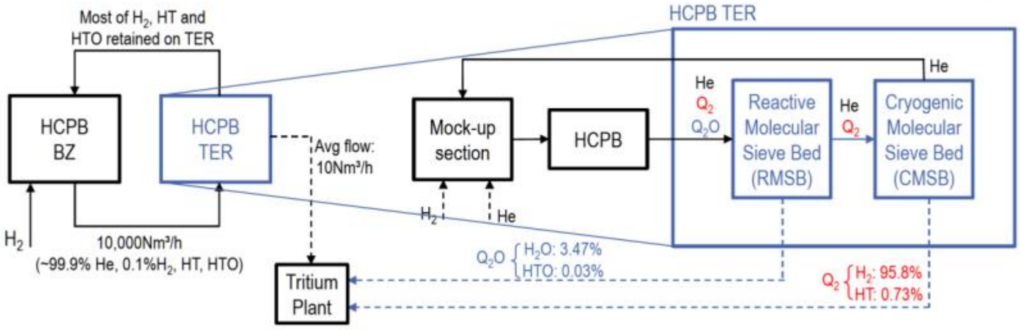

- Selected TER technology: cryogenic approach (higher TRL)
- Purge gas chemistry: He + 0.1%H_2 => permeating Q_2 species => T permeation
- Alternative chemistry: He + x% H_2O ("wet" purge gas) => non-permeating Q_2O species => T permeation reduced orders of magnitude, but fast corrosion of EUROFER97 and safe use with beryllides to be assessed
- TER technology for wet purge gas can also be based on RMSB

4. Plant Integration: HCPB PHTS and BoP

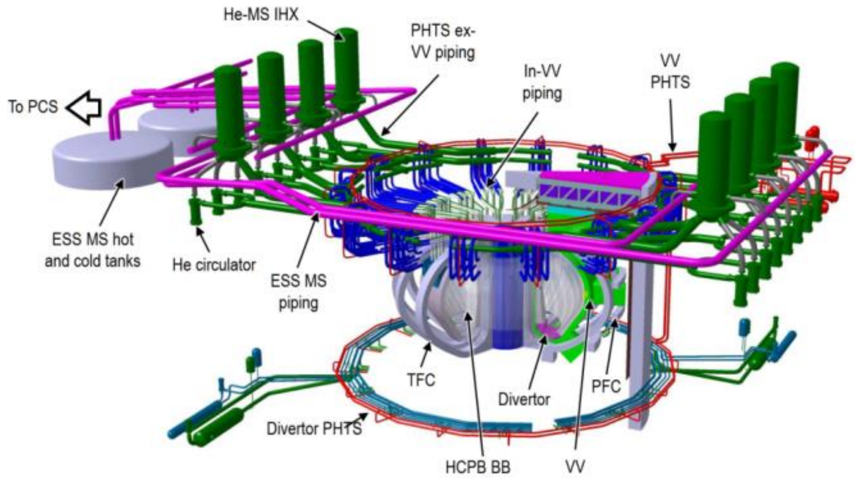

- BoP = PHTS + IHTS(ESS) + PCS ; PHTS: 8 loops ; 1 loop = 1 IHX + 2 circulators
- High BoP TRL ⇔ $P_{1circ,el}$ <6MW ⇔ Δp_{PHTS} <3 bar (for P_{fus}≈2GW)
- Δp_{inVV}≈0.8 bar; Δp_{exVV}≈1.9 bar; Δp_{PHTS}≈2.7 bar => **$P_{pump,el}$ ≈90MW ($P_{1circ,el}$ ≈5MW)**

Outline

KIT Karlsruhe Institute of Technology

1. HCPB BL2017 v1: Design Architecture
2. Performance: Neutronics, Thermo-hydraulics, Thermo-mechanics
3. Plant Integration: HCPB TER and HCPB PHTS & BoP
4. DEMO Relevancy of the ITER HCPB-TBS
5. Summary and Outlook Towards the CD Phase

5. DEMO Relevancy of the ITER HCPB-TBS

KIT Karlsruhe Institute of Technology

- Technical Performance Assessment EU DEMO through ITER TBM:

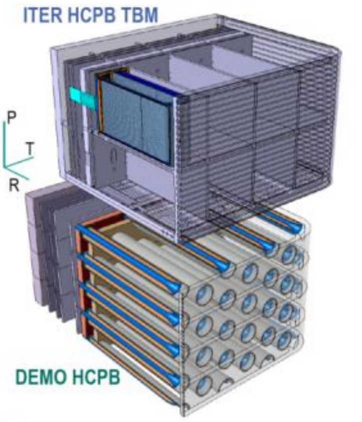

	ITER CDR HCPB TBM	DEMO PCD HCPB
Coolant	He	He
• Pressure / Tin / T_{out}	80 bar / 300°C / 500°C	80 bar / 300°C / 520°C
Steel		
• Type	EUROFER97	EUROFER97
BFMs		
• CB / Li6	Li_4SiO_4 / 90%	Li_4SiO_4+Li_2TiO_3 / 60%
• T_{max} CB / PF	920 °C / ~63%	920 °C / ~63%
• NMM	Be	$Be_{12}Ti$
• T_{max} NMM / PF	650 °C / ~63%	- / blocks
Purge gas		
• Chemistry / Pressure	He + 0.1%H_2 / 4 bar	He + 0.1%H_2 / 2 bar
FW		
• Length x thickness	3m x 29mm	~3m x 20mm
• Channels section	(15 x 15)mm	~(12 x12)mm, variable
• Mass flow / speed	100 g/s / 80 m/s	~50 g/s / ~50m/s
• HTC / augmentation	6400 W/m²K / no	8000 W/m²K / yes
BU / Pin		
• T x P x R | Ø / pitch	(205 x 205 x 480)mm	Ø80mm / 130mm
• Mass flow per unit	~50 g/s	~20 g/s
Stiffening grids		
• Channel section	(6 x 10)mm	-
• HTC / Δp	4400 W/m²K / 0.24 bar	-

- Functionality ("act-alike" philosophy) is maintained
- Expected that EU TBM RoX to DEMO will still be very relevant despite changes

Outline

KIT Karlsruhe Institute of Technology

1. HCPB BL2017 v1: Design Architecture
2. Performance: Neutronics, Thermo-hydraulics, Thermo-mechanics
3. Plant Integration: HCPB TER and HCPB PHTS & BoP
4. DEMO Relevancy of the ITER HCPB-TBS
5. **Summary and Outlook Towards the CD Phase**

15 20/09/2019 Francisco A. Hernández et al., 20th International Workshop on CBBI, KIT CN

EUROfusion

6. Summary and Outlook Towards CD Phase

KIT Karlsruhe Institute of Technology

- Current reference design: fuel-breeder pin in hexagonal prismatic $Be_{12}Ti$ blocks
- Basic key performance indicators (neutronics, thermo-hydraulics, thermo-mechanics) show promising results
- "Interface-friendly" design => helps to keep high TRL of key interfacing systems (TER and BoP)
- Design to be presented at the PCD phase Gate Review => starting point for CD phase

  - You're welcomed for a further discussion at ISFNT (Poster P1-083, Monday 23rd)!

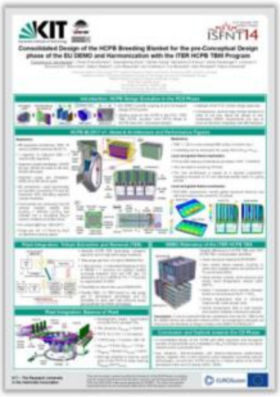

16 20/09/2019 Francisco A. Hernández et al., 20th International Workshop on CBBI, KIT CN

EUROfusion

Design and R&D Status of Tritium Extraction System for HCCR-TBM

Mu-Young Ahn[a], Seungyon Cho[a], Soon Chang Park[a], Seok-Kwon Son[a],
Youngmin Lee[a], Yi-Hyun Park[a], Duck Young Ku[a], Chang-Shuk Kim[a], Jongil Kim[a],
Alice Ying[b]

[a]National Fusion Research Institute, Daejeon, Republic of Korea

[b]Mechanical and Aerospace Engineering Dep., University of California, Los Angeles

Tritium Extraction System (TES) is one of major ancillary systems of Korean Helium Cooled Ceramic Reflector (HCCR) Test Blanket System (TBS) to achieve technical and operational objectives of Test Blanket Module (TBM) program in ITER. Main functions of the TES are to extract tritium produced in breeding zone of the HCCR-TBM by using a low pressure helium purge gas with small amount of hydrogen and to recover tritium for measurement before routing to Tritium Accountancy System in the TBS then to tritium processing systems in ITER. In this paper, progress of the TES design is summarized including main processes adopted, description for the components, layout of the system, operational procedures, engineering analyses results, etc. And then, R&D efforts to support and to validate the design are addressed. In particular, performance of large-scale Cryogenic Molecular Sieve Bed (CMSB) which is one of the main processes adopted for adsorption and desorption of hydrogen isotopes in the circuit is discussed.

20th International Workshop on Ceramic Breeder Blanket Interactions, Sept. 18-20, 2019, KIT, Germany

CBBI-20

Design and R&D Status of Tritium Extraction System for HCCR-TBM

M.-Y. Ahn[1], S. Cho[1], S. C. Park[1], S. K. Son[1], Y. Lee[1], Y.-H. Park[1], D. Y. Ku[1], C.-S. Kim[1], J. Kim[1], A. Ying[2]

[1] National Fusion Research Institute (NFRI), Daejeon, Rep. of Korea
[2] University of California, Los Angeles (UCLA), Los Angeles, USA

과학기술정보통신부 Ministry of Science and ICT

KOREA DOMESTIC AGENCY

Outline

1. Introduction
2. Progress of TBM Design
3. Progress of TES Design
4. Status of TES R&Ds
5. Summary

Overview of TBM Program

- Principal Functions of Breeding Blanket in Fusion Reactors
  - Tritium breeding to ensure tritium self-sufficiency
  - Power extraction at high temperature
  - Radiation shielding

Test Blanket Module (TBM) Program : ITER provides ports for testing to demonstrate breeding blanket functions

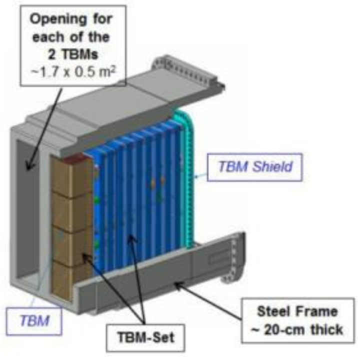

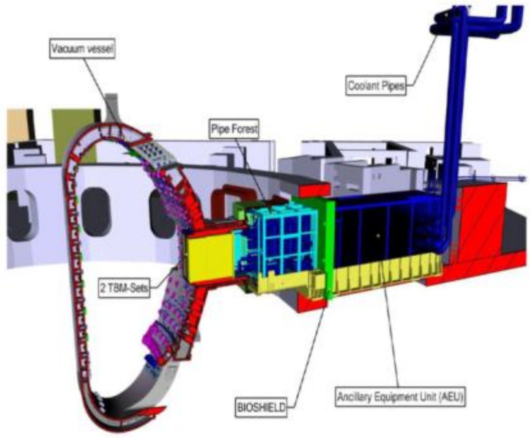

KO TBM Program

- HCCR-TBS consists of TBM-set and its ancillary systems
  - Helium Cooling System (HCS), Coolant Purification System (CPS), Tritium Extraction System (TES), Tritium Accountancy System (TAS), Neutron Activation System (NAS), Pipe Forest (PF), Ancillary Equipment Unit (AEU), I&C and Connection Pipes

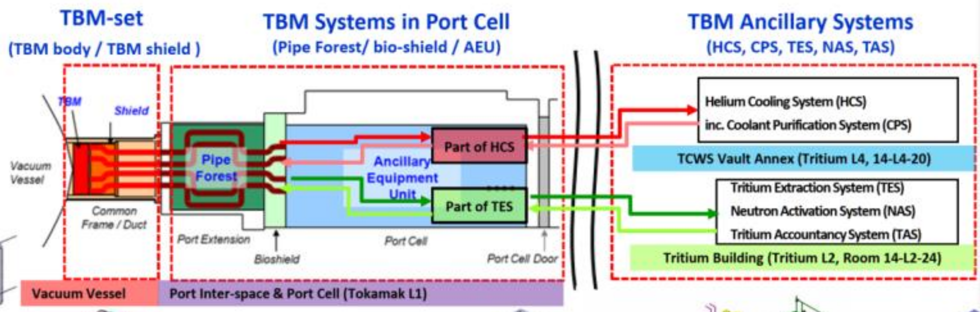

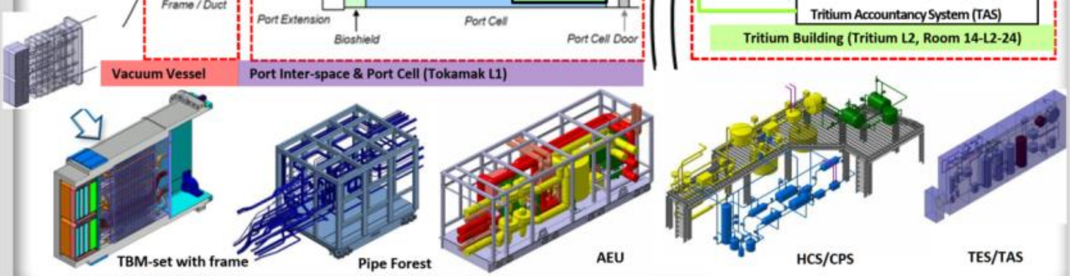

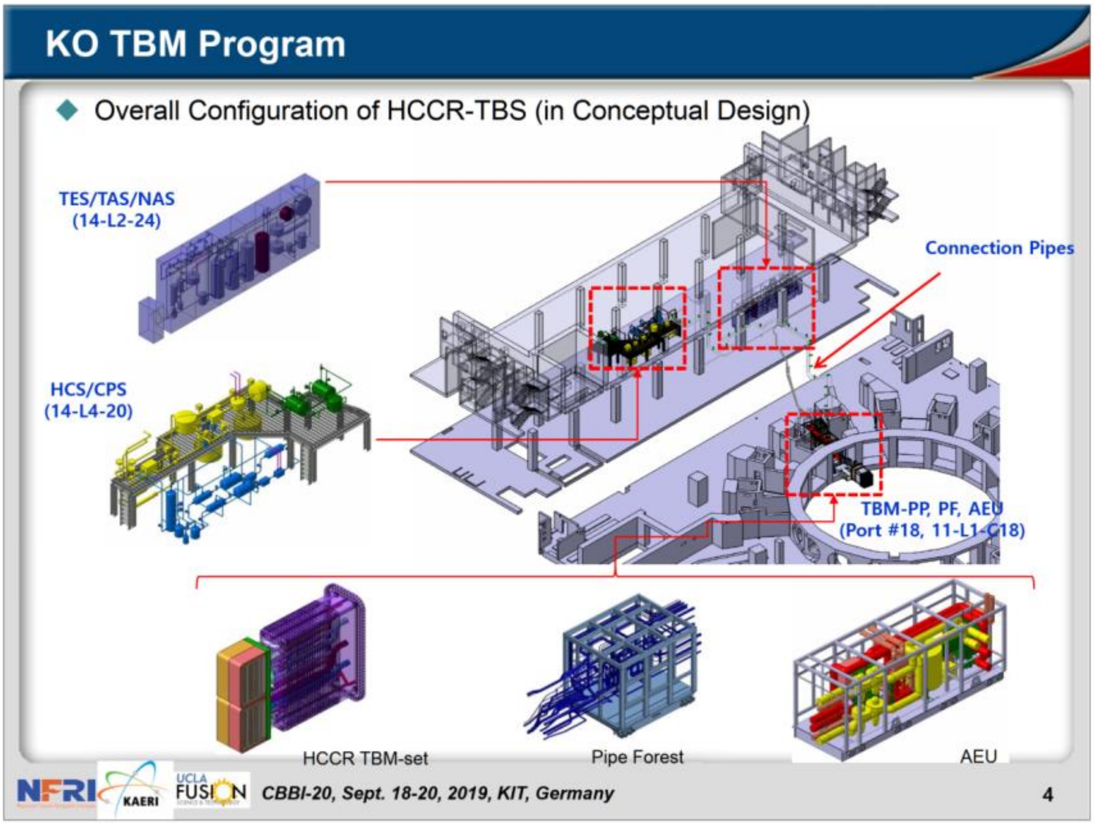

KO TBM Program
Overall Configuration of HCCR-TBS (in Conceptual Design)
TES/TAS/NAS
(14-L2-24)
HCS/CPS
(14-L4-20)
Connection Pipes
TBM-PP, PF, AEU
(Port #18, 11-L1-C18)
HCCR TBM-set
Pipe Forest
AEU
NFRI
KAERI
UCLA FUSION
CBBI-20, Sept. 18-20, 2019, KIT, Germany
4

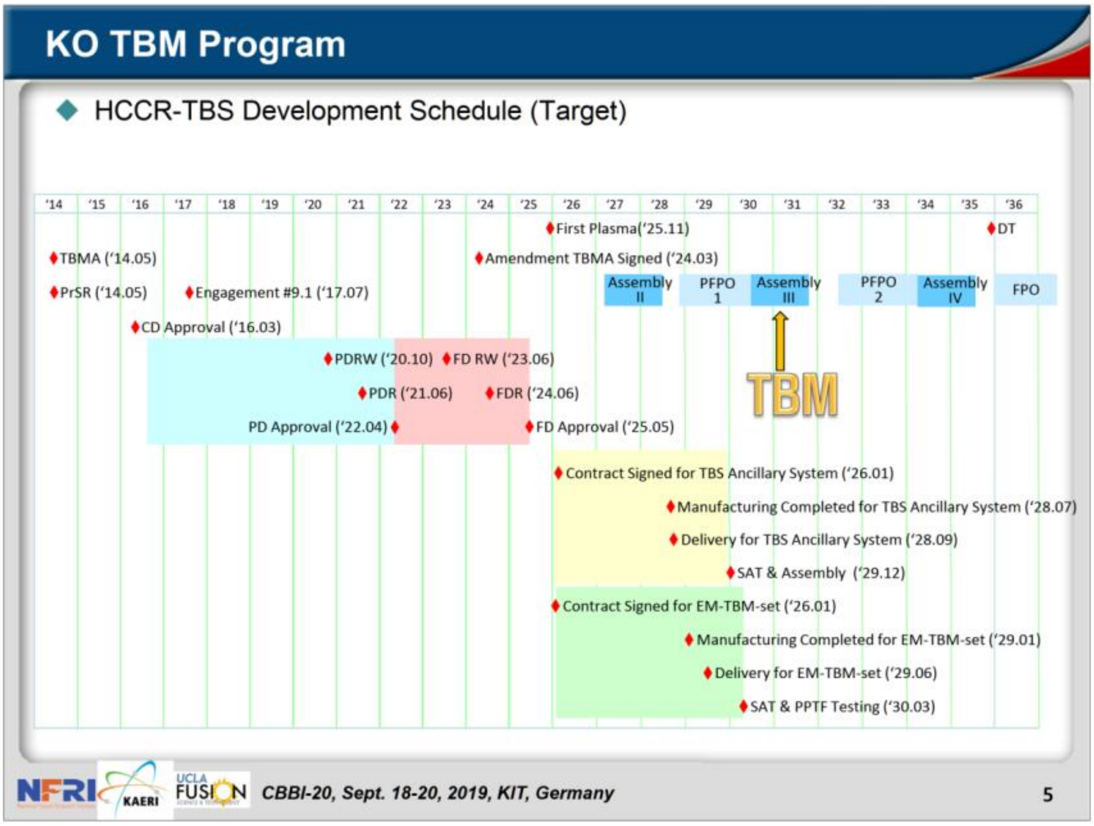

KO TBM Program
HCCR-TBS Development Schedule (Target)
'14 '15 '16 '17 '18 '19 '20 '21 '22 '23 '24 '25 '26 '27 '28 '29 '30 '31 '32 '33 '34 '35 '36
First Plasma('25.11)
DT
TBMA ('14.05)
Amendment TBMA Signed ('24.03)
PrSR ('14.05)
Engagement #9.1 ('17.07)
Assembly II
PFPO 1
Assembly III
PFPO 2
Assembly IV
FPO
CD Approval ('16.03)
PDRW ('20.10)
FD RW ('23.06)
PDR ('21.06)
FDR ('24.06)
TBM
PD Approval ('22.04)
FD Approval ('25.05)
Contract Signed for TBS Ancillary System ('26.01)
Manufacturing Completed for TBS Ancillary System ('28.07)
Delivery for TBS Ancillary System ('28.09)
SAT & Assembly ('29.12)
Contract Signed for EM-TBM-set ('26.01)
Manufacturing Completed for EM-TBM-set ('29.01)
Delivery for EM-TBM-set ('29.06)
SAT & PPTF Testing ('30.03)
NFRI
KAERI
UCLA FUSION
CBBI-20, Sept. 18-20, 2019, KIT, Germany
5

Outline

1. Introduction
2. Progress of TBM Design
3. Progress of TES Design
4. Status of TES R&Ds
5. Summary

TBM Concept

- Design parameters for Helium Cooled Ceramic Reflector (HCCR) TBM-set

Parameter	Values
FW heat flux	0.3 MW/m^2
Neutron wall load	0.78 MW/m^2
Thermal Power	0.98 MW (TBD)
Structural material	KO-RAFM (ARAA) (< 550°C), 0.01% Zr Improved creep and impact resistances
Breeder	Li_2TiO_3 (< 920°C, TBD), ~80 kg 70% enrichment Li-6
Multiplier	Be (< 650°C), ~100 kg
Reflector	Graphite (<1200°C) Reduce the Be Multiplier up to 50%
Size	1670(P) x 462(T) x 605(R) (mm)
Coolant	8 MPa He, 1.14 kg/s (Nominal) 300°C inlet / 500°C outlet
Purge gas	He with 0.1 % H_2
TBM-shield	316L(N)-IG Block/Cooling Channels ITER FW/BLK-PHTS (70°C, 4 MPa)

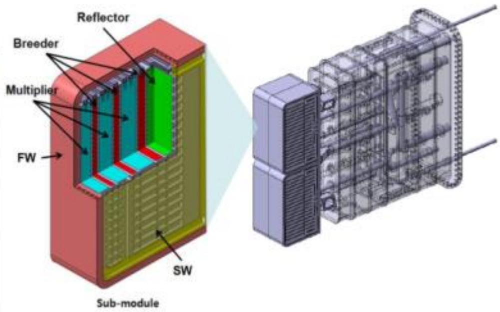

- Four-sub-module Concept
  - Manufacturability
  - Transportation of Irradiated TBM for PIE
  - Reduction of EM Force
  - Endurance of Internal Over-pressure
- Graphite Pebbles as Neutron Reflector
  - Reduce the Amount of Be Multiplier up to 50%
  - Reduce the difficulty of handling Be
  - Decrease of Cost
  - Comparable Nuclear Performance

TBM Design Status

- Since CD approval (Mar. 2016), series of PD designs have been evolved
  - Performance analyses were carried out for various load cases and load combinations

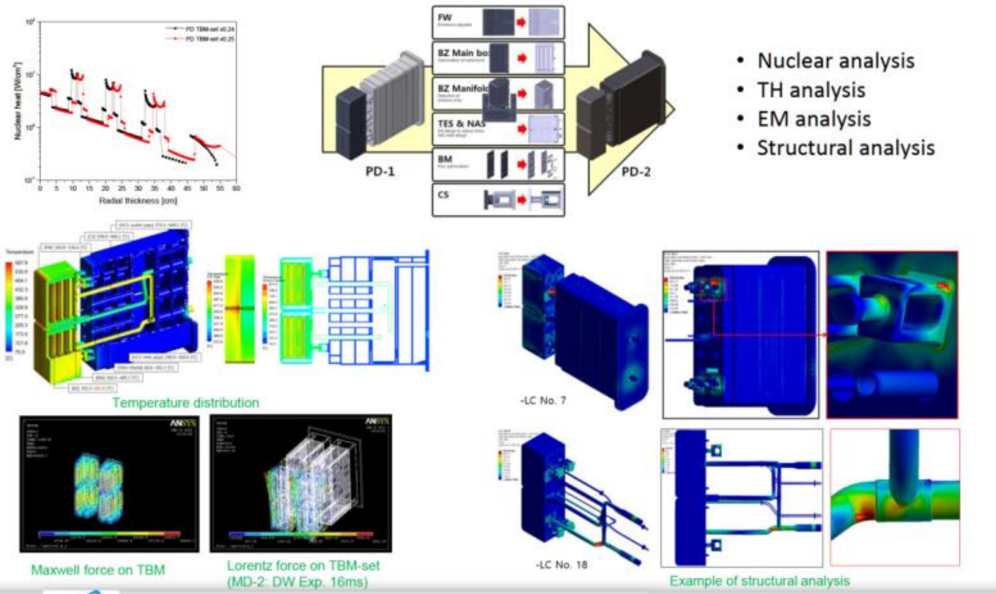

NFRI KAERI UCLA FUSION *CBBI-20, Sept. 18-20, 2019, KIT, Germany* 8

Tritium Production

- Since CD approval (Mar. 2016), series of PD designs have been evolved
  - Performance analyses were carried out for various load cases and load combinations
  - Tritium production up to ~25 mg/day should be extracted from the TBM by TES

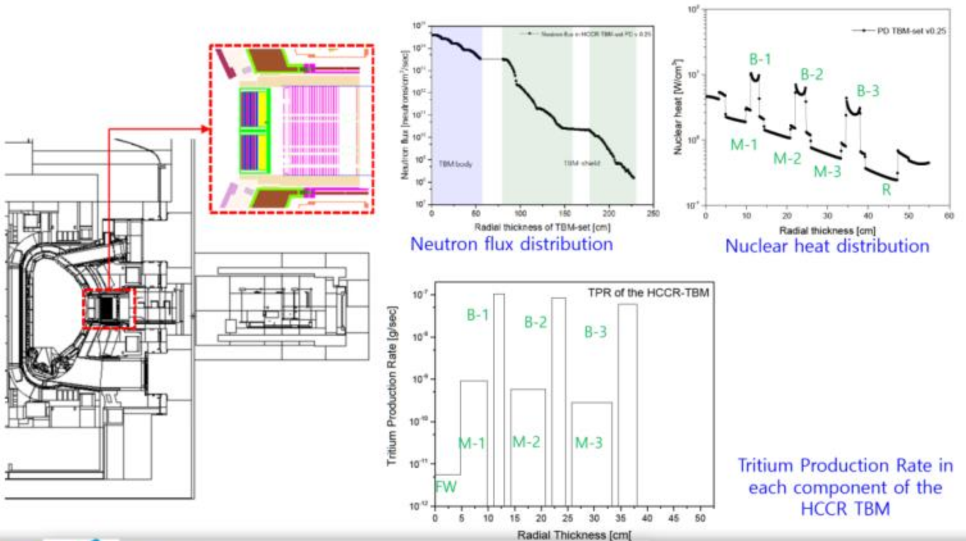

NFRI KAERI UCLA FUSION *CBBI-20, Sept. 18-20, 2019, KIT, Germany* 9

Outline

1. Introduction
2. Progress of TBM Design
3. Progress of TES Design
4. Status of TES R&Ds
5. Summary

Tritium Extraction System

- Functions of the Tritium Extraction System (TES)
  - To extract tritium produced in the breeder & multiplier pebble beds by the purge gas
  - To control chemical compositions of the purge gas
  - To remove impurities (Q2, N2, CO, CQ4, TBD)
  - To recover tritium for the accountancy in Tritium Accountancy System (TAS)

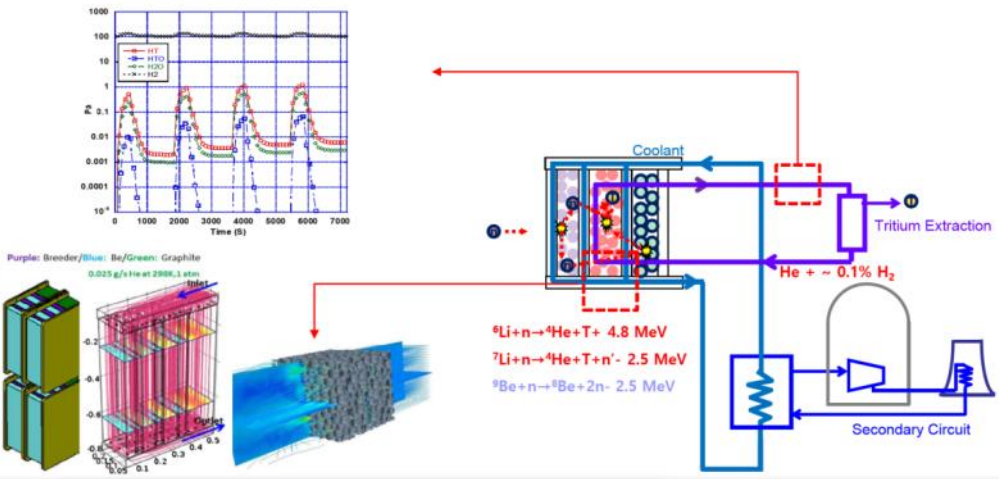

Tritium Extraction System

- Functions of the Tritium Extraction System (TES)
  - To extract tritium produced in the breeder & multiplier pebble beds by the purge gas
  - To control chemical compositions of the purge gas
  - To remove impurities (Q_2, N_2, CO, CQ_4, TBD)
  - To recover tritium for the accountancy in Tritium Accountancy System (TAS)

Parameters	Values
Tritium production rate	~25 mg/day (continuous back to back with duty 0.25)
Purge gas property	(TBD)
Swamping ratio	He : H2 = 1000 : 1
Mass flow rate	> 0.1 g/s (> 2Nm³/h)
At TBM inlet	Room temperature with 1 bar
At TBM outlet	~450 °C with 0.9 bar
Composition (molar fraction)	(TBD)
H2	981.8 vppm
HT	18.2 vppm
HTO	1.8 vppm
H2O	~8 vppm
Other impurities	~10 vppm
Extraction	(TBD)
Extraction efficiency	> 90%
H2	> 2.1 mole/day
HT	~ 0.04 mole/day
HTO	~ 0.004 mole/day
H2O	~ 0.02 mole/day

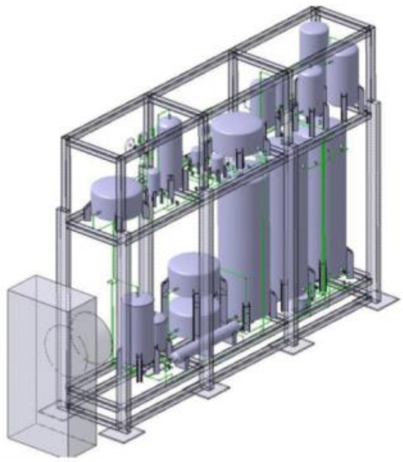

Main Process

- During adsorption phase Q2 and Q2O are adsorbed to CMSBs and AMSBs, respectively

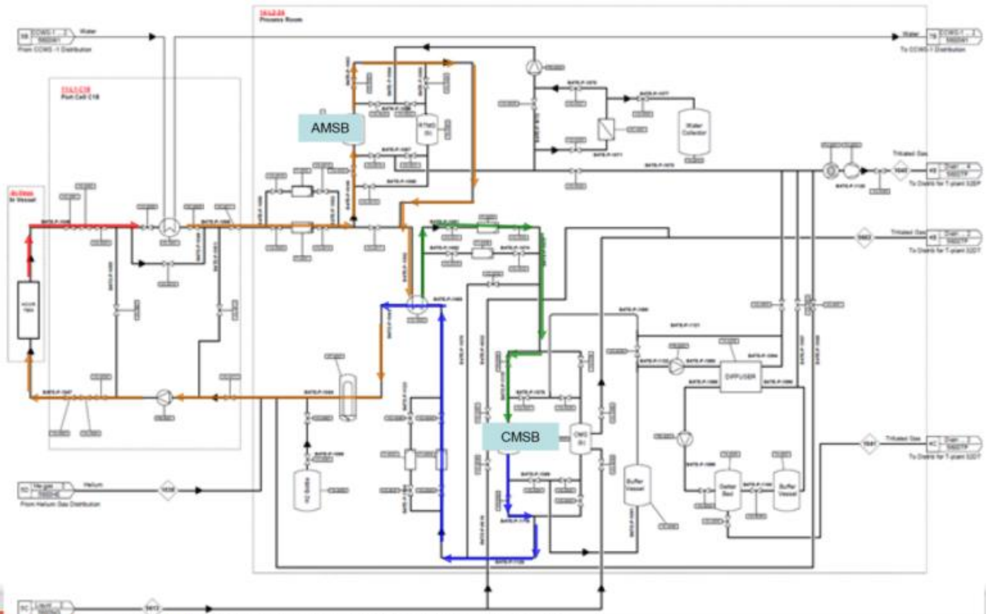

Main Process

- During desorption phase regenerated hydrogen isotopes are purified at the diffuser and stored in the getter bed

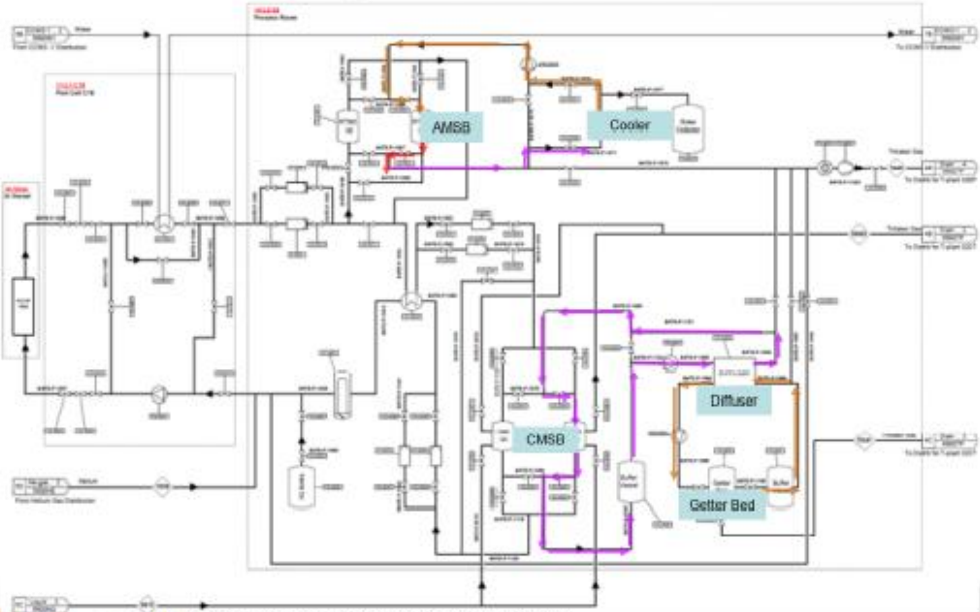

NFRI KAERI FUSION *CBBI-20, Sept. 18-20, 2019, KIT, Germany* 14

Engineering Analysis

- Steel structure and pipe analyses performed for series of PD designs
  - HCCR-TBS System Load Specifications for Ancillary Systems
  - Design Seismic Floor Response Spectr in the Tokamak Complex
  - NUREG-800 Section 3.7.2 Siesmic System Analysis

Event Cat.	States	Load conditions	Initiating event	Concatenated event	# of events
IV	POS + SL-2 + Internal fire	DW, Pres-O, ThO	SL-2	Internal fire	1
	Hot standby + SL-2 + Internal fire	DW, Pres-H, ThH	SL-2	Internal fire	1
	Cold standby +SL-2 + Internal fire	DW, Pres-C, ThC	SL-2	Internal fire	1
	Outgassing +SL-2 + Internal fire	DW, Pres-G, ThG	SL-2	Internal fire	1
	STM +SL-2 + Internal fire	DW, Pres-S, ThS	SL-2	Internal fire	1
	LTM + SL-2 + Internal fire	DW, Pres-L, ThL	SL-2	Internal fire	1

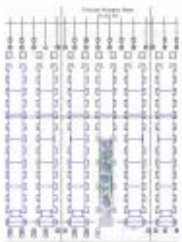

NFRI KAERI UCLA FUSION *CBBI-20, Sept. 18-20, 2019, KIT, Germany* 15

Engineering Analysis

- Steel structure and pipe analyses performed for series of PD designs
  - ANSI/AISC N690 Safty-related Structure for Nuclear Facilities (TBD)
  - ANSI/AISC ASD Manual of Steel Construction Allowable Stress Design (TBD)

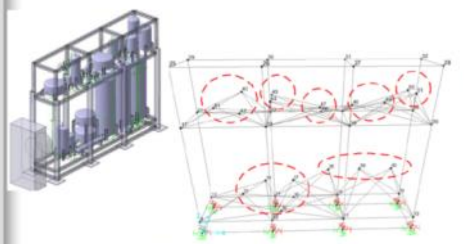

Mass point of the analysis model

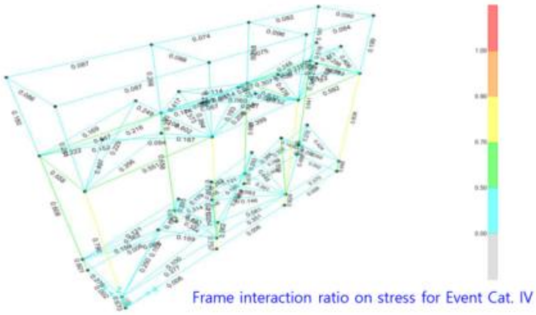

Frame interaction ratio on stress for Event Cat. IV

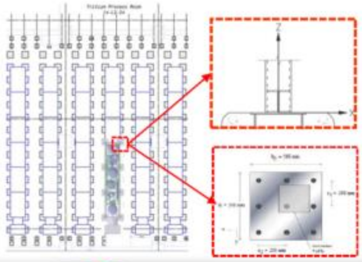

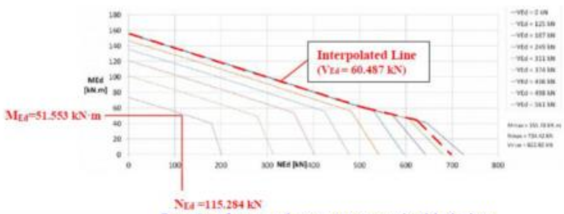

Reaction force and moment on embedded plate

CBBI-20, Sept. 18-20, 2019, KIT, Germany **16**

Engineering Analysis

- Steel structure and pipe analyses performed for series of PD designs
  - ASME B31.3 (TBD)

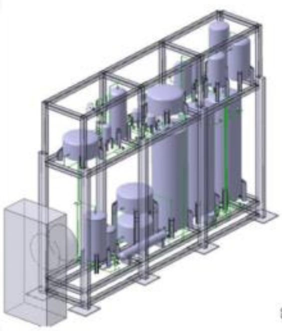

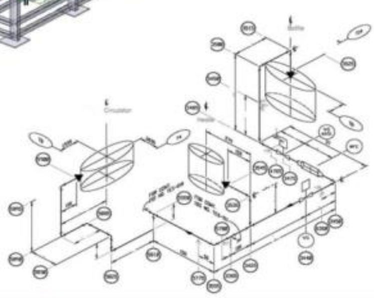

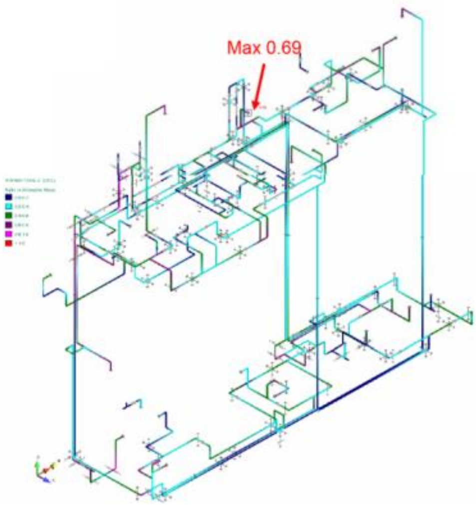

Stress distribution for load combination W+P3+T3+SL-2

CBBI-20, Sept. 18-20, 2019, KIT, Germany **17**

Outline

1. Introduction
2. Progress of TBM Design
3. Progress of TES Design
4. Status of TES R&Ds
5. Summary

Objectives of R&Ds

- In order to validate and support the design of TES, various R&Ds have been conducted and are planned
  - Validation of TES process
  - Performance evaluation of the components (incl. lifetime, failure rate, etc.)
  - Build-up know-how for TES operations

PGLoop

- PGLoop facility is in operation in NFRI
  - Basic tests for unit process, and integral test for adsorption and desorption envisaged for the TES of HCCR-TBS
  - Gas circulation module, gas control module, AMSB module, CMSB module, diffuser & storage module, vacuum module, etc.

PGLoop

- PGLoop facility is in operation in NFRI

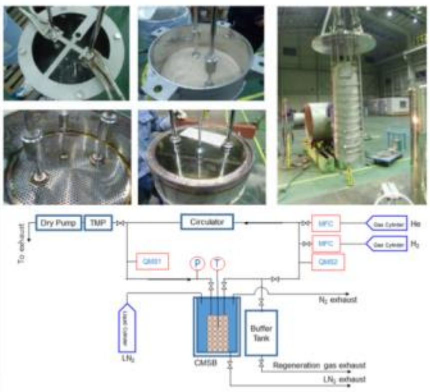

Hydrogen adsorption and breakthrough curve for large-scale CMSB

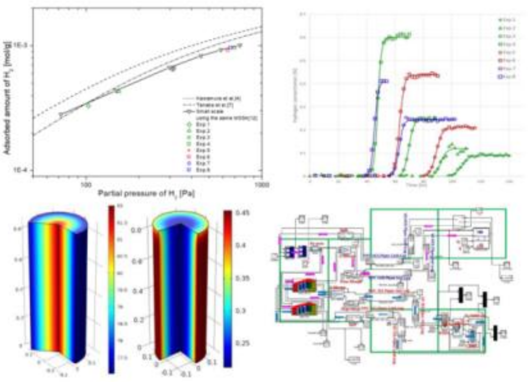

Computation of temp. and adsorption amount using T-dynamic model in devleopment

  - Large-scale hydrogen adsorption performance comparable to the TBS-relevant scale were demonstrated using the CMSB module
    - Size effect on the adsorption is not large for the current CMSB design
    - The adsorbed amount of hydrogen depends only on hydrogen partial pressure as reported by other small-scale studies
  - Desorption performance of the CMSB is being tested

HYPER

- HYPER facility for permeation experiments
  - Permeation experiments for structural materials including ARAA, Korean RAFM steel
  - Tests for the component-related permeation issues also foreseen

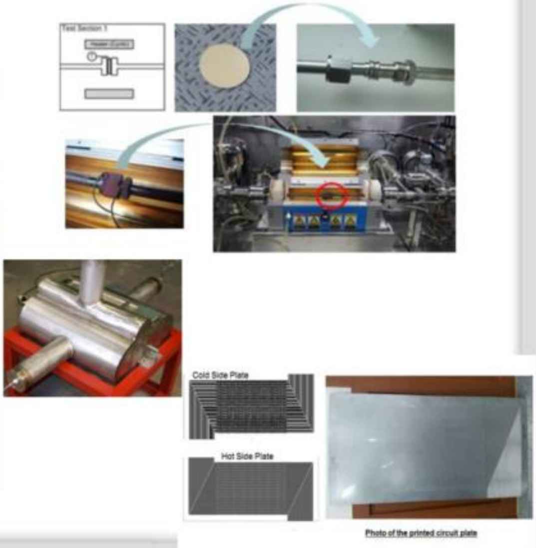

Outline

Summary

- TBM program is to test the concept of breeding blanket for DEMO and fusion power plant, which is very an important role in KO domestic fusion energy development roadmap.
- Current design status of KO HCCR TBM and TES is introduced. Since CD approval ('16.03), KO TBM Team has been preparing PD design.
- R&Ds to validate and support the TES design have been conducted and are planned with the major objectives including validation of TES process, performance evaluation of the components and build-up know-how for TES operations. The recent activities have demonstrated large-scale hydrogen adsorption, one of the main processes adopted in TES, using PGLoop facility

Thank you for your attention!

Lithium-6 Enrichment using Innovative Electrodialysis with Lithium Ionic Conductor for ITER-TBM

Tsuyoshi Hoshino, Kenji Morita

National Institutes for Quantum and Radiological Science and Technology (QST), 2-166, Obuchi, Omotedate, Rokkasho-mura, Kamikita-gun, Aomori, 039-3212, Japan

The tritium as a fuel for fusion reactors is produced by the neutron capture reaction of lithium-6 (^{6}Li). However, natural Li contains only about 7.8 % ^{6}Li, and the enrichment of ^{6}Li up to 90% is required for the fusion reactor. The amalgamation process using mercury is the only ^{6}Li enrichment technology in practical use overseas; however, because mercury is toxic, this method cannot be industrialized in Japan. Other methods have very low separation efficiencies and are unfit for mass production. Because it is difficult to import ^{6}Li from overseas, the establishment of a ^{6}Li enrichment technology that is unique to Japan is an issue of top priority for the realization of fusion reactors.

Therefore, we have proposed a new and innovative process that uses an electrodialysis with lithium ionic conductor, thereby establishing an innovative Li isotope separation technology. While lithium ions can move through the lithium ionic conductor by electrodialysis, the higher mobility of ^{6}Li ions due to its lighter mass than that of ^{7}Li ions enables ^{6}Li to be enriched on the cathode side. Principle demonstration was completed. Then a long-term evaluation test of the lithium-6 enrichment was performed as a next step.

The new method involves the use of $Li_{0.29}La_{0.57}TiO_3$ (LLTO) as an Li isotope separation membrane (LISM) whereby only Li ions permeate from the positive electrode side to the negative electrode side during electrodialysis. The area and thickness of the LISM are 25 cm^2 (5.0 cm × 5.0 cm) and 0.5 mm, respectively. The positive side of the dialysis cell was filled with 0.1M LiOH solution. With the electrode area being set to 16 cm^2, the relationship between the ^{6}Li separation coefficient and the electrodialysis time was investigated by ICP-AES and ICP-MS.

Measurements of the Li ion concentration at the negative electrode side as a function of electrodialysis duration showed that the Li recovery ratio increased to 47.8% after 132 days. Moreover, we obtained a maximum of 1.06 for the ^{6}Li isotope separation coefficient. This result showed that the ^{6}Li isotope separation coefficient of this method is the same as that of the amalgamation process using mercury (1.06). Thus, this method has the potential to be a superior ^{6}Li enrichment method to produce 90% enriched tritium breeder for ITER-TBM.

20th International Workshop onCeramic Breeder Blanket Interactions
18 – 20 September 2019, KIT Campus North

Lithium-6 enrichment using innovative electrodialysis with lithium ionic conductor for fusion reactor

Tsuyoshi HOSHINO, Kenji MORITA

QST

National Institutes for
Quantum and Radiological Science and Technology

1/20

Introduction

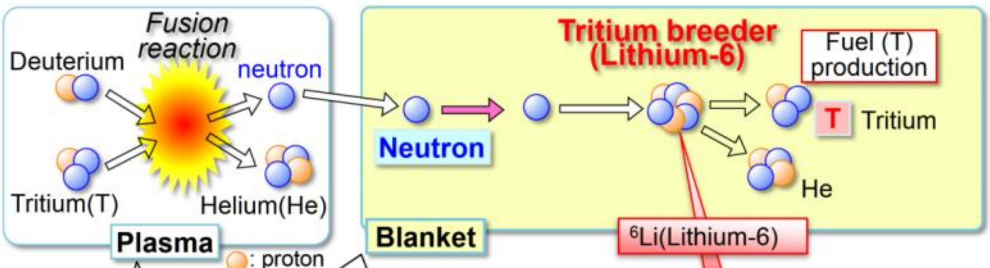

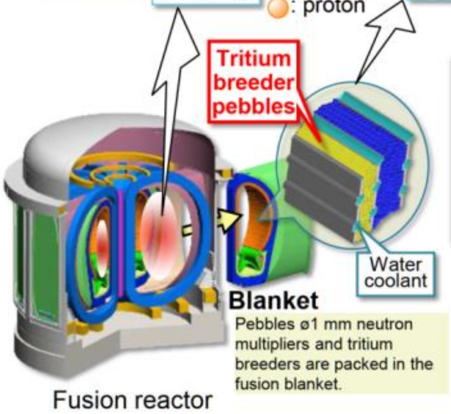

1)Tritium needed as a fuel for fusion reactors is produced via neutron capture by lithium-6 (^{6}Li).
2)However, natural Li contains only about 7.8%
3)^{6}Li Enrichment of ^{6}Li up to 90% is required for adequate tritium breeding in fusion reactors

1: Lithium Recovery
2: ^{6}Li Separation Technology is needed.

2/20

QST

1: Lithium Recovery Technology

3/20

Lithium resources

QST

In South America, lithium is recovered from salt lakes.

Pending issue

Lithium reserve :
South America (80%)

reserve : 30 million tons

Li is recovering from these salt lake for 1-2 years.

Suitable land for Li recovery from these salt lake is limited.

High altitudes

Li demand will exceeds supply in 2025.

Innovative technology of Li recovery is needed.

4/20

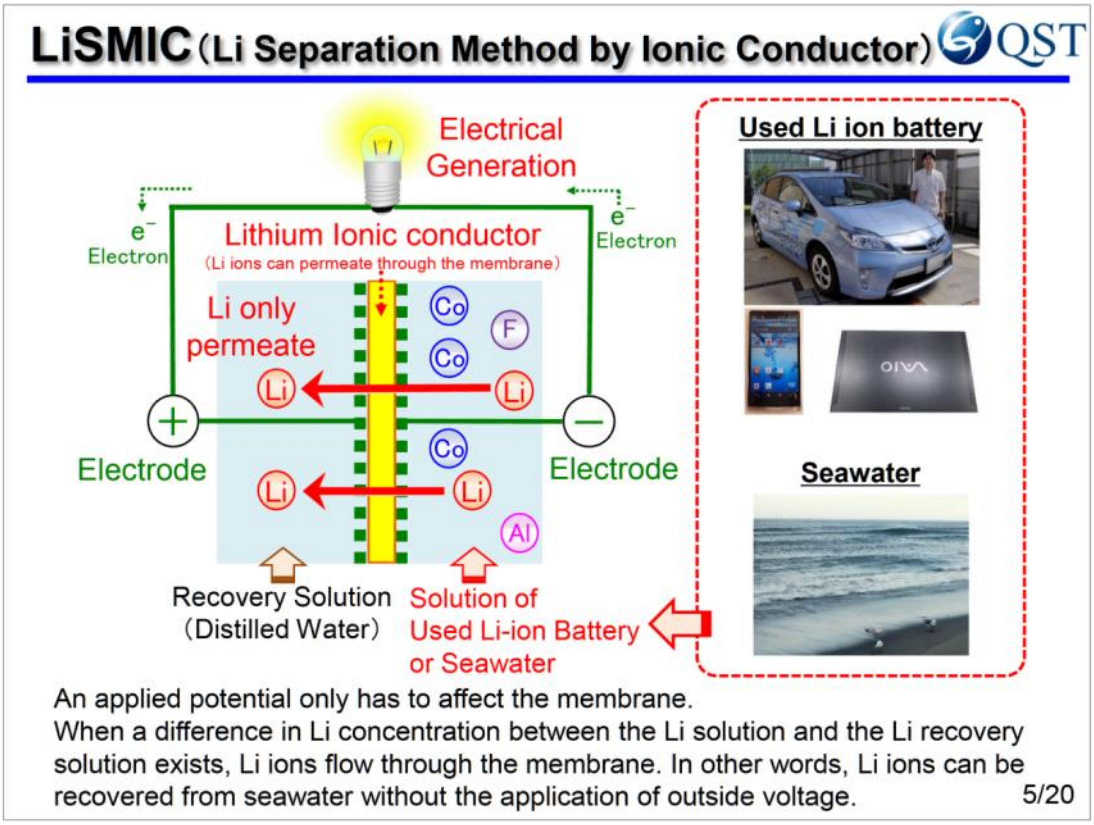
LiSMIC (Li Separation Method by Ionic Conductor)
QST
Electrical Generation
e⁻
Electron
e⁻
Electron
Lithium Ionic conductor
(Li ions can permeate through the membrane)
Li only permeate
Li
Li
Co
F
Co
Co
Al
+
−
Electrode
Electrode
Recovery Solution
(Distilled Water)
Solution of
Used Li-ion Battery
or Seawater
Used Li ion battery
Seawater
An applied potential only has to affect the membrane.
When a difference in Li concentration between the Li solution and the Li recovery solution exists, Li ions flow through the membrane. In other words, Li ions can be recovered from seawater without the application of outside voltage.
5/20

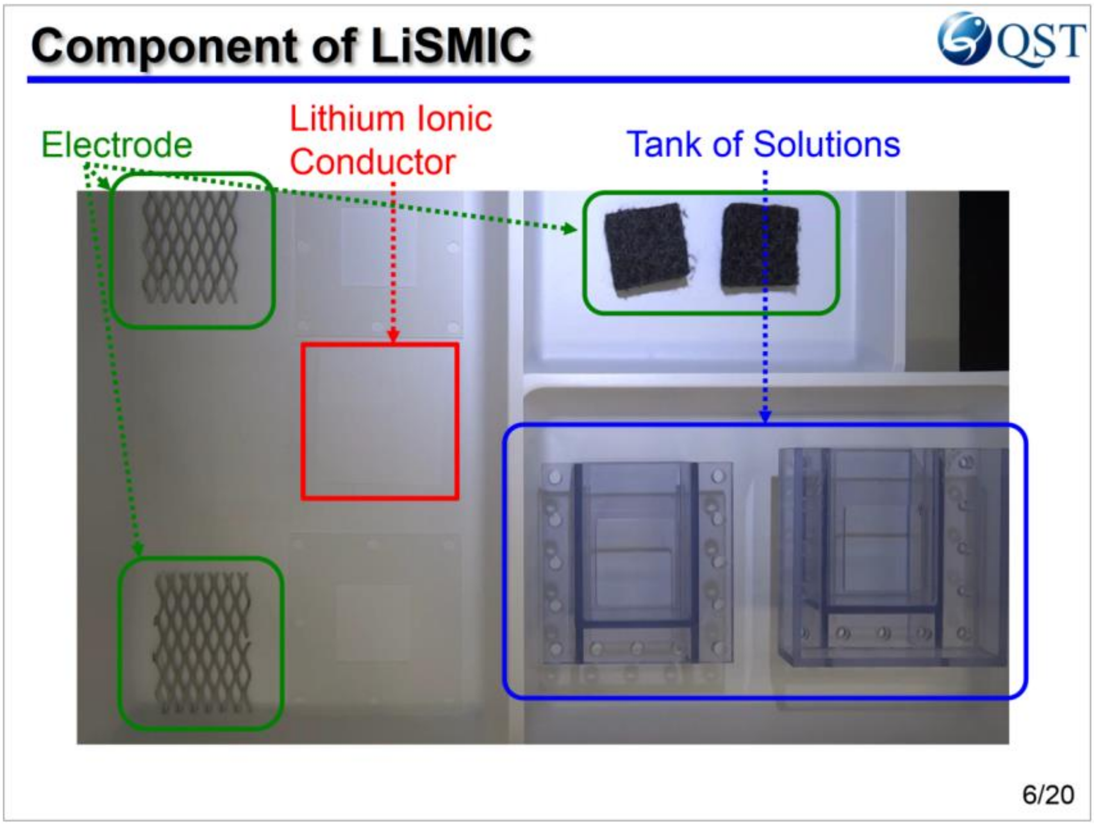
Component of LiSMIC
QST
Electrode
Lithium Ionic Conductor
Tank of Solutions
6/20

Device of LiSMIC

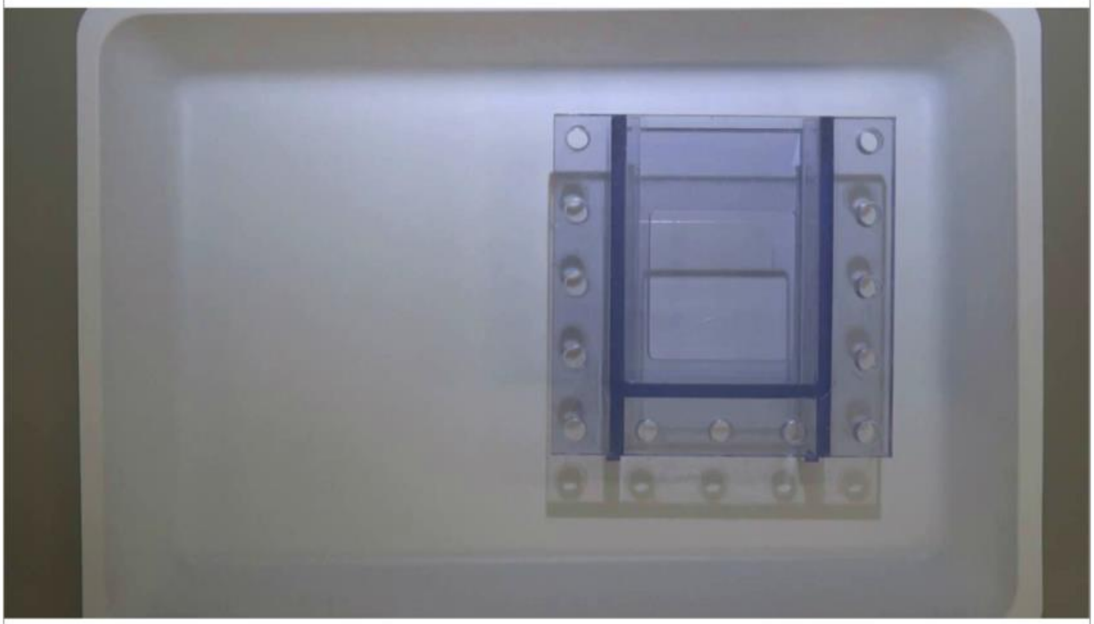

7/20

Electrical Power

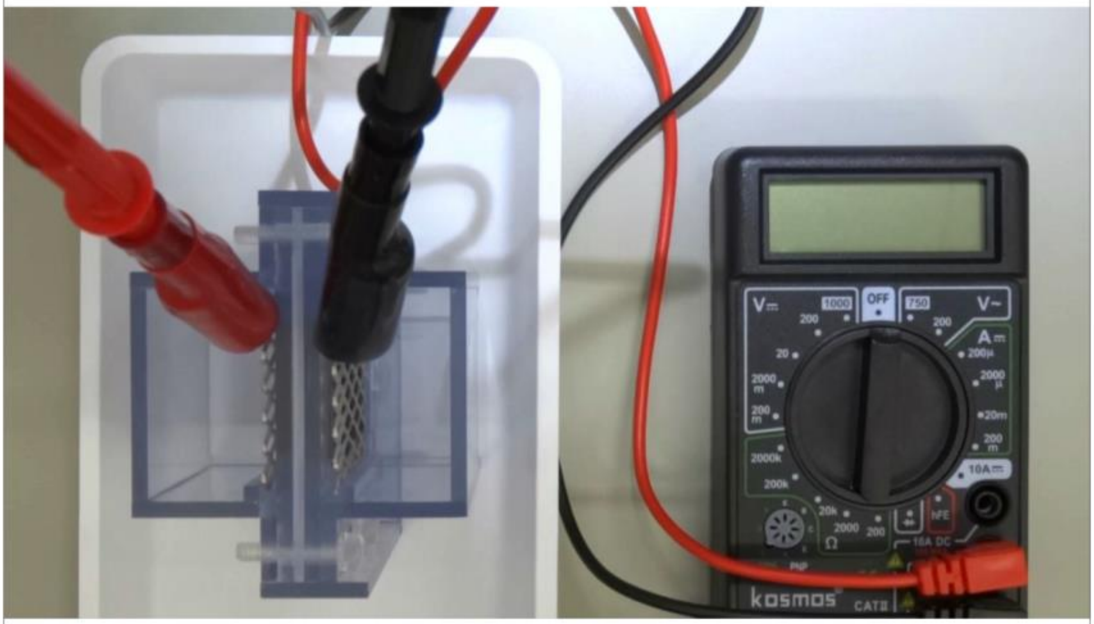

8/20

Lithium Recovery

QST

Positive Electrode Side

LISM: $La_{0.57}Li_{0.29}TiO_3$

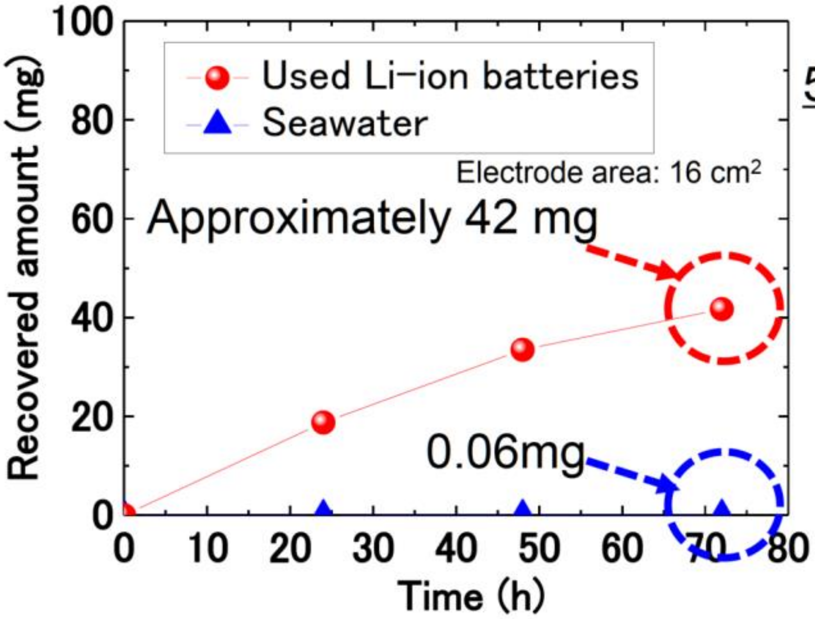

5 V

9/20

QST

2: ^{6}Li Enrichment

10/20

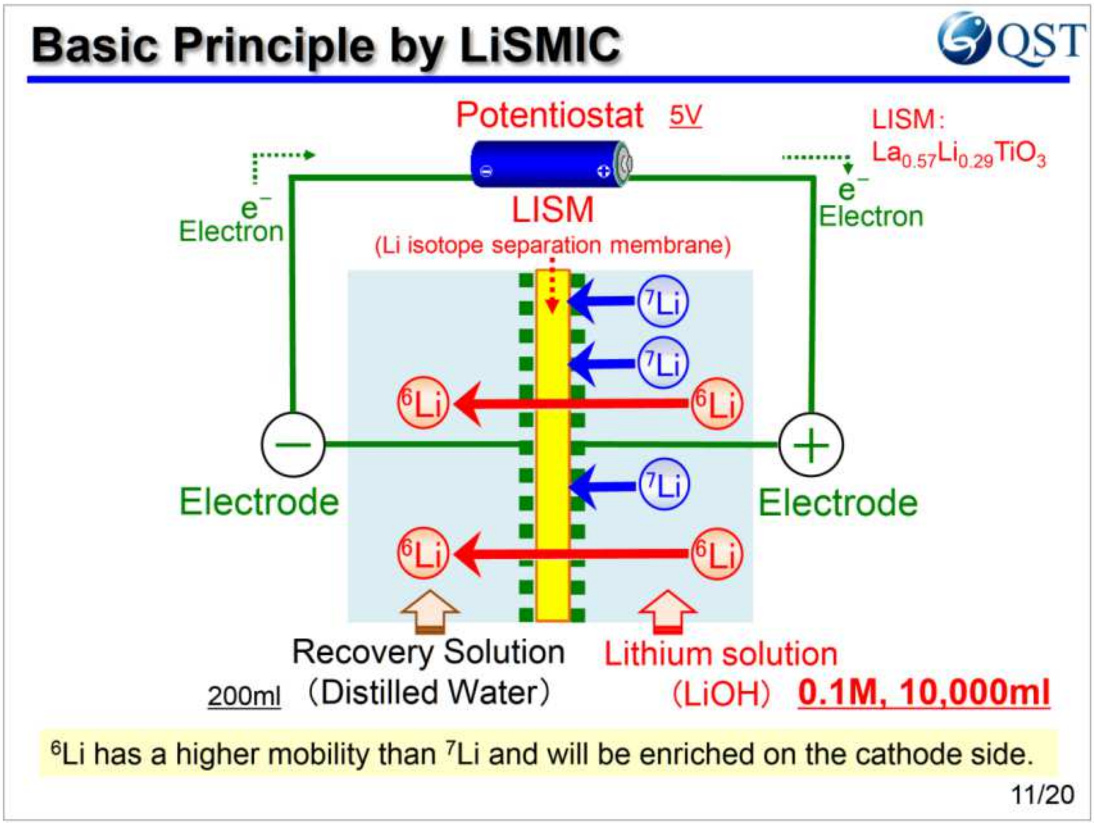
Basic Principle by LiSMIC
QST
Potentiostat 5V
LISM: $La_{0.57}Li_{0.29}TiO_3$
e^- Electron
e^- Electron
LISM
(Li isotope separation membrane)
^7Li
^7Li
^6Li
^6Li
Electrode
Electrode
^7Li
^6Li
^6Li
Recovery Solution
200ml (Distilled Water)
Lithium solution
(LiOH) 0.1M, 10,000ml
^6Li has a higher mobility than ^7Li and will be enriched on the cathode side.
11/20

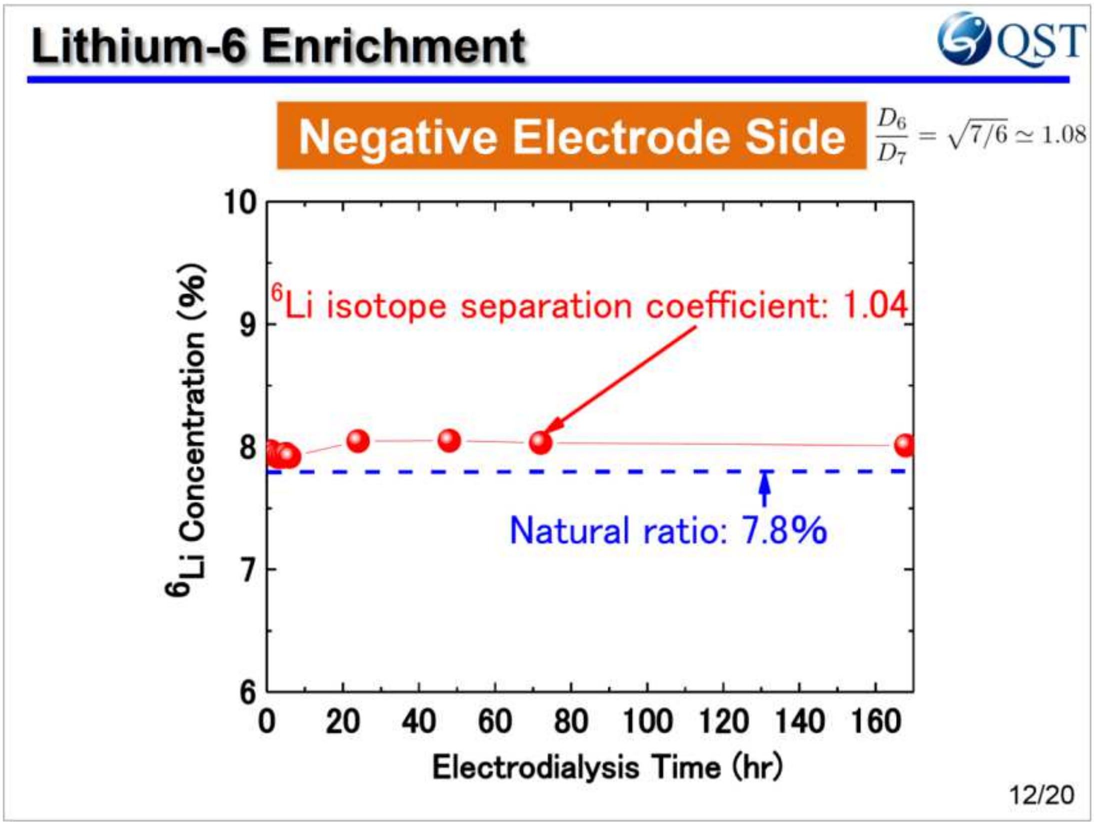
Lithium-6 Enrichment
QST
Negative Electrode Side
$\frac{D_6}{D_7} = \sqrt{7/6} \simeq 1.08$
^6Li isotope separation coefficient: 1.04
Natural ratio: 7.8%
^6Li Concentration (%)
Electrodialysis Time (hr)
10
9
8
7
6
0
20
40
60
80
100
120
140
160
12/20

Lithium-6 Enrichment

QST

Positive Electrode Side

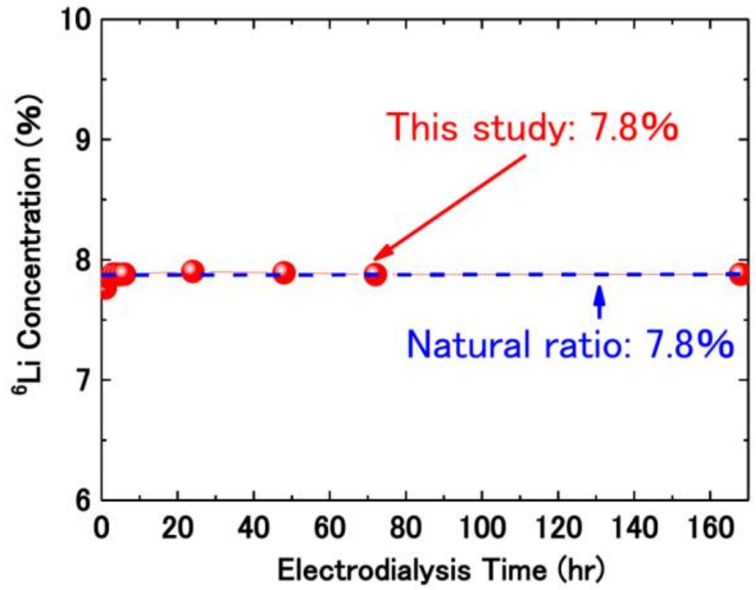

13/20

Long-Term Experimental

QST

Negative Electrode Side

Theoretical coefficient $\frac{D_6}{D_7} = \sqrt{7/6} \simeq 1.08$

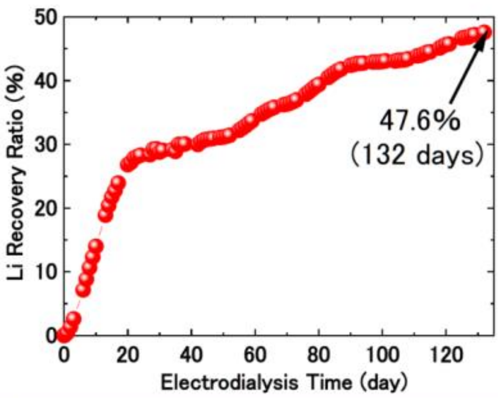

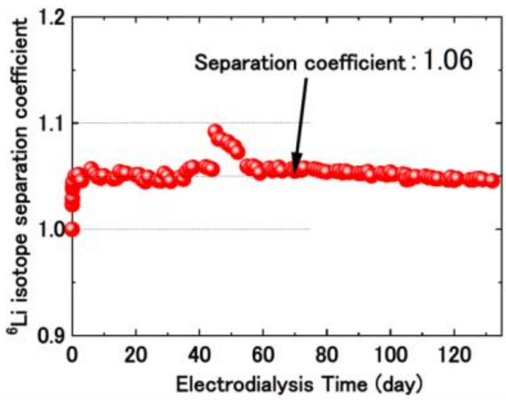

This result showed that the ^{6}Li isotope separation coefficient of this method is the same as that of the amalgamation process using mercury (1.06).

14/20

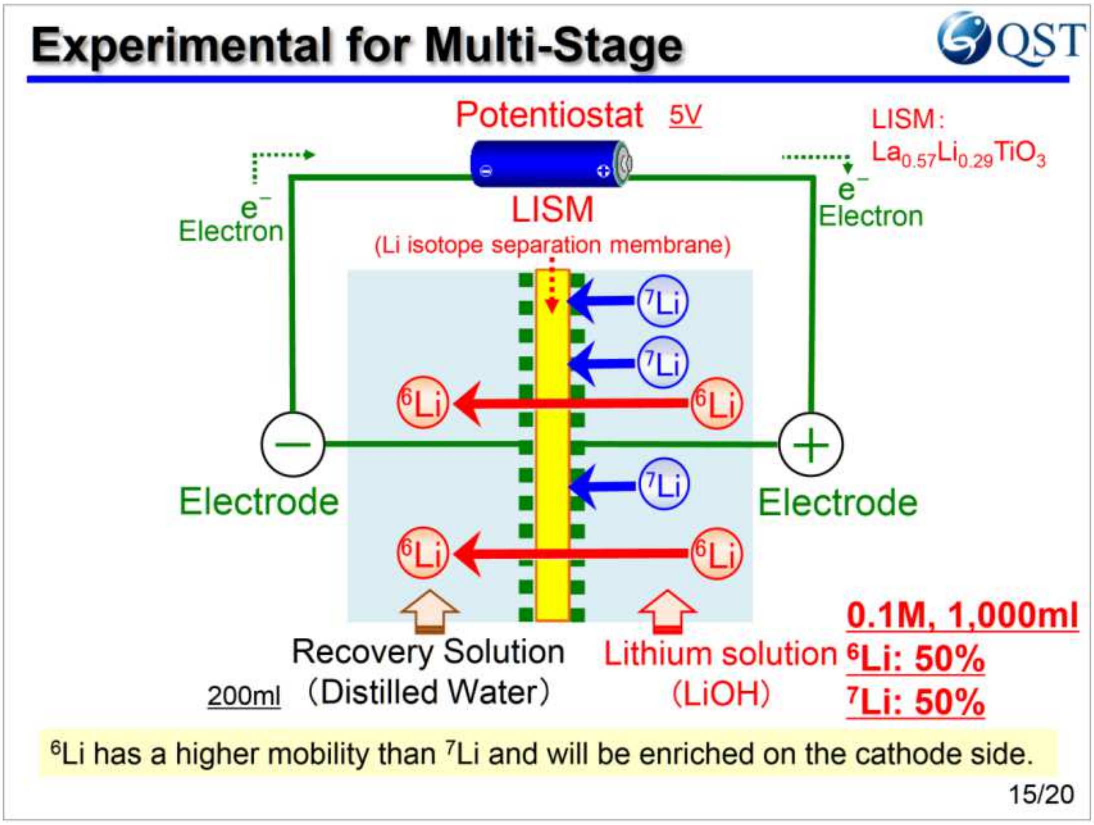
Experimental for Multi-Stage
QST
Potentiostat 5V
LISM: $La_{0.57}Li_{0.29}TiO_3$
e^- Electron
e^- Electron
LISM
(Li isotope separation membrane)
^7Li
^7Li
^6Li
^6Li
Electrode
Electrode
^7Li
^6Li
^6Li
0.1M, 1,000ml
Recovery Solution
200ml (Distilled Water)
Lithium solution
(LiOH)
^{6}Li: 50%
^{7}Li: 50%
^{6}Li has a higher mobility than ^{7}Li and will be enriched on the cathode side.
15/20

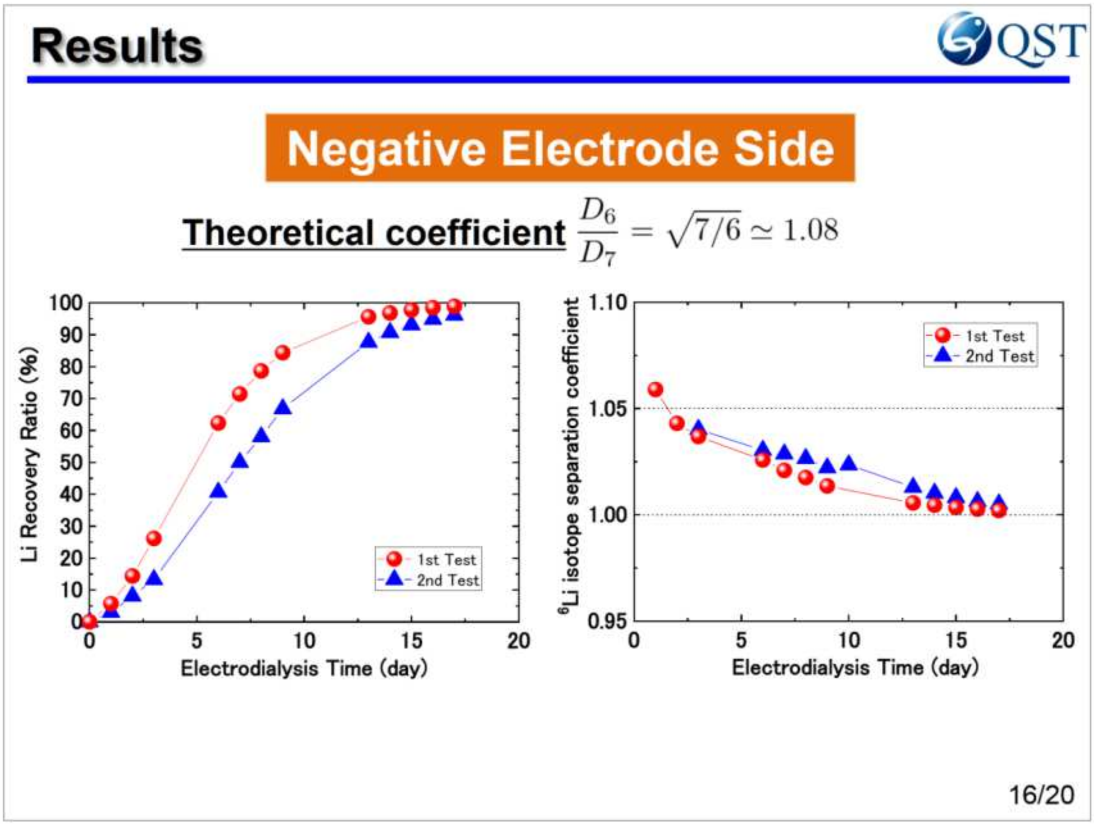
Results
QST
Negative Electrode Side
Theoretical coefficient $\frac{D_6}{D_7} = \sqrt{7/6} \simeq 1.08$
Li Recovery Ratio (%)
Electrodialysis Time (day)
1st Test
2nd Test
^{6}Li isotope separation coefficient
Electrodialysis Time (day)
1st Test
2nd Test
16/20

Results

Negative Electrode Side

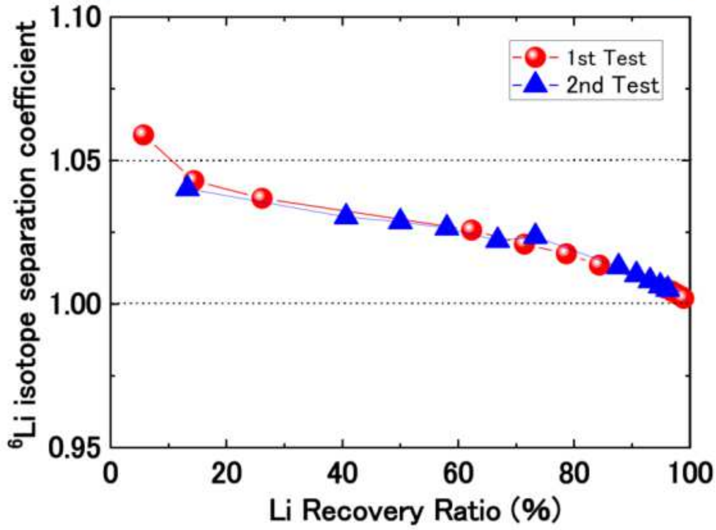

Suitable Li recovery ratio of ^{6}Li isotope separation coefficient is around 50 %.

17/20

Conclusion

18/20

Conclusion

・Using $Li_{0.29}La_{0.57}TiO_3$ (LLTO) as the Li ionic superconductor was prepared, and the relationship between the ^6Li separation coefficient and the LiSMIC time was investigated.

・After LiSMIC, we obtained a maximum of 1.06 for the ^6Li isotope separation coefficient.

・This result showed that the ^6Li isotope separation coefficient of this method is the same as that of the amalgamation process using mercury (1.06).

・Preliminary test of Multi-stage was performed successfully.

・Thus, LiSMIC has the potential to be a superior ^6Li enrichment method to produce 90% enriched tritium breeder for fusion reactors.

19/20

Thank you for your kind attention !

20/20

Computational Analyses of Fast Ion Conductors for Efficient Separation of Lithium-6

Kenji Morita, Tsuyoshi Hoshino

Rokkasho Fusion Institute, National Institute for Quantum and Radiological Science and Technology (QST), 2-166 Oaza Obuchi Aza Omotedate, Rokkasho, Aomori, 039-0212, Japan.

Lithium-6 (^{6}Li) is an indispensable element for providing tritium as a fuel for fusion reactors through the neutron capture reaction. However, its fraction is only about 7.6% in nature, such that the remaining is ^{7}Li. Thus, an efficiently separation and concentration method is demanded because up to 90% enrichment of ^{6}Li is required in order to have adequate tritium breeding in many fusion reactor concepts. While various methods such as amalgam, eletromigration and chromatography were examined, most of them are not practically applicable or may cause environment hazards. Recently, one of the authors (T.H.) has proposed to apply electrodialysis of aqueous solution containing Li ions by making use of fast Li-ion conductors as a separation membrane. The different mobility of ^{6}Li and ^{7}Li due to the lighter mass of ^{6}Li allows for faster permeation of ^{6}Li from one solution to the other through the membrane, resulting in slightly higher ^{6}Li fraction. Properly repeating the procedure may lead to the desired enrichment.

To achieve the efficient separation, the choice of the ion-conducing material is of central importance. Solid electrolytes exhibiting high ionic conductivity such as lithium lanthanum titanate (LLTO) are promising candidates. In this work we focus on inorganic solid electrolytes. According to the transient state theory which is the classical theory of the ionic transport in solid, the separation efficiency which can be characterized by the ratio of the diffusion coefficient of ^{6}Li and ^{7}Li is related to the inverse of the mass ratio, $D_6/D_7 \sim \sqrt{m_7/m_6} \sim 1.08$. However, actual efficiency can take a larger or smaller value since it depends on detailed conduction mechanism of Li ions. Thus, it is desirable to understand the conduction mechanism of Li ions and to identify the one maximizing the separation efficiency.

For this purpose, we conduct ab-initio molecular dynamics simulations of ^{7}Li and ^{6}Li transport in ion-conducting materials with the VASP code which is based on the density functional theory. We examine several fast Li-ion conductors which are found by explicitly calculating ionic conductivity after screening from randomly selected materials from the Inorganic Crystal Structure Database (ICSD). By comparing the results of those materials, we discuss the relationships among the diffusion coefficient, conduction mechanism, and the separation efficiency to find out the optimal condition for the efficient isotope separation.

Computational Analyses of Fast Ion Conductors for Efficient Separation of Lithium-6

Kenji Morita

(Rokkasho Fusion Inst. QST)

Collaborator: Tsuyoshi Hoshino (QST)

Acknowledgement: Numerical works are done with IFERC-CSC

QST

^{6}Li: Indispensable for Nuclear Fusion

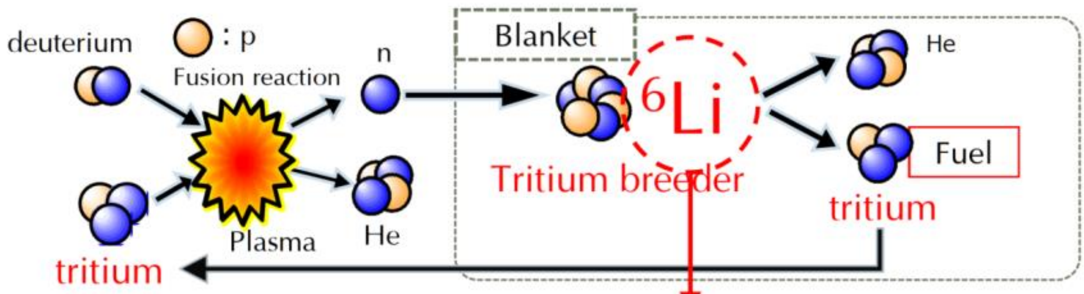

Fusion needs tritium

Li: Extract from brine, seawater etc…
^{6}Li: only 7.6% fraction in nature – enrichment necessary

QST

Novel ^{6}Li Separation Technique

- Electrodialysis using ionic conductor

See T. Hoshino's talk for experimental details

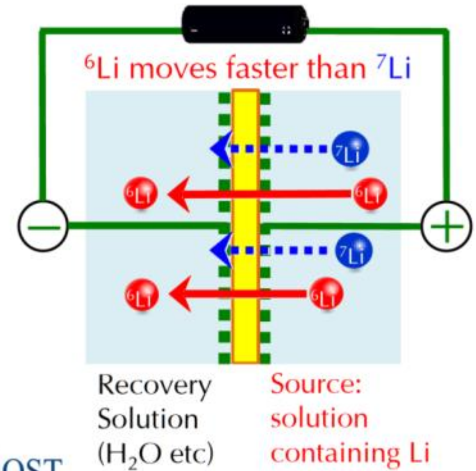

Li ionic conductor : crucial role

- Pass Li only
- Faster conduction, more efficient
- Understand conduction mechanism → finding suitable materials
- Transition state theory (classical jump):

$$D_6/D_7 \sim \sqrt{m_7/m_6} \simeq 1.08$$

Many-body effects can enhance the separation efficiency*

*see e.g., : K. Kobayashi and T. Hoshino, Fusion Eng. Des. 136, 205 ('18)

QST

Goal: Finding Fast (Large $D_{6,7}$) and Efficient (D_6 / D_7 > 1.08) Li-ion conductors

from Computational Approaches

QST

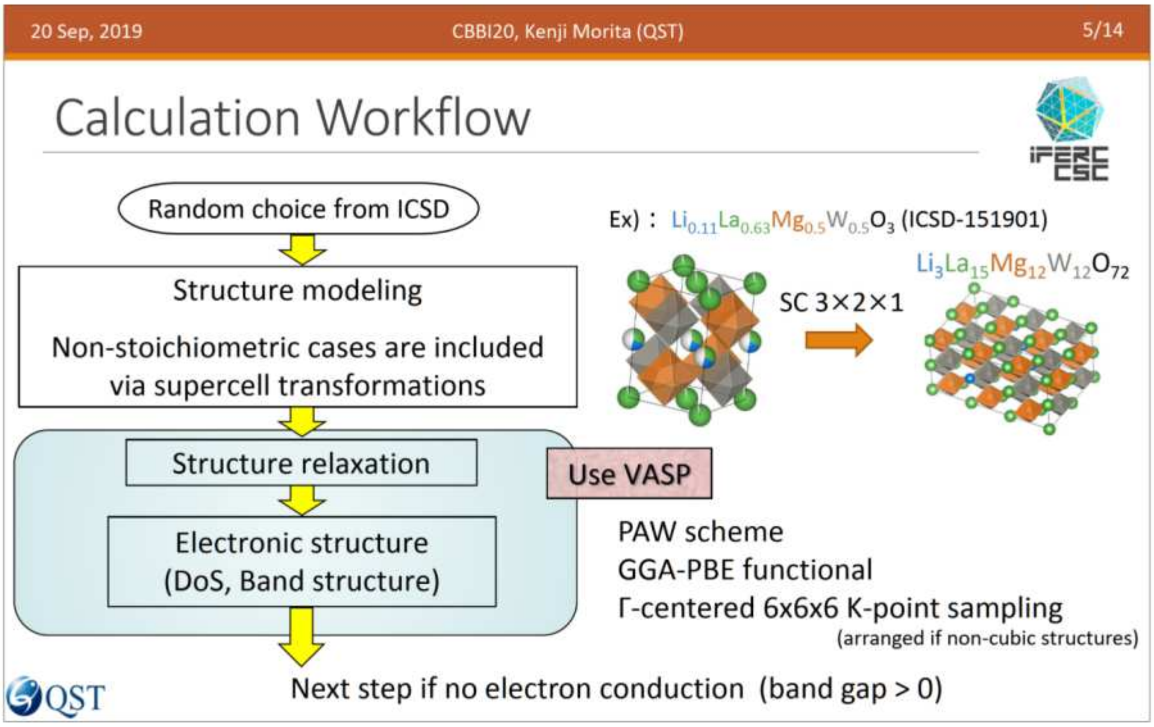
20 Sep, 2019
CBBI20, Kenji Morita (QST)
5/14
Calculation Workflow
Random choice from ICSD
Structure modeling
Non-stoichiometric cases are included via supercell transformations
Structure relaxation
Electronic structure (DoS, Band structure)
Ex) : $Li_{0.11}La_{0.63}Mg_{0.5}W_{0.5}O_3$ (ICSD-151901)
SC 3×2×1
$Li_3La_{15}Mg_{12}W_{12}O_{72}$
Use VASP
PAW scheme
GGA-PBE functional
Γ-centered 6x6x6 K-point sampling
(arranged if non-cubic structures)
Next step if no electron conduction (band gap > 0)
QST

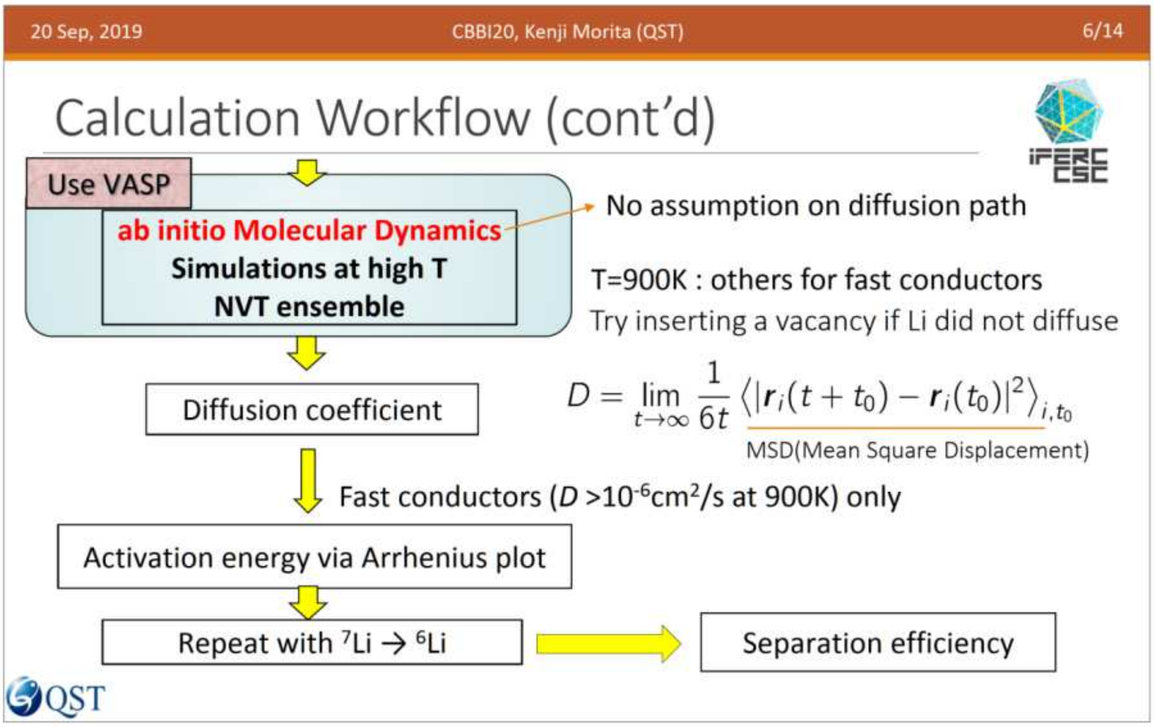
20 Sep, 2019
CBBI20, Kenji Morita (QST)
6/14
Calculation Workflow (cont'd)
Use VASP
ab initio Molecular Dynamics
Simulations at high T
NVT ensemble
No assumption on diffusion path
T=900K : others for fast conductors
Try inserting a vacancy if Li did not diffuse
Diffusion coefficient
$D = \lim_{t\to\infty} \frac{1}{6t} \underbrace{\langle |\boldsymbol{r}_i(t+t_0) - \boldsymbol{r}_i(t_0)|^2 \rangle_{i,t_0}}_{\text{MSD(Mean Square Displacement)}}$
Fast conductors ($D > 10^{-6} cm^2/s$ at 900K) only
Activation energy via Arrhenius plot
Repeat with $^7Li \rightarrow {}^6Li$
Separation efficiency
QST

Material Screening (Random)

Li Conduction Property	Vacancy Insertion	# of Structures	Comment
Nonzero Bandgap		67	out of 122
No Li conduction	✓	18	
Slow Li Conduction		1	$D \sim 10^{-7}$ cm^2/s at 900K
	✓	6	
Fast Li Conduction		10	6 melt at high T
	✓	6	Potentially useful for partial substitution

Machine learning will improve the screening...(next step)

QST

Numerical Results: MSD of a Slow Conductor

- Ex.1 : tetragonal LLZO (Garnet/ICSD-183684), T=900K

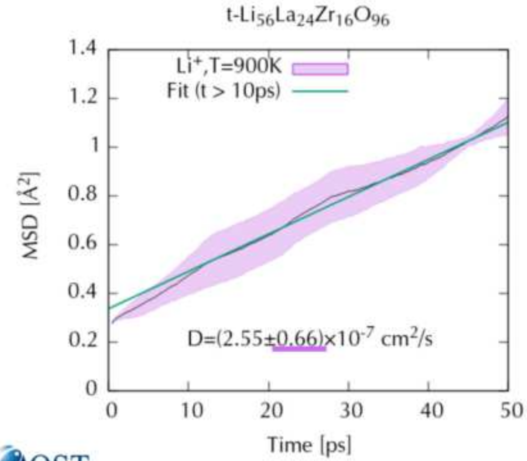

- ✓ Simulation time: 84ps (42,000 steps)
- ✓ Error estimation is important to discuss isotope effect
- ✓ Statistical errors of MSD (band) and Diffusion coefficients estimated by the Jackknife method
- ✓ $D = (2.55 \pm 0.66) \times 10^{-7}$ cm^2/s :
  - Slow conductor
  - Still large stat. error

QST

Numerical Results: Isotope effect

- Ex.1 : tetragonal LLZO (Garnet/ICSD-183684), T=900K

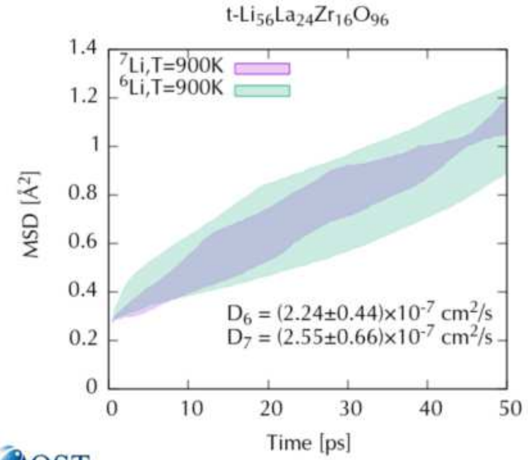

✓ Simulation time

^{7}Li 84ps (42,000 steps)

^{6}Li 129ps (64,500 steps)

$D_6/D_7 = 0.878 \pm 0.283$

Consistent with 1.08

Clearly, need more statistics to say something....

QST

Numerical Results: MSD of a Fast Conductor

- Ex.2 : LGPS (known Li-superionic sulfide/ICSD-188886)

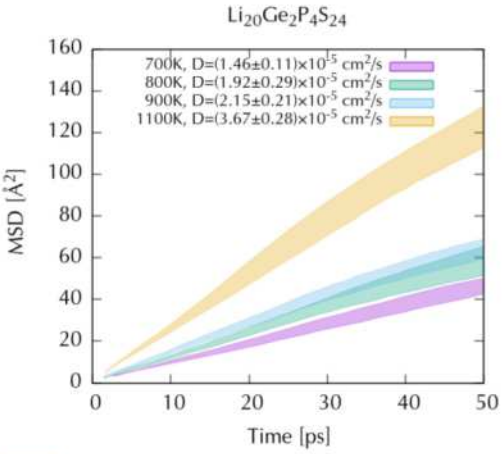

✓ Simulation time: 163-536 ps

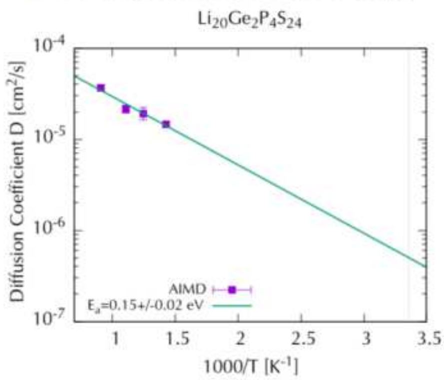

QST

Numerical Results: MSD of a Fast Conductor

- Ex.2 : LGPS (known Li-superionic sulfide/ICSD-188886)

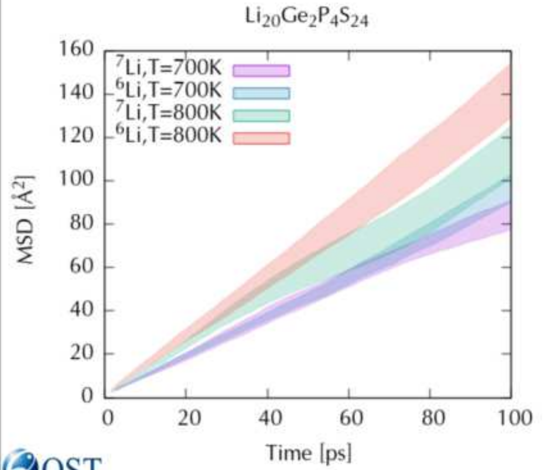

- ✓ MSD overlap even with longer simulation time
- ✓ Temperature dependence of D_6/D_7: statistically <u>not significant</u>

Temperature [K]	D_6/D_7
700	1.218±0.111
800	1.216±0.216
900	1.346±0.249
1100	1.043±0.191

QST

Comparison of ^{6}Li and ^{7}Li diffusion

- Probability distribution of displacement $|d\boldsymbol{r}| = \langle|\boldsymbol{r}_i(t+t_0) - \boldsymbol{r}_i(t_0)|\rangle_i$

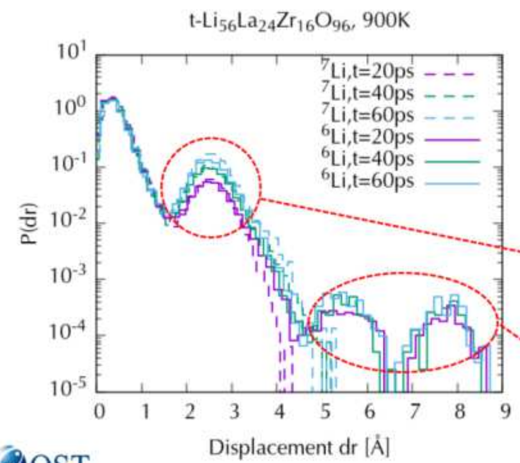

LLZO : Vacancy migration

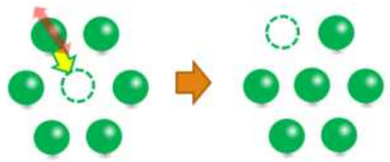

Jump to neighboring sites

^{6}Li exhibit further jumps

Too small probability to affect D_6

QST

Comparison of ^{6}Li and ^{7}Li diffusion

- Probability distribution of displacement $|d\boldsymbol{r}| = \langle |\boldsymbol{r}_i(t+t_0) - \boldsymbol{r}_i(t_0)| \rangle_i$

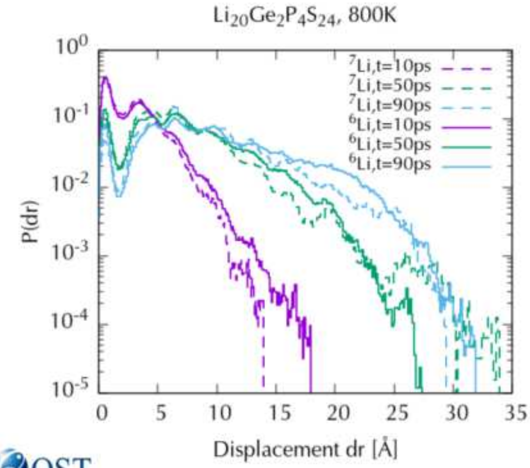

LGPS Diffusion mechanism: interstitial
Smoother distribution

Wider distribution of ^{6}Li:
Faster diffusion expected
Note: Width $\propto$ Dt

QST

Summary and Outlook

- Isotope effect in Li-ion conductors
- Computational search scheme for fast ion conductors with efficient separation capability
- Ab initio MD simulation : error estimation is important! Computationally expensive to see the difference in the diffusion coefficients D_6 and D_7
- Probability distribution shows differences between ^{6}Li and ^{7}Li depending on diffusion mechanism

- Future plan: Machine Learning (training with computed data) for screening
- Identification of diffusion path of fast ion conductors : more accurate estimation of D_6/D_7

QST

Lithium-6 availability and an assessment of enrichment strategies

Julia M. Heuser[a], Regina Knitter[a], Sehila M. Gonzalez de Vicente[b]

[a]Institute for Applied Materials (IAM), Karlsruhe Institute of Technology (KIT), 76021 Karlsruhe, Germany

[b]Department of Nuclear Sciences and Applications, International Atomic Energy Agency (IAEA), 1400 Vienna, Austria

For future fusion reactors, tritium and deuterium are intended to be used as fuel. While deuterium is abundant in seawater and can be implemented in the fusion reaction directly, tritium has to be bred from lithium. Therefore, a sufficient supply of lithium will be of crucial importance for all tritium breeding materials. For fusion technology, materials enriched with the isotope Li-6 are required to produce tritium by an exothermic reaction with thermal neutrons. Depending on the breeder material, enrichments in Li-6 of 60–90 % are required to ensure an adequate tritium breeding ratio of slightly above one for a self-sustained fusion reaction. Since natural lithium contains only 7.6 % Li-6 beside 92.4 % Li-7, efficient Li-6 enrichment and procurement strategies are needed.

In this survey, firstly the availability of lithium will be examined. Secondly the need of Li-6 for future fusion technology will be as assessed. Here, the focus will be on the EU solid breeder concept and the possible usage of advanced ceramic breeder materials consisting of Li_4SiO_4 with additions of Li_2TiO_3 in helium cooled pebble bed (HCPB) blankets. Moreover, several isotope separation methodologies will be described and discussed with regard to achieving an efficient Li-6 enrichment. In this regard, the different methods will be compared and evaluated with respect to fusion technology.

As the lithium resources appear to provide enough raw material, this topic is often neglected in fusion technology. This study should help to understand the necessity of finally taking into account the Li-6 supply on the path to DEMO and subsequent future fusion power plants.

Karlsruhe Institute of Technology

Lithium-6
availability and an assessment of enrichment strategies

Julia M. Heuser, Regina Knitter, Sehila M. Gonzalez de Vicente

INSTITUTE FOR APPLIED MATERIALS – IAM-ESS

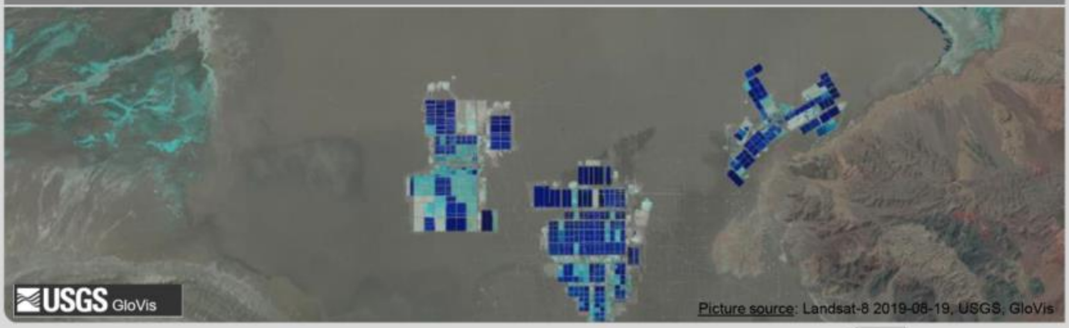

KIT – The Research University in the Helmholtz Association

www.kit.edu

Karlsruhe Institute of Technology

Part I: Global lithium availability

Part II: Lithium-6 enrichment strategies

2 20.09.2019 CBBI-20 – Heuser et al.: Lithium-6 availability and an assessment of enrichment strategies IAM-ESS

Lithium availability

Resources 61 Mt
Naturally occurring lithium, which is or might become of economic interest.

Reserves 14 Mt
Part of resources that can be economically extracted with current technologies.

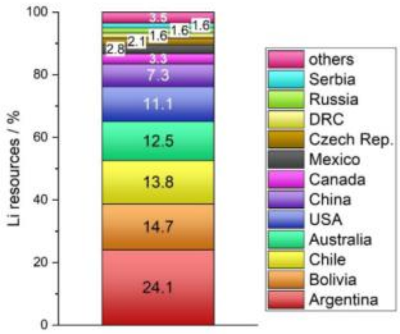

others = Zimbabwe, Mali, Spain, Brazil, Germany, Peru, Portugal, Austria, Finland, Kazakhstan, and Namibia; each country <1 %

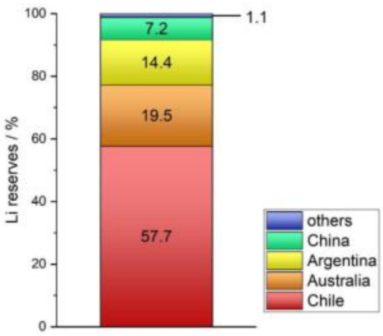

others = Zimbabwe, Brazil, and USA; each country <1 %

Data source: U.S. Geological Survey 2019

3 20.09.2019 CBBI-20 – Heuser et al.: Lithium-6 availability and an assessment of enrichment strategies IAM-ESS

Lithium sources

Brines	Minerals	Seawater
e. g. in Chile, Argentina, Bolivia, China, USA	e. g. in Australia, China, USA	global
200-1500 ppm	17-20 ppm, up to 60 ppm	0.17 ppm
• Production from salt lakes • Potential sources: geothermal and oilfield brines	• Production from pegmatites (spodumene (Al-silicate)) • Potential sources: hectorite (clay) and jadarite (B-silicate)	• Not considered as resource!

4 20.09.2019 CBBI-20 – Heuser et al.: Lithium-6 availability and an assessment of enrichment strategies IAM-ESS

Lithium from brines

- Solar evaporation for 1–2 years
- No flexible response to market changes
- High Mg/Li and SO_4/Li increase the production costs
- Mainly Li_2CO_3
- Largest deposit: “Li-triangle”, Southamerica

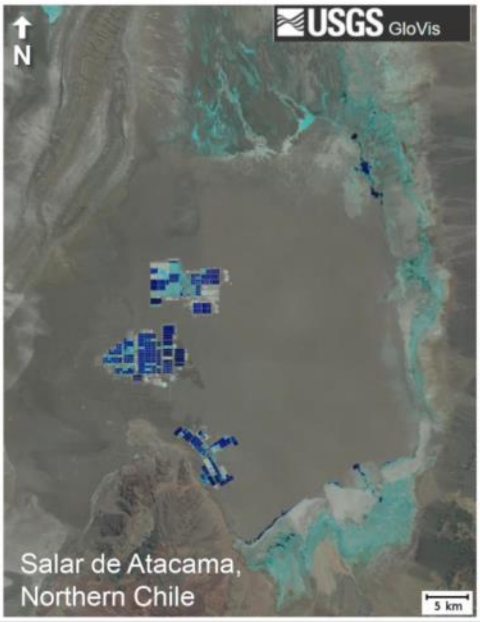

Picture source: Landsat-8 2019-08-19, USGS, GloVis

5 20.09.2019 CBBI-20 – Heuser et al.: Lithium-6 availability and an assessment of enrichment strategies IAM-ESS

Lithium extraction from brines

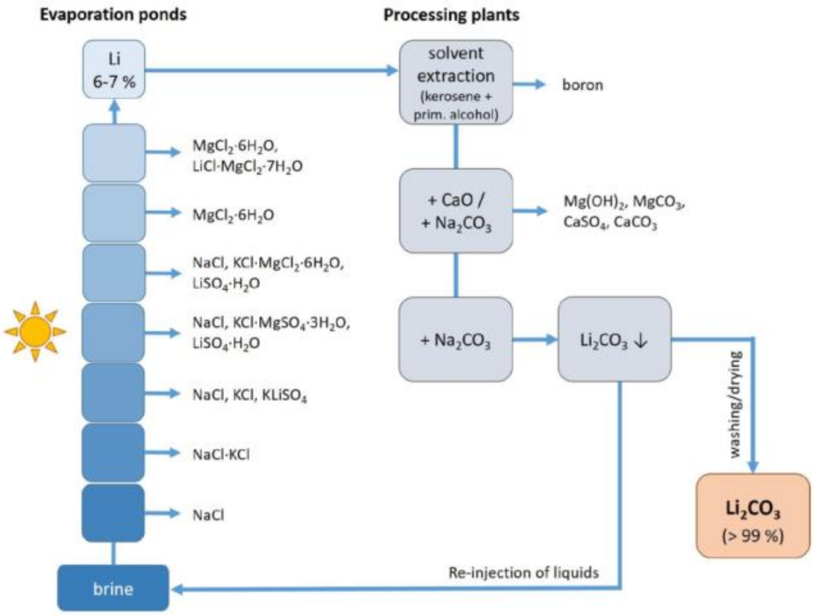

Further information e. g. in:
Garrett, *Handbook of lithium and nat. calcium chloride*, Elsevier (2004)
Choubey et al., Miner. Eng. 89 (2016) 119–137

6 20.09.2019 CBBI-20 – Heuser et al.: Lithium-6 availability and an assessment of enrichment strategies IAM-ESS

Lithium from minerals

KIT Karlsruhe Institute of Technology

- Main mineral: spodumene
- Advantage: low Mg/Li
- Li_2CO_3, LiOH
- Largest deposit: Greenbushes, Australia

Please find photos of the largest deposit "Greenbushes" in Australia here:
http://en.tianqilithium.com; https://www.mindat.org/loc-11514.html; www.miningglobal.com

7 20.09.2019 CBBI-20 – Heuser et al.: Lithium-6 availability and an assessment of enrichment strategies IAM-ESS

Lithium extraction from minerals

KIT Karlsruhe Institute of Technology

- Chemical extraction methods such as:
  - Sulfation
  - Carbonation
  - Chlorination
  - Fluorination
  - Alkali digestion

Example for spodumene:

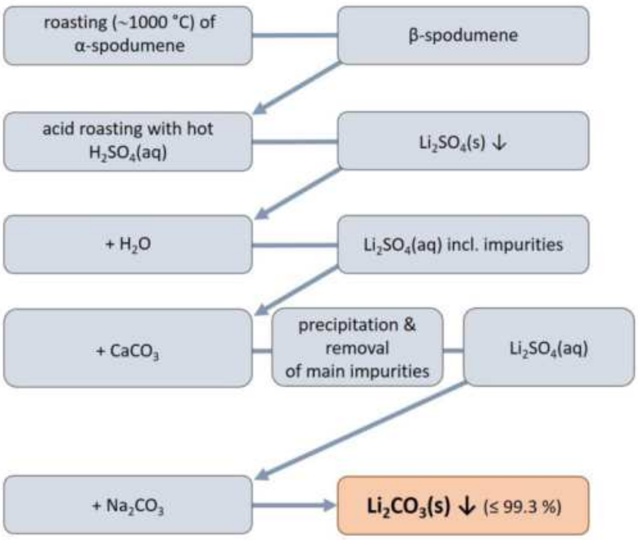

Further information e. g. in:
Garrett, *Handbook of lithium and nat. calcium chloride*, Elsevier (2004)
Choubey et al., Miner. Eng. 89 (2016) 119–137

8 20.09.2019 CBBI-20 – Heuser et al.: Lithium-6 availability and an assessment of enrichment strategies IAM-ESS

Lithium production

KIT Karlsruhe Institute of Technology

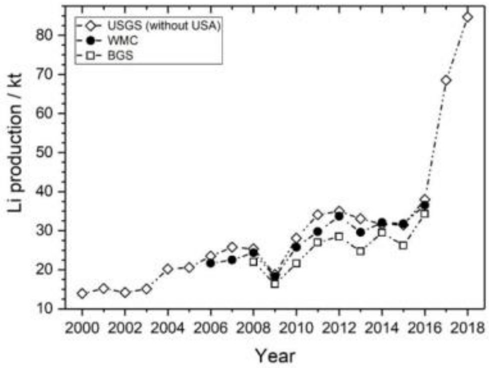

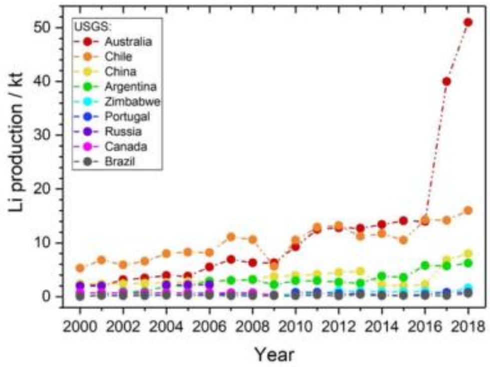

- Global Li production increased significantly since 2016 due to an intensified spodumene production in Australia
- 4 countries dominate the production with > 90 % *(AUS, CHL, ARG, CHN)*
- 4 producers dominate the supply with > 80 % *(Albemarle, SQM, Tianqi, FMC)*

Data sources: USGS = U. S. Geological Survey, WMC = World Mining Congress, BGS = British Geological Survey

9 20.09.2019 CBBI-20 – Heuser et al.: Lithium-6 availability and an assessment of enrichment strategies IAM-ESS

Lithium consumption

KIT Karlsruhe Institute of Technology

- Battery industry overtook ceramics & glass sector in 2015
- Further rapid grow in battery sector
- Expected growth of traditional industries with GDP

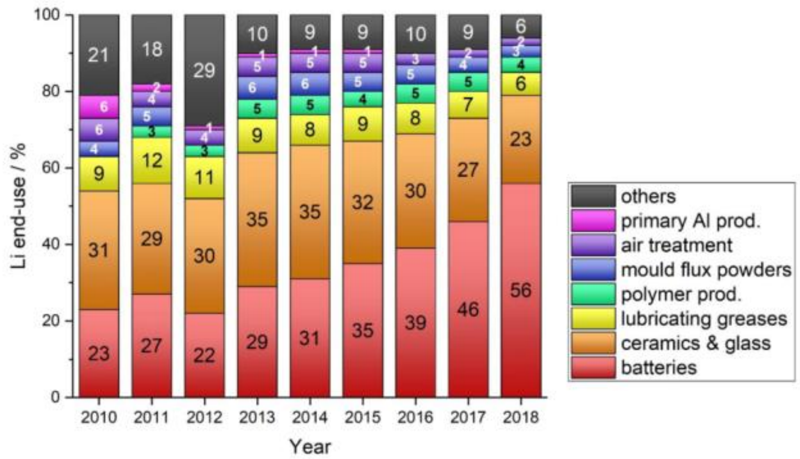

Data source: U.S. Geological Survey 2011–2019

10 20.09.2019 CBBI-20 – Heuser et al.: Lithium-6 availability and an assessment of enrichment strategies IAM-ESS

Lithium needs for fusion

- DEMO power plant considering the 2 most promising blanket concepts

- **HCPB** (60 % Li-6)
  65-LOS + 35-LMT
  134 t CB needed:
  25 t Li, incl. 14 t Li-6

- **WCLL** (90 % Li-6)
  Pb-16Li
  ~8204 t LB needed:
  46 t Li, incl. 41 t Li-6

- DEMO lifetime: ~7-8 FPY; blanket lifetime: ~3 FPY
- Reprocessing of CB possible after ~15 a → not applicable for DEMO

> 3× blanket fillings required
> Amount of Li-nat needed represents ~1 % of global production of ~85 kt (estd. for 2018)

CB = ceramic breeder; LB = liquid breeder
LOS = Li_4SiO_4; LMT = Li_2TiO_3

Part I: Global lithium availability

Part II: Lithium-6 enrichment strategies

Lithium isotope separation strategies

Chemical exchange reactions	Electrochemical separation	Others
• Ion exchange • Complexation • Amalgamation • Intercalation • Liquid ammonia based separation	• Electrolysis • Electrophoresis, electromigration & electrodialysis • Electrodeposition • Insertion / intercalation	• Electromagnetic isotope separation (EMIS) • Laser isotope separation (LIS) • Thermal diffusion • Distillation • Fractional crystallisation • Zone melting • Radiofrequency spectroscopy

13 20.09.2019 CBBI-20 – Heuser et al.: Lithium-6 availability and an assessment of enrichment strategies IAM-ESS

Chemical exchange reactions

Ion exchange

- Inorganic ion exchangers
  - zeolites, hydrated metal oxides, zirconium phosphates, titanates
  - preferential uptake of Li-6

Complexation

- (Poly)cyclic organic complexing agents
  - Li extraction is isotope selective; usually with a preferred uptake of Li-6

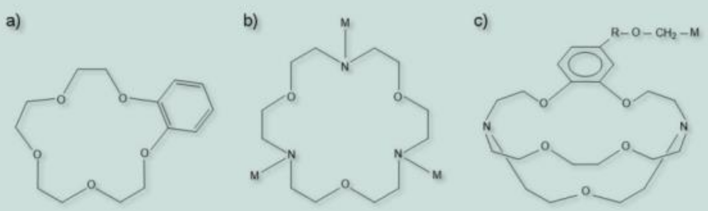

a) Benzo-15-crown-5 ether (B15C5) b) N3O3 azacrown ether c) [2B,2,1] cryptand

14 20.09.2019 CBBI-20 – Heuser et al.: Lithium-6 availability and an assessment of enrichment strategies IAM-ESS

Chemical exchange reactions

KIT Karlsruhe Institute of Technology

Amalgamation

- Li-6 has a higher affinity for mercury
- Columns: $^7Li\,(Hg) + {}^6LiOH\,(aq) \rightleftharpoons {}^6Li\,(Hg) + {}^7LiOH\,(aq)$
- Decomposer: $Li\,(Hg) + H_2O \underset{-Hg}{\rightarrow} LiOH + ½\,H_2$

Historical background:

- Production scale
- COLEX was main process for Li-6 in the USA (enrichment up to 95.5 %)
- >300 t Hg were released to the environment

Please find a schematic of the COLEX process here:
U. S. DOE, *Linking Legacies - Connecting the Cold War nuclear weapons production processes to their environmental consequences*, rep.-no. F2002-00544 (1997) appendix-B, fig. B-7.

15 20.09.2019 CBBI-20 – Heuser et al.: Lithium-6 availability and an assessment of enrichment strategies IAM-ESS

Electrochemical separation

KIT Karlsruhe Institute of Technology

Electrochemical insertion/intercalation

- Li-6 is preferentially inserted in the cathode or
- Li-6 is preferentially intercalated in a graphite anode

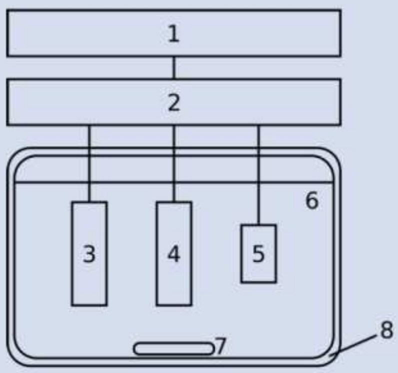

1) data acquisition unit
2) current supply
3) cathode *(e. g., Ga, Zn, Sn, SnO_2; $LiCoO_2$)*
4) anode *(e. g., Li; graphite)*
5) optional reference electrode
6) electrolyte sol. *(e. g., EC:MEC (1:2))*
7) optional stirrer
8) electrolytic cell

EC = ethylene carbonate,
MEC = methyl ethyl carbonate

16 20.09.2019 CBBI-20 – Heuser et al.: Lithium-6 availability and an assessment of enrichment strategies IAM-ESS

Others

EMIS

- Calutron = *California university cyclotron*
- Main purpose: enrichment of U-235
- 235 isotopes of 56 elements by 1987 (3 kg of Li)

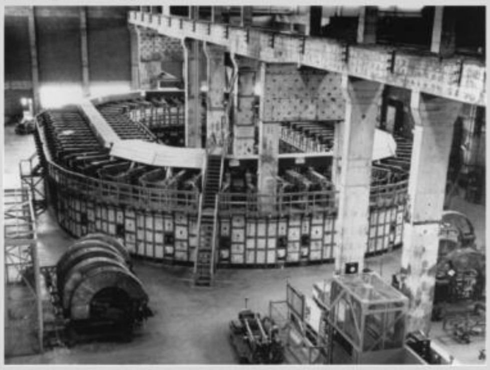

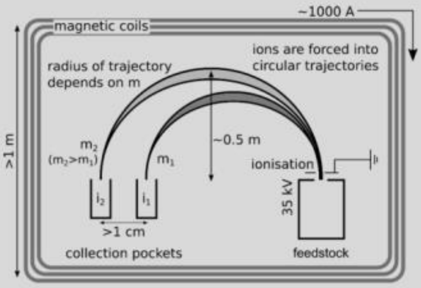

Photos by: U. S. DOE; schematic mod. after: Mazur, PhD thesis, Springer (2016)

Evaluation of Li IS strategies

- 7 criteria were chosen for the assessment
- Direct comparison of published IS strategies is challenging due to
  - degree of given information
  - time of the experiments and the resp. state-of-the-art technologies
- 1st stage assessment using a simple 3-point system (-1, 0, 1)
  - 0 = neutral incl. when no information is given or no profound assumption can be made
- Interpretation of the assessment results

Evaluation of Li IS strategies

Techniques...

- ... with **high potential**:
  - complexation (organic) and
  - amalgamation (COLEX).

- ... with **low potential**:
  - radiofrequency spectroscopy,
  - fractional crystallisation,
  - zone melting,
  - distillation,
  - thermal diffusion,
  - electrodeposition,
  - EMIS (calutron), and
  - LIS (e. g., MAGIS).

- ... with **medium potential**:
  - liquid ammonia based techniques,
  - electrochemical techniques (electrophoresis/-migration/ -dialysis, insertion/intercalation),
  - amalgamation (ELEX and OREX)
  - intercalation, and
  - ion exchange (inorganic).

Conclusions

- Global lithium resources comprise 61 Mt
  - Found in minerals and brines; seawater is not considered
- Accessible global lithium reserves amount to 14 Mt
  - ➢ With a static production of 85 kt/a there is sufficient Li for 165 a

- Existing strategies were compared and evaluated considering selected criteria.
  - main drawbacks: low efficiencies, high energy consumption, and/or low technical maturity
  - only 2 strategies have the potential to be used in the near future as Li-6 enrichment process:
    - complexation of Li-6 with organic agents
    - amalgamation in a COLEX-type process
  - a COLEX-type process could be implemented with the lowest effort in the near future; mistakes resulting in environmental disasters in the past should not lead to a banishment of this process.

Challenges...

... in fusion technology with regard to lithium

- Establishment on the global lithium market
- Assurance of lithium and in particular Li-6 supply

The »fusion community« should not rely on the U.S. stockpile of Li-6 and the time to think about an appropriate Li-6 enrichment process has come!

21 20.09.2019 CBBI-20 – Heuser et al.: Lithium-6 availability and an assessment of enrichment strategies IAM-ESS

Thank you for your attention!

EUROfusion

This work has been carried out within the framework of the EUROfusion Consortium and has received funding from the Euratom research and training programme 2014-2018 and 2019-2020 under grant agreement No 633053. The views and opinions expressed herein do not necessarily reflect those of the European Commission.

22 20.09.2019 CBBI-20 – Heuser et al.: Lithium-6 availability and an assessment of enrichment strategies IAM-ESS

KIT Scientific Working Papers
ISSN 2194-1629